

VOLUME 68

AUGUST, 1964

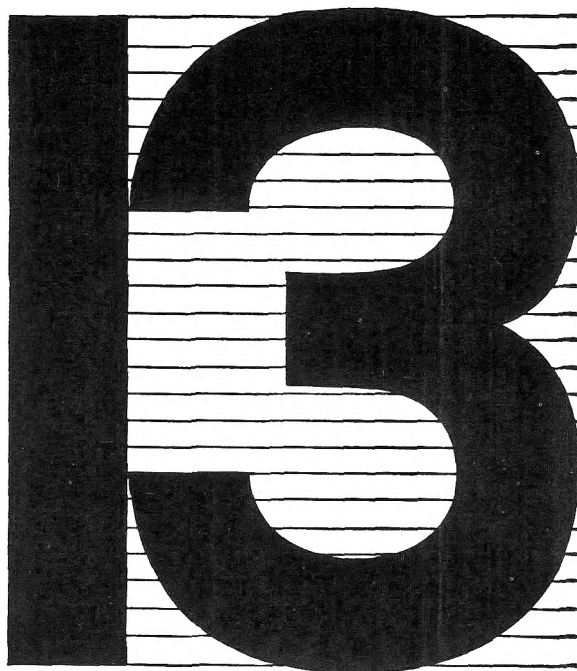
NUMBER 8

THE JOURNAL OF

PHYSICAL

CHEMISTRY

PUBLISHED MONTHLY BY THE AMERICAN CHEMICAL SOCIETY



13 Spectroquality Solvents Now Available for Use In FAR UV

	Cut-Off*
SG2726 Acetonitrile	188 m μ
SG2825 Cyclohexane	193 m μ
SG5089 Glycerol	203 m μ
SG5234 Heptane	193 m μ
SG5093 Hexane	190 m μ
SG2859 Methanol	204 m μ
SG2857 iso-Propyl Alcohol	205 m μ
SG5916 2,2,4-Trimethylpentane	194 m μ
SG5696 2-Methylbutane	191 m μ
SG2858 iso-Butyl Alcohol	207 m μ
SG7602 Cyclopentane	192 m μ
SG2466 Pentane	189 m μ
SG2272 Butyl Alcohol	206 m μ

Low residue 0.0005% max. Low moisture 0.05 max. Low fluorescence less than 0.5% as quinine base. All are typically much less. It has been known for some time that spectra obtained in the region between 160 m μ and 210 m μ are very intense and often highly characteristic. Much valuable information can be gained by exploration in this area. However, the lack of commercially available solvents that are essentially free of impurities with high absorptivity in the far UV has discouraged use of this region.

Now, all MC&B Spectroquality Solvents devoid of intrinsic absorption characteristics in the far UV region, and some with inherent absorptivity in this area, are available with cut-offs that extend well into the far UV.*

We hope that these Spectroquality Solvents will stimulate renewed interest in far UV exploration. The development of these solvents is the result of MC&B's continuing effort to provide the best solvents for spectrophotometry, fluorometry and other precise techniques

*Cut-offs determined with 1-cm cell path using high purity nitrogen as a reference. A cell path of 0.01 cm is recommended in practice to increase the utility of these solvents.

Division of The Matheson Co., Inc.
Norwood (Cincinnati) O., East Rutherford, N. J.



THE JOURNAL OF
PHYSICAL
CHEMISTRY

Volume 68

MAY—AUGUST, 1964

PAGES 983—~~2034~~ 2384

W. ALBERT NOYES, JR., *Editor*

L. O. MORGAN, *Associate Editor*

CHARLES R. BERTSCH, *Senior Production Editor*

RICHARD H. BELKNAP, *Director of Fundamental Journals Division*

EDITORIAL BOARD

A. O. ALLEN
J. BIGEISEN
L. F. DAHL
B. P. DAILEY
F. S. DANTON
D. D. ELEY
J. R. FRESCO

C. J. HOCHANADEL
C. KEMBALL
W. KLEMPERER
A. D. LIEHR
S. C. LIND
F. A. LONG
J. L. MARGRAVE
J. P. McCULLOUGH

W. J. MOORE
R. G. PARR
G. PORTER
J. E. RICCI
M. B. WALLENSTEIN
W. WEST
B. ZIMM

EASTON, PA.
MACK PRINTING COMPANY
1964

THE JOURNAL OF
PHYSICAL CHEMISTRY

Volume 68, Number 8 August, 1964

Microwave Absorption and Molecular Structure in Liquids. LVIII. The Dielectric Relaxations, Infrared Spectra, and Intramolecular Hydrogen Bonding of 2,6-Dichloro- <i>p</i> -nitroaniline and Four Substituted Phenols	Arthur A. Antony, Francis K. Fong, and Charles P. Smyth	2035
Commentary on Scavenging Plots in Radiation Chemical Studies of Liquid Cyclohexane	Cornelius E. Klots, Y. Raef, and Russell H. Johnsen	2040
Localization of Torsional Oscillation about Carbon-Carbon Bonds in Long-Chain Molecules in Aqueous Solutions	A. J. B. Spaul and M. R. Nearn	2043
A Few Cases of Electron Emission and Transfer in Heterogeneous Media	A. Bernas	2047
Induced Dipole Moments of Inorganic Complex Ions	Reiner Kollrack	2052
Oxide-Coated Electrodes. II. Aluminum in Alkaline Solutions and the Nature of the Aluminate Ion	Robert C. Plumb and James W. Swaine, Jr.	2057
The Molecular Structure in Surface Films of Unsaturated 1-Monoglycerides on Water as Related to Three-Dimensional States	D. R. Merker and B. F. Daubert	2064
The Binding of Phenols by Hair. I	M. M. Breuer	2067
The Binding of Phenols by Hair. II. Volume Changes Accompanying the Dilution of Aqueous Solutions of Phenols	M. M. Breuer	2074
The Binding of Phenols by Hair. III. Volume Changes Accompanying Binding of Phenols by Hair	M. M. Breuer	2081
Radiation Chemistry of Oxalate Solutions in the Presence of Oxygen over a Wide Range of Acidities	Z. D. Draganić, I. G. Draganić, and M. M. Kosanić	2085
Equilibrium Studies with the Chelating Ion-Exchange Resin Dowex A-1	Donald E. Leyden and A. L. Underwood	2093
Studies of Anion Adsorption on Platinum by the Multipulse Potentiodynamic (M.p.p.) Method. I. Kinetics of Chloride and Phosphate Adsorption and Associated Charge at Constant Potential	S. Gilman	2098
Studies of Anion Adsorption on Platinum by the Multipulse Potentiodynamic (M.p.p.) Method. II. Chloride and Phosphate Desorption and Equilibrium Surface Concentrations at Constant Potential	S. Gilman	2112
Sensitization by Nitrous Oxide to Radiation-Induced Cross Linking of Polyethylene	Yoichi Okada	2120
Conductance Study of Model Hydrogen Bonding Solutes in Aqueous Solutions at 25°	H. Olin Spivey and Fred M. Snell	2126
The Reduction of Nitrite by Molybdenum(V)	Jean A. Frank and Jack T. Spence	2131
Proton Magnetic Resonance Studies of Hydrogen Bonding of 2-Propanol with <i>N</i> -Methylacetamide and <i>N,N'</i> -Dimethylacetamide	Fujio Takahashi and Norman C. Li	2136
Hydrogen Bonding Studies of <i>N</i> -Methylacetamide and Some Thiols	Raj Mathur, Sung M. Wang, and Norman C. Li	2140
Diaphragm-Cell Method for Constant Mass Diffusion Measurements. Interionic Diffusion and Friction Coefficients in Molten Silver Nitrate-Sodium Nitrate Mixtures	Richard W. Laity and Melvin P. Miller	2145
The Kinetics of the Decarboxylation of Malonanilic Acid in Polar Solvents	Louis Watts Clark	2150
X-Ray Studies of Hydrogen-Silver-Palladium Electrodes	S. D. Axelrod and A. C. Makrides	2154
Absorption of Hydrogen by Silver-Palladium Alloys	A. C. Makrides	2160
The Reaction of Hg 6(³ P ₁) Atoms with Vinyl Chloride	M. G. Bellas, J. K. S. Wan, W. F. Allen, O. P. Strausz, and H. E. Gunning	2170

No. **29** in the
**ADVANCES IN
 CHEMISTRY
 SERIES**

PHYSICAL PROPERTIES OF CHEMICAL COMPOUNDS—III

This handbook of basic data contains 456 full-page tables on 434 aliphatic compounds and 22 miscellaneous compounds and elements—all carefully worked out by R. R. Dreisbach of The Dow Chemical Co.

It is a sequel to **PHYSICAL PROPERTIES—II** (Advances No. 22), which covers 476 organic straight-chain compounds, and **PHYSICAL PROPERTIES—I** (Advances No. 15), which presents data on 511 organic cyclic compounds.

This series provides you with a breadth of data that you can get in no other way. For each compound 15 physical properties are given: purity—freezing point—vapor pressure—liquid density—vapor density—refractive index—rate of change of boiling point with pressure—latent heat of fusion—latent heat of evaporation—critical values—compressibility—viscosity—heat content—surface tension—solubility. Parameters are also furnished for interpolating and extrapolating determined data for almost all the compounds. To get this information by ordinary means you would have to seek out many sources.

PHYSICAL PROPERTIES—III offers the extra advantage of a cumulative index to **all three volumes** (1443 compounds and elements). Use it and the earlier compilations to save yourself hours of laboratory time, and to answer questions quickly.

489 pages.

Cloth bound.

Price: \$6.50

PHYSICAL PROPERTIES—II — 491 pages • cloth bound • price: \$6.50

PHYSICAL PROPERTIES—I — 536 pages • cloth bound • price: \$5.85

Order from:

Special Issues Sales/American Chemical Society/1155 Sixteenth Street, N.W./Washington 6, D.C.

Isotopic Fractionation of Hydrogen between Water and the Aqueous Hydroxide Ion Karl Heinzinger and Ralph E. Weston, Jr.	2179
Radiolysis of Solid Solutions of Acrylamide and Propionamide G. Adler, D. Ballantine, R. Ranganthan, and T. Davis	2184
Radiolysis of Cyclohexane. V. Purified Liquid Cyclohexane and Solutions of Additives S. K. Ho and G. R. Freeman	2189
Investigation of the Vanadium-Hydrogen System by X-Ray Diffraction Techniques Arnulf J. Maeland	2197
Electrodialytic Polarization of Ion-Exchange Membrane Systems H. P. Gregor and Marvin A. Peterson	2201
The Adsorption of Aromatic Vapors on Water Surfaces M. Blank and R. H. Ottewill	2206
Exchange and Diffusion of Ions in Glass R. H. Doremus	2212
Self-Diffusion in Tin at High Pressure C. Coston and N. H. Nachtrieb	2219
Anion Exchange of Metal Complexes. XIV. The Effect of Acidity on the Sorption of Lanthanides from Lithium Nitrate Solutions. Y. Marcus and M. Givon	2230
The Critical Temperature and Coexistence Curve for Bismuth Chloride J. W. Johnson and Daniel Cubicciotti	2235
A Zeroth-Order Approximation for Bond Energies, Hybridization States, and Bond Ionicities. I. Diatomic Molecules and A ⁺ -B ⁻ Crystals Ricardo Ferreira	2240
Voltammetric Study of the Volmer Reaction on Platinum in Sulfuric Acid Solution. I. Dependence of the Exchange Current Density upon the Hydrogen Coverage at 30° M. W. Breiter	2249
Voltammetric Study of the Volmer Reaction on Platinum in Sulfuric Acid Solution. II. Temperature Dependence and Heat of Activation M. W. Breiter	2254
The Measurement of Molecular Weight Distribution in Polymers by Cross Linking-Solubility Methods William W. Graessley	2258
The Continuous Absorption Spectra of Chlorine, Bromine, Bromine Chloride, Iodine Chloride, and Iodine Bromide Daniel J. Seery and Doyle Britton	2263
Isolated Helical Macromolecules Arthur V. Tobolsky	2267
The Filtration of Amorphous and Sized Crystalline Silica Suspensions Flocculated by High Polymers Jacqueline C. Kane, Victor K. La Mer, and Henry B. Linford	2273
Molecule-Wall Collisions in Porous Media at Low Gas Pressure William S. Horton	2278
The Differential Thermal Analysis of Perchlorates. VI. Transient Perchlorate Formation during the Pyrolysis of the Alkali Metal Chlorates Meyer M. Markowitz, Daniel A. Boryta, and Harvey Stewart, Jr.	2282
A Mass Spectrometric Study of Some Alkyl-Substituted Phosphines Yasuo Wada and Robert W. Kiser	2290
Enthalpy Changes in the Reaction of Hydrogen(I), Nickel(II), and Copper(II) Ions with Some α -Amineoximes James C. Wang, John E. Bauman, Jr., and R. Kent Murmann	2296
Energies of Disorientation in Solid Carbon Monoxide and Nitrous Oxide Marian Whitney Melhuish and Robert L. Scott	2301
Activity Coefficients of Electrolytes at Intermediate Concentrations and the "Cube-Root" Law J. E. Desnoyers and B. E. Conway	2305
A Study of Irradiation-Induced Active Sites on Magnesium Oxide Using Electron Paramagnetic Resonance Jack H. Lunsford	2312
Electron Paramagnetic Resonance of Some Nitrogen-Bonded Copper Chelates A. K. Wiersema and J. J. Windle	2316
Activity Coefficients in Aqueous Three-Component Electrolyte Solutions by Equilibrium Ultracentrifugation Richard M. Rush and James S. Johnson	2321
The Heat and Entropy of Formation of Boron(I) Fluoride(g) Jay Blauer, M. A. Greenbaum, and Milton Farber	2332
Sublimation and Thermodynamic Properties of Zinc Oxide Donald F. Anthrop and Alan W. Searcy	2335
Kinetics of Reaction of Elemental Fluorine. II. The Fluorination of Hafnium Carbide and Hafnium Boride A. K. Kuriakose and J. L. Margrave	2343
A Torsion Effusion Study of the Reaction of Graphite with Oxides of Thorium and Zirconium John R. Hollahan and N. W. Gregory	2346
The Near-Infrared Transitions of the Trivalent Lanthanides in Solution. III. Promethium(III) W. T. Carnall, P. R. Fields, and G. E. Toogood	2351

NOTES

Heat of Formation of (HOBO), Jay A. Blauer and Milton Farber	2357
---	------

Appearance Potentials of the Difluoromethylene Positive Ion	W. C. Steele	2359
Comparison of the Photo- and Radiation-Sensitized <i>cis-trans</i> Isomerizations of Polybutadiene	Morton A. Golub	2360
The Effect of Pressure on the Benzylation of 1-Methyl-2-naphthoxide Ion	W. J. le Noble	2361
The Monomerization Rate of Dithionite Ion in Aqueous Solution	S. Lynn, R. G. Rinker, and W. H. Corcoran	2363
The Structure of Rhombohedral Sulfur	J. Donohue and S. H. Goodman	2363
The Photochemistry of α -Keto Acids and α -Keto Esters. III. Photolysis of Pyruvic Acid in the Vapor Phase	George F. Vesley and Peter A. Leermakers	2364
The Rotatory Dispersion of Quartz	Leonard I. Katzin	2367
The Kinetics of Bromine Exchange between Bromide and Bromoacetate Ions	F. J. Johnston	2370
Association between Silver and Chloride Ions in Aqueous Solution	M. J. Insley, G. D. Parfitt, and A. L. Smith	2372
Double Layer Capacity in the Presence of Leucoriboflavin	T. Biegler and H. A. Laitinen	2374
Limiting Isothermic Heats of Adsorption of <i>n</i> -Butane, <i>n</i> -Pentane, and <i>n</i> -Hexane on Graphitized Carbon Black	G. C. Chirnside and C. G. Pope	2377
The Dipole Moments and Polarizabilities of Nitrogen Dioxide and Nitrogen Tetroxide	James E. Boggs	2379
Generation of Acidity in Silica Gel by Ionizing Radiation	C. Barter and C. D. Wagner	2381
The Dipole Moment of Trifluoronitrosomethane	James E. Boggs, DeWitt Coffey, Jr., and Jeff C. Davis, Jr.	2383

AUTHOR INDEX

- | | | | | |
|---------------------------------|-------------------------|-------------------------|-----------------------------|--------------------------|
| Adler, G., 2184 | Daubert, B. F., 2064 | Ho, S. K., 2189 | Maeland, A. J., 2197 | Scott, R. L., 2301 |
| Allen, W. F., 2170 | Davis, J. C., Jr., 2383 | Hollahan, J. R., 2346 | Makrides, A. C., 2154, 2160 | Searcy, A. W., 2335 |
| Anthrop, D. F., 2335 | Davis, T., 2184 | Horton, W. S., 2278 | Marcus, Y., 2230 | Seery, D. J., 2263 |
| Antony, A. A., 2035 | Desnoyers, J. E., 2305 | Insley, M. J., 2372 | Margrave, J. L., 2343 | Smith, A. L., 2372 |
| Axelrod, S. D., 2154 | Donohue, J., 2363 | Johnsen, R. H., 2040 | Markowitz, M. M., 2282 | Smyth, C. P., 2035 |
| Ballantine, D., 2184 | Doremus, R. H., 2212 | Johnson, J. S., 2321 | Mathur, R., 2140 | Snell, F. M., 2126 |
| Barter, C., 2381 | Draganić, I. G., 2085 | Johnson, J. W., 2235 | Melhuish, M. W., 2301 | Spaull, A. J. B., 2043 |
| Bauman, J. E., Jr., 2296 | Draganić, Z. D., 2085 | Johnston, F. J., 2370 | Merker, D. R., 2064 | Spence, J. T., 2131 |
| Bellas, M. G., 2170 | Farber, M., 2332, 2357 | Kane, J. C., 2273 | Miller, M. P., 2145 | Spivey, H. O., 2126 |
| Bernas, A., 2047 | Ferreira, R., 2240 | Katzin, L. I., 2367 | Murmann, R. K., 2296 | Steele, W. C., 2359 |
| Biegler, T., 2374 | Fields, P. R., 2351 | Kiser, R. W., 2290 | Nachtrieb, N. H., 2219 | Stewart, H., Jr., 2282 |
| Blank, M., 2206 | Fong, F. J., 2035 | Klots, C. E., 2040 | Nearn, M. R., 2043 | Strausz, O. P., 2170 |
| Blauer, J., 2332, 2357 | Frank, J. A., 2131 | Kollrack, R., 2052 | Okada, Y., 2120 | Swaine, J. W., Jr., 2057 |
| Boggs, J. E., 2379, 2383 | Freeman, G. R., 2189 | Kosanić, M. M., 2085 | Ottewill, R. H., 2206 | Takahashi, F., 2136 |
| Boryta, D. A., 2282 | Gilman, S., 2098, 2112 | Kuriakose, A. K., 2343 | Parfitt, G. D., 2372 | Tobolsky, A. V., 2267 |
| Breiter, M. W., 2249, 2254 | Givon, M., 2230 | Laitinen, H. A., 2374 | Peterson, M. A., 2201 | Toogood, G. E., 2351 |
| Breuer, M. M., 2067, 2074, 2081 | Golub, M. A., 2360 | Laity, R. W., 2145 | Plumb, R. C., 2057 | Underwood, A. L., 2093 |
| Britton, D., 2263 | Goodman, S. H., 2363 | La Mer, V. K., 2273 | Pope, C. G., 2377 | Vesley, G. F., 2364 |
| Carnall, W. T., 2351 | Graessley, W. W., 2258 | Leermakers, P. A., 2364 | Raef, Y., 2040 | Wada, Y., 2290 |
| Chirnside, G. C., 2377 | Greenbaum, M. A., 2332 | le Noble, W. J., 2361 | Ranganthan, R., 2184 | Wagner, C. D., 2381 |
| Clark, L. W., 2150 | Gregor, H. P., 2201 | Leyden, D. E., 2093 | Rinker, R. G., 2363 | Wan, J. K. S., 2170 |
| Coffey, D., Jr., 2383 | Gregory, N. W., 2346 | Li, N. C., 2136, 2140 | Rush, R. M., 2321 | Wang, J. C., 2296 |
| Conway, B. E., 2305 | Gunning, H. E., 2170 | Linford, H. B., 2273 | | Wang, S. M., 2140 |
| Corcoran, W. H., 2363 | Heinzinger, K., 2179 | Lunsford, J. H., 2312 | | Weston, R. E., Jr., 2179 |
| Coston, C., 2219 | | Lynn, S., 2363 | | Wiersema, A. K., 2316 |
| Cubicciotti, D., 2235 | | | | Windle, J. J., 2316 |

Microwave Absorption and Molecular Structure in Liquids. LVIII.**The Dielectric Relaxations, Infrared Spectra, and Intramolecular****Hydrogen Bonding of 2,6-Dichloro-*p*-nitroaniline and****Four Substituted Phenols^{1,2}**

by Arthur A. Antony,³ Francis K. Fong, and Charles P. Smyth

Frick Chemical Laboratory, Princeton University, Princeton, New Jersey (Received April 20, 1964)

The dielectric constants and losses of dilute benzene solutions of 2,6-dibromophenol, 2,6-dibromo-*p*-nitrophenol, 2,6-dichloro-*p*-nitrophenol, 2,4-dibromophenol, and 2,6-dichloro-*p*-nitroaniline have been measured at 20, 40, and 60° at several microwave frequencies and used to calculate the dielectric relaxation times. The infrared spectra in the OH stretching region have been measured for solutions of 2,6-dibromo-*p*-nitrophenol, 2,6-dibromophenol, 2,4-dibromophenol, and *o*-bromophenol. 2,6-Dibromo-*p*-nitrophenol and 2,6-dichloro-*p*-nitrophenol behave as rigid molecules, but 2,6-dibromophenol can be treated in terms of two relaxation times, one due to molecular rotation and the other due to OH group rotation. 2,4-Dibromophenol probably has more than two relaxation times. The dipole moment of this molecule can be interpreted in terms of the two conformations in which the OH is coplanar with the benzene ring.

Previous work⁴ on the dielectric relaxation of chloroform in solution indicates that hydrogen bonding increases the dielectric relaxation time. Substitution of halogens in the *ortho* position in phenol should result in an intramolecular hydrogen bond and, therefore, an increased barrier to internal rotation. In order to confirm the presence of an intramolecular hydrogen bond and in order to ascertain the relative strength of this bond in the compounds studied, infrared spectroscopic measurements have been made in the region of the OH stretching fundamental of the phenols. The

unexpectedly large band widths observed in benzene solution prompted some additional infrared studies, which are also reported in this paper.

(1) This research was supported by the Office of Naval Research, the National Science Foundation, and the U. S. Army Research Office (Durham). Reproduction, translation, use, or disposal in whole or in part by or for the United States Government is permitted.

(2) This paper represents part of the work submitted by A. A. Antony to the Graduate School of Princeton University in partial fulfillment of the requirement for the degree of Doctor of Philosophy.

(3) Allied Chemical Fellow, 1961-1962; Woodrow Wilson Fellow, 1959-1960.

Experimental

Purification of Materials. Five compounds obtained from Eastman Kodak Co. were treated as follows: 2,6-dibromophenol was shaken with decolorizing charcoal, filtered, and then recrystallized from ether; 2,6-dibromo-*p*-nitrophenol, 2,6-dichloro-*p*-nitrophenol, and 2,6-dichloro-*p*-nitroaniline were recrystallized from ether; 2,4-dibromophenol was recrystallized from chloroform. The following melting points were obtained: 2,6-dibromophenol, 54.8–55.3°; 2,6-dibromo-*p*-nitrophenol, 143–144°; 2,6-dichloro-*p*-nitrophenol, 122.5°, decomposition accompanying melting; 2,6-dichloro-*p*-nitroaniline, 193.5–194.4°; 2,4-dibromophenol, 38–40°. *o*-Bromophenol from Matheson Coleman and Bell was used without further purification. Reagent grade benzene and carbon tetrachloride from Baker and Adamson were also used without further purification. Cyclohexane from Matheson Coleman and Bell was fractionally distilled.

Apparatus. Dielectric constants and losses were measured by methods previously described.^{5–7} Infrared spectra were measured on a Perkin-Elmer 421 grating spectrometer.

Results

Slopes a_0 , a' , a_D , and a'' were obtained by plotting the static dielectric constants ϵ_0 , the high frequency dielectric constants ϵ' , the refractive indices for the sodium D-line, and the losses ϵ'' of the solutions against the concentrations of the polar solutes. Values of the distribution parameter α and the most probable relaxation time τ_0 were obtained from Cole-Cole plots of a' against a'' .^{8,9} In Table I the experimental values for a_0 , a' , and a'' are listed. In Table II the values for α , a_D , a_∞ , and τ_0 are listed.

Because of the very low solubility of 2,6-dichloro-*p*-nitroaniline in benzene, measurements were made only on the saturated solution and τ_0 was obtained from the frequency at maximum loss from a plot of $\epsilon_S'' - \epsilon_B''$ against log frequency, where ϵ_S'' is the loss of the solution and ϵ_B'' is the loss of benzene. Table III lists the OH stretching fundamental frequencies and half-band widths measured in the infrared region. Some of the values listed are taken from the literature. The frequency associated with the nonhydrogen-bonded OH is listed under the column "Free" and that associated with the hydrogen-bonded OH under the column "Bonded." The band width at half-height is given under $\Delta\nu_{1/2}$.

Discussion

All of the compounds discussed in this paper may be expected to show intramolecular hydrogen bonding.

Table I: Slopes for the Dependence of Dielectric Constant and Loss on Concentration in Benzene Solution

Wave length, cm.	20°		40°		60°	
	a'	a''	a'	a''	a'	a''
2,6-Dibromophenol (0–0.0195)						
1 25	1.9	1.05	2.2	1.20	2.4	1.33
3 22	3.2	1.57	3.5	1.49	3.5	1.43
10 0	5.0	1.53	4.9	1.10	4.9	0.87
575 m.	5.9		5.5		5.2	
2,6-Dibromo- <i>p</i> -nitrophenol (0–0.0125)						
1 25	1.6	1.75	2.1	1.88	2.0	2.23
3 22	2.69	3.4	3.7	3.9	4.6	4.4
10 0	8.9	7.25	11.1	6.2	12.0	4.44
25 0	15.8	5.04	14.6	3.75	13.5	2.55
50 0	16.7	2.98	15.1	2.10	13.9	1.4
575 m.	17.66		16.00		14.32	
2,4-Dibromophenol (0–0.0125)						
3 22	1.8	0.72	1.8	0.66		
10 0	2.5	0.63	2.35	0.43		
25 0	2.05	0.35	2.75	0.28		
50 0	3.05	0.20	2.8	0.18		
575 m.	3.1		2.85			
2,6-Dichloro- <i>p</i> -nitrophenol (0–0.0158)						
1 25	2.63	1.4	2.68	1.70	2.58	1.70
3 22	3.37	2.98	3.71	3.28	4.05	3.67
10 0	7.31	6.06	8.54	5.21	9.22	3.98
575 m.	15.96		13.96		11.84	
2,6-Dichloro- <i>p</i> -nitroaniline						
	$\epsilon_S'' - \epsilon_B''$		$\epsilon_S'' - \epsilon_B''$		$\epsilon_S'' - \epsilon_B''$	
1.25	0.0122		0.0164		0.0192	
3.22	0.0220		0.0235		0.0246	
10.0	0.0327		0.0268		0.0198	

If halogens are substituted in both the 2- and the 6-positions, the OH or NH₂ group can be intramolecularly bonded to either position and, in an alternating electric field, might acquire enough energy to break the bond to one halogen, jump over the barrier to internal rotation, and form a hydrogen bond to the other halogen. This behavior would manifest itself by a second intramolecular relaxation time, in addition to that associated with the over-all molecular rotation. It would

(4) A. A. Antony and C. P. Smyth, *J. Am. Chem. Soc.*, **86**, 152 (1964).

(5) W. M. Heston, Jr., A. D. Franklin, E. J. Hennelly, and C. P. Smyth, *ibid.*, **72**, 3443 (1950).

(6) D. A. Pitt and C. P. Smyth, *J. Phys. Chem.*, **63**, 582 (1959).

(7) L. M. Kushner and C. P. Smyth, *J. Am. Chem. Soc.*, **71**, 1401 (1949).

(8) K. S. Cole and R. H. Cole, *J. Chem. Phys.*, **9**, 341 (1941).

(9) C. P. Smyth, "Dielectric Behavior and Structure," McGraw-Hill Book Co., New York, N. Y., 1955, Chapter II.

Table II: Slopes, a_D , for the Dependence of the Square of the Refractive Index on Concentration, Infinite Frequency Intercepts a_∞ , Relaxation Times τ_0 , Distribution Parameters α , and Dipole Moments μ

t , °C.	a_D	a_∞	τ_0 , 10^{-12} sec.	α	$\mu \times$ 10^{18}
2,6-Dibromophenol					
20	0.6	1.50	23	0.13	
40		1.51	18	0.12	
60		1.50	14	0.12	
2,6-Dibromo- <i>p</i> -nitrophenol					
20	1.0	1.68	56	0.03	3.32
40		1.68	44	0.04	
60		1.68	28	0.06	
2,4-Dibromophenol					
20	0.36	0.85	23	0.24	1.35
40		0.83	22	0.28	
2,6-Dichloro- <i>p</i> -nitrophenol					
20	0.45	2.40	69	0	3.04
40		2.35	49	0	
60		2.30	32	0	
2,6-Dichloro- <i>p</i> -nitroaniline					
20			61		
40			40		
60			23		

Table III: OH Fundamental Stretching Frequencies and Half-Band Widths

Solute	Solvent	Bonded		Free ν , cm. ⁻¹
		ν , cm. ⁻¹	$\Delta\nu^{1/2}$, cm. ⁻¹	
2,6-Dibromo- <i>p</i> -nitrophenol	C ₆ H ₁₂	3496	16	
	CCl ₄	3492	31	
	C ₆ H ₆	3473	67	
2,6-Dibromophenol	CCl ₄	3514	36	
	C ₆ H ₆	3499	55	
2,4-Dibromophenol	CCl ₄ ^a	3528	23	3597
	C ₆ H ₆	3512	62	
<i>o</i> -Bromophenol	CCl ₄ ^a	3529	19	3604
	C ₆ H ₆	3515	50	
Phenol	CCl ₄ ^b			3614
	C ₆ H ₆ ^b			3558

^a I. Brown, G. Eglinton, and M. Martin-Smith, *Spectrochim. Acta*, **18**, 1593 (1962). ^b G. M. Huggins and G. C. Pimentel, *J. Phys. Chem.*, **60**, 1615 (1956).

thus be feasible to analyze the most probably relaxation time τ_0 into a relaxation time τ_1 due to over-all molecular rotation and another relaxation time τ_2

associated with internal group rotation. The infrared measurements in every case indicate the presence of intramolecular hydrogen bonding. The solutions were dilute enough so that no intermolecular bonding between solute molecules was expected, and no infrared peak characteristic of such a bond was found.

2,6-Dibromophenol. It was possible to analyze the data for this compound into two relaxation times by the double arc method.¹⁰ The results of this analysis are listed in Table IV. A dipole moment of 2.26 D. is calculated for this molecule from bond moments.¹¹ A value of 1.46 D. was used for the *m*-dibromo contribution. The OH bond moment was assumed to be 1.51 D. and the CO moment 0.99 D. A COH angle of 115° was assumed. The moment μ along the direction of the CO bond is 1.82 D. and the moment μ_2 perpendicular to this is 1.36. If Debye behavior is assumed for both the over-all molecular and the intramolecular relaxation processes, $C_1/C_2 = (\mu_1/\mu_2)^2$, which gives C_2 as 0.36. This is close to the observed value at 20° in Table IV. The temperature dependence of C_2 may be due to a greater rate of increase of the relaxation of the hydrogen-bonded group with rising temperature, although the actual values of C_2 are higher than expected.

Table IV: Relaxation Times (10^{-12} sec.) by the Double Arc Method for 2,6-Dibromophenol

t , °C.	τ_1	τ_2	C_2
20	39.2	12.7	0.40
40	35.2	10.3	0.54
60	26.5	10.0	0.57

The relaxation time associated with hydroxyl group rotation is larger than the value reported for compounds in which intramolecular bonding is absent. Some values which have been reported are 3.2×10^{-12} sec. for 2-naphthol,¹⁰ 3.5×10^{-12} sec. for 2,6-dimethylphenol,^{12,13} and 8.4×10^{-12} sec. for 2,4,6-trichlorophenol.¹³ A much higher barrier to internal rotation in the 2,4,6-trichlorophenol molecule is the result of the intramolecular hydrogen bond. The OH group rotation relaxation time is slightly higher for the bromo-substituted compound (Table IV) than for the chloro-substituted compound. Conclusions drawn

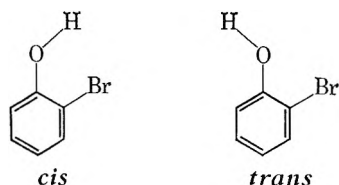
(10) F. K. Fong and C. P. Smyth, *J. Phys. Chem.*, **67**, 226 (1963).

(11) C. P. Smyth, "Dielectric Behavior and Structure," McGraw-Hill Book Co., New York, N. Y., 1955, Chapter X.

(12) F. K. Fong and C. P. Smyth, *J. Am. Chem. Soc.*, **85**, 1565 (1963).(13) A. Aihara and M. Davies, *J. Colloid Sci.*, **11**, 671 (1956).

from infrared measurements concerning the relative strengths of the intramolecular hydrogen bonding of the OH group to the two halogens in these compounds are ambiguous.¹⁴⁻²⁰ The dielectric studies suggest that the hydrogen bonding is stronger in the case of the bromo-substituted compound. However, the relaxation times associated with group rotation in the two compounds were not calculated by the same method, and the difference between the two values is, perhaps, too small to permit conclusions as to the relative strengths of the two intramolecular hydrogen bonds.

2,4-Dibromophenol. Because of the small polarization of this compound, no attempts were made to analyze the data for it into more than one relaxation time. The large value of the distribution parameter indicates that more than one mechanism is contributing to dielectric relaxation. In addition to the relaxation time associated with molecular rotation, one might expect two relaxation times associated with group rotation, one involving breaking the intramolecular hydrogen bond and rotation of the OH group to the *trans* position, and the other involving rotation of the OH from the *trans* position to the *cis* position. The *cis-trans* rotation would be expected to have a larger relaxation time than the *trans-cis* rotation since the breaking of a hydrogen bond is necessary for the former.



The orientation polarization, obtained from the Cole-Cole arc at 20°, is 38.15 cc. This corresponds to a dipole moment of 1.35 D., according to eq. 1.²¹

$$\frac{C_1 M_1 + C_2 M_2}{d C_2} \left[\frac{\epsilon_0 - 1}{\epsilon_0 + 2} - \frac{\epsilon_\infty - 1}{\epsilon_\infty + 2} \right] = \frac{4\pi N}{9kT} \mu^2 \quad (1)$$

Using the bond moments given above, the dipole moment is calculated to be 0.37 D. with OH in the *cis* configuration and 2.64 D. with it in the *trans* configuration. The intermediate value is an indication that both species are present.

Equation 2 can be used to estimate the fraction of molecules in the *trans* conformation.

$$P = x P_{trans} + (1 - x) P_{cis} \quad (2)$$

P is the measured polarization, x the fraction of molecules in the *trans* conformation, and P_{trans} and P_{cis} the calculated polarizations for the *trans* and *cis* forms,

respectively. Approximately 20% of the molecules are in the *trans* form. This is very close to the result obtained²² for *o*-bromophenol.

*2,6-Dibromo-*p*-nitrophenol.* Attempts were made to obtain two relaxation times by the double arc method¹⁰ used for the 2,6-dibromophenol. It was impossible to obtain two relaxation times. The expected dipole moment¹¹ along the axis of symmetry is 2.16 D., and the component perpendicular to this axis is 1.36 D. One would, therefore, expect a value of about 0.2 for C_2 , assuming Debye behavior for the group relaxation. The virtual absence of a contribution to the relaxation time due to the OH group rotation, while a considerable contribution is observed in the absence of the nitro group, indicates that the carbon-oxygen bond is considerably stiffened by the presence of the nitro group in the *para* position. This is not unexpected. The nitro group is an electron-withdrawing group, and, in the *para* position, it aids the resonance interaction of the hydroxyl oxygen with the benzene ring, as evidenced by an increase of 0.70 in the dipole moment of the *p*-nitrophenol above the calculated value. The resultant double-bond character of the C-O bond appears to be sufficient to hinder strongly rotation of the OH in the applied field. Because of the increased resonance interaction between the oxygen and benzene, a stronger intramolecular hydrogen bond is expected. That this is the case is indicated by the fact that the OH stretching absorption occurs at a lower frequency for 2,6-dibromo-*p*-nitrophenol than for 2,6-dibromophenol. The increased hydrogen bond strength further hinders the internal OH rotation.

*2,6-Dichloro-*p*-nitrophenol.* The relaxation time of 2,6-dichloro-*p*-nitrophenol is larger than that of 2,6-dibromo-*p*-nitrophenol, in spite of the fact that the bromine atoms are larger than the chlorine atoms. This could conceivably arise from a greater lowering of relaxation time by OH rotation in the bromo compound, although the effect is too small to permit a separation into two relaxation times. The dipole

(14) G. Rossmly, W. Luttkie, and R. Mecke, *J. Chem. Phys.*, **21**, 1606 (1953).

(15) A. W. Baker, *J. Am. Chem. Soc.*, **80**, 3598 (1958).

(16) A. W. Baker and W. W. Kaeding, *ibid.*, **81**, 5904 (1959).

(17) O. Wulf, E. Jones, and L. Deming, *J. Chem. Phys.*, **8**, 753 (1940).

(18) L. Pauling, *J. Am. Chem. Soc.*, **58**, 94 (1936).

(19) D. A. Jones and J. G. Watkinson, *Chem. Ind. (London)*, 661 (1960).

(20) I. Brown, G. Eglinton, and M. Martin-Smith, *Spectrochim. Acta*, **18**, 1593 (1962).

(21) C. P. Smyth, "Dielectric Behavior and Structure," McGraw-Hill Book Co., New York, N. Y., 1955, pp. 18, 55.

(22) J. H. Richards and S. Walker, *Trans. Faraday Soc.*, **57**, 412 (1961).

moment of 2,6-dichloro-*p*-nitrophenol, as calculated by eq. 1 is 3.04 D., while that for 2,6-dibromo-*p*-nitrophenol is 3.32. Bond moment calculations¹¹ lead one to expect a dipole moment of 2.53 D. for 2,6-dichloro-*p*-nitrophenol, as compared to 3.04 observed (Table II), and 2.55 for 2,6-dibromo-*p*-nitrophenol, as compared to 3.32 observed. The C-NO₂ bond moment was taken as 3.98 D., and the moment due to the *m*-dichloro substituents was taken as 1.48, the moment of *m*-dichlorobenzene. The other values used have been given previously in this paper. The measured dipole moment 3.04 is greater than that expected from bond moments alone because of the large mesomeric moment, a situation similar to that in 2,6-dibromo-*p*-nitrophenol. The difference between the calculated and the observed moments (D.) of *p*-nitrophenol is 0.70, while, for 2,6-dichloro-*p*-nitrophenol, it is only 0.51, and, for 2,6-dibromo-*p*-nitrophenol, it is 0.77.

2,6-Dichloro-p-nitroaniline. The relaxation times for this compound are calculated from the loss *vs.* log frequency curves. The values at 40 and 60° are more accurate than that at 20° since the experimental points lie on both sides of the maxima. These relaxation times are not to be considered as reliable as those determined from the Cole-Cole arcs for the other compounds. One would expect 2,6-dichloro-*p*-nitrophenol and 2,6-dichloro-*p*-nitroaniline to have about the same relaxation time. The fact that the aniline has a smaller relaxation time may indicate a contribution from NH₂ group rotation, but this should be small in view of the large mesomeric moments of *p*-nitroaniline and *N,N*-dimethyl-*p*-nitroaniline,¹¹ which indicate a considerable amount of double-bond character in the C-N bond. Several molecules containing the NH₂ group have, however, been found to have somewhat lower relaxation times than the corresponding molecules with OH groups.^{10,12,23}

Infrared Investigation. The OH stretching frequency of the *o*-halophenols is shifted to considerably lower frequencies than that of phenol. For phenol in benzene, it is shifted to a frequency 56 cm.⁻¹ lower than that for phenol in carbon tetrachloride. On the other hand, in the *o*-halophenols, the difference between the OH frequencies in benzene and in carbon tetrachloride is 19 cm.⁻¹ or less. Thus, the position of the OH frequency indicates intramolecular bonding between the hydroxyl and halogen groups in both benzene and car-

bon tetrachloride solution. The OH band for 2,6-dibromophenol occurs at a lower frequency than that for 2,4-dibromophenol, indicating that the intramolecular hydrogen bond is stronger in 2,6-dibromophenol than in 2,4-dibromophenol or *o*-bromophenol.

For *o*-bromophenol in benzene, a small shoulder is observed on the high frequency side of the band at 3515 cm.⁻¹. This is probably due to the "free" OH band, which is shifted into the region of the intramolecularly bonded OH band because of hydrogen bonds to the benzene solvent molecules. Not even a shoulder is observed for 2,4-dibromophenol. Because of the inductive effect of the additional bromine group and because of the fairly large breadth of both the "free" and the bonded peak, the "free" peak is probably completely masked by the bonded peak.

All of the intramolecularly bonded OH bands are significantly broader in benzene than in carbon tetrachloride. In general, when intermolecular hydrogen bonding causes a shift to a lower frequency, it also causes band broadening²⁴; and the stronger the bond, the broader the band. It is unlikely that the intramolecular hydrogen bond is stronger in benzene solution than in carbon tetrachloride solution. The band broadening could result from a perturbation on the intramolecular hydrogen bond exerted by the π -electrons of the benzene molecule. Thus, the benzene molecules might increase the number of possible intramolecularly bonded configurations. Similarly, the band for 2,6-dibromo-*p*-nitrophenol is broader in carbon tetrachloride than in cyclohexane because of the forces exerted by the C-Cl dipoles. The solute-solvent interaction due to the ability to form hydrogen bonds might also explain why the relaxation times are slightly larger than expected in comparison with other molecules of similar size and shape. For example, the relaxation time of 2,6-dibromophenol for molecular rotation is 39.2×10^{-12} sec. at 20° in benzene, which is considerably larger than the value 18.0×10^{-12} sec. reported²⁵ for α -bromonaphthalene at 20° in benzene, although the latter is a larger molecule.

(23) E. L. Grubb and C. P. Smyth, *J. Am. Chem. Soc.*, **83**, 4879 (1961).

(24) C. M. Huggins and G. C. Pimentel, *J. Phys. Chem.*, **60**, 1615 (1956).

(25) H. Hufnagel, *Z. Naturforsch.*, **15a**, 723 (1960).

Commentary on Scavenging Plots in Radiation Chemical

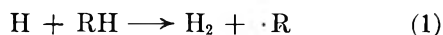
Studies of Liquid Cyclohexane¹

by Cornelius E. Klots, Y. Raef, and Russell H. Johnsen

*Department of Chemistry and the Institute of Molecular Biophysics,
Florida State University, Tallahassee, Florida (Received April 15, 1964)*

Hydrogen yields from X-irradiated liquid cyclohexane in the presence of a variety of potential hydrogen atom scavengers have been measured and analyzed within the framework of an assumed scavenging mechanism. Only oxygen- and iodine-containing solutions are amenable to this interpretation, other solutes showing a more complicated concentration dependence. The role of a molecular detachment process is delineated.

The work of Dewhurst² and Burton³ has strongly implied that thermally diffusing hydrogen atoms are important in the radiation chemistry of the liquid aliphatics. From this premise and its corollary that much of the radiolytically produced hydrogen originates in the reaction



Hardwick⁴ has developed techniques of seemingly unprecedented potency for determining both the yields of such hydrogen atoms and the rate of their abstraction reaction relative to scavenging by a suitable additive (see ref. 4 and intermediate papers). During the course of some earlier work in this laboratory,⁵ it appeared worthwhile to exploit this technique to determine the relative scavenging efficiencies of various aromatic agencies. The initial results, in a cyclohexane medium, were of sufficient interest to justify their extension to a larger number of scavengers. The data are presented in this paper and permit an operational commentary on scavenging studies of this type. In brief, they suggest that mechanistic conclusions are not to be so easily reached as has been previously suggested.

Experimental

Eastman Kodak spectral grade, Fisher spectral grade, and Phillips research grade cyclohexane were all used, both as received and after purification by sulfuric acid or gas-liquid chromatography. Radiolytic yields of hydrogen were identical from all sources

except when chromatography indicated an obvious olefinic impurity. Five-milliliter samples were degassed and sealed off in Pyrex ampoules, mounted on a turntable, and irradiated at room temperature with X-rays generated by 3-Mev. electrons. Typical doses were 0.1 Mrad and were monitored by a sample of pure cyclohexane, for which a $G_0(\text{H}_2) = 5.55$ was assumed.⁶ Electron density corrections were made when significant. Hydrogen yields were measured, as gas volatile at -196° , with a McLeod gauge, except in the case of added oxygen; here hydrogen yields were determined by injecting the volatile gases onto a 6-ft. charcoal column at room temperature, using a thermal conductivity detector and nitrogen as a carrier gas.

Solutions were prepared volumetrically. The solutes were Eastman Kodak spectral or research grade, when available. In the case of oxygen, a Henry's law constant, $K = 7.3 \times 10^2$ (atm.), was estimated from analogous solubilities in the literature.

Results and Discussion

The qualitative influence of free-radical scavengers on radiolytic hydrogen yields led early workers to the

(1) This work was supported in part by the U. S. Atomic Energy Commission under contract No. AT-(40-1)-2001, and the Division of Biology and Medicine, U. S. Atomic Energy Commission.

(2) H. A. Dewhurst, *J. Phys. Chem.*, **62**, 15 (1958).

(3) G. Meshitsuka and M. Burton, *Radiation Res.*, **10**, 499 (1959).

(4) (a) T. J. Hardwick, *J. Phys. Chem.*, **64**, 1623 (1960); (b) T. J. Hardwick, *ibid.*, **66**, 1611 (1962).

(5) C. E. Klots and R. H. Johnsen, *ibid.*, **67**, 1615 (1963).

(6) P. J. Dyne and J. A. Stone, *Can. J. Chem.*, **39**, 2381 (1961).

concepts of scavengeable and nonscavengeable sources of hydrogen.^{2,7} The distinction between these two sources is best illustrated by the employment of a so-called scavenging plot^{4,8} in which the reduction in hydrogen yield (ΔG) is plotted as a function of solvent-scavenger concentration ratio. A steady-state kinetic treatment provides the analytically convenient form

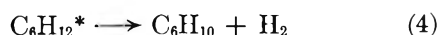
$$(\Delta G)^{-1} = A(1 + B[\text{hydrocarbon}]/[\text{scavenger}]) \quad (2)$$

Hydrogen reductions must be corrected for the fractional dose absorbed by the additive. In this paper, the customary method utilizing the electron fraction approximation has been followed, in the absence of the information necessary for a more appropriate procedure.⁹ The graphically-derived parameter (A) then provides a measure of $G(H)$, the hydrogen atoms which are presumed to react according to eq. 1 in the absence of scavengers. The rate constant for this reaction (k_1) relative to that for the assumed scavenging mechanism



is then given by parameter B . Finally, from the derived value of $G(H)$, and the observed $G_0(\text{H}_2)$, an estimate of the "nonscavengeable" hydrogen is obtained.

Before embarking upon a discussion of the present results, it will be useful to establish an upper limit for $G(H)$ in the cyclohexane system. Dicyclohexyl is obtained with a $G = 1.95$ as a primary product.⁶ This is most plausibly attributed to the combination of cyclohexyl radicals since its appearance can be quenched by the addition of a variety of scavengers.¹⁰⁻¹² If we make the nontrivial^{13,14} assumption that the recently measured disproportionation-combination ratio ($=1.31$) for cyclohexyl radicals¹⁵ is applicable here, the yield of cyclohexene *via* disproportionation is easily obtained. From the observed initial yield,⁶ $G(\text{C}_6\text{H}_{10}) = 3.27$, it follows that an additional source of cyclohexene exists with a $G = 0.72$. A yield of this magnitude is in excellent agreement with the observed cyclohexene production in heavily scavenged solutions^{6,10,16} and consistent with the first-order yield of D_2 from C_6D_{12} .¹⁷ Dyne¹⁸ has argued forcibly for a molecular detachment mechanism



The rather satisfactory convergence of three quite independent pieces of evidence, aside from delineating the extent of this reaction, lends further justification to our assumption concerning the origin of dicyclohexyl. It thus seems unnecessary to postulate^{19,20}

mechanisms involving an ion-molecule condensation directly to dimeric product in liquid cyclohexane.

The above prelude serves to establish that only $\sim 15\%$ of the total hydrogen yield is to be assigned to reaction 4. The source of the remaining hydrogen, which might conceivably arise entirely through reaction 1, is now to be considered. In Fig. 1, the hydrogen yields from oxygen- and iodine-scavenged solutions are presented. They take the correct analytical form with intercepts indicating a $G(H) \simeq 1.96$. This is in excellent agreement with, and confirms, previous studies using iodine.^{3,12} If the scavenging mechanism is accepted, then the slopes yield k_1/k_3 (oxygen) = 4.4×10^{-4} , k_1/k_3 (iodine) = 2.6×10^{-4} . Such an interpretation would, however, be at odds with hydrogen yields from isotopic mixtures,^{17,21} in which a

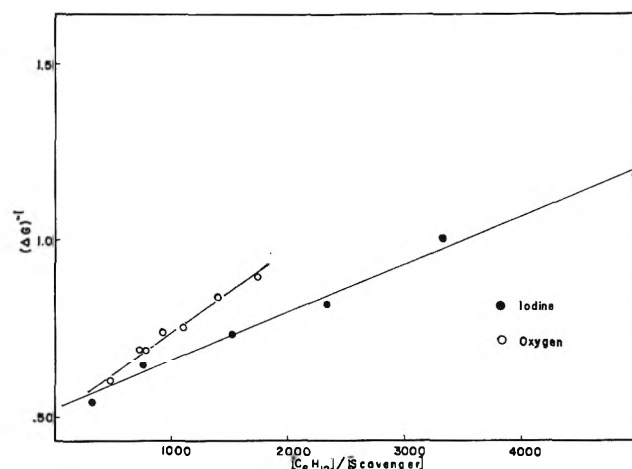


Figure 1. Hydrogen yields from oxygen- and iodine-scavenged liquid cyclohexane.

- (7) M. Burton and W. N. Patrick, *J. Phys. Chem.*, **58**, 421 (1954).
- (8) G. E. Adams, J. H. Baxendale, and R. D. Sedgewick, *ibid.*, **63**, 854 (1959).
- (9) C. E. Klots, *J. Chem. Phys.*, **39**, 1571 (1963).
- (10) H. A. Dewhurst, *J. Phys. Chem.*, **63**, 813 (1959).
- (11) E. S. Waight and P. Walker, *J. Chem. Soc.*, 2225 (1960).
- (12) L. J. Forrestal and W. H. Hamill, *J. Am. Chem. Soc.*, **83**, 1535 (1961).
- (13) It is probable, but not imperative,¹⁴ that the reactions of cyclohexyl radicals formed adjacent to each other, as may well be the case here, will be identical with those of freely diffusing species.
- (14) P. S. Dixon, A. P. Stefani, and M. Szwarc, *J. Am. Chem. Soc.*, **85**, 2551 (1963).
- (15) C. E. Kloos and R. H. Johnsen, *Can. J. Chem.*, **41**, 2702 (1963).
- (16) A. MacLachlan, *J. Am. Chem. Soc.*, **82**, 1005 (1960).
- (17) P. J. Dyne and W. M. Jenkinson, *Can. J. Chem.*, **39**, 2163 (1961).
- (18) P. J. Dyne, *J. Phys. Chem.*, **66**, 767 (1962).
- (19) F. Williams, *Trans. Faraday Soc.*, **57**, 755 (1961).
- (20) L. Kevan and W. F. Libby, *J. Chem. Phys.*, **39**, 1288 (1963).
- (21) M. Burton and J. Chang, 137th National Meeting of American Chemical Society, Cleveland, Ohio, April, 1960.

role for iodine other than scavenging is indicated. The present authors are not prepared to resolve this conflict; we note, however, that previously established rate constants²² for these solutes indicate that if bulk-diffusing hydrogen atoms are produced in these solutions, they will be scavenged with at least the indicated efficiency. A $G(H) \simeq 2.0$ must then represent a *maximum* yield for such species.

Reference to Fig. 2 will reveal a somewhat more complex situation. Despite the variety of conventional scavengers used, in no case is the expected

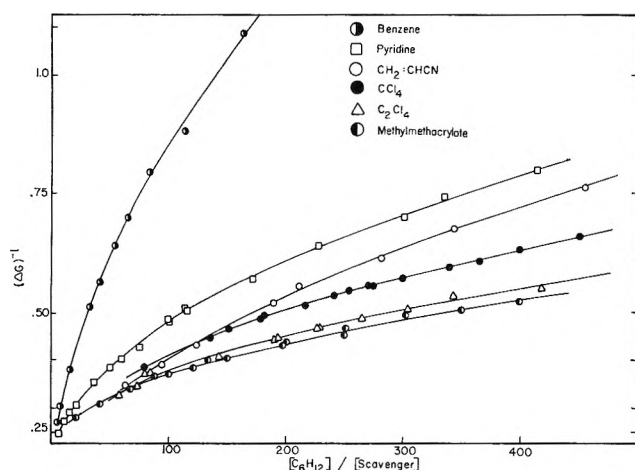
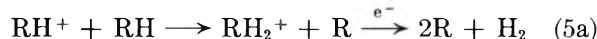


Figure 2. Hydrogen yields from cyclohexane solutions containing a variety of organic scavengers.

analytical form obtained. Tangents to the observed curves at concentrations $\sim 1\%$ do show a remarkable tendency to extrapolate to a $G(H) \sim 3.2$, as previously suggested.^{4b,8} The curvature observed at high solute concentrations, however, persists throughout the concentration range studied, introducing an element of arbitrariness into any kinetic analysis. This is most dramatically illustrated in the case of benzene. Additional data of ours, at lower benzene concentrations (not shown), indicate a prolonged curvature and eventually merge with those given by Stone.²³ The resultant plots are thus ambiguous with respect to a mechanistic interpretation. The reader may convince himself that the more obvious sources of systematic error—scavenger depletion and residual impurities in the cyclohexane—will lead to curvature of a sign opposite to that obtained. We are therefore of the opinion that hydrogen yield data do not warrant the simplicity of interpretation previously accorded them. Indeed, it is quite possible that the seemingly well-behaved data of Fig. 1 merely reflect the higher dilutions used. In any case, no special significance can be attached to any intercept derived from the data of Fig. 2.

One might reconcile the above difficulties with a strict free radical interpretation by invoking a role for spur penetration at high solute concentrations, as suggested by indications of nonhomogeneous effects in alkane radiolyses.^{24,25} Our present results, however, are equally consistent with evidence that solutes may act in a manner other than through their assigned scavenging role.²⁶ As evaluated above, the molecular detachment process, together with freely diffusing hydrogen atoms (presumably formed by simple bond rupture), is not sufficient to account for the observed hydrogen yields. An additional mechanism, involving kinetically hot hydrogen atoms, has often been invoked,^{4b,12,27} but has been criticized recently by one of us.²⁸ Such considerations do not exclude the possible role of electronically excited hydrogen atoms.²⁹ There is by now, however, considerable evidence that significant yields of charge separation exist momentarily or are readily induced in the liquid alkanes.^{12,30,31} This suggests immediately the often-considered possibility of an ion-molecule mechanism, written in the (perhaps naive) stoichiometric form



or more discreetly



We note that because of the only transient nature of the charge separations (as evidenced by the low ion yields from such media³²), any distinction between these two mechanisms becomes operationally blurred.³³ They do have the virtue of generating the cyclohexyl radicals necessary for our previously assumed disproportionation-combination reactions. They also provide a basis for the apparent mobile character of primary excitations in aliphatic media^{26,30} by virtue of a charge migration process. More immediately, at least some of the results of Fig. 2 may then be under-

(22) J. H. Sullivan, *J. Chem. Phys.*, **30**, 1292 (1959); J. K. Thomas, *J. Phys. Chem.*, **67**, 2593 (1963).

(23) J. A. Stone and P. J. Dyne, *Radiation Res.*, **3**, 353 (1962).

(24) J. W. Falconer, *Nature*, **198**, 985 (1963).

(25) J. W. Falconer and M. Burton, *J. Phys. Chem.*, **67**, 1643 (1963).

(26) P. J. Dyne, J. Denhartog, and D. R. Smith, *Discussions Faraday Soc.*, **36**, 135 (1964).

(27) V. V. Voevodskii and Y. N. Molin, *Radiation Res.*, **17**, 366 (1962).

(28) C. E. Klots, *J. Chem. Phys.*, **41**, 117 (1964).

(29) R. Platzman, *Radiation Res.*, **17**, 419 (1962).

(30) T. J. Hardwick, *J. Phys. Chem.*, **66**, 2132 (1962).

(31) W. H. Hamill, *et al.*, *Discussions Faraday Soc.*, **36**, 169 (1964).

(32) G. R. Freeman, *J. Chem. Phys.*, **39**, 988 (1963).

(33) Hamill has mentioned, however (ref. 12), that reaction 5a has not been observed for cyclohexane in the mass spectrometer.

stood in terms of the classical charge-transfer mechanism of "protection." Alternatively, electron attachment to a solute could affect (5a) in a variety of ways^{12,31,34} and also would be expected to modify the course of (5b). In this last instance, we envisage the mechanism (in the room temperature liquid) as essentially that of quenching with only transient charge separation.³⁵ Thus, while the nonselective use of scavenger

plots in radiation chemistry may be criticized on operational grounds, their failure may also be understood, we suggest, in terms of the over-all pattern of recent experimental developments.

(34) J. Roberts and W. H. Hamill, *J. Phys. Chem.*, **67**, 2446 (1963); R. H. Schuler, *ibid.*, **61**, 1472 (1957); P. R. Geissler and J. E. Willard, *J. Am. Chem. Soc.*, **84**, 4627 (1962).

(35) D. K. Majumdar and S. Basu, *J. Chem. Phys.*, **33**, 1199 (1960).

Localization of Torsional Oscillation about Carbon-Carbon

Bonds in Long-Chain Molecules in Aqueous Solutions

by A. J. B. Spaul and M. R. Nearn¹

Chemistry Department, Brunel College, London, W.3, England (Received April 3, 1963)

The temperature dependence of adsorption of 1-butanol and 1-hexanol at the air-water interface has been studied at low surface pressures (between 0.2 dyne cm.⁻¹ and 6 dynes cm.⁻¹), and the thermodynamic data reported show that the adsorption is essentially an entropic process. The recent statistical thermodynamic argument of Aranow and Witten, that the origin of the entropy arises from the transition of a molecule upon a change of environment from the state of hindered internal rotation to the state of internal torsional oscillation, cannot account for the experimental value.

Introduction

Recently Aranow and Witten² have suggested that aqueous solutions of long-chain hydrocarbons can be regarded as a special class of nonideal solution, where hydrogen bonds between water molecules form a cage surrounding a given long-chain hydrocarbon and prevent complete rotation around a carbon-carbon bond, thus confining a particular bond to the configuration it is in initially. They showed how this could account for a number of phenomena, in particular Traube's rule of surface tension. The argument of Aranow and Witten predicts that the free energy of adsorption from aqueous solution to the liquid-air interface is an entropy effect and that this arises from the changed behavior of the hydrocarbon molecules. This theory has been discussed by Hansen and Smolders³ and Higgs,⁴ who point

out that no accurate data on the temperature dependence of adsorption isotherms exist to demonstrate whether the suggestion of Aranow and Witten is a valid conclusion.

We report some thermodynamic parameters for the adsorption of 1-butanol and 1-hexanol from aqueous solution to the air-water interface and discuss the theory of Aranow and Witten in the light of our results.

(1) This work is to be submitted in partial fulfillment for the degree of M.Sc. of the University of London by M. R. Nearn.

(2) R. H. Aranow and L. Witten, *J. Phys. Chem.*, **64**, 1643 (1960); *J. Chem. Phys.*, **35**, 1504 (1961).

(3) R. S. Hansen and C. A. Smolders, *J. Chem. Educ.*, **39**, 167 (1962).

(4) M. Higgs, *J. Chem. Phys.*, **35**, 1504 (1961).

Experimental

Surface tension measurements were made using a drop volume method, the drops being formed on a stainless steel tip. The experimental technique was similar to that described by Matijević and Pethica.⁵ The probable error in the value of the drop volume for water, at 20°, from about 14 runs with three drops per run was less than $\pm 0.02\%$. The same result was obtained for the probable error in the drop volume for water, from about the same number of runs, at the other temperatures stated in this note. The surface tensions of solutions of sodium chloride at temperatures used in this note agreed with values as published.⁶ Sodium chloride, A.R. grade, purified in the manner described by Matijević and Pethica⁵ was used. The surface tension of benzene measured at 20° agreed with the value stated by Harkins.⁷ B.D.H. extra pure benzene purified in the manner described by Jones and Mill was used.⁸ Each "point" in Fig. 1 and 2 represents determinations in at least four runs with three drops per run. The temperature of the thermostat was controlled to $\pm 0.01^\circ$. We found our surface tension measurements could be reproduced with an accuracy of ± 0.06 dyne cm^{-1} . The alcohols were obtained from Fluka, A.G. and Bucks S.C., Switzerland. They were stated to 99% pure or better. Using gas-phase chromatography, the alcohols were shown to be homogeneous and pure within the specification stated by the manufacturer. Water having a specific conductance of less than 1μ mho was obtained by distillation of laboratory distilled water from alkaline permanganate and was further re-distilled from dilute phosphoric acid.

Theoretical

Precise definitions of heats of adsorption of vapors on solids have been given by Everett.⁹ This work has been extended for adsorption at the liquid-air interface by Pethica,¹⁰ and for adsorption of ionic systems at the perfectly polarized interface by Parsons.¹¹ Developing the concept of surface fugacity Betts and Pethica have obtained thermodynamic parameters¹² that have a precise significance as required by the work of Everett and Parsons. An alternative approach is as follows.¹³

We express the surface pressure in virial form

$$\pi A = RT + \pi a \quad (1)$$

applicable at low values of π , where a is the two-dimensional second virial coefficient and A is the total area. This is analogous to the Amagat equation for gases at low pressures. For an aqueous solution of alcohol x , sufficiently dilute that activity may be replaced by concentration, the Gibbs adsorption equation for a

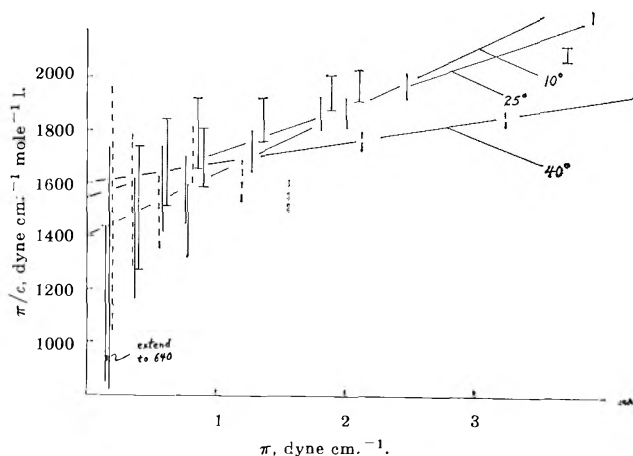


Figure 1. 1-Hexanol: \square , 10°; \square , 25°; \square , 40°.

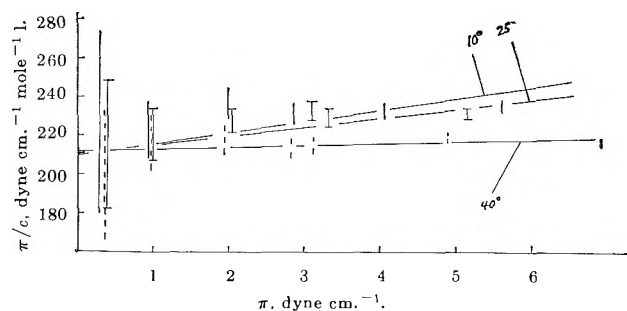


Figure 2. 1-Butanol: \square , 10°; \square , 25°; \square , 40°.

plane thin interface at constant temperature and pressure is given by

$$\frac{d\pi}{\Gamma_x} = RT d \ln c_x \quad (2)$$

where Γ_x is the surface excess of alcohol x with respect to the surface excess of water $\Gamma_1 = 0$, and c_x is the bulk concentration. Equation 1 may be written in the form

$$\frac{1}{\Gamma_x} = a + \frac{RT}{\pi}$$

or

(5) E. Matijević and B. A. Pethica, *Trans. Faraday Soc.*, **54**, 1382 (1958).

(6) International Critical Tables.

(7) W. D. Harkins, "The Physical Chemistry of Surface Films," Reinhold Publishing Corp., New York, N. Y., 1952, p. 79.

(8) D. C. Jones and G. S. Mill, *J. Chem. Soc.*, 213 (1957).

(9) D. H. Everett, *Trans. Faraday Soc.*, **46**, 453 (1950).

(10) B. A. Pethica, *ibid.*, **51**, 1402 (1955).

(11) R. Parsons, *Can. J. Chem.*, **37**, 308 (1959).

(12) J. J. Betts and B. A. Pethica, *Trans. Faraday Soc.*, **56**, 1515 (1960).

(13) This analysis is essentially that of Prof. R. S. Hansen.

$$\frac{d\pi}{\Gamma_x} = a d\pi + RT d \ln \pi \quad (3)$$

Comparing eq. 2 with 3, we obtain

$$RT d \ln \pi - RT d \ln c_x = -a\pi \quad (4)$$

Let $(\pi/c_x)_0 = \lim_{c \rightarrow 0} (\pi/c_x)$, eq. 4 can be integrated

to give

$$\pi/c_x = (\pi/c_x)_0 \exp(-a\pi/RT)$$

or

$$= (\pi/c_x)_0 (1 - a\pi/RT) \quad (5)$$

to first order. The standard chemical potential of x, $\Delta\mu_x^\circ$, is given by the expression

$$-RT \ln (\pi/c_x)_0 = \Delta\mu_x^\circ$$

where the standard states are at 1 mole l.⁻¹ for the bulk phase and a surface pressure of 1 dyne cm.⁻¹ for the surface phase. The standard integral heat of adsorption of x, ΔH_x° , is obtained from

$$\left(\frac{\partial \Delta\mu_x^\circ/T}{\partial T}\right)_P = -\frac{\Delta H_x^\circ}{T^2}$$

Hence, the standard chemical potentials, heats and entropies of adsorption in this work and in the work of Betts and Pethica have the same thermodynamic significance.

Results

Equation 5 requires that at low surface pressure, the ratio of surface pressure to concentration as a function of surface pressure should be linear. The results are shown in Fig. 1 and 2. The error in the ratio of surface pressure to concentration is drawn; the "points" should also be expanded along the abscissa to show the error in the surface pressure. For both systems the slope is positive, with a greater slope for 1-hexanol than for 1-butanol; therefore, *a* is negative and the interaction of the adsorbed molecule is attractive. The origin of these attractive forces is discussed by Davies and Rideal,¹⁴ and they give an empirical expression for calculating the cohesive surface pressure; accepting this we would expect that for the same temperature the slope for 1-hexanol would be greater than for 1-butanol.

In fitting the data obtained for the surface pressure to concentration ratio as a function of surface pressure, we are justified on the grounds of continuity in claiming that both slopes and intercepts at the three temperatures should be ordered, so that (intercept)_{10°} < (intercept)_{25°} < (intercept)_{40°} and (slope)_{10°} > (slope)_{25°} > (slope)_{40°}. The thermodynamic parameters are given in Table I.

Table I: Thermodynamic Parameters at 25°

	$\Delta\mu_x^\circ$, kcal. mole ⁻¹	ΔH_x° , kcal. mole ⁻¹	ΔS_x° , cal. deg. ⁻¹ mole ⁻¹
1-Butanol	-3.15	0.19	±1.5 11.2
1-Hexanol	-4.33	0.67	16.8

Ward¹⁵ has discussed Traube's rule and has emphasized the importance of the initial linear region of the surface tension curve $(-d\gamma/dc)_{c \rightarrow 0}$. He further notes that although the homologous series of fatty acids has been investigated more frequently than any other, there is considerable disagreement between the different values, with divergences in some cases of several hundred per cent. More recently Posner, Alexander, and Anderson¹⁶ have made an extensive study of the temperature dependence of adsorption isotherms of the homologous series of primary alcohols. Their experimental results show a scatter greater than the precision they claim for the method used; this suggests that their alcohols were impure. The thermodynamic parameters they report are to this extent unreliable since their method of calculation depends on the value of Traube's constant, for this homologous series. Although our data are sufficiently accurate for our argument, we feel it would be desirable to develop a technique to measure surface tension with an accuracy of an order of magnitude better than can be obtained using the drop volume method. At least the challenge exists.

Discussion

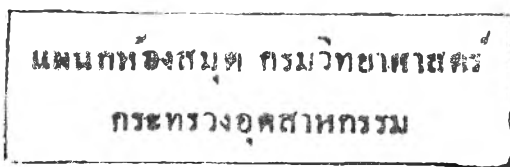
The theoretical argument of Aranow and Witten has two contentions that may be stated as follows

- (i) $|\Delta H_x^\circ| \ll |\Delta\mu_x^\circ| \approx |T\Delta S_x^\circ|$
- (ii) $\Delta S_x^\circ = nR \ln 3 + \Delta$ (6)

where *n* is the number of carbon-carbon bonds and Δ is a term arising from entropy contributions other than those due to rotation.

From the thermodynamic data we report, it appears that the first contention of Aranow and Witten is correct. Their second contention depends on the value of Δ . We consider that the most significant contribution to Δ is that due to the loss of one degree of translational freedom when the molecule is restricted to a plane, and we obtain its value in the following manner.¹⁷

(14) J. T. Davies and E. K. Rideal, "Interfacial Phenomena," Academic Press New York, N. Y., 1961, p. 230.
 (15) A. F. H. Ward, *Trans. Faraday Soc.*, **42**, 399 (1946).
 (16) A. M. Posner, J. R. Anderson, and A. E. Alexander, *J. Colloid Sci.*, **7**, 623 (1952).



In a study of the adsorption of insoluble vapors on water surfaces, Jones and Ottewill¹⁸ find that the entropy changes could be accounted for as being approximately equivalent to the loss in the adsorbed state of one degree of translational freedom. The standard states chosen were a pressure of 1 atm. for the gas phase and a surface area per molecule of $22.53T \text{ \AA}^2$ for the surface phase. From their data the same conclusion is reached as to the value of the entropy change if the standard states chosen are 1 atm. and surface pressure of 1 dyne cm.⁻¹. For these standard states

$$-\Delta G_s^\circ = RT \ln (\pi/p)_0$$

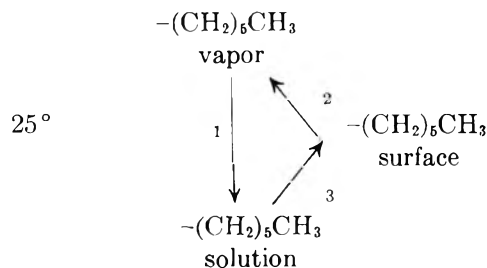
and

$$\left(\frac{\partial \Delta G_s^\circ}{\partial T}\right)_P = -\Delta S_s^\circ$$

where ΔG_s° and ΔS_s° are the standard free energy and the standard entropy of adsorption from the vapor to surface, respectively, and $(\pi/p)_0$ is the ratio of surface pressure to vapor pressure, extrapolated to zero vapor pressure. The experimental value of ΔS_s° for *n*-hexane in the temperature range 0–15° is $-14.6 \text{ cal. deg.}^{-1} \text{ mole}^{-1}$. This may be compared with a value of $-14.2 \text{ cal. deg.}^{-1} \text{ mole}^{-1}$ calculated, at 7.5°, from the Sackur–Tetrode equation, for the standard state translational entropy of the molecule in the gas phase and the two dimensional analog for the standard state translational entropy of the molecule in the surface. A similar agreement is found between the experimental and the calculated values of the entropies of adsorption for the other hydrocarbons in their work.

For the homologous series of primary alcohols Aveyard¹⁹ has shown that certain thermodynamic parameters quoted by Butler²⁰ are incorrect. In particular, he finds that, at 25°, the entropy of hydration ΔS_H° is $-3.7 \text{ cal. deg.}^{-1} \text{ mole}^{-1}$ per CH_2 group, for the standard states of 1 atm. for the gas phase and 1 mole l.⁻¹ for the aqueous phase.

Consider the following cycle



From the work of Aveyard we find that for step 1 the entropy of hydration is $-22.2 \text{ cal. deg.}^{-1} \text{ mole}^{-1}$. On the basis of the work of Jones and Ottewill we are justi-

fied in computing the value of step 2; and this is found to be $13.3 \text{ cal. deg.}^{-1} \text{ mole}^{-1}$. In this work we find that for step 3 the entropy of adsorption is $16.8 \text{ cal. deg.}^{-1} \text{ mole}^{-1}$. Therefore, Δ is approximately $-6.7 \text{ cal. deg.}^{-1} \text{ mole}^{-1}$. If the Sackur–Tetrode contribution, Δ , is subtracted from our experimental value of $16.8 \text{ cal. deg.}^{-1} \text{ mole}^{-1}$ we obtain a “nonideal” part of $23.5 \text{ cal. deg.}^{-1} \text{ mole}^{-1}$ for the entropy of adsorption of $-(\text{CH}_2)_6\text{CH}_3$ on to the water–air interface. This may be compared with $4.2 \text{ cal. deg.}^{-1} \text{ mole}^{-1}$, the value calculated from eq. 6 ($n = 5$). We conclude that the second contention of Aranow and Witten is not valid.

Frank and Evans²¹ suggested that the water molecules immediately near a hydrocarbon form an ordered ice-like structure or “iceberg.” Frank and Evans did not define their concept precisely. In describing their model for the thermodynamic properties of aqueous solutions of hydrocarbons, Némethy and Scheraga²² state, “the basic assumption of the model consists of the requirement that the probability of finding a cluster be somewhat greater in the neighborhood of solute hydrocarbon molecules than at a point in the bulk pure water. Thus the solute molecule is *partially* surrounded by the hydrogen bonded water network of a cluster.” Both these concepts are similar in that the presence of the hydrocarbon molecule brings about an increase in the order of local water molecules. The argument of Aranow and Witten implies that the hydrocarbon molecule has no significant effect upon the structure of adjacent water. If the adsorption of hydrocarbons from aqueous solution at the liquid–air interface is an entropy effect there are current two views as to its origin. One is the effect of the changed behavior of the hydrocarbon, and the other is the effect of the changed behavior of water molecules when the hydrocarbon is removed to the surface. We tentatively suggest that as a further possibility the entropy of adsorption from aqueous solution to the liquid–air interface is a composite one having its origin partly in both these effects. This idea is germinal in the paper by Némethy and Scheraga.²³

Acknowledgment. We thank Dr. D. H. Haydon for

(17) The method is essentially that suggested by Dr. B. A. Pethica.

(18) D. C. Jones and R. H. Ottewill, *J. Chem. Soc.*, 4076 (1955).

(19) R. Aveyard, Ph.D. Thesis, University of Sheffield, England, 1962.

(20) J. A. V. Butler, “Chemical Thermodynamics,” MacMillan and Co., Ltd., London, 1946, p. 388.

(21) H. S. Frank and M. W. Evans, *J. Chem. Phys.*, **13**, 507 (1945).

(22) G. Némethy and H. A. Scheraga, *ibid.*, **36**, 3401 (1962).

(23) G. Némethy and H. A. Scheraga, *J. Phys. Chem.*, **66**, 1773 (1962).

many helpful suggestion, Mr. L. Saggars and the Glaxo Research Unit for help with apparatus, and the Chemi-

cal Society, London, for a grant toward the purchase of chemicals.

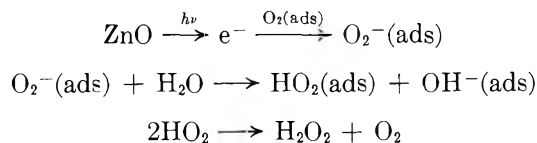
A Few Cases of Electron Emission and Transfer in Heterogeneous Media

by A. Bernas

*Laboratoire de Chimie Physique de la Faculté des Sciences de Paris, Orsay, France
(Received July 22, 1963)*

Photochemical reactions which involve a solid and a liquid phase may be studied with various objectives in view: (1) the possibility of inducing reactions which are not observed under homogeneous conditions; and (2) the possibility of inducing electron transfer from the absorbing solid to the liquid phase. We have been mostly interested in the last topic. Photoirradiations of aqueous aerated suspensions of zinc oxide in the absorption region of the oxide are known to give rise to the reduction of the adsorbed oxygen molecules and to the subsequent formation of hydrogen peroxide. Our own experiments have confirmed that the H_2O_2 production (1) is increased when appreciable quantities of interstitial Zn atoms are present, and (2) is smaller when fluorescent oxide samples are used. These two observations substantiate an electron migration mechanism. Outgassed water and a few other liquids of high or low electron affinity have also been irradiated under conditions in which ZnO is the only absorbing species. From our experimental results (H_2 and H_2O_2 measurements in the case of water and initiation of polymerization reactions in all cases) it appears that dissociation of the solvent may occur and that chemisorption of the latter is neither a necessary nor a sufficient condition. This sensitized photolysis implies an energy transfer, presumably an electron transfer and capture. Other possible photoemissive oxides are being tested.

Since the electronic theory of catalytic action, first established for metals and alloys, has been extended to semiconductors,¹⁻⁴ it appears that photochemical reactions occurring at semiconductor surfaces may be used to investigate electron attachment mechanisms. Zinc oxide is a well-known extrinsic, n-type semiconductor; and the formation of hydrogen peroxide in photoirradiated aqueous suspensions of ZnO, where the oxide is the only absorbing species, has been studied for some time.⁵⁻¹⁰ Following these various studies, it has been generally agreed that photoexcited electrons migrate to the surface of the solid oxide and can reduce adsorbed oxygen molecules. A scheme such as the following would be operative



However the question arises whether, in absence of oxygen, such an electron transfer could affect the sol-

- (1) M. McD. Baker and G. I. Jenkins, *Advan. Catalysis*, **7**, 1 (1955).
- (2) K. Hauffe, *ibid.*, **7**, 213 (1955).
- (3) Th. Wolkenstein, Conference on Phenomena of Catalysis and Adsorption, Moscow, July, 1955; "Théorie électronique de la catalyse sur les semi-conducteurs," Masson, Paris, 1961.
- (4) G. M. Schwab, *Advan. Catalysis*, **9**, 229 (1957).
- (5) C. N. Chari and M. Qureshi, *J. Indian Chem. Soc.*, **21**, 97, 297 (1944).

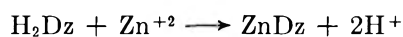
vent—chemisorbed or not on the solid oxide—and this is the problem we were concerned with. Before describing the experiments performed with degassed ZnO suspensions, some of the results we obtained from aerated suspensions will be given briefly.

Experimental

Materials. Triply distilled water, twice distilled IG Farben acrylonitrile, Merck or New Jersey Zinc Co. zinc oxide, Riedel de Hähn Sb_2O_3 , and Johnson Matthey WO_3 were used. In the case of degassed ZnO suspensions, only the Merck oxide was utilized. The zinc oxide was repeatedly washed, filtered on a $35\text{-}\mu$ sieve, and then vacuum-dried.

Irradiations. Two medium pressure mercury vapor lamps, a Philips HPW 125 w. and a Hanovia UVS 500 w., have been used successively. When not only the oxide but the solvent or the monomer were absorbent in the region 3000–3500 Å, the 3650–3660 Å. doublet was isolated by means of a thiocyanate complex solution. Absorption curves of various complex solutions are represented in Fig. 1, and it can be seen that the frequency corresponding to the rapid drop in transmission can be continuously shifted by modifying the CO^{+2} concentration. The thermal stability of the filter solutions was excellent, and the stability under irradiation was satisfactory. No filter solution was needed in the case of aqueous suspensions, except when quantum yields for H_2O_2 production were evaluated. In the case of CCl_4 and CH_3I suspensions, 0.05 M CO^{+2} solutions were used. Intensity measurements were performed in homogeneous solutions, using the ferrioxalate reduction method. Oxide suspensions were magnetically stirred and maintained in a constant temperature bath of $20 \pm 1^\circ$.

Analytical. H_2O_2 was titrated by the classical iodide method in a neutral or slightly acid buffered solution, or in acid solution by the Ti^{+4} complex formation. In acid solution ZnO was dissolved and H_2O_2 might be titrated without preliminary separation of the oxide. Zn^{+2} was estimated with dithizone reagent which reduces Zn^{+2} .



Gas analysis was performed with the aid of an α -meter gage¹¹ where the ionization currents supplied by an α -emitter are linear functions of the pressure in the α -meter, the slopes being different for different gases. Experimentally, the total gas volume was measured with a McLeod gage, and the CO_2 was condensed in a liquid nitrogen trap. In the case of a binary mixture, $\text{H}_2\text{-O}_2$, e.g., the proportion of the two gases was directly deduced from the standardizing

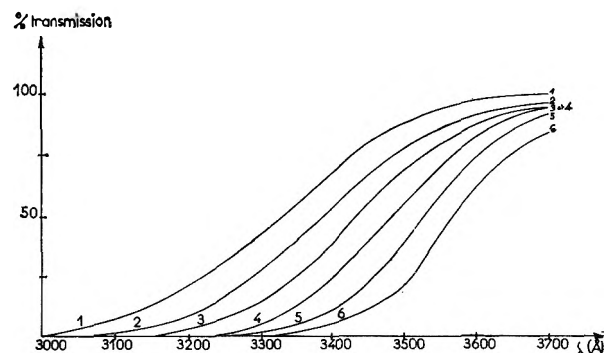


Figure 1. Absorption curves of various cobalt thiocyanate complex solutions: 1, 0.01 M CO^{+2} ; 2, 0.017 M CO^{+2} ; 3, 0.025 M CO^{+2} ; 4, 0.033 M CO^{+2} ; 5, 0.05 M CO^{+2} ; 6, 0.01 M CO^{+2} ; 2 M SCN^- ; $\epsilon = 2$ mm.

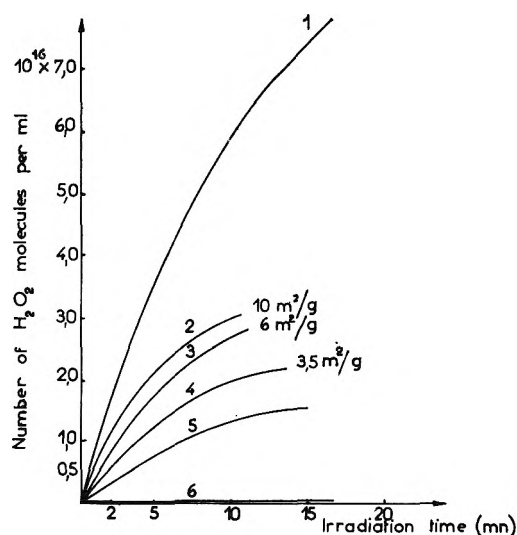


Figure 2. H_2O_2 production vs. time of irradiation for various specimens of ZnO ($\theta = 16^\circ$, Co^{+2} 0.017 M filter solution): curve 1, ZnO prepared from the metal and containing large quantities of interstitial Zn^0 ; curves 2–4, New Jersey Zinc Co. specimens of known surface areas; curve 5, fluorescent ZnO; curve 6, ZnO–MgO phosphor.

curves of the α -meter. The determination may be confirmed by direct measurement of H_2 after its diffusion through a palladium foil. The sensitivity of gas detection was of the order of 1 mm.³ STP.

(6) (a) V. I. Veselovsky and D. M. Schub, *Zh. Fiz. Khim.*, **26**, 509 (1952); (b) *ibid.*, **31**, 1721 (1957).

(7) (a) J. G. Calvert, *et al.*, *J. Am. Chem. Soc.*, **75**, 2850 (1953); (b) *ibid.*, **76**, 2757 (1954).

(8) M. C. Markham and K. J. Laidler, *J. Phys. Chem.*, **57**, 363 (1953).

(9) G. A. Korsunovsky, *Zh. Fiz. Khim.*, **31**, 2351 (1957); **34**, 510 (1960).

(10) E. Beranek, *et al.*, *Collection Czech. Chem. Commun.*, **25**, 358, 369 (1960).

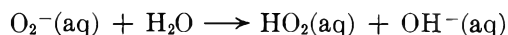
(11) M. Lefort, *Bull. soc. chim. France*, 239 (1960).

Results

Aerated Aqueous ZnO Suspensions. The quantity of H_2O_2 produced vs. time of irradiation for various specimens of ZnO is represented in Fig. 2. In particular, Fig. 2 illustrates (1) that the reaction is a surface reaction (*cf.* curves 2–4 obtained with increasing specific area, (2) that a fluorescent sample containing electron traps is not very efficient, and (3) that a specimen containing large quantities of Zn atoms in interstitial position leads to large quantities of H_2O_2 .

As already known from previous investigations, the initial quantum yield, as well as the stationary state plateau, depends on the chemical composition of the oxide, which is not necessarily stoichiometric, and on the superficial topography of the solid sample. Initial quantum yields amount to about 0.20–0.35, and it may be suggestive to point out that an analogous value was found by Collins¹² for the photoconductivity of ZnO in the same wave length region. These observations substantiate an electron transfer mechanism. Valence electrons of interstitial Zn atoms or Zn^+ ions are photoexcited and transferred to adsorbed oxygen molecules as suggested by the reduced efficiency of vacuum-heated oxides or degassed suspensions.

As to the photochemical or radiochemical formation of hydrogen peroxide in an homogeneous liquid phase, it seems justified to disregard a reaction such as



in which O_2 is not in an adsorbed but a dissolved state. The $\text{p}K$ value of HO_2 (~ 2.5 – 4) would greatly favor the existence of the basic form O_2 at pH 7; and the free energy of the reaction, estimated from values given by Latimer,¹³ turns out to be about +10 kcal./mole.

However, from what we have seen above, such a reaction may occur at a solid–liquid interface where adsorption heats modify the energy balance; and it should be considered also in the radiation chemistry of heterogeneous systems. In such conditions, H and OH would not be necessary precursors for H_2O_2 .

Degassed Aqueous Suspensions of ZnO. (a) Gas Analysis. Figure 3 shows that even for thoroughly degassed suspensions by successive cycles of freezing, pumping, and thawing, dissolved oxygen which originates from initially adsorbed molecules is still present. As can be seen, $[\text{O}_2]$ decreases with increasing time of irradiation which reveals a photoadsorption process. From the work of Kwan and Fujita¹⁴ such a process is known to occur for specimens prepared from the metal. If the ZnO samples are previously vacuum-heated for 14 hr. at 400° (10^{-2} mm. pressure), the quan-

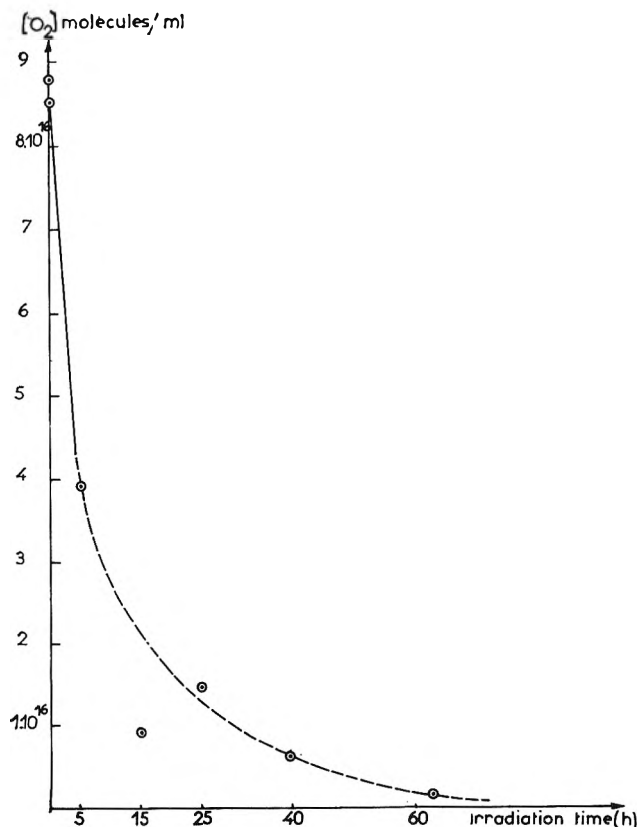
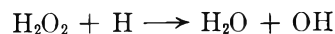


Figure 3. Dissolved oxygen as a function of irradiation time.

tity of measured dissolved O_2 is decreased; but in some cases such a treatment results in the chemical reduction of the oxide forming Zn metal which would ultimately reduce water.

Experiments where dissolved O_2 consumption and H_2O_2 production have been measured simultaneously (Fig. 4) indicate that a large percentage of the consumed O_2 does not reappear as H_2O_2 . Since it has been verified that H_2O_2 is not masked through its adsorption at the surface of the oxide, one must conclude either that photoadsorbed O_2 molecules do not necessarily generate H_2O_2 or that H_2O_2 produced in equivalent quantity may itself be reduced through atomic H.



With the low intensity Philips lamp, no H_2 has been found, but under irradiation with the 500-w. Hanovia small quantities of molecular hydrogen are detectable which increase with time of irradiation as shown in

(12) R. J. Collins and D. G. Thomas, *Phys. Rev.*, **112**, 1, 388 (1958).

(13) W. M. Latimer, "Oxidation Potentials," 2nd Ed., Prentice Hall, New York, N. Y.

(14) Y. Fujita and T. Kwan, *Bull. Chem. Soc. Japan*, **31**, 380 (1958).

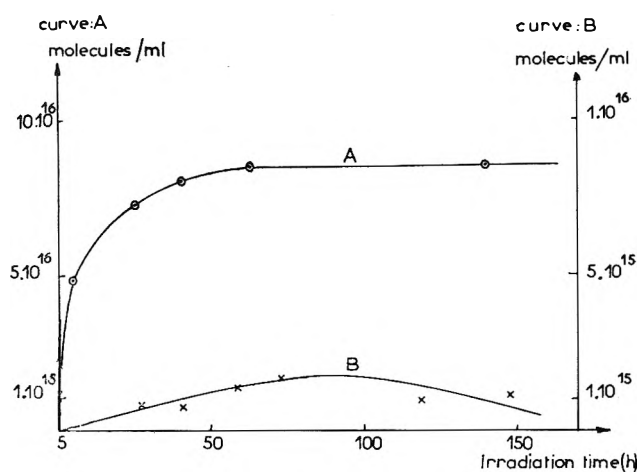
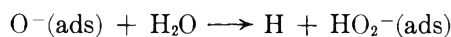


Figure 4. Dissolved oxygen consumption (A), H_2O_2 formation (B).

Fig. 5. The linear portion of the curve corresponds to the production of 2×10^{-6} mole l^{-1} hr^{-1} , which according to homogeneous phase intensity measurements, would lead to a quantum yield of the order of 10^{-5} .

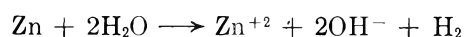
Such a low value is not surprising since, if the solvent is not chemisorbed, the observed quantum yield should be a combination of a photoelectric quantum yield, which may be of the order of 10^{-2} , and of an electron capture cross section which may also be very low if estimated according to experimental determinations in the gas phase.

We cannot think of any mechanism whereby H_2 could accompany O_2 or oxygen atom reduction. A very questionable step such as



would insert water oxygen into H_2O_2 which is contrary to the experimental findings of Calvert.⁷

Two origins for H_2 may then be thought of: an electron transfer to water molecules with their subsequent dissociation into H and $\text{OH}^-(\text{aq})$ or a reduction of water by zinc atoms. Zinc atoms could possibly be formed either by diffusion of interstitial Zn under irradiation or by electron diffusion resulting in Zn^{+2} neutralization at the surface of the oxide. Such a reduction of water



would form one Zn^{+2} per H_2 evolved.

Zn^{+2} ions have been titrated in blank and irradiated solutions. The observed increase in Zn^{+2} concentration appears hardly significant and about 100 times smaller than the quantity of H_2 molecules produced

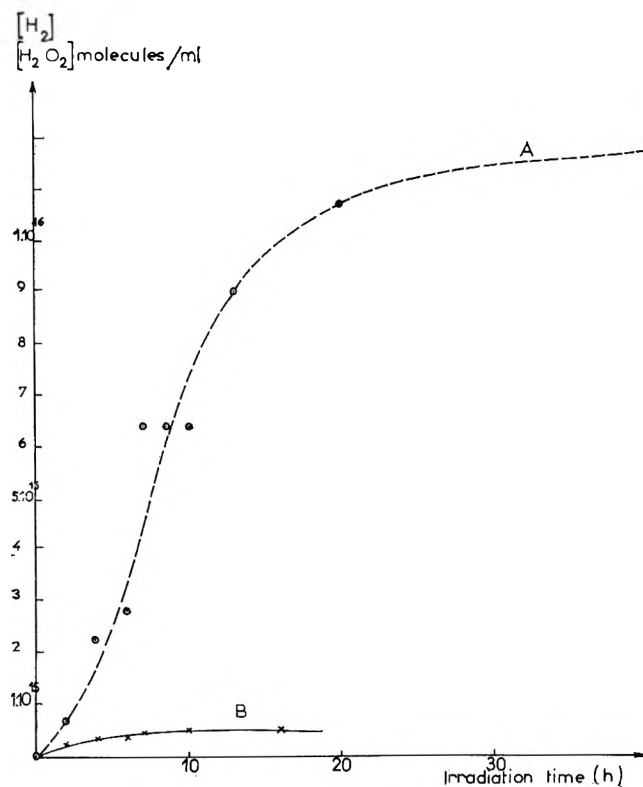


Figure 5. H_2 evolution as a function of irradiation time (A), H_2O_2 formation as a function of irradiation time (B).

under the same conditions. However, the possibility is not ruled out that Zn^{+2} formed in the previous reaction may remain incorporated in the oxide lattice which would prevent its titration in the liquid phase. We therefore turned to other solvents which cannot be reduced by zinc and to other oxides, the metal of which cannot reduce water. For these various systems, a polymerization reaction was used as a test for free-radical production, thus of solvent photosensitized dissociation.

(b) *Polymerization Reactions.* If a monomer which is not itself absorbent is added to the aqueous ZnO suspension, a polymerization is observed under 3660 \AA illumination.¹⁵ Acrylonitrile, $\text{CH}_2=\text{CH}-\text{CN}$, a water-soluble monomer, was utilized in our experiments. The polymer yield *vs.* time of irradiation is given in Fig. 6 (400 mg. of ZnO being suspended in 38 ml. of a solution containing 1.8 mole % of monomer). The polymer yield plotted as a function of the quantity of oxide used is represented in Fig. 7 for the pure monomer and for an aqueous monomer solution for 24-hr. irradiation.

(15) The mechanism of the polymerization reactions observed under such conditions will be discussed in more detail elsewhere: *J. Chim. Phys.*, to be published.

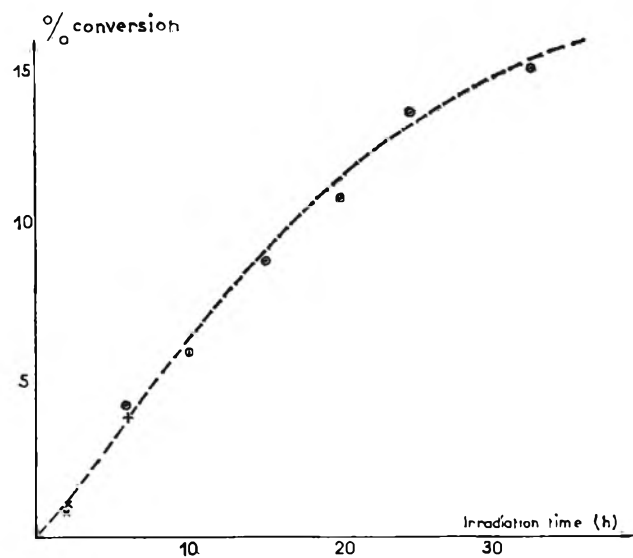


Figure 6. Photosensitized polymerization of acrylonitrile in aqueous suspensions of ZnO. Polymer yield vs. time of irradiation.

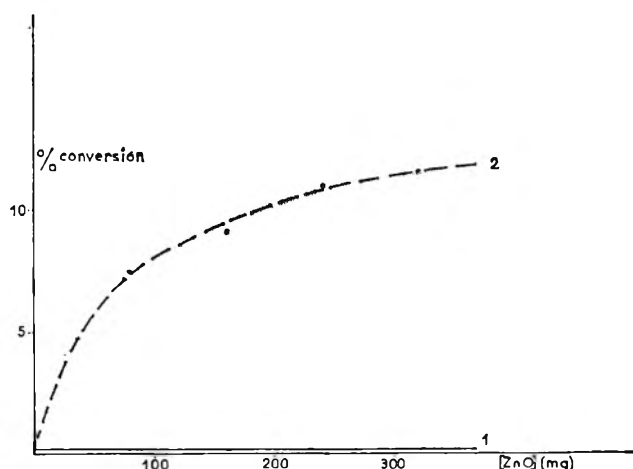


Figure 7. Polymer yield vs. quantity suspended ZnO: curve 1, pure acrylonitrile; curve 2, aqueous solution of acrylonitrile.

From these curves two conclusions may be drawn: (1) the polymerization reaction cannot be due to chemisorption of the monomer followed by its dissociation since the amount of polymer formed from pure acrylonitrile is independent of ZnO concentration, and (2) the presence of water is a necessary condition for the polymer yield to reach an appreciable level.

One must then conclude that either the solvent or a molecule derived from the solvent must participate in the initiation of the polymerization. Since the quantity of H_2O_2 produced is not affected by the presence of monomer and since the number of polymer chains initiated turns out to be five to ten times greater

than the number of H_2O_2 molecules formed, it must be concluded that neither the OH^\bullet or HO_2^\bullet precursors of H_2O_2 nor the OH derived from H_2O_2 decomposition are involved. Free radicals formed by direct dissociation of the water must then be responsible for the chain initiation.

ZnO Suspensions in Various Organic Liquids. If water is replaced by various other liquids—transparent in the wave length region used—one finds no photosensitizing action of ZnO in the case of benzene, ethanol, or chloroform, whereas a polymerization reaction is induced for ZnO suspensions in CH_3I and CCl_4 .

These last experiments where a reduction of the solvent through zinc atoms cannot occur reinforce the suggestion of an electron transfer from the oxide to the liquid. We have not found any data about methyl iodide adsorption on ZnO; but, from Kipling's¹⁶ measurements, CCl_4 is bound to the oxide surface through reversible physical adsorption whereas ethanol is more strongly adsorbed. Chemisorption of the solvent would then be neither a necessary nor a sufficient condition for an electron transfer process to occur.

Aqueous Suspensions of WO_3 and Sb_2O_3 . When WO_3 or Sb_2O_3 are treated and irradiated in aqueous suspensions in the same conditions as ZnO the same type of polymer yield curves is obtained, as shown in Fig. 8, which further substantiates an electron transfer to water molecules and suggests that specific heat of adsorption of water on the oxide is not the determining factor of the reaction.

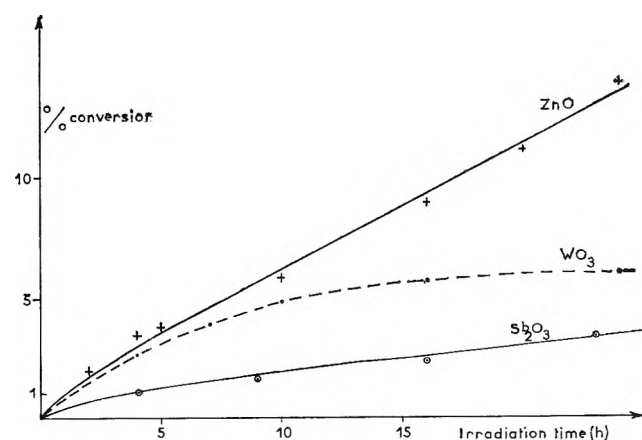


Figure 8. Polymer yield vs. time of irradiation for ZnO (solid line with cross), for WO_3 (dashed line), and for Sb_2O_3 (solid line with dot).

(16) Kipling, et al., *J. Chem. Soc.*, 834 (1957).

In conclusion, experiments in heterogeneous media such as those just described should permit at least qualitative studies of electron capture by liquids, and they may provide means of inducing photochemical reactions which are not observed under homogeneous conditions.

Finally, in case where the liquid is absorbent and

photolyzed, the suspended solid particles might be used at room temperature as a trapping medium for the unstable intermediates produced, whether ions or radicals.

Acknowledgment. We are grateful to Drs. Lefort and Bouby for their help in the gas analysis.

Induced Dipole Moments of Inorganic Complex Ions

by Reiner Kollrack

*Scientific Staff, Pratt & Whitney Aircraft Division, United Aircraft Corporation, East Hartford, Connecticut
(Received October 2, 1963)*

The induced dipole moment of a fluorine ion has been calculated for the complex ions $[M^{IV}F_6]^{2-}$, $[M^{II}F_6]^{4-}$, $[M^{III}LF_6]^{2-}$, $[M^{III}L_5F]^{2+}$, and *trans*- $[M^{III}L_4F_2]^+$ using ligand field theory (L = dipole molecule like H₂O or NH₃). The dipole moment of a given F⁻ ligand is induced by the inhomogeneous electric field which is caused by the influence of the other ligands and the central ion.

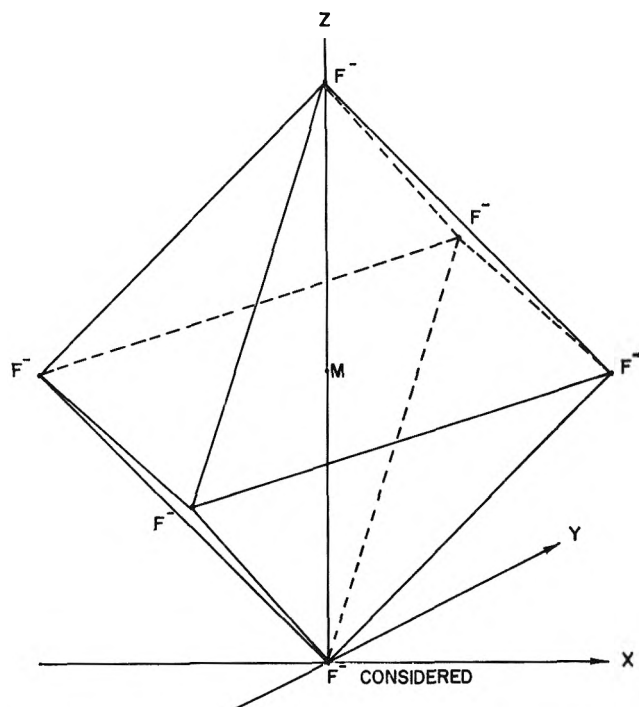
Introduction

During the past 12 years, ligand field theory has been applied to explain properties of inorganic complex compounds.¹⁻¹³ All ligand field theory calculations, however, lack exact information concerning the two parameters: the distances between the central ion and the ligands and the induced dipole moments of the ligands (the induced dipole moment of the central ion is negligible). Heretofore, the induced dipole moments have always been arbitrarily assigned. In the present paper, the former rough estimations of the induced dipole moments will be replaced by far more accurate calculations.

Usually, induced dipole moments of atomic species are calculated or measured only for *homogeneous* electric fields by determination of the polarizability, as the polarizability is not defined for inhomogeneous fields (*i.e.*, it is not unique). In the case of inorganic complex compounds, any given ligand is affected by the inhomogeneous electric field due to the electric charges and/or dipoles of the central ion and the other ligands.

For a complex ion of the type $[M^{III}F_6]^{3-}$ such an induced dipole moment of a fluorine ligand was first calculated by Hartmann and Kollrack.^{14,15} This paper presents the induced dipole moments of fluorine

- (1) H. Hartmann and F. E. Ilse, *Z. physik. Chem.*, **6**, 768 (1951).
- (2) H. Hartman and F. E. Ilse, *Z. Naturforsch.*, **69**, 751 (1951).
- (3) F. E. Ilse, Thesis, University of Frankfurt, Frankfurt, Germany, 1947.
- (4) H. Hartmann and H. Fischer-Wasels, *Z. physik. Chem.*, **4**, 297 (1955).
- (5) H. Hartmann, "Theorie der chemischen Bindung," Springer Verlag, Berlin, Germany, 1954.
- (6) C. K. Jørgensen, *Acta Chem. Scand.*, **12**, 903 (1958).
- (7) L. E. Orgel, *J. Chem. Phys.*, **23**, 1819 (1955).
- (8) L. E. Orgel, *J. Chem. Soc.*, 4756 (1952).
- (9) C. J. Ballhausen and C. K. Jørgensen, *Kgl. Danske Videnskab. Selskab. Mat. fys. Medd.*, **29**, No. 14, 1955.
- (10) C. K. Jørgensen, *Mol. Phys.*, **2**, 96 (1959).
- (11) C. Furlani and A. Furlani, *J. Inorg. Nucl. Chem.*, **19**, 51 (1961).
- (12) R. E. Hamm, R. Kollrack, G. L. Welch, and R. H. Perkins, *J. Am. Chem. Soc.*, **83**, 340 (1961).
- (13) D. M. Grant and R. Kollrack, *J. Inorg. Nucl. Chem.*, **23**, 25 (1962).

Figure 1. Sketch of the complex ion $[MF_6]$.

ions in following complex ions: $[M^{IV}F_6]^{2-}$, $[M^{II}F_6]^{4-}$, $[M^{III}LF_5]^{2-}$ (only the F^- ion in transposition to the dipole ligand L is considered), $[M^{III}L_5F]^{2+}$, and *trans*- $[M^{III}L_4F_2]^+$. The different values of the resulting dipole moments, which depend on the type of complex ion considered, are discussed.

Calculations

Basic Model. Ligand field theory considers the central ion and the ligands as point charges and/or point dipoles. The calculations of the induced dipole moment itself are based on the concept that the electron cloud of one given F^- ion is distorted by the influence of the aforementioned electric field, so that the center of the negative charge of the F^- ion no longer coincides with the center of the positive charge. We assume the nucleus to be completely unchanged. Thus, the length of the induced dipole is given by the distance between the nucleus and the center of the electron cloud. Figure 1 shows an octahedral complex ion. The nucleus of the F^- ion under consideration is taken as the origin of a Cartesian coordinate system. The other five ligands are either F^- ions or "dipole molecules" such as H_2O or NH_3 as mentioned before.

The electron cloud is represented by the proper eigenfunction of the F^- ion. From quantum mechanics it follows that

$$D = \int \psi^{0*} z \psi^0 d\tau \quad (1)$$

$$\psi^0 = \psi_0^0 + \sum_l' \frac{H_l^0}{E_0^0 - E_l^0} \psi_l^0 \quad (2)$$

$$H_l^0 = \int \psi_l^{0*} \mathbf{H}' \psi_0^0 d\tau \quad (3)$$

where

ψ^0 = eigenfunction of the perturbed F^- ion in the ground state

ψ_0^0 = eigenfunction of the unperturbed (free) F^- ion in the ground state

ψ_l^0 = eigenfunction of the unperturbed F^- ion in the l th excited state

D = length of the induced dipole

E_0^0 = energy of the unperturbed F^- ion in the ground state

E_l^0 = energy of the unperturbed F^- ion in the l th excited state

z = operator corresponding to the coordinate z

Σ' = summation over all possible l values except $l = 0$

\mathbf{H}' = perturbation operator representing the electric field

Calculations for the Free F^- Ion. In this section, the atomic states of a free F^- ion are determined. For the ground state of a free F^- ion and those twelve lowest excited states which are pertinent, the electron configuration and the designation of the resulting atomic states are presented in Table I.

Table I

$(1s^2, 2s^2)2p^6 \rightarrow$	1S	(E_0^0)
$2p^6 3s \rightarrow$	1P	(E_1^0)
$2p^6 3p \rightarrow$	1D	(E_2^0)
	1P	(E_3^0)
$2p^6 3d \rightarrow$	1D	(E_4^0)
	1F	(E_5^0)
	1P	(E_6^0)
$2p^6 4s \rightarrow$	1P	(E_7^0)
$2p^6 4p \rightarrow$	1D	(E_8^0)
	1P	(E_9^0)
$2p^6 4d \rightarrow$	1D	(E_{10}^0)
	1F	(E_{11}^0)
	1P	(E_{12}^0)

All triplet terms resulting from these electron configurations and all terms resulting from electron configurations with less than five 2p electrons, *e.g.*, $(1s^2,$

(14) H. Hartmann and R. Kollrack, to be published in *Theoretica chimica Acta*.

(15) R. Kollrack, Thesis, University of Frankfurt, Frankfurt, Germany, 1959.

$2s^2)2p^43p^2$, are omitted, since their corresponding H_l^0 values in eq. 3 are zero.

The E_l^0 values were calculated in the usual way according to Slater as

$$E_l^0 = E_l + \Sigma I_l + \Sigma C_l - \Sigma A_l \quad (4)$$

for $l = 0, 1, \dots, 12$

where

$$E_l = -1/2 \sum_i \frac{(Z - \sigma_i)^2}{n_i'^2}$$

and Z = atomic number, σ_i = screening constant for the i th electron, n_i' = effective principle quantum number of the i th electron.

E_l is the energy of the free F^- ion without consideration of the electron interaction. The terms ΣI_l , ΣC_l , ΣA_l result from the electron interaction provided Russell-Saunders coupling is valid.

The integrals I_l have the form

$$I_l = \int_0^\infty R_l^2 \frac{\sigma_l}{r} r^2 dr$$

The integrals C_l and A_l are the usual Coulomb and exchange integrals, respectively, according to Slater. These integrals can be broken down into sums of standard integrals of the general form

$$\int_0^\infty \int_0^\infty R_{(1)}^2 R_{(2)}'^2 \frac{r^{<k}}{r^{k+1}} r^2 r'^2 dr dr'$$

and

$$\int_0^\infty \int_0^\infty R_{(1)} R_{(1)}' R_{(2)} R_{(2)}' \frac{r^{<k}}{r^{k+1}} r^2 r'^2 dr dr'$$

respectively, where $R_l, R_{(1,2)}, R_{(1,2)}'$ are the radial functions of the proper Slater one-electron eigenfunctions. This method is described in detail for the configuration p^2 by Pauling and Wilson.¹⁶

The radial functions of the Slater one-electron eigenfunctions have the form

$$R = A r^{n'-1} e^{-fr}$$

with

$$f = \frac{Z - \sigma}{n'}$$

where A is a normalization factor.

The f -value for a $2p$ electron (ground state) determined by Slater's¹⁷ semiempirical rule is 2.42. Morse¹⁸ has calculated 2.35 for this f -value. In the present paper the value 2.40 is used. The f -values for $3s$, $3d$, $4s$, $4d$ electrons (excited states) have been calculated by minimization of the aforementioned E_l^0

terms; 0.8 has been found for the f -values of the $3s$ and $3d$ electrons; 0.6 for the f -values of the $4s$ and $4d$ electrons.

The numerical calculations were confined to the differences $E_0^0 - E_l^0$, since only these differences are of interest here. The results of these rather lengthy calculations are

$$E_0^0 - E_1^0 = -0.11 \text{ a.u. (atomic units)}$$

$$E_0^0 - E_4^0 = -0.12 \text{ a.u.}$$

$$E_0^0 - E_5^0 = -0.12 \text{ a.u.}$$

$$E_0^0 - E_6^0 = -0.13 \text{ a.u.}$$

$$E_0^0 - E_7^0 = -0.14 \text{ a.u.}$$

$$E_0^0 - E_{10}^0 = -0.14 \text{ a.u.}$$

$$E_0^0 - E_{11}^0 = -0.14 \text{ a.u.}$$

$$E_0^0 - E_{12}^0 = -0.14 \text{ a.u.}$$

Calculations for the Perturbed F^- Ion. In this paper, "the weak field method" is applied in all ligand field theory calculations. Subsequently, Slater eigenfunctions are used as eigenfunctions. The quantum mechanical formalism used is described by Condon and Shortley.¹⁹ In eq. 3, the eigenfunctions ψ_l^0 belonging to the atomic states $^1S, ^1P, ^1D, \dots$ are represented by the atomic eigenfunctions $\Psi(S, L, M_S, M_L)$ where S = spin quantum number, L = angular momentum quantum number, M_S = quantum number of the component of S in a field, and M_L = magnetic quantum number. According to the ligand field theory formalism, the atomic eigenfunctions are replaced by the proper linear combinations of these atomic eigenfunctions which belong to the corresponding irreducible representations of the respective symmetry cases. The symmetry depends on the type of the complex ion considered; *i.e.*, the symmetry of the aforementioned electric field induced by the central ion and the five ligands. For further evaluation the atomic eigenfunctions of these linear combinations are replaced by antisymmetrized products of one-electron eigenfunctions using the formalism of Gray and Wills²⁰ with the sign of each product determined by the method of Ufford and Shortley.²¹ It has been

(16) L. Pauling and E. B. Wilson, "Introduction to Quantum Mechanics," McGraw-Hill Book Co., New York, N. Y., 1935.

(17) J. C. Slater, *Phys. Rev.*, **36**, 57 (1930).

(18) P. M. Morse, L. A. Young, and E. S. Haurwitz, *ibid.*, **48**, 948 (1935).

(19) E. U. Condon and G. H. Shortley, "The Theory of Atomic Spectra," Cambridge University Press, London, England, 1953.

(20) N. M. Gray and L. A. Wills, *Phys. Rev.*, **38**, 248 (1931).

(21) C. W. Ufford and G. H. Shortley, *ibid.*, **42**, 167 (1932).

found that the method of Gray and Wills applied without consideration of the rule of Ufford and Shortley leads to incorrect results here. Thus, the value of the induced dipole moment has been calculated to be zero. The present method follows the outline of Ufford and Shortley. Usually, all matrix elements of the x -component of an angular momentum vector are taken as real and positive. For such a purely algebraic calculation of a matrix representing electrostatic interaction or any second-order perturbation, one must determine what this choice of positive signs implies in the phase of the eigenfunctions considered as sums. Wigner²² has given a general formula for the pertinent states which result from the addition of any two angular momentum vectors. The rule of Ufford and Shortley follows the scheme given by Wigner's formula. Thus, the integrals $\int \psi_i^{0*} \mathbf{H}' \psi_0^0 d\tau$ are replaced by sums of integrals of the form $\int \phi_m^* \mathbf{H}' \phi_n d\tau$, where ϕ_m and ϕ_n are the proper, antisymmetrized products of one-electron eigenfunctions. The perturbation operator \mathbf{H}' can be written as $\sum_i \mathbf{H}_i$, where \mathbf{H}_i is the

perturbation operator representing the aforementioned electric field influencing the i th electron of the considered F^- ligand. These many-electron integrals can be broken down into one-electron integrals according to Condon and Shortley¹⁹

$$\int \phi_m^* \sum_i \mathbf{H}_i \phi_n d\tau = 0$$

for ϕ_m and ϕ_n differing in more than one set of quantum numbers, *i.e.*, more than one one-electron eigenfunction.

$$\int \phi_m^* \sum_i \mathbf{H}_i \phi_n d\tau = \pm \int a^k \mathbf{H}_k b^k d\tau$$

for ϕ_m and ϕ_n differing in one set of quantum numbers represented here by a^k and b^k . The sign depends on the number of necessary permutations.

$$\int \phi_m^* \sum_i \mathbf{H}_i \phi_n d\tau = \sum_i \int a^i \mathbf{H}_i a^i d\tau$$

for ϕ_m and ϕ_n being equal.

The resulting one-electron integrals can now be evaluated. The perturbation operator \mathbf{H}_i consists of two parts

$$\mathbf{H}_i = \mathbf{V}_i + \mathbf{V}_{D_i}$$

where \mathbf{V}_i represents that part of the electric field which is induced by the charges of the central ion and the five aforementioned ligands (see Fig. 1), and \mathbf{V}_{D_i} represents that part of the electric field which is induced by the dipoles of the five ligands. Thus

$$\int a^i \mathbf{H}_i b^i d\tau = \int a^i \mathbf{V}_i b^i d\tau + \int a^i \mathbf{V}_{D_i} b^i d\tau \quad (5)$$

with

$$\int a^i \mathbf{V}_{D_i} b^i d\tau = \frac{d}{dR_j'} \int a^i \mathbf{V}_i b^i d\tau$$

where R_j' = distance between the considered F^- ligand and one of the other five ligands ($j = 2, 3, \dots, 6$). Furthermore

$$\mathbf{V}_i = \sum_j \frac{Q_j}{r_{ij}} \quad (6)$$

where Q_j = charge of the central ion ($j = 1$) or one of the five F^- ligands ($j = 2, 3, \dots, 6$), and r_{ij} = distance between the i th electron and the central ion ($j = 1$) or one of the five F^- ligands ($j = 2, 3, \dots, 6$).

According to Slater, r_{ij} is developed into²³

$$\frac{1}{r_{ij}} = \sum_{k=0}^{\infty} \sum_{m=-k}^{m=+k} \frac{(k-|m|)!}{(k+|m|)!} \frac{r_{<}^k}{r_{>}^{k+1}} P^{|m|}_{k(\cos \delta_i)} P^{|m|}_{k(\cos \delta_j)} e^{im(\phi_i - \phi_j)}$$

Results

The calculations in the present paper are confined to cases for which the aforementioned electric field is of tetragonal symmetry. Similar calculations for electric fields of lower symmetries are possible but far more complex and less accurate.

The final results are (given in atomic units)

1. For $[M^{III}L_5F]^{2+}$

$$\mu = \frac{8.782}{R^2} - \frac{22.555}{R^4} - \frac{4.872}{R_L^3} \mu_L - \frac{1.719}{R_L^5} \mu_L$$

2. For *trans*- $[M^{III}L_4F_2]^+$

$$\mu = \frac{8.157}{R^2} - \frac{22.085}{R^4} - \frac{0.732}{R^3} \mu + \frac{0.940}{R^5} \mu - \frac{4.354}{R_L^3} \mu_L - \frac{2.658}{R_L^5} \mu_L$$

3. For $[M^{III}LF_5]^{2-}$ (only the F^- ion in transposition to the L molecule is considered because of the symmetry)

$$\mu = \frac{4.635}{R^2} - \frac{23.206}{R^4} - \frac{4.141}{R^3} \mu - \frac{2.563}{R^5} \mu - \frac{0.731}{R_L^3} \mu_L + \frac{0.909}{R_L^5} \mu_L$$

(22) E. Wigner, "Gruppentheorie," Vieweg, Braunschweig, Germany, 1931.

(23) H. Eyring, J. Walter, and G. E. Kimball, "Quantum Chemistry," John Wiley and Sons, Inc., New York, N. Y., 1959.

4. For $[M^{II}F_6]^{4-}$

$$\mu = \frac{0.819R^3 - 15.25R}{R^5 + 4.872R^2 + 1.718}$$

5. For $[M^{IV}F_6]^{2-}$

$$\mu = \frac{5.72R^3 - 30.75R}{R^5 + 4.872R^2 + 1.718}$$

where μ = induced dipole moment of the considered F^- ion, μ_L = permanent (total) dipole moment of the L molecule (the induced dipole moment of L has been neglected), R = distance between central ion and F^- ligand, and R_L = distance between central ion and L ligand.

In Fig. 2, the values of the induced dipole moment, μ , are plotted as a function of the distance, R , where $R_L = 3.5$ a.u. and $\mu_L = 1.0$ a.u. (R -values under 3.0 a.u. do not exist for the complex ions considered.)

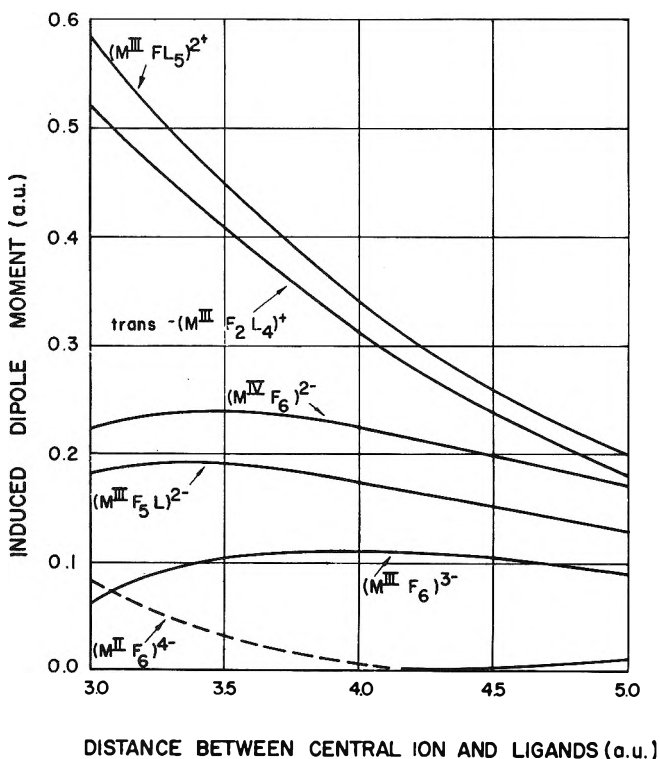


Figure 2. Induced dipole moments of F^- ligands in various complex ions as functions of the distance between central ions and ligands.

For comparison the values of μ were calculated under the assumption that only the component of the aforementioned electric field along the z -axis ($C_{\infty v}$ symmetry) influences the F^- ion. This approximation has often been used. In Table II, the μ -values for

$R = 3.5$ a.u., $R_L = 3.5$ a.u., $\mu_L = 1.0$ a.u. are presented for both the exact case with a field of tetragonal symmetry and the approximation with a field of $C_{\infty v}$ symmetry. The latter values agree with the experimental μ -values (taken from the polarizability of an F^- ion) within 8%.

Table II

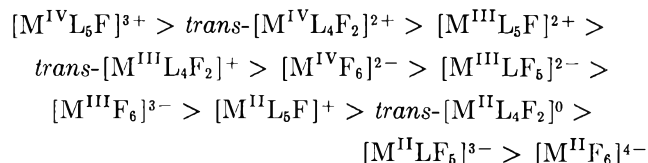
	$[M^{III}L_6F]^{2+}$	$trans-[M^{III}L_4F_2]^+$	$[M^{III}F_6]^{3-}$	$[M^{IV}F_6]^{2-}$
Tetragonal	0.45	0.41	0.10	0.24
$C_{\infty v}$	1.81	1.66	0.81	1.41

Discussion

The results show very clearly that the application of the aforementioned approximation produces induced dipole moment values which are about three to four times too large. Such an approximation, therefore, is no longer appropriate. For any complex ion, the exact μ -values calculated by the present method will always be much smaller than the μ -values determined by this approximation.

In this paper only complex ions with the coordination number 6 have been discussed. The treatment of complex ions with the coordination number 4 is similar.

The values of the induced dipole moment generally depend strongly on the "ratio" of the influence of the central ion (on the considered ligand) to the influence of the five other ligands. The strong influence of the central ion together with the weak influence of the other five ligands means that the electric field approaches $C_{\infty v}$ symmetry. Here, the resulting dipole moment will be relatively large. On the other hand, the larger the "inhomogeneity" of the electric field (strong influence of the ligands, weak influence of the central ion) the smaller will be the induced dipole moment. Thus, a series with decreasing μ -values can be stated for the complex ions considered



where $\mu_L = 1$ a.u., $R = 3.5$ a.u., $R_L = 3.5$ a.u. In general, ion ligands show stronger influence than dipole ligands.

The aforementioned ratio also determines whether or not there is a maximum for the curves in Fig. 2 (μ as a function of R) for the considered values of R .

The dashed curve for $[M^{II}F_6]^{4-}$ in Fig. 2 indicates that here the influence of the five ligands dominates at small values of R . Contrary to the configuration

of the dipoles calculated for the other four complex ions, $[M^{II}F_6]^{4-}$ here shows the positive pole of the induced dipole of an F^- ligand faces the central ion.

Oxide-Coated Electrodes. II. Aluminum in Alkaline Solutions and the Nature of the Aluminate Ion¹

by Robert C. Plumb and James W. Swaine, Jr.

Worcester Polytechnic Institute, Worcester, Massachusetts (Received October 1, 1963)

An investigation of the electrode potentials of evaporated aluminum films as a function of oxidation time has given the reversible electrode potentials for the aluminum–aluminate ion system. The potentials have been studied over the pH range from 10.5 to 13.8. Using the observed dependence of electrode potential upon the over-all concentration of aluminum in the solution and the pH, it is shown that the electrode reaction below a pH of 12.4 consists of the addition of aluminum ions from the metal to the aluminate anion. Above a pH of 12.4 the reaction is directly between hydroxyl ions in solution and the metal ions from the metal. Possible structures for the aluminate anion are discussed. The aluminate ion is shown to be a polymeric anion of composition $(OH^-)_2[Al(OH)_4^-]_n$, in which the $Al(OH)_4^-$ units are, most likely, linked together by two hydroxyl bridges and each aluminum ion is surrounded by six hydroxyl ions. The chain length is of the order of $n = 40$ to $n = 100$.

Introduction

A technique for determining the effects of oxide films upon electrode potentials was described in a previous publication.² Those studies showed that the electrode potentials of aluminum in acidic and neutral solutions varied in a systematic way with the period of air oxidation. Electrode potentials measured after known and variable periods of air oxidation could be extrapolated to zero oxidation time to obtain potentials characteristic of the electrode in particular solutions. Using (1) an assumed electrode reaction and (2) well-established free energies of formation and of reaction determined by thermochemical techniques, one can predict *a priori* three quantities: (1) the standard electrode potential for the reaction, (2) the variation of electrode potential with pH, and (3) the variation of

electrode potential with metal ion concentration in solution. The potentials obtained by extrapolating the experimentally measured potentials to zero oxidation time agree quantitatively with those potentials predicted *a priori* from thermodynamic data in all three respects showing that the observed potentials are thermodynamic potentials.

Accepting the capability of measuring reversible potentials, one can anticipate using these potentials to study the nature of ions in solution. This communication describes our findings on the behavior of the

(1) From a dissertation submitted by J. W. S. in partial fulfillment of the requirements for the degree of Doctor of Philosophy in chemistry.

(2) R. C. Plumb, *J. Phys. Chem.*, **66**, 866 (1962).

aluminum electrode in alkaline solutions and the nature of the aluminate ion.

The nature of the aluminate ion has been the subject of much discussion and speculation. It has generally been assumed to be mononuclear, such as AlO_2^- , or a hydrated form of this species. Using potentiometric titrations, in which the number of "bound" hydroxyl ions per aluminum ion is determined from the measured pH and the known additions of base, Sillén and co-workers³ have concluded that, at least at high pH, the aluminate ion is mononuclear and of the form $\text{Al}(\text{OH})_4^-$. There seems to be little doubt about the correctness of the assertion that the ligands contribute approximately four negative charges for each tripositive aluminum ion. It is not clear that the potentiometric titration is sufficiently sensitive to determine whether or not the ligand-metal ion ratio results from an associated species containing a larger number of ligand and metal ions or from the mononuclear species proposed. Bode⁴ found no evidence for colloidal particles in sodium aluminate solution in an investigation using light scattering measurements. He found that the mobility of the aluminate ion was comparable with that of the lithium cation and the acetate anions, and on the basis of conductivity measurements found no evidence for the existence of ionic species other than AlO_2^- . Contrary to these observations Brintzinger⁵ found, by dialysis in KOH solutions, the molecular weight of the aluminate ion to be consistent with either $\text{Al}_2(\text{OH})_{10}^{-4}$ or $\text{Al}_2\text{O}_2(\text{OH})_8^{-6}$. Jahr⁶ found it necessary to assume the existence of both polymerized and monomeric forms, depending on the pH, in order to interpret diffusion in aluminate solutions. His results indicated that aluminum had a coordination number of four or six depending upon the conditions prevailing in the solution. Recently, Lippincott⁷ and co-workers measured the Raman spectra of the aluminate ion and found it consistent with T_d symmetry even though ν_3 , of symmetry species F_2 , which should be active in the Raman effect, was not observed. N.m.r. studies of the aluminum cation in aqueous solutions have not been capable of distinguishing between a coordination number of four and six.^{8,8a} Baldwin and Taube⁹ concluded that the hydration number of the aluminum ion in aqueous solution was about six from isotopic dilution measurements in a flow system. It is apparent that the nature of the aluminate ion is still not clear.

We will show, in the discussion to follow, that the reversible potentials of aluminum in aluminate ion solution cannot be interpreted in terms of electrode reactions involving the conventional model of a tetrahedrally coordinated aluminate ion. The potentials

may be interpreted quantitatively (both with respect to dependence on metal ion concentration and dependence on pH) by a model in which the metal ions are octahedrally coordinated and linked together in a polymeric anion structure by hydroxyl bridges.

Experimental

The General Experimental Technique. The experimental apparatus used for studying the effects of oxide films upon electrode potentials has been described in a previous publication² and only the essential features of the experiments will be reviewed here. Initially oxide-free metal surfaces are generated by evaporating the metal from a filament onto a glass microscope slide under vacuum. In a rapid sequence of events the vacuum is broken with ambient atmosphere, the sample is removed from the vacuum chamber, and, after a predetermined lapse of time, an electrolyte in contact with a reference electrode is brought in contact with the metal surface and the transient in potential is recorded on an oscilloscope. The lapse of time between the first exposure to the atmosphere and the contact with the electrolyte is variable upward from a minimum of 0.2 sec. There are brief initial phase charging transients which may be corrected for by extrapolation, there are changes in potential as a result of oxidation or dissolution of oxide in the electrolyte, and there are effects upon the potential as a result of the oxide film present when the cell is first completed.

The only major modification of the transient potential apparatus has been a change in the cell design to increase the capabilities of the equipment. Whereas in the previous design one data point, at a particular oxide film thickness and with a particular electrolyte, was obtained, it is now possible to obtain three separate data points on a particular metal film evaporation. This has been achieved by forming three separate miniature cells with the single common metal film.

The Transients in Potential. Two distinguishable types of transients were obtained with aluminum in basic solutions. The type of transient observed in the pH range from 10.5 to 11.1 is shown in Fig. 1a. In this

(3) (a) C. Brosset, *Acta Chem. Scand.*, **6**, 910 (1952); (b) C. Brosset, G. Biedermann, and L. G. Sillén, *ibid.*, **8**, 1917 (1954).

(4) H. Bode, *Z. anorg. allgem. Chem.*, **269**, 44 (1952).

(5) H. Brintzinger, *ibid.*, **256**, 98 (1948).

(6) K. F. Jahr, *Naturwissenschaften*, **38**, 302 (1951).

(7) E. R. Lippincott, J. A. Pselos, and M. C. Tobin, *J. Chem. Phys.*, **20**, 536 (1952).

(8) J. A. Jackson, J. F. Lemons, and H. Taube, *ibid.*, **32**, 553 (1960).

(8a) NOTE ADDED IN PROOF.—After this paper was submitted, n.m.r. measurements by Connick and Fiat indicating a coordination number of six for the aluminum ion were published [*ibid.*, **39**, 1349 (1963)].

(9) H. W. Baldwin and H. Taube, *ibid.*, **33**, 206 (1960).

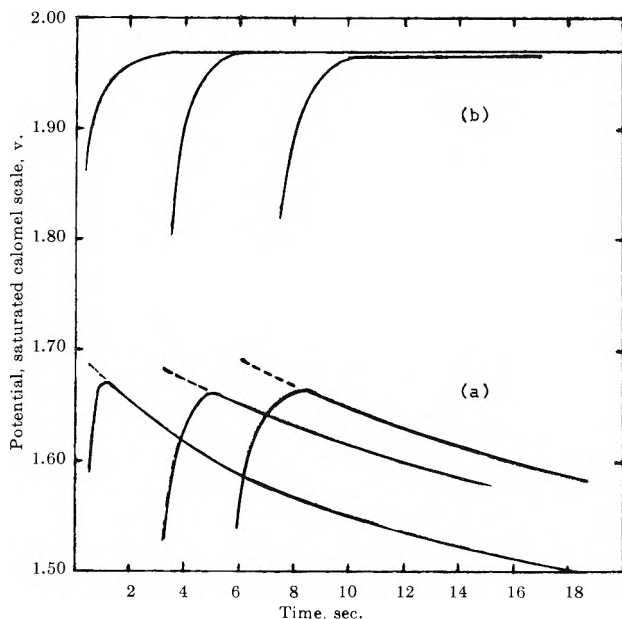


Figure 1. The transients in potential observed when alkaline solutions are brought into contact with an evaporated aluminum film after three different periods of air oxidation. (a) Type of transient observed in pH range from 10.5 to 11.1. (b) Type of transient observed in pH range above 11.1.

type of transient the potential reaches a maximum shortly after contact with the electrolyte and then decreases as further oxidation of the metal surfaces takes place in the solution. The initial portion of the transient is probably a phase charging transient. The time constant for this increases with increasing oxide film thickness. Extrapolation of the transient through the phase charging region to the moment of contact of the electrolyte with the metal surface gives a potential which is found to be independent of the oxidation time. The type of transient found in the pH range from 11.1 to 13.8 is shown in Fig. 1b. The potential rises to a maximum which is independent of both the oxidation time and the continued contact of the electrolyte with the metal film. The time constant for the initial transient increases with increasing oxide film thickness, but the steady value of the potential is independent of the initial oxide film thickness. Probably the initial transient is a mixture of effects caused by phase charging and oxide dissolution.

Below a pH of about 10.5 the transients are complicated and difficult to interpret. In this pH region there is considerable tendency for the oxide film to grow in the electrolyte so that the metal becomes more and more passive. However, the competition between oxide dissolution and oxide growth seems to be critically balanced and we have found it difficult to get reproducible measurements.

The small saturated calomel electrodes required for the miniaturized cells exhibited junction potentials as a result of contact with the alkaline aluminate electrolytes. These junction potentials amounted to 20 or 30 mv. and were reproducible for a given electrolyte. They were determined by comparison to a reference calomel electrode and the data were corrected. The potential measurements, after correction for the junction potentials, were reliable to ± 5 mv. except where the transients posed special problems in analysis.

Solutions Studied. Most of the solutions were prepared from H_2SO_4 with $Al_2(SO_4)_3$ and the addition of NaOH to the appropriate pH. The concentration of the sulfate ion was $0.0057 M + 1.5 M_{Al}$ in most cases. The concentrations of the aluminum ion were 0.0072 , 0.00072 , and $0.000072 M$. Sulfate was chosen as the principal anion because it was found to have negligible tendency to coordinate with the aluminum in comparison with the tendency of the hydroxyl ion present in the solution. The pH values of the solutions were determined with a Beckman Type E2 glass electrode using $Ca(OH)_2$ standards having a pH of 12.45 (based on NBS measurements supplied by Beckman Instruments, Inc.). Corrections to the pH were made for Na^+ ion concentrations. Potentials were also measured with a phosphate electrolyte at a pH of 11.5 but these did not agree with the sulfate electrolyte. It was demonstrated that the sulfate ion concentrations did not affect the electrode potentials by measurements at a pH of 11.6 with an electrolyte consisting of $0.0072 M$ sodium aluminate which had been prepared free of sulfate. In the high pH region it was found that the potentials were independent of the aluminate ion concentration. Measurements at high pH were made over a range of three decades of aluminate ion concentration with the ordinary sulfate electrolyte and also with a pure $1 M$ sodium hydroxide solution containing no sulfate or aluminate.

Experimental Results. The experimental results are shown in Fig. 2. It is seen that in the lower pH region the electrode potentials depend in a systematic way upon the aluminate ion concentration and upon the pH. At a pH of about 12.4 the potential becomes less sensitive to the aluminate ion concentration and above this pH' the potential is independent of the aluminate ion concentration and changes less drastically with the pH. In the pH range from 10.5 to about 12.4 the experimental data can be fitted with the empirical relationship

$$E_{\text{sat. cal.}} = 0.5099 + \frac{0.0591}{3} \log [\text{aluminate ion}] + 2(0.0591) \text{ pH}$$

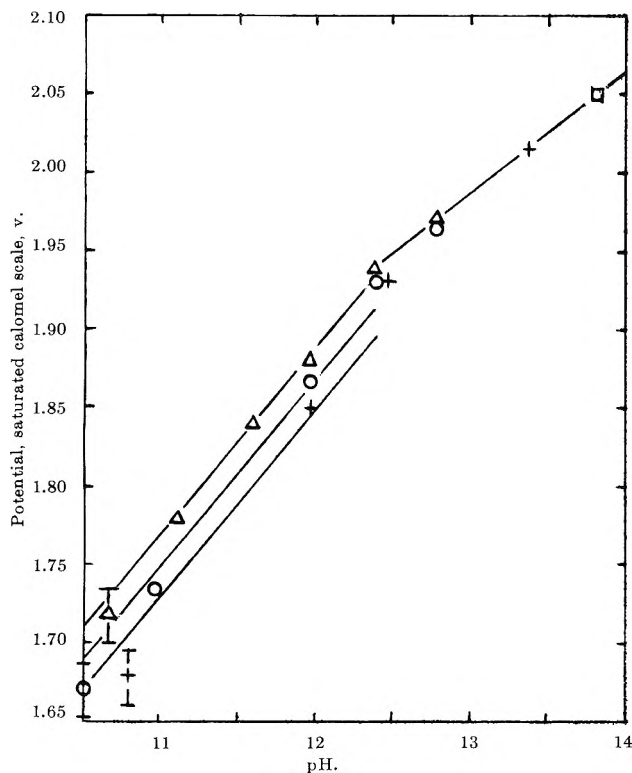


Figure 2. The potentials obtained by extrapolation to zero oxide film thickness for an aluminum electrode in a variety of electrolytes. Points experimental. Curves according to empirical relationships given in text. \square , NaOH; Δ , $7.16 \times 10^{-3} M Al^{3+}$; \circ , $7.16 \times 10^{-4} M Al^{3+}$; $+$, $7.16 \times 10^{-5} M Al^{3+}$.

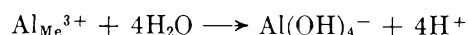
The constant, 0.5099, was chosen to provide the best fit to the data in 0.00716 M solutions. A surprising feature of the results in this pH region is that the potential tends to increase with increasing aluminate ion concentration rather than decrease. The curves drawn on Fig. 2 represent this empirical equation. In the pH range from 12.4 to 13.8 the experimental data may be fitted by the equation

$$E_{\text{sat. cal.}} = 0.962 + \frac{4}{3}(0.0591) \text{ pH}$$

In this region the potentials are independent of the aluminate ion concentration.

Interpretation of Results

The most obvious electrode reaction to test against the experimental data is obtained assuming that the anionic species in solution is the monomer $Al(OH)_4^-$.



The potential for this reaction should be given by

$$E = E^\circ - \frac{0.059}{3} \log [Al(OH)_4^-] + \frac{4}{3}(0.059) \text{ pH}$$

The experimental results do not agree with this expression. In the high pH range the dependence upon pH is correct but there is no observed dependence upon the concentration of the aluminate ion. In the low pH range the potential varies at the rate of 0.059/3 v. per decade of aluminate ion concentration but the potential is observed to increase with increasing aluminate ion concentration whereas the equation predicts a decrease. In the low pH range the observed dependence on pH ($2[0.059]$ v. per pH unit) does not agree with that predicted by the equation. Thus, the above hypothetical electrode reaction cannot be correct.

In order to explain the fact that the potential increases with increasing aluminate ion concentration it is necessary to assume that the aluminate ion is a reactant in the electrode reaction. Thus, an aluminum ion from the metal, entering the solution, must react with aluminate ions forming some type of polynuclear complex. In the high pH range, in order to explain the lack of dependence of the potential upon aluminate ion concentration it is necessary to assume that the product of the electrode reaction is in equilibrium with the aluminate ion concentration in such a way that the concentration of the product of the electrode reaction is quite independent of the over-all concentration of the aluminate ion.

One may use the observed pH dependence to arrive at the number of protons displaced by an aluminum ion entering the solution from the metal. Thus, in the low pH range six protons must be released when an aluminum atom reacts at the electrode. In the high pH range four protons must be released per aluminum atom. One may use these observations as a starting point in deducing the nature of the electrode reactions. The behavior of the electrode potentials with respect to the concentration of the aluminate ion in solution and the pH is explicable if one assumes that the aluminate ion in solution exists as a polymeric anion. Several alternative structures for the polymeric anion are possible. We will first describe the general characteristics which are necessary in order to be consistent with the experimental observations.

Since the aluminate ion bears a negative charge, it is not surprising that it would react with the positively charged aluminum ion entering the solution from the metal. In the low pH range the reaction can be considered as that of an aluminum ion from the electrode reacting with a site of a polymeric aluminate anion to produce a branched polymeric structure. The number of active sites which the polymer will present to the ion

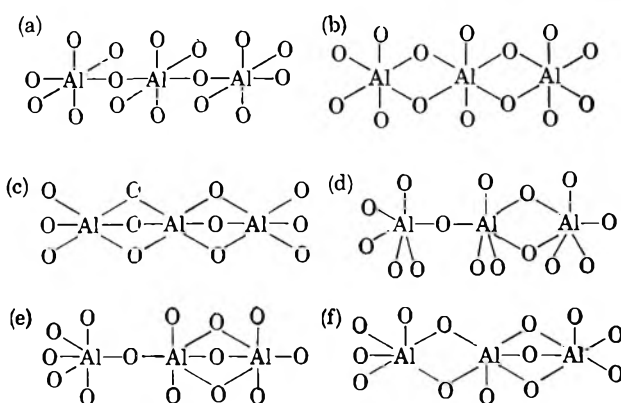
will be proportional to the over-all aluminate concentration in the solution. Thus, the observed dependence of the electrode potential upon aluminate ion concentration will result. The reaction of an aluminum ion with an active site must be of such a form that a net of six protons are displaced for each aluminum ion reacting. It is attractive to think that the same polymeric structure persists at high pH values. The observed results at high pH may be explained if an aluminum ion from the electrode reacts with hydroxyl ions to form $\text{Al}(\text{OH})_4^-$ which then reacts with a polymer chain end without any further proton displacement. Such a reaction will produce potentials which are dependent in the observed manner on the hydrogen ion concentration and, if the chains are long enough, will be approximately independent of the over-all aluminate ion concentration.

The change in the nature of the reaction observed in the vicinity of pH 12.4 is reasonable. The hydroxyl ion concentration at pH of 12.4 is of the order of the magnitude of 0.01 M. Below this pH the negatively charged sites on the aluminate ion outnumber the hydroxyl ions in the solution and one would expect that a reaction of aluminum with the polymer directly would predominate. Above the pH of 12.4, hydroxyl ions are outnumbering the negatively charged active sites on the polymer and one would expect that aluminum ions would react directly with hydroxyl ions. One would expect that the transition from one reaction to the other would take place at lower pH values for dilute aluminate ion solutions and higher pH values for concentrated solutions. There is some evidence in the experimental data that such is the case.

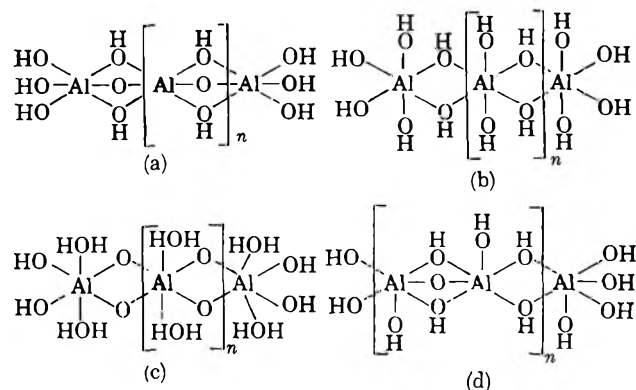
The Selection of Possible Polymeric Anion Structures.

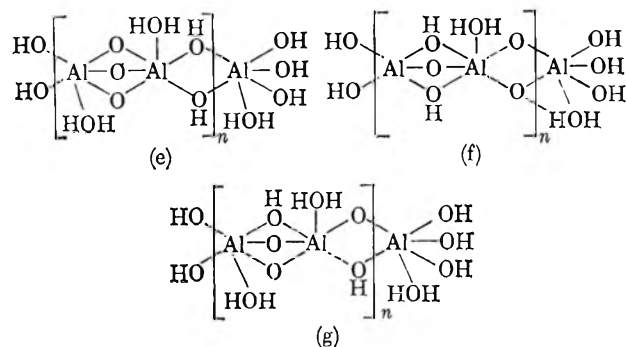
The ratio of bound hydroxyl ions to aluminum ions is useful information to establish the nature of the polymeric anion in more detail. From Brosset's data^{3a} one finds that in the pH range above 10.5 the number of bound hydroxyl ions per aluminum ion is 4.10 ± 0.05 . The conditions with which possible polymeric structures must comply are that the building of bridged chains must produce six protons, and addition to chain ends must produce four protons. It is reasonable to assume that the coordination number of the aluminum must be four or six. We will refer to skeletal structures for the polymer in which we will neglect explicit mention of the positions of hydrogen atoms. There are four simple skeletal structures having aluminum with a coordination number of four. These involve double bridges between aluminum atoms, single bridges between aluminum atoms, alternate single and double bridges, and alternate single and triple bridges. It can be demonstrated that building branched chains from

any of these four structures by reaction of aluminum ions from the metal with active sites will displace only four protons instead of the necessary six protons so that aluminum with a coordination number of four does not appear to be a reasonable possibility, at least in the low pH region. It is possible that aluminum has a coordination number of six in the low pH region and changes to a coordination number of four at high pH values but this does not seem likely. For octahedrally coordinated aluminum the possible skeletal structures are shown below.



It is reasonable to assume that the bridging oxygen atoms may be either O or OH but oxygen atoms in similar bonding positions should have the same number of hydrogen atoms attached to them. It also is reasonable to assume that all the nonbridging oxygen in a particular structure must be of one type, either OH or H_2O . It can be seen that skeletal structures (a) and (d) must violate these assumptions in order to have an over-all composition of $\text{Al}(\text{OH})_4^-$. Using the observed dependence of potential upon pH and the number of protons involved in the electrode reactions one can systematically eliminate many of the possible structures. Seven polymer structures which are consistent with the experimental facts are





The Electrostatic Energy of a Polymeric Anion. It is useful to estimate the electrostatic energy of a polymeric anion of the type which we have proposed because, without *a priori* knowledge, one might expect that the electrostatic energy would be so great that the ion could not exist. One is interested in the difference in electrostatic energy of a linear array of negative charges in an atmosphere of an equivalent number of positive charges and an array of individual positive and negative charges which are not localized as in the polymer. A crude estimate of the energy of the ionized monomeric species is obtainable by assuming a b.c.c. lattice of alternating positive and negative charges at distances predicted from the over-all concentration of the solution (at $10^{-3} M$ the distance between charges is about 100 Å.). Using the Madelung constant for a b.c.c. lattice and the dielectric constant of water one obtains -0.844 kcal./mole. An approximation of the electrostatic energy of the polymer is obtainable assuming a polymeric anion containing 27 negative charges arrayed along a line with a separation of 5 Å. with the polymeric anion centered in a cubic lattice containing a total of 27 positive charges distributed over 64 lattice points. The electrostatic energy for this model is $+1.91$ kcal./mole. The difference between the electrostatic energy of the polymeric and the monomeric model is $+2.75$ kcal./mole. It is apparent, since hydrogen bonds have an energy of the order of 8 kcal./mole, that the electrostatic repulsive energy of the polymeric species is small compared to the total bond energy which might be obtained from the bridged type of structure.

Raman Spectra of the Aluminate Ion. Lippincott and co-workers⁷ interpreted their measurements on the Raman spectra of the aluminate ion as favoring T_d symmetry for monomeric aluminum ions. Neither T_d symmetry nor O_h symmetry was completely consistent with the spectrum they observed. With T_d symmetry one expects to find four fundamentals, whereas in O_h symmetry one expects to find three Raman active fundamental vibrations, in each case ignoring the motions of the hydrogen atoms. Of course

the symmetry cannot be precisely O_h since the over-all composition of the ion is $Al(OH)_4^-$. If it were D_{4h} there would be no change in selection rules from those found for O_h but the E_g and the F_{2g} vibration would be split into components. Only two Raman lines were observed in Lippincott's work but, from estimates of the force constants and predictions of the frequencies he argued that T_d was the appropriate symmetry. It is necessary to inquire if the proposed polymeric structure for the anion is any less or more consistent with the spectra than the free monomeric ion models. To determine the selection rules for the fundamental vibrations of a one-dimensional repetitive structure (line group) one determines the selection rules for the point group isomorphous with the factor group of the line group.¹⁰ Three of the seven polymer structures (a), (b), and (c) would be linear and would produce a small number of Raman active fundamentals. The second one (b) seems most reasonable to us because it involves only one kind of ligand, that is OH^- . The factor group of the line group of that structure is isomorphous with the point group D_{2h} . The correlation table for the vibrations under D_{2h} symmetry with the vibrations under O_h is shown in Table I.

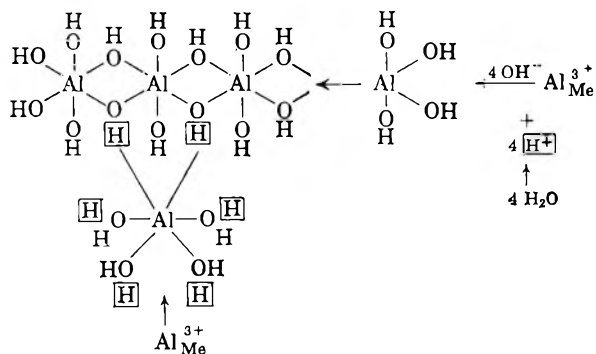
Table I

O_h	Raman activity		D_{2h}	Raman activity
A_{1g}	+	→	A_g	+
E_g	+	→	$2A_g$	+
$F_{1u}(1)$	0	→	$B_{1u} + B_{2u} + B_{3u}$	0
$F_{1u}(2)$	0	→	$B_{1u} + B_{2u} + B_{3u}$	0
F_{2g}	+	→	$B_{1g} + B_{2g} + B_{3g}$	+
F_{2u}	0	→	$B_{1u} + B_{2u} + B_{3u}$	0

If the symmetry was that of the free ion, O_h , there would be three Raman fundamentals. Six Raman fundamentals are predicted for the D_{2h} polymer. However, it is to be noted, that the changes in the spectra in going from O_h to D_{2h} are caused by splitting of the degeneracies of fundamentals and not by changes in the selection rules for particular modes of vibration. Thus, if the effects of next-nearest neighbors around the aluminum ions are small, as seems reasonable, one would observe only three lines for the polymer. Further studies of the Raman spectrum of the aluminate ion and, in particular, attempts to interpret the spectrum in terms of the model which we propose, would be desirable.

(10) M. C. Tobin, *J. Chem. Phys.*, **23**, 891 (1955).

The Electrode Reactions. Using the doubly bridged polymer in which each aluminum ion is surrounded by six hydroxyl ions we believe that the two electrode reactions take place as shown schematically in the following diagram.



The protons displaced are shown in boxes. The direct reaction between an active site on the aluminate polymer, four water molecules, and an aluminum ion produces a branched structure in which the bonding is similar to that in the straight chain polymer except that the bonding role of two of the hydrogen atoms is replaced by an aluminum ion. We suppose that the branched polymer is metastable with respect to the linear polymer since it involves a greater spacial concentration of negative charge. The reaction to produce the branched chains requires two adjacent hydroxyl bridges. For a linear polymer with n aluminum ions there will be $n - 1$ of these positions. Therefore, the electrode reaction which describes this process should depend directly on the aluminum concentration and the aluminum concentration will appear as a reactant. At high pH values where the aluminum reacts directly with hydroxyl ions in solution a net of four protons are produced. One expects the free $\text{Al}(\text{OH})_4^-$ to be in equilibrium with the polymer. The concentration of the monomeric species will be only weakly dependent on the over-all aluminate ion concentration in the solution so that where this direct reaction between aluminum ions and hydroxyl ions predominates it may be expected that the potential is independent of the over-all aluminum ion concentration.

The Measured Ratio $\text{OH}^-_{\text{bound}}/\text{Al}^{3+}$. Brosset, working at 40° and with two concentrations of aluminate ion, found that above a pH of 10.5 the ratio of hydroxyl ligands to aluminum ions was somewhat greater than four. The over-all composition of the polymeric anion which we favor is $(\text{OH})_2[\text{Al}(\text{OH})_4^-]_n$. The existence of such a polymeric anion is consistent with Brosset's measurements and one can calculate the chain length from the measured ratio. Brosset's observa-

tions are in Table II together with values of the chain length derived from them.

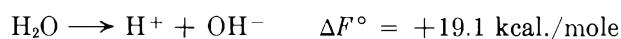
Table II

Aluminate ion concentration, M	$\text{OH}^-_{\text{bound}}/\text{Al}^{3+}$, initial ^a	$\text{OH}^-_{\text{bound}}/\text{Al}^{3+}$, final ^a	Chain length, final
0.00221	4.056	4.049	40
0.0111	4.034	4.018	100

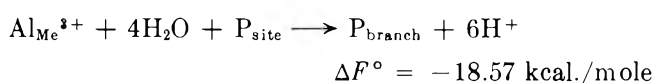
^a Initial values obtained a few minutes after introducing base, final values obtained several hours after introducing base.

There are two significant trends in the ratios. First, it is noted that the ratio decreases with time as the solution stands. We believe that this results from branched chains in the polymeric structure initially obtained which readjust slowly as the negatively charged anionic groups migrate to the chain ends. Second, there is a decrease in the ratio with increasing aluminum ion concentration in the solution. This is consistent with the expectation that in more concentrated solutions the chain length will be longer. We have done experiments similar to Brosset's in which we confirm the results on the ratio in the pH range which Brosset covered and we find similar behavior through a pH of 12.

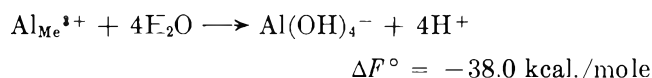
The Thermodynamic Properties of the Aluminate Polymer. The standard electrode potentials, on the hydrogen scale, for the reactions in the low and high pH ranges are, respectively, 0.2684 v. and 0.7205 v., and the free energies are -18.57 kcal./mole and -49.84 kcal./mole. One may estimate the free energy of formation of an $\text{Al}(\text{OH})_4^-$ monomeric unit from water and metal from the fact that the hydrated, neutral species present in acidic solution has a free energy of formation of -57.1 kcal./mole and the anion differs primarily by the removal of an additional proton. Thus, one obtains -38.0 kcal./mole using the free energy for



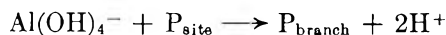
One finds by dividing the reaction



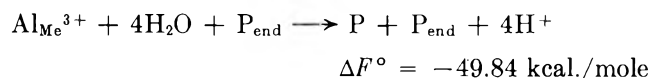
into



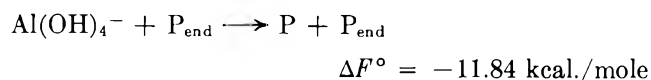
and



that the free energy for formation of a branch is +19.4 kcal./mole. Similarly, for the reaction at high pH one may divide the reaction



into parts and obtain for the association of the polymer



Acknowledgments. This work was supported by the U. S. Atomic Energy Commission under Research Contract AT(30-1) 2479.

The Molecular Structure in Surface Films of Unsaturated 1-Monoglycerides on Water as Related to Three-Dimensional States¹

by D. R. Merker and B. F. Daubert

Department of Chemistry, University of Pittsburgh, Pittsburgh, Pennsylvania
(Received November 20, 1963)

The relationship of the molecular structure in monolayers of unsaturated 1-monoglycerides to three-dimensional states is discussed. Monolayers of *cis*-monoglycerides were in the expanded state under all the conditions studied and extremely stable. The physical properties of the monolayers in this state resemble in certain respects the physical properties of three-dimensional liquids. An expanded monolayer of 1-monoelaidin was transformed under pressure to a condensed state with a limiting area of 24 Å.². This area was in close agreement with the cross-sectional area calculated for a hypothetical liquid crystal from density and X-ray data. The correlation indicates that the orientation of the molecules in the condensed monolayer of 1-monoelaidin approximates the orientation in the anhydrous three-dimensional crystal.

Introduction

The effect of unsaturation in monolayers of fatty acids on water has been studied extensively.²⁻⁷ The unsaturated C₁₈ acids occupy much greater areas per molecule than does stearic acid at the same temperature. Hughes⁴ has suggested that expansion is caused by the attraction of water for the double bonds. Sneider, *et al.*,⁶ have found that the area of the *cis* C₁₈ acids at negligible pressure increases as the unsaturation increases. They have suggested that this effect and the stability of the expanded monolayers are caused by a progressively greater curl of the unsymmetrical molecules.

This investigation was undertaken in part to ascertain if either of the above-mentioned theories is applicable to the unsaturated 1-monoglycerides. It was

(1) The authors extend their appreciation to Swift and Co. for a research grant that made this work possible.

(2) E. K. Rideal and R. K. Schofield, *Proc. Roy. Soc. (London)*, **110**, 170 (1926).

(3) E. K. Rideal and A. Hughes, *ibid.*, **140**, 253 (1933).

(4) A. Hughes, *J. Chem. Soc.*, 338 (1933).

(5) J. Marsden and E. K. Rideal, *ibid.*, 1163 (1938).

(6) V. L. Sneider, R. T. Holman, and G. O. Burr, *J. Phys. Colloid Chem.*, **53**, 1016 (1949).

(7) E. D. Goddard and A. E. Alexander, *Biochem. J.*, **47**, 331 (1950).

also desired to compare the results with those previously reported for saturated 1- and 2-monoglycerides.⁸

Experimental

Oleic acid was isolated from olive oil by the method of Brown and Shinowara.⁹ Elaidic acid was prepared by the isomerization of oleic acid with sodium nitrite. Linoleic acid was prepared by the debromination in ether of tetrabromostearic acid, which was obtained by brominating the unsaturated acids isolated from corn oil. Linolenic acid was prepared by the debromination in pyridine of hexabromostearic acid, which was obtained by brominating the unsaturated acids isolated from linseed oil.

Oxalyl chloride was used to prepare the corresponding acid chlorides, which were treated with 1,2-isopropylidene glycerol according to the method of Daubert and Baldwin.¹⁰ Acid hydrolysis yielded 1-monoolein (m.p. 35.0–35.5°, iodine value 71.0), 1-monoelaidin (m.p. 57.5–58.5°, iodine value 70.3), 1-monolinolein (m.p. 14.5–15.5°, iodine value 143.2), and 1-monolinolenin (m.p. 12.6–13.8°, iodine value 213.9).

The densities, determined by the displacement of iso-octane in a pycnometer, of 1-monoolein and 1-monoelaidin in the solid state at 0° were 1.043 and 1.058, respectively. Average cross-sectional areas calculated from these densities and X-ray long spacings of 49.5 Å. and 50.5 Å.^{11,12} were 22.9 Å.² for 1-monoolein and 22.4 Å.² for 1-monoelaidin. Theoretical average cross-sectional areas for these compounds in a hypothetical liquid crystalline state as calculated from the X-ray long spacing data and extrapolated densities of 0.958 for 1-monoolein and 0.962 for 1-monoelaidin in a liquid state at 20° were 25.0 Å.² and 24.4 Å.², respectively.

Force-area data for the monolayers were obtained as described in a previous publication.⁸ In order to retard autoxidation 0.12% hydroquinone was added to the distilled water in the trough of the Langmuir film balance as suggested by Rideal and Hughes.³ Compression was begun as soon as possible after evaporation of the benzene, which was used as a solvent for spreading the monolayers. Several determinations were made on distilled water, which did not contain an antioxidant, but the results were unchanged.

The force-area curves showed that the monolayers of the *cis* unsaturated monoglycerides were expanded and occupied areas of similar magnitude at a given temperature and pressure. The limiting areas at 24.3° and negligible pressure for 1-monoolein, 1-monolinolein, and 1-monolinolenin were 72, 74, and 76 Å.²/molecule, respectively. At 4.0° these critical areas decreased slightly but the curves were basically unaltered. The

monolayers were extremely stable and collapsed at 30–34 Å.² and 45–50 dynes/cm. The pressure then remained constant and did not fall with time indicating that the monolayers were in equilibrium with an oil lens of equal spreading pressure.

A monolayer of 1-monoelaidin at 24.3° and negligible pressure also was expanded and occupied 70 Å.²/molecule. However, this monolayer transformed to a liquid condensed state at 30 Å.² and 42 dynes/cm. At 4.0° the transformation occurred at approximately 16 dynes/cm. The limiting area for the condensed state at 4.0° was 24 Å.² and the relative compressibility expressed as the reciprocal slope of the isotherm was 0.073 cm.³/dyne. The limiting area of 24 Å.² agrees well with the cross-sectional area calculated for a hypothetical liquid crystal from the X-ray long spacing of the three-dimensional unit cell and the extrapolated density of the three-dimensional liquid. There were no discontinuities on further compression and the fluid monolayer finally collapsed at 58 dynes/cm. and 21.5 Å.².

Discussion of Results

The molecular orientation in the expanded monolayers of monoglycerides appears to be independent of the type or degree of unsaturation. Complete solvation of the glyceryl groups probably is responsible for the formation of the expanded state and its characteristic areas because the monolayers of saturated monoglycerides also occupy an average cross-sectional area of 70–75 Å.²/molecule in this state.⁸ The magnitude of this area indicates that the orientation differs radically from that in the anhydrous crystals in which the average cross-sectional area per molecule is approximately 23 Å.².

The extremely high stability of unsaturated monoglycerides in the expanded state is remarkable and appears to be related to the force of double bond interaction as well as to the strong hydrophilic nature of the glyceryl groups. It is very significant that the spreading pressure remained constant and did not fall with time after the monolayers collapsed at 30–35 Å.². At this point a two-dimensional monolayer and a three-dimensional oil lens are in equilibrium and conceivably could be alike in molecular orientation.

(8) D. R. Merker and B. F. Daubert, *J. Am. Chem. Soc.*, **80**, 516 (1958).

(9) J. B. Brown and G. Y. Shinowara, *ibid.*, **59**, 6 (1937).

(10) B. F. Daubert and A. R. Baldwin, *ibid.*, **66**, 997 (1944).

(11) L. J. Filer, S. S. Sidhu, B. F. Daubert, and H. E. Longenecker, *ibid.*, **66**, 1333 (1944).

(12) M. G. R. Carter and T. Malkin, *J. Chem. Soc.*, 554 (1947).

The force-area curve for a sample of 1-monolinolenin, which was aged in contact with air for 1 week, showed that oxidation of the double bonds increased the limiting area in the expanded state to a greater extent than does the introduction of double bonds. Therefore, the packing of the chains could be quite compact even in the expanded state.

The densities of the C_{18} unsaturated monoglycerides in the three-dimensional liquid state were greater at any given temperature than the density of 1-monostearin.⁸ The monoglycerides in the liquid state thus become more compact with increasing unsaturation and asymmetry. It is well known that unsaturated monoglycerides and fatty acids are more stable as liquids than as solids at ordinary temperatures and atmospheric pressure but the corresponding saturated compounds under the same conditions have a greater tendency to be in the solid state. The same analogy exists in the monolayers. 1-Monostearin is in the liquid condensed state at 20°,⁸ but 1-monolein remains in the expanded state at all pressures. Therefore, in this respect the expanded monolayers are similar to the three-dimensional liquids.

The results are interesting in relation to the theories proposed by Hughes⁴ and Sneider⁶ for the expanded monolayers of unsaturated compounds. In regard to the theory of Hughes it is noteworthy that essentially the same pressure was required to reduce the area to any given point for the three *cis* unsaturated monoglycerides. If the attraction of water for the double bonds is instrumental in the formation of these expanded monolayers, one would expect that a much greater pressure would be required to reduce the area

to a given point for the more highly unsaturated compounds. The results, likewise, were not entirely compatible with the theory of chain curling. However, the magnitude of the areas within the expanded state are such that rotation of the chains should be possible except at the double bonds.¹³

The condensed monolayer of 1-monoelaidin resembled those of saturated 1-monoglycerides. Apparently the orientation of the molecules in this state is similar to that in the three-dimensional crystal but the monolayer is liquid crystalline because of partial interaction with the substrate. Transformation of state probably does not occur in the case of the *cis* compounds, because the cohesive forces that would exist if the monolayer were condensed simply are not great enough to appreciably aid the mechanical force in effecting a stable rearrangement of the polar group. The introduction of double bonds into the hydrocarbon chain lowers the stability of the liquid condensed state just as it lowers the melting point of the anhydrous crystals and increases the stability of the liquid. The densities of 1-monolein and 1-monoelaidin in the solid state were found to be lower than the density of 1-monostearin.⁸ The reverse situation, as mentioned above, exists for the liquids. The instability of the three-dimensional crystals and the liquid condensed monolayers of unsaturated monoglycerides is additional support for the theory⁸ that the molecular structures in these states are similar.

(13) J. G. Kirkwood, *Publ. Am. Assoc. Advan. Sci.*, No. 2, 15 (1943).

Binding of Phenols by Hair. I

by M. M. Breuer¹

Gillette Research Laboratories, Reading, Berkshire, England (Received December 3, 1963)

The binding by hair of five different phenolic compounds was studied. The results indicate that the adsorption occurs on the peptide groupings of the polypeptide chains, probably by formation of H bonds. Resorcinol was found to exhibit unique binding characteristics among the compounds studied. From the experimental data presented, conclusions can also be drawn regarding the water binding sites and the mechanism of hydration of hair. Changes in adsorption isotherms of resorcinol were found when the hair was "treated" with HCl. These changes point to the occurrence of transformations in the *tertiary* hair structure below the pH range 2.4–2.6.

Introduction

The adsorption of phenols on wool and hair has been studied by several workers. Thus, Zahn² found that reversible changes occur in the mechanical properties of wool when it is dipped at 25° into solutions of phenols. Chipalkatti, Giles, and Vallance^{3a} measured the adsorption of many compounds, among them phenols, on wool and other textile fibers from aqueous and nonaqueous solutions. The data gathered by these authors, however, were far from being sufficient to allow the postulation of a binding mechanism for phenols on wool. Reports of other investigations carried out on this subject contain only scanty data mostly of a qualitative nature; the interpretation of these data is very difficult.^{3b}

In the present study, adsorption isotherms of various phenols on hair were measured at a number of temperatures. On the basis of the experimental results, a model is suggested for the binding mechanism of phenolic compounds. The behavior of resorcinol is shown to differ markedly from that of the other phenols studied.

Experimental

Materials. Brown "De-Meo" Caucasian hair was used in all experiments. The hair was purified by extracting it in a Soxhlet apparatus with chloroform and acetone consecutively for 24 hr. each. Subsequently, it was soaked in distilled water for 6 days, the water being changed twice a day. The hair was then allowed to dry while hanging in the atmosphere.

Chemicals. Where available, B.D.H. Analar grade

materials were used for all experiments; in all other cases B.D.H. laboratory reagent grade chemicals were used after recrystallization.

Methods. The adsorption measurements were carried out in the following manner. About 0.5 g. of hair was weighed into a test tube equipped with a ground-glass stopper and dried *in vacuo* over P₂O₅ for 16 hr. The test tube was stoppered in a dry cabinet and weighed; then a known volume of an accurately prepared aqueous solution of a phenol or HCl was added. A set of such tubes was subsequently placed in a thermostatically controlled bath and left there until equilibrium was attained, which, as a rule, required 24 hr. After the equilibrium had been completed, aliquot quantities of the solutions were withdrawn and, after suitable dilution, the phenol concentrations were measured. The amounts of phenols bound to the hair (\bar{r}) were calculated from the decreases in concentrations and the volumes of the solutions originally added.⁴

The concentrations of the phenolic solutions were obtained by measuring their optical densities by means

(1) Unilever Research Laboratory, Isleworth, Middlesex, England.

(2) H. Zahn, *Z. Naturforsch.*, **213**, 286 (1947).

(3) (a) W. R. Chipalkatti, C. H. Giles, and D. G. M. Vallance, *J. Chem. Soc.*, 4375 (1954); (b) a detailed bibliography is given in this reference.

(4) Simultaneously with the adsorption of phenols, a hydration of the hair also takes place. The volume of the "free" phenolic solution is therefore slightly less than the volume of the original solution, and the calculated amounts of the phenol adsorbed in hair are thus lower than the real values. An estimate of this error showed that it must be less than 2% and no correction was applied. The values of \bar{r} were reproducible within $\pm 10^{-4}$ mole g.⁻¹. This was established by carrying out many repeated experiments under identical conditions.

of a Hilger Uvispek spectrophotometer at the wavelength of the maximum absorbancy of the phenol in question. The values of the latter are available in the literature.⁵ Calibration curves were prepared for the individual phenols and the molar extinction coefficients calculated. Adherence to the Lambert-Beer law was found in all cases, within the concentration ranges studied (10^{-3} to 10^{-6} mole/l.).

The water adsorption measurements were carried out by exposing weighed samples of hair to atmospheres of constant humidities and determining the weight increases of the hair samples. The attainment of equilibrium was ascertained by taking weighings at several time intervals. No further weight change was observed after 10 days.

An Electronic Instruments Ltd. direct reading pH meter was used for the pH measurements. The reproducibility of the measurements was within 0.1 pH unit.

The mechanical properties of single hair fibers were measured using an Instron extensometer. The work required for stretching to 30% extension was determined with fibers totally immersed in distilled water.

Results

In each experiment, r , the quantity of bound phenolic compound (measured in moles/g. of hair), was calculated and plotted against f , the equilibrium concentration (moles/l.) of the phenolic compound in solution. Two types of isotherms were obtained; resorcinol, catechol, and pyrogallol each yielded a curve convex with regard to the f -axis in its entire course, whereas phenol and hydroquinone gave slightly sigmoid curves (for a typical isotherm, see Fig. 1 and 2). The difference between the two types of adsorption isotherms can be better demonstrated by plotting $1/r$ against $1/f$. Resorcinol, catechol, and pyrogallol then yield straight lines (typical curves are shown in Fig. 3), whereas phenol and hydroquinone give pronounced sigmoids (for typical curves, see Fig. 4). All of the isotherms represent fully reversible processes at the temperatures and concentrations studied, confirming Zahn's similar previous results.²

The mechanical properties of single fibers, although influenced by the binding of phenols, were entirely restored after washing out of the phenols.

For the interpretation of these results, we now consider the relevant theoretical treatments of systems of this type. Thus, Klotz⁶ derived equations for various types of binding equilibria of small molecules to proteins in the following manner. Postulating a model where the small molecules are bound on independent, fixed, and equivalent sites (*i.e.*, Langmuiric

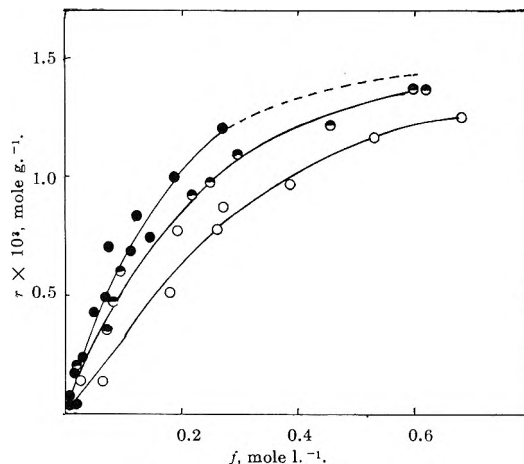


Figure 1. Binding isotherms of resorcinol hair: O, 2°; ◐, 26°; ●, 37°.

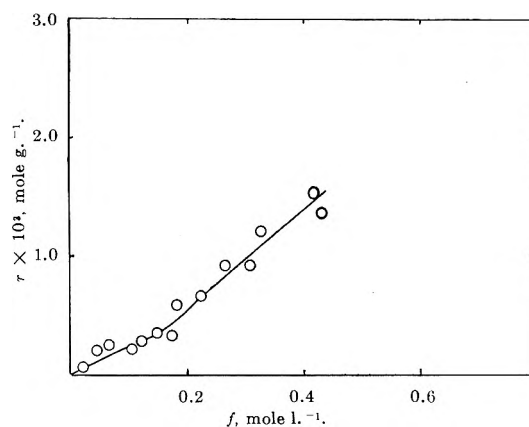


Figure 2. Binding isotherms of hydroquinone on hair.

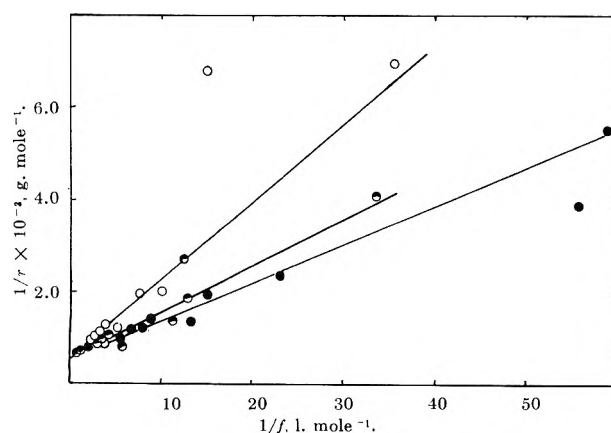


Figure 3. Reciprocal plots of resorcinol binding isotherms: O, 2°; ◐, 26°; ●, 37°.

(5) H. E. Ungnade, "Organic Electronic Spectral Data," Interscience Publishers, Inc., New York, N. Y., 1960.

(6) I. M. Klotz in "Proteins," Vol. 1B, H. Neurath and K. Bailey, Ed., Academic Press, Inc., New York, N. Y., 1953, pp. 724-804.

Table I: Binding Constants and Thermodynamic Quantities of Hair-Phenol Interactions

Compound	T , °K.	$n \times 10^3$, mole g. ⁻¹	K , mole ⁻¹ l.	ΔF , cal. mole ⁻¹	ΔH , kcal. mole ⁻¹	ΔS , e. u.
Phenol	275	5.2	0.21	+858	+15.85	+50.5
	299	5.2	1.82	-358		
Hydroquinone	275	4.5	1.83	+91	+3.09	+10.9
	299	4.5	1.32	-166		
Catechol	275	4.6	1.05	-25	+3.21	+12.0
	299	4.6	1.69	-312		
Resorcinol	275	1.8	3.50	-815	+2.50	+12.0
	299	1.8	5.75	-1050		
	311	1.8	6.80	-1220		
Pyrogallol	275	4.8	0.91	+50	+2.12	+7.82
	299	4.8	1.25	-137		
Resorcinol and acid- treated hair	275	5.0	1.26	-126	-2.43	-8.75
	299	5.0	0.89	+84		
Catechol and acid- treated hair	275	4.6	1.26	-126	+3.96	+14.8
	299	4.6	2.20	-472		

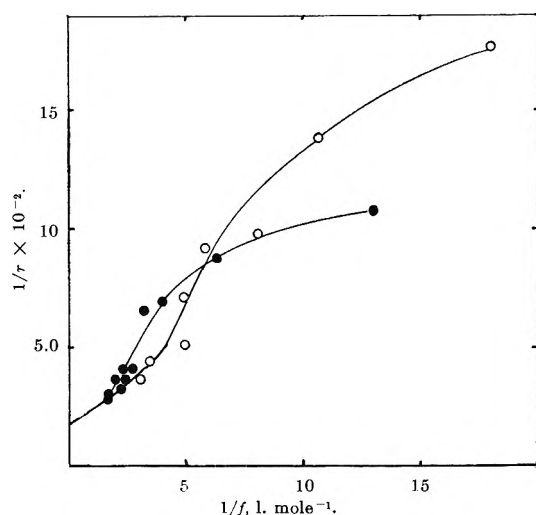


Figure 4. Reciprocal plots of phenol binding isotherms: O, 2°; ●, 26°.

isotherm), he obtained the equation

$$\frac{1}{r} = \frac{1}{Knf} + \frac{1}{n} \quad (1)$$

where n and K are the number of sites and the equilibrium constant of binding of each individual site, respectively. The straight lines obtained in $1/r$ vs. $1/f$ plots in the cases of resorcinol, catechol, and pyrogallol, therefore, indicate that this type of binding mechanism operates with these compounds. From the slopes and the intercepts of the lines, the n and K values for the individual phenols were obtained and are given in Table I (columns 2 and 3).

The curves of Fig. 4 show that this simple model is not adequate for the interpretation of the adsorption

data of phenol and hydroquinone, and a slightly more complicated model is used, therefore, to account for the experimental results. In this model it is assumed that the binding occurs on fixed sites with equal intrinsic binding constants, but that the sites are not independent and that interaction occurs between two molecules bound to adjacent sites.⁷ This interaction can have either a facilitating or hindering influence depending on the nature of the interacting forces. Thus, if electrostatic repulsion forces (for instance) are involved, the adsorption on the second site will be hindered. Should, however, van der Waals attraction forces exist, the binding next to an occupied site will be facilitated.

If we introduce the quantity

$$\omega = \frac{\Delta F_i}{RT} \quad (2)$$

(where ΔF_i , R , and T are the free energy of interaction, the gas constant, and the absolute temperature, respectively) we obtain the adsorption equation⁷

$$f \left(\frac{n}{r} - 1 \right) = \frac{\exp 2\omega r/n}{K} \quad (3)$$

$$2.303 \frac{\omega r}{n} = \log K + \log f \left(\frac{n}{r} - 1 \right) \quad (4)$$

When the quantities $\log f((n/r) - 1)$ were calculated from the phenol-hair and hydroquinone-hair adsorption data and plotted against r/n , straight lines were obtained, suggesting that the modified model is the correct one. (For typical curves, see Fig. 5.) From

(7) R. Fowler and E. A. Guggenheim, "Statistical Thermodynamics," Cambridge University Press, London, 1956, p. 429.

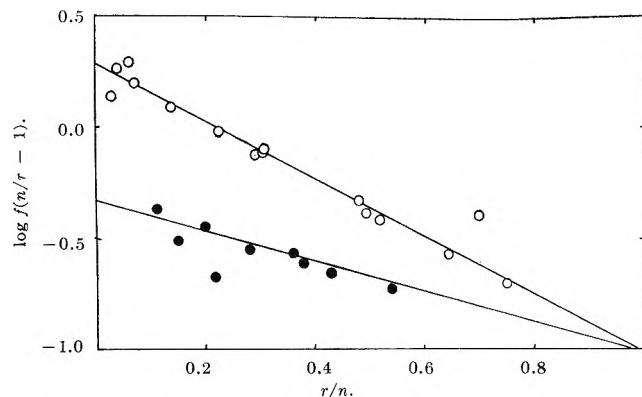


Figure 5. Phenol binding data represented according to eq. 4: ●, 2°; ○, 26°.

the intercept and slope of each line, the appropriate values of K and ω were evaluated. The values are given in Tables I and II, respectively.

Table II: Values of the Thermodynamic Quantities of Next-Neighbor Interactions

	T , °K.	ω	ΔF_i , cal. mole ⁻¹	ΔH_i , kcal. mole ⁻¹	ΔS_i , e.u.
Phenol	275	-0.92	-505	+5.12	+20.4
	299	-1.49	-895		
Hydroquinone	275	-1.90	-1040	-6.94	-21.4
	299	-0.82	-490		

An alternative method for the evaluation of small molecule binding data has been suggested by Schumaker and Cox.⁸ Their method of representation of the experimental data provides additional information on the hydration properties of the protein. Schumaker and Cox pointed out that a serious error in the value of K is possible if the calculations are carried out on the tacit assumption that changes in the solute concentration of the solution do not influence the amounts of water which are bound to the protein. These workers derived the equations

$$\alpha = \frac{-r55.51}{f} \quad (5)$$

and

$$\alpha = \Sigma \lambda_i + n \frac{1 - K55.51}{1 + Kf} \quad (6)$$

The quantity α is known as the degree of preferential hydration. It is equal to the number of water molecules which would need to be released or bound in order

to restore the same solute to solvent ratio at the binding site as the one which exists in the solution. The symbol λ_i represents the number of sites of the i th type, capable of binding water but incapable of adsorbing solute molecules; n and K are the number of solute binding sites which can also bind solvent molecules and the appropriate equilibrium constant, respectively.

With the help of eq. 5 and 6, it is possible to check the correctness of the values calculated for K by means of eq. 1. Furthermore, one may also calculate the number of sites in hair which bind water only.

Using the experimental values of r and f and calculated values of K , the values of α were calculated and plotted against the quantity $1 - 55.51K/(1 + fK)$ (Fig. 6). Straight lines passing through the origin were obtained in all cases. It is obvious therefore that the water- and phenol-binding sites in hair are the same (since λ_i is always positive and $\Sigma \lambda_i = 0$), and no exclusively water-binding sites exist. The values of the slopes give the number of sites available for the binding of phenolic compounds. In case of the resorcinol-virgin hair system, the value $n = 1.7 \times 10^{-3}$ mole/g. of hair was obtained; in all other cases (*i.e.*, catechol or pyrogallol on virgin hair, catechol or resorcinol on acid-treated hair), the value $n = 4.8 \times 10^{-3}$ mole/g. of hair resulted.

These figures are in very good agreement with those obtained by extrapolation from eq. 1. It also follows

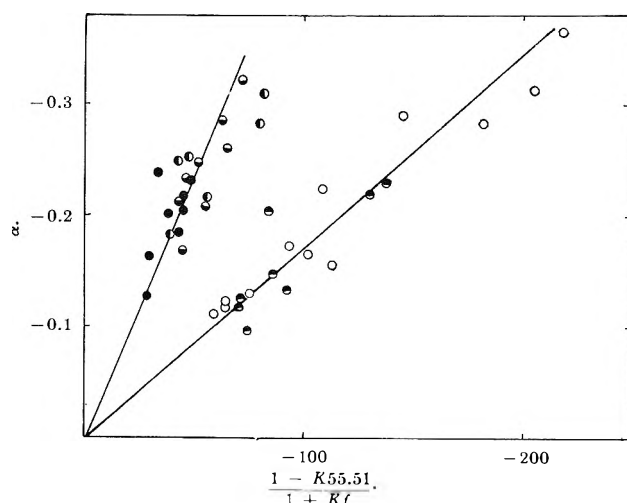


Figure 6a. Plot of binding data according to the Schumaker-Cox equation—phenols on virgin hair: ○, 1.75°, resorcinol; ●, 26°, resorcinol; ●, 2°, catechol; ○, 20°, catechol; ●, 2°, pyrogallol.

(8) V. N. Schumaker and D. T. Cox, *J. Am. Chem. Soc.*, **83**, 2445 (1961).

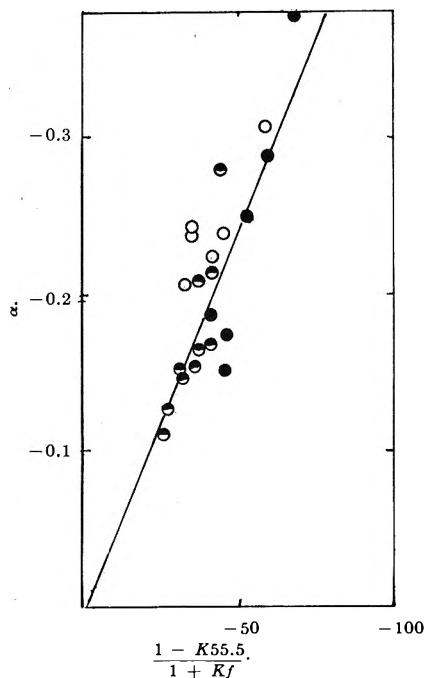


Figure 6b. Plot of binding data according to the Schumaker-Cox equation—phenols on acid-treated hair: ●, 2°, catechol; ◐, 2°, resorcinol; ○, 26°, resorcinol.

from the above data that the values calculated for K by means of eq. 1 are correct.

The enthalpy and entropy changes ΔH and ΔS of the various phenol bindings and next-neighbor interactions were calculated from isotherms obtained at different temperatures (column 5 and 6, Table I and II) using the well-known thermodynamic relations

$$\Delta F = RT \ln K \quad (7)$$

$$\Delta F = \Delta H - T\Delta S \quad (8)$$

The heats and entropies of adsorption are positive in all cases and are of very similar magnitudes, except for the binding of phenol itself, which exhibits significantly higher ΔH and ΔS values.⁹

The binding of phenols on hair did not induce any changes in the pH of solutions in equilibrium. The initial pH of the solutions, if not otherwise stated, was adjusted to a value between 5.50 and 5.80 and remained unchanged (within ± 0.1 pH unit) during the entire duration of the experiment. It can be concluded therefore that no change in the state of ionization of the protein occurs.

The adsorption of resorcinol was also measured from solutions containing increasing concentrations of HCl (Fig. 7). No change in the shape of the isotherm occurred until a critical pH value (pH ~ 2.4) was reached; at pH lower than 2.4, n was found to have

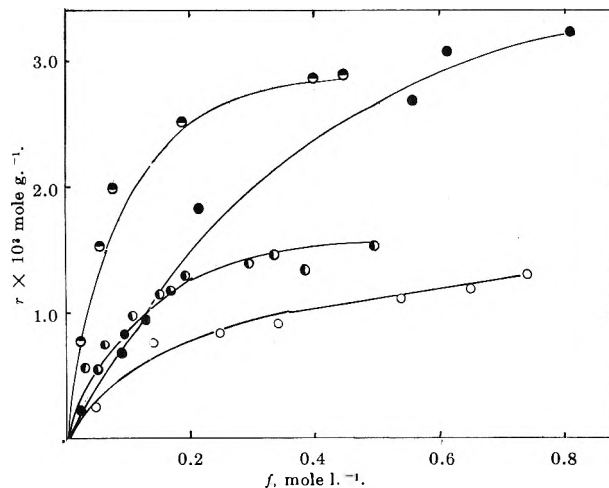


Figure 7. Resorcinol binding isotherms at different pH values: ●, pH 1.0; ◐, pH 2.3–2.7; ○, pH 2.7–2.9; ●, pH 3.2–4.0.

twice the normal value. These results suggest that at or below this critical pH, irreversible structural changes occur in the hair. The irreversibility of the change of resorcinol binding capacity has been further demonstrated by measuring resorcinol and catechol binding on acid-treated hair. In these experiments the hair was soaked in 0.1 N HCl for 12 hr. and subsequently washed free of HCl with distilled water until no positive reaction for Cl^- was observed. The isoelectric point for the acid-treated hair was found to be 3.80 in contrast to the value of 5.60–5.80 for the untreated hair. The value of n for resorcinol in the acid-treated hair increased to 4.5×10^{-3} mole/g. in line with the n values observed with other phenols. The ΔH and ΔS values for resorcinol adsorption on acid-pretreated hair were entirely different from those obtained with untreated hair. It is especially interesting to note the reversal of signs of both the enthalpy and entropy of resorcinol binding. No significant changes in the values of ΔH and ΔS were observed in the case of catechol.

The effect of acid treatment on hair was further investigated. The amount of HCl absorbed by hair was determined as a function of the pH of the solution in the absence of neutral salts (Fig. 8, curve A). The maximum acid binding capacity was found to be 8.2×10^{-4} equivalent/g. of hair, in good agreement with the

(9) The ΔH and ΔS values stated in Tables I and II might be in error up to about 20%. This, however, does not alter the main conclusions which can be drawn from an inspection of these thermodynamic quantities: (a) the entropies and the enthalpies of binding are positive; (b) the values of ΔH and ΔS for phenol are higher than for the other phenols investigated; and (c) acid treatment of hair causes a reversal of signs in the values of both ΔH and ΔS in the case of resorcinol, but does not influence the thermodynamic quantities of other phenol-binding processes.

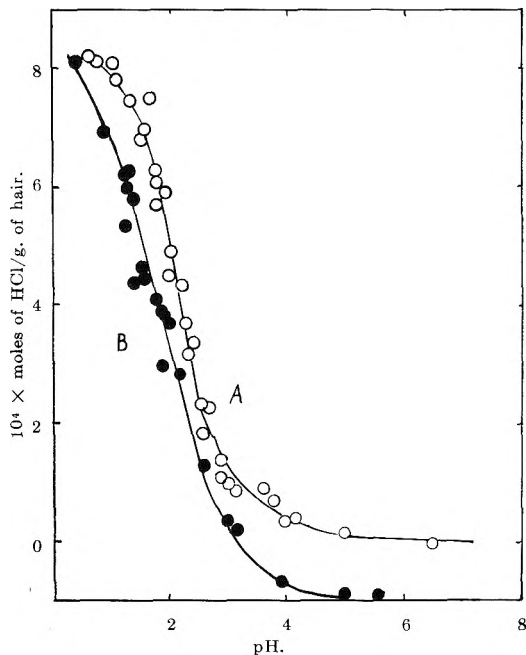


Figure 8. HCl titration curve of virgin and acid-treated hair: O, virgin hair; ●, acid-treated hair.

values found for wool. When, however, the back titration was carried out from low toward high pH values, a different curve was obtained (Fig. 8, curve B). Any subsequent titrations with the same hair specimen followed curve B whether carried out from high to low or low to high pH values; curve B was also obtained when the HCl adsorption of acid-treated hair was measured. The difference between curves A and B is due to the fact that curve B represents the titration curve of an increased number of carboxylic groups (*i.e.*, 9.5×10^{-4} mole/g. of hair as against 8.2×10^{-4} mole/g. of hair titrated on curve A). Exposure to low pH (less than 2.0) causes, therefore, the appearance of 1.30×10^{-4} mole/g. of hair of new acidic groups.¹⁰

The water binding capacities of both native and acid-treated hair were measured (Fig. 9). The acid-treated hair was found to have lower water uptake capacity (at a given humidity) than the native hair. The difference between the two curves amounted to a decrease in the water binding, 0.01 g. of water/g. of hair or 5×10^{-4} mole of water/g. of hair.

The work required to stretch a single fiber to 30% extension was also measured before and after HCl treatment (*i.e.*, soaking in 0.1 N HCl and subsequent washing out of the acid). It was found that on the average, a decrease of 4.2% in the required stretching work results from the acid treatment. A subsequent second acid treatment, however, restores the stretching work required to a value only 2% less than that of the

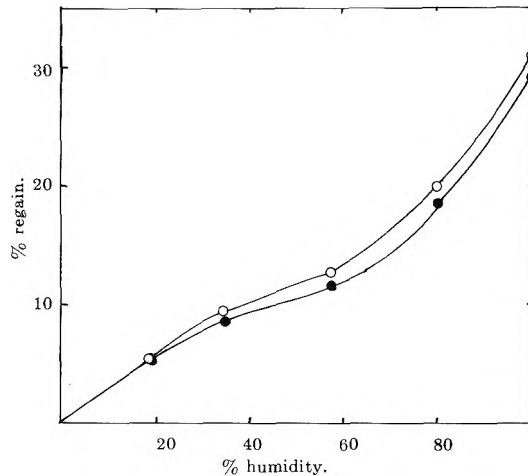


Figure 9. Water adsorption isotherms of virgin and acid-treated hair at 25°: O, virgin hair; ●, acid-treated hair.

original stretching work. The same recovery of tensile strength was also observed without HCl treatment, but only after a sufficient lapse of time (48 hr.).

Untreated and acid-treated hair did not exhibit any differences in their X-ray diffraction patterns.

Discussion

The number of the sites capable of binding phenolic compounds far exceeds the number of ionizing groups in hair (about 0.8×10^{-3} mole/g. of each of acidic and basic groups). It seems, therefore, that groups other than the carboxylic and basic groups are responsible for the binding of the phenolic compounds. Zahn² suggested the possibility that the peptide linkages may act as sites for phenol adsorption. The total number of peptide groupings in hair is about 8.60×10^{-3} mole/g. of hair.¹¹ The fraction of peptide linkages which stay hydrogen bonded, even when brought into contact with water, has been determined in wool by

(10) In order to account for the appearance of new acid-binding groups, the following three alternative explanations can be suggested: (a) some amide groups are present in virgin hair, which are hydrolyzed to carboxylic groups; (b) some of the carboxylic groups in virgin hair are in the form of Ca or Mg salts and get freed after exposure to low pH values; or (c) in virgin hair some of the acid groups are buried in hydrophobic regions of the protein and only become unmasked when the polypeptide chains unfold under the influence of an exposure to low pH medium. The third possibility seems the most plausible in view of the following considerations. The number of new acid-binding groups is the same after a relatively short exposure to acid (15 min.) as after a long acid treatment (24 hr.). This result implies that the amide groups in hair are completely hydrolyzed at room temperature within 15 min., a result which does not seem likely. Finally, together with the appearance of new acidic groups, other properties of hair (*e.g.*, resorcinol binding capacity, volume changes accompanying the adsorption of various phenols—see part III) also undergo changes, implying that some deeper structural changes also accompany the appearance of the new acidic groups.

(11) P. Alexander and R. F. Hudson, "Wool," Chapman and Hall Ltd., London, 1954.

Burley, Nicholls, and Speakman¹² from measurements of the rates of hydrogen exchange reactions and was found to be 14% of the total amount, *i.e.*, about 7.40×10^{-3} mole/g. of bonds are readily accessible. Additional support for the number of accessible peptide bonds is found from the analysis of water adsorption curves of hair. The number of fixed water binding sites in hair can be calculated from Chamberlain and Speakman's¹³ data, using Hill's equation,¹¹ giving the value 6.12×10^{-3} mole/g.⁻¹ sites. The corresponding figure for wool is 6.80×10^{-3} mole/g.⁻¹. The difference is in accordance with the view that hair has higher degree of order than wool.¹¹

The relatively close correspondence between the numbers of water- and phenol-binding sites (6×10^{-3} mole/g. and about $4.5\text{--}5.0 \times 10^{-3}$ mole/g., respectively, Table I) suggests that they are identical and are presumably the peptide groups. The observation that these numbers are slightly less than the total available peptide sites suggests that not all the latter are equally accessible to water and to the phenolic compounds. The difference can be easily explained on the assumption that some of the peptide linkages will be hindered by bulky side groups and will not be readily accessible to the larger aromatic molecules.

The fact that the resorcinol- and water-binding sites seem to be identical (since water could not be displaced from other types of site by the resorcinol—a conclusion which follows from Fig. 6) strongly implies that resorcinol is attached by two of its phenolic hydroxyls to the polypeptide chain.

It is postulated, therefore, that the two meta-hydroxyls of resorcinol form H bonds with two consecutive peptide groups of polypeptide chains. It can be demonstrated on molecular models that this type of binding is easily feasible for resorcinol; the angles of both bonds are about $110\text{--}120^\circ$, in agreement with the values found for similar bonds in other systems.¹⁴ Compounds containing two phenolic hydroxyl groups in the *ortho* or *para* positions, on the other hand, can be fitted to two consecutive peptide groups of the polypeptide chains with two H bonds only if a smaller value is assumed for the $\text{C}=\text{O} \cdots \text{H}-$ bond angle.

Examination of the values of enthalpies and entropies (Table I) reveals the fact that the positive entropy changes are the driving forces in the binding of phenols to hair; the enthalpies of binding are unfavorable. The source of the positive entropy changes must be sought in the release of hydration water possibly from both the polypeptide chain of hair and from the phenolic molecules.

The adsorption of the subsequent molecules of phenol and hydroquinone are facilitated by a next-neighbor

interaction process. The thermodynamic quantities of these interactions show that different mechanisms are at work in the cases of phenol and hydroquinone. In the former case, the positive values of the interaction entropy and enthalpy (see Table II) point toward a mechanism in which the adsorption of a phenol molecule on a neighboring site to an occupied site will squeeze out the remainder of the hydration water from around the phenol group and bring about a hydrophobic-type interaction between the two benzene rings.

With hydroquinone, the negative values of interaction entropies and enthalpies point rather to an interaction where the hydration shells are not disturbed. In one of the models which can be postulated, the hydroquinone molecule can be assumed to be bound through hydrogen bonds to the peptide links while the rest of the molecule is directed from the polypeptide chain. It can further be assumed that the neighboring molecules are interacting through their *para*-substituted hydroxyl groups.

It is difficult to account for the nature of changes which occur in hair near the critical pH region, at ~ 2.4 , and which causes the changes in resorcinol adsorption characteristics. No significant differences could be seen in the X-ray diffraction patterns of the untreated and acid-pretreated hair, and therefore probably only the tertiary structure is involved. The same conclusion may be drawn from the fact that the adsorption characteristics of resorcinol are affected by the acid treatment, while those of catechol are not, since a more fundamental structural modification would be expected to affect the adsorption characteristics of all the phenols. The change in the signs of the entropy and enthalpy of adsorption of resorcinol on pretreated hair can be taken as an indication that the attachment of a resorcinol molecule induces a smaller loss of hydration water and consequently is more loosely attached to the polypeptide chain. In any case, the foregoing again demonstrates the differences which exist between resorcinol and the rest of the phenols, with regard to their adsorption on hair. Our results also confirm that the great majority of peptide bonds in hair are easily accessible, and consequently only a small fraction can be regarded as bound in an organized structure.

Finally, it has been shown in the present work

(12) R. W. Burley, C. H. Nicholls, and J. B. Speakman, *J. Textile Inst. Trans.*, **46**, 427 (1954).

(13) N. H. Chamberlain and J. B. Speakman, *Z. Elektrochem.*, **37**, 375 (1931).

(14) G. C. Pimentel and A. L. McClellan, "The Hydrogen Bond," Reinhold Publishing Corp., New York, N. Y., 1960.

that only 4.8×10^{-3} equivalent of water/g. of hair is firmly bound to hair (Fig. 6) and that this hydration water is replaced by phenolic compounds in a molar proportion of 1:1 in the case of most of the phenols, and 2:1 in the case of resorcinol,¹⁵ also that no preferential hydration on other sites occurs or, in other words, the rest of the water adsorbed by hair contains solutes (phenolic compounds) in the same proportion as in the external solution. This water can, therefore, be regarded only as included solution.

Acknowledgments. The author wishes to thank Dr. A. D. Jenkins for many valuable suggestions and discussions, Mr. G. E. Jones for his skillful technical assistance, Dr. E. Graminski for permission to refer to his results, and the Management of Gillette Industries Ltd. for permission to publish this paper.

(15) The displacement of water, in these ratios, was also demonstrated directly by Dr. E. Graminski of Harris Research Laboratories, Washington, D. C. Dr. Graminski showed that hair samples containing increasing amounts of phenols had proportionally lower water uptake at a given humidity.

The Binding of Phenols by Hair. II. Volume Changes Accompanying the Dilution of Aqueous Solutions of Phenols

by M. M. Breuer¹

Gillette Research Laboratories, Reading, Berkshire, England (Received December 3, 1963)

Volume changes occurring during the dilution of saturated water solutions of five phenols are reported. The data are interpreted in terms of a multiple association process, and values for the association constants are calculated. The results suggest that both hydrogen bonds and hydrophobic linkages are formed during the association processes.

Introduction

The need for the present investigation arose in the course of our work on the mechanism of sorption of phenolic compounds on keratin.^{2a} In order to follow the processes which occur during the sorption of phenolic molecules, the volume changes accompanying these processes which occur during the sorption of phenolic molecules were measured by means of a sensitive dilatometric technique.^{2b}

It became apparent, however, that the mere dilution of phenol solutions also causes volume changes which promised to be useful for the study of the molecular structure of aqueous phenolic solutions.

Experimental

The experimental procedures described by Kasarda and Kauzmann³ were followed with minor alterations.

a. The Dilatometers. These were designed originally by Screenivasaya and Bhagvat⁴ and subsequently modified by Linderstrom-Lang and Lanz⁵ and by Johansen and Thygesen.⁶ The dilatometers used in this work were made by Mr. E. C. Collingwood of this laboratory. They consist of an inverted Y-shaped lower part and an upper part consisting of a precision bore capillary of 0.05-cm. diameter, fused to a B14

(1) Unilever Research Laboratory, Isleworth, Middlesex, England.

(2) (a) See part I, M. M. Breuer, *J. Phys. Chem.*, **68**, 2061 (1964); (b) see part III, M. M. Breuer, *ibid.*, **68**, 2081 (1964).

(3) D. D. Kasarda, Ph.D. Thesis, Princeton University, 1961.

(4) M. Screenivasaya and K. Bhagvat, *Ergeb. Enzymforsch.*, **6**, 234 (1937).

(5) K. Linderstrom-Lang and H. Lanz, *Compt. rend. trav. lab. Carlsberg*, **21**, 315 (1938).

(6) G. Johansen and J. E. Thygesen, *ibid.*, **26**, 369 (1948).

ground glass cone at one end and to a capillary stopcock continuing in another B14 ground glass cone at the other end. By means of the latter cone, the dilatometer could be attached to a vacuum line and evacuated.

b. Constant Temperature Bath. Volume changes of the order of 10^{-4} cm.³ were expected, and in order to obtain reproducible results, a high degree of temperature control was required. The thermostat consisted of a lagged glass container (diameter 30 cm., height 41 cm.) heated by an electric blade heater regulated through a Variac, and stirred with a four-blade stirrer driven by a standard laboratory motor. The temperature was controlled by a standard toluene thermoregulator (Gallenkamp TM.550) equipped with a proportionating head (Type Tol.3C) and connected to an A.E.I. electronic relay (Type EA4T). The thermoregulator was set to 28°. Temperature fluctuations were measured by means of a toluene thermometer (a 30-cm.³ bulb fused to a 0.05-cm. capillary tubing and filled with distilled toluene). The height of the toluene column was read, with reference to a fixed mark on the capillary, by means of a cathetometer accurate to 0.002 cm. The toluene thermometer was calibrated against a Beckmann thermometer and was easily capable of detecting a temperature difference of 2.5×10^{-4} °. The temperature of the thermostat remained constant to within 0.01° during the duration of an experiment. To minimize the errors caused by temperature fluctuations, each dilatometer was calibrated against the toluene thermometer. The dilatometer was filled with 10 ml. of distilled water and petroleum ether in the usual fashion (see Dilatometric Technique) and the variations in the meniscus level were plotted against the readings of the toluene thermometer. The readings of the height of the petroleum ether column were corrected during each experiment by means of this calibration curve to a constant temperature.

c. Materials. All chemicals used were of analytical or reagent grade purity. The special hydrophilic grease, used for the lubrication of the inner part of the dilatometer joints (which are in contact with petroleum ether), was prepared according to the procedure given by Kasarda³: 3.5 g. of sodium stearate was heated with 100 ml. of glycerol until a clear solution was obtained, the solution was filtered while hot, and then cooled.

d. Dilatometric Technique. Measured volumes of reagent solution of known concentration and of water were introduced into the first and second arm of the dilatometer, respectively. The dilatometer was then filled up to about two-thirds of its volume with petroleum ether (boiling range 100–120°) and attached to a vacuum line; it was evacuated and kept under

static vacuum while tapped to facilitate the escape of trapped air bubbles. The vacuum was then broken and the procedure repeated several times until no more evolution of air bubbles could be observed from either the water or the reagent solution. After disconnecting from the vacuum line, the dilatometer was filled completely with petroleum ether and immersed in the thermostat. It was allowed to stand for 1 to 2 hr. in order to achieve thermal equilibrium. The height of the meniscus in the capillary was then adjusted by means of a capillary pipet.

The position of the meniscus, relative to a fixed mark on the capillary, was observed at frequent time intervals with a cathetometer, simultaneously taking readings of the toluene thermometer.

When the meniscus had become virtually stationary, the reagent was tipped over into the arm of the dilatometer containing the water. Good mixing was achieved by shaking the dilatometer for several minutes. The dilatometer was subsequently replaced in the thermostat and the observations of the height of meniscus were resumed. The mixing was repeated several times until no significant volume changes could be observed. Generally, two mixings sufficed and the experiment could be concluded about 5 hr. after the first mixing. A number of experiments were run over a 24-hr. period; no significant changes were observed, however, between the position of the meniscus after 5 and 24 hr.

The reagent solutions were removed after completion of the experiment and the final concentration of the reagent in the solution determined spectrophotometrically (see Experimental part of ref. 2a). Several blank experiments with both arms filled with 5 ml. of water were carried out to test the performance of the dilatometers. No volume changes were observed in these experiments.

Results and Discussion

The changes in ϕ (the apparent molal volumes), $\Delta\phi$, with concentration for the five phenols investigated, are given in Fig. 1 and 2. The values of $\Delta\phi$ were calculated from the experimental volume changes, ΔV by means of the equation

$$\phi_0 - \phi = \Delta\phi = \frac{\Delta V}{n} \quad (1)$$

where n and ϕ_0 denote the number of moles of phenolic compound present in the dilatometer and the value of ϕ at infinite dilution, respectively.

The solutions of resorcinol and hydroquinone show a steady expansion on dilution (Fig. 1), those of phenol exhibit positive volume changes with a maximum at 0.8 mole/l., while saturated solutions of catechol and

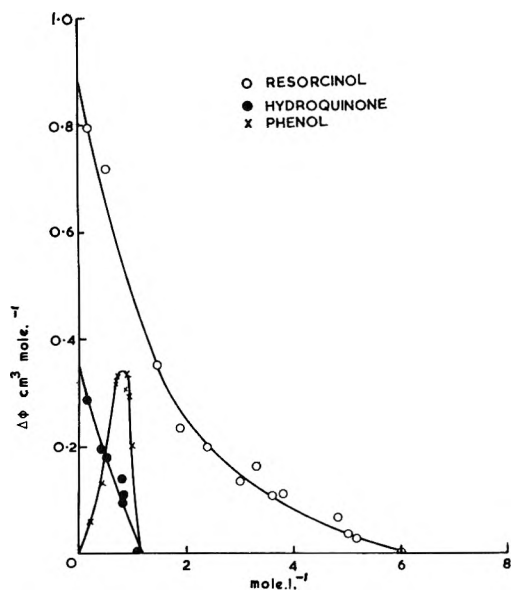


Figure 1. Changes of the apparent molal volumes of resorcinol, hydroquinone, and phenol as a function of the concentrations.

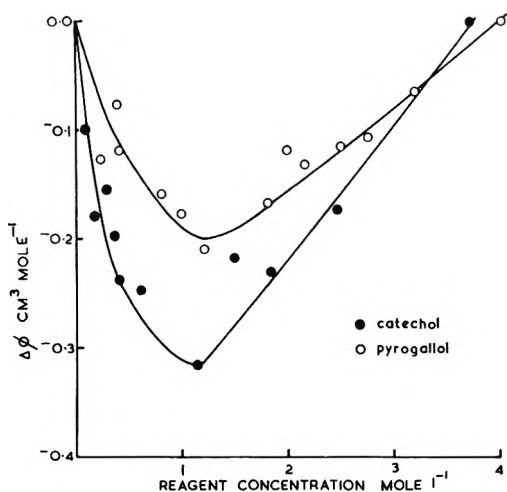


Figure 2. Changes of the apparent molal volumes of catechol and pyrogallol as a function of the concentrations.

pyrogallol contract, reaching a minimum molal volume in the vicinity of 1.20 mole/l. (Fig. 2).

A comparison between the changes in the molal volumes of phenols during dilution of their aqueous solutions and those which occur when 1 mole of phenolic compound is transferred from the liquid state into aqueous solution (the molal volume change due to solution), suggests that only minor changes occur in the hydration state of the phenol during the dilution process.

The differences between \bar{V} , the partial molal volumes in water, and V_0 , the molal volumes in the liquid state,

Table I

	V_0 , cm. ³ /mole	\bar{V} , cm. ³ /mole	$\bar{V} - V_0$, cm. ³ /mole
Phenol	87.5	75.0	-12.5
Catechol	87.5	63.0	-24.5
Resorcinol	86.2 (88.3) ^a	65.0	-21.2 (-23.3)

^a Calculated from the partial molal volume in ethyl acetate.

are of the order 12–20 cm.³/mole, *i.e.*, about 15 to 20 times larger than the maximum value of measured $\Delta\phi$ (Table I).^{7–9}

In order to explain the volume changes during dilution, a multiple association process is postulated. The available thermodynamic data can be interpreted in agreement with this model. Cavellero and Indelli¹⁰ determined the activity coefficients of hydroquinone, resorcinol, and catechol by a cryoscopic technique in aqueous solutions, in the concentration range 0 to 1 mole/l. According to Prigogine and Defay,¹¹ in a dicomponent system, where one of the components (the solute) undergoes a reversible multiple association process, the ratio β of the activity coefficients of the solute, γ_1 , and the solvent, γ_2 , is equal⁶ to the fraction of the unassociated solute molecules.^{12,13}

(7) The values of \bar{V} were calculated from Harkins and Grafton's density data⁸; V_0 at 25° was obtained by extrapolating to 25° the tabulated densities of liquid phenols,¹⁰ measured above their melting points, using the equations

$$d_{\text{phenol}} = 1.05021 - (t - 50^\circ) \times 9.39 \times 10^{-4}$$

$$d_{\text{catechol}} = 1.0680 - (t - 200^\circ) \times 10.58 \times 10^{-4}$$

$$d_{\text{resorcinol}} = 1.0800 - (t - 200^\circ) \times 9.50 \times 10^{-4}$$

(t denotes the temperature in °C.).

(8) M. D. Harkins and E. H. Grafton, *J. Am. Chem. Soc.*, **47**, 1331 (1925).

(9) J. Timmermans, "Physico Chemical Constants of Pure Organic Compounds," Elsevier Publishing Co., Inc., New York, N. Y., 1950.

(10) L. Cavellero and A. Indelli, *Gazz. chim. ital.*, **88**, 369 (1958).

(11) T. Prigogine and R. Defay, "Chemical Thermodynamics," Longmans, Green and Co., London, 1954.

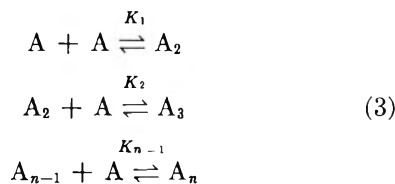
(12) This relation is, however, only valid if γ_1 and γ_2 refer to an asymmetrical system of reference, *i.e.*, when $\lim_{X_2 \rightarrow 1} \gamma_1 = 1$ and

$\lim_{X_1 \rightarrow 0} \gamma_2 = 1$, and the mixture of complexes is regarded as an

ideal solution. (X_1 and X_2 denote the mole fractions of solute and solvent, respectively.) Prigogine and Defay's treatment was derived for a two-component system, in which only one component is associated. Although water is an associated liquid, for the purpose of the present discussion, it is assumed that no significant changes occur in its degree of association during the dilution process, and therefore Prigogine and Defay's treatment is applicable. This assumption seems to be reasonable in view of the high water concentrations (20–55 moles/l.). Its validity is also supported by recent infrared measurements of aqueous solutions of electrolytes by Buijs and Choppin.¹³ These authors found that in aqueous electrolyte solutions, the degree of H bonding of water is affected mainly

$$\beta = \frac{\gamma_1}{\gamma_2} \quad (2)$$

In a stepwise multiple association of the general type



assuming that

$$K_1 = K_2 = K_{n-1} = K \quad (4)$$

the value of K is given by

$$K = \frac{1 - \sqrt{\beta}}{\beta x} \quad (5)$$

where x is the solute concentration in mole fraction units.

Using Cavellero and Indelli's data, $(1 - \sqrt{\beta})/\beta$ was calculated and plotted against x (Fig. 3). The data on both hydroquinone and resorcinol, which have identical activity coefficients at a given concentration, yielded a straight line, giving the value $K = 19 = 0.312$ (l./mole).

From the available calorimetric data on the heats of dilution of resorcinol and hydroquinone at 0° ,¹⁴ the apparent molal enthalpy of dilution of these phenols was calculated as a function of the concentrations. Using the value $K = 0.312$ (mole/l.)⁻¹, the corresponding values for β were computed and plotted against h . A straight line was obtained (Fig. 4), from the

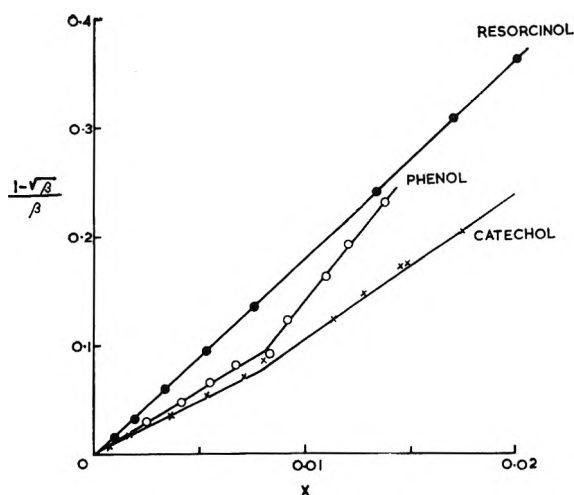


Figure 3. Plot of the quantity $(1 - \sqrt{\beta})/\beta$ against x .

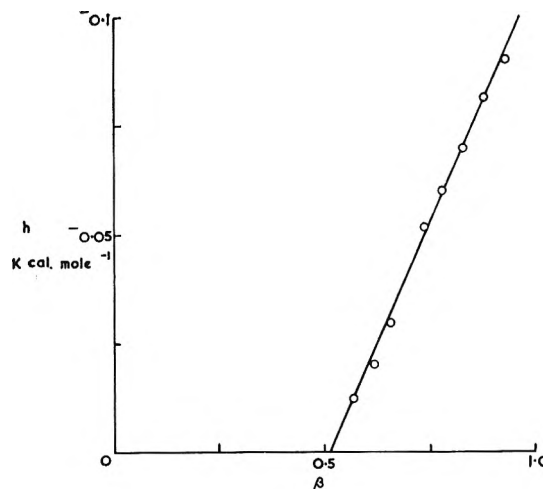


Figure 4. The apparent molal heat of dilution of resorcinol as a function of β .

slope of which the value $\Delta h = -220$ cal./mole is obtained for the heat of association between $\beta = 0$ and $\beta = 1$. Using the well-known relationship

$$\Delta S = R \ln K + \frac{\Delta h}{T} \quad (6)$$

the value $\Delta S = -3.05$ e.u./mole was obtained for the entropy of association.

The negative value of enthalpy change which accompanies the formation of an H bond (which is assumed to be the bond of association) between two phenolic hydroxyls in aqueous solutions of resorcinol is surprising in view of the available thermodynamic data which indicate a higher enthalpy of formation for a phenol-water H bond than for a phenol-phenol H bond.¹⁵ This problem has been discussed recently by Némethy, Steinberg, and Scheraga.¹⁶ These authors showed that this apparent contradiction can be explained. In liquid water, only a fraction of the

by the electrostatic potential in the vicinity of the ion. Relatively large monovalent ions (*e.g.*, potassium ion) have much smaller effect than small ions (*e.g.*, Li). The degree of association of the water, in the case of most of the electrolytes investigated, stayed practically constant in the concentration range above 1 M solution. It appears, therefore, safe to assume that in the solutions, the degree of association of the water remains unchanged, to a good approximation, with the dilution of the solutes.

(13) G. R. Choppin and K. Buijs, *J. Chem. Phys.*, **39**, 2042 (1963).

(14) "International Critical Tables," McGraw-Hill Book Co., Inc., New York, N. Y.

(15) R. M. Badger and R. C. Greenough, *J. Phys. Chem.*, **65**, 2088 (1961).

(16) G. Némethy, I. Z. Steinberg, and H. A. Scheraga, *Biopolymers*, **1**, 43 (1963).

possible hydrogen bonds is actually formed.¹⁷⁻²¹ Similarly, only a fraction of the hydroxy groups of phenols will be bonded to water in aqueous solutions, even at high dilutions. In an aqueous medium, when 1 mole of phenol-phenol H bond is formed, only $K_{sp}/(1 + K_{sp})$ mole of phenol-water bond will be broken. (The symbol K_{sp} denotes the equilibrium constant of the reaction $\text{water} + \text{phenol-hydroxyl} \rightleftharpoons \text{water-phenol complex}$.) The value of ΔH , the net enthalpy change accompanying the formation of phenol-phenol hydrogen bond in an aqueous medium is therefore given by

$$\Delta H = \Delta H_{pp} - \frac{K_{sp}}{1 + K_{sp}} \Delta H_{sp} \quad (7)$$

where ΔH_{pp} and ΔH_{sp} denote the enthalpy changes of the phenol-phenol H-bond formation and the phenol-water H-bond formation, respectively.

In a similar manner, the experimental $\Delta\phi$ -values can be correlated with the calculated β -values. Resorcinol and hydroquinone give straight lines when $\Delta\phi$ is plotted against β (Fig. 7); furthermore, both sets of experimental data can be represented on a single curve, provided the value of $\Delta\phi$ for the saturated hydroquinone solution is set equal to the $\Delta\phi$ -value obtained for resorcinol solution of the same concentration. It appears from Fig. 5 that the formation of an H bond in an aqueous medium is accompanied by a contraction of the apparent molal volume by 1.05 cm.³/mole.

The various available data on aqueous catechol solutions can be treated in an entirely similar way. Again using Cavellero and Indelli's data,¹⁰ $(1 - \sqrt{\beta})/\beta$ was calculated and plotted against x (Fig. 3). A broken straight line was obtained, yielding, from the slopes of the two sections, the association constants $K_1 = 9 = 0.15$ (mole/l.)⁻¹ (for the low concentration range) and $K_2 = 12 = 0.212$ (mole/l.)⁻¹ for the higher concentration range. The respective heats and entropies of association, calculated from the values of K_1 and K_2 and the heats of dilution (Fig. 6) in an analogous way as described before, are +650 cal./mole, +1600 cal./mole, +1.53 e.u./mole, and +4.65 e.u./mole.

The change in the values of the association constants, enthalpies and entropies in the concentration range at about $x = 0.008$ (at 0°) can be attributed to a difference in the mechanism between dimer and the trimer (or polymer) formation. The ratio of concentrations of dimers $[A_2]$ and trimers $[A_3]$ in a multiple equilibrium is given by¹¹

$$\frac{[A_3]}{[A_2]} = [A_1]K = \beta K \quad (8)$$

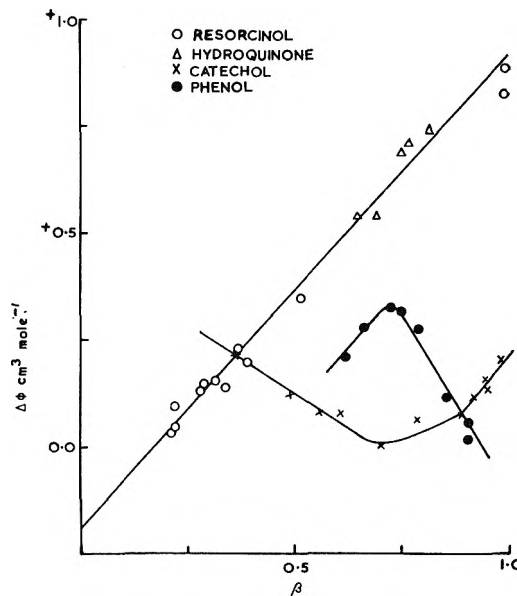


Figure 5. Plot of $\Delta\phi$ as a function of β .

Substituting $x = 0.008$, $K = 12$, $\beta = 0.86$ into eq. 8 yields

$$\frac{[A_3]}{[A_2]} = 0.082 \quad (9)$$

indicating that a considerable formation of trimers occur in this region.

An inspection of molecular models (Fig. 7) of dimers and trimers of resorcinol, hydroquinone, and catechol reveals that in a trimer or catechol, unlike in those of the two other phenols, the benzene rings of the molecules 1 and 3 can come into close proximity and thus participate in a hydrophobic bond. This additional interaction probably accounts for the higher value of the association constant K_2 .

(17) Conflicting views can be found in the literature regarding the degree of hydrogen bonding in water. Némethy and Scheraga¹⁸ estimate the fraction of free hydroxyls, on the basis of statistical-mechanical calculations, as high as 50%. This figure is supported by the conclusion reached by Buijs and Choppin¹⁹ from infrared measurements. On the other hand, Pauling's estimate²⁰ for the fraction of free hydroxyls in water from the specific heat of water is only 15%. A similar value has also been derived by Luck²¹ on the basis of infrared measurements. For the discussion in the present paper, however, the absolute value of unassociated hydroxyl groups is of secondary importance only. The validity of the argument that even in relatively concentrated aqueous solutions of phenols only a fraction of the phenolic hydroxyls (presumably 50-80%) will be hydrogen bonded to water seems to be established.

(18) G. Némethy and H. A. Scheraga, *J. Chem. Phys.*, **36**, 3382 (1962).

(19) K. Buijs and G. R. Choppin, *ibid.*, **39**, 2035 (1963).

(20) L. Pauling, "The Nature of the Chemical Bond," Cornell University Press, Ithaca, N. Y., 1960.

(21) W. Luck, *Ber. deut. Bunsenges.*, **67**, 186 (1963).

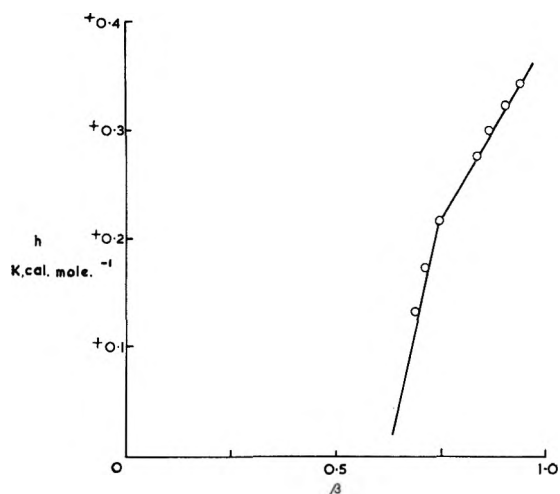
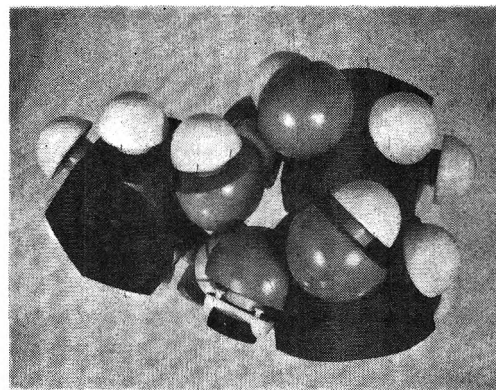


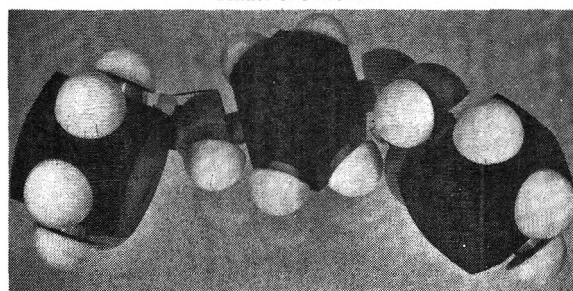
Figure 6. The apparent molal heat of dilution of catechol as a function of β .

According to Némethy and Scheraga's theory of aqueous hydrocarbon solutions,²² the hydrophobic solute increases the "ice-likeness" of water, *i.e.*, increases the H-bonded fraction of water molecules. A hydrophobic interaction between hydrocarbon groups, on the other hand, reduces the surface of water-hydrocarbon contact, and causes positive enthalpy and entropy changes. Némethy and Scheraga estimated the respective enthalpy and entropy changes involved in the formation of a hydrophobic bond between two phenyl radicals,²² to be in the range +0.3 to +0.8 kcal./mole and +1.6 to +7.5 e.u./mole, depending on the strength of the bond. The differences between the heats and entropies of dimerization and trimerization of catechol (+950 cal./mole and +3.12 e.u./mole) are in good agreement with these estimates.

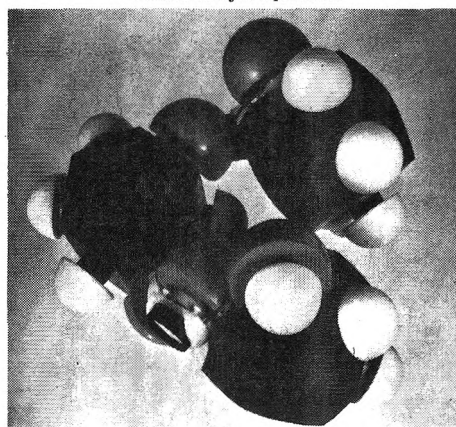
The dilatometric results, obtained with catechol solutions, also support the above picture. Using the respective values of K_1 and K_2 for the appropriate concentration ranges, the curve $\Delta\phi$ vs. β was constructed (Fig. 5). Two intersecting lines with slopes of opposite signs were obtained. In the low concentration region (presumably dimerization) $d\Delta\phi/d\beta = -1.05$ cm.³/mole, identical with the value obtained for resorcinol and hydroquinone. The dimerization of catechol seems thus to follow identical mechanism to that of the other two difunctional phenols. In the higher concentrations region, however, the volume change becomes positive, giving $d\Delta\phi/d\beta = +0.65$ cm.³/mole. Assuming that the trimer (or higher polymer) formation occurs through the simultaneous formations of a hydrophobic and an H bond, the volume change due to the hydrophobic bond is +1.70 cm.³/mole.



Trimer of catechol.



Trimer of hydroquinone.



Trimer of resorcinol.

Figure 7. Molecular models of trimers of catechol, hydroquinone, and resorcinol.

According to Némethy and Scheraga,²² a volume change of this order is expected when 2.5 moles of water are removed from contact with a hydrophobic side chain, and agrees well with an entropy change of 3.12 e.u./mole.

Pyrogallol shows similar $\Delta\phi$ vs. concentration curve to that of catechol (Fig. 2). No thermodynamic data were available, however, and therefore the quantitative treatment of the data was not attempted.

The dilution data on phenol can be also treated in

(22) G. Némethy and H. A. Scheraga, *J. Phys. Chem.*, **66**, 1773 (1962).

an entirely similar way as those of catechol. Jones and Bury²³ reported freezing point measurements obtained on aqueous phenol solutions. These cryoscopic data yielded a broken line on the $(1 - \sqrt{\beta})/\beta$ vs. x plot. (Fig. 3). The association constants calculated from the slopes were $K_1 = 9.30$ and $K_2 = 21.6$, respectively. The $\Delta\phi$ vs. β curve also gave a broken line with slopes $+1.67$ cm.³/mole for the high dilution region and -1.10 cm.³/mole for the low dilution region (Fig. 5). These results suggest that in the case of phenol, the initial association steps (*i.e.*, the dissociation) occur through a hydrophobic bond formation. The value for the molal volume change $+1.67$ cm.³/mole compares well with the 1.70 cm.³/mole calculated for the hydrophobic bond in the case of catechol. Badger and Greenough¹⁵ found evidence from infrared measurement for the existence of a phenol dimer in which the two phenyl rings overlap and consequently interact. The hydroxyl groups are bridged with one water molecule through two hydrogen bonds. The formation of this type of dimer seems to be in agreement with dilatometric measurements, since no direct phenol-phenol hydrogen bond is present and thus the observed volume change is due entirely to the hydrophobic bond formation. Apparently, the formation of higher-mers occurs through phenol-phenol H bonds and this must be responsible for the -1.10 cm.³/mole slope, observed in the higher concentration region.

Support for these processes can also be found from the surface tension measurements of phenol solutions. Campbell and Campbell²⁴ found that the surface tension of aqueous phenol solutions drops strongly up to about 6% (~ 0.70 mole/l.) and does not change afterward with concentration. It seems that the

monomeric phenol shows a high surface activity or hydrophobicity, but on dimerization, its tendency to further hydrophobic interaction is reduced.

The observed decrease in the molar volume of resorcinol by 1.05 cm.³/mole, as a consequence of its association with another resorcinol molecule, through hydrogen bond formation, can be correlated with the calorimetrically determined heat of dilution data.¹⁴ The energy required to diminish the bond length of an H bond can be estimated from the compressibility of ice²⁰ and is given by the equation

$$\Delta E = 12\Delta D^2 \quad (10)$$

where ΔE and ΔD denote the increase in the bond energy in kcal./mole units and the decrease of the bond length in Å. units, respectively. Assuming that 1.20 Å., the diameter of an O atom, also represents the diameter of an H bond, the volume change of -1.05 cm.³/mole (-1.68 Å.³/bond) corresponds to $\Delta D = 0.145$ Å., giving the increase in the bond energy (from eq. 10) as -0.248 kcal./mole, in good agreement with the value of -0.220 kcal./mole, computed from the calorimetric data.

In conclusion, it can be said that dilatometric measurements, especially if used in connection with thermodynamic data, can yield valuable information on the structure of aqueous solutions of nonelectrolytes.

Acknowledgment. The author wishes to thank Mr. R. Lee for his skillful technical assistance and the Management of Gillette Industries Ltd. for permission to publish this paper.

(23) E. R. Jones and C. R. Bury, *Phil. Mag.*, **4**, 1125 (1927).

(24) A. N. Campbell and J. R. Campbell, *J. Am. Chem. Soc.*, **59**, 2481 (1937).

The Binding of Phenols by Hair. III. Volume Changes

Accompanying Binding of Phenols by Hair

by M. M. Breuer¹

Gillette Research Laboratories, Reading, Berkshire, England (Received December 3, 1963)

The volume changes occurring during the binding of four phenolic compounds to "De Meo" hair have been measured. The results suggest that the binding of the phenols disorganizes the hydration layer of the hair. The nature of the binding forces between hair and the phenolic compounds is also discussed.

Introduction

The binding of phenols to hair is accompanied by a simultaneous release of hydration water and by positive enthalpy and entropy changes.² These results indicate that the entropy increase, which occurs as a consequence of changes in the hydration layers of the keratin, and of the phenols, is the driving force in these sorption processes. The measurement of the volume changes accompanying these interactions promises to be a useful method for studying the hydration changes.³

Experimental

The purification of De Meo hair, the preparation of acid-treated hair, and the experimental procedures have been described previously.^{2,4}

Results

The volume changes accompanying the binding processes, ΔV_s were calculated from ΔV_T , the total measured volume change, and from ΔV_D , the known value of the volume change which occurs during the dilution of the aqueous reagent solution.

$$\Delta V_s = \Delta V_T - \Delta V_D \quad (1)$$

The values of ΔV_s are plotted as a function of f , the concentration of the phenolic compound in equilibrium, in Fig. 1-4. The latter quantity was determined spectrophotometrically from solution samples which were withdrawn from the dilatometers after completion of the experiments.²

In the case of phenol both the data obtained with virgin and acid-treated hair can be represented on a single curve, having a broad plateau as a maximum and dropping suddenly to negative values (Fig. 1).

The behavior of resorcinol is exceptional, insofar as it is the only phenol studied which causes volume contraction when adsorbed by hair. The binding curves for virgin and acid-treated hair are similar in shape (Fig. 2), but the sorption processes on acid-treated hair are accompanied by larger volume contractions.

The results obtained with catechol and pyrogallol are qualitatively very similar (Fig. 3 and 4); in both cases the sorption processes are accompanied by volume expansions. In the case of acid-treated hair ΔV_s increases smoothly with f , but for virgin hair the curves exhibit maxima and minima.

The volume changes accompanying the binding of the various phenols can also be represented as a function of r , the amount of phenol bound to hair in moles/g. The values of r were computed from the appropriate binding constants.² The apparent molal volumes of the various phenols, ϕ , are functions of their concentrations. In order to obtain a more uniform picture of the volume changes which occur during the sorption of the various phenols, it appears more useful to compute the value of $\Delta V_s'$, the volume change which occurs when phenols in a standard hydration state, chosen arbitrarily as the hydration state at infinite dilution, are transferred from solutions into hair. The value of $\Delta V_s'$ was calculated from the known dependence⁴ of ϕ on f by means of the equation

- (1) Unilever Research Laboratory, Isleworth, Middlesex, England.
- (2) See part I, M. M. Beuer, *J. Phys. Chem.*, **68**, 2067 (1964).
- (3) J. Rasper and M. Kauzmann, *J. Am. Chem. Soc.*, **84**, 1771 (1962).
- (4) See part II, M. M. Breuer, *J. Phys. Chem.*, **68**, 2074 (1964).

$$\Delta V_s' = \Delta V_s - (\phi_i - \phi)r \quad (2)$$

where ϕ_i denotes the apparent molal volume of the phenol in question at infinite dilution.

In Fig. 5, 6, 7, and 8 the values $\Delta V_s'$ are represented as a function of r for phenol, resorcinol, catechol, and pyrogallol, respectively. It is evident from Fig. 5-8 that virgin hair and acid-treated hair differ in their behavior; whereas in the case of the former, plots of $\Delta V_s'$ vs. r exhibit maxima which are followed, at critical values of r , by an abrupt fall to a minimum (volume contraction), the $\Delta V_s'$ against r plots for the latter are generally smooth curves composed of two fairly linear sections with moderately different slopes. Phe-

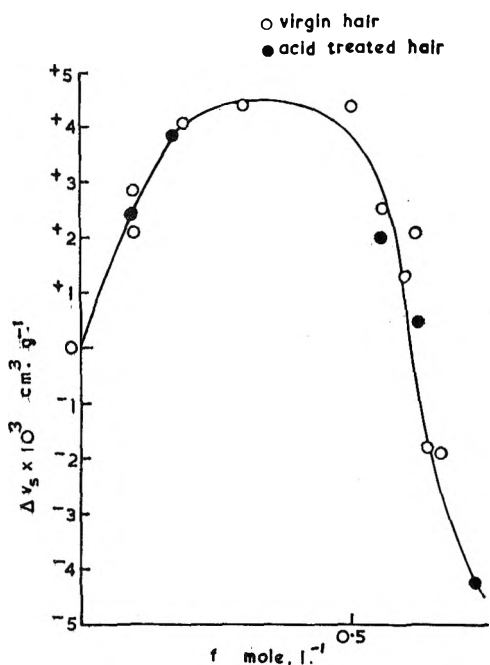


Figure 1. The volume change accompanying binding of phenol as a function of the concentration.

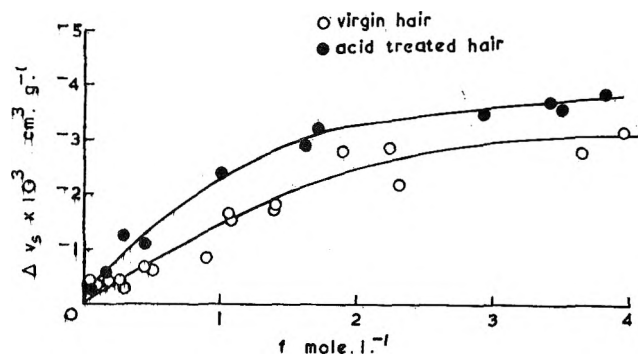


Figure 2. The volume changes accompanying the binding of resorcinol as a function of the concentration.

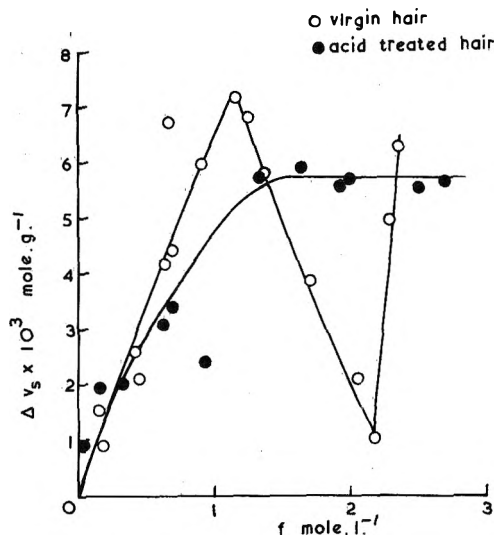


Figure 3. The volume changes accompanying the binding of catechol as a function of the concentration.

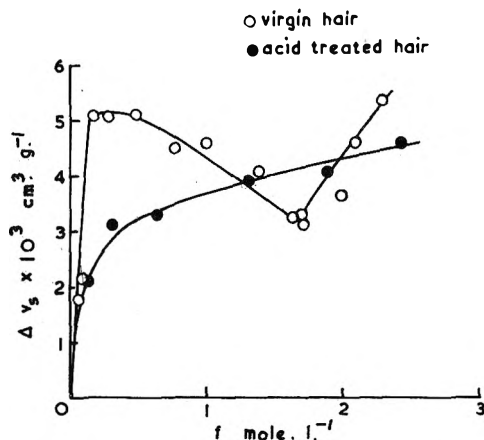
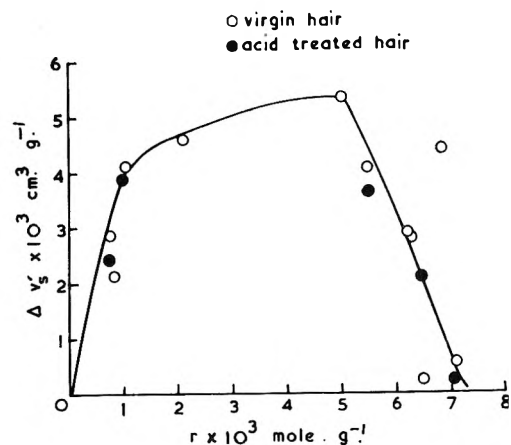
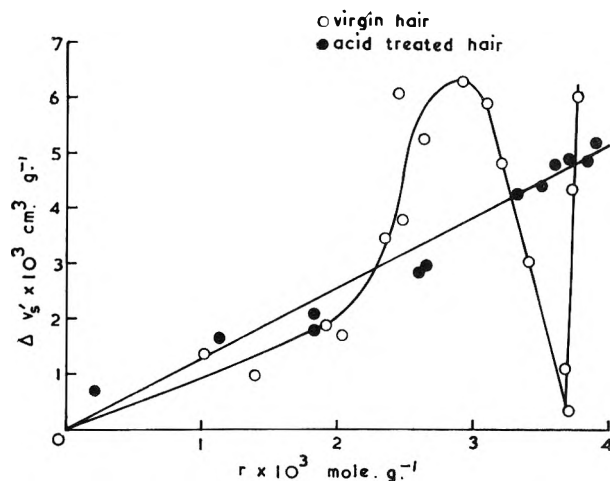
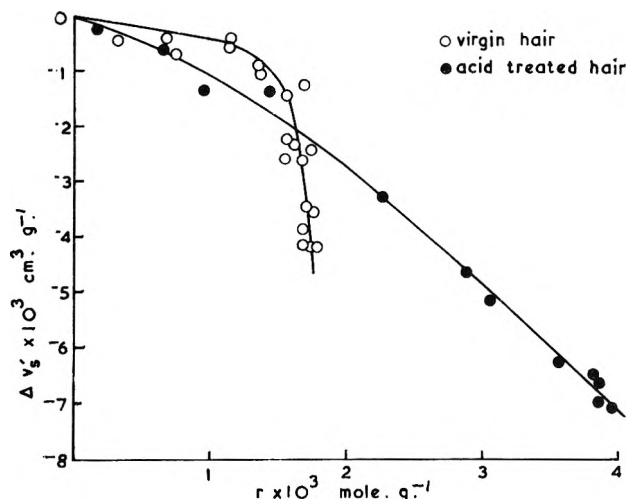
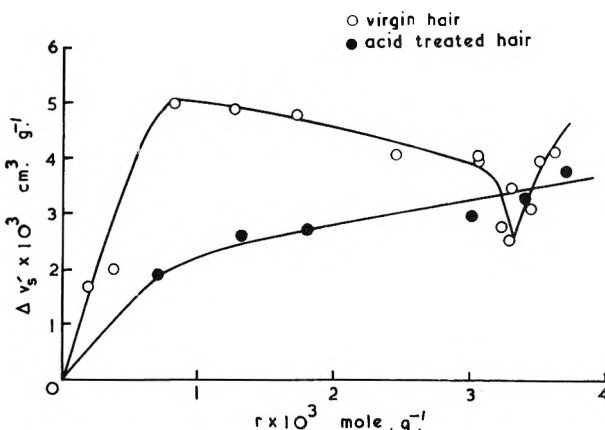


Figure 4. The volume changes accompanying the binding of pyrogallol as a function of the concentration.

nol seems to exhibit an exceptional behavior, as it gives identical curves for virgin and acid-treated hair.

Discussion

The quantity $\Delta V_s'$ can be regarded as being composed of two terms: (a) the change occurring in the apparent molal volume of the phenol as a consequence of its transfer from the aqueous solution into its new environment and its attachment to the hair, and (b) the volume change reflecting on the structural changes which occur in keratin as a consequence of the phenol-keratin interaction (e.g., changes in tertiary structure, hydration layer, etc.). For a given compound, it can be assumed *a priori*, that the magnitude of $\Delta V_s'$ will be the same, irrespective of the value of r (assuming


 Figure 5. Plot of $\Delta V_s'$ against r for phenol.

 Figure 7. Plot of $\Delta V_s'$ against r for catechol.

 Figure 6. Plot of $\Delta V_s'$ against r for resorcinol.

 Figure 8. Plot of $\Delta V_s'$ against r for pyrogallol.

that no phenol-phenol interaction is present between the bound molecules). This seems to be a reasonable assumption in view of Langmuir characteristic of the absorption isotherm.² The causes for the deviation from linearity of the $\Delta V_s'$ vs. r curves can be attributed therefore to changes which occur in the hair and its hydration structure.

One of the most striking differences between virgin and acid-treated hair is the sudden volume contraction which occurs in virgin hair after a certain amount of resorcinol, catechol, or pyrogallol is adsorbed. The most plausible explanation for this volume contraction in virgin hair is the occurrence of a disorganization process in certain parts of the hair structure, involving an exposure to water of hitherto buried polypeptide side chains. The exposure of both polar and nonpolar side chains to contact with water involves volume contraction as a consequence either of electrostriction

(polar group-water interactions) or an increase of the ice-like structure of water (nonpolar group-water interaction). On the basis of the available data, however, no distinction can be made between these two alternatives. The absence of similar volume contraction phenomena with acid-treated hair indicates that these denaturation processes also occur during the soaking of hair in 0.1 N HCl. Further support for this view comes from results which show that acid-treated hair has a higher acid binding capacity (about 11% more) and lower water retention (at given humidity) than virgin hair.²

Also, the fact that larger positive volume changes accompany the binding of pyrogallol and, to a lesser extent, that of catechol to virgin hair than to acid-treated hair, is very interesting. This different binding behavior suggests that virgin and acid-treated hair differ in their surface structure (hydration structure)

rather than in their inner structure. Both the X-ray diffraction patterns and the mechanical properties of virgin and acid-treated hair are practically identical. (The 30% index, *i.e.*, the work needed to stretch a hair fiber to 30% of its original length, is only 2% less for acid-treated hair than for virgin hair.²)

On the basis of the above dilatometric results, it seems as if virgin hair possesses a different hydration layer (different in structure and possibly in extent) from that of acid-treated hair. Adsorption of phenols brings about a collapse of this "extra" hydration layer to varying extents, depending on the nature of the phenol in question.

It is also interesting to note in this connection that acid-treated hair has a lower water uptake, at a given humidity, than virgin hair by about 4×10^{-4} mole/g. of hair.² These findings seem to support Klotz's hypothesis⁵ at least to a limited extent, which states that proteins in their native state are surrounded by organized water layers (icebergs), which may collapse during reactions with other compounds.

The $\Delta V_s'$ vs. r plots, especially in the case of acid-treated hair, also provide some qualitative information concerning the nature of the binding forces between the phenolic compounds and hair. Thus, after the initial adsorption of 1.4×10^{-3} mole/g. of resorcinol, the binding of any additional resorcinol is accompanied by 2 cm.³/mole volume contraction. This negative volume change, and the fact that both the enthalpy and the entropy of resorcinol-keratin interaction are negative quantities,² strongly suggest an H-bond formation between resorcinol and keratin. On the other hand, the positive slopes observed with catechol and pyrogallol on the $\Delta V_s'$ against r plots indicate that, although H-bond formation may exist, hydrophobic

interactions are more important.⁶ These results are in good qualitative agreement with the solution properties of these three phenols.⁴ The more positive initial slopes observed in the case of all the above-mentioned three phenols with acid-treated hair (Fig. 6, 8) might be due to the existence of "icebergs" or more limited extents.

Finally, the results with phenol indicate that in this case an entirely different adsorption mechanism is at work. The close resemblance between the $\Delta V_s'$ vs. r curve and the curve representing the change of apparent molal volume of phenol as a function of concentration in aqueous solution,⁴ suggest that phenol-phenol interactions play an important role during the sorption process. Both the dilatometric results and the absorption isotherms (indicating strong next-neighbor interactions)² point toward a mechanism in which only few phenol molecules bind directly to the polypeptide chains. These molecules seem to act as nuclei for a crystallization or condensation process for other phenol molecules, forming phenol crystallites or droplets in the pores of the hair. This hypothesis is also supported by the fact that hair adsorbs much larger quantities of phenol, given the same reagent concentration, than any of the other phenolic compounds studied.²

Acknowledgment. The author wishes to thank Mr. R. Lee for his skillful technical assistance and the Management of Gillette Industries Ltd. for permission to publish this paper.

(5) I. M. Klotz, *Science*, **128**, 815 (1958).

(6) G. Némethy and H. A. Scheraga, *J. Chem. Phys.*, **36**, 3701 (1962); *J. Phys. Chem.*, **66**, 1773 (1962).

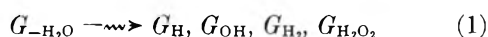
Radiation Chemistry of Oxalate Solutions in the Presence of Oxygen over a Wide Range of Acidities

by Z. D. Draganić, I. G. Draganić, and M. M. Kosanic

Institute of Nuclear Sciences "Boris Kidrič," Vintcha, Yugoslavia (Received December 27, 1963)

The radiation yields of carbon dioxide, molecular hydrogen, and hydrogen peroxide formed were measured at 50 mM oxalic acid and 0.75 mM oxygen concentrations, over the pH range from 1.61 to 9.85. The results obtained are quantitatively consistent with a simple scheme which allows the determination of the primary free radical and molecular yields in the pH region studied. A cube root dependence of the measured molecular hydrogen yields on oxalic acid concentration has been observed.

It is often assumed that the radical and molecular products of the γ -radiolysis of water, which are available to react with solutes 10^{-8} sec. after the passage of ionizing radiation, can be represented by the following relation



where G denotes the corresponding radiation chemical yield. The true identity and structure of short-lived species, formed in the initial processes of the radiation decomposition of water and denoted as H atoms and OH radicals, are still a matter of discussion. Recent experiments on reducing species in water give an experimental evidence for the existence of hydrated electrons,^{1,2} while the existence of hydrogen atoms has been proved kinetically on many other occasions.³ The nature of the oxidizing OH radical, especially in alkaline solutions, seems less certain. Therefore, G_H and G_{OH} in relation 1 represent the yields of H and OH species of their chemical equivalents.

The yields in relation 1, which are also called the primary radical and molecular yields, have been thoroughly measured in acid media, especially in 0.8 N H_2SO_4 ; it appears to be well known in neutral media as well.³ There are few complete data obtained on a single system for a high pH.^{4,5} Measurements on the same system in a large region of pH (acid, neutral, alkaline) are also still very rare.⁶⁻¹⁰ The reason for this is the difficulty of choosing a suitable system; salts of metal ions are usually hydrolyzed at higher pH, whereas with organic compounds analytical chemistry

of the products formed in microquantities is often unsatisfactory or does not even exist.

The scarcity of, and the discrepancy in, the results published so far moved us to carry out measurements on one system in all three pH regions (acid, neutral, alkaline). The data we obtained in our previous work with aqueous oxalic acid solutions,^{11,12} especially the complete material balance for acid medium in the presence of oxygen,¹³ indicated that this system could be used.

The results presented here cover the pH region from 1.61 to 9.85, while experiments at pH higher than this are in progress.

Experimental

Solutions. The oxalic acid ($H_2C_2O_4 \cdot 2H_2O$) is an A.R. grade Merck product which was recrystallized before use.

- (1) G. Czapski and H. A. Schwarz, *J. Phys. Chem.*, **66**, 471 (1962).
- (2) E. J. Hart and J. W. Boag, *J. Am. Chem. Soc.*, **84**, 4090 (1962).
- (3) A. O. Allen, "The Radiation Chemistry of Water and Aqueous Solutions," D. Van Nostrand Co., Inc., New York, N. Y., 1961.
- (4) M. Haissinsky and P. Patigny, *J. chim. phys.*, **59**, 675 (1962).
- (5) M. Haissinsky, *ibid.*, in press.
- (6) E. J. Hart, *J. Am. Chem. Soc.*, **76**, 4198 (1954).
- (7) F. S. Dainton and D. B. Peterson, *Proc. Roy. Soc. (London)*, **A276**, 443 (1962).
- (8) F. S. Dainton and W. S. Watt, *Nature*, **195**, 1294 (1962).
- (9) M. Daniels and J. Weiss, *J. Chem. Soc.*, 2467 (1958).
- (10) J. T. Allan and G. Scholes, *Nature*, **187**, 218 (1960).
- (11) I. G. Draganić, *J. chim. phys.*, **56**, 9 (1959).
- (12) I. G. Draganić, *Nucleonics*, **21**, 33 (1963).
- (13) I. G. Draganić, *J. chim. phys.*, **56**, 16 (1959).

The water used was distilled in a continuous system, first from alkaline permanganate, then from acid dichromate, and, finally, without any additive.

Attempts were made to attain the least possible quantity of CO_2 in the solution before irradiation. Therefore, except in some cases for the sake of comparison or simplicity, commercial oxalates were not used; all solutions were made from oxalic acid with the addition of specially prepared NaOH. For this purpose metallic sodium (A.R. grade Carlo Erba product) was first washed with diethyl ether and then quickly cut. Waste parts were removed and pieces of about 0.5 g. in weight were dissolved in triply distilled water. This operation was performed in a nitrogen atmosphere and the flask was put in an ice-cold bath. After dissolution of the quantity needed, the concentration of the hydroxide prepared was determined by using an automatic buret connected with the flask.

To prepare the solution of the given pH, a desired quantity of hydroxide was poured into an oxalic acid solution deaerated previously. This was done by means of the automatic buret and in a nitrogen atmosphere. The solution was deaerated once more the measured quantity of oxygen was introduced, and finally the irradiation vessels were filled.

The irradiation vessels are 60-mm. long Pyrex cylindrical ampoules, 18-mm. i.d. They end in a normal B₇ joint located at the end of a narrow 45-mm. long neck, 2-mm. i.d. Eight ampoules are placed on a 250-cm.³ flask from which the solution is poured simultaneously into all ampoules. With the standard vacuum line the flask is connected to an Edwards "Speedivac" pump, to the supply of oxygen, and to the differential manometer. This device permits deaeration of the solutions and introduction of a given quantity of oxygen by simple operations. The ampoules are filled up to the top so that no gas phase remains and then closed with a cap which has a corresponding normal joint. This simplifies the subsequent procedure of introducing samples into the gas chromatograph. Tests have proved that the ampoules need not be sealed.

The pH of the solutions was varied only by the additions of different NaOH quantities, determined from the neutralization curve. A Beckman GS pH meter and a Beckman E 2 electrode were employed in the measurement.

The quantity of oxygen in the solution was 0.75 (± 0.05) mM, so that even after the longest irradiation more than half of the oxygen initially present remained. The oxygen quantity was varied only where its concentration effect was investigated.

Irradiations. Our radiation unit with 2000 c. of radioactive cobalt served as the radiation source.¹⁴

The dose rate was 2.3×10^{19} e.v. ml.⁻¹ hr.⁻¹, determined by the Fricke dosimeter with $G(\text{Fe}^{3+}) = 15.5$. No correction was introduced ($< 2\%$) by the electronic density difference between the dosimetric solutions and the ones studied.

Analyses. The gas products CO_2 and H_2 were determined by gas chromatography with helium or argon as carrier gases in a silica gel column. A Perkin-Elmer 154 DG instrument and procedures enabling precise measurements of 1–2 mm.³ were used.¹⁵

The amounts of H_2O_2 were spectrophotometrically measured by the iodide method developed by Ghormley.¹⁶ The extinction coefficient of 25,810 l. mole⁻¹ cm.⁻¹ was determined at 24°. The presence of oxalic acid slowed down the iodide oxidation so that the extinctions were read on the spectrophotometer about 0.5 hr. after the preparation of the solution. An unirradiated sample of oxalic acid with reagent, treated in the same way as the one studied, was used as the reference solution. When hydrogen peroxide had to be measured in a series of irradiated samples, to avoid errors due to the oxidation of iodide in the reference solution, we measured the unknown samples against the references which were prepared simultaneously with the ones studied.

The amount of oxalate ions decomposed was spectrophotometrically determined from the concentration difference in the nonirradiated and irradiated solutions by the use of copper benzidine.¹⁷ For each pH, a corresponding wave length and extinction coefficient were taken.

Results

General. Only carbon dioxide, hydrogen peroxide, and hydrogen have been found in the studied solutions irradiated at low absorbed doses. Their amounts depend on the dose absorbed and the initial pH of the irradiated solution. The proportionality with the doses absorbed in the studied region (from 0.75×10^{18} to 4.65×10^{18} e.v. ml.⁻¹) can be seen in Fig. 1. The pH influence is shown in Fig. 2, where the G values are averages of a series of measurements at the given pH.

Molecular oxygen consumption data are included only to check the reaction scheme proposed. They have been obtained by electrochemical measurements in separate experiments with the same system and will be presented in full detail elsewhere.¹⁸

(14) B. B. Radak and I. G. Draganić, *Bull. Inst. Nucl. Sci. "Boris Kidrič,"* 13, 77 (1962).

(15) Lj. Petković, M. Kosanić, and I. Draganić, *ibid.*, 15, 9 (1964).

(16) C. J. Hochanadel, *J. Phys. Chem.*, 56, 587 (1952).

(17) Z. D. Draganić, *Anal. Chim. Acta*, 28, 394 (1963).

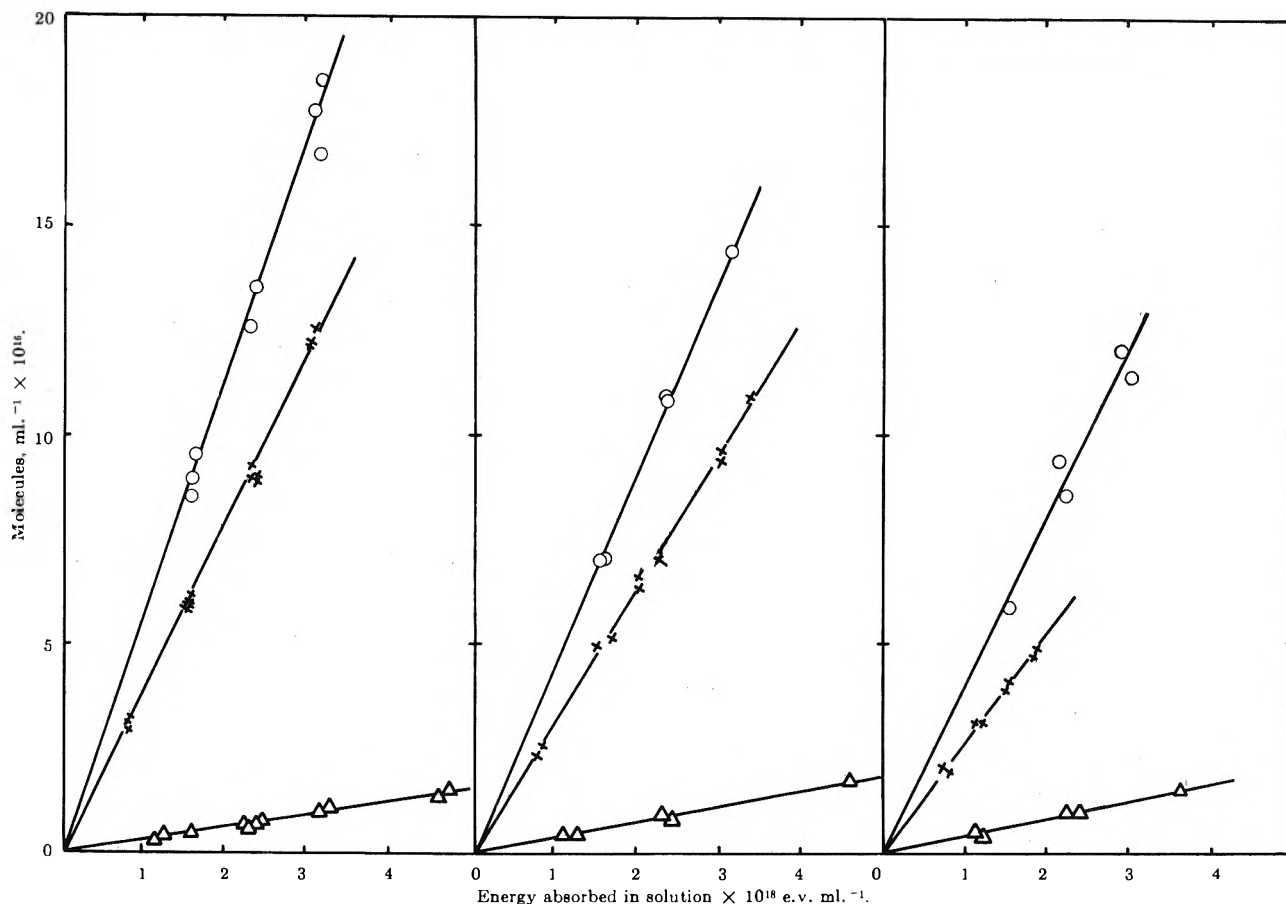


Figure 1. The absorbed dose influence on the formation of CO_2 , H_2 , and H_2O_2 in 50 mM oxalic acid solutions, in acid, neutral, and alkaline media; 0.75 (± 0.05) mM O_2 initially present: O, CO_2 ; X, H_2O_2 ; Δ , H_2 .

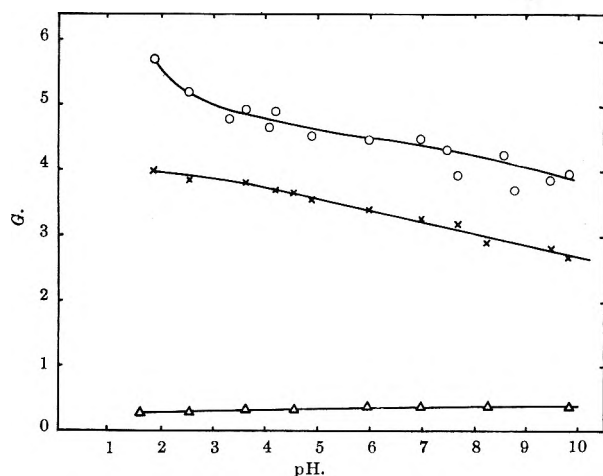


Figure 2. Irradiation yields of CO_2 , H_2O_2 , and H_2 measured in 50 mM $\text{H}_2\text{C}_2\text{O}_4$ with 0.75 \pm 0.05 mM O_2 present; the pH influence: O, CO_2 ; X, H_2O_2 ; Δ , H_2 .

Some experiments concern the determination of the decomposition yields of oxalate ion. They could not be performed in the absorbed dose region where the initial

mechanism has been studied; up to 100 times higher energy input was needed to obtain measurable concentration differences in the nonirradiated and irradiated samples.

The products which may be formed in the radiolysis of oxalate solutions, such as formic, glycolic, glyoxalic, and tartaric acids or some aldehydes, have been checked.

All the measurements were carried out in 50 mM oxalic acid solutions, except in the cases where the concentration effect was investigated. This relatively large concentration was taken so that the sodium hydroxide concentration should not be higher than that of the solute studied. Besides, this concentration lies within a larger region wherein the radiation yield of the oxalic acid decomposition measured by CO_2 and H_2O_2 formation is not visibly influenced by the initial solute concentration as can be seen in Table I.

Products in Liquid Phase. As can be seen in Fig. 2, yields of hydrogen peroxide measured in the studied solutions decrease from 4.00 to 2.78 with increasing pH

(18) D. Ovcin, O. Mičić, and I. Draganić, to be published.

Table I: The Influence of Oxalate Ion Concentration on Measured Yields of CO₂, H₂, and H₂O₂^a

Concentration, mM	G(CO ₂)	No. of determinations	G(H ₂)	No. of determinations	G(H ₂ O ₂)	No. of determinations
Oxalic acid ^b						
10	5.45	6	0.39	7	3.70	8
25	5.65	9	0.36	7	3.86	8
50	5.76	9	0.34	17	4.00	14
100	5.98	6	0.28	7	3.92	8
200	6.70	6	0.26	7	4.06	8
600	0.19	7
Potassium oxalate ^b						
10	4.10	4	0.41	12	3.00	8
25	4.39	4	0.41	7	3.13	14
50	4.50	4	0.40	7	3.19	8
100	4.48	4	0.39	12	3.18	14
200	5.02	4	0.38	12	3.22	14
600	0.35	6

^a Absorbed doses between 0.75×10^{18} and 4.65×10^{18} e.v. ml.⁻¹. ^b Irradiated solutions: oxalic acid (natural pH 2.7–0.8) and commercial potassium oxalate (natural pH 7.0–7.7). Oxygen present $0.75 (\pm 0.05)$ mM.

from 1.61 to 9.85. The experiments carried out in the absence of radiation have proved that the instability of H₂O₂ in alkaline medium (pH ~10) does not visibly influence our measurement.

Spot test reactions¹⁹ on formic, glycolic, glyoxalic, and tartaric acids, as well as on aldehydes, were negative. The consumption of oxygen has been followed polarographically during irradiation with a dropping mercury electrode. Some results obtained are given in Table II and will be presented in full detail elsewhere with other results of electrochemical measurements performed in oxalic acid solutions at different pH values.¹⁸

Products in Gas Phase. The results given in Fig. 2 show that carbon dioxide yields decrease from 5.76 to 3.98 with increasing pH of the irradiated solution from 1.61 to 9.85. It should be mentioned that blank test corrections in CO₂ measurements may be very important for high precision and good reproducibility, especially when very small amounts of gas are formed as in the case of high pH values. Even a careful preparation of sodium hydroxide and the solution studied did not enable us to obtain reproducible initial amounts of CO₂, and a blank test correction was made for each run. Out of eight samples from each batch, three or four were nonirradiated and taken as blanks. Usually these corrections were about $0.4 (\pm 0.1) \times 10^{16}$ CO₂ ml.⁻¹ in acid medium (pH 1.61) and $1.5 (\pm 0.5) \times 10^{16}$ CO₂ ml.⁻¹ in alkaline (pH 9.85).

Table II^a: Influence of pH on Molecular Oxygen Consumption¹⁸

pH	G(-O ₂)	No. of determinations
3.6	3.06	5
7.0–8.0 ^b	2.40	7
8.7–9.3 ^b	2.23	5

^a Irradiated solutions: 50 mM oxalic acid, the initial pH adjusted with sodium hydroxide; 0.3 mM of air oxygen initially present. Absorbed doses between 0.47×10^{18} and 10×10^{18} e.v. ml.⁻¹. ^b In the case where two pH values are given, the first value refers to the initial one, the second is the pH measured after irradiation.

Table III: The Effect of Oxygen Concentration on Measured Yields of H₂

Irradiated solution ^a	Oxygen concentration, mM	G(H ₂)	No. of determinations
H ₂ C ₂ O ₄ , pH 1.61	0.00	0.46	5
H ₂ C ₂ O ₄ , pH 1.61	0.048	0.36	4
H ₂ C ₂ O ₄ , pH 1.61	0.063	0.35	4
H ₂ C ₂ O ₄ , pH 1.61	0.077	0.35	6
H ₂ C ₂ O ₄ , pH 1.61	0.075	0.34	3
H ₂ C ₂ O ₄ , pH 1.61	0.098	0.33	6
H ₂ C ₂ O ₄ , pH 1.61	0.341	0.33	3
H ₂ C ₂ O ₄ , pH 1.61	0.790	0.34	17
H ₂ C ₂ O ₄ , pH 1.61	1.020	0.34	6
H ₂ C ₂ O ₄ + 0.08 N H ₂ SO ₄	0.750	0.32	6
H ₂ C ₂ O ₄ + 0.8 N H ₂ SO ₄	0.750	0.31	6
H ₂ C ₂ O ₄ + NaOH, pH 4.55	0.00	0.45	6
H ₂ C ₂ O ₄ + NaOH, pH 4.55	0.750	0.37	5
H ₂ C ₂ O ₄ + NaOH, pH 7.00	0.800	0.40	5
H ₂ C ₂ O ₄ + NaOH, pH 9.85	0.056	0.41	5
H ₂ C ₂ O ₄ + NaOH, pH 9.85	0.058	0.41	5
H ₂ C ₂ O ₄ + NaOH, pH 9.85	0.750	0.40	5

^a Irradiated solutions: 50 mM oxalic acid. Oxygen present in concentrations between 0.00 and 1.02 mM.

The yields of molecular hydrogen, measured in 50 mM oxalic acid aqueous solutions, increase from 0.34 to 0.40 with a pH increase from 1.61 to 9.85 and the presence of 0.75 mM of oxygen. As can be seen in Table I,

(19) F. Feigl, "Spot Tests," Elsevier Publishing Co., Amsterdam, 1954.

measured molecular hydrogen yields depend on initial oxalic acid concentration. We also studied the effect of initial oxygen concentration on molecular hydrogen formation in 50 mM oxalic acid solutions at different pH values. The results are summarized in Table III.

For the sake of simplicity in preparation, we used commercial potassium oxalate in studying the oxalate ion concentration effect at pH 7. In that case the CO_2 blanks were doubled but the measured radiation yields (Table I) agree with the yields measured in the solution prepared from oxalic acid and sodium hydroxide as previously described.

Radiation Yields in the Noninitial Irradiation Conditions. The decomposition yield of oxalate ions could be useful in considering the radiolysis mechanism of oxalic acid solutions. However, for the determination of $G(-\text{C}_2\text{O}_4^{2-})$ much longer irradiations were needed to obtain measurable concentration differences in the nonirradiated and irradiated samples. In such cases oxygen was bubbled through the solution during irradiation. The yields thus measured are not initial since the absorbed doses are up to 100 times higher than those with which the initial yields were measured. In order to relate the decomposition yield to the formation yields initially measured, also CO_2 and H_2O_2 were measured in the noninitial irradiation conditions.

In acid medium, as shown in our earlier work,¹³ the quantities of the products formed under these conditions are linearly proportional to the dose absorbed, and the yields of carbon dioxide and hydrogen peroxide were equal to initial yields. The oxalate decomposition yield was practically equal to $0.5G(\text{CO}_2)$ in the whole region studied, indicating a complete transformation to carbon dioxide.

In neutral medium the CO_2 yield measured under noninitial conditions was about 12% smaller than corresponding initial yield. The formation of H_2O_2 was linearly proportional only at very low absorbed doses, where the yield observed was in agreement with the initial one. At higher doses the decomposition took place, and a decrease of the yield has been observed with the increase of the dose absorbed. The oxalate decomposition yield was about 25% smaller than $0.5G(\text{CO}_2)$, measured under the same conditions.

Different experiments have been performed in order to elucidate why in neutral medium $G(-\text{C}_2\text{O}_4^{2-})$ is smaller than $0.5G(\text{CO}_2)$. The observed ratio $\text{CO}_2 \text{ formed} / \text{C}_2\text{O}_4^{2-} \text{ decomposed} > 2$ should be considered apparent since one decomposed molecule of oxalic acid cannot give more than two CO_2 molecules. This ratio points to the formation of a compound which reacts with copper benzidine similarly to oxalate ions and decreases the extinction difference of the nonirradiated and irradi-

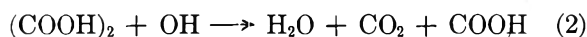
ated solution, thus apparently decreasing the oxalate ion decomposition yield. As copper benzidine reagent is not specific for oxalic acid and other acids may react (in the known cases molar absorptivities are smaller than for oxalic acid), we tried to identify the products which may be formed in the radiolysis of oxalic acid: formic, glycolic, glyoxalic, and tartaric acids. Different spot test reactions have been used. This with β, β' -dinaphthol and gallic acid¹⁹ indicate the presence of tartrate. The presence of hydrogen peroxide interferes less in the case when gallic acid is used as reagent; yellow-green coloration indicates the presence of μgram amounts. However, the color intensity does not seem to increase visibly with the absorbed dose and no quantitative measurements of such low concentration could be performed. In order to get larger amounts of the unknown products for not more than 15% decomposition, we have also irradiated more concentrated solutions (200 and 600 mM). The observation was as in 50 mM solutions. It is interesting to note that the values obtained here by precipitating thorium oxalate and measuring it as an oxide after ignition are in agreement with the values spectrophotometrically obtained. This means that the product formed precipitates as oxalic acid does. Since formic, glycolic, and glyoxalic acids do not precipitate, this product may be a more complicated molecule which could be precipitated with thorium as oxalic acid (such as tartaric acid).

The yield of unknown product (or products) observed at greater doses does not seem to be significant, as can be easily seen if some points are taken into consideration. First, the 25% difference between the decomposition yield and $0.5G(\text{CO}_2)$ in neutral medium is certainly a serious indication that some other product is present with oxalic acid in irradiated solution. However, the possible error is large although the accuracy of the spectrophotometric method used is $\pm 2\%$; in neutral medium the decomposition yield is considerably smaller than in acid medium. (Also, the concentration differences to be measured are considerably smaller, only up to 15%. For larger decompositions nonlinearity with absorbed dose has been observed.) Second, tartrate yield estimated from spot test reaction with gallic is of the order of $10^{-2} G$ unit. Third and most important, the difference between the CO_2 yield measured at initial and noninitial conditions is small. The 12% difference observed is in fact much smaller if the correction for pH change during irradiation is taken into account. Due to the extensive decomposition of oxalate and partial removal of CO_2 formed, pH changes have been as large as two pH units during larger irradiations; thus the carbon dioxide yield should be expected to be smaller than the initial one.

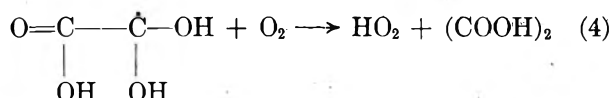
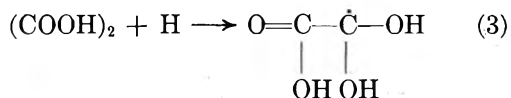
Discussion

Mechanism. Results obtained at low doses show that the decomposition of oxalate ions in the presence of oxygen gives only carbon dioxide and hydrogen peroxide. The build-up of these products at higher doses may lead to a change in the reaction mechanism and formation of some other products, as often observed in aqueous solutions. This could also explain our observations at higher doses. However, they do not seem to be significant for the initial mechanism; the oxygen consumption data confirm the complete material balance. Therefore, in considering the reaction scheme we will take into account only the products formed and measured in initial conditions.

Oxalic acid reacts efficiently with OH radicals



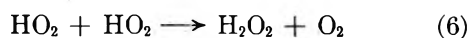
Data on the oxalic acid concentration influence on molecular yields measured in irradiated solutions (Table I) indicate that oxalic acid also reacts with H atoms; the increase in the solute concentration decreases the molecular hydrogen yield. As carbon dioxide and hydrogen peroxide yields essentially do not change in the studied region, reactions 3 and 4 may occur.



Free radicals formed in reaction 2 disappear by reaction with oxygen present in the solution in a large excess



Hydrogen peroxide is formed in reaction 6.



The usual kinetic treatment gives

$$G(-\text{H}_2\text{C}_2\text{O}_4) = G_{\text{OH}} \quad (7)$$

$$G(\text{CO}_2) = 2G_{\text{OH}} \quad (8)$$

$$G(\text{H}_2\text{O}_2) = G_{\text{H}_2\text{O}_2} + 0.5(G_{\text{OH}} + G_{\text{H}}) \quad (9)$$

$$G(\text{H}_2) = G_{\text{H}_2} \quad (10)$$

If the relation giving the material balance of the primary yields of water radiolysis induced by γ -radiation is taken into consideration

$$G_{\text{H}} + 2G_{\text{H}_2} = G_{\text{OH}} + 2G_{\text{H}_2\text{O}_2} \quad (11)$$

then, relations 8, 9, 10, and 11 make possible the calculation of the primary radical and molecular yields of water radiolysis from the measured yields of CO_2 , H_2O_2 , and H_2 . Therefore, with some simple mathematical operations and rearrangements, we have

$$G_{\text{OH}} = 0.5G(\text{CO}_2) \quad (12)$$

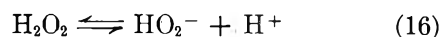
$$G_{\text{H}_2} = G(\text{H}_2) \quad (13)$$

$$G_{\text{H}} = G(\text{H}_2\text{O}_2) - G(\text{H}_2) \quad (14)$$

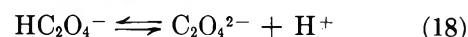
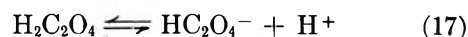
$$G_{\text{H}_2\text{O}_2} = 0.5[G(\text{H}_2\text{O}_2) + G(\text{H}_2) - 0.5G(\text{CO}_2)] \quad (15)$$

Nature of Reacting Species in the Oxalic Acid-Oxygen Solutions at Different pH Values. Relations 12-15 can be used in the whole pH region studied, since the change in the nature of the reacting species, by the increase of pH from 1.61 to 9.85, does not seem to affect the reaction mechanism.

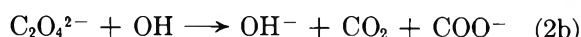
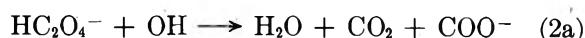
The molecular species in the irradiated solutions are hydrogen, hydrogen peroxide, oxalic acid, and oxygen. The first two, once formed, do not participate in the reaction. Even if a dissociation like (16) suggested for alkaline medium does exist, it does not



seem to influence the reaction scheme. It also exerts no influence on the analytical method employed in our case for the determination of hydrogen peroxide. There is only a considerable change in the nature of oxalic acid, since with the increase of pH we have ions in the solution instead of molecules. Values of



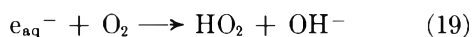
$\text{p}K_1 = 1.2$ and $\text{p}K_2 = 4.2$, for reactions 17 and 18, respectively, mean that above $\text{pH} \sim 5$ essentially only $(\text{COO}^-)_2$ ions are present in the solution. However, the experimental results presented here suggest that the ionic form does not affect the decomposition due to reaction 2. It is probably because, according to the degree of dissociation, other reactions take place, such as



The pH may exert influence only with a change in the nature of the OH radicals, especially by a possible substitution of the neutral hydroxyl radical by a basic form. This does not appear to be the case within the pH region that has been investigated here.

However, it can be noticed that the influence of the oxalic acid concentration on measured molecular hy-

drogen yields is less evident in neutral and alkaline than in acid media. It is probably because in that pH region the solvated electrons are the main reducing species. As they react faster with O_2 than with $(COO^-)_2$ ions, reactions 3 and 4 are probably replaced by



Large hydrogen peroxide yields measured at higher pH values indicate that reactions in which H_2O_2 is formed are practically the same as reactions 5 and 6, proposed for acid medium.

It is worth mentioning here that our experimental results, as well as those obtained by Daniels and Weiss⁹ show that it is not necessary to pay attention to a possible HO_2 radical dissociation for which Uri²⁰ estimates $pK \sim 2$.

Molecular Hydrogen Yields. Our experimental results are in accordance with $G(H_2)$ measured under similar conditions in aqueous solutions of formic acid with oxygen present⁶ where, according to the mechanism proposed, $G(H_2) = G_{H_2}$. However, the data given in Table I indicate an oxalic acid concentration influence. Figure 3 shows cube root plots for lowering the measured molecular hydrogen yields by increasing oxalic acid concentration. This observation, made also on many other systems,³ indicates the kinetics in which a second-order radical recombination reaction competes with first-order radical destruction reactions while the radicals diffuse outward from the center.

As can be seen in Fig. 3 hydrogen yields are higher in neutral medium and much less affected by oxalate ion concentration than in acid medium. It seems here that the formation of molecular hydrogen goes less disturbed through reaction 20 than the molecular

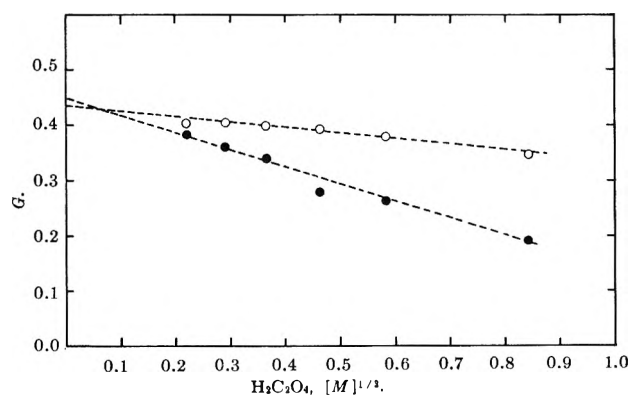
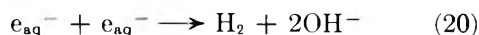
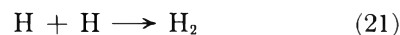


Figure 3. Cube root plots: measured molecular hydrogen yields as a function of oxalic acid concentration; $O_2 = 0.75 \pm 0.05$ mM; ●, acid solutions (natural pH 2.1–0.8); ○, neutral solutions (natural pH 7.0–7.7).



hydrogen formation in acid medium, where reaction 21 takes place in competition with reaction 3.



Extrapolation to zero scavenger concentration in Fig. 3 gives the value 0.45 as the primary molecular hydrogen yield in acid medium and 0.43 in neutral. However, this difference is small and it is within the limits of experimental error. The other results obtained for alkaline medium also indicate 0.45 as a probable primary hydrogen yield in the whole pH region studied.

As can be seen in Table III, measured hydrogen yields are independent of the amount of oxygen present in a very large concentration region. However, it can be noticed that $G(H_2)$ increases when oxygen concentration falls to zero.

Primary Radical and Molecular Yields in Water γ -Radiolysis for pH 1.61–9.85. Using the experimental results given in Fig. 1 and eq. 12, 14, and 15 we can calculate G_{OH} , G_H , and $G_{H_2O_2}$. The results in Table I indicate that the corrected values in Fig. 3 should be used in relation 13 to primary molecular hydrogen calculations. We used these corrected values without introducing corresponding corrections in measured hydrogen peroxide yields, since the data in Table I do

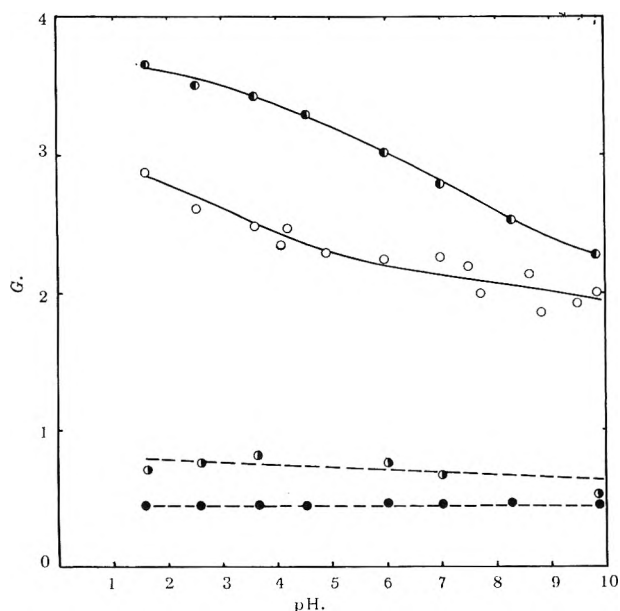


Figure 4. The primary radical and molecular yields in water γ -radiolysis, for pH 1.61 to 9.85, derived from the oxalic acid-oxygen system: ○, H; ○, OH; ●, H_2O_2 ; ●, H_2 .

(20) N. Uri, *Chem. Rev.*, 50, 379 (1952).

not show a visible oxalic acid concentration influence on $G(\text{H}_2\text{O}_2)$. Figure 4 summarizes the results obtained for primary yields in water γ -radiolysis in the pH region studied.

From the radiolysis mechanism presented with the reactions 2-6 one can deduce

$$G(-\text{O}_2) = 0.5(G_{\text{H}} + G_{\text{OH}}) \quad (22)$$

The $G(-\text{O}_2)$ values calculated from the eq. 22 and the data given in Fig. 4 are 2.97, 2.38, and 2.19 for pH 3.6, 7.5, and 9.0, respectively. As can be seen, they are in good agreement with experimental data presented in Table II.

Remarks. The values for free radical yields, calculated from the oxalic acid-oxygen system, are in good agreement with the values derived from other systems in acid and neutral solutions.³ However, it may be noticed that our radical yields are slowly but continually decreasing above pH ~ 3 .

In alkaline medium (pH ~ 10), our values for free radical yields are somewhat smaller than Cheek and Linnenbom's values²¹ (at pH 13) and much smaller than the other results published for pH 13.⁴⁻⁸

In agreement with many published results,^{3,7,8} although not with all,^{4,5} our molecular yields do not seem to change considerably with increasing pH. Nevertheless, a distinction should be made between G_{H_2} and $G_{\text{H}_2\text{O}_2}$ in which case a greater decrease of the latter is apparent.

Acknowledgment. The authors wish to thank Dr. A. O. Allen for his helpful suggestions and discussion of this work. Thanks are also due to Mrs. M. Marović and Mr. V. Jovanović for their technical assistance in the experiments.

(21) C. H. Cheek and V. J. Linnenbom, *J. Phys. Chem.*, **67**, 1856 (1963).

Equilibrium Studies with the Chelating Ion-Exchange Resin Dowex A-1¹⁻³

by Donald E. Leyden and A. L. Underwood

Department of Chemistry, Emory University, Atlanta, Georgia (Received January 9, 1964)

The apparent ionization constants of the iminodiacetic acid groups of the chelating ion-exchange resin Dowex A-1 have been measured in 0.1 *M* and in 1 *M* sodium chloride solution. Despite the fact that the ionogenic groups are situated in a styrene-divinylbenzene copolymer matrix, the measured values are of the same magnitude as those of the simple monomeric analog, benzyloiminodiacetic acid. However, the pH dependence of metal ion distribution coefficients is not predictable from the pK_a values using the customary treatment applied to monomeric chelons. Experimental distribution coefficients as functions of pH are reported. From the temperature dependence of the *D* values, "formal" values of ΔH and of ΔS have been calculated for the exchange process.

Introduction

Attempts to "tailor-make" ion-exchange resins for specificity have achieved only limited success. Clearly a more realistic goal is a resin exhibiting a more modest selectivity; separations will then be accomplished through ingenuity based upon a detailed knowledge of its properties and of the coordination chemistry of ions in solution. Dowex A-1, a chelating resin with iminodiacetic acid groups attached to a styrene-divinylbenzene copolymer matrix, although it interacts with many metal ions, is inherently much more selective than conventional cation exchangers. Numerous analytical applications of Dowex A-1 have been reported, involving mainly the removal of di- and trivalent cations from solutions of the alkalis and alkaline earths, based upon the marked selectivity of the resin toward ions of greater complexing ability. The resin first became generally available in 1959; in 1962 a considerable change in the manufacturing process led to an improved product.⁴

In view of the widespread interest in the resin, the literature is noticeably scanty with regard to the fundamental data needed to place the use of Dowex A-1 on a sound basis. The first dissociation constant of the acid form of Dowex A-1 was measured by Marinsky and Krasner,⁵ and distribution coefficients for several metal ions in the presence of sulfosalicylate and of citrate at several pH values have been reported.⁶ Unfortunately, it is doubtful that the 5-hr. contact between resin and solution in the latter study was sufficient for

the attainment of equilibrium. Turse and Rieman studied the kinetics of several exchange processes with Dowex A-1.⁷ It was found that in the case of ions that could form chelates the rate of exchange was not diffusion controlled (as is usual with conventional resins), but, rather, was governed by the rate of the chelation reaction itself. More recently, Heitner-Wirguin and Markovits have reported that exchange rates are governed by diffusion processes under conditions of low pH where the resin is considerably more shrunken than in the studies of Turse and Rieman.⁸

The principal drawbacks to the use of Dowex A-1, *viz.*, slow kinetics and pronounced swelling behavior, are indeed serious. Nevertheless, because the resin has found application despite its limitations, it is desirable to report our measurements of the ionization of

(1) This investigation was supported by the National Science Foundation through Research Grant GP-1974.

(2) Presented in part before the Division of Analytical Chemistry, 145th National Meeting, American Chemical Society, New York, N. Y., September, 1963.

(3) Taken from a dissertation submitted by Donald E. Leyden in partial fulfillment of the requirements for the Ph.D. degree, Emory University, 1963.

(4) R. M. Wheaton, Physical Research Laboratory, Dow Chemical Co., Midland, Mich., private communication.

(5) J. A. Marinsky and J. Krasner in "Radioisotopes in the Physical Sciences and Industry," International Atomic Energy Agency, Vienna, 1962, p. 503.

(6) R. D. Szidon and J. S. Fritz, U. S. Atomic Energy Commission Report IS-340, May, 1961.

(7) R. Turse and W. Rieman, III, *J. Phys. Chem.*, **65**, 1821 (1961).

(8) C. Heitner-Wirguin and G. Markovits, *ibid.*, **67**, 2263 (1963).

the iminodiacetic acid groups and equilibrium values of the distribution coefficients for several cations at various pH and temperature values. Such data, along with kinetic information, are needed in planning the most intelligent use of the resin, and may prove useful in evaluating improved chelating resins should they be developed.

Experimental

Conditioning and Properties of the Resin. A.R. grade Dowex A-1 was obtained from the J. T. Baker Chemical Co. in the sodium form as 50- to 100-mesh beads.⁹ The material was washed five times with deionized water, decanting the "fines" each time; then the material was air-dried until free-flowing and was stored. The moisture content was determined by drying samples (which were not used in subsequent work) to constant weight at 100°. The wet and dry densities (1.07 and 1.30, respectively, at 25°) were measured in a conventional manner.¹⁰ The capacity of the resin stated by the supplier for lot No. 28366 was 3.96 mequiv. per g. of dry, sodium-form resin, based upon the uptake of tetraamminecopper(II) ion. This value was verified within 2% by a potentiometric titration of a sample of the resin converted to the hydrogen form and suspended in 90% 2-propanol. The titrant was tetra-*n*-butylammonium hydroxide in the same solvent, and the electrodes were glass and calomel. The titration curve exhibited two "breaks" and equilibrium was established fairly rapidly (about 30 min.), two characteristics not seen in comparable aqueous titrations of the resin. The capacity of the resin by this method was 3.88 mequiv. per g. of dry, sodium-form resin. Such a titration enables assessment of the extent of conversion of the resin to the hydrogen form, since two useful "breaks" are obtained representing the bifunctional acidity of the iminodiacetic acid group.

Measurement of Apparent pK_a Values. Samples of Dowex A-1 were titrated with sodium hydroxide using essentially the technique described by Topp and Pepper,¹¹ where each point on the titration curve is obtained by equilibration of an individual portion of resin with a given quantity of base. The ionic strengths of the solutions were held at either 1 or 0.1 by appropriate additions of sodium chloride. Carbon dioxide was carefully excluded by outgassing the solutions with purified nitrogen. The samples were rotated in sealed tubes for 7 days in a water bath at $25 \pm 0.05^\circ$; preliminary work indicated that the pH values actually became constant in about 2 days. After equilibration, the pH was measured *in situ* as rapidly as possible, using a Leeds and Northrup Model 7401 pH meter with No. 124138 miniature pH electrodes. In cases where it

was needed, the sodium ion concentration was obtained by passing an aliquot of the solution through a column of Dowex 50 cation exchanger in the hydrogen form, titrating the acid solution, and correcting for the titratable acidity present before passage through the column. Moisture content of the resin phase after equilibration was estimated by drying to constant weight at 100° a weighed portion of the resin which had been freed of superficial water by a blotting technique with filter paper as described by Gregor, *et al.*^{12,13}

The pK_a values of benzyliminodiacetic acid, the closest monomeric analog of Dowex A-1, were not available in the literature for comparison with the values for the resin. A sample of this acid, obtained from Columbia Organic Chemicals Co., Inc., Columbia, S. C., was recrystallized four times from water and dried *in vacuo* at 100° for 5 hr. Potentiometric titrations under nitrogen were performed with potassium hydroxide on $10^{-2} M$ solutions of the acid in the presence of 0.1 *M* and of 1 *M* sodium chloride. Each value reported is based upon five experiments.

Measurement of Distribution Coefficients of Cations. Because of the slow kinetics with Dowex A-1, batch equilibrations were deemed more suitable than column techniques for measuring distribution coefficients. Preliminary experiments in which equilibrium was approached from both directions established that 18–24 hr. was sufficient for equilibration with the cation solutions. In the work reported here, the contact period was 48 hr. Weighed quantities of about 500 mg. of the hydrogen-form resin and 60-ml. portions of various solutions were placed in sealed tubes and rotated in a water bath at $25 \pm 0.05^\circ$. Each solution contained 50 ml. of a 0.001 *M* solution of the cation as nitrate and 10 ml. of buffer solution, to which solid potassium nitrate was added to obtain the desired ionic strength. The ionic strength was 0.1 except in the case of copper, where three values were studied (see Fig. 1). The buffers were as follows: pH 1, potassium nitrate–nitric acid; pH 2 to 6, potassium acid phthalate–potassium hydroxide; pH 7, potassium dihydrogen phosphate–potassium hydroxide. After the equilibration period,

(9) "Dowex Chelating Resin A-1," Product Data, Index No. 056209, J. T. Baker Chemical Co., Phillipsburg, N. J.

(10) R. Kunin, "Ion Exchange Resins," 2nd Ed., John Wiley and Sons, Inc., New York, N. Y., 1958, p. 325.

(11) N. E. Topp and K. W. Pepper, *J. Chem. Soc.*, 3299 (1949).

(12) H. P. Gregor, K. M. Held, and J. Bellin, *Anal. Chem.*, **23**, 620 (1951).

(13) Moisture content by this method is not so accurate as that obtained by extrapolation of a wet weight–relative humidity curve, but it is adequate for the purpose here; a 5% error in the moisture determination leads to an error of about 0.05 pK_a unit when the degree of neutralization is about 0.5.

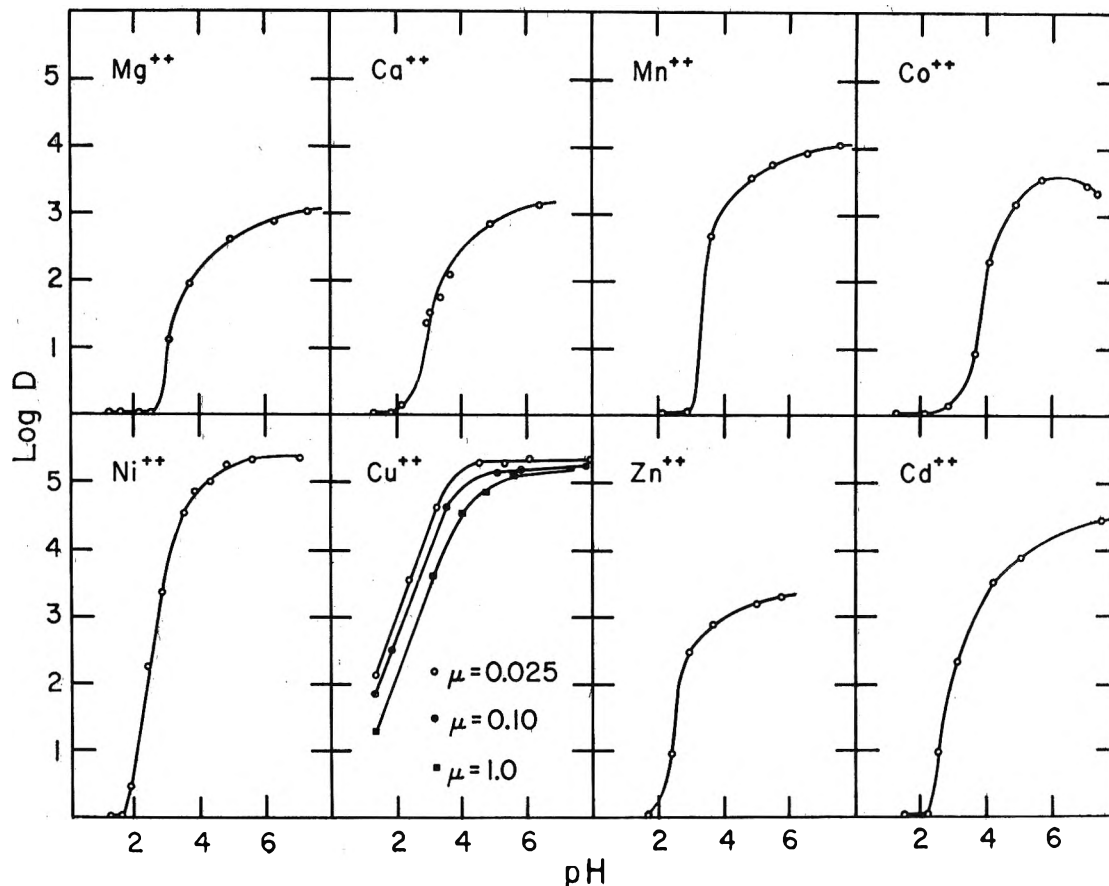


Figure 1. Distribution of cations as a function of pH for Dowex A-1 ($\mu = 0.10$ for all cases except as noted for Cu^{2+}).

the pH value was measured, the solution was filtered, and the resin was rinsed rapidly with deionized water. The solution and rinse were combined and analyzed for metal ion concentration using reliable spectrophotometric and EDTA titrimetric procedures.

Measurement of Temperature Dependence of Distribution Coefficients. To about 1 g. of Dowex A-1 in the sodium form was added 200 ml. of a 0.01 M solution of the cation to be investigated; the solution was buffered at pH 3 and its ionic strength was adjusted to 0.05 with potassium nitrate. The mixture was stirred for 48 hr. in a flask with a water jacket through which constant-temperature water was pumped. A 10-ml. aliquot of the solution was withdrawn for analysis, after which the temperature was raised to a new value and the procedure repeated.

Infrared Measurements. Portions of sodium-form Dowex A-1 were converted to other desired forms by passing large excesses of various metal nitrate solutions through small columns containing the resin. The samples were thoroughly rinsed with deionized water and dried at 100°, after which they were ground to pass 200 mesh and further dried for 24 hr. at 100°.

About 0.2-mg. portions of the resin samples were mixed with 300-mg. portions of dried, 200-mesh spectral grade potassium bromide. The mixtures were pressed into disks in an evacuated die at about 120,000 p.s.i. Spectra were recorded using a Perkin-Elmer Model 137 Infracord spectrophotometer. To make certain that important information was not being overlooked for lack of resolution, some of the spectra were also run on a Perkin-Elmer Model 421 spectrophotometer.

Results and Discussion

Apparent pK_a Values of Dowex A-1. Apparent pK_a values were obtained from the titration curves and auxiliary data using the equation

$$pK_a = \text{pH} + \log [\text{Na}^+] - \log \frac{[\bar{X}]}{2} \quad (\alpha = 0.5)$$

The derivation of this equation and an interpretation of its significance are given by Helfferich.¹⁴ The term $[\bar{X}]$ represents the total concentration of ionogenic groups, both undissociated and dissociated, and α is

(14) F. Helfferich, "Ion Exchange," McGraw-Hill Book Co., Inc., New York, N. Y., 1962, p. 84.

the degree of dissociation. pK_a values for Dowex A-1 are shown in Table I, where also may be seen the values for benzyliminodiacetic acid. It should be noted that the values for Dowex A-1 in Table I are

Table I: pK_a Values for Dowex A-1 and for Benzyliminodiacetic Acid^a

System	pK_{a_1}	pK_{a_2}
Dowex A-1 in 0.1 M NaCl ^b	2.92	
Dowex A-1 in 0.1 M NaCl	2.97 ± 0.06	8.55 ± 0.18
Dowex A-1 in 1 M NaCl	2.96 ± 0.16	8.58 ± 0.06
Benzyliminodiacetic acid in 0.1 M NaCl	2.43 ± 0.02	8.90 ± 0.06
Benzyliminodiacetic acid in 1 M NaCl	2.27 ± 0.09	8.69 ± 0.06

^a Uncertainties are expressed in terms of the confidence interval of the mean for a probability level of 0.90. ^b Ref. 5.

based upon data obtained at the midpoints of the buffer regions of the titration curves. If pK_{a_1} is calculated from various points along the first buffer region, the value increases with increasing per cent neutralization. In the case of pK_{a_2} , the value increases to the midpoint of the second stage of neutralization and then diminishes. Some pK_a values corresponding to several degrees of neutralization are shown in Table II. This

Table II: Variation of pK_a Values for Dowex A-1 with Degree of Neutralization in 1 M NaCl

α	pK_{a_1}	pK_{a_2}
0.125	2.37	7.47
0.250	2.42	7.90
0.500	2.96	8.58
0.750	3.04	8.54
0.875	3.50	8.45

inconstancy of pK_a with degree of neutralization has been observed with other polymeric acids.¹⁵⁻¹⁸ Although it has not been studied in detail in the present work, it may be noted that there is a hysteresis effect in the resin titration, *i.e.*, slightly different pK_a values are obtained from titrations of sodium-form resin with acid, even in 1 M sodium chloride solution.

It must be emphasized that the pK_a values obtained in a study such as this pertain only to phenomena observed in the aqueous phase in contact with the resin. Conditions within the resin pores and the character of the ionogenic groups within the resin cannot be deduced from the analysis of the aqueous phase. How-

ever, the apparent pK_a values found for Dowex A-1 are seen to differ by considerably less than an order of magnitude from the values for the monomeric analog, benzyliminodiacetic acid. This encourages the application to Dowex A-1 of a treatment normally employed in describing the chemistry of monomeric chelating agents such as EDTA. For example, one might hope to deduce from the pK_a values of Dowex A-1 the effect of pH upon the distribution coefficients for various cations. Normally, the "effective" stability constant of a metal chelate increases with increasing pH, becoming maximal (and equal to the "absolute" stability constant) when the ligand is essentially completely ionized. Applying this idea to Dowex A-1, it might be predicted that the distribution coefficients for the several cations would rise with increasing pH and become maximal around pH 10 to 11. It will be seen below, however, that maximal distribution coefficients are in fact obtained at a much lower pH value, *viz.*, 4-5. Actually, it is in this region that the first ionization of Dowex A-1 becomes essentially complete. The explanation of this discrepancy is not clear, but the most obvious conclusion is that both ionogenic groups of Dowex A-1 are not involved in chelating metal ions, although one is restrained from an easy acceptance of this by the uncertainty about the situation actually obtaining within the pores of the resin.

pH Dependence of Distribution Coefficients. In this discussion, the function considered is the distribution coefficient, D , defined by

$$D = \frac{\text{amt. of metal ion per g. of dry resin}}{\text{amt. of metal ion per ml. of solution}}$$

The variation of D values with pH is obviously extremely important in planning separations utilizing Dowex A-1. Figure 1 shows plots of $\log D$ vs. pH for several metals. It is readily seen that all of the cations studied show similar behavior, exhibiting D values which become maximal at pH 4-5. Although the individual values differ considerably, the slopes of the curves in the pH region 1-4 are so steep that good pH control would be necessary in attempting separations on the basis of D values in this region. The pronounced peak in the cobalt curve has been seen before in a similar connection.¹⁹

(15) R. Arnold and J. T. G. Overbeek, *Rec. trav. chim.*, **69**, 192 (1950).

(16) A. Oth and P. M. Doty, *J. Phys. Chem.*, **56**, 43 (1952).

(17) A. Katchalsky, *J. Polymer Sci.*, **7**, 393 (1951).

(18) H. P. Gregor, L. B. Lutinger, and E. M. Loebel, *J. Phys. Chem.*, **59**, 34 (1955).

(19) H. P. Gregor, M. Taifer, L. Citarel, and E. I. Becker, *Ind. Eng. Chem.*, **44**, 2834 (1952).

Table III: Thermodynamic Values for Cations Exchanged on Dowex A-1

Exchange system	$-RT \ln D$, kcal./mole			$-\Delta H$, kcal./mole			ΔS , e.u.		
	30°	50°	70°	30°	50°	70°	30°	50°	70°
$\text{Cu}^{+2}\text{-Na}^+$	-3.20	-3.46	-2.64	0.692	0.626	0.783	12.9	12.7	10.0
$\text{Co}^{+2}\text{-Na}^+$	-2.53	-2.75	-2.97	0.865	0.820	0.818	11.2	11.0	11.0
$\text{Ni}^{+2}\text{-Na}^+$	-3.34	-3.61	-3.86	0.865	0.951	1.05	13.9	14.1	14.3
$\text{Zn}^{+2}\text{-Na}^+$	-3.78	-4.17	-4.45	0.240	0.434	0.465	13.4	14.0	14.1

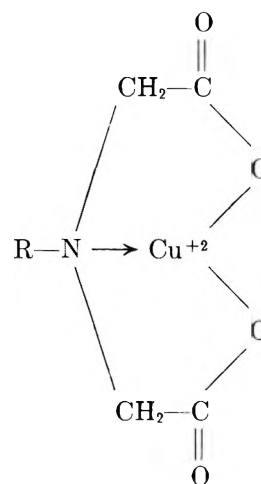
Temperature Dependence of Distribution Coefficients.

Values of thermodynamic functions for exchanges involving several cations are given in Table III. These values were calculated from the measured distribution coefficients at 20, 40, 50, 60, and 80°, utilizing plots of $1/T$ vs. $\log D$. Within the sensitivity of the analytical methods employed, there was no variation of D with temperature for calcium and magnesium.

The heats of exchange found for conventional ion-exchange resins are generally less than 2 kcal./mole.²⁰ It is interesting that small ΔH values were found in this study as well. This should not be interpreted as indicating that the bonding is of the same type with both conventional and chelating resins, however, because the complicated ion-exchange phenomenon involves several processes each of which may contribute to the measured ΔH value in a degree which is difficult to evaluate. The main value of the measurements reported here lies in the disclosure that the distribution coefficients are relatively insensitive to temperature, a fact which may be of practical importance to users of the resin.

It must be emphasized that the values in Table III are not standard thermodynamic values. They are, however, pertinent values for conditions under which the resin might normally be used. The enthalpy values represent the heat of the transfer of the metal ion from the aqueous phase to the resin in the normal manner of exchange. For a metal ion at very low concentration, the value of D would relate to the equilibrium constant of the exchange reaction, and $-RT \ln D$ might be associated with a standard free energy change by making certain assumptions.²¹ Under the conditions of this study, however, the values are "formal" ones, valid only in comparable situations.

Infrared Measurements. In most discussions of Dowex A-1 in the literature, it is tacitly assumed that chelates involving two five-membered rings are formed, similar to those of iminodiacetic acid itself.



There is little evidence, however, that this is indeed the case, and it is difficult to apply to an ion-exchange resin the standard techniques used to elucidate chelation in solution or in crystalline solids. Although it was hoped that infrared spectra might be helpful, our results are inconclusive. The sodium, potassium, and hydrogen forms of the resin exhibit a split carbonyl peak at 1620 and 1730 cm^{-1} . With the manganese, copper, cobalt, and nickel forms, there is a single broad peak at about 1580 cm^{-1} . One cannot say from the spectrum whether there is more than one type of carboxyl group present. There are no observable shifts in the C-H region of 3000 cm^{-1} which, according to Sawyer and Paulsen,²² are observed when the sodium salt of EDTA forms chelates with complex-forming cations.

(20) Reference 14, p. 166.

(21) K. A. Kraus and R. J. Raridon, *J. Phys. Chem.*, **63**, 1901 (1959).

(22) (a) D. T. Sawyer and P. J. Paulsen, *J. Am. Chem. Soc.*, **80**, 1597 (1958); (b) *ibid.*, **81**, 816 (1959).

Studies of Anion Adsorption on Platinum by the Multipulse Potentiodynamic (M.p.p.) Method. I. Kinetics of Chloride and Phosphate Adsorption and Associated Charge at Constant Potential¹

by S. Gilman

General Electric Research Laboratory, Schenectady, New York (Received January 13, 1964)

A multipulse potentiodynamic (m.p.p.) method has been developed which allows the rapid determination of the extent of anion adsorption as a function of time at constant potential. The rapid kinetics of chloride and phosphate adsorption leads to diffusion control under our experimental conditions. An oxidative current is found to flow during the rapid adsorption of chloride from solution at 0.7 v. This current may correspond to a change in valence state of the surface.

Introduction

Adsorption of anions on platinum has previously been studied by a variety of nonvoltammetric techniques. These methods, most commonly applied to platinized platinum, include: (1) observation of the effect of anion adsorption on hydrogen deposition^{2,3}; (2) measurement of the electrode potential shift resulting on addition of the adsorbable ion to a solution of sulfuric or perchloric acids⁴⁻⁶; (3) measurement of the pH or conductivity change of a relatively small volume of liquid, caused by displacement of hydrogen ions from the ionic double layer by anions⁷; (4) direct determination by quantitative analysis of anions lost from solution⁸; and (5) direct determination of anion surface concentration by means of radioactive tracers.⁹⁻¹¹ The results reported for any particular anion vary with surface preparation, pH, potential, etc. One fairly clear-cut conclusion is that the halide ions specifically adsorb, with the extent of adsorption increasing as one descends down the series to the higher atomic weights.¹² Perchlorate ion is assumed to adsorb very slightly or not at all.

Recently, Breiter¹³ made measurements of the capacity of a smooth platinum wire in perchloric-hydrochloric acid solutions under the conditions of periodically varying potential. This method served to bring the electrode to a more reproducible surface state than generally accomplished in the nonvoltam-

metric measurements of his predecessors. One disadvantage of the method is that it suffers from the inability to assign quantitative interpretation to the measured capacities.

The purpose of this study was to develop methods for the study of ion adsorption along the same lines as previously applied to CO¹⁴⁻¹⁶ and "oxygen adsorp-

(1) This work was made possible by the support of the Advanced Research Projects Agency (Order No. 247) through the U. S. Army Engineer Research and Development Laboratories under contract No. DA-44-009-ENG-4909.

(2) (a) B. Ershler, *Acta Physicochim. URSS*, **7**, 327 (1937); (b) *Zh. Fiz. Khim.*, **13**, 1092 (1939).

(3) B. Ershler, G. Deborin, and A. Frumkin, *Acta Physicochim. URSS*, **8**, 565 (1938).

(4) A. Obrucheveva, *Zh. Fiz. Khim.*, **32**, 2155 (1958).

(5) A. Obrucheveva, *Dokl. Akad. Nauk SSSR*, **141**, 1463 (1961).

(6) A. Obrucheveva, *ibid.*, **142**, 859 (1962).

(7) A. Shlygin, A. Frumkin, and V. Medvedovsky, *Acta Physicochim. URSS*, **4**, 911 (1936).

(8) I. Kolthoff and T. Kameda, *J. Am. Chem. Soc.*, **51**, 2888 (1929).

(9) N. Balaschova, *Electrochim. Acta*, **7**, 559 (1962).

(10) N. Balaschova, *Z. physik. Chem. (Leipzig)*, **A207**, 340 (1957).

(11) K. Schwabe, *Electrochim. Acta*, **6**, 223 (1962).

(12) A. N. Frumkin, "Advances in Electrochemistry and Electrochemical Engineering," Vol. 3, John Wiley and Sons, Inc., New York, N. Y., 1963, Chapter 5.

(13) M. W. Breiter, *Electrochim. Acta*, **8**, 925 (1963).

(14) S. Gilman, *J. Phys. Chem.*, **66**, 2657 (1962).

(15) S. Gilman, *ibid.*, **67**, 78 (1963).

(16) S. Gilman, *ibid.*, **67**, 1898 (1963).

tion."¹⁷ Such a "multipulse potentiodynamic" approach has the advantage, when successfully applied, of providing simple initial boundary conditions and allowing for quantitative interpretation of data. Two anions of different nature were chosen for this study. Chloride is highly adsorbed and is an oxidizable ion. Phosphate is relatively slightly adsorbed and is non-oxidizable. The study resulted in development of the desired quantitative methods for measurement of anion adsorption. These methods permit the measurement of kinetics of adsorption and desorption, and determination of equilibrium surface coverages as a function of potential. Part I of this series will deal mainly with the development of methods and with the study of adsorption kinetics. Part II will deal mainly with determination of equilibrium surface coverages. The solutions studied were 1 *N* in perchloric acid and relatively dilute in hydrochloric or phosphoric acid.

Experimental

Equipment and Chemicals. The electronic equipment, glassware, and electrodes have been described previously.¹⁴ The working electrode was a length of C.P. platinum wire of 0.064 cm.² geometric area. The saturation hydrogen coverage, Q_{H}^{S} , determined as previously described¹⁵ was 0.272 mcoulomb/cm.², suggesting a roughness factor of approximately 1.3. Q_{H}^{S} was not found to vary appreciably during the measurements, suggesting little or no etching of the surface in the dilute solutions used under pulsed conditions. The working electrode was treated with hot chromic acid cleaning solution for several minutes and thoroughly washed in distilled water before each day of experimentation. Solutions were made with permanganate-treated, triply distilled water and A.R. grade perchloric, hydrochloric, and phosphoric acids. All measurements were made in a bath thermostated to 30°. All potentials are referred to a reversible hydrogen electrode in 1 *N* perchloric acid. Graphical areas were measured using an Ott polar planimeter.

Procedure. The potential functions employed are diagrammed in Fig. 1. The procedure during each step of each sequence is summarized in Table I along with the significance of the procedure. All HCl solutions were made using a stock solution of 1 *N* perchloric acid.

Results and Discussion

I. Establishment of a Reproducible Surface Condition. The general requirements of a surface pretreatment are: (1) removal of previously adsorbed species, including impurities originally dissolved in the electrolyte; (2) protection (blocking) of the surface against the readsorption of material while the solution

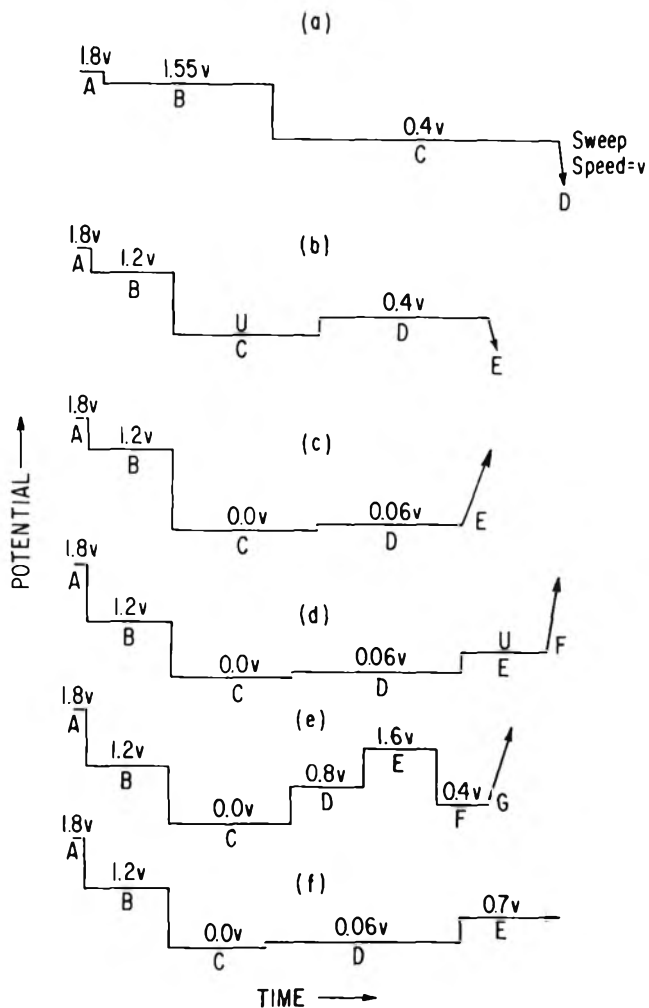


Figure 1. Potential-time sequences applied to the working electrode.

near the surface is being brought into concentration equilibrium with the bulk; (3) rapid removal of the "surface protection" of (2), so that adsorption may commence from essentially zero time. These requirements are met for a solution of 1 *N* perchloric acid of ordinary purity¹⁵ by means of sequence I of Table I.

The criteria previously employed for a reproducibly clean surface are constancy of (1) saturation hydrogen coverage, Q_{H}^{S} ,^{15,17} (2) "oxygen adsorption," Q_{O} ,^{15,17} and (3) differential electrode capacity.¹⁷ According to these criteria the surface is reproducibly clean (to within a few per cent of fractional surface) for 10 msec. $< T_c < 10$ sec. in an unstirred solution without pre-electrolysis, and for longer periods of time employing pre-electrolysis with an auxiliary electrode.¹⁵ It is not possible to use sequence I of Table I for the study of

(17) S. Gilman, *Electrochim. Acta*, 9, 1025 (1964).

Table I: Procedures Followed during Potential Sequences

Se- quence no.	Fig. no.	Step no., refers to Fig.	Procedure	Purpose
I	1a	A	(1) Bubble argon through solution with paddle stirring for 15 sec.	(1) To remove previously adsorbed species from the electrode surface and to deposit passive "oxygen" film which hinders readsorption
		B	(2) Bubbling and stirring continued for 0.5 min. Solution allowed to become quiescent for 1.5 additional min.	(2) To retain passive film deposited during step A, while sweeping away rejected impurities and molecular oxygen generated in step A. Final quiescence of solution limits mass transport to linear diffusion (at small values of time)
		C	(3) The solution is unstirred. Step C is chosen of duration T_c	(3) The passive film is largely reduced during the first few milliseconds, exposing a reproducibly clean surface
		D	(4) Apply linear cathodic pulse of sweep speed v . Measure current-time trace	(4) To measure the charge corresponding to hydrogen deposition for any time, T_c
II	1b	A	(1) Bubble argon through solution with paddle stirring for 2 sec.	(1) To remove previously adsorbed species from the surface (other than large quantities of anions), and to deposit "passive oxygen" on the surface which protects surface against readsorption
		B	(2) Continue bubbling and stirring for 15 sec.	(2) To retain passive film while molecular oxygen and other impurities from step (A) are swept away and diluted. The potential is too low for discharge of chloride ions
		C	(3) Bubble and stir for additional 0.5 min. Allow solution to become quiescent for 1.5 min.	(3) The passive film is largely reduced during the first few msec. when U is chosen less than 0.4 v. At sufficiently low values of U (less than ~ 0.06 v.) anions are desorbed and swept away while stirring. Also deposited hydrogen serves to block the surface against adsorption. Allowing the solution to become quiescent limits the rate of mass transport to ordinary diffusion
		D	(4) Step D is of 10-sec. duration	(4) Adsorbed hydrogen is removed within the first few msec. Dissolved hydrogen is depleted to some small calculable level
		E	(5) Apply cathodic linear sweep of speed $v = 30$ v./sec., and measure resulting current-time trace	(5) To measure the charge corresponding to hydrogen deposition under these conditions of electrode pre-treatment
III	1c	A	(1) Same as II(1)	(1) Same as II(1)
		B	(2) Same as II(2)	(2) Same as II(2)
		C	(3) Bubbling and stirring continued for 0.5 min. Allow solution to become quiescent for 1.5 min.	(3) Passive oxygen film is reduced and adsorbed chloride is desorbed. A monolayer of adsorbed hydrogen helps block the surface against the adsorption of impurities. The potential is too low for the adsorption of the anions under study
		D	(4) Step D is of 10-sec. duration	(4) The concentration of dissolved hydrogen adjacent to the surface is gradually reduced toward a value corresponding to equilibrium with 0.01 atm. of hydrogen. This makes the hydrogen oxidation current negligible in the next step
		E	(5) Apply linear anodic sweep of speed v , and measure current-time trace	(5) ΔQ_0 and hence the amount of anion adsorbed may be measured from the traces obtained

Table I (Continued)

Se- quence no.	Fig. no.	Step no., refers to Fig.	Procedure	Purpose
IV	1d	A-D	(1)-(4) Same as for sequence III	(1)-(4) Same as for sequence III
		E	(5) Potential step of duration T_E	(5) To allow anions to adsorb at potential U under well-defined conditions
		F	(6) Apply anodic linear sweep of speed v , and measure resulting current-time trace	(6) The current-time traces may be interpreted to reveal the extent of adsorption at potential U during preceding step
V	1e	A-C	(1)-(3) Same as for sequence III	(1)-(3) Same as for sequence III
		D	(4) Solution unstirred. Step of 10-sec. duration	(4) To adsorb anions corresponding to the maximum surface coverage for 0.8 v.
		E	(5) Step E applied for time interval T_E	(5) To test possible oxidation or repulsion of the anions adsorbed at 0.8 v.
		F	(6) Step F applied for 10 msec.	(6) To sufficiently reduce "oxygen" deposited in the previous step so that no correction need be made for "oxygen" in step G
		G	(7) Apply step G with $v = 1000$ v./sec. Measure the resulting current-time trace	(7) To determine if step E has exerted an effect on the trace obtained during step G
VI	1f	A-D	(1)-(4) Same as III, steps 1-4	(1)-(4) Same as III, steps 1-4
		E	(5) Step E applied and left "on" indefinitely. The resulting current-time trace is recorded in the presence and in the absence of dissolved chloride	(5) To measure the flow of current which accompanies adsorption of chloride at 0.7 v.

anion adsorption since considerable surface coverage with the anion will result during step C due to the positive potential involved. Therefore, a modified scheme had to be developed. In sequence II of Table I, a brief treatment at 1.8 v. serves to clean oxidizable impurities off the surface while minimizing the extent of chloride discharge. Step B serves to transport away and dilute any oxygen or chlorine (in the presence of HCl) produced during step A. The potential of step B is too low for additional release of either oxygen or chlorine. In step C, the potential is chosen so that θ_{Cl^-} (fractional surface coverage with specifically adsorbed chloride) is zero and so that adsorbed atomic hydrogen serves as a protective film against impurity adsorption while the solution is vigorously stirred for equilization of solution concentrations. To determine the efficacy of steps A-C of sequence II, the potential was next brought to 0.4 v. in step D. At this potential, adsorbed hydrogen is immediately removed from the surface, and adjacent dissolved hydrogen is gradually depleted. In step E, a cathodic linear potential sweep was applied and the charge corresponding to hydrogen deposition Q_H was measured in the usual way.¹⁵ The values of Q_H obtained in this manner for different

values of U in 1 *N* perchloric acid (absence of Cl^-) are compared with Q_H^S (obtained by means of sequence I $T_c = 10$ msec.) in Table II. It is seen that Q_H has a value within 2% of Q_H^S if $U \leq 0.02$ v., and decreases sharply above this potential. The larger values of Q_H obtained are ascribed to the action of the (nearly) complete hydrogen layer and perhaps the negative potential in preventing adsorption of impurities from solution. It should be noted that when potential U of sequence II is taken as 0.4 v., we have a sequence identical with I with $T_c = 130$ sec. with intensive stirring during the

Table II: The Variation in Hydrogen Deposition with Pretreatment Potential U , Sequence II, Table I

U , v.	$\frac{Q_H^S - Q_H}{Q_H^S} \times 100$, %
-0.04	0.0
0.00	1.6
+0.02	2.0
+0.05	10.0
+0.10	19.0
+0.40	19.4

first 30 sec. As already noted, noticeable decrease in Q_H are observed for $T_e > 10$ sec., with no stirring, under these conditions.

If "oxygen adsorption" is measured by substituting an anodic linear sweep for the negative sweep of step E, no variations of Q_o (area under the "oxygen adsorption" curve) is observed for $U \leq 0.02$ v.

While pre-electrolysis was found to increase the period of constancy of $Q_H^{S,15}$ by sequence I, Table I, it was actually found to have the reverse effect when sequence II was used. This is probably due to conversion of original impurities to impurities which have a greater tendency to adsorb at potentials below 0.4 v. (step C of sequence II). Hence, pre-electrolysis was not further employed in this study.

II. Chloride Adsorption and Discharge during an Anodic Linear Potential-Time Sweep. Sequence III of Table I was used in this study. (Steps A, B, and C were adjusted to the potentials and duration which led to a reproducible surface state in section I. Step D was introduced to minimize the concentration of dissolved hydrogen during the next step.) The concentration of HCl in 1 N perchloric acid, was varied from 0 to 0.1 N for any value of the sweep speed, v . A concentration sequence for $v = 40$ v./sec. appears in Fig. 2. Traces for 0.1 N HCl and $v = 4$ and 40 v./sec. appear in Fig. 3. In Fig. 2 for zero HCl concentration, we obtain the usual current-potential trace for platinum in 1 N perchloric acid.¹⁸ Excluding double-layer charging, the currents (and area in millicoulombs) lying to the left of 0.4 v. are due to oxidation of adsorbed hydrogen and hydrogen dissolved in the solution adjacent to the electrode. The currents (and area) to the right of 0.8 v. are due to "oxygen adsorption" (and finally, oxygen evolution) on the surface. As the concentration of HCl is increased, both the hydrogen and oxygen regions are affected. These will be discussed separately.

A. Hydrogen Region. The effect of increasing Cl^- concentration on the hydrogen region is to make the curve shift towards the left and to increase the size of the maxima. Such qualitative effects have already been observed in experiments employing periodic potential-time sweeps¹³ and in the measurement of charging curves.¹² The hydrogen maxima are generally regarded as an expression of surface heterogeneity.¹² The shifts in the hydrogen maxima with the adsorption of anions are generally regarded as due to changes in the heat of adsorption of hydrogen.¹² The largest effects upon the hydrogen region in Fig. 2 are observed for 0.01 N HCl. The equilibrium surface concentration of adsorbed chloride depends only on the potential at fixed concentration and the rate is determined by mass transport.¹⁹ Further the dependence of

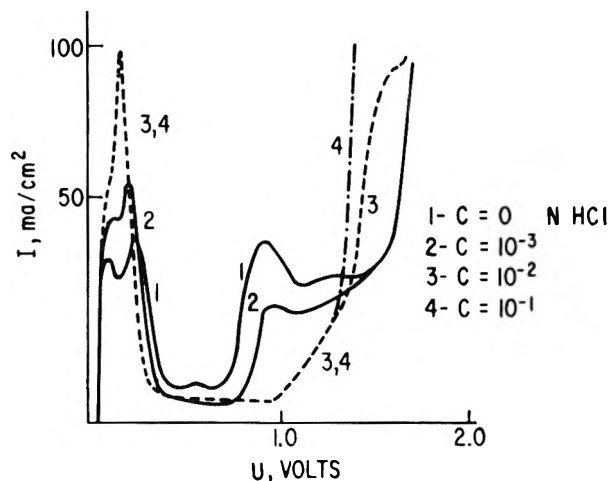


Figure 2. Anodic current-potential traces obtained for HCl solutions in 1 N perchloric acid using sequence III, Table I; sweep speed, $v = 40$ v./sec.

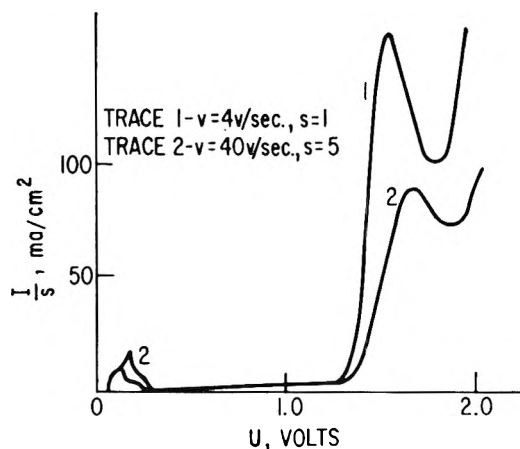


Figure 3. Anodic current-potential traces obtained for 0.1 N HCl in 1 N perchloric acid, using sequence III, Table I.

surface coverage on concentration of the solution is slight.¹⁹ Hence, the significance of traces 3 and 4 is that approximately equilibrium surface coverage is achieved at these concentrations (0.01 and 0.1 N HCl) whereas it is not for trace 1 (0.001 N HCl).

At equilibrium, $\theta_{Cl^-} = 0$ at $U = 0.06$ v.,¹⁹ which is the potential at which these anodic sweeps were initiated. An important question is whether the total amount of hydrogen deposited on the surface at $U = 0.06$ v. and removed during the sweep is affected by chloride adsorption. To investigate this possibility, the anodic traces for $v = 40$ and 400 v./sec. were

(18) F. G. Will and C. A. Knorr, *Z. Elektrochem.*, **64**, 258 (1960).

(19) S. Gilman, part II of this series, *J. Phys. Chem.*, **68**, 2112 (1964).

Table III: Charge, Q_H' , Passed in the Region $0.06 \leq U \leq 0.7$ v. of the Current-Potential Curve (see Fig. 2)

n, v./sec., step E, sequence III, Table I	Concn. HCl, N	Q_H' , mcoulomb/ cm. ²	
40.0	0	0.324	} Av. = 0.325, } av. deviation = } $\pm 0.3\%$
40.0	0.0100	0.326	
40.0	0.100	0.324	
400	0	0.312	} Av. = 0.311, } av. deviation = } $\pm 1.2\%$
400	0.00100	0.304	
400	0.0100	0.312	
400	0.100	0.316	

integrated from 0.06 to 0.7 v. The upper potential was chosen large so as to include any possible overlap of hydrogen into the "double-layer region." Values of total charge Q_H' are summarized in Table III. From the table, we see that Q_H' remains constant to within an average deviation of 0.3% at 40 v./sec., and to within an average deviation of 1.2% at 400 v./sec. The quantity Q_H' includes charge corresponding to the oxidation of hydrogen deposited at 0.06 v. and to the charging of the ionic double layer.^{12,13} It appears that Q_H' also includes some charge corresponding to a change in valence of the surface (see section VI). This latter quantity can contribute a maximum of approximately 8% to Q_H' and must be compensated for by combined decreases in the electrode capacitance and in the amount of hydrogen adsorbed at 0.06 v. for Q_H' to remain constant. Hence, the amount of hydrogen deposited at 0.06 v. must stay constant to within 8% as the concentration of dissolved chloride increases.

B. "Oxygen Adsorption" Region. The maximum values of θ_{Cl^-} obtained for potentials above 0.8 v. are approximately the equilibrium values for 0.8 v.¹⁹ Smaller values of θ_{Cl^-} are determined by the rate of mass transport.¹⁹ Hence, for traces 3 and 4 of Fig. 2 we might judge that the similarity of the traces in the oxygen adsorption region are due to maximum values of θ_{Cl^-} . Trace 2 differs from traces 3 and 4 because of the smaller θ_{Cl^-} values obtained. We see that for trace 2, total oxidation current up to 1.6 v. is noticeably decreased, compared with trace 1 (no chloride). Retardation of platinum surface oxidation by chloride was previously observed by Ershler.²⁰ Traces 1 and 2 merge in the high-current region where oxygen is evolved. For traces 3 and 4, we see that although the surface oxidation current is even more drastically reduced below approximately 1.3 v., additional current is passed at higher potentials. Traces 1 and 2 of Fig. 3 reveal that this additional current reaches a maximum

at ~ 1.5 v. for $v = 4$ v./sec., and obviously corresponds to the evolution of molecular chlorine ($E_o = 1.36$).²¹ From $v = 4$ v./sec. (trace 1, Fig. 3) to $v = 40$ v./sec. (trace 2, Fig. 3), the peak current rises only as the square root of 8 rather than 10, as predicted for linear diffusion under conditions of continuously varying potential.²² Also the calculated peak currents are only 0.6 of the calculated maximum value, indicating partial kinetic control of the chloride discharge reaction under these conditions.

In summary, we see that the effect of dissolved chloride ion on the anodic current potential curves described in sections A and B above is: (1) chloride adsorbs in the hydrogen region and affects the shape of the curve, but not the total amount of hydrogen deposited (to within 8%); (2) chloride adsorbs on the surface and decreases the amount of "oxygen" deposited, Q_o ; (3) chloride is oxidized to chlorine and provides additional charge, Q_{Cl_2} , at potentials above 1.3 v. The scheme employed in the remainder of this study is to increase the sweep speed v , relative to the concentration of HCl so that Q_{Cl_2} becomes negligible compared with ΔQ_o . Then ΔQ_o is used as a measure of θ_{Cl^-} .

III. Measurement of Fractional Surface Coverage with Chloride Ion through Measurement of $\Delta Q_o'$. We saw in section IIB that during an anodic sweep, adsorbed chloride tended to cause a decrease in surface oxidation charge, ΔQ_o , and to provide additional charge Q_{Cl_2} due to chlorine evolution. The experiments described above are further complicated by the fact that adsorption occurs over the entire range of potentials covered by the potential sweep rather than at fixed potential. Hence, modification of the procedure is required in order to obtain more quantitative information on chloride adsorption. This is accomplished by means of sequence IV of Table I, using a solution of 10^{-4} N HCl in 1 N perchloric acid.

In step C of sequence IV, the surface is completely bare of Cl^- . This is established by noting that the same current-time trace (for higher values of v) may be obtained during step F both in the presence and absence of dissolved chloride (see also ref. 19). During step D, dissolved hydrogen is depleted so that the hydrogen oxidation current will be negligible during step F. In step E, the potential is raised to $U = 0.7$ v., and adsorption of chloride is allowed to occur at constant potential either for 10 sec. (resulting in the equilibrium value of θ_{Cl^-} for this potential) or for 10 msec. ($\theta_{Cl^-} = \sim 0$).

(20) B. Ershler, *Zh. Fiz. Khim.*, **14**, 357 (1940).

(21) N. A. Lange, "Handbook of Chemistry," 10th Ed., McGraw-Hill Book Co., New York, N. Y., 1961.

(22) P. Delahay, "New Instrumental Methods in Electrochemistry," Interscience Publishers, Inc., New York, N. Y., 1954.

Finally sweep F is applied and the current-time trace recorded. If v is sufficiently large, additional adsorption or discharge of chloride during the sweep will be negligible compared with the charge equivalent of θ_{Cl^-} for $U = 0.7$ v. To determine a minimum suitable range for v , let us assume semi-infinite linear diffusion of Cl^- to the surface. Then the rate of transport of Cl^- to the surface, expressed as a current, I_{Cl^-} , will be²³

$$I_{\text{Cl}^-} = nFAD_{\text{Cl}^-}^{1/2}C_{\text{Cl}^-}/\pi^{1/2}t^{1/2} \quad (1)$$

and the corresponding charge Q_{Cl^-} is

$$Q_{\text{Cl}^-} = \int_0^t I_{\text{Cl}^-} dt = 2nFAD_{\text{Cl}^-}^{1/2}C_{\text{Cl}^-}t^{1/2}/\pi^{1/2} \quad (2)$$

where n = number of electrons involved in the process following transport, F = Faraday constant, A = electrode area in $\text{cm}^2 = 0.064$, D_{Cl^-} = diffusion constant of $\text{Cl}^- = 2.03 \times 10^{-5} \text{ cm}^2/\text{sec}$. (25° value used²⁴), C_{Cl^-} = concentration of Cl^- in moles/ cm^3 , t = diffusion time in sec. Choosing $C_{\text{Cl}^-} = 10^{-7}$ mole/ cm^3 , $t = T_F$ (duration of sweep F, sequence IV), and $n = 1$ (chloride discharge reaction), then the maximum charge due to chlorine evolution during sweep F, Q_{Cl_2} , is,

$$Q_{\text{Cl}_2} = Q_{\text{Cl}^-} = 0.05T_F^{1/2} \text{ mcoulomb}/\text{cm}^2 \quad (3)$$

Assuming that $Q_{\text{H}}^{\text{S}} = 0.3 \text{ mcoulomb}/\text{cm}^2$ is equivalent to a (hypothetical) full monolayer of chloride ions, we might attempt to limit Q_{Cl_2} to $0.003 \text{ mcoulomb}/\text{cm}^2$, and correspondingly limit T_F to 4 msec.

Figure 4 shows the results obtained for $v = 9, 90,$ and 900 v./sec . The top trace for each value of v is obtained for $T_E = 10 \text{ msec}$. (virtually no adsorption of Cl^- at 0.7 v .) and the bottom trace for $T_E = 10 \text{ sec}$. The hatched area between traces will be called $\Delta Q_o'$. Then

$$\Delta Q_o' = \Delta Q_o + \Delta Q_o'' + Q_{\text{Cl}_2} + Q_{\text{Cl}_2}' + \Delta Q_{\text{cap}} \quad (4)$$

where ΔQ_{cap} = the difference in capacitive charge included under the upper and lower traces of Fig. 4; ΔQ_o = diminution of Q_o caused by chloride adsorbed at 0.7

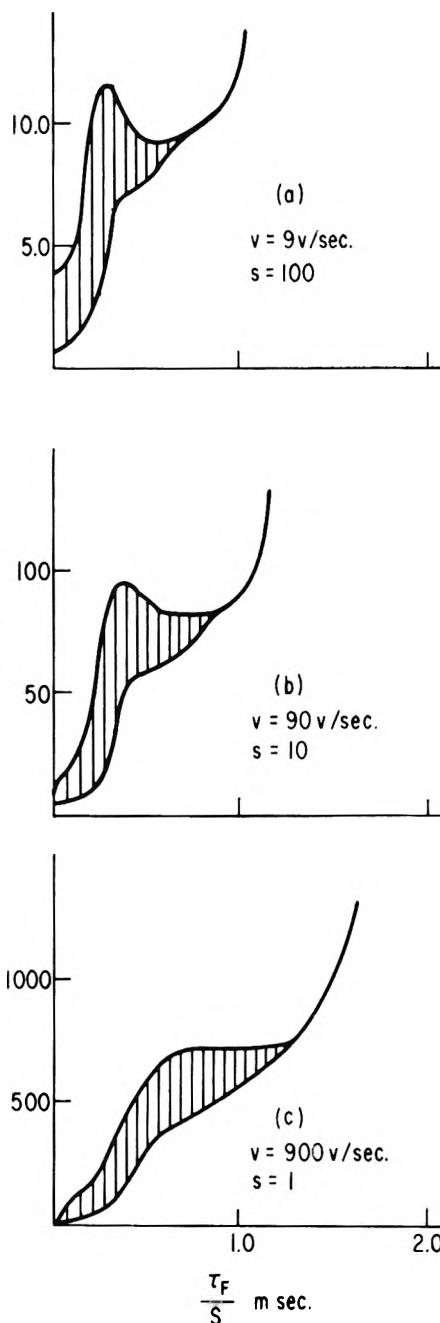


Figure 4. "Oxygen adsorption" traces obtained in the presence of $10^{-4} N$ HCl in $1 N$ perchloric acid, using sequence IV, Table I. The upper traces were obtained for an adsorption time, T_E , of 10 msec . The lower traces were obtained for $T_E = 10 \text{ sec}$. The hatched areas are values of $\Delta Q_o'$.

v ; $\Delta Q_o''$ = additional diminution of Q_o caused by chloride adsorbed during sweep F; Q_{Cl_2} = charge

Table IV: Frequency Dependence of $\Delta Q_o'$

v , v./sec.	$\Delta Q_o'$, mcoulomb/ cm^2
1800	0.228
900	0.226
180	0.222
90	0.224
36	0.224
18	0.238
9	0.238

(23) H. A. Laitinen and I. M. Kolthoff, *J. Am. Chem. Soc.*, **61**, 3344 (1939).

(24) R. Parsons, "Handbook of Electrochemical Constants," Butterworth and Co. Ltd., London, 1959.

corresponding to discharge of chloride transported to the electrode during sweep F; $Q_{Cl_2}' =$ charge corresponding to discharge during sweep F of chloride adsorbed at $U = 0.7$ v. It will be demonstrated below that $Q_{Cl_2}' = 0$. Therefore, as v is increased $\Delta Q_o'$ ought to be expected to approach $\Delta Q_o + \Delta Q_{cap} \approx \Delta Q_o$ since all the remaining terms depend on mass transport. Table IV summarizes the results for a wide range of values of the sweep speed, v . At $v = 180$ v./sec., the duration of the sweep is approximately 4 msec., which eq. 3 suggested for virtual elimination of transport considerations. However, we see that $\Delta Q_o'$ remains constant to within 1% average deviation down to $v = 36$ v./sec. ($T_F = 30$ msec.) and does not increase greatly down to $v = 9$ v./sec. This large range of constancy (where $\Delta Q_o' \sim \Delta Q_o$) is likely due in part to two factors. (1) Adsorption during step F occurs during both the sweep corresponding to $T_E = 10$ msec. and 10 sec. Since $\Delta Q_o'$ is given by the difference in area under these sweeps, the adsorptions tend to cancel each other. (2) The partial surface oxidation which occurs during the early part of sweep F tends to repress further adsorption of chloride during the remainder of the sweep and hence effectively reduces T_F . The results suggest that ΔQ_o is a quantity which may be precisely measured over a large range of values of v .

IV. *Kinetics of Adsorption of Chloride Ion from Solution at Constant Potential.* In section III, it was shown that adsorption of chloride ion at 0.7 v. caused a decrease in "oxygen adsorption" as measured by application of a subsequent anodic potential-time sweep of sufficient speed v . By means of sequence IV of Table I it is possible to measure ΔQ_o as a function of adsorption time, T_E at potential U . A solution of 10^{-3} N HCl in 1 N perchloric acid was chosen since at this concentration of chloride adsorption is virtually complete within 100 msec., allowing us to assume the conditions of semi-infinite linear diffusion even for our wire electrode. A sweep speed $v = 1000$ v./sec. was chosen. The 1-msec. duration of this sweep provides an effective maximum uncertainty of less than 1 msec. on the time scale, and becomes negligible (because of dependence on the square root of time) after the first few msec. A sequence of current-time traces for various values of T_E appear in Fig. 5. ΔQ_o for any value of T_E is taken as the area enclosed by the trace for that value of T_E , by the trace for $T_E = 0$ (measured in absence of chloride ion), and the dashed line. A plot of ΔQ_o vs. $T_E^{1/2}$ appears in Fig. 6 where excellent linearity is apparent. If we assume that ΔQ_o is determined by mass transport, then

$$\Delta Q_o = Q_{Cl^-} \quad (5)$$

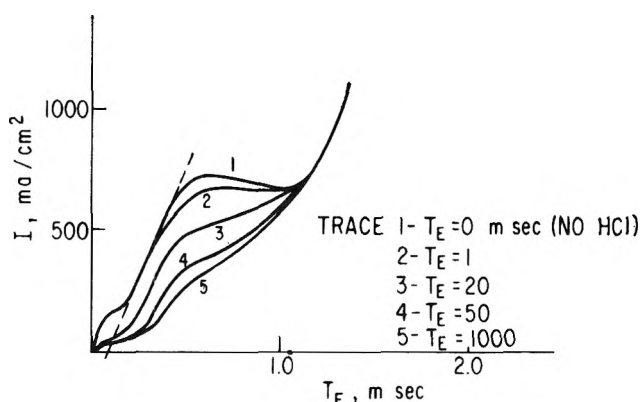


Figure 5. Sequential "oxygen adsorption" traces for 10^{-3} N HCl in 1 N perchloric acid at $U = 0.7$ v.; traces obtained by means of sequence IV, Table I. ΔQ_o for any value of T_E is obtained by measurement of the area bounded by trace 1, the dashed line, and the trace corresponding to T_E .

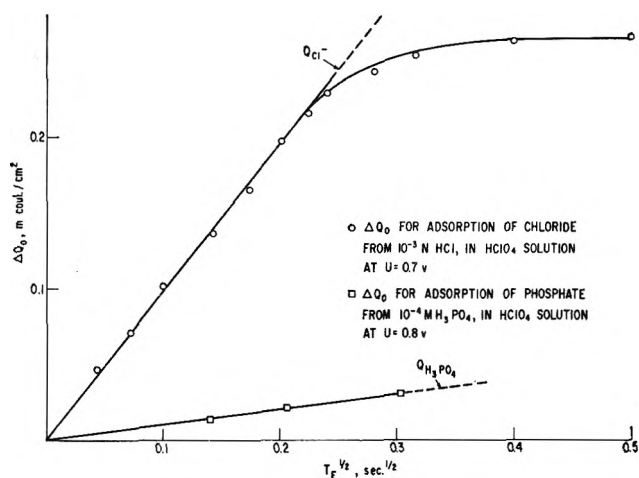


Figure 6. Analysis of the charge-time data obtained in the adsorption of chloride and phosphate from solution at constant potential.

where Q_{Cl^-} has been defined by eq. 2. Taking " t " of eq. 2 equal to T_E and $n = 2$ (one equivalent of chloride prevents the "adsorption" of two equivalents of "oxygen") we obtain a linear plot of ΔQ_o vs. $T^{1/2}$ which exactly fits the experimental points of Fig. 6 up to high values of ΔQ_o . The results establish the measurement of ΔQ_o as a precise and linear measure of the amount of chloride ions adsorbed. This is further supported by the constancy of ΔQ_o with varying sweep speed (section III). Since the adsorption is diffusion controlled even in the several msec. range, the rate constant for the adsorption may not be obtained. It may merely be said to exceed the usual limitation of the multipulse potentiodynamic method,¹⁵ i.e., 1 cm./sec. ΔQ_o reaches a

plateau value of 0.267 mcoulomb/cm.², equivalent to the adsorption of 0.134 mcoulomb/cm.² of chloride ion.

Since the results presented above demonstrate a simple relationship between the amount of chloride adsorbed and the "adsorbed oxygen" film, it is in principle possible to determine the structure of the chloride adlayer from a knowledge of the "oxide" stoichiometry, and the extent of a full chloride monolayer. The latter information may not be obtained since "oxygen adsorption" limits chloride adsorption in the high potential range.¹⁹ The "oxide" stoichiometry is still a matter of controversy.

V. *The Anodic Current Associated with Chloride Adsorption.* The idea that chloride ion is specifically adsorbed on platinum, implicit in the work of previous investigations,¹⁻¹¹ is distinct from the suggestion recently made by Peters and Lingane^{25a} that a platinum chloride film is formed on the surface in hydrochloric acid solutions. The latter concept calls for the flow of oxidative charge (1 faraday of electricity/equivalent of chloride "adsorbed"). The structure of the two different species obtained in the absence and presence of an oxidative process may be generalized by



where S^0 and S^{m+} are platinum surface sites with the indicated valences. If S is taken as one-half a platinum atom and m is taken as one, we would have PtCl_2 stoichiometry, but not necessarily PtCl_2 structure. The direct test of whether structure A or B results upon "adsorption"^{25b} of chloride ions is to measure the flow of oxidative current during the adsorption, since only structure B requires the flow of noncapacitive current. Peters and Lingane^{25a} have reported that they do obtain chronopotentiograms indicating a Faradaic process between 0.55 and 0.85 v. (against a hydrogen electrode). The arrest is obtained only after employing a particular pretreatment sequence. On the other hand, Breiter¹³ did not observe a wave corresponding to platinum chloride formation, upon application of a continuous triangular potential-time sweep to his electrode.

In this work, as in Breiter's¹³ no discrete platinum chloride wave was observed (see Fig. 2) under the condition of measurement of chloride ion adsorption. Hence, if the surface does undergo valence change during or after the adsorption step at potentials lower than 0.8 v. and during the application of a linear anodic potential-time sweep, the corresponding current must be small and largely compensated for by a diminution of the charge stored on the surface as hydrogen and/or in

the ionic double layer as capacitive charge. To eliminate such compensating effects and to seek out a possible small oxidative current during adsorption of chloride ions, sequence VI of Table I was employed. This sequence employs our knowledge of the rate of chloride ion adsorption and of the maximum surface coverage with chloride ion at 0.7 v., to measure the small oxidative current which flows during the adsorption.

At the end of step D of sequence VI of Table I, the concentration of dissolved molecular hydrogen near the electrode surface corresponds to equilibrium with 0.01 atm. of hydrogen (Nernst equation). Assuming applicability of Henry's law, the effective concentration of hydrogen, C_{H_2} , is one-hundredth of the value at 1 atm. or 7.6×10^{-9} mole/cm.³.²¹ In step E, the electrode potential is raised to 0.7 v. and in the presence of chloride ion, five processes are possible: (1) oxidation of previously adsorbed hydrogen; (2) oxidation of dissolved molecular hydrogen; (3) adsorption of chloride ions accompanied by electron transfer; (4) dissolution of platinum; (5) discharge of the ionic double layer. Steps 2 and 3 are diffusion controlled. The current corresponding to step 2 is given by an equation similar to eq. 1. Taking $C_{\text{H}_2} = 7.6 \times 10^{-9}$ mole/cm.³, $D_{\text{H}_2} = 4.1 \times 10^{-5}$ cm.²/sec.,²⁶ and $n = 2$, we obtained for the diffusion current of molecular hydrogen

$$I_{\text{H}_2} = 0.0053T_E^{-1/2} \text{ ma./cm.}^2 \quad (6)$$

At the beginning of step E, the current which flows in the first 0.6 msec. both in the presence and absence of chloride ion is orders of magnitude larger than predicted by eq. 6 and hence corresponds mainly to the oxidation of previously adsorbed hydrogen. The area under the curve up to $T_E = 1$ msec. both in the presence and absence of dissolved chloride has the value 0.31 mcoulomb/cm.², which is close to the value obtained for Q_{H} in section IIA when $v = 400$ v./sec. (Table II). In the absence of dissolved chloride, the current in the 1-100-msec. range approaches the value given by eq. 6 and therefore corresponds entirely to the oxidation of molecular hydrogen. In the presence of dissolved HCl, electrode process 3-5 are possible in addition to (1) and (2) and we do indeed observe a "hump" in the current-time trace over a range of HCl concentrations

(25) (a) D. G. Peters and J. J. Lingane, *J. Electroanal. Chem.*, **4**, 193 (1962). (b) Adsorption in quotation marks is taken to signify the possibility of a buildup of a surface excess of ions with the passage of Faradaic current, so that a surface chloride is formed. The quotation marks will be dropped henceforth except for emphasis and the term will be used to signify a surface excess of anions with or without the passage of Faradaic current.

(26) G. Tammann and V. Jessen, *Z. anorg. allgem. Chem.*, **179**, 125 (1929).

(Fig. 7). The differences in current, ΔI , between traces 1 and 2 of Fig. 7a-d are plotted in Fig. 8 against $T^{-1/2}$. If " n " is taken as $1/2$ in eq. 1, the resulting value of I_{Cl^-} is the current which would flow if two equivalents of chloride ion "adsorbed" resulted in the flow of 1 faraday of oxidative charge. A plot of I_{Cl^-} vs. $T^{-1/2}$ appears in Fig. 8. It is observed that ΔI tends to approach I_{Cl^-} especially at the higher concentrations. In the paragraphs below, we will present arguments to support the conclusion that ΔI is a gross oxidative current corresponding to a change in valence of the surface platinum atoms (electrode process 3).

The sign and magnitude of the capacitive current which might flow during the adsorption of chloride ions at 0.7 v. must be estimated in order to gauge its contribution to ΔI . The total charge Q_c stored in the ionic double layer may be expressed in terms of the differential capacity C_θ

$$Q_c = \int_{U_0}^U C_\theta dU \quad (7)$$

where C_θ is the differential capacity for any fixed value of θ_{Cl^-} and is a function of U . U_0 is the value of U at the zero point of charge and depends on θ_{Cl^-} .

Then

$$I_c = \frac{\partial Q_c}{\partial t} = \frac{\partial}{\partial t} \left[\int_{U_0}^U C_\theta dU \right]_U \quad (8)$$

where I_c is the capacitive current which flows at constant potential due to adsorption of chloride ions. Experimental plots of C_θ vs. U are available^{13,17} for $\theta_{Cl^-} = 0$. Similar capacitance-potential plots for constant $\theta_{Cl^-} > 0$ are neither available nor easily derived. However, a plot¹³ of capacitance vs. potential where θ_{Cl^-} increases with potential reveals that the differential capacitance drops with increase of θ_{Cl^-} at any value of $U > \sim 0.4$ v. Hence, I_c must be negative, and the experimental values of ΔI obtained from Fig. 7 must be gross oxidative currents. It may be the negative capacitive current which is responsible for the smaller (than diffusion-controlled) values of ΔI at short times. This would tend to give the current-time traces of Fig. 7 the appearance of a maximum at short time. The total negative charge released by the double layer upon adsorption of the equilibrium amount of chloride ions is given by

$$\Delta Q_c = \int_a^{0.7} C_{\theta=0} dU - \int_b^{0.7} C_{\theta=\text{equilibrium}} dU \quad (9)$$

where " a " and " b " are for corresponding zero points of charge for the two different surface states and are assumed approximately equal. If we choose the values of capacity reported by Breiter¹³ for zero and 10^{-2} N HCl

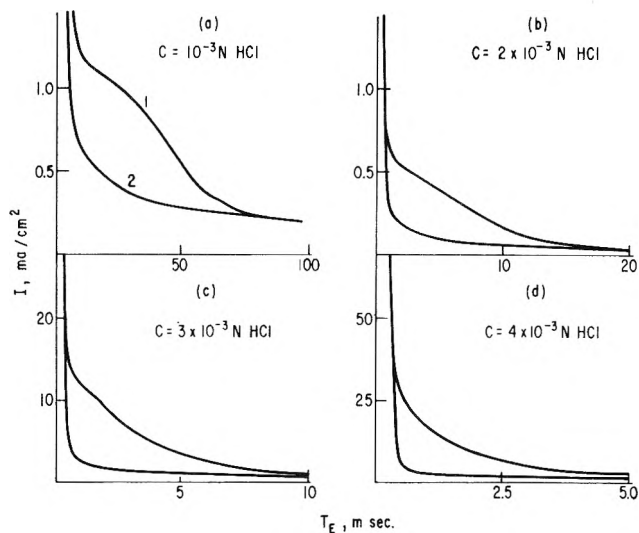


Figure 7. Transient current-time traces obtained at 0.7 v. in the presence (upper traces) and in the absence (lower traces) of dissolved chloride. Sequence VI, Table I, was employed.

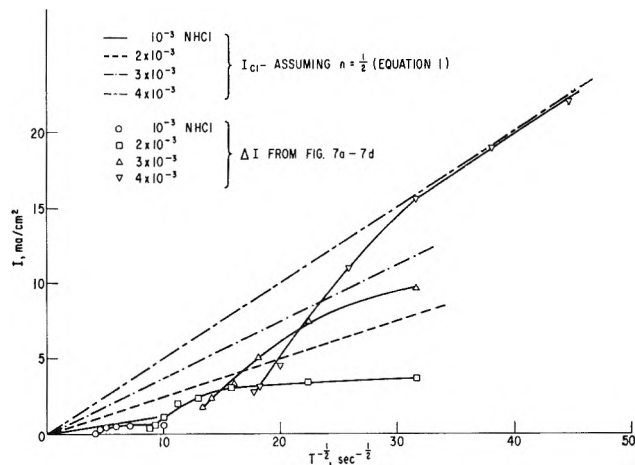


Figure 8. Analysis of the anodic current measured during adsorption of chloride ion at 0.7 v.

solutions in 1 N HClO₄, integration of the difference in capacities to a potential of 0.7 v. should give us a minimum value of ΔQ_c [since the values of θ_{Cl^-} in Breiter's experiments do not correspond to the (larger) equilibrium value for 0.7 v.]. The value of ΔQ_c so obtained is 0.016 mcoulomb/cm.². The integration of the charge between traces 1 and 2 of Fig. 7a-d results in a value of 0.027 mcoulomb/cm.² = $\int \Delta I dt$. The sum of the minimum estimated value of ΔQ_c and $\int \Delta I dt$ is 0.04 mcoulomb/cm.². This figure approaches the value of charge which would be passed if one electron were passed through the external circuit for each two chloride ions adsorbed, or $Q_o/4 = 0.06$ mcoulomb/cm.².

Hence, it is likely that the capacitive current can account for some of the deviations of the experimental points of Fig. 8 from the linear diffusion plot of I_{Cl^-} .

We have thus far established that during the adsorption of chloride ion at 0.7 v., an oxidative current flows corresponding approximately to 0.5 faraday/equivalent of chloride ion adsorbed. This flow of current must correspond to either electrode process 3 or 4. If dissolution of platinum (process 4) did occur, we would not expect the retardation of oxygen adsorption to follow linear diffusion laws precisely as observed in section IV. That dissolution is not a general problem when measurement is made in dilute HCl solution is not surprising. Ershler²⁷ measured dissolution rates which did not exceed a few tenths of a milliamper on a 30 cm.² electrode in an HCl solution as concentrated as 0.1 *N*. Having ruled out the other possibilities, we are led to the conclusion that the current which flows at 0.7 v. during the adsorption of chloride ions corresponds to formation of less than a monolayer of material with an average stoichiometry of SCl_2^- where the platinum surface site "S" has an effective valence of +1. In a sense, this resembles adsorption of chloride as a complex ion.

One may next inquire whether some such electron transfer occurs over the entire range of chloride adsorption, or simply ensues at some potential less than 0.7 v., as a reaction between previously adsorbed chloride and the zerovalent surface. Since the total amount of chloride "adsorbed" depends on the potential,¹⁹ studies at much lower potentials would involve even smaller passage of oxidative charge and become increasingly more difficult to follow. Studies of the oxidative current at potentials larger than 0.7 v., would involve correction for surface oxidation and again would become more difficult. Such extensions of this work must likely await improved knowledge of the necessary double-layer charging correction.

VI. *Further Consideration of the "Platinum Chloride" Wave.* As already indicated, Peters and Lingane^{25a} obtained a distinct chronopotentiogram for platinum in 1 *N* HCl in the potential range 0.55–0.85 (against reversible hydrogen) which they ascribed to the formation of $PtCl_2$. (No actual measurement of the ratio of chlorine to platinum was made however.) In this work, evidence was also found for a valence change in the surface platinum atoms at 0.7 v., which signifies that at least at this potential electron transfer accompanies ion adsorption. However, no distinct "chloride wave" appears in the voltammetric traces of Fig. 2 or in similar experiments by Breiter,¹³ although the "adsorption" of chloride is clearly detected in both cases. To help resolve the anomaly, sequence IV of

Table I was employed with $v = 4$ v./sec.; the concentration of HCl was 0.1 *N*. To duplicate the conditions of Peters and Lingane,^{25a} U was chosen at 0.246 v. (potential of the saturated calomel electrode). When the electrode was held at 0.246 v. for $T_E = 10$ sec., the trace obtained (trace 1 of Fig. 9) was similar to traces 3 and 4 of Fig. 2, exhibiting no discernible "chloride wave." When T_E was chosen as 15 min. with the solution stirred with a paddle stirrer, a wave (trace 2 of Fig. 9) did appear beginning at ~ 0.45 v. (maximum at 0.75 v.) and must correspond to the Peters and Lingane wave. The surface state of the recently pretreated electrode of trace 1 is usually referred to as "active" and that of trace 2 as "inactive."¹² A qualitative explanation of the two different voltammetric behaviors may be made on that basis.

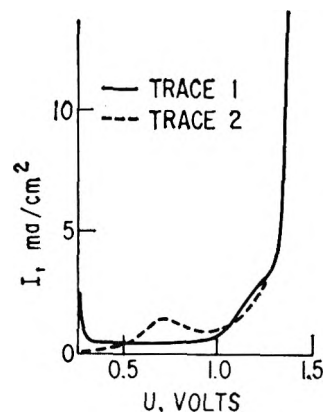


Figure 9. Anodic current-potential traces obtained for 0.1 *N* HCl in 1 *N* $HClO_4$ solution using sequence IV, Table I, $v = 4$ v./sec. The initial potential, $U = 0.246$ v. Trace 1, U held for $T_E = 10$ sec.; trace 2, U held for $T_E = 15$ min.

(1) In trace 1 of Fig. 8 the current measured in the potential range between approximately 0.3 and 0.95 v. corresponds to a slight amount of hydrogen atom discharge, double-layer charging, and electron transfer involving chloride ions. These charges are all small (compared with a monolayer of hydrogen), and merge, resulting in an almost constant current, and no obvious "wave."

(2) In trace 2 of Fig. 9, the "inactive" electrode has no hydrogen adsorbed on its surface (note the appearance of a small hydrogen peak at 0.25 v. in trace 1, and its absence in trace 2). Further, the capacitance of the "inactive" electrode is quite small¹⁷ as is verified by observing that the current which flows between 0.25 and 0.45 v. of trace 2 is extremely small. Therefore,

(27) B. Ershler, *Acta Physicochim. URSS*, **19**, 139 (1944).

no appreciable current flows until the "chloride wave" commences at 0.45 v. While adsorption of chloride commences from 0.125 v. on the "active" electrode,¹⁹ it is possible that no adsorption of chloride occurs on the "inactive" electrode below 0.45 v., with or without the passage of charge.

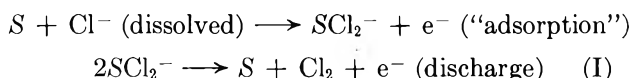
Gilman^{15,17} has presented evidence that the several manifestations of platinum surface "inactivity" (reduction in capacitance, decrease in hydrogen adsorption, higher overvoltage for oxygen "adsorption") may be correlated with adsorption of impurities from the solution during the first 1000 sec. following electrode pretreatment. Further work would be required to test the same hypothesis on the system involving chloride ions.

VII. Nonoxidizability of Preadsorbed Chloride at Elevated Potentials. By means of sequence V, Table I, chloride was adsorbed at 0.8 v. from a $10^{-4} M$ solution of HCl in 1 *N* perchloric acid (step D). The potential was then brought to 1.6 v. for a period of time, T_E . The "adsorbed oxygen" on the surface was next reduced by means of a 10-msec. pulse at 0.4 v. (step F). When sweep G ($v = 1000$ v./sec.) was applied, the same trace was obtained for $T_E = 0$ or 10 sec., and the constant value of ΔQ_0 was 0.19 mcoulomb/cm.². This result suggests no noticeable oxidation of the preadsorbed chloride ions for $T_E = 1$ sec., subject to the following possibilities for re-adsorption of chloride ion during step F: (1) dissolved chloride may be adsorbed from the $10^{-4} M$ HCl solution; (2) chlorine gas produced by discharge of dissolved chloride ions during step E may be reduced back to dissolved chloride ions during step F and re-adsorbed; (3) chlorine gas generated by discharge of adsorbed chloride ions during step E may be reduced back to dissolved chloride ions during step F and re-adsorbed. We may immediately discard complications from possibilities (1) and (2) by noting that the total contribution of dissolved chloride and chlorine from these possibilities may not exceed that of 10^{-4} equiv./l. of HCl (the initial HCl concentration). From eq. 5 and 2, such a concentration of HCl can contribute only 0.01 mcoulomb/cm.² to Q_0 , which is small compared to the observed value of ΔQ_0 retained after step E. For possibility (3), if all of the adsorbed chloride ions were to be discharged early during step E, the resulting chlorine would tend to diffuse away during the remainder of the 10-sec. step. During the 10-msec. duration of step F, only a portion of the chlorine would have sufficient time to diffuse back to the surface where it could be reduced and re-adsorbed. The observed constancy of ΔQ_0 for $T_E = 0$ and 10 sec., argues against any such rapid discharge of adsorbed chloride ions during step E. This confirms the conclusion (al-

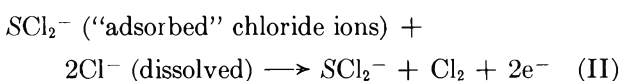
ready proposed in section III) that no appreciable oxidation of previously adsorbed chloride ions occurs during a fast linear anodic sweep (which is always chosen of duration much smaller than 1 sec.).

When a very small amount of chloride ions was pre-adsorbed from a $10^{-6} N$ HCl solution, some removal of the chloride at 1.8 v. was observed after 15 sec., suggesting some very small rate of removal for small values of chloride surface coverage. It is possible that this effect might involve an extremely slow rate of platinum dissolution, rather than simple discharge of adsorbed chloride ions.

The tendency of an adsorbed halide ion to resist discharge as the halogen might in general be ascribed to stabilization by the very forces that bind it to the surface. The evidence for actual change in valence of the surface at a potential of 0.7 v. (presented in section V) suggests that at potentials this great, or greater, a chloride-like species is formed on the surface. Hence, it is somewhat intuitive that simple oxidation of the chloride would no longer be possible. Since "adsorbed" chloride is found not to discharge at potentials above the value of E_0 for the chloride-chlorine couple (1.36 v.), the generation of molecular chlorine may not proceed through the mechanism

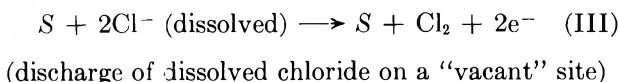


but may proceed by either of two alternative paths



(discharge of dissolved chloride ions on "adsorbed" chloride)

or



Arbitrary reaction orders were chosen for paths II and III.

It is well known¹² that the adsorbability of iodide ions on platinum is even greater than that of chloride ions. Osteryoung, *et al.*,²⁸ failed to detect the presence of adsorbed iodide on a platinum electrode by oxidation of iodide during application of an anodic linear sweep. This result need not be taken, as they suggests,²⁹ as evidence that iodide does not adsorb. An alternative explanation which does not contradict the previous

(28) R. A. Osteryoung, G. Lauer, and F. C. Anson, *J. Electrochem. Soc.*, **110**, 926 (1963).

literature¹² is that the iodide which *was already* adsorbed before application of each anodic pulse could not be removed during the anodic sweep as is the case for chloride ions. A reduction in the amount of oxygen "adsorbed" at higher potentials than used in their experiments would be anticipated on the basis of experience with the chloride system.

VIII. Kinetics of Adsorption of Phosphoric Acid from Perchloric Acid Solution. Experiments similar to those described for chloride ion in section IV were performed for a solution of $10^{-4} M$ phosphoric acid in 1 *N* perchloric acid. U of sequence IV was chosen at 0.8 v. Typical traces appear in Fig. 10. The maximum value of ΔQ_o , produced by phosphoric acid adsorption is approximately an order of magnitude less than that produced by chloride at 0.7 v., hence extreme reproducibility of the "oxygen adsorption" trace is required. This was accomplished by recalibration of the oscilloscope before each individual measurement and by measuring the reduction in oxygen adsorption for each subsequent time relative to the value obtained for $T_E = 10$ msec. Resulting values of ΔQ_o are plotted against $T_E^{1/2}$ in Fig. 6.

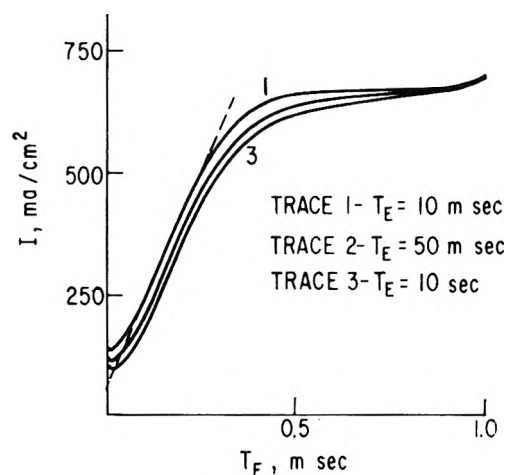


Figure 10. Sequential "oxygen adsorption" traces for $10^{-4} M$ phosphoric acid in 1 *N* perchloric acid at $U = 0.8$ v. Traces were obtained by use of sequence IV, Table I.

The plot is linear as was the case for chloride adsorption and again suggests diffusion control. For phosphoric acid, we can assume that it is undissociated acid which is transported to the electrode because of the strong acid conditions, and that conversion to the ionic form occurs either during or just preceding the adsorption step. We may then write an expression for ΔQ_o similar to eq. 5

$$\Delta Q_o = Q_{H_3PO_4} \quad (10)$$

$Q_{H_3PO_4}$ may be expressed by an equation similar to eq. 2

$$Q_{H_3PO_4} = 2nFAD_{H_3PO_4}^{1/2}C_{H_3PO_4}T_E^{1/2}/\pi^{1/2} \quad (11)$$

where, as before, n is the number of equivalents of "oxygen" retarded by the adsorption of 1 mole of ions. We have no previous knowledge of whether the ion adsorbs in the dihydrogen phosphate, monohydrogen phosphate, or phosphate form. Let us assume that it is the valence of the anion which determines the surface bond and hence the extent of retardation of oxygen "adsorption." Then since n has the value 2 for the singly-charged chloride ion, the corresponding value of n for the three different phosphate species might be $n = 2, 4,$ and $6,$ respectively. Hence, if we knew the diffusion constant for undissociated phosphoric acid under these conditions, we could determine n from the slope of the plot of Fig. 10. Unfortunately, the required diffusion constant is not known. However, the slope of the plot corresponds exactly to the value obtained using the diffusion constant for chloride ion and $n = 2$. To get the same result for $n = 4$ we would have to assume a diffusion constant for phosphoric acid $1/4$ that for chloride ion, which seems unlikely. Hence, the available evidence suggests that phosphoric acid adsorbs as the dihydrogen phosphate ion.

We have already seen that the gross anodic current which flows during the adsorption of chloride ion is equivalent to less than one-half the calculated diffusion current. Hence, the total charge passed is less than $\Delta Q_o/4$. For the very small amounts of phosphate ion adsorbed and the resulting small values of ΔQ_o measured, it would, at this time, be extremely difficult to measure a possible oxidative current.

Summary

(1) A pretreatment potential sequence has been devised for use in solutions containing adsorbable anions. The pretreatment results in an extremely reproducible electrode surface with zero initial surface concentration of the anion.

(2) Adsorption of chloride or phosphate ions causes a decrease in "oxygen adsorption," ΔQ_o , during an anodic linear potential-time sweep. ΔQ_o is constant over a wide range of sweep speeds and is directly proportional to the amount of anions adsorbed.

(29) After submission of this paper for publication, Osteryoung and Anson presented iodide radiotracer data at a Gordon Conference (February, 1964). These data lead them to conclude that iodide is indeed adsorbed during the application of an anodic linear sweep, but is not "electroactive." This seems to confirm the similarity of the chloride and iodide systems.

(3) The adsorption kinetics of chloride and phosphate ions is so rapid as to be diffusion controlled even in the millisecond range of observation.

(4) The addition of chloride ion to perchloric acid does not perceptibly alter the amount of hydrogen which may be deposited on the surface at 0.06 v.

(5) *Adsorbed* chloride ion is resistant to discharge as molecular chlorine at potentials well above the reversible chloride-chlorine potential both during the application of an anodic linear sweep, and when held at constant high potential. Phosphate ion is also not desorbed at high potentials.

(6) The oxidative current which flows during the adsorption of chloride ion at 0.7 v. appears to correspond to the formation of a surface complex ion. It is such stabilization of the anion which may possibly best explain the retardation of oxygen "adsorption" and of anion discharge.

Acknowledgment. The author is pleased to acknowledge the helpful assistance of R. W. Kopp and J. T. Adamchick. Thanks are extended to Drs. D. Vermilyea and M. W. Breiter for helpful discussions.

Studies of Anion Adsorption on Platinum by the Multipulse Potentiodynamic (M.p.p.) Method. II. Chloride and Phosphate Desorption and Equilibrium Surface Concentrations at Constant Potential¹

by S. Gilman

General Electric Research Laboratory, Schenectady, New York (Received January 13, 1964)

When a platinum electrode is allowed to adsorb chloride ions at 0.8 v. and the potential is then lowered, it is possible to follow changes in the "oxygen adsorption" trace as a function of desorption time at the lower potential. The results indicate that desorption is rapid and terminates at the equilibrium surface coverage for the lower potential. Since adsorption in the range $0 < U \leq 0.8$ v. is reversible, it is possible to measure equilibrium adsorption of chloride and phosphate ions as a function of solution concentration and potential in this range. The results for chloride ions suggest a Temkin adsorption isotherm. Because of irreversible "oxygen adsorption" above 0.8 v., the surface coverage with anions at any potential above 0.8 v. is a function of path and may vary from a maximum (corresponding to the equilibrium value for 0.8 v.) to zero. Studies of nonequilibrium adsorption in the high potential range indicate that increasing surface coverage with "oxygen" results in decreasing surface coverage with the anion.

Introduction

The preceding paper in this series² dealt with the development of an multipulse potentiodynamic (m.p.p.) method for the study of ion adsorption. This paper presents discussion of further adaptation of the m.p.p. method to provide information on ion desorption and equilibrium surface coverage over a wide range of conditions.

Experimental

Equipment and Reagents. Equipment, reagents, etc., have been described in the preceding paper.² As previously, solutions of hydrochloric or phosphoric acid were prepared by addition of the concentrated acid to a stock solution of 1 *N* perchloric acid. The working electrode was the same used previously² with $Q_{\text{H}}^{\text{S}} = 0.272$ mcoulomb/cm.².

Procedures. Potential sequences applied to the working electrode are diagramed in Fig. 1 (time durations are not to scale). The procedures employed during each step of Fig. 1 are summarized in Table I. As previously, all measurements were made at 30°, and all

potentials are referred to a reversible hydrogen electrode immersed in 1 *N* perchloric acid.

Results

I. Chloride Desorption Kinetics. Sequence I of Table I was employed in making these measurements. The solution studied was 10^{-4} *M* HCl in 1 *N* perchloric acid. The procedure followed through steps A–D of the sequence was intended to provide a clean surface free of adsorbed chloride ion and with the concentration of dissolved hydrogen in the adjacent solution extremely small. This latter condition is required to eliminate (effectively) the hydrogen oxidation current during the measurement of "oxygen adsorption" traces. Procedural steps 1–4 and 5a–7a result in obtaining a "blank" ($\theta_{\text{Cl}^-} = 0$) "oxygen adsorption" trace when sweep G is applied. Procedural steps 1–4 and 5b–7b result in the corresponding trace for the maxi-

(1) This work was made possible by the support of the Advanced Research Projects Agency (Order No. 247) through the U. S. Army Engineer Research and Development Laboratories under Contract No. DA-44-009-ENG-4909.

(2) S. Gilman, part I of this series, *J. Phys. Chem.*, **68**, 2098 (1964).

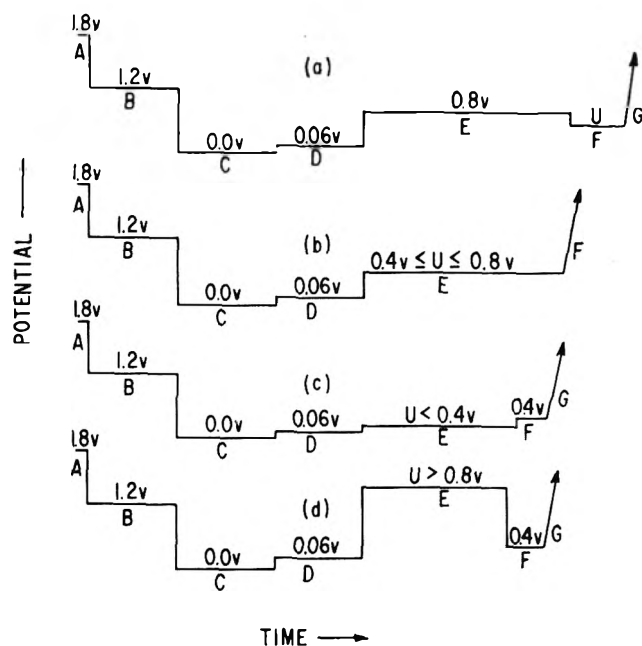


Figure 1. Potential sequences used in the measurement of chloride and phosphate ion adsorption.

imum value of θ_{Cl^-} obtainable at 0.8 v., when T_F is chosen equal to zero. Traces corresponding to these two different situations appear in Fig. 2 (traces 4 and 1, respectively; trace 1 actually is for a value of T_F somewhat greater than zero). The area bounded by traces 1 and 4 of Fig. 2 and the dashed line defines a quantity $\Delta Q_o'$ as previously discussed.² Under the conditions just described $\Delta Q_o' = \Delta Q_o$ and is proportional to the surface coverage with chloride ions.² If, after maximum chloride adsorption is allowed to occur at 0.8 v., T_F is made greater than zero, with $U < 0.8$ v., $\Delta Q_o'$ is observed to decrease (Fig. 2 corresponds to $U = 0.4$ v.) signifying *desorption* of chloride at potential U . Figure 3 is a plot of $\Delta Q_o'$ against the log of desorption time, T_F , for desorption potentials, U , of 0.4 and 0.6 v. The value of $\Delta Q_o'$ obtained after 10 sec. of *desorption* is (within a few per cent) the same as the maximum values of ΔQ_o obtained during *adsorption* at the same values of U . The same observation may be made for U as low as 0.1 v., where the equilibrium value of $\Delta Q_o'$ is zero (no adsorbed chloride). Hence, the adsorption of chloride in the range $0 \text{ v.} < U \leq 0.8 \text{ v.}$ is reversible.

In attempting to determine the *kinetics* of desorption from our experimental data, we must first make the following observations.

(1) During previous studies² of the *adsorption* of chloride at constant potential, the experiment was begun with a low (equal to bulk) concentration of dis-

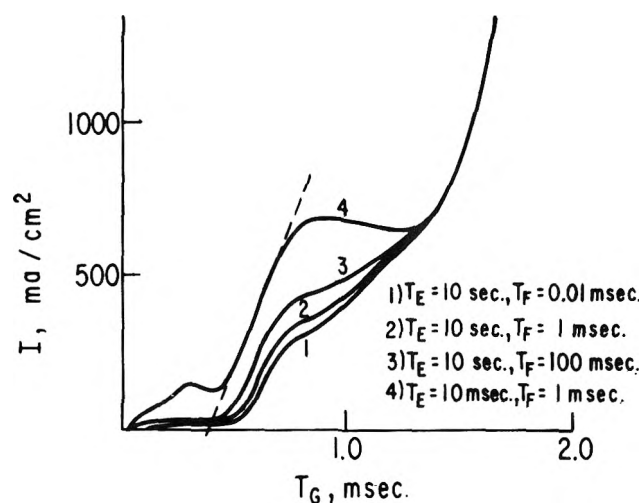


Figure 2. "Oxygen adsorption" traces obtained during desorption of chloride ions at $U = 0.4$ v. (sequence I of Table I; T_F is the desorption time).

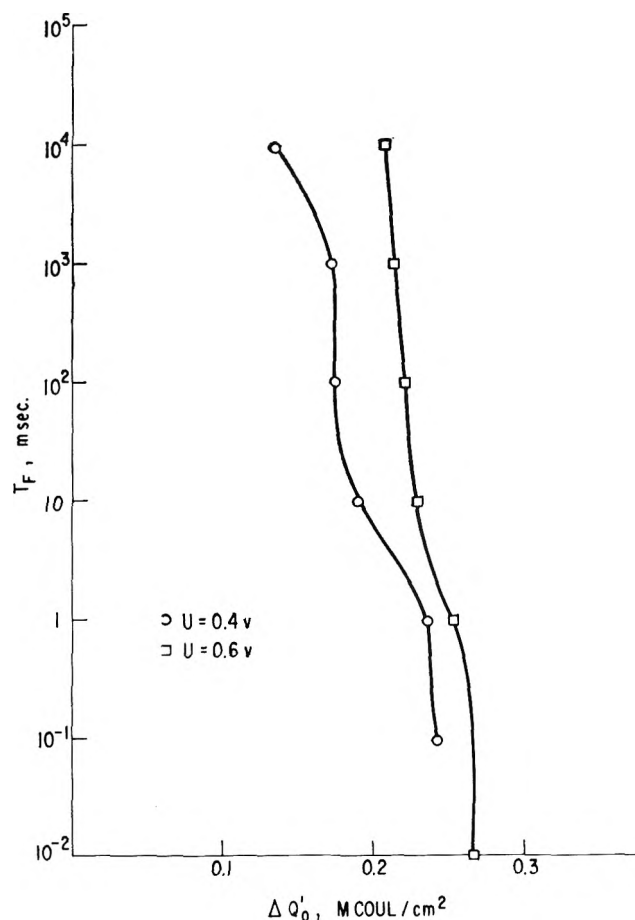


Figure 3. Variation of $\Delta Q_o'$ with desorption time, T_F , at potential U . Solution was $10^{-4} M$ HCl, $1 N$ HClO₄.

solved chloride adjacent to the surface. As the adsorption progressed, the solution of chloride adjacent to

Table I: Potential Sequences and Procedures Used in Measuring Anion Adsorption

Se- quence no.	Fig. no.	Step ^a	Procedure	Purpose
I	1a	A	(1) $T_A = 2$ sec. with paddle stirring and argon bubbled through the electrolyte	(1) To remove impurities and to deposit a protective "oxygen" film which protects the surface until step C
		B	(2) $T_B = 15$ sec. with paddle stirring and argon bubbling	(2) To sweep away any molecular oxygen and chlorine generated during step A while retaining the "oxygen" film
		C	(3) Stir for 0.5 min. Allow the solution to become quiescent for 1.5 additional min.	(3) To reduce the concentration of chloride (or phosphate) on the surface to zero. Desorbed material is swept into the bulk. Transport of material from the electrolyte is controlled by ordinary diffusion at the end of this step
		D	(4) $T_D = 10$ sec.	(4) To reduce the concentration of dissolved hydrogen adjacent to the electrode surface
		E	(5a) $T_E = 10$ msec.	(5a) To bring the potential of the electrode to 0.8 v., without allowing sufficient time for the adsorption of an appreciable amount of anions
			(5b) $T_E = 10$ sec.	(5b) To allow for the maximum (equilibrium) amount of adsorption at 0.8 v.
		F	(6a) $T_F = 1$ msec.	(6a) To bring the electrode potential to the value " U " without allowing sufficient time for the (appreciable) adsorption of anions
			(6b) $T_F =$ variable	(6b) To allow for variable extent of desorption of anions at potential U
		G	(7a) Apply linear anodic sweep of speed 2000 v./sec. and measure current-time trace	(7a) To obtain "oxygen adsorption" trace corresponding to zero surface coverage with anion ("blank" experiment)
			(7b) Same as (7a)	(7b) To obtain "oxygen adsorption" trace corresponding to variable surface coverage with the anion obtained by desorption of the anion at potential U for variable time, T_F
II	1b	A-D	(1)-(4) Same as sequence I, (1)-(4)	(1)-(4) Same as sequence I, (1)-(4)
		E	(5a) $T_E = 10$ msec.; $0.4 \leq U \leq 0.8$ v.	(5a) To bring the electrode to " U " without allowing sufficient time for appreciable adsorption of anions from solution
			(5b) $T_E = 10$ sec., with paddle stirring	(5b) To allow maximum (equilibrium) adsorption of anions at potential U
		F	(6a) Apply linear anodic sweep of speed $v = 1000$ v./sec. and measure the current-time trace corresponding to steps 1-4 and 5a	(6a) To obtain "oxygen adsorption" trace corresponding to zero surface coverage with the anion ("blank" trace)
			(6b) Apply linear anodic sweep and measure the current-time trace corresponding to steps 1-4 and 5b	(6b) To obtain "oxygen adsorption" trace corresponding to maximum (equilibrium) surface coverage with the anion
III	1c	A-D	(1)-(4) Same as sequence I, (1)-(4)	(1)-(4) Same as sequence I, (1)-(4)
		E	(5a) $T_E = 10$ msec., $U < 0.4$ v.	(5a) To bring the electrode potential to " U " without allowing sufficient time for appreciable adsorption of anions from solution
			(5b) $T_E = 10$ sec.	(5b) To allow maximum (equilibrium) adsorption of anions at potential U
		F	(6a) and (6b) $T_F = 10$ msec.	(6a) and (6b) To remove hydrogen which remains on the surface from potential step E, without allowing sufficient time for adsorption of appreciable anions from solution

Table I (Continued)

Se- quence no.	Fig. no.	Step ^a	Procedure	Purpose
		G	(7a) Apply linear anodic sweep of speed $v = 2000$ v./sec. and measure the current-time trace corresponding to steps 1-4 and 5a-6a (7b) Apply linear anodic sweep and measure the current-time trace corresponding to steps 1-4 and 5b-6b	(7a) To obtain "oxygen adsorption" trace corresponding to zero surface coverage with the anion ("blank" trace) (7b) To obtain the "oxygen adsorption" trace corresponding to maximum (equilibrium) surface coverage with the anion at potential U
IV	1d	A-D	(1)-(4) Same as sequence I, (1)-(4)	(1)-(4) Same as sequence I, (1)-(4)
		E	(5a) $T_E = 10$ msec.; $U > 0.8$ v. (5b) $T_E = 10$ sec.	(5a) To bring the electrode to potential U without allowing sufficient time for appreciable adsorption of anions from solution (5b) To allow maximum adsorption of anions at potential U
		F	(6a) $T_F = 1$ msec. (6b) $T_F = 1$ msec.	(6a) To remove "oxygen" deposited on the surface during potential step E, without allowing time for appreciable adsorption of anions from solution (6b) To remove "oxygen" deposited during potential step E, while allowing a minimum amount of time for the desorption of anions and diffusion away from the surface
		G	(7a) Apply linear anodic sweep of speed $v = 2000$ v./sec. and measure the current-time trace corresponding to steps 1-4 and 5a-6a (7b) Apply linear anodic sweep and measure the current-time trace corresponding to steps 1-4 and 5b-6b	(7a) To obtain "oxygen adsorption" trace corresponding to zero surface coverage with anions (7b) To obtain "oxygen adsorption" trace corresponding to maximum (but nonequilibrium) surface coverage with anions established after application of potential step $U > 0.8$ v.

^a "T" with the appropriate subscript indicates the duration of a particular step; e.g., T_A is the duration of step A.

the electrode was further *depleted*. Throughout the experiment, therefore, there was no appreciable diffusion of chloride to the surface during the short linear anodic pulse used to measure the adsorption which preceded the pulse. Hence, $\Delta Q_o'$ was equal to ΔQ_o , which is proportional to chloride surface coverage.

(2) During *desorption* of chloride, the concentration of dissolved chloride initially adjacent to the surface is equal to the small bulk value, but must soon increase greatly with time. Hence, $\Delta Q_o' \neq \Delta Q_o$ and is not an accurate measure of chloride surface coverage until the dissolved chloride concentration adjacent to the surface diminishes sufficiently by diffusion into the bulk of the solution.

Consideration (2) leads us to the conclusion that the values of $\Delta Q_o'$ plotted in Fig. 3 serve as a guide only to the *upper limit* of chloride surface coverage as a function of desorption time. A rather complicated analysis of the data would be required to obtain actual quantita-

tive information. One extreme possibility is that there is instantaneous desorption of excess (compared to equilibrium) chloride and that $\Delta Q_o'$ is a measure of diffusion of the desorbed chloride into the bulk.

II. *Measurement of Equilibrium Chloride Surface Coverage in the Range $0.4 \leq U \leq 0.8$ v.* Sequence II of Table I and a 10^{-4} of solution of HCl in 1 *N* perchloric acid was used in making these measurements. The procedure was similar to that used previously in following adsorption as a function of time.² Procedural steps 1-4 and 5a-6a were used to obtain the "blank" "oxygen adsorption" trace. Steps 1-4 and 5b-6b were used to obtain the "oxygen adsorption" trace corresponding to maximum θ_{Cl^-} . The choice of $T_E = 10$ sec. with mechanical stirring was found to give maximum adsorption throughout the concentration range studied. For concentrations $\geq 10^{-4}$ *M* HCl, maximum surface coverage was achieved within 10 sec. without mechanical stirring, whereas mechanical stirring was

required for sufficient transport at lower concentrations. The values were ascertained as maximum by varying T_E over another decade of time and observing constancy of the "oxygen adsorption" trace. To determine if the maximum values were indeed equilibrium values, sequence I of Table I was used (mechanical stirring added to step 6b with $T_F = 10$ sec.) and desorption measured at 0.4 and 0.7 v. The desorption values of ΔQ_o were found to be almost identical with the adsorption values at each concentration. Results are plotted in Fig. 4 and 5, with surface coverage expressed in terms of the fractional surface coverage, θ_{Cl^-} , defined as

$$\theta_{Cl^-} = \Delta Q_o / 2Q_H^S \quad (1)$$

θ_{Cl^-} has the formal significance of fractional surface coverage if the full surface coverage situation is arbitrarily taken as equivalent to having one adsorbed chloride ion per hydrogen adsorption site. The results may be alternatively expressed in terms of equiv./cm.² by multiplying by Q_H^S/F (or 2.82×10^{-9}), where F is the Faraday constant and Q_H^S has the value 2.72×10^{-4} coulomb/cm.² as already noted.

III. *Measurement of Equilibrium Chloride Surface Coverage in the Range $0 < U \leq 0.4$ v.* Sequence III of Table I was used in making these measurements. Procedural steps 1-4 and 5a-7a were used in obtaining the "oxygen adsorption blank" trace, while steps 1-4 and 5b-7b were used in obtaining the trace corresponding to maximum surface coverage at potential U . The procedure differs from that of the preceding section in the addition of potential step F, which was intended to remove adsorbed hydrogen (deposited at potential U)³ which would ordinarily interfere with measurement of the "oxygen adsorption" traces. These measurements must result in exact values of θ_{Cl^-} in accordance with the following considerations.

(1) Sufficient time is allowed for the equilibrium adsorption of chloride at potential U .

(2) Potential step F (0.4 v.) which follows potential U is greater than potential U . Hence, the tendency is for additional chloride to adsorb during step F. However, diffusion does not allow for appreciable adsorption of chloride under these conditions (10 msec., 10^{-4} M HCl). Hence, the value of θ_{Cl^-} achieved at potential U is maintained through steps F and G.

Values of θ_{Cl^-} obtained in this potential range are plotted in Fig. 5. It may be noted that the values obtained in the potential range $0.150 \leq U \leq 0.4$ v. fall on a straight line connecting these data with those of the higher potential range. No adsorption is observed at $U \leq 0.125$, hence there is a fairly vertical rise in θ_{Cl^-} between 0.125 and 0.150 v. The values of θ_{Cl^-} ob-

tained for the potential range $0 < U \leq 0.4$ v. are equilibrium values since they may also be obtained by means of sequence I of Table I (desorption).

IV. *Measurement of Nonequilibrium Chloride Surface Coverage in the Potential Range $0.8 < U < 1.6$ v.* Measurements of θ_{Cl^-} in this potential range were accomplished by means of sequence IV of Table I. The sequence is very similar to that used in section III, except that step F is only of 1-msec. duration and intended to remove "adsorbed oxygen" (rather than adsorbed hydrogen) which is encountered in this potential range.³ Because step F (0.4 v.) is of lower potential than U , accurate values of θ_{Cl^-} cannot be expected throughout the potential range due to some desorption of chloride during step F. The extent of uncertainty of the data is covered in the following paragraphs.

(1) The apparent value of θ_{Cl^-} at 0.9 v. is greater than the equilibrium value for 0.4 v., therefore desorption must occur during potential step F. Since the value of θ_{Cl^-} at 0.9 v. is less than the equilibrium value for 0.8 v., the extent of desorption must be less than that noted after 1 msec. in section I, when the potential was stopped from 0.8 to 0.4 v. This provides us with the upper limit of uncertainty for 0.9 v., which is indicated in Fig. 5 (cross-hatched square). The smooth curve for θ_{Cl^-} was drawn through the average of the apparent maximum and minimum values at 0.9 v.

(2) The apparent value of θ_{Cl^-} for 1.1 v. is less than the equilibrium value for 0.4 v.; therefore, no desorption could occur during step F, and the value of θ_{Cl^-} is accurate.

(3) The apparent value of θ_{Cl^-} at 1.0 v. is not much larger than the equilibrium value for 0.4 v. Hence, only slight effective desorption could occur during step F. This will be considered negligible with respect to the maximum uncertainty noted for 1.1 v. Hence, there is considerable uncertainty only in the value of θ_{Cl^-} at 0.9 v., and this is not great enough to affect the over-all shape of the curve in this potential range.

V. *Measurement of Phosphate Adsorption in the Potential Range $0 < U < 1.6$ v.* Procedures similar to those reported above (sections II and IV, respectively) were employed in obtaining equilibrium phosphate surface coverages in the range $0.4 \leq U \leq 0.8$ v., and nonequilibrium surface coverages in the range $0.8 < U < 1.6$ v. The solution used was 10^{-4} M metaphosphoric acid in 1 N perchloric acid. The values obtained are reported in Fig. 5 in terms of $\theta_{\text{phosphate}}$ which is defined as follows

$$\theta_{\text{phosphate}} = \Delta Q_o / 2Q_H^S \quad (2)$$

(3) F. G. Will and C. A. Knorr, *Z. Elektrochem.*, **64**, 258 (1960).

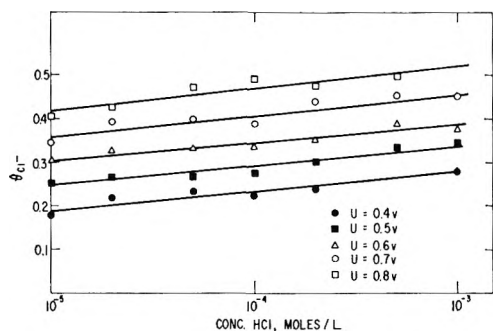


Figure 4. Variation in chloride ion surface concentration with concentration and potential.

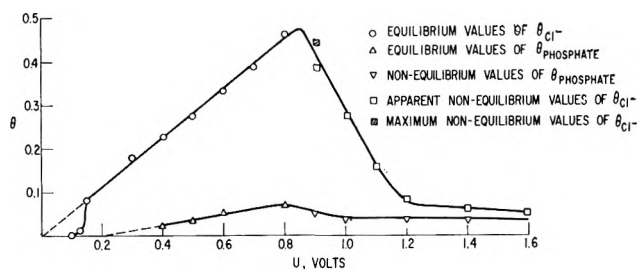


Figure 5. Variation in chloride and phosphate ion adsorption with potential for $10^{-4} M$ solutions of the acid.

This *arbitrary* definition is equivalent to assuming that a complete monolayer of phosphate corresponds to a surface having each hydrogen adsorption site covered with an adsorbed $H_2PO_4^-$ ion. $\theta_{\text{phosphate}}$ is a valid measure of the *relative surface excess of phosphate ion even if the assumption is incorrect*.

Discussion

I. Chloride Desorption Kinetics. The data in Fig. 3 are obtained when chloride is adsorbed at 0.8 v. and desorbed at a lower potential U . The final point obtained in such an experiment corresponds to the maximum amount of chloride adsorbed at potential U (starting with zero surface coverage) and indicates that chloride adsorption-desorption is *reversible* in the potential range below 0.8 v.

Regarding the values of $\Delta Q_0'$ in Fig. 3 as an indication of maximum surface coverage at any time, we may make the following qualitative observations on the kinetics of desorption at potential U . (1) More than half the equilibrium desorption for the potentials studied is accomplished within 10 msec. (2) Some desorption occurs before 1 msec. More quantitative interpretation of the data has not yet been attempted.

II. Constant Potential Isotherms for Chloride Adsorption. The data obtained for reversible adsorption of chloride ion over a wide range of concentrations appear

in Fig. 4. The data can be approximately represented as a family of parallel lines. Such a linear relationship between surface coverage log and concentration of adsorbate (at constant potential) suggests a Temkin isotherm relationship.⁴ The slope of the plot is approximately equivalent to a decrease in fractional surface coverage of 0.05 per order of magnitude decrease in concentration. This suggests that appreciable adsorption of chloride might be observed at chloride concentrations much lower than $10^{-5} M$ if sufficient time is allowed for mass transport and the solution is sufficiently free of impurities.

III. Equilibrium Chloride Surface Coverage in the Potential Range $0 < U \leq 0.8$ v. Values of θ_{Cl^-} obtained for this potential range and for a solution of $10^{-4} M$ HCl in 1 *N* perchloric acid are plotted in Fig. 5. Two aspects of the plot are noteworthy. (1) An almost vertical rise in θ_{Cl^-} occurs in the potential range between 0.125 and 0.150 v. (average = 0.138 v. = U_0). (2) The plot is fairly linear between 0.150 and 0.8 v. These features will be further discussed in the paragraphs below.

While U_0 may be *close* to the "zero point of charge" as previously suggested for anion adsorption by Frumkin,⁵ it need not be identical with that potential because of specific properties of the ion itself, as pointed out by Bockris, *et al.*⁶ If the simplifying assumption is made that U_0 is a zero point of charge, the following explanation for the vertical rise in surface coverage at U_0 may be offered.

(1) U_0 is the zero point for platinum in our electrolyte corresponding to the surface state which exists before the adsorption of chloride ion.

(2) When the earliest adsorption of chloride occurs at U_0 , the zero point shifts to a new, more negative value, U_0' corresponding to the new surface state. This means that U_0 is now considerably more positive to the new zero point of charge, and additional adsorption occurs. U_0' the (approximate) new zero point would then be obtained by back extrapolation of the $\theta_{Cl^-}-U$ plot (to obtain the x intercept (0.0 v.)).

It would be valuable to be able to compare the results reported here with that of previous investigators using different techniques. Unfortunately, as already observed by Parsons⁷ much of the work done in this area

(4) B. M. W. Trapnell, "Chemisorption," Butterworth and Co. Ltd., London, 1955.

(5) A. N. Frumkin, "Advances in Electrochemistry and Electrochemical Engineering," Vol. 3, Interscience Publishers, Inc., New York, N. Y., 1963, Chapter V.

(6) J. O'M. Bockris, M. A. V. Devanathan, and K. Muller, *Proc. Roy. Soc. (London)*, A274, 55 (1963).

(7) R. Parsons, "Modern Aspects of Electrochemistry," Vol. 1, Academic Press, Inc., New York, N. Y., 1954.

has been done under conditions of dubious surface preparation and without control of the potential. Some comparison, however, is possible with the work of Slygin, Frumkin, and Medvedovsky.⁸ These investigators studied the adsorption of chloride from a solution of 1 *N* NaCl and 0.01 *N* HCl. Platinized platinum was used and the adsorption was followed by following the changes of solution pH which accompanied "coadsorption" of hydrogen ions on the surface. Employing their values and the surface roughness factor suggested by Frumkin, the value obtained by Slygin, *et al.*,⁸ was approximately half the value reported here. This must be considered fair agreement under the conditions of uncertain comparative surface area.

IV. Nonequilibrium Chloride Surface Coverage at Potentials above 0.8 v. As the potential is increased above 0.8 v., the surface of platinum is covered to an increasing extent with "adsorbed oxygen."³ "Oxygen" deposited in the higher potential region is not reduced until the potential is made lower than approximately 0.8 v.³ It is due to this passive film and its irreversible nature that chloride adsorption in the high potential range is also irreversible.

We have already seen that if chloride is adsorbed at 0.8 v., the resulting surface coverage will be retained even if the potential is suddenly raised to 1.6 v.² This is because the adsorbed chloride is neither (rapidly) desorbed, nor oxidized, but in fact, partially protects the platinum surface against "oxygen adsorption." Conversely if the potential is stepped to 1.6 v. in a dilute chloride solution (resulting in very slight chloride adsorption) and then the potential is lowered to some value above 0.9 v., no additional adsorption occurs because of the protective nature of the "oxygen film." By choosing the path by which a potential is set in the range above 0.8 v., it is therefore possible to arrive at any surface coverage between that for approximately 0.8 v. and zero. The results recorded in Fig. 5 correspond to the special situation where the surface was initially bare of chloride and of "oxygen" (at 0.06 v.). The potential was then brought to the particular value, $U > 0.8$ v., whereupon "oxygen" deposition and chloride adsorption began immediately. The former is quite rapid (approximately dependent on the log of time) and reaches an apparent "steady state" within milliseconds.⁹ Hence most of the adsorption of chloride under our conditions in the high potential range occurs after the surface oxidation has gone to "steady state." Under these conditions θ_{Cl^-} for $U > 0.8$ v. is therefore a reflection of the amount of chloride which can adsorb on the *partially* "oxidized" surface. From this point of view, we see that the extent of surface oxidation which occurs after 10 sec. at 1.2 v. is sufficient

to exert the maximum blocking effect on chloride adsorption. This effect could be due to actual physical blocking of the surface or to some more indirect effect. The stoichiometry of the "oxygen" film is still a matter of controversy. The most that can now be said is that almost a monolayer of blocking "oxide" is *possible* at 1.2 v. if we assume the stoichiometry of the film to correspond to PtO.⁹

V. Adsorption of Phosphate in the Potential Range $0 < U < 1.6$ v. The amount of phosphate reversibly adsorbed at any potential in the range below 0.8 v. is less than a fifth that of the chloride (Fig. 5). While the concentration of the phosphoric acid is the same as that of the HCl (10^{-4} *M*), the effective concentration of the dihydrogen phosphate ion is only approximately 7.5×10^{-8} , calculated on the basis of the appropriate ionization constant (7.5×10^{-3}),¹⁰ while HCl is assumed completely dissociated. If we assumed that the dependence of the amount of phosphate adsorbed on concentration is similar to that of chloride, the difference in ion concentrations is still not large enough to explain the large differences in adsorbabilities of the ion at constant potential. As for chloride, the amount of nonequilibrium phosphate adsorbed during application of a potential step adsorbed in the potential range above 0.8 v., decreases with increasing potential. In spite of the small amounts adsorbed at lower potentials, almost the same limit is observed for the two ions at the high potential end. A simple explanation for this is that the low surface coverages achieved in the high potential end are the result only of the "blocking" effect of the "oxygen" which determines the *maximum* number of *sites* available for ion adsorption at the higher potentials. The amount actually adsorbed is therefore independent of the adsorbability of the particular ion, so long as the adsorbability *exceeds* the available sites.

As for chloride, phosphate surface coverage in the potential range above 0.8 v. can be adjusted to *any* value between the *maximum* of Fig. 5 and *zero*, by choice of the *path* by which the final potential is established.

Summary

(1) Chloride and phosphate adsorption at $U \leq 0.8$ v. is *reversible*. Depending on initial conditions, there will be adsorption or desorption of ions until the equilibrium surface concentration corresponding to the new potential is established.

(8) A. Slygin, A. Frumkin, and V. Medvedovsky, *Acta Physicochim. URSS*, **4**, 911 (1936).

(9) S. Gilman, *Electrochim. Acta*, **9**, 1025 (1964).

(10) N. A. Lange, "Handbook of Chemistry," 10th Ed., McGraw-Hill Book Co., New York, N. Y., 1961.

(2) The desorption of chloride on going from higher potentials (higher surface coverages) to lower potentials (both potentials lower than 0.8 v.) is rapid (some desorption observed within milliseconds).

(3) The amount of chloride adsorbed at constant potential depends on the concentration of dissolved chloride in a manner suggesting a Temkin isotherm.

(4) At a concentration of 10^{-4} M HCl, there is no chloride adsorbed below 0.125 v. There is a sudden rise in chloride adsorption between 0.125 and 0.150 v., which might be ascribed to a sudden change in the potential of the zero point of charge. From 0.150 to

0.8 v., the amount of chloride which is reversibly adsorbed varies approximately linearly with potential. Phosphate adsorbs to a considerably smaller extent, and the low-potential discontinuity if it occurred would not be detectable. Above 0.8 v., "oxygen adsorption" occurs. The irreversibility of the latter process causes an irreversibility in anion adsorption above this potential. The general rule is that the "adsorption" of "oxygen" will interfere with the adsorption of anions, and *vice versa*. The surface coverage with anions in this range (0.8–1.6 v.) therefore depends upon the path taken to reach the particular potential.

Sensitization by Nitrous Oxide to Radiation-Induced

Cross Linking of Polyethylene

by Yoichi Okada

Central Research Laboratory, Sumitomo Bakelite Co., Ltd.,
Totsuka, Yokohama, Japan (Received January 13, 1964)

γ -Ray irradiation of polyethylene in an atmosphere of nitrous oxide (N_2O) yields a greater degree of cross links and of *trans*-vinylene unsaturation than does irradiation *in vacuo*. This sensitization is caused by N_2O molecules dissolved in polyethylene solid. N_2O was consumed at a large G -value, of the order of 10^3 , and nitrogen and water were formed. The amounts of nitrogen and water obtained were stoichiometrically equivalent to the loss of N_2O , *i.e.*, $N_2O \xrightarrow{+2H} N_2 + H_2O$. Two hydrogen atoms come from polyethylene. This material balance also shows that the cross links formed due to the sensitization are C-C bonds as in the case of vacuum irradiation. The increments of cross links and unsaturation increase monotonically with increase in N_2O concentration in the solid. The efficiency per N_2O molecule, however, gradually decreases with increase in N_2O concentration. Since the dissolved N_2O forms only about 0.1 wt. % in the solid, the absorption of radiation energy by the N_2O is so little that it can be ignored in comparison with the absorption by the polymer. The large G -value for the consumption of N_2O suggests that a part of absorbed energy by the polymer transfers to the N_2O molecule. It is not strange, if such an energy transfer occurs, that a greater number of N_2O molecules is efficiently excited and abstracts two hydrogen atoms from polymer chain segments in a closed vicinity. The abstraction results in the formation of cross links and unsaturation.

1. Introduction

Recently we presented evidence that¹⁻⁴ the low density polyethylene irradiated in an atmosphere of nitrous oxide (N_2O) gives higher yields of cross links and unsaturation (*trans*-vinylene) than the polymer irradiated *in vacuo*. This effect of nitrous oxide may be called "sensitization." The increment due to the nitrous oxide was 44% for cross links and 87% for unsaturation at a pressure of 600 mm.⁴ The formations of cross links and unsaturation are the main chemical changes which occur when irradiated *in vacuo*. Being one of the most soluble gases in the polymer among inorganic gases,^{5,6} nitrous oxide serves not only as an atmosphere for the polymer but also as an additive. The sensitization is certainly a reaction in the polymer solid between polyethylene chains and nitrous oxide dissolved in it. In polyisobutylene, on the other hand, the nitrous oxide reduces the amount of radiation degradation.⁷ The nitrous oxide dissolved forms only 0.1-0.2

wt. % in these polymers at 600 mm. It is interesting that the evident chemical change is caused by the very small amount of dissolved gas. Xenon shows a similar effect to nitrous oxide on polyethylene,⁴ but the effect of xenon is rather weak. This paper presents the results of further researches about the effect of nitrous oxide on polyethylene and our hypothesis on the mechanism of the sensitization.

2. Experimental

The experimental technique was nearly the same as in the preceding work,²⁻⁵ unless otherwise noted. In

- (1) Y. Okada and A. Amemiya, *J. Polymer Sci.*, **50**, S22 (1961).
- (2) Y. Okada, *J. Appl. Polymer Sci.*, **7**, 695 (1963).
- (3) Y. Okada, *ibid.*, **7**, 703 (1963).
- (4) Y. Okada, *ibid.*, **8**, 467 (1964).
- (5) Y. Okada, *ibid.*, **7**, 1153 (1963).
- (6) A. S. Michaels and H. J. Bixler, *J. Polymer Sci.*, **50**, 393 (1961).
- (7) Y. Okada, *J. Appl. Polymer Sci.*, **7**, 1791 (1963).

most cases, Sumikathene L-70 film (0.3 mm. thick), low density polyethylene, was packed in an ampoule (ca. 30 cc.) and was irradiated with γ -rays from cobalt-60 source. The material balance of nitrous oxide was given by enclosing a known amount of nitrous oxide in an ampoule before irradiation and by analyzing the gas present in the ampoule after irradiation. Since various gases were formed during irradiation (for example, evolved hydrogen from polyethylene), the gas in the ampoule was separated into two fractions by passing through several U-tubes dipped in liquid nitrogen. The freezing point of nitrous oxide is -102.4° and the boiling point is -89.5° . In addition, the component which freezes at Dry Ice temperature was separated again from the condensed fraction in the U-tubes. Each fraction was analyzed by mass spectrometry.

3. Results

3.1. Material Balance of Nitrous Oxide. The consumption of nitrous oxide could not be detected in the previous work, probably because the amount of film and the dose were too little. In the present study, as shown in Table I, a greater amount of film was closely

Table I: Consumption of Nitrous Oxide

Expt.	Film, g.	Packing ratio, g./cc.	Initial N_2O , mole $\times 10^4$	$G(-N_2O)$	Formation of H_2O , mg.	Formation ^a of N_2 , mole $\times 10^4$	$G(H_2)$
1	0	0	9.98	10-0
2	18.0	0.64	6.95	1710	12.3 (12.5) ^b	7.37	3.1
3	20.0	0.65	11.4	2280	19.5 (20.5) ^b	11.0	3.4
4	20.0	0.68	0	3.1

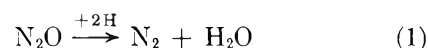
^a Moles $N_2 = X_{N_2}(\text{moles}_{\text{total gas}} - \text{moles}_{\text{hydrocarbons}})$. X_{N_2} = mole fraction of N_2 in the uncondensed fraction at liquid nitrogen temperature. ^b Calculated yield (equivalent to the initial amount of N_2O).

packed and subjected to a total dose of 5×10^7 r. Packing ratio (column 3) is the term applied to the weight of film packed in a unit volume of ampoule.

In the absence of film (expt. 1), the reduction of N_2O pressure could not be observed within the limit of error (ca. 2%). The radiolysis of nitrous oxide in gas phase was reported by several investigators.^{8,9} $G(-N_2O)$ is at most equal to 12, and the radiolytic products are nitrogen, oxygen, nitric oxide, and nitrogen dioxide. In the presence of a greater amount of film, on the contrary, the enclosed nitrous oxide was completely consumed during irradiation. The component which did

not freeze at Dry Ice temperature did not contain nitrous oxide but was a mixture of various hydrocarbons evolved from polyethylene. Large G -values are given for the disappearance of nitrous oxide in column 5. The G -values would become still larger if the dose when the nitrous oxide was all consumed were measured. Estimation of G -value is based on the assumption that the consumption was proportional to the irradiation time and the useful energy for the consumption was only the one absorbed by the gas dissolved in the polymer solid. Such a large G -value, however, seems unnatural except for the case of a chain reaction. But a chain reaction mechanism cannot account for this large value, because each gas molecule is closely surrounded by polymer chains and therefore can hardly collide with another nitrous oxide molecule which is located far away. It is unreasonable to assume that the consumption is due only to the energy absorbed directly by the dissolved gas.

The component which was condensed at Dry Ice temperature was water, and its weight is shown in column 6. Its vapor pressure, freezing point, and the color change of silica gel show that it was undoubtedly water. The yield of water was stoichiometrically equivalent to the loss of nitrous oxide. The uncondensed fraction at liquid nitrogen temperature, on the other hand, was a mixture of hydrogen and nitrogen. The yield of nitrogen was also stoichiometrically equivalent of the loss of nitrous oxide (column 7). The material balance of nitrous oxide, therefore, should be written as eq. 1.



Here 2H does not mean an evolved hydrogen as mentioned later on. The cross links formed due to nitrous oxide, from this viewpoint, should be composed of a so-called C-C bond as in case of the vacuum irradiation, for apparently the nitrous oxide or its fragments did not chemically add to polyethylene. A different type of bridge, for example C-NH-C or C-N(NO)-C, should not be formed. The increment of cross links, at expt. 3, was 24%, and that of unsaturation was 43%. If the G -values for the formation of cross links and unsaturation, at the vacuum irradiation are equal to 2.0 and 1.7, respectively,¹⁰ the moles of cross links in excess of that of the vacuum irradiation become 4.8×10^{-4} , and that of unsaturation 7.3×10^{-4} . Since the reacted moles of nitrous oxide is 11.4×10^{-4} , nitrous

(8) P. Harteck and S. Dondes, *Nucleonics*, **14**, No. 3, 66 (1956).

(9) N. T. Williams and H. Essex, *J. Chem. Phys.*, **16**, 1153 (1948).

(10) A. Chapiro, "Radiation Chemistry of Polymeric Systems," Interscience Publishers, Inc., New York, N. Y., 1962, pp. 414, 433.

oxide must be lost one by one corresponding to the excess formations of cross links and unsaturation.

3.2. Packing Ratio of Film. Variations of gel fraction and the packing ratio of film were studied here. In Fig. 1 the increments (%) of the reciprocal of $s + s^{1/2}$ are plotted. Here s is the sol fraction. From Charlesby's relation¹¹ between $s + s^{1/2}$ and the reciprocal of dose ($1/r$), the probability (density) of cross linking (q_0) can be shown in the form

$$q_0 = (p_0 + 1/u_1 r)/(s + s^{1/2}) \quad (2)$$

where u_1 is the number-average degree of polymerization; p_0 is the probability of main-chain scission and is nearly constant.⁴ Thus, q_0 can be given relatively by the reciprocal of $s + s^{1/2}$. Strictly speaking, the above treatment should be reasonable in the dose range where Charlesby's relation gives a straight line. The error owing to a little deviation from the straight line, however, may be roughly compensated when the plot is shown as a relative value to that for the vacuum irradiation.

The initial low value in Fig. 1 is probably due to the radiolytic products of nitrous oxide in the gas phase,¹⁻³ for these products diffuse into the polymer solid and inhibit the cross linking of the polymer. It seems quite reasonable that the effect of radiolytic products becomes distinct when the amount of film is small, especially in the case of thin film. The decrease of curves, on the contrary, when the amount of film increases, should be

due to the rapid consumption of nitrous oxide during irradiation. Both the gas pressure and the gas concentration in the solid must be gradually decreased; 0.3- and 0.03-mm. thick films were not made of the same material. Not only the cross links, but the unsaturation decreased with an increase in the amount of film. The increment of unsaturation, at the packing ratio of 0.36, was only 70% of the value at the packing ratio of 0.01.

3.3. X-Rays from Linear Electron Accelerator. Under γ -radiation from a cobalt-60 source, as previously reported,³ the increment of gel fraction is independent of dose rate over a range of $5.0 \times 10^4 \sim 6.5 \times 10^6$ r./hr. Although the report was concerned only with the film of 0.03-mm. thickness, a similar behavior also was observed in the case of film 0.3 mm. thick. Here an irradiation of very high dose rate was tested by using a linear electron accelerator. By attaching a platinum target to the accelerator, a series of pulsed X-rays of 4- μ sec. duration, repeated at 150 or 250 pulses/sec., was emitted. Since the X-rays were emitted only for a period equivalent to about 0.1% of irradiation time, there would be considerable variations in dose rate. The average rate was nearly 1×10^7 r./hr., and the rate during the pulses possibly exceeded 1×10^{10} r./hr.

Under vacuum and in nitrous oxide (600 mm.), 0.9 g. of the film 0.3 mm. thick was irradiated to about a dose of 2×10^7 r. The increment of cross links, the increment of reciprocal of $s + s^{1/2}$, was approximately 25%. This value seems to be somewhat lower than that obtained using the cobalt-60 source (*ca.* 44%). Nitrous oxide, as mentioned above, must be supplied into the polymer solid by diffusion from the gas phase, as the gas is consumed during irradiation. Then, the independence of dose rate to the gel fraction, observed in the case of the cobalt-60 source, must be attributed to the sufficiently rapid diffusion of nitrous oxide compared with its consumption. The lower value of increment observed here, on the other hand, may be accounted for by assuming that the diffusion process becomes a rate-determining step due to the high dose rate.

3.4. Gas Pressure of Nitrous Oxide. In the former study³ of the variations of gel fraction with gas pressure, the gel fraction forms a curve which initially increases with pressure, passes through a maximum, and decreases at high pressure. The decrease at high pressure must be attributed to the depressive effect¹⁻³ of radiolytic products of nitrous oxide, for a significant amount of these products is formed in the gas phase at

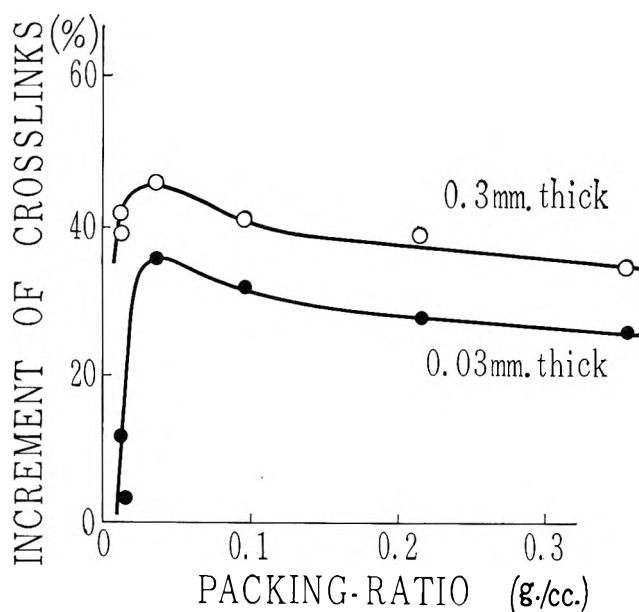


Figure 1. Effect of amount of film. Two films were irradiated together in the same ampoule to a dose of 2×10^7 r. at a constant dose rate of 1.05×10^6 r./hr. Initial pressure of nitrous oxide was 600 mm.

(11) A. Charlesby and S. H. Pinner, *Proc. Roy. Soc. (London)*, **A249**, 367 (1959).

high pressure. In order to observe the net dependence of the sensitization on the gas pressure, therefore, the experiment should be carried out under conditions where the effect of these products can be ignored. Here, the weight of film inserted in the ampoule was raised to 4 g. (2 g. of 0.3 mm. thick and 2 g. of 0.03 mm. thick) as against 0.54 g. in the former study, and the dependence was examined in a limited pressure range up to 1000 mm. as against 5000 mm. in the former study.

As shown in Fig. 2, the increment of reciprocal of $s + s^{1/2}$ and also the increment of unsaturation increase with the pressure monotonically. The reciprocal of $s + s^{1/2}$ should be relatively equivalent to the probability of cross linking or to the G -value, as mentioned above. Although the thin film was added in the ampoule for the purpose of protecting the thick film against the depressive effect of radiolytic products, the thin film also showed a similar behavior with pressure. The feature that the plots increase monotonically with the pressure seems to be quite natural since the gas concentration in the polymer solid should increase

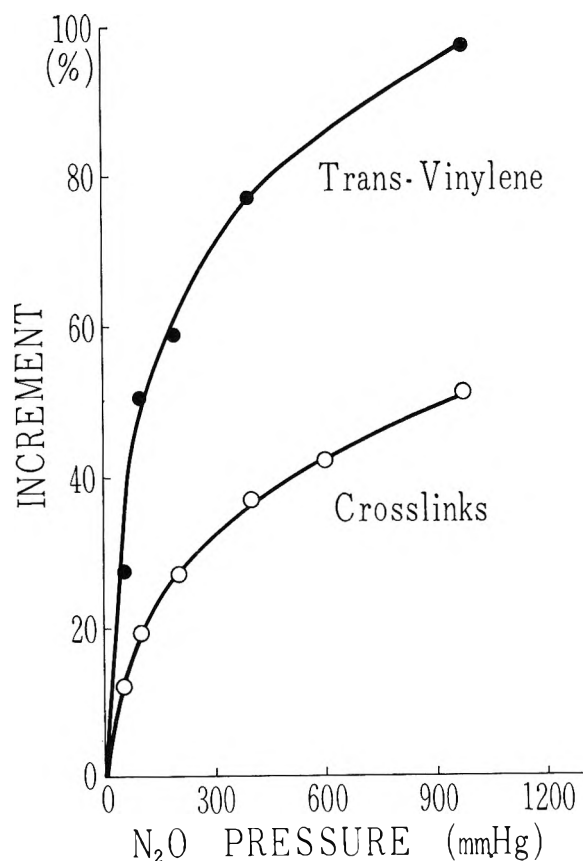


Figure 2. Effect of N_2O pressure. The increments of cross links and unsaturation for 0.3-mm. thick film are shown. Total dose: 2×10^7 r. Dose rate: 5.1×10^6 r./hr.

with the pressure. The increment of unsaturation is nearly twice as much as that of cross links. In the preceding study,⁴ a similar relation was observed.

3.5. Type of Polyethylene. A low density film, Sumikathene L-70 (ICI process), was mainly examined during the former studies. Petrothene-206 showed an increase in gel fraction in an atmosphere of nitrous oxide.² However, no examination had ever been carried out for a high density film, *i.e.*, Marlex-50 or Hizex-7000 (Ziegler process, prepared by Mitsui Chemicals Co.). One gram of each film was inserted in an ampoule and was irradiated to a dose of 2×10^7 r. in various pressures of nitrous oxide. The thickness of film was 0.3 mm. for Sumikathene and 0.1 mm. for the other films. The measurement of gel fraction was carried out at 130° in xylene for 3 days. Figure 3, as Fig. 2, shows the variations of increment of cross links against the gas pressure. All four curves increase with the pressure monotonically and are convex upward. The high density film, roughly speaking, gives somewhat smaller increments than the low density ones, which may be attributed to the low amorphous content of the former. However, this mutual relation is rather meaningless, for the increment is given as a relative value.

3.6. Type of Gas. In the preliminary study⁵ a little increase in gel fraction was observed in atmospheres of the following gases: krypton, carbon monoxide, water vapor, methane, ethane, propane, and bu-

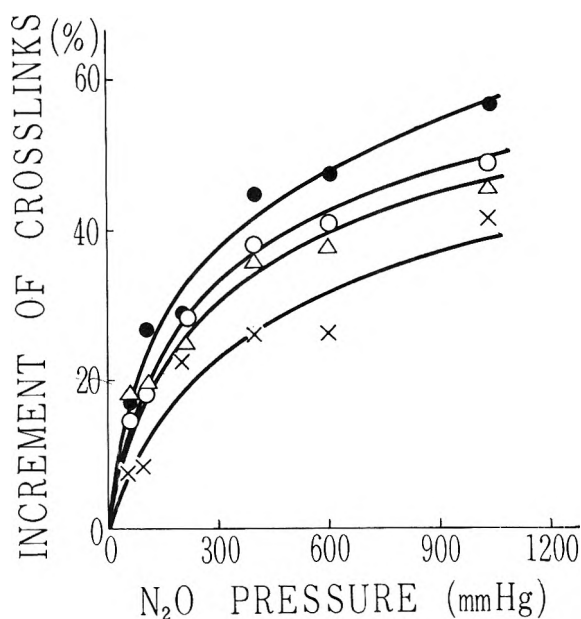


Figure 3. Type of polyethylene: ●, Petrothene-206; ○, Sumikathene L-70; Δ, Marlex-50; ×, Hizex-7000. Dose rate: 5.1×10^6 r./hr.

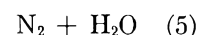
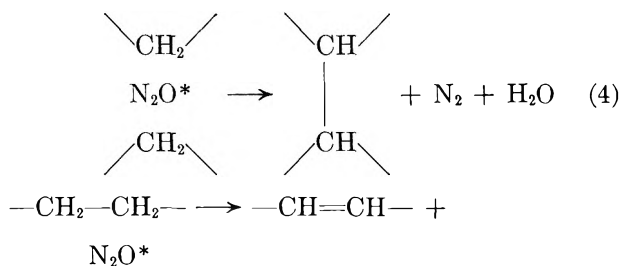
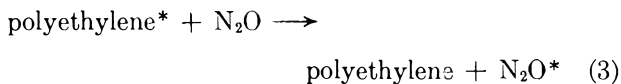
tane. However, no subsequent examination gave any evidence that these seven gases are effective in sensitizing the formations of cross links and unsaturation. Even at 5 atm. pressure, the gel and the unsaturation formed in krypton were in accord with those formed under vacuum when subjected to doses over $2 \times 10^7 \sim 1 \times 10^8$ r. Similar results were obtained, respectively, in the atmospheres of carbon monoxide and of saturated hydrocarbons at a pressure of 600 mm. In the case of water vapor, on the other hand, a little increase in gel fraction was again observed when irradiated at 80° up to a dose of 5×10^7 r. While the gel fraction was 87.7% (0.03-mm. thick film) and 87.9% (0.3 mm.) in vacuum irradiation, it was 89.2% (0.03 mm.) and 89.4% (0.3 mm.) in water vapor. Nevertheless, no increase was observed in unsaturation. Thus, in the present stage, the species which evidently show the sensitizing effect are limited to nitrous oxide and xenon. We can scarcely find any reliable reason why a little increase in gel fraction was observed in the preliminary test for the other several gases. The data on the vacuum irradiation which were adopted as the standard for comparison in the preliminary test may have been unsuitable. A supplementary test for argon and nitrogen confirmed their ineffectiveness. Furthermore, carbon dioxide and hydrogen sulfide gave a depressive effect to the gel formation.

4. Discussion

4.1. *Mechanism of Sensitization.* The over-all reaction of sensitization results in the formation of C-C cross links and *trans*-vinylene unsaturation in polyethylene, and the formation of water and nitrogen from nitrous oxide. The experiment confirms that the sensitizing reaction occurs between the nitrous oxide molecule dissolved in the polymer solid and the surrounding polymer chain segments. The dissolved gas molecule, however, forms only a very small weight fraction in the solid. The radiation energy absorbed by the dissolved gas, therefore, is so little that the energy can be disregarded in comparison with that absorbed by the polymer solid. Accordingly, the G -value for the disappearance of nitrous oxide and for the excess formation of cross links and unsaturation becomes extremely large, of the order of 10^3 , if it is calculated on the assumption that the dissolved nitrous oxide only reacts due to the directly absorbed energy. Though such large G -values are often seen in the case of a chain reaction, the reaction in question cannot be a chain reaction as suggested above. As a conclusion, the energy directly absorbed does not contribute to the reaction to any detectable extent but the efficiency of

energy absorbed by the polymer itself must be enhanced by the nitrous oxide in some way.

Our results, from this viewpoint, can be readily accounted for by assuming the occurrence of energy transfer (especially an excitation transfer) from the polyethylene chain to the nitrous oxide molecule. Provided most of the nitrous oxide molecules are electronically excited owing to the energy transfer, and these excited molecules act on the polymer chain segments nearby, it is not strange that a notable chemical change is induced, however low the concentration of nitrous oxide may be. The formation of water and the disappearance of nitrous oxide corresponding to the excess formation of cross links and unsaturation indicate that two hydrogen atoms are abstracted from the polymer chains by the excited nitrous oxide molecule. The formation of cross links and unsaturation is nothing but a dehydrogenation from the polymer. Hence, the reaction scheme can be expressed as follows



Equation 3 shows the localization of excitation energy to the dissolved nitrous oxide molecule. Equation 4 shows the abstraction of hydrogen atoms from the different polymer chains, but eq. 5 shows dehydrogenation from the same chain. The formation of cross links and unsaturation, therefore, can be given by essentially the same mechanism. If an oxygen atom is formed in the polymer solid as a result of the dissociation of excited nitrous oxide, the oxygen probably abstracts two hydrogen atoms from the surrounding polymer chains. However, the details of the dehydrogenation process are still obscure.

Nitrous oxide has a molecular structure which is a resonance hybrid between two polarized structures,¹² and it shows various absorption spectra^{13,14} in the near-

(12) H. J. Emeléus and J. S. Anderson, "Modern Aspects of Inorganic Chemistry," 2nd Ed., Routledge, London, 1952, p. 323.

(13) H. Spomer and L. G. Bonner, *J. Chem. Phys.*, **8**, 33 (1940).

(14) M. Zelikoff, K. Watanabe, and E. C. Y. Ihn, *ibid.*, **21**, 1643 (1953).

and far-ultraviolet regions, *i.e.*, the continuous absorption between 3000 and 2400 Å. and absorption at 1820, 1450, 1285, 1178, and 1080 Å., etc. The lowest excitation level of a series of *n*-paraffin of increasing length, on the other hand, extrapolates to near 1750 Å. In addition, nitrous oxide shows a high solubility and a strong affinity (heat of solution: 2 kcal./mole) for polyethylene. These relations between the mutual species, polyethylene and nitrous oxide, would be favorable to the occurrence of excitation transfer. The possibility of charge transfer from polyethylene to nitrous oxide, however, remains questionable, for the ionization potential of nitrous oxide (12.9 e.v.) is higher than the extrapolated value (10.2 e.v.) from the potentials of *n*-paraffins.

The radiation-induced cross linking, generally speaking, must be reduced when an energy transfer occurs from the polymer chain to an additive if the localized energy to the additive is dissipated without inducing any chemical reaction. Linear paraffins are protected against cross linking¹⁵ by attaching a naphthyl group to the alkyl chain. It may be possible then that nitrous oxide plays the role of reducing the cross linking to some extent on one hand, and enhancing the cross linking to a greater extent on the other. In any case, the efficiency of absorbed energy by the polymer solid must be increased due to the occurrence of energy transfer. This explanation is not so unusual, for a greater part of absorbed energy is, by nature, dissipated as heat or light without inducing any chemical reaction.

The plots in Fig. 2 and 3 are not linear with the gas pressure. The slope of curves gradually decreases with an increase in the pressure. This behavior seems to be an essential nature of the sensitizing reaction, for the gas concentration should be proportional to the pressure in this range.⁶ This sort of concentration dependence is often seen in the system in which an energy transfer takes place. It seems reasonable that the efficiency of an additive molecule decreases when another additive molecule exists in the vicinity. If the sensitization were a chain reaction, in this connection, the curves would be concave upward.

4.2. Supplementary Discussion. It is considered to be the most reasonable idea, in the present stage, that the sensitizing reaction involves the excitation transfer process. Whether or not any other idea is possible, however, is a question. The contribution of polymer radicals or evolved hydrogen to this reaction can be disregarded because the probability of their collision with the nitrous oxide molecule should be low in the solid and because nitrous oxide itself is a relatively inert chemical species. When nitrous oxide gas was introduced into the ampoule after the

vacuum irradiation, the excess formation of cross links was not observed. Besides, in a range between -80 and 100° , the excess formation occurred almost equally.³ There remains, on the contrary, a small possibility that the thermalized secondary electron formed in the polymer solid contributes to the excess formation of cross links and unsaturation. The sub-excitation electron¹⁶ may yet be capable of exciting the nitrous oxide, for the lowest excited level of polyethylene is higher than that of nitrous oxide. Moreover, nitrous oxide can capture the thermalized electron and form a negative ion, because nitrous oxide has an electron affinity.¹⁷⁻¹⁹ If most of the nitrous oxide molecules are selectively excited through these processes, the dehydrogenation may take place from the polymer chains.

Nothing but the occurrence of excitation transfer can account for the appreciable chemical effect induced by a very small amount of xenon dissolved in the solid. The solubility of xenon and its heat of solution in polyethylene are estimated to be nearly the same as those of nitrous oxide, probably because the Lennard-Jones potential of both gases are accidentally close together.⁶ Xenon can accept only high excitation energy from polyethylene, for the lowest excited level of xenon (1470 Å.) is somewhat higher than that of polyethylene. It is difficult to assume the contribution of thermalized electrons in the case of xenon.

The effect of nitrous oxide on polyisobutylene can easily be accounted for by assuming an energy transfer process from the polymer chain to the nitrous oxide. Polyisobutylene also has a saturated hydrocarbon structure, and its gas solubility is much the same as polyethylene.²⁰ It seems reasonable to account for the effect of nitrous oxide on both polymers by assuming essentially the same mechanism. The fate of localized energy to the nitrous oxide and the material balance of nitrous oxide, in the case of polyisobutylene, will be discussed in a forthcoming paper.²¹ It may be difficult to assume the contribution of thermalized electrons in this case.

Acknowledgment. The author wishes to thank Professor A. Amemiya (University of Tokyo) and his

-
- (15) P. Alexander and A. Charlesby, *Nature*, **173**, 578 (1954).
 - (16) R. L. Platzman, *Radiation Res.*, **2** (1), 1 (1955).
 - (17) R. K. Curran and R. E. Fox, *J. Chem. Phys.*, **34**, 1590 (1961).
 - (18) G. J. Schulz, *ibid.*, **34**, 1778 (1961).
 - (19) F. S. Dainton and D. B. Peterson, *Proc. Roy. Soc. (London)*, **A267**, 443 (1962).
 - (20) S. Prager and F. A. Long, *J. Am. Chem. Soc.*, **73**, 4072 (1951).
 - (21) Y. Okada, a forthcoming paper.

group, especially K. Katsuura, for many helpful discussions and suggestions during this work. Thanks

are also given to T. Ito for his assistance in the experimental work.

Conductance Study of Model Hydrogen Bonding Solutes in Aqueous Solutions at 25°

by H. Olin Spivey¹ and Fred M. Snell

Department of Biophysics, State University of New York, Buffalo, New York (Received January 15, 1964)

Conductance measurements at 25° on dilute aqueous solutions of ethanoltrimethylammonium chloride, trimethylpropylammonium bromide, and N-methylbetaineamide chloride have been made. The limiting equivalent conductances of the cations with potential hydrogen bonding sites are compared with those of cations (alkyl analogs) of similar size and shape but lacking these sites. It is concluded that either the hydroxyl and amide groups on these cations are not associated with water molecules during transport or there exist mechanisms which compensate for their presence. Comparison of these data with mobility measurements on hydroxyl or amide containing nonelectrolytes in solution suggests that the affinity of solute hydrogen bonding groups for water molecules is affected by the neighboring atomic groups of the solute.

Hydrogen bond interactions between solute and solvent molecules may significantly affect both equilibrium and transport properties of these solutions. The purpose of this study is to assess, by means of conductance measurements, the extent of such interactions in the case of aqueous solutions of certain model solutes containing hydroxyl or amide groups.

Experimental

Materials. Ethanoltrimethylammonium chloride, $(\text{Me}_3\text{NEtOH})\text{Cl}$, and trimethylpropylammonium bromide, $(\text{Me}_3\text{NPr})\text{Br}$, obtained from Eastman Co. and N-methylbetaineamide chloride, $(\text{Me}_3\text{NCH}_2\text{CO}\cdot\text{NH}\cdot\text{CH}_3)\text{Cl}$, obtained from Starks Associates of Buffalo, N. Y. were recrystallized four to five times from isopropyl alcohol or a 50 vol. % mixture of benzene-isopropyl alcohol. Portions from the last two recrystallizations of each salt were stored *in vacuo* over P_2O_5 until needed. Potassium chloride (A.R. grade)

was recrystallized twice by hydrogen chloride precipitation from water, then dried, and fused in an inert atmosphere. It was tested and found free of hydroxyl ion contamination.² These crystals were used as the primary standard in titrations and conductance measurements. Distilled water from the building supply was further distilled, once from dilute sulfuric acid and then from a potassium hydroxide-potassium permanganate solution in an all-glass still. This latter distillation provided water for the conductivity solutions as well as steam for cleaning glass vessels.

(1) (a) This article is based on a thesis submitted by H. Olin Spivey to Harvard University in partial fulfillment of the requirements for the Ph.D. degree, 1963; (b) the work was begun at Harvard University and completed at the State University of New York at Buffalo; (c) Massachusetts Institute of Technology, Cambridge, Mass. 02139.

(2) G. D. Pinching and R. G. Bates, *J. Res. Natl. Bur. Std.*, **37**, 311 (1946).

Specific conductances between 1 and 2×10^{-7} ohm $^{-1}$ cm. $^{-1}$ were obtained for the water in all experiments.

Apparatus. One quartz and one Vycor flask cell of Shedlovsky design and 1-l. size were used for the conductance measurements together with apparatus described elsewhere.³ We feel that some improvements in performance were achieved in the construction of a solid state proportional temperature regulator and an inductance ratio arm bridge. Also, special Teflon pipets of 5- and 25-ml. capacity were constructed which offered advantages of quantitative transfer of small amounts of stock solution from solution weight bottles with negligible conductance contamination. The thermostat was maintained within $\pm 0.001^\circ$ of the same reference temperature for all experiments, as judged by a Beckmann differential thermometer. The absolute temperature of the bath was $24.97 \pm 0.02^\circ$ as measured by an N.B.S. calibrated, mercury in glass thermometer.

Procedure. A stock solution (0.05–0.10 *M*) of the salt to be studied was made by weight and successive portions were transferred from the solution weight bottles to the water or solution in the conductance cell, by means of the appropriate Teflon pipet. Conductance measurements were made on the resulting solutions covering the concentration range 10^{-4} – 2×10^{-2} *M*. Nitrogen gas, which was cleaned and equilibrated with water by passage through a set of gas dispersion bottles, was passed through the cell prior to and during the measurements in order to maintain the conductance at a stable minimum. Differential potentiometric titrations with silver nitrate solutions⁴ and duplicate density measurements were made on portions of the stock solution to determine concentrations accurately in molarity units (moles/l.).

Equivalent conductance values at each concentration were calculated after correcting for background conductance and polarization resistances and the resulting data were used to evaluate the unknown parameters in the Fuoss–Onsager equations⁵

$$\Lambda = \Lambda_0 - S\sqrt{c} + Ec \log c + (J - F\Lambda_0)c \quad (1)$$

unassociated electrolytes

$$\Lambda = \Lambda_0 - S\sqrt{\gamma c} + E\gamma c \log \gamma c + (J\gamma - K_A f_{\pm}^2 \Lambda \gamma - F\Lambda_0)c \quad (2)$$

associated electrolytes

Least-squares analyses of both equations were obtained using a program of Kay⁶ transcribed for an IBM 1620 computer.

Results

Three potassium chloride conductance experiments, each with eight concentration points, provided a test of our procedure along with cell constant calibrations.⁷ Cell constants with a standard deviation of 0.02% or better were obtained in each of the experiments. The first two experiments using the Vycor and quartz cells, respectively, were made just prior to the studies on the quaternary salts; the last one with the quartz cell was performed following these studies. Average cell constants found in each experiment are 1.0271

Table I: Equivalent Conductances of Quaternary Salts in Water at 25°

10 ² <i>c</i> (Me ₃ NEtOH)Cl	Λ	10 ² <i>c</i> (Me ₃ NPr)Br	Λ	10 ² <i>c</i> (Me ₃ NCH ₂ CO-NH-CH ₃)Cl	Λ
Run 1, 3 × ReX, V. ^a		Run 1, 4 × ReX, Q.		Run 1, 3 × ReX, Q.	
2.2797	110.43	2.7305	110.19	0.25937	108.45
4.1352	108.98	5.0237	108.54	3.5477	104.69
5.8827	107.94	7.0715	107.36	6.4844	102.98
7.5747	107.09	9.1693	106.33	9.1828	101.76
9.1443	106.41	11.866	105.21	11.492	100.86
		15.564	103.81	13.500	100.19
Run 2, 3 × ReX, Q.		Run 2, 5 × ReX, V.		Run 2, 4 × ReX, V.	
0.47715	112.65	0.41915	113.03	0.46232	107.97
1.3443	111.35	1.2242	111.75	2.3276	105.66
3.5268	109.39	3.8324	109.32	4.3952	104.14
5.4154	108.22	6.0223	107.90	6.7616	102.85
7.2402	107.29	8.1522	106.80	8.8613	101.87
		10.919	105.57	10.389	101.26
		14.173	104.32		
Run 3, 4 × ReX, V.		Run 3, 5 × ReX, Q.			
4.2698	108.93	0.81194	112.36		
5.0642	108.41	1.6625	111.25		
8.0669	106.90	4.5959	108.81		
10.640	105.87	7.6727	107.07		
14.002	104.61	11.1416	105.52		
19.017	103.17				

^a Abbreviations: V., Vycor cell; Q., quartz cell; ReX, times recrystallized.

(3) See ref. 1a, pp. 26–28, 51–54.

(4) D. A. MacInnes, "The Principles of Electrochemistry," Dover Publications, New York, N. Y., 1961, p. 306.

(5) R. M. Fuoss and F. Accascina, "Electrolytic Conductance," Interscience Publishers, Inc., New York, N. Y., 1959, pp. 195, 234.

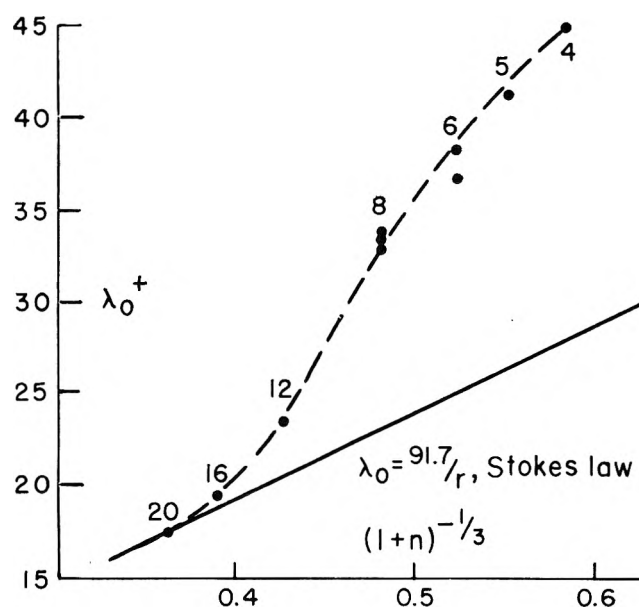
(6) R. L. Kay, *J. Am. Chem. Soc.*, **82**, 2099 (1960); we are grateful to Dr. Kay for sending us his revised program in 1962.

(7) J. E. Lind, J. J. Zwolenik, and R. M. Fuoss, *ibid.*, **81**, 1557 (1959).

Table II: Conductance and Density Results

	$\Lambda_0 \pm \sigma(\Lambda_0)^a$	Conductance			Density			
		$\sigma(\Lambda)^b$	$\delta\bar{\Lambda}^b$	$(J - F\Lambda_0)^c$	$10^3 m^d$	α	$\bar{V}_0 \pm 5^e$	$\bar{V}_0^+ \pm 5^e$
(Me ₃ NEtOH)Cl	114.55 ± 0.01	0.02	0.00	96.9	1.6070	0.012	127	109
(Me ₃ NPr)Br	114.84 ± 0.01	0.02	0.00	57.2	7.2649	0.037	145	120
(Me ₂ NCH ₂ CO·NH·CH ₃)Cl	109.80 ± 0.01	0.01	0.00	93.1	4.0246	0.023	145	127

^a Λ_0 , limiting equivalent conductance. ^b σ and $\delta\bar{\Lambda}$, standard and mean deviation. ^c $J - F\Lambda_0$, term from eq. 1. ^d m , moles/kg. of solution at which density, $d = 0.99707 + \alpha m$, was measured. ^e \bar{V}_0 (ml./mole), partial molal volume of the salt at infinite dilution; $\bar{V}_0^- = 18$ and 25 for Cl^- and Br^- , respectively (K. H. Stern and E. S. Amis, *Chem. Rev.*, **59**, 1 (1959)), for calculations of the partial molal volumes of the cations, \bar{V}_0^+ .

**Figure 1.** Ionic conductance as inverse function of size.

Ion	n	λ_0^+	Ion	n	λ_0^+
[Me ₄ N] ⁺	4	44.9	[Me ₂ NCH ₂ CO·NH·CH ₃] ⁺	8	33.4 ^a
[Me ₃ NEt] ⁺	5	41.2 ^b	[Et ₄ N] ⁺	8	32.7
[Me ₃ NEtOH] ⁺	6	38.2 ^a	[Pr ₄ N] ⁺	12	23.4
[Me ₃ NPr] ⁺	6	36.7 ^a	[Bu ₄ N] ⁺	16	19.5
[Me ₂ N(EtOH) ₂] ⁺	8	33.6 ^b	[Am ₄ N] ⁺	20	17.5

^a This study. ^b Ref. 9. All other λ_0^+ values from ref. 13, p. 463. The broken curve represents the corrected Stokes law (ref. 13 and Discussion); the line representing the uncorrected Stokes law, $\lambda = 91.7/r(\text{Å})$, was estimated assuming 0.5 Å . change for each four $-\text{CH}_2$ groups removed from Am_4N^+ to which $r = 5.3 \text{ Å}$. was assigned (ref. 13). Chloride and bromide limiting conductances were taken as 76.4 and 78.1, respectively, for calculating λ_0^+ values (ref. 13, p. 463), which are probably all accurate to within $\pm 0.1 \lambda$ unit.

cm.^{-1} , Vycor cell; 0.62887 and 0.62872 cm.^{-1} , quartz cell, listed in order of determination.

Equivalent conductances, Λ , and molarities, c , calculated from the experimental measurements on the quaternary salt solutions are given in Table I. Table II lists values of equivalent conductances at

infinite dilution with their standard deviations, $\sigma(\Lambda_0)$, and the standard and mean deviations of all experimental points, $\sigma(\Lambda)$ and $\delta\bar{\Lambda}$, respectively, from the unassociated electrolyte eq. 1. In these calculations all data for a given salt were used in evaluation of the terms in eq. 1. Remaining columns in Table II give density data from duplicate measurements and partial molal volumes at infinite dilution, \bar{V}_0 , calculated from apparent molal volumes, ϕ , and use of the Redlich equation,⁸ $\phi = \bar{V}_0 + 1.86\sqrt{c}$. Figure 1 shows cation limiting conductance values, λ_0^+ , derived from these and similar measurements of others plotted as a function of n , the number of atoms other than hydrogen in the groups attached to the quaternary nitrogen. Table III summarizes various radii for cations of interest, calculated as indicated footnotes of Table III.

Table III: Ionic Radii, Å .

	r_a^a	r_b^b	r_v^c	r_c^d
[Me ₃ NEtOH] ⁺	2.40	3.72	3.5	2.9-3.9
[Me ₃ NPr] ⁺	2.50	3.77	3.6	2.9-3.9
[Me ₂ NCH ₂ CO·NH·CH ₃] ⁺	2.74	3.93	3.7	2.9-4.7
[Et ₄ N] ⁺	2.80	3.92		4.0
[Me ₂ N(EtOH) ₂] ⁺	2.73	3.90		2.2-4.0

^a $r_a = 0.820|z|/\lambda_0\eta_0$, Stokes law radius. ^b r_b = corrected Stokes radius, ref. 13. ^c $r_v = 10^8[(3/4\pi N_A)\bar{V}_0^+]^{1/3}$. ^d r_c estimated from Courtauld molecular models as minor-major semi-axes, assuming ellipsoid of revolution.

Discussion

Experimental Accuracy. Our conductance values for potassium chloride solutions are within 0.02% standard deviation of the equation suggested by Lind, Zwolenik, and Fuoss⁷ as best representing selected data from the literature. The close agreement between Λ_0 -values obtained using the quartz or Vycor

(8) O. Redlich, *J. Phys. Chem.*, **67**, 496 (1963).

cell for the quaternary salt experiments further corroborates the accuracy of the cell constants used. Duplicate potentiometric titrations with silver nitrate solutions were made on each stock solution of quaternary salt except for N-methylbetaineamide chloride, $3 \times \text{ReX}$, where one of the titrations was lost. Silver nitrate solutions were standardized by duplicate titrations with potassium chloride solutions prior to each stock solution determination. At least two end point determinations were made for each titration. Standard deviations of concentrations calculated from all end points averaged 0.01% and never exceeded 0.025% for the stock solutions. For each standardization, a 0.01% agreement between weight determined concentrations and titration determined concentrations of silver nitrate was obtained, giving additional evidence of the purity of potassium chloride which served as the standard for the conductance data.

The above considerations would lead us to judge that the errors in Λ - and Λ_0 -values of these measurements are not in excess of $\pm 0.05 \Lambda$ unit. To our knowledge, the only cation in these experiments which has been similarly studied is $[\text{Me}_3\text{NEtOH}]^+$. Varimbi and Fuoss⁹ report a $\lambda_0^+ = 38.4$; Fleming¹⁰ reports $\lambda_0^+ = 42.0$, to be compared with the value of 38.2 herein reported.

Conductance Equation. As indicated in Table II, the data for each salt studied can be represented by the unassociated electrolyte eq. 1 within a standard deviation of 0.02% and negligible mean deviation, *i.e.*, the data are randomly distributed about this equation. Analysis of the data by the associated electrolyte equation provided association constants less than unity which are negligible in dilute solutions and of the order of experimental precision. However, more recent theoretical and experimental considerations¹¹ have indicated that association constants less than 40 may be in considerable error and that in general, little physical significance may be attached to the distance of closest approach parameter, a , derived from J . We, therefore, report only the lumped coefficient of the linear term in the Fuoss-Onsager equation, $(J - F\Lambda_0)c$. These uncertainties in the higher order terms have little effect on the intercept, Λ_0 , however.

Molecular Interpretations. Each hydroxyl group has the potentiality of two hydrogen bonds, and the amide groups the possibility of three (not to mention the possibility of secondary hydration). On the other hand, Courtauld molecular models and the derived radii, r_c , listed in Table III indicate that, unless there are special compensating mechanisms, a single water molecule hydrogen bonded to the hydroxyl or amide

groups of the model cations would lower their mobilities¹² below that of the alkyl analogs of comparable size. This lowering would be at least one λ -unit and probably two or more, judging from the effect of an added $-\text{CH}_2$ on λ_0^+ seen in Fig. 1 in the region $n = 6-8$. Instead, we have found quite similar, but slightly higher mobilities for the model cations ($n = 6$ and 8) than for their alkyl analogs. This is most simply interpreted as evidence that the $-\text{OH}$ and $-\text{CO-NH-CH}_3$ groups of these solutes are not hydrogen bonded to water.

We consider the data next in terms of classical hydrodynamic theories. The dashed curve in Fig. 1 is drawn through the conductance values of the symmetrical tetraalkylammonium ions with $n = 4, 8, 12, 16,$ and 20 and represents the corrected Stokes law suggested by Robinson and Stokes.¹³ This curve demonstrates the experimental fact that as the radii of solute particles decreases (below 5 \AA . in water) relative to the solvent, the mobility of the particles increases progressively faster than predicted by the linear Stokes law, $\lambda = 91.7/r(\text{\AA})$. Thus, corrected Stokes radii, r_h , calculated for the ions of interest here, (Table III)¹³ differ still less in percentage than the mobilities, due to the nonlinear relation between them. For example, the 4.1% mobility difference between $[\text{Me}_3\text{NEtOH}]^+$ and $[\text{Me}_3\text{NPr}]^+$ requires only a 1.3% difference in r_h or 0.05 \AA . Furthermore, on the assumption that there is negligible solvent interaction with the symmetrical alkylammonium ions (or interaction similar to that of other ions), deviations from this curve may be attributed to molecular asymmetry and/or specific solvent interactions. Indeed, the low mobility of the $[\text{Me}_3\text{NPr}]^+$ ion compared to the symmetrical cations seen in Fig. 1 is not unexpected, considering its asymmetry and the effects of rotational Brownian motion. Thus, the small differences that are found in the cation mobilities seem explicable in terms of existing hydrodynamic theories without invoking any specific interaction with solvent molecules.¹⁴

(9) J. Varimbi and R. M. Fuoss, *J. Phys. Chem.*, **64**, 1335 (1960).

(10) R. Fleming, *J. Chem. Soc.*, 4914 (1960).

(11) D. J. Karl and J. Dye, *J. Phys. Chem.*, **66**, 477 (1962); R. M. Fuoss and L. Onsager, *ibid.*, **66**, 1722 (1962); R. L. Kay and J. Dye, *Proc. Natl. Acad. Sci. U. S.*, **49**, 5 (1963); H. O. Spivey, *ref. 1a*, p. 7 ff.

(12) Mobility, $u = 6.466 \times 10^9 \lambda / |z|$ (cm. sec.⁻¹ dyne⁻¹), see, *e.g.*, *ref. 13*, pp. 42, 43.

(13) R. A. Robinson and R. H. Stokes, "Electrolyte Solutions," 2nd Ed., Butterworth and Co., Ltd., London, 1959, pp. 123-125.

(14) Radii derived from the partial molal volumes, v_v , are consistent with this view as well as reasonable in comparison with the other radii, though molecular interpretations from these small differences are certainly questionable.

Alternative explanations should be considered which might permit hydrogen bond interactions of water to the cations without causing a decrease of their mobility. Thus, *e.g.*, $\text{Me}_3\text{N}^+\text{Pr}$ ions might be surrounded by solvent with a larger local viscosity than the bulk value due to the structure promoting effect of the nonpolar groups as suggested by Frank and Evans.¹⁵ Indeed, viscosity¹⁶ and heat capacity¹⁷ measurements on the symmetrical quaternary ions do indicate an unusually large structure promoting influence of these cations on aqueous solutions. In contrast, such a structured region about the more polar $[\text{Me}_3\text{N}(\text{EtOH})]^+$ ion might be prevented or less favored by solvent interactions with the hydroxyl group. The ideas of Samoilov¹⁸ whereby the frequency of exchange between water molecules adjacent to a solute is increased may lead to the same result. Also, the attraction between the charge on the nitrogen and the polar functional groups may cause a sufficient contraction in radius to mask the effects of bound water. It seems unlikely, however, that these special mechanisms could compensate for the effects of bound water molecules (particularly for two or more) in the case of each model solute.

Finally, we compare these ideas and results with those from related studies of others. Viscosity measurements on the system dimethylacetamide and water¹⁹ and dimerization constant measurements of N-methylacetamide in water, in comparison with measurements in dioxane, carbon tetrachloride, or benzene,²⁰ have been interpreted as evidence for water hydrogen bonded to these amides. It is likely, however, that the high concentrations of amides in water encountered in these experiments (7–12 M) could prevent the normal hydrogen bond structure of water and hence shift the equilibrium in favor of solute–solvent interactions on this basis. On the other hand, Longworth²¹ calculates hydration numbers at infinite dilution of 3.0, 2.5, and 1.9 for acetamide, methylacetamide, and dimethylacetamide, respectively; for hydroxy

compounds, hydration numbers of approximately one molecule per hydroxyl group are found. If these hydration numbers are accepted and attributed to hydrogen bonding, comparison with our conductance data, where little evidence of hydrogen bonding appears, suggests that such interactions may be affected by neighboring atomic groups of the solute. Such differences in behavior between the cations of this study and the nonelectrolyte solutes in other studies mentioned might be due to the charge on the nitrogen atom interfering with the neighboring hydrogen bonding sites or they may be due to alternative mechanisms as referred to above. In any case, they indicate that a variety of behavior may be observed with such solutes in water and suggest that considerable caution should be used in deductions and generalizations based on these models.

Acknowledgments. We wish to express our thanks to Dr. Robert A. Spangler for advice and assistance on electronic problems, Mr. Edward Gill for assistance with some of the measurements, and Mr. Basilio Scofidio for work on the computer program and calculations. We are also grateful to Dr. T. Shedlovsky for timely help in regard to the potentiometric titrations and construction of the conductance cells. Economic support for this study was provided in part by U. S. Public Health Service Research Grant RG-6730 and Training Grant 571GM718.

(15) H. S. Frank and M. W. Evans, *J. Chem. Phys.*, **13**, 507 (1945).

(16) E. Hückel and H. Schaaf, *Z. physik. Chem. (Frankfurt)*, **21**, 326 (1959).

(17) H. S. Frank and W. Y. Wen, *Discussions Faraday Soc.*, **24**, 133 (1957).

(18) O. Ya. Samoilov, *ibid.*, **24**, 141 (1957).

(19) R. C. Petersen, *J. Phys. Chem.*, **64**, 184 (1960).

(20) I. M. Klotz and J. S. Franzen, *J. Am. Chem. Soc.*, **84**, 3461 (1962); M. Davies and D. K. Thomas, *J. Phys. Chem.*, **60**, 767 (1956); G. E. Hibberd and A. E. Alexander, *ibid.*, **66**, 1854 (1962).

(21) L. G. Longworth, *ibid.*, **67**, 689 (1963), and personal communication.

The Reduction of Nitrite by Molybdenum(V)¹

by Jean A. Frank² and Jack T. Spence

Chemistry Department, Utah State University, Logan, Utah (Received January 16, 1964)

The kinetics and mechanism of the reduction of nitrite by Mo(V) in aqueous solution have been investigated. It was found that NO was produced in stoichiometric amounts during the reduction. The reaction was determined to be first order with respect to nitrite and hydrogen ion and zero order with respect to Mo(V) in the pH range 5.0–7.5. A negative salt effect on the reaction rate was observed. The activation energy, free energy, and entropy for the reaction have been determined. A mechanism, involving the formation of NO⁺ from HNO₂ as the rate-determining step, has been developed.

Molybdenum has been shown to participate in the enzymatic reduction of nitrate to nitrite.³ The subsequent biological reduction of nitrite to hyponitrite is apparently mediated by an iron and copper containing enzyme,⁴ but little is known concerning its properties. It is perhaps significant that a nitrite-reducing system obtained from bacteria has been reported to convert nitrite to nitric oxide,⁵ but whether or not a metal is involved is not yet known.

Recently, considerable interest has been shown in the ability of molybdenum to catalyze the reduction of nitrate by various reducing agents in strong acid.^{6–9} It has been reported that Mo(V) will reduce hydroxylamine to ammonia in acid¹⁰ and that it acts as a catalyst for the reduction of hydroxylamine by stannous chloride, again under strongly acidic conditions.¹¹ No reports have appeared, however, concerning the reduction of nitrite by Mo(V).

There have been a number of studies concerning the reduction of nitrite or nitrous acid. The reactions with ferrous ion¹² and with metallic copper^{13,14} have both been investigated. In addition, the reductions by sulfite, oxalate, formate, sulfamate, iodide, and several other species have been reported.¹⁵ Of particular interest, because of the nature of the intermediate, is the study of Anbar and Taube of the rate of exchange of oxygen between nitrite and water.¹⁶

Preliminary work in this laboratory, undertaken as part of a study of possible models for nitrate reductase, indicated that Mo(V) reduces nitrite to nitric oxide at a considerably faster rate than it reduces nitrate to nitrite.¹⁷ Because of its relation to nitrate reduction

and its possible biochemical significance, the reaction was investigated in detail.

Experimental

Materials. Molybdenum(V) stock solutions in HCl were prepared and standardized as previously reported.¹⁸ The chloride ion concentrations and the ionic strength of the solutions were maintained constant by the addition of the proper amount of a stock solution of NaCl, prepared from Baker and Adamson reagent grade NaCl.

(1) Journal Paper No. 384, Utah State Agricultural Experiment Station.

(2) Abstracted from the thesis submitted by J. A. Frank in partial fulfillment of the requirements for the Ph.D. degree, Utah State University, 1963.

(3) D. J. D. Nicholas and A. Nason, *J. Biol. Chem.*, **211**, 183 (1957).

(4) D. J. D. Nicholas, *Nature*, **179**, 800 (1957).

(5) T. Yamanaka, A. Otaand, and K. Okunuki, *Biochim. Biophys. Acta*, **53**, 294 (1961).

(6) G. P. Haight, Jr., *Acta Chem. Scand.*, **15**, 2012 (1961).

(7) G. P. Haight, Jr., P. Mohliner, and A. Katz, *ibid.*, **16**, 221 (1962).

(8) G. P. Haight, Jr., and A. Katz, *ibid.*, **16**, 659 (1962).

(9) J. M. Kolthoff and J. Hodara, *J. Electroanal. Chem.*, **5**, 2 (1963).

(10) G. P. Haight, Jr., and A. C. Swift, *J. Phys. Chem.*, **65**, 1921 (1961).

(11) G. P. Haight, Jr., and C. V. Frankenberg, *Acta Chem. Scand.*, **15**, 2026 (1961).

(12) E. Abel, H. Schmid, and I. Pollak, *Monatsh.*, **69**, 125 (1936).

(13) Y. Komuro and K. Kato, *Bull. Aichi Gakugei. Univ.*, **2**, 43 (1953).

(14) Y. Komuro and K. Kato, *Chem. Abstr.*, **48**, 1122 (1952).

(15) T. A. Turney and G. A. Wright, *Chem. Rev.*, **59**, 497 (1959).

(16) M. Anbar and H. Taube, *J. Am. Chem. Soc.*, **76**, 6243 (1954).

(17) J. T. Spence and J. A. Frank, *ibid.*, **85**, 116 (1963).

(18) J. T. Spence and G. Kallos, *Inorg. Chem.*, **2**, 710 (1963).

In order to obtain reproducible results, the stock solutions of Mo(V) were aged for 12 days before use. Standard solutions of NaNO₂ were prepared from Baker and Adamson reagent grade material that had been dried *in vacuo* over P₂O₅. Before use these solutions were analyzed for nitrite concentration by the method of Shinn.¹⁹ Phosphate buffers were prepared from reagent grade KH₂PO₄ and NaOH and adjusted to the proper pH and ionic strength. Helium, used for flushing the reaction vessels, was obtained from Matheson Co. Its purity (99.99%) was found to be sufficient and no deoxygenation treatment was required. Nitric oxide was obtained in lecture bottles from Matheson Co. All other chemicals used were reagent grade.

Methods. A silica spectrophotometric cell, which could be evacuated, was joined to a specially constructed reaction vessel for measurement of Mo(V) concentrations. This was essential because Mo(V) is easily oxidized by atmospheric oxygen. The buffer and sodium nitrite solutions were added to the vessel and flushed with helium for 30 min. The proper amount of Mo(V) stock solution, which had also been deoxygenated, was then added and mixed with a helium stream. The moment of mixing was recorded as zero time. A stopcock at the bottom of the vessel was opened to allow the solution to flow into the evacuated cell. The cell was then sealed with an oxygen torch and placed in a constant temperature bath. The concentration of Mo(V) was determined by removing the cell momentarily from the thermostat and reading its absorbance at 289 m μ in a Beckman DU spectrophotometer against a blank containing buffer and sodium nitrite. For following nitrite concentrations with time, helium was bubbled continuously through the reaction vessel under a slight positive pressure and samples of the proper volume were withdrawn through a rubber diaphragm using a hypodermic syringe. The sample was then analyzed for nitrite.¹⁹ When a run had a large excess of nitrite, the sample was prepared as above; but the sealed cell was allowed to remain in the spectrophotometer compartment for the entire reaction, due to the increased rate. The temperature in the compartment was maintained constant by the use of thermospacers. Unless one reactant was in large excess, duplicate runs were made, one being analyzed for Mo(V) and the other for nitrite.

Runs were made at five pH values, from 4.68 to 7.50, to determine the effect on the rate. Lower pH values were not used because of the rapidity of the reaction and because of the autodecomposition of nitrite, which becomes appreciable in acidic solutions. Higher values were not used because of the great decrease in reaction rate and because of the tendency of Mo(V) to precipitate as the hydroxide in basic solution.

Kinetic measurements were also made at four temperatures, 20, 35, 42, and 50°, to obtain the activation energy for the reaction. Runs which contained initially both the products, Mo(VI) and NO, were made in order to investigate possible effects on the rate. Runs were made containing 1 M Na₂SO₄ in addition to the reactants to investigate ionic strength effects.

Gas measurements to determine the stoichiometry of the reaction were made with a Warburg constant volume respirometer, using the procedure of Umbreit, Burris, and Stauffer.²⁰ The buffer containing the nitrite was measured into the single arm Warburg flask and the Mo(V) stock solution was measured into the side arm. The flask was shaken under a flow of helium in the thermostat for 1 hr. and then closed off. Thirty minutes were allowed to establish equilibrium before the initial reading of the manometer was made. The Mo(V) and nitrite solutions were mixed immediately after this reading and the flask shaken in the bath for the desired time. The final reading on the manometer was then taken. Identical solutions were prepared and the concentrations of Mo(V) and nitrite were determined with time as described.

All pH measurements were made with a Beckman expanded scale pH meter. Rate constants and the activation energy were obtained from the slope of the proper plots, using the method of least squares.

Results

Stoichiometry. Previous work, using gas chromatography, had identified the gas produced in the reduction of nitrite by Mo(V) as nitric oxide.¹⁷ Furthermore, no appreciable amounts of other nitrogen oxides were detected.

In the present work, the average value for the number of moles of NO produced for each mole of nitrite consumed, measured at various reaction times, was found to be 1.02 with a standard deviation of ± 0.03 . In all cases, the concentrations of Mo(V) and nitrite were found to be the same, within experimental error, at equal reaction times.

Kinetics. The over-all order of the reaction was determined from the runs containing equal amounts of Mo(V) and nitrite, at different total concentrations. It was found that under these conditions the half-lives for each run were the same, indicating an over-all first-order reaction. When the results were plotted as first-order reactions, straight lines were obtained for initial

(19) M. B. Shinn, *Ind. Eng. Chem., Anal. Ed.*, **13**, 33 (1941).

(20) W. W. Umbreit, R. H. Burris, and J. T. Stauffer, "Manometric Techniques," 3rd Ed., Burgess Publishing Co., Minneapolis, Minn., 1957.

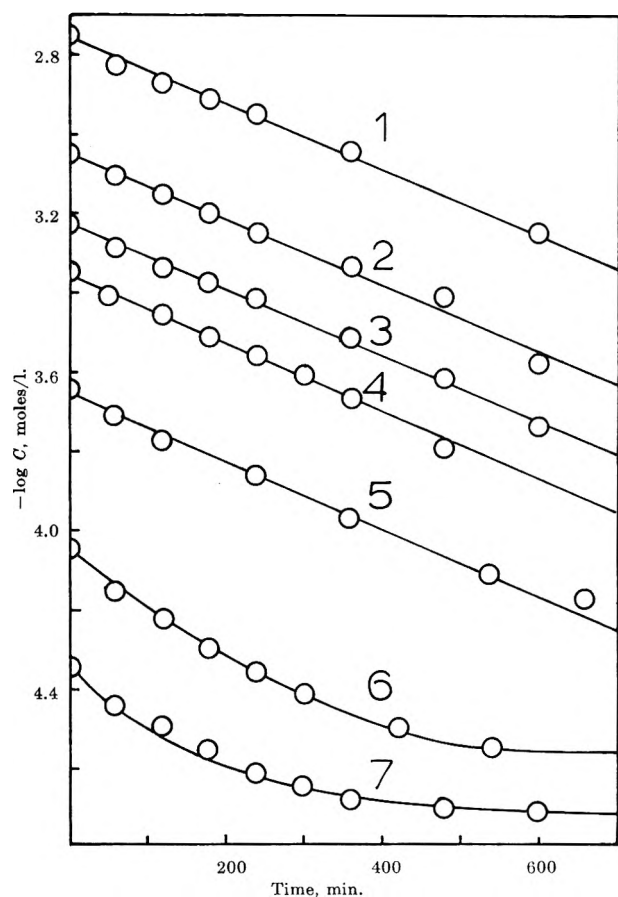


Figure 1. First-order plots for equal concentration runs; $-\log C$ ($C = [\text{Mo(V)}] = [\text{NO}_2^-]$) is plotted vs. time. Numbers refer to runs as listed in Table I. $T = 35^\circ$, pH 6.23, 0.05 M phosphate buffer, $\mu = 0.77$.

concentrations of 1.80×10^{-3} to $2.25 \times 10^{-4} M$ (Fig. 1). Below this concentration, considerable deviation from the first-order plots was observed; however, no other simple order equations would fit the data in this region of low concentration.

The order with respect to each reactant was determined from runs in which the concentration of one reactant was in large excess. When Mo(V) was in excess, the same half-life was obtained as in the equal concentration runs. When nitrite was in excess, the rate was independent of Mo(V) concentration, indicating a reaction first order in nitrite and zero order in Mo(V), within the above concentration range. The first-order rate constant obtained from the run with excess Mo(V) agreed very well with the first-order rate constant of the equal concentration run containing the same nitrite concentration. The rate constant obtained from the run with excess nitrite was found also to be in excellent agreement with the other results. (In this case, the zero-order rate constant, k' , obtained from the equation,

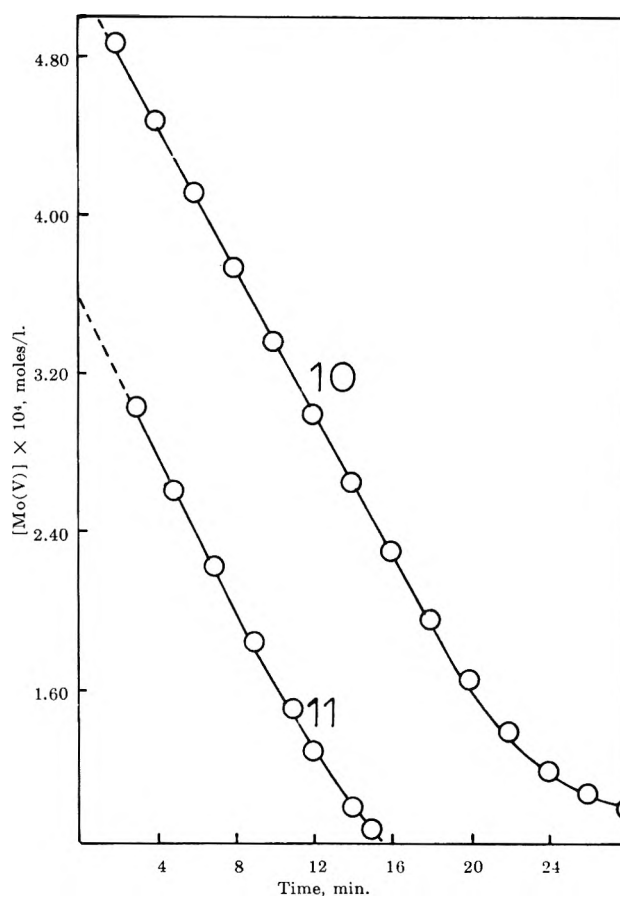


Figure 2. Zero-order plots for runs with excess NO_2^- ; concentration of Mo(V) is plotted vs. time. Numbers refer to runs as listed in Table I. $T = 35^\circ$, pH 6.23, 0.05 M phosphate buffer, $\mu = 0.77$.

rate = $k[\text{NO}_2^-] = k'$, was divided by $[\text{NO}_2^-]$ in order to obtain the first-order constant, k .) In the runs with excess nitrite, the plot of concentration of Mo(V) vs. time gave a straight line until the Mo(V) concentration had fallen to approximately $10^{-4} M$, in agreement with the results of the equal concentration runs (Fig. 2).

It was observed that the rate was strongly dependent on pH, increasing rapidly with an increase in acid concentration. The data gave good first-order plots in all cases, indicating that the order did not change with pH. The reaction was found to be first order with respect to hydrogen ion concentration. This was determined by plotting the data according to the equation, rate = $k_1[\text{NO}_2^-][\text{H}^+]^n$, and observing that consistent values of k_1 were obtained only for $n = 1$.

It was found that the rate of the reaction was unaffected by the presence of the products, NO or Mo(VI).

It was found that an increase in ionic strength produced a significant decrease in the rate but did not affect the order. Because of the high ionic strength necessary

for the reactions ($\mu = 0.77$) no further attempts were made to study this effect quantitatively.

The activation energy for the reaction was determined from the runs at four temperatures at the same pH, concentration, and ionic strength. The Arrhenius plot for this data is shown in Fig. 3. From the slope of the line the activation energy was determined to be 10.6 kcal. From the frequency factor obtained from the intercept, a value of ΔS^* of -16.4 e.u. was obtained and ΔF^* was calculated from Eyring's rate equation to be 15.6 kcal.

Table I: Rate Constants

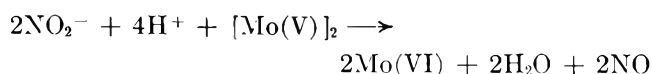
Run ^a	[Mo(V)] ₀ × 10 ⁴ , moles/l.	[NO ₂ ⁻] ₀ × 10 ⁴ , moles/l.	pH	T, °C.	k ₁ × 10 ⁻³ , moles/l. min. ⁻¹
1 ^b	18.0	18.0	6.23	35	3.24
2 ^b	9.00	9.00	6.23	35	3.29
3 ^b	6.00	6.00	6.23	35	3.29
4 ^b	4.50	4.50	6.23	35	3.31
5 ^b	2.25	2.25	6.23	35	3.38
6 ^b	0.900	0.900	6.23	35	...
7 ^b	0.450	0.450	6.23	35	...
8 ^b	9.00	4.50	6.23	35	3.41
9 ^b	18.0	0.132	6.23	35	3.23
10 ^b	5.12	100.00	6.23	35	3.13
11 ^b	3.67	100.00	6.23	35	3.23
12 ^b	17.6	17.6	7.50	35	3.10
13 ^b	9.00	9.00	5.90	35	3.00
14 ^b	4.50	4.50	5.90	35	2.95
15 ^b	9.26	9.26	5.04	35	3.21
16 ^b	9.00	9.00	4.68	35	3.03
17	9.00	9.00	6.23	20	1.52 mean
18	4.50	4.50	6.23	20	
19	9.00	9.00	6.23	42	4.79 mean
20	4.50	4.50	6.23	42	
21	9.00	9.00	6.23	50	7.00 mean
22	4.50	4.50	6.23	50	
23 ^c	18.0	18.0	6.23	35	1.07
24 ^c	9.00	9.00	6.23	35	1.34

^a All runs made in 0.05 M phosphate buffer with $\mu = 0.77$.

^b Average value of k_1 for runs 1-16 with standard deviation: $k_1 = 3.20 \pm 0.14$. ^c Runs 23 and 24 contained 1.00 mole/l. of Na₂SO₄.

Discussion

The stoichiometric data indicate that the over-all reaction is relatively simple and can be represented as



(The exact species of Mo(V) and Mo(VI) present in aqueous solution are unknown; but it appears that Mo(V) exists as a dimer²¹ and that both species occur as oxyanions.)

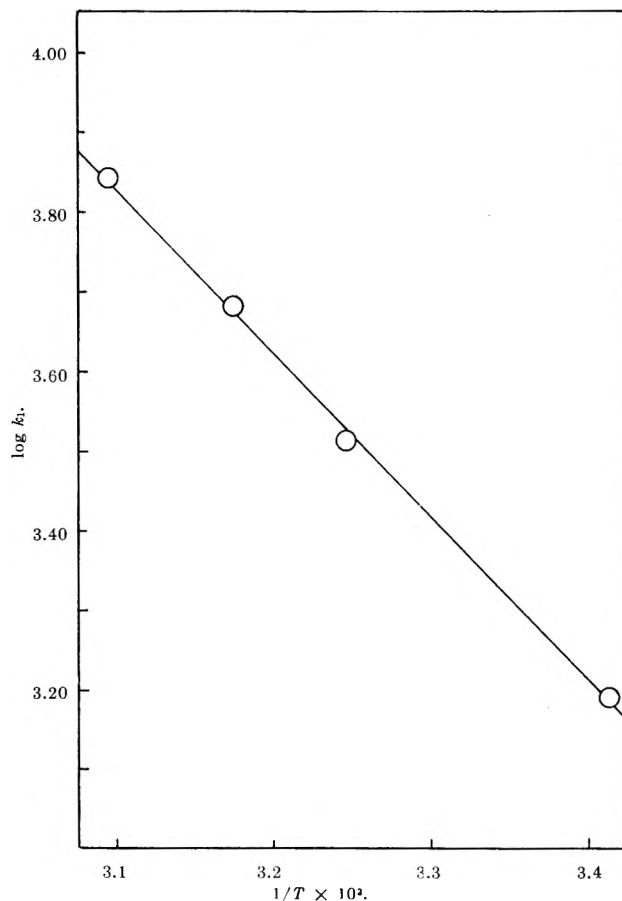


Figure 3. Arrhenius plot of temperature dependence of rate constant: $\log k_1$ is plotted vs. $1/T$. pH 6.23, 0.05 M phosphate buffer, $\mu = 0.77$.

In the concentration range from 1.80×10^{-3} to 2.25×10^{-4} M the reaction is first order in nitrite, first order in H^+ , and zero order in Mo(V). The rate-determining step, therefore, must involve the decomposition of either nitrite ion, nitrous acid, or some species formed from H^+ and NO_2^- into an intermediate species which reacts quickly with Mo(V) to give the products. (In the pH range studied, the nitrite is present predominantly as nitrite ion since K_a for nitrous acid is 4.0×10^{-4} . Since the nitrite analysis measures total nitrite; this is equivalent to measuring the nitrite ion concentration.)

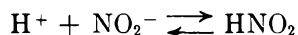
This gives the experimental rate law

$$\text{rate} = k_1[\text{H}^+][\text{NO}_2^-] \quad (1)$$

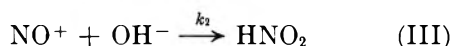
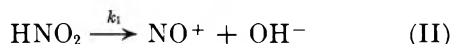
The reactive intermediate cannot be HNO_2 since the rate of formation of HNO_2 from H^+ and NO_2^- would be considerably greater than the over-all rate of the reaction. Although there is no direct evidence to support

(21) G. P. Haight, Jr., *J. Inorg. Nucl. Chem.*, 24, 663 (1962).

it, NO^+ is a reasonable possibility for the intermediate. This species has been proposed for various other reactions of nitrous acid.^{13,14,16} The following possible mechanism, based on NO^+ as the reactive intermediate, is proposed.



$$K_a = [\text{H}^+][\text{NO}_2^-]/[\text{HNO}_2] \quad (\text{I})$$



Nitrous acid, in equilibrium with H^+ and NO_2^- , decomposes in the rate-controlling step (reaction II) into NO^+ and OH^- . In a subsequent fast step (reaction IV) the NO^+ reacts with Mo(V) to give the products.

The rate of the reaction is given by

$$\text{rate} = k_3[\text{NO}^+][\text{Mo(V)}] \quad (2)$$

Applying the steady-state condition to $[\text{NO}^+]$

$$\frac{d[\text{NO}^+]}{dt} = 0 = k_1[\text{HNO}_2] -$$

$$k_2[\text{NO}^+][\text{OH}^-] - k_3[\text{NO}^+][\text{Mo(V)}] \quad (3)$$

$$[\text{NO}^+] = \frac{k_1[\text{HNO}_2]}{k_2[\text{OH}^-] + k_3[\text{Mo(V)}]} \quad (4)$$

Replacing $[\text{HNO}_2]$ and $[\text{OH}^-]$ from their respective equilibria and substituting for $[\text{NO}^+]$ in eq. 2

$$\text{rate} = \frac{k_3 k_1 [\text{H}^+] [\text{NO}_2^-] [\text{Mo(V)}] / K_a}{k_2 K_w / [\text{H}^+] + k_3 [\text{Mo(V)}]} = \frac{k_1 / K_a [\text{H}^+]^2 [\text{NO}_2^-] [\text{Mo(V)}]}{k_2 K_w / k_2 + [\text{H}^+] [\text{Mo(V)}]} \quad (5)$$

When $(k_2/k_3 K_a) \ll [\text{H}^+][\text{Mo(V)}]$, this simplifies to

$$\text{rate} = \frac{k_1}{K_a} [\text{H}^+] [\text{NO}_2^-] \quad (6)$$

This expression is identical with the experimental rate law in the concentration range 1.80×10^{-3} to 10^{-4} M.

The nature of the species of Mo(V) involved in the reaction is uncertain. There is evidence that at the pH and concentrations employed in this work it is present primarily as a dimer.²¹ Whether it reacts in this form or as a monomer is unknown. If NO^+ reacts with

the dimer, $[\text{Mo(V)}]_2$, the same rate expression is obtained, except $[\text{Mo(V)}]$ is replaced by $[\text{Mo(V)}]_2$.

The cause of the deviation from second-order kinetics when the total Mo(V) concentration drops below 10^{-4} M is unknown. It may be that the first term in the denominator of eq. 5 becomes significant at this concentration. At present, however, this cannot be determined since the exact species of Mo(V) involved in the reaction is unknown. Further work to elucidate the nature and reactions of Mo(V) species in dilute solution is planned.

The experimental entropy of activation, $\Delta S^* = -16.4$ e.u., is in agreement with the proposed mechanism since it implies a greater degree of order in the transition state than in the reactants. Such a situation would arise because of the separation of charge occurring in the transition state as the neutral molecule decomposes into NO^+ and OH^- , with a subsequent increase in ordering of solvent molecules. It should be noted that the experimental ΔS^* was calculated from the experimental rate constant. If the proposed mechanism is correct, this rate constant (k) involves the actual rate constant (k_1) and the ionization constant for HNO_2 (K_a)

$$k = k_1 / K_a$$

$$\Delta S^*_{\text{exptl}} = \Delta S^*_{\text{rate det. step}} - \Delta S_{\text{ionization of HNO}_2}$$

The experimental ΔS^* thus involves the entropy of ionization of nitrous acid, which is calculated from standard thermodynamic functions²² to be -5.4 e.u. If a correction is made for this, ΔS^* becomes -21.8 e.u.

The proposed mechanism is in agreement with the experimental rate data in the concentration range in which it can be experimentally verified. Furthermore, other kinetic studies on reactions of nitrous acid are in agreement with the results and strengthen the postulate of NO^+ as the reactive intermediate.

Acknowledgment. Thanks are expressed by the authors for financial support from funds administered by the Agriculture Research Center of Stanford Research Institute in the name of The James G. Boswell Foundation and the Public Health Service, grant GM 08347-2, Division of General Medical Sciences, National Institutes of Health.

(22) F. D. Rossini, D. D. Wagman, W. H. Evans, S. Levine, and I. Jaffe, "Selected Values of Chemical Thermodynamic Properties," National Bureau of Standards Circular, U. S. Government Printing Office, Washington, D. C., 1952.

Proton Magnetic Resonance Studies of Hydrogen Bonding of 2-Propanol with N-Methylacetamide and N,N'-Dimethylacetamide¹

by Fujio Takahashi and Norman C. Li

Chemistry Department, Duquesne University, Pittsburgh, Pennsylvania (Received January 27, 1964)

Proton magnetic resonance studies are reported of hydrogen bonding between the OH proton of 2-propanol and the hydrogen acceptors, N-methylacetamide and N,N'-dimethylacetamide, and of self-association of 2-propanol, all in CCl₄ medium. Data on the variation of the OH proton frequency as a function of the concentration of the N-substituted acetamides at different temperatures are treated graphically in a manner which permits the determination of the equilibrium constant of a 1:1 complex, K , between 2-propanol and the N-substituted acetamide. The enthalpy changes on hydrogen bond formation were determined to be -4.1 and -2.4 kcal./mole for N-methylacetamide and N,N'-dimethylacetamide, respectively.

Introduction

As part of an extensive program in this laboratory on the use of nuclear magnetic resonance method for the study of hydrogen bonding in relatively noninteracting solvents, this paper presents the results of thermodynamic studies of hydrogen bonding of 2-propanol with N-methylacetamide and N,N'-dimethylacetamide as hydrogen acceptors in CCl₄. Mathur, *et al.*,² have shown that for an equilibrium between a monomeric hydrogen donor, M, and a hydrogen acceptor or electron donor, D, to form a 1:1 complex, MD, the following equation may be derived when $d \gg (MD)$

$$\frac{1}{\nu - \nu_f} = \frac{1}{K(\nu_c - \nu_f)} \frac{1}{d} + \frac{1}{(\nu_c - \nu_f)} \quad (1)$$

In eq. 1 ν is the measured proton magnetic resonance (p.m.r.) frequency of the hydrogen-bonding proton at a concentration d of D, ν_f and ν_c are the characteristic frequencies of M and MD, respectively, and K is the association constant

$$K = (MD)/(M)d \quad (2)$$

When 2-propanol is used as the hydrogen donor, eq. 1 has to be modified since self-association of the alcohol occurs, and this may affect the equilibrium involving its 1:1 complex formation with the N-substituted acetamide, D.

For the purpose of studying the extent of self-association of the alcohol, we have determined the p.m.r. frequency of the OH proton of 2-propanol as a function of its concentration in CCl₄ and at various temperatures. The results are included in this paper.

Modification of Eq. 1 for 2-Propanol. Let C' be the concentration of 2-propanol which is *not* hydrogen bonded to N-substituted acetamide, x be the fraction of this concentration which is in the form of monomer, M, and C be the total concentration of the alcohol. Then

$$C = C' + (MD) \quad (3)$$

$$(M) = xC' \quad (4)$$

Since hydrogen-bonding equilibria usually involve very rapid reactions, we may assume the observed frequency of OH in 2-propanol to be the weighted average of ν' and ν_c , so that

$$\begin{aligned} \nu &= (C'/C)\nu' + ((MD)/C)\nu_c \\ &= \nu' + \frac{(MD)}{C}(\nu_c - \nu') \end{aligned} \quad (5)$$

(1) This investigation was supported by P.H.S. research Grant No. GM-10539-01 from the National Institute of General Medical Sciences, Public Health Service.

(2) R. Mathur, E. D. Becker, R. B. Bradley, and N. C. Li, *J. Phys. Chem.*, **67**, 2190 (1963).

In eq. 5 ν' is the weighted average frequency of the 2-propanol which is *not* hydrogen bonded to the N-substituted acetamide. From eq. 2-5, the following equation, which is a modified form of eq. 1 is obtained

$$\frac{1}{\nu - \nu'} = \frac{1}{K(\nu_c - \nu')} \frac{1}{dx} + \frac{1}{(\nu_c - \nu')} \quad (6)$$

From eq. 6, a plot of $1/(\nu - \nu')$ vs. $1/dx$ yields a straight line, from which the values of $(\nu_c - \nu')$ and K can be determined separately. When $x = 1$, $\nu' = \nu_t$, then eq. 6 and 1 become identical.

Experimental

Materials. N-Methylacetamide, N,N'-dimethylacetamide, and 2-propanol were distilled twice; and the fractions boiling at 205, 165, and 82°, respectively, were collected. Carbon tetrachloride was Fisher Spectro-analyzed Certified Reagent liquid.

Preparation of Samples. Samples were prepared by the same methods as described in the previous paper.²

P.m.r. Measurements. All the p.m.r. spectra were obtained with a Varian Associated Model A-60 n.m.r. spectrometer. During the running of the spectra the temperature remained constant to within $\pm 1^\circ$, as indicated by the separation in c.p.s. between two peaks in ethylene glycol or methanol.

Chemical shifts of the OH signal in 2-propanol were measured with respect to tetramethylsilane as an internal standard in the manner described in a previous paper.² The reported shifts at 36° are accurate to about 0.2 c.p.s. At lower temperatures the signals are broader so that the uncertainty is greater.

Results

A. Self-Association of 2-Propanol. The experimental frequency data for solutions of 2-propanol are given in Table I. Plots of ν' vs. concentration of 2-propanol at constant temperature indicate that the limiting frequency at zero concentration is 46 c.p.s. in the temperature range 14-40°. At zero concentration the alcohol is a monomer, so that we may take 46 c.p.s. as the monomer frequency, ν_t . Likewise, plots of ν' vs. temperature for $C' = 0.050$, 0.0375, and 0.025 M indicate that ν_t is also about 46, if we assume that for these dilute solutions at high temperatures, the alcohol is a monomer.

At high concentrations of 2-propanol, trimers and higher polymers became predominant. From the results of Table I, it is safe to assume that below 0.05 M and at temperatures higher than 14°, dimers, rather than trimers and higher polymers, predominate. In the low concentration region therefore, we may assume

Table I: Frequency of OH Signal in 2-Propanol in CCl_4 ^a

(A) At 35°						
	C', M (concn. of 2-propanol)					ν' , c.p.s.
	0.050					51.1
	0.111					59.6
	0.222					94.1
	0.443					144.7
	0.665					173.4
	0.886					193.2
	1.108					203.6
(B) At various temperatures						
Temp., °C.	ν' , c.p.s., at various values of C'					ν' , c.p.s. Neat 2- propanol
	0.50 M	0.075 M	0.050 M	0.0375 M	0.025 M	
						352.0 (-32°)
						342.3 (-14°)
-10	258.2		115.5			
-6.5			102.0			
-3	239.7					
0			86.1			332.6
+6	222.2					
14	202.7		61.9	51.6	49.1	320.9 (15°)
21			56.6	51.8	49.3	
24	184.6			49.7	47.6	
29		55.2	52.9	48.8		
36			51.1	48.6	47.8	
40	140.4	52.2	49.9	47.6	46.7	301.7 (39°)

^a No N-substituted acetamide present.

that the observed frequency of OH is a weighted average of monomer and dimer, and the following equation can be written

$$\nu = \frac{(M)}{C'} \nu_t + \frac{C' - (M)}{C'} \nu_2 \quad (7)$$

In view of eq. 4, eq. 7 becomes

$$x = \frac{\nu_2 - \nu'}{\nu_2 - \nu_t} \quad (8)$$

where ν_2 is dimer frequency. Since ν_2 cannot be determined in a direct manner, we have estimated it by use of the equation

$$\nu_2 = \nu_t + \frac{1}{2} (\nu_p - \nu_t) \quad (9)$$

where ν_p is the polymer frequency and is taken to be the extrapolated frequency of the OH signal in *neat* 2-propanol at its freezing point, -89.5° . From the results of Table I, the extrapolated value of ν_p is 380 c.p.s. Since ν_t is 46, ν_2 is calculated to be 213 c.p.s., and eq. 8 becomes

$$x = \frac{213 - \nu'}{213 - 46} \quad (10)$$

The justification of eq. 9 is that infrared spectra data have indicated that as hydrogen-bonded polymers become larger, the hydrogen bonds become stronger,³⁻⁵ and that for the OH stretching mode the change in frequency $\Delta\nu$ for dimer formation is approximately half as big as $\Delta\nu$ for polymer formation. Thus, Kuhn³ finds that $\Delta\nu$ for dimeric phenol and dimeric 2-butanol is 136 and 129 cm.^{-1} , respectively, whereas for polymeric phenol and polymeric 2-butanol $\Delta\nu$ is 270 and 243, respectively.

It may be assumed that in the limiting that $(1 - x) = 0$, dimers, rather than trimers, are formed. Therefore, in a plot of $(1 - x)/x^2C'$ vs. $(1 - x)$, the intercept should be equal to $2K_2$, where K_2 is the equilibrium constant for the formation of dimer: $2M = M_2$. Such a plot at 36° yields the value $K_2 = 0.2 M^{-1}$. The plot has a large slope, which indicates that there is strong interaction in the higher association steps, that is, once a dimer is formed, a trimer or higher polymer is formed more readily. Similar observation has been reported by Klotz and Franzen⁶ for the self-association of N-methylacetamide from infrared data.

B. Hydrogen Bonding between 2-Propanol and N-Substituted Acetamide. The chemical shifts of the OH signal of 2-propanol in CCl_4 solutions containing 0.05 M 2-propanol and various amounts of N-methylacetamide were determined at various temperatures between 0 and 36° . Table II lists the results obtained.

Table II: 2-Propanol-N-Methylacetamide

<i>d</i> , M	$\nu_{\text{obsd.}}$ c.p.s.	<i>d</i> , M	$\nu_{\text{obsd.}}$ c.p.s.
36°		24°	
0.434	201.7	0.440	227.3
0.564	214.6	0.572	242.4
0.869	238.3	0.881	260.9
1.736	265.0	1.761	283.1
14°		0°	
0.445	240.9	0.453	267.6
0.579	253.7	0.589	276.7
0.891	271.5	0.906	291.4
1.786	291.5	1.811	305.5

In the treatment of data, we assume that C' , the concentration of 2-propanol not hydrogen bonded to N-methylacetamide, is so small that in eq. 6 we may set $x = 1$ and $\nu' = \nu_t$, which is 46. Plots of $1/(\nu - \nu_t)$ vs. $1/d$ for the temperatures 0– 36° are shown in Fig. 1. The straight lines were obtained by least-

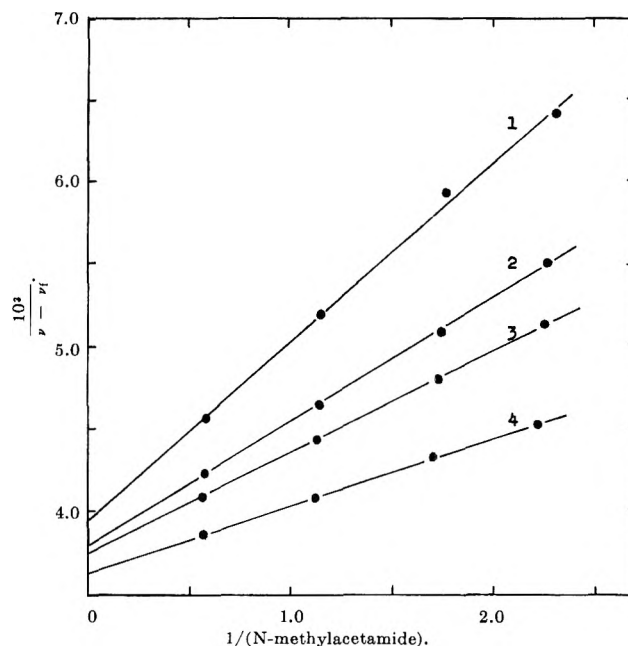


Figure 1. Plots of $10^3/(\nu - \nu_t)$ vs. $1/(\text{N-methylacetamide})$ at (1) 36° ; (2) 24° ; (3) 14° ; (4) 0° .

square calculation. The values of ν_c and K obtained from the intercept and slopes of these lines are summarized in Table III(A). Figure 2 gives a plot of $\log K$ vs. $1/T$, the slope of which yields a value of -4.1 kcal./mole for the enthalpy of hydrogen bond formation.

Table III: Thermodynamic Data for 2-Propanol Hydrogen Bonding to Acetamides

Temp., $^\circ\text{C.}$	<i>K</i> , M	ν_c	
		c.p.s.	p.p.m.
(A) N-Methylacetamide			
36	3.61	300	5.00
24	5.02	310	5.17
14	6.01	314	5.23
0	8.94	321	5.35
(B) N,N'-Dimethylacetamide			
40	2.23	252	4.20
29	2.56	258	4.30
21	2.88	260	4.33

(3) L. P. Kuhn, *J. Am. Chem. Soc.*, **74**, 2494 (1952).

(4) C. M. Huggins, G. C. Pimentel, and J. N. Shoolery, *J. Phys. Chem.*, **60**, 1311 (1956).

(5) R. F. Badger, *J. Chem. Phys.*, **8**, 288 (1940); E. R. Lippincott and R. Schroeder, *ibid.*, **23**, 1099 (1955).

(6) I. M. Klotz and J. S. Franzen, *J. Am. Chem. Soc.*, **84**, 3461 (1962).

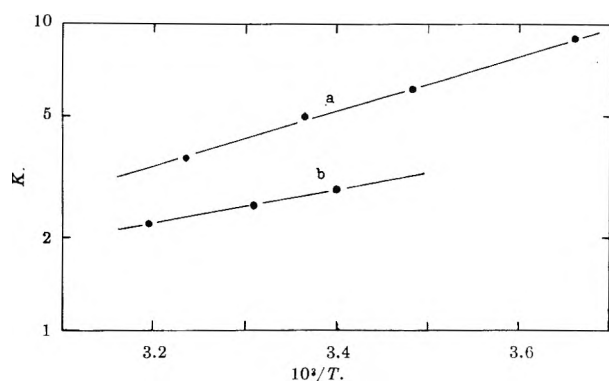


Figure 2. Plots of $\log K$ vs. $10^3/T$ for 2-propanol hydrogen bonding to (a) N-methylacetamide; (b) N,N'-dimethylacetamide.

The chemical shifts of the OH signal of 2-propanol in CCl_4 solutions containing 0.20 M 2-propanol and various amounts of N,N'-dimethylacetamide were determined at three different temperatures, and the results are listed in Table IV. In this case, a higher concentra-

Table IV: 2-Propanol-N,N'-Dimethylacetamide, 2-Propanol 0.20 M

40°				29°			
<i>d</i> , M	ν , c.p.s.	ν'	<i>x</i>	<i>d</i> , M	ν	ν'	<i>x</i>
1.055	194.9	49.9	0.977	1.069	208.8	50.9	0.971
1.177	200.2	49.2	0.981	1.191	209.5	50.8	0.971
1.679	210.3	48.0	0.988	1.700	221.5	49.0	0.982
2.107	217.1	47.4	0.992	2.134	226.9	48.5	0.985
3.609	230.0	46.6	0.996	3.656	238.8	47.3	0.992
21°							
1.079	216.0	53.1	0.957				
1.204	215.8	53.4	0.956				
1.718	227.4	50.0	0.976				
2.156	232.6	49.2	0.981				
3.692	242.9	47.7	0.990				

tion of 2-propanol, 0.20 M, is necessary because at lower concentration the OH signal would overlap that of the N-CH₃ signal from N,N'-dimethylacetamide. Because of the higher concentration used, it is no longer valid to set $x = 1$. Treatment of the data is as follows: from eq. 3 and 5, the following equation is derived

$$\frac{C'}{C} = \frac{\nu_c - \nu}{\nu_c - \nu'} \quad (11)$$

The value of ν_c is obtained from the intercept of a $1/(\nu - 46)$ vs. $1/d$ plot (eq. 1). This value of ν_c , together with the frequency ν listed in Table IV and an

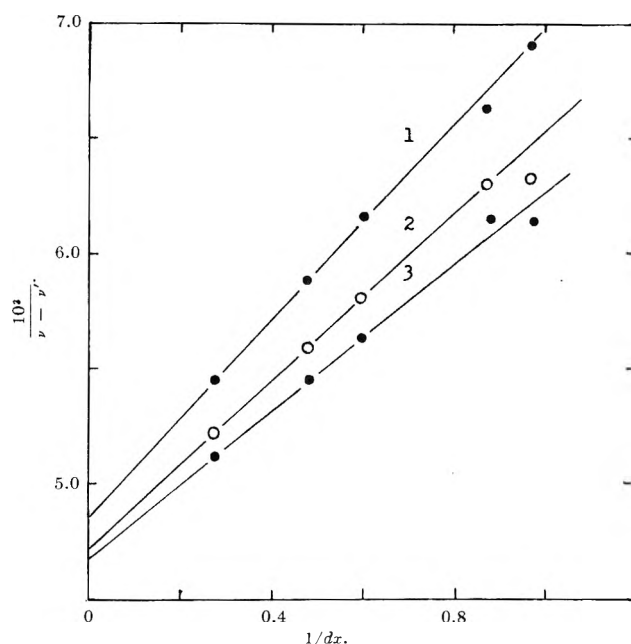


Figure 3. Plots of $10^3/(\nu - \nu')$ vs. $1/dx$ for 2-propanol hydrogen bonding to N,N'-dimethylacetamide at (1) 40°; (2) 29°; (3) 21°.

assumed value of ν' , was inserted in eq. 11 in order to calculate C' . From the calculated value of C' and the data of Table I(B), ν' can be obtained. If the assumed value of ν' is correct, then the ν' calculated from C' and results of Table I(B) should be in agreement with it. If they do not agree, then different values are assumed until the correct value of ν' is obtained. x is then calculated by eq. 10. The values of ν' and x are included in Table IV. Plots of $1/(\nu - \nu')$ vs. $1/dx$ (eq. 6) for three different temperatures are shown in Fig. 3. The values of ν_c and K obtained from intercepts and slopes of these lines are summarized in Table III(B). Figure 2(b) gives plots of $\log K$ vs. $1/T$, the slope of which yields a value of -2.4 kcal./mole for enthalpy of hydrogen bonding between 2-propanol and N,N'-dimethylacetamide.

Discussion

In an infrared study of hydrogen bonding in alcohol-base systems, Becker⁷ suggested that at the low total concentration of alcohol (he used 0.02 M) the equilibrium constant of hydrogen bond formation can be corrected for self-association of alcohol by dividing K by g , the fraction of alcohol in the form of monomer at a total concentration of 0.02 M with no base present. It is interesting to note that this suggestion is similar to the relationship between eq. 6 and 1 of this paper,

(7) E. D. Becker, *Spectrochim. Acta*, 17, 436 (1961).

except that x is the fraction of alcohol in the form of monomer at a concentration of alcohol which is *not* hydrogen bonded to a base, C' . In our treatment of the data for the N-methylacetamide system, we have assumed $x = 1$. This assumption is justified because with the known value of K_2 for the self-association of 2-propanol and with the value of K listed in Table II(A), both at 36° , it can be shown that the monomer concentration is equal to C' (C 0.05 M for the 2-propanol-N-methylacetamide system).

The value of ΔH for 2-propanol-N-methylacetamide is consistent with the values of alcohol to dimethylformamide (-3.7 to -3.9 kcal./mole).⁷ In the case of N,N'-dimethylacetamide the value of ΔH seems low but cannot be explained at present.

Several authors^{2,7-9} have made the assumption and have tested the assumption in treating the p.m.r. data, that the hydrogen bond shifts do not vary with temperature. The small variation in ν_c with temperature in Table III indicates that the assumption is open to further investigation.

Acknowledgment. The authors are very deeply grateful to Dr. E. D. Becker for a number of helpful suggestions.

(8) C. M. Huggins, G. C. Pimentel, and J. N. Shoolery, *J. Chem. Phys.*, **23**, 1244 (1955).

(9) J. C. Davis, Jr., K. S. Pitzer, and C. N. R. Rao, *J. Phys. Chem.*, **64**, 1744 (1960).

Hydrogen Bonding Studies of N-Methylacetamide and Some Thiols¹

by Raj Mathur, Sung M. Wang, and Norman C. Li

Chemistry Department, Duquesne University, Pittsburgh, Pennsylvania (Received January 27, 1964)

A proton magnetic resonance study of hydrogen bonding between benzenethiol and N-methylacetamide as hydrogen acceptor, all in CCl_4 , in the temperature range -18 to 37° has been made. The hydrogen bond shift, Δc , and enthalpy of hydrogen bond formation, $-\Delta H$, are determined to be 1.8 p.p.m. and 0.9 kcal./mole, respectively. The 1:1 hydrogen-bonded complex is weaker than the benzenethiol dimethylformamide complex previously investigated by Mathur, *et al.*:² $\Delta c = 2.2$ p.p.m., $-\Delta H = 1.8$ kcal./mole. Over a 0.8 M concentration range of N-methylacetamide at 37° , the SH frequency of 0.05 M benzenethiol changes by 10 c.p.s., while that of 0.1 M *t*-butyl mercaptan changes by only 3 c.p.s. N-Methylacetamide is shown to undergo extensive self-association; however, the self-association does not interfere with its hydrogen bonding with 0.05 M benzenethiol. The effects of metal ions on the p.m.r. spectra of N-methylacetamide suggest that the binding site toward Cu(II) and zinc ions is the carbonyl oxygen, and not the nitrogen atom.

Introduction

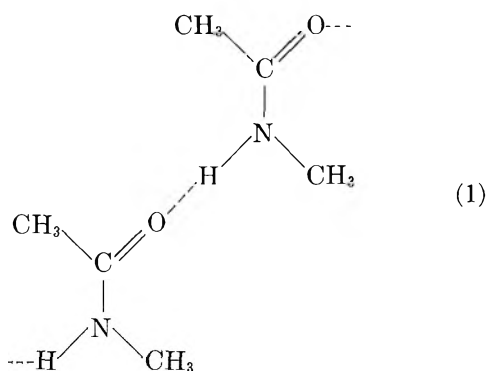
Mathur, *et al.*,² recently reported the results obtained on proton magnetic resonance (p.m.r.) studies of hydrogen bonding between benzenethiol as hydrogen donor and several hydrogen acceptors. For the acceptors, they chose only compounds which are monomeric in carbon tetrachloride solution. It was con-

sidered of interest to study hydrogen bonding between the same hydrogen donor, but use a hydrogen acceptor

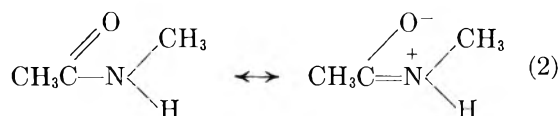
(1) This investigation was supported by P.H.S. research Grant No. GM-10539-01 from the National Institute of General Medical Sciences, Public Health Service.

(2) R. Mathur, E. D. Becker, R. B. Bradley, and N. C. Li, *J. Phys. Chem.*, **67**, 2190 (1963).

which undergoes extensive self-association. For this purpose, N-methylacetamide (NMA) was chosen because its self-association has been extensively studied by several investigators³⁻⁶ and because it is the simplest model compound representative of the peptide amide group. NMA aggregates into dimers, trimers, and higher oligomers; and the aggregation may be represented as



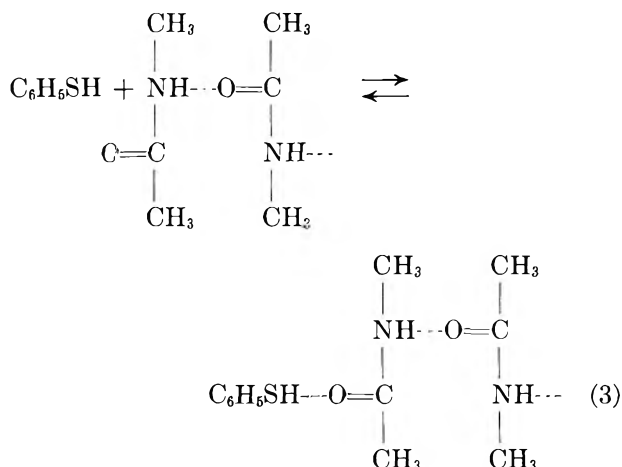
Resonance structures of NMA have been shown to be³



and the hydrogen atom of the NH group tends to form a strong hydrogen bond. In the polypeptide chain in proteins, we may expect similar resonance of the peptide amide group, which may account in part for the strong tendency of the polypeptide chain to form hydrogen bonds both intermolecularly and intramolecularly. The investigation of hydrogen bonding of thiols to NMA was carried out with the hope that these may serve as model systems to the hydrogen bonding of thiol group in cysteine and glutathione, to the peptide amide group in proteins.

This paper presents the results obtained on p.m.r. studies using benzenethiol and NMA by measuring the change in SH frequency when benzenethiol was kept constant at 0.05 M in the presence of NMA in the concentration range 0.3-2.4 M, all in CCl₄, in the temperature range -18 to 37°. Similar studies were carried out with propanethiol and *t*-butyl mercaptan. However, no quantitative values of equilibrium constants were obtained, either because the SH frequency did not change appreciably on hydrogen bonding or because the SH signal is obscured by other signals in the system.

The hydrogen bonding of NMA with benzenethiol may be represented as shown in eq. 3



The degree of aggregation of the acetamide increases with concentration. Thus, the environment of the NH group changes, resulting in changes in the NH frequency. In hydrogen bonding with benzenethiol, the environment of a bonded NH group undergoes an additional change because of its nearness to a carbonyl group which is hydrogen bonded to SH (see eq. 3). It becomes of interest therefore to measure the NH frequency over a wide concentration range of NMA at various temperatures, in the absence and presence of thiols. The results are presented.

Because of resonance in (2) and because oxygen is more electronegative than nitrogen, it may be expected that the hydrogen acceptor site is the carbonyl oxygen, rather than the nitrogen atom. Li, *et al.*,⁷ have shown that changes in the p.m.r. spectra on adding paramagnetic and diamagnetic metal ions to amino acids and peptides can be used to provide information on the nature of metal binding sites. In order to see whether the metal binding site corresponds with the hydrogen acceptor site, we have investigated the effect of metal salts on the p.m.r. spectra of NMA. The results are included in this paper.

Experimental

Materials. N-Methylacetamide was purchased from Eastman Organic Chemicals. It was purified by double distillation at 160° and dried over phosphorus pentoxide in an evacuated desiccator. Carbon tetrachloride and benzenethiol were treated in a manner described by

(3) S. Mizushima, T. Simanouti, S. Nagakura, K. Kuratani, M. Tsuboi, H. Baba, and O. Fujioka, *J. Am. Chem. Soc.*, **72**, 3490 (1950).

(4) M. Davies and D. K. Thomas, *J. Phys. Chem.*, **60**, 767 (1956).

(5) J. B. Hasted, G. H. Haggis, and P. Hutton, *Trans. Faraday Soc.*, **47**, 577 (1951).

(6) I. M. Klotz and J. S. Franzen, *J. Am. Chem. Soc.*, **84**, 3461 (1962).

(7) N. C. Li, R. Scruggs, and E. D. Becker, *ibid.*, **84**, 4650 (1962).

Mathur, *et al.*² Propanethiol and *t*-butyl mercaptan were distilled in a nitrogen atmosphere. All reagents after distillation were kept under nitrogen.

Preparation of Samples for Hydrogen-Bonding Studies. Samples were prepared as described earlier.² Since NMA is highly hygroscopic, its stock solution was made by adding the solid to volumetric flask inside the dry-box, and then the flask was taken out and weighed. Solutions containing NMA alone were prepared in the same manner, except that a trace⁸ of HCl was not added.

The molarity of the solutions, at temperatures other than room temperature, was calculated from the change in density with temperature of carbon tetrachloride.

P.m.r. Measurements. P.m.r. spectra were obtained with a Varian Associates Model A-60 n.m.r. spectrometer. The SH and NH proton frequencies were measured as described earlier,² by putting two side bands of tetramethylsilane (TMS) on either side of the signal. At temperatures below room temperature, the Varian Associates low temperature kit together with the variable temperature controller was used. Temperature variation was found to be $\pm 1^\circ$ during measurements. The accuracy in measuring the peak positions of the SH proton signal is estimated to be ± 0.2 c.p.s., while that for the NH frequency is about ± 1 c.p.s. The half-width of the NH signal at room temperature is about 17 c.p.s., and about 14 c.p.s. below room temperature. In certain metal complexation studies using 99.8% D₂O as medium, sealed capillary containing benzene was used as an external reference. Although bulk diamagnetic susceptibility corrections should be applied when an external reference is used,⁹ we have not made such corrections since our interest is in the *relative* effects of a metal ion on the two methyl proton signals in NMA. In other metal complexation studies, using methanol as medium, TMS was used as internal reference.

Results

A. Hydrogen-Bonding Studies. Table I records the results obtained with 0.05 *M* benzenethiol in the presence of various concentrations of NMA at four different temperatures. Plots of $1/(\nu - \nu_f)$ vs. $1/d$ were made in the manner described by Mathur, *et al.*,² for hydrogen bonding of benzenethiol to several hydrogen acceptors. The equation used is

$$\frac{1}{\nu - \nu_f} = \frac{1}{K\Delta c} \frac{1}{d} + \frac{1}{\Delta c} \quad (4)$$

where ν is the measured SH proton frequency at a concentration, d , of NMA, ν_f is the frequency at $d = 0$, Δc is the difference in frequency between the hydrogen-

Table I: SH Proton Frequency of 0.05 *M* Benzenethiol in the Presence of Various Concentrations, d , of NMA^a

d, M	$\nu, \text{c.p.s.}$	d, M	$\nu, \text{c.p.s.}$
37°		22°	
0	194.4	0	195.0
0.799	204.5	0.802	205.9
1.198	208.3	1.203	210.5
1.598	212.1	1.604	214.4
2.396	219.6	2.406	222.1
2.796	222.6		
$K = 0.13$		$K = 0.14$	
8°		18°	
0	195.9	0	196.7
0.816	207.9	0.841	210.7
1.223	212.5	1.261	216.2
1.631	217.7	1.681	220.0
2.447	226.1	2.522	232.2
$K = 0.15$		$K = 0.17$	

^a All frequencies are downfield, relative to TMS.

bonded benzenethiol-NMA complex and the uncomplexed benzenethiol monomer, and K is the association constant for eq. 3. From the intercept and slope of a $1/(\nu - \nu_f)$ vs. $1/d$ plot, the values of K and Δc can be separately determined. The value of Δc is 110 c.p.s. or 1.8 p.p.m. and is virtually independent of temperature. The values of K are included in Table I, for the various temperatures. A plot of $\log K$ vs. $1/T$ is linear. The enthalpy of hydrogen bond formation, $-\Delta H$, between benzenethiol and NMA is calculated to be 0.9 kcal./mole, and is probably accurate to ± 0.2 kcal./mole. The SH frequencies of 0.1 *M* *t*-butyl mercaptan in the presence of various concentrations of NMA are listed in Table II. The molarities of the solutions are those for 25° only.

An extensive series of experiments was carried out on measuring the NH frequency of NMA in the absence and presence of 0.05-0.1 *M* of benzenethiol, propanethiol, and *t*-butyl mercaptan. The data obtained for NMA in the absence of thiol are listed in Table III. Values for concentrations below 0.4 *M* are not reported since the signal becomes too broad. The NH frequency of NMA in the presence of the thiols is not

(8) HCl was added to bring about rapid proton exchange and to ensure a sharp SH peak. Mathur, *et al.*,² have shown that this amount of HCl (5 p.p.m. in the final solution) did not alter the SH frequency. The amount of water introduced by addition of aqueous HCl was only $5 \times 10^{-3}\%$ and is negligible.

(9) J. A. Pople, W. G. Schneider, and H. H. Bernstein, "High Resolution Nuclear Magnetic Resonance," McGraw-Hill Book Co., New York, N. Y., 1959.

Table II: SH Proton Frequency of 0.1 *M* *t*-Butyl Mercaptan in the Presence of Various Concentrations of NMA

<i>d</i> , <i>M</i>	ν , c.p.s.		
	80°	36°	-18°
0	96.8	96.6	96.5
0.206	97.8	97.6	
0.412	98.6	98.2	98.3
0.618	99.1	98.8	98.8
0.824	99.6	99.4	99.7

Table III: NH Proton Frequency of NMA in the Absence of Any Thiol

<i>d</i> , <i>M</i>	ν , c.p.s.	<i>d</i> , <i>M</i>	ν , c.p.s.
-17°		-9.5°	
0.419	502.8	0.416	497.1
0.692	504.8	0.686	501.0
0.922	507.9	0.915	503.7
1.048	507.8	1.040	503.7
1.677	508.8		
2.516	508.7	2.495	505.2
3.229	508.8	3.202	506.5
0°		10°	
0.411	488.8	0.407	479.9
0.679	493.6	0.671	487.5
		0.894	490.7
1.028	496.5	1.016	491.0
1.645	499.0	2.439	495.4
3.167	500.1	3.130	496.4
-20.5°		37°	
0.662	481.1	0.394	455.0
		0.650	467.0
		0.866	472.2
		0.984	474.0
1.004	484.7	1.575	479.3
		2.362	481.5
3.091	491.3	3.031	483.0

appreciably different from that in the absence of the thiols.¹⁰

The SH frequency of 0.2 *M* propanethiol in CCl₄ was determined to be 72.5 c.p.s. at 36°. In the presence of NMA, the SH signal is superimposed by other proton signals, so that further studies of hydrogen bonding between NMA and propanethiol were discontinued.

B. Metal Complexation Studies. Li, *et al.*,⁷ Cohn and Hughes,¹¹ and Mathur and Li¹² show that paramagnetic metal ions selectively broaden the p.m.r. lines of nuclei which are adjacent to the sites of binding because the magnetic field of the ion decreases the relaxation time of the nuclei and because the complexed ligand

is exchanging rapidly with the free ligand in solution. Diamagnetic metal ion, on the other hand, selectively cause the downfield shift of the p.m.r. lines of nuclei adjacent to the binding site.

Relative to benzene as external reference, solutions of 0.75 *M* NMA in 99.8% D₂O at room temperature exhibit a HDO signal at 1.88 p.p.m., and two signals at 3.85 and 4.53 p.p.m. all upfield from benzene. These are ascribed to N-CH₃ and CH₃CO protons, respectively. D₂O was used as solvent to reduce the obscuring resonance of H₂O. However, exchange of the labile NH proton in NMA with solvent and the H₂O present in 99.8% deuterium oxide, introduce sufficient protons to give a HDO resonance. In the presence of 10⁻³ *M* MnSO₄, the HDO line is broadened to the extent that it becomes unobservable, while the signals at 3.85 and 4.58 p.p.m. are broadened by about 17 and 22%, respectively. Solutions of 0.7 *M* N-ethylacetamide exhibit three signals: $\delta = 3.33$ (quartet), 4.55 (singlet), and 5.42 (triplet), ascribed to the CH₂, CH₃CO, and CH₃ of the ethyl group, respectively. In the presence of 10⁻³ *M* MnSO₄, all three signals are broadened and the broadening *seems* to increase slightly in the order for $\delta = 5.42, 3.33, 4.55$. However, because metal complexation in aqueous solution is not stable and because the three signals are of three different multiplicities, it is not possible to state in quantitative terms the extent of broadening.

For the purpose of demonstrating a greater effect of metal ion on the p.m.r. spectra of NMA, we carried out experiments using methanol as solvent at -10°. TMS was used as internal reference and all signals are downfield from it. Figure 1 and 2 show the results obtained. In Fig. 1 and 2, the signals at $\delta = -1.92$ and -2.70 p.p.m. are ascribed to the CH₃CO and N-CH₃ protons, respectively. It is seen that the presence of a paramagnetic metal ion exerts a greater broadening effect on the $\delta = -1.92$ signal than on the -2.70 p.p.m. signal. The presence of the diamagnetic zinc ion causes the -1.92 p.p.m. signal to move downfield to a greater extent than the -2.70 p.p.m. signal.

Discussion

From Table I it is seen that the value of ν_t , the SH frequency at *d* = 0, is virtually independent of temperature (a change of only 2.3 c.p.s. over a 55° change),

(10) For instance, the NH frequencies of 0.411 *M* NMA at 0° in the presence of 0.05 *M* benzenethiol and 0.1 *M* *t*-butyl mercaptan are 490.6 and 489.1 c.p.s., respectively. The NH frequencies of 1.645 *M* NMA at 0° in the presence of 0.05 *M* benzenethiol and 0.2 *M* propanethiol are 499.6 and 498.9 c.p.s., respectively.

(11) M. Cohn and T. R. Hughes, Jr., *J. Biol. Chem.*, **237**, 176 (1962).

(12) R. Mathur and N. C. Li, *J. Am. Chem. Soc.*, **86**, 1289 (1964).

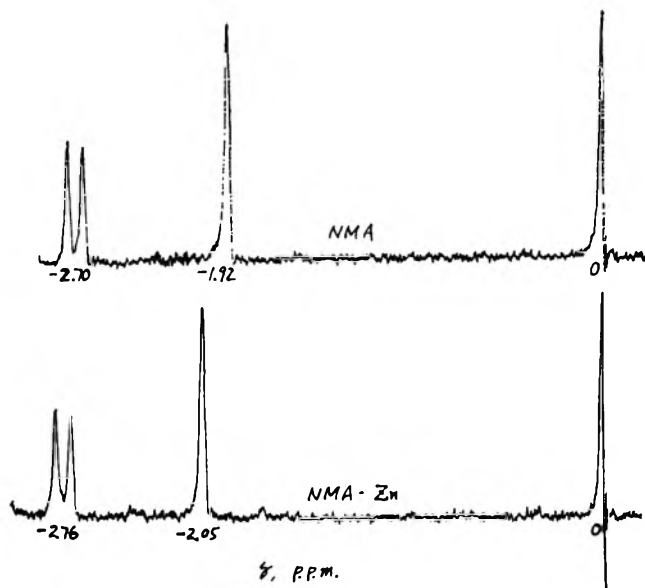


Figure 1. 0.4 *M* NMA (top); 0.4 *M* NMA, 1.2 *M* ZnCl₂ (bottom). Methanol as medium, -10°. TMS reference.

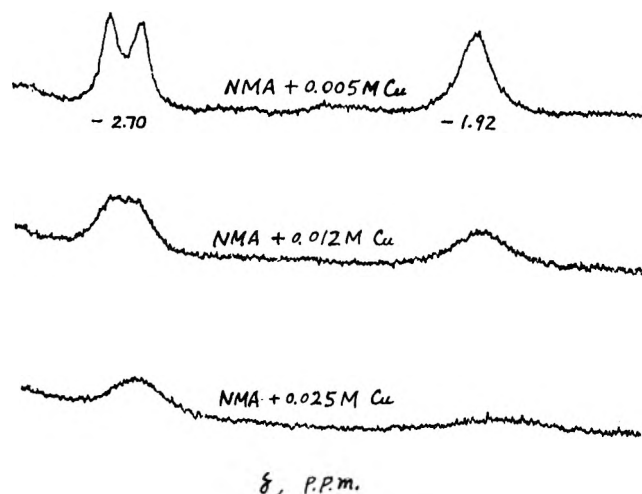


Figure 2. 0.8 *M* NMA and its Cu(II) complexes. Methanol as medium, -10°. TMS reference.

so that 0.05 *M* benzenethiol may be considered only very slightly dimerized. This is in agreement with the findings of Mathur, *et al.*,² and of Spurr and Byers¹³ from infrared work. The values of $-\Delta H = 0.9$ kcal./mole, $K_{22^\circ} = 0.14$ l. mole⁻¹, and $\Delta c = 1.8$ p.p.m. for the benzenethiol-NMA system may be compared with the values of $-\Delta H = 1.8$ kcal./mole, $K_{26^\circ} = 0.24$ l. mole⁻¹, and $\Delta c = 2.2$ p.p.m. found for the benzenethiol-dimethylformamide system.² The hydrogen bonding in the benzenethiol-NMA system therefore is very weak and at 22° in the presence of 1 *M* NMA, only 12% of the benzenethiol is complexed. It is only because

of the large hydrogen-bonding shift, $\Delta c = 110$ c.p.s. or 1.8 p.p.m., and the precision of p.m.r. frequency measurements that the equilibrium can be studied.

From Table II it is seen that ν_t for *t*-butyl mercaptan changes by only 0.3 c.p.s. over a 78° change, and that at a given temperature, over a NMA concentration range of 0.8 *M*, the SH frequency changes by only 3 c.p.s. These indicate that the SH in *t*-butyl mercaptan is a weak hydrogen donor, probably because of the inductive and steric hindrance effects of the *t*-butyl group.

The data of Table III show that the NH proton frequency of a 1 *M* NMA solution decreases by about 34 c.p.s. when the temperature increases by 54°. This very large temperature effect on NH proton frequency as compared to that on SH proton frequency indicates strongly that NMA is extensively associated. At 37° the NH proton frequency increases by 28 c.p.s. over a NMA concentration range of 0.4–3 *M*, whereas over the same concentration range at -17°, the frequency increases by only 6 c.p.s. This indicates that at 37° the aggregation of NMA changes rapidly from dimer, trimer to higher oligomers, whereas at -17° the aggregation of NMA has virtually reached its peak at concentrations higher than 1 *M*. From the constancy of the NH proton frequency at -17° over a 1–3 *M* concentration range, it is perhaps justifiable to estimate that the characteristic NH proton frequency for the fully aggregated NMA form is in the region of 510 c.p.s., or 8.5 p.p.m. Since CCl₄ freezes at -22°, we did not extend our study to lower temperatures. Klotz and Franzen⁶ have derived a method of treatment of data for calculating the dimerization constant of NMA from their infrared data. The same method could be adapted to our p.m.r. data. Unfortunately, however, the NH proton signal becomes too broad at concentrations below 0.4 *M*, so that it becomes impossible to extrapolate any function to zero concentration, where the highest aggregation may be assumed to be a dimer. It is possible that in a laboratory where double resonance facilities are available, that the NH frequency can be determined at very low concentrations of NMA.

From (3) it may be inferred that the extensive self-association of NMA would not interfere with hydrogen bonding between benzenethiol and NMA. This expectation is fully supported by the following experimental facts: (a) in spite of the very large temperature effect on the NH proton frequency of NMA, the value of Δc for the benzenethiol-NMA system remains virtually independent of temperature; (b) the NH proton

(13) R. A. Spurr and H. F. Byers, *J. Phys. Chem.*, **62**, 425 (1958).

frequency of NMA is not appreciably affected by the presence of thiols.

The effects of paramagnetic and diamagnetic metal ions indicate that the carbonyl oxygen, rather than the nitrogen, in NMA is the coordination site to these metal ions. This is the first experimental evidence of the binding site in NMA toward Cu(II) and zinc ions. It is of interest to note that n.m.r. studies have shown¹⁴ that the added proton in dimethylformamide is also preferentially attached to the oxygen rather than the nitro-

gen, so that the binding site toward Cu(II) and zinc ions in NMA is analogous to the binding site toward proton in dimethylformamide.

Acknowledgment. The authors are indebted to Dr. Edwin D. Becker, of the National Institutes of Health, for reading the manuscript.

(14) J. D. Roberts, "Nuclear Magnetic Resonance," McGraw-Hill Book Co., New York, N. Y., 1959, pp. 70, 71.

Diaphragm-Cell Method for Constant Mass Diffusion Measurements.

Interionic Diffusion and Friction Coefficients in Molten

Silver Nitrate-Sodium Nitrate Mixtures¹

by Richard W. Laity and Melvin P. Miller

Frick Chemical Laboratory, Princeton University, Princeton, New Jersey (Received January 23, 1964)

A diffusivity method is described for systems in which constant volume cannot be maintained. Results are presented for dilute solutions of AgNO_3 in NaNO_3 at 310° : the mass-fixed diffusion coefficient of Ag^+ is independent of concentration, the mean of eight determinations being $(1.96 \pm 0.09) \times 10^{-5} \text{ cm.}^2 \text{ sec.}^{-1}$; the ordinary (volume-fixed) and "thermodynamic" diffusion coefficients increase with increasing concentration of Ag^+ ; the silver-sodium friction coefficient is smaller than either of the cation-anion friction coefficients and apparently somewhat smaller than the sodium-sodium friction coefficient in pure NaNO_3 at the same temperature.

In attempting to account for the observed characteristics of equivalent conductivity (Λ) isotherms in binary fused salt mixtures, two additional transport parameters are of particular importance.² One is a type of transference number (P , or ϕ as originally designated) which Aziz and Wetmore³ first used to describe results of Hittorf-type experiments on the system AgNO_3 - NaNO_3 . The other is the ordinary diffusion coefficient (D_{12}) which characterizes the rate at which like-charged ions interdiffuse. Although Aziz and Wetmore's method for P apparently gave inaccurate results,

procedures subsequently developed have yielded satisfactory values of this quantity in a number of systems.⁴ On the other hand, the only values of D_{12} we have found in the literature⁵ were obtained by a method of

(1) (a) Supported in part by U. S. Atomic Energy Commission Contract No. AT(30-1)-2644; (b) based on the Ph.D. Thesis of Melvin P. Miller, Princeton University, 1962.

(2) R. W. Laity, *Ann. N. Y. Acad. Sci.*, **79**, 997 (1960).

(3) P. M. Aziz and F. E. W. Wetmore, *Can. J. Chem.*, **30**, 779 (1952).

(4) See chapter by A. Klemm in "Molten Salt Chemistry," M. Blander, Ed., Interscience Publishers, New York, N. Y., 1964.

questionable validity.⁶ In the present work an application of the diaphragm-cell technique is described which has yielded new diffusion data for the system $\text{AgNO}_3\text{-NaNO}_3$ at 310° in the range 2–8 mole % AgNO_3 . This is the only simple mixture of fused salts for which both thermodynamic activity coefficients and reliable values of Λ and P are currently available. Combined with experimental values of D_{12} , such information makes it possible to calculate the "thermodynamic mutual diffusion coefficient" and the interionic friction coefficients.²

Experimental

Method. A modification of the diaphragm-cell technique developed by Northrup and Anson⁷ was devised for this work. Due to slight but continuous gas evolution resulting from thermal decomposition of the melt, constant electrolyte volume could not be maintained in each compartment by sealing or stoppering. The simplest alternative was to keep both compartments open to atmospheric pressure, providing a cell arrangement that closely approximated a condition of constant mass. The drift in the relative concentrations of the mixtures on opposite sides of the diaphragm could be monitored continuously by following the e.m.f. between silver electrodes dipping into each compartment.

Materials. Baker and Adamson reagent grade silver nitrate and sodium nitrate were found to be adequate for use without further purification.

Apparatus. The cell consisted of two concentric cylindrical Pyrex compartments, 25 and 50 mm. in diameter, respectively. The former, about 30 cm. in length, had a "medium" porosity Pyrex fritted disk sealed into one end. Figure 1 shows the experimental arrangement, with both compartments supported vertically in a larger vessel containing the constant temperature bath (eutectic of sodium and potassium nitrates) set into the cavity of an electric tube furnace.

The magnetic stirring bars located in the bottom of each compartment could both be rotated from below by the powerful horseshoe magnet which was operated by a motor underneath the furnace. The bath itself was stirred from above as indicated in Fig. 1. Constant temperature ($\pm 0.5^\circ$) was maintained in the bath by a mercury-to-wire thermoregulator which controlled the input to a small auxiliary immersion heater (neither shown in Fig. 1), while a constant voltage was fed to the furnace windings.

The electrodes consisted of coils of 8-mm. silver wire attached to long platinum leads which were sealed through Pyrex glass tubing. The stoppers supporting the electrodes from above had slits to permit rapid pressure equilibration with atmosphere. All e.m.f.

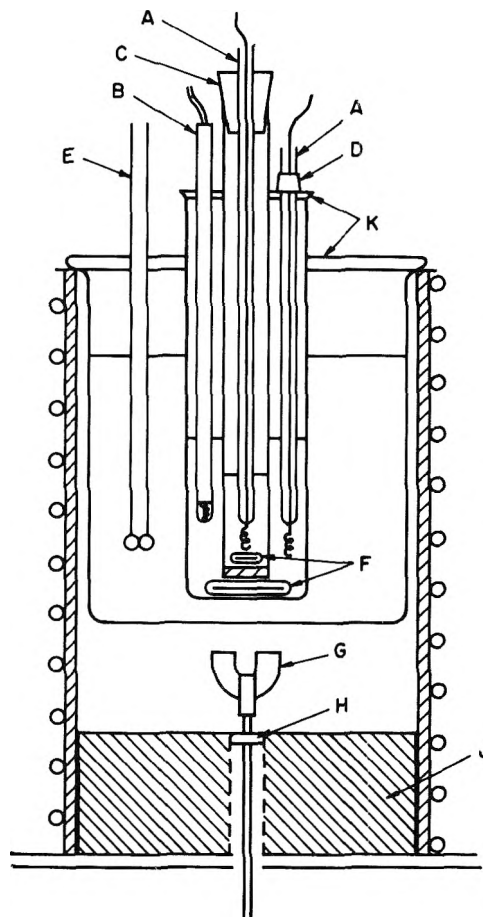


Figure 1. Constant-mass diaphragm cell arranged in furnace cavity: A, electrodes; B, thermocouple; C and D, stoppers with slits; E, stirrer; F, magnetic stirring bars; G, alnico magnet; H, ball bearing; J, firebrick; K, transite covers.

measurements were made with a Leeds and Northrup Type K potentiometer.

Procedure. The cell was filled as follows. First, a mixture of AgNO_3 and NaNO_3 was melted in the outer compartment. Most of this (about 30 g.) was drawn into the inner compartment by applying suction. Additional salt (120 g.) of the approximate composition desired in the outer compartment (1–10 mole % richer in NaNO_3 than that in the inner) was added until the outer liquid level was slightly above the inner. Stirring in both compartments was initiated and the cell was left standing at least 12 hr. to establish hydrostatic equilibrium between compartments.

(5) L. H. Harrison, Thesis, University of Munich, 1911, and A. Hoechberg, Thesis, University of Frankfurt, 1915, both given in W. Jost, "Diffusion in Solids, Liquids and Gases," Academic Press, New York, N. Y., 1952, p. 63 ff.

(6) M. P. Miller, Ph.D. Thesis, Princeton University, 1962.

(7) J. H. Northrup and M. L. Anson, *J. Gen. Physiol.*, 12, 543 (1929).

A diffusion run consisted of taking e.m.f. readings at frequent intervals over a period of 24–72 hr. and removing the contents of each compartment for analysis immediately after the last reading. The salt mixtures were then dissolved in water and aliquots were titrated for total Ag^+ (Volhard method) and for total cations measured by H^+ displaced from Dowex 50 cation-exchange resin.

Cell Constant. The effective length-to-area ratio of the diffusion path had to be determined in a separate experiment. Several methods were tried. Diffusion coefficients reported here are based on the cell constant obtained by measuring the resistance across the diaphragm of an aqueous 0.1 *M* KCl solution of known specific conductivity. The electrodes were mercury pools that effectively sealed the electrolyte inside the diaphragm by complete contact with the two faces. Although this determination was performed at 25°, calculation indicated that the cell constant at the 310° temperature of the diffusion experiments should differ by less than 0.1%. Therefore, no correction factor was applied. Measurements carried out before and after each run were generally in good agreement.

Other approaches to determination of the cell constant included measurements of (1) diffusion in the same cell at 25° of an aqueous KCl solution of known diffusion constant, (2) conductance across the diaphragm of molten NaNO_3 , (3) tracer-diffusion of pure molten NaNO_3 using labeled sodium ions. Although the reproducibility of each of these methods was poorer than that of the aqueous conductance method, all results obtained showed substantial agreement. The best value was 0.735 cm.^{-1} .

Analysis of Diffusion Data

Boundary Conditions. The condition of hydrostatic equilibrium requires that there be virtually no pressure drop across the diaphragm. Instead of maintaining constant volume, therefore, the levels of the two solutions initially at different densities must approach one another as their compositions are equalized by diffusion. To see what restriction is imposed on the fluxes of AgNO_3 and NaNO_3 by this boundary condition, it is useful to divide the cell contents conceptually into three parts: V_A , the volume of liquid in the inner compartment; V_B , that in the outer compartment above the level of the diaphragm; and V_C , the volume below the diaphragm.

If the inner compartment was positioned so that the magnitude of V_C was comparable with V_B , a significant increase in the mass of liquid below the diaphragm would occur as the density of the outer compartment was increased by diffusion. An equal decrease would

develop in the total mass of liquid in $V_A + V_B$. Since it is the distribution of this constantly changing mass between V_A and V_B that is responsible for maintaining hydrostatic equilibrium across the diaphragm, it is apparent that the boundary conditions for such an arrangement would be rather complicated. However, if V_C is diminished until it becomes negligible compared to V_B (by lowering the inner compartment), a very simple boundary condition is approached in which the mass of liquid in each compartment remains constant. For the values of V_A , V_B , and V_C used in the present work the error introduced in the calculation of D by assuming this latter condition was shown⁶ to be less than 1%.

Rate of Change of Concentration. To evaluate the diffusion coefficient (see next section) it is necessary to know the "initial" composition of each compartment, *i.e.*, the composition at a known time interval before the end of the run, but after steady-state diffusion conditions have been established. This is obtained from e.m.f. readings as follows. The e.m.f. measured between the silver electrodes is that of a concentration cell with transference. For AgNO_3 – NaNO_3 mixtures it is related to composition by⁸

$$E = \frac{RT}{F} \ln \frac{X_{1A}}{X_{1B}} + \frac{RT}{F} \ln \frac{\gamma_{1A}}{\gamma_{1B}} \quad (1)$$

where X_{1A} and X_{1B} represent the mole fractions of AgNO_3 in the inner and outer compartments, respectively, and the γ 's are the corresponding activity coefficients. (The absence of a term involving a transference number results from the characteristic transport behavior ($P = X_2$) of this system.⁴)

From the measured e.m.f. and the analytical results at the end of a diffusion run it is possible to evaluate the activity coefficient term in eq. 1. The concentrations X_{1A}' and X_{1B}' for any previously measured e.m.f., E' , can then be evaluated by a method of successive approximations: first, assume that the activity coefficient term is constant for the small concentration changes occurring during diffusion

$$\frac{RT}{F} \ln \frac{X_{1A}'}{X_{1B}'} \approx E' - \frac{RT}{F} \ln \frac{\gamma_{1A}}{\gamma_{1B}} \quad (2)$$

Now since the mass of salt in each compartment remains constant during diffusion, we can make use of the formula weights M_1 and M_2 of the two salts to derive

$$\frac{X_{1A}'}{X_{1B}'} = \frac{(n_{1A} + \Delta n_1)[M_2 n_B + (M_1 - M_2)\Delta n_1]}{(n_{1B} - \Delta n_1)[M_2 n_A - (M_1 - M_2)\Delta n_1]} \quad (3)$$

where Δn_1 is the number of moles of AgNO_3 that dif-

(8) R. W. Laity, *J. Am. Chem. Soc.*, **79**, 1849 (1957).

fused out of compartment A after its concentration was X_{1A}' ; $n_A = n_{1A} + n_{2A}$ and $n_B = n_{1B} + n_{2B}$ are the total numbers of moles in compartments A and B, respectively, at the end of the run.

Employing the approximate value of X_{1A}'/X_{1B}' obtained from eq. 2, eq. 3 can be solved for Δn_1 . This is used to calculate approximate values of X_{1A}' and X_{1B}' .

The activity coefficient ratio associated with X_{1A}' and X_{1B}' is obtained from the known thermodynamic behavior of the system. In $\text{AgNO}_3\text{-NaNO}_3$ the terminal analyses of diffusion cells at a number of different compositions were consistent with a previous report that⁸

$$RT \ln \frac{\gamma_{1A}}{\gamma_{1B}} = A(X_{2A}^2 - X_{2B}^2)$$

where A is about 800 cal./mole. From the preceding calculation a new value of the activity coefficient term can be used in eq. 2. Repeating the calculation by putting the resulting value for X_{1A}'/X_{1B}' into eq. 3, better approximations are now obtained for Δn_1 , X_{1A}' , and X_{1B}' . The cycle is repeated (three or four times) until values of X_{1A}' and X_{1B}' obtained from successive calculations show no significant difference.

Solution of the Diffusion Equation. When the cell has compartments of fixed volume, V_A and V_B , the diffusion coefficient D can be calculated from experimental data using an integrated form of Fick's second law

$$\ln \frac{\Delta C_1^0}{\Delta C_1} = \frac{1}{\kappa} \left(\frac{1}{V_A} + \frac{1}{V_B} \right) Dt \quad (4)$$

where ΔC_1^0 and ΔC_1 are the initial and final differences in concentration (moles per unit volume) of diffusant between compartments A and B, κ is the cell constant, and t is the time of the diffusion process. For the constant mass boundary condition the volumes of liquid in each compartment vary slightly during diffusion. As a result, the relation of D to experimental variables becomes much more complicated. For the conditions employed in the present work it was found that eq. 4 could be substituted for the more rigorous relation by using the mean values of V_A and V_B . These quantities are obtained from the initial and final quantities of salt in each compartment and the known densities of the mixtures.⁹ The error introduced by this simplification was less than 1%.

Results and Discussion

Results of the eight runs carried out at 310° are listed in Table I. (A few runs at higher temperatures were attempted; these showed poorer reproducibility, apparently due to the increased rate of silver-catalyzed decomposition of the melt at the electrodes.) The

column headed \bar{X}_1 gives the mean composition during each run, obtained by averaging the mean compositions of the two compartments at the beginning and end of the run. At the highest value of \bar{X}_1 (8 mole % AgNO_3) the initial concentration in the inner compartment was 13 mole %. Concentrations higher than this were not attempted due to the difficulty of obtaining accurate e.m.f. measurements without having too great a concentration span between compartments for the results to be meaningful (see eq. 1). The column headed D_1^M gives the mass-fixed diffusion coefficient of Ag^+ obtained from experimental data using eq. 4. D_{12}^V is the volume-fixed or "ordinary" diffusion coefficient of either ion. The latter is calculated from D_1^M and the known molar volumes⁹ and masses of the salts by standard methods.¹⁰ D_{12}' , the thermodynamic mutual diffusion coefficient,¹¹ is obtained from the relation

$$D_{12}' = D_{12}^V \left/ \left(1 + \frac{d \ln \gamma_i}{d \ln X_i} \right) \right.$$

where the subscript i refers to either salt. The last column of Table I gives values of the interionic friction coefficient r_{12} calculated from the relation¹²

$$\frac{D_{12}'}{RT} = \frac{1}{r_{12} + X_{2'}r_{13} + X_{1'}r_{23}} \quad (5)$$

The cation-anion friction coefficients r_{13} and r_{23} were taken to be equal in accord with the results of transference experiments,⁴ the values being based on the conductance measurements of Wetmore, *et al.*⁹

The principal source of error in the present work was in the determination of e.m.f. Readings tended to fluctuate over several hundredths of a mv., but the accuracy was apparently worse than this, as indicated by comparison of each final e.m.f. reading with that calculated from analysis of the cell contents. Discrepancies were as great as 0.70 mv. and averaged ± 0.27 mv. This was considerably poorer precision than had been obtained previously in this laboratory,⁸ but the error was apparently a random function of electrode "stability" which could not be eliminated. It leads to an average uncertainty of $\pm 3.5\%$ in the calculated values of D_1^M .

From Table I it is seen that there is no systematic trend in the variation of D_1^M with concentration, fluctuations about the mean value of 1.97×10^{-5} cm.²

(9) J. Byrne, H. Fleming, and F. E. W. Wetmore, *Can. J. Chem.*, **30**, 922 (1952).

(10) R. P. Wendt and L. J. Gosting, *J. Phys. Chem.*, **63**, 1287 (1959).

(11) R. W. Laity, *ibid.*, **63**, 80 (1959).

(12) The general expression is correctly given first in footnote 7 of R. W. Laity, *ibid.*, **67**, 671 (1963).

Table I: Results of Diffusion Measurements in $\text{AgNO}_3\text{-NaNO}_3$ at 310°

Run no.	\bar{X}_1	$D_1^M \times 10^6$, cm. ² sec. ⁻¹	$D_{12}^V \times 10^6$, cm. ² sec. ⁻¹	$D_{12}' \times 10^6$, cm. ² sec. ⁻¹	$r_{12} \times 10^{-8}$, joules sec. cm. ⁻² mole ⁻¹
1	0.0239	1.98	2.03	2.10	0.41
2	.0292	1.95	2.01	2.09	0.42
3	.0319	1.89	1.95	2.04	0.56
4	.0378	1.74	1.80	1.90	0.90
5	.0442	2.10	2.20	2.34	-0.05
6	.0540	1.98	2.09	2.25	0.11
7	.0625	1.90	2.02	2.20	0.22
8	.0770	2.17	2.33	2.59	-0.44
Averages	.0451	1.96 ± 0.09	2.05 ± 0.11	2.19 ± 0.16	0.27 ± 0.31

sec.⁻¹ averaging about $\pm 4.5\%$. We conclude that D_1^M is nearly independent of concentration over the range studied. The other two diffusion coefficients, D_{12}^V and D_{12}' , show a tendency to increase with concentration that is confirmed by the correspondingly greater average deviations. This behavior is to be expected from the physical properties of the system (mass, molar volume, and thermodynamic behavior) if the value of D_1^M is constant. Since all three diffusion coefficients must extrapolate to the same value at infinite dilution, the best figure for this limiting value is given by the average of D_1^M .

The only diffusion results previously reported for this system are the 1911 figures of Harrison⁵ on mixtures of about the same composition. Although he worked at temperatures $20\text{--}70^\circ$ higher, extrapolation to the temperature of this work gives a D_{12}^V value about twice the average of these found here. This is not surprising, since the Harrison method is expected to suffer from convective mixing of the solutions.⁶ On the other hand, a chronopotentiometric study of Ag^+ in NaNO_3 carried out in this laboratory¹³ appears to confirm the validity of the present results. Extrapolation of values obtained at 315 , 340 , and 360° gives $D_{\text{ch}} = (1.96 \pm 0.05) \times 10^{-5}$ cm.² sec.⁻¹ for solutions at 310° containing $0.04\text{--}0.4$ mole % AgNO_3 . (At infinite dilution the chronopotentiometric diffusion coefficient D_{ch} becomes identical with the other three.¹⁴)

The large fluctuations in the figures listed for r_{12} illustrate the extreme sensitivity of this friction coefficient to the precision of the diffusion data from which it is calculated. From the mean of D_1^M , the infinite dilution value of r_{12} is estimated to be $(0.72 \pm 0.23) \times 10^8$ joules sec. cm.⁻² mole⁻¹. The increase in D_{12}' with concentration implies a downward trend in r_{12}' but it appears unlikely that the latter actually becomes negative in this range. Moreover, a systematic uncertainty that results from the possible error in the values of r_{13} used in eq. 5 makes negative values of r_{12}

even more unlikely. Experimental uncertainty in the transference results on which these quantities are based is such that setting r_{13} equal to r_{23} gives a *maximum* value for the former. r_{13} may be as much as 13% lower than r_{23} and it is only the latter quantity that is known accurately from conductance measurements in this region. It follows from eq. 5 that figures as much as 0.5×10^8 joules sec. cm.⁻² mole⁻¹ *greater* than those listed for r_{12} in Table I would still be consistent with experimental data.

In view of such uncertainties it is difficult to draw reliable conclusions about r_{12} from the results of our measurements. However, one or two general conclusions appear to be warranted. It is apparent that in dilute solutions of AgNO_3 in NaNO_3 the value of this cation-cation friction coefficient increases as infinite dilution is approached, but remains considerably smaller than either of the cation-anion friction coefficients. The sodium nitrate coefficient r_{23} is 4.23×10^8 joules sec. cm.⁻² mole⁻¹ at infinite dilution, while the silver nitrate coefficient r_{13} may lie anywhere between 3.68 and 4.23×10^8 . Perhaps even more significant is the observation that it now appears probable that the silver-sodium friction coefficient at infinite dilution in NaNO_3 is smaller than the sodium-sodium coefficient r_{22} in the pure salt. The latter is calculated from self-diffusion results¹⁵ to be 1.25×10^8 at 310° . It had been expected² that r_{12} and r_{22} might be about equal in view of the apparent equality of r_{13} and r_{23} . The present results seem to warrant the speculation that r_{13} does not equal r_{23} after all, but instead lies nearer the low end of the range permitted by the transference results. The correspondingly higher value that is

(13) R. W. Laity, K. Kawamura, and J. D. McIntyre, to be published.

(14) R. W. Laity and J. D. McIntyre, theoretical results to be published.

(15) A. S. Dworkin, R. B. Escue, and E. R. Van Artsdalen, *J. Phys. Chem.*, **64**, 872 (1960).

then calculated for r_{12} (between 1.0 and 1.2×10^8 at infinite dilution) prompts us to replace our former anticipation of equal values for the two cation-cation coefficients with an alternative suggestion: at infinite dilution the ratios r_{12}/r_{22} and r_{13}/r_{23} may be found nearly the same when more accurate data are available for this system. The interionic friction coefficients in-

volving Ag^+ called for by this conjecture have the following values at 310° : $r_{12} = 1.1 \times 10^8$, $r_{13} = 3.8 \times 10^8$ joules sec. cm.⁻² mole⁻¹.

Acknowledgment. The authors are indebted to Mr. L. Chen, who performed some of the calculations on the IBM-7090 computer.

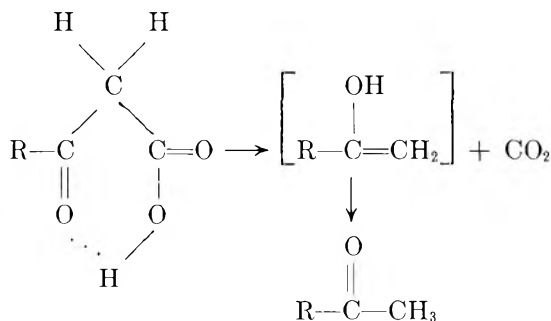
The Kinetics of the Decarboxylation of Malonanilic Acid in Polar Solvents

by Louis Watts Clark

Department of Chemistry, Western Carolina College, Cullowhee, North Carolina
(Received January 30, 1964)

Kinetic data are reported for the decarboxylation of malonanilic acid in 11 polar solvents, namely, *m*-cresol, *p*-cresol, *o*-cresol, 1,4-butanediol, 2,3-butanediol, 1,3-butanediol, acetanilide, aniline, *N*-ethylaniline, quinoline, and 8-methylquinoline. The activation parameters for the reaction are calculated and compared with those for malonic acid and other related acids. The results indicate that the mechanism of the decarboxylation of malonanilic acid is *not* the same as that for malonic acid, but that the malonanilic acid apparently functions as a nucleophilic agent.

Kinetic studies have been carried out on the decarboxylation of several β -keto acids, including acetoacetic acid and α,α -dimethylacetoacetic acid.¹ Results of these studies suggest that the mechanism probably involves a chelated six-membered ring, which loses CO_2 to form an enol, the enol then reverting to the more stable tautomeric form

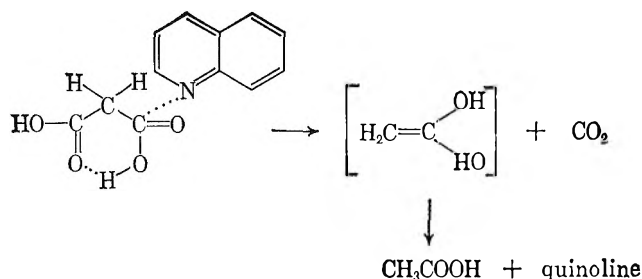


Because of the importance of β -keto acids in enzymic reactions detailed information on the effect of solvents and other factors on the reaction would be highly desirable. However, these compounds are generally so unstable that their preparation, separation, and purification are unfeasible.

On the basis of results obtained in studies on the decarboxylation of malonic acid in quinoline and other solvents Fraenkel and co-workers proposed a cyclic mechanism for the reaction yielding the enol of acetic acid which then tautomerized.²

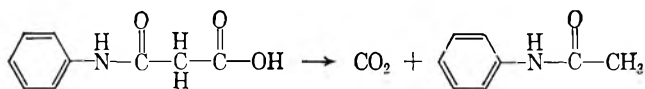
(1) (a) E. M. P. Widmark, *Acta med. Scand.*, **53**, 393 (1920); *Chem. Abstr.*, **15**, 2763 (1931); (b) K. J. Pedersen, *J. Am. Chem. Soc.*, **51**, 2098 (1929); (c) *ibid.*, **60**, 595 (1938).

(2) G. Fraenkel, R. L. Belford, and P. E. Yankwich, *ibid.*, **76**, 15 (1954).



They believed that, in the activated state, a nucleophilic atom of solvent molecule coordinated with one of the electrophilic carbonyl carbon atoms of the acid facilitating cleavage. Subsequent studies on the decarboxylation of malonic acid and its derivatives in a wide variety of solvents have confirmed the reasonableness of the proposed mechanism.³

Although malonic acid and its derivatives resemble β -keto acids in having a keto group in the β -position, they differ from β -keto acids in the possession of a second carboxyl group. It is well known that dicarboxylic acids tend to polymerize *via* hydrogen bond past the dimer stage.⁴ For this reason it would be desirable to have a fairly stable β -keto acid having only one terminal carboxyl group. A compound which answers this description is malonanilic acid. It is well known that this compound easily undergoes thermal decarboxylation yielding acetanilide and CO_2 according to the equation



Since this compound held promise of affording some valuable and interesting data on the behavior of β -keto acids, a sample of it was prepared and a careful investigation was carried out in this laboratory on the kinetics of its decarboxylation in various solvents. The results of this study are reported herein.

Experimental

The malonanilic acid used in this research was prepared by the method of Rügheimer,⁵ which consists of heating equivalent amounts of malonic acid and aniline at 105° for 1 hr. After recovering the product, recrystallizing it three times from water, and drying it for 2 hr. at 100° , it melted with decomposition at 130° (cor.); lit.⁶ m.p. 132° (uncor.).

Analytical Data. A 0.7834-g. sample of the malonanilic acid was dissolved in 40 ml. of distilled water and was titrated with 0.1000 *N* NaOH using a Model H2 Beckman pH meter to determine the end point. The calculated pH at the end point is 7.85, based on the reported ionization constant of malonanilic acid at 25° .⁷

The observed end point determined graphically was also 7.85. A 44.18-ml. portion of base was required for neutralization, indicating a purity of 99.0% for the sample.

The solvents were reagent grade and were distilled at atmospheric pressure immediately before use. Approximately 60 ml. of solvent were used in each experiment.

The apparatus and technique have been described previously.⁸ The use of a completely transistorized temperature control unit enabled the temperature of the oil bath to be kept constant to $\pm 0.005^\circ$. The evolved CO_2 was collected in a 50-ml. buret calibrated by the U. S. Bureau of Standards. The temperature of the water surrounding the buret was controlled to $\pm 0.05^\circ$, using a water circulator, heater, mercury thermoregulator, and electronic relay.

A 0.3219-g. sample of malonanilic acid was used in each decarboxylation experiment. This is the amount required to furnish 40.0 ml. of CO_2 at STP on complete reaction, calculated on the basis of the actual molar volume of CO_2 at STP, namely, 22,267 ml.

Results

The decarboxylation of malonanilic acid gave good first-order kinetics over the greater part of the reac-

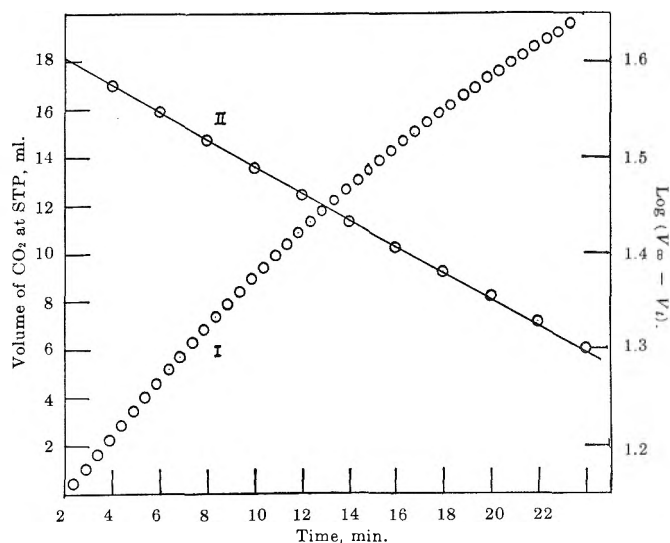


Figure 1. Decarboxylation of 0.3219 g. of malonanilic acid in 60 ml. of *m*-cresol at 124.79° (cor.). Line I, volume of CO_2 at STP; line II, $\log (V_\infty - V_t)$.

(3) L. W. Clark, *J. Phys. Chem.*, **67**, 2602 (1963), and many previous papers in this series.

(4) W. Hückel, "Theoretical Principles of Organic Chemistry," Vol. II, Elsevier Publishing Co., New York, N. Y., 1958, p. 329.

(5) L. Rügheimer, *Ber.*, **17**, 736 (1884).

(6) R. Seifert, *ibid.*, **18**, 1358 (1885).

(7) W. Ostwald, *Z. physik. Chem.*, **3**, 370 (1889).

(8) L. W. Clark, *J. Phys. Chem.*, **60**, 1150 (1956).

tion in most of the solvents. During the latter part of the reaction in the hydroxylic solvents the logarithmic plot deviated to a slight extent from linearity, due, presumably, to a slow solvolysis reaction. However, this did not affect the accuracy of the calculation of the specific reaction velocity constants in these solvents. Duplicate determinations of the rate constant in the same solvent at the same temperature did not differ by more than 1% in any case (Fig. 1).

In Table I are shown the average values of the rate

Table I: Apparent First-Order Rate Constants for the Decarboxylation of Malonanilic Acid in Various Solvents

Solvent	Temperature, °C., cor.	$k \times 10^4$, sec. ⁻¹
<i>m</i> -Cresol	119.69	3.05
	129.95	9.26
	139.75	24.6
<i>p</i> -Cresol	120.49	3.7
	129.95	10.5
	138.37	25.4
<i>o</i> -Cresol	117.69	2.90
	130.05	12.56
	135.65	22.8
1,4-Butanediol	108.04	3.52
	118.46	8.25
	128.12	17.6
2,3-Butanediol	109.57	3.51
	120.39	9.97
	129.45	23.4
1,3-Butanediol	106.97	2.78
	117.29	8.86
	126.84	24.8
Acetanilide	115.35	7.31
	122.35	13.4
	133.71	26.1
Aniline	104.14	3.95
	113.95	10.3
	122.25	24.6
N-Ethylaniline	96.06	1.55
	105.44	4.67
	114.35	12.63
Quinoline	98.64	5.31
	108.84	12.4
	118.05	24.3
8-Methylquinoline	102.74	2.69
	112.96	7.48
	122.06	17.8

constants for the reaction in the various solvents at the different temperatures studied. The apparent first-order rate constants were calculated from the slopes of the experimental logarithmic plots.

Table II shows the parameters of the absolute reaction rate equation⁹

$$k = \frac{\kappa T}{h} e^{\Delta S^*/R} e^{-\Delta H^*/RT}$$

calculated from the data in Table I. Included also are corresponding data for malonic acid where available.

Table II: Activation Parameters for the Decarboxylation of Malonic Acid and Malonanilic Acid in Several Solvents

Solvent	Malonic acid		Malonanilic acid	
	ΔH^* , kcal./mole	ΔS^* , e.u./mole	ΔH^* , kcal./mole	ΔS^* , e.u./mole
<i>m</i> -Cresol	32.3	+3.2	33.2	+9.4
<i>p</i> -Cresol	29.8	-2.4	34.0	+11.54
<i>o</i> -Cresol	24.2	-16.5	35.5	+15.5
1,4-Butanediol			23.7	-12.7
2,3-Butanediol			28.1	-1.5
1,3-Butanediol			32.6	+10.4
Acetanilide			21.1	-19.15
Aniline	26.9	-4.5	27.6	-1.5
N-Ethylaniline	26.0	-6.6	31.9	+10.0
Quinoline	26.7	-2.4	21.0	-17.5
8-Methylquinoline	24.4	-10.5	28.5	+0.4

Discussion

It will be observed in Table II that the values of the entropy of activation for the decarboxylation of malonanilic acid in the various solvents (with the exception of quinoline) are higher than those for malonic acid. This would be expected considering the fact that the parent compound, containing two carboxyl groups, tends to polymerize past the dimer stage,⁴ whereas the derivative, with only one carboxyl group, would probably exist in the dimer form. It will be noted also in Table II that the values of the enthalpy of activation for the decarboxylation of malonanilic acid in the various solvents (quinoline again excepted) are likewise higher than those for malonic acid.

As already mentioned the mechanism of the decarboxylation of malonic acid in polar solvents apparently involves the formation of an activated complex between the acid and solvent, a pair of unshared electrons on the nucleophilic atom of the solvent coordinating with the electrophilic center situated on the carbonyl carbon atom of the acid. If the reactant is electrophilic, then an increase in basicity of the solvent will increase the attraction between solute and solvent and therefore lower the energy of reaction.¹⁰ This lowering

(9) S. Glasstone, K. J. Laidler, and H. Eyring, "The Theory of Rate Processes," McGraw-Hill Book Co., Inc., New York, N. Y., 1941, p. 14.

(10) K. J. Laidler, "Chemical Kinetics," McGraw-Hill Book Co., Inc., New York, N. Y., 1950, p. 138.

of the energy of activation with increasing basicity of solvent is demonstrated by the data in Table II in the case of the malonic acid reaction, but not in the reaction of malonanilic acid.

If one considers the cresols, the methyl group on the nucleus exerts a $+I$ effect which will make the cresols less acidic than phenol. This effect will be the most pronounced when the methyl group is in the *ortho* position, somewhat less when it is in the *para* position, and least pronounced when it is in the *meta* position. The order of increasing nucleophilicity of the cresols will be, therefore, *m*-cresol, *p*-cresol, *o*-cresol. It will be observed in Table II that the enthalpy of activation for the malonic acid reaction the cresols decreases regularly with increasing nucleophilicity of solvent, whereas for malonanilic acid it *increases*.

If we consider next aniline and its derivatives, an ethyl group on the amino nitrogen atom exerts a $+I$ effect increasing the effective negative charge on the nitrogen, whereas an acetyl group exerts a $-I$ effect, decreasing the negative charge. In other words, in this group of solvents, the nucleophilicity of the solvent increases in the order: acetanilide, aniline, *N*-ethyl-aniline. Again it will be observed in Table II that the enthalpy of activation for the malonic acid reaction decreases in this group of solvent with increasing basicity, whereas, for malonanilic acid, it *increases*.

Due to the inductive effect of the methyl group on the 8-position in quinoline, 8-methylquinoline would be expected to be more basic than quinoline. Furthermore, the methyl group would tend to sterically hinder the formation of the activated complex, leading to a decrease in the entropy of activation. In these two solvents, malonic acid shows the expected decrease in the enthalpy of activation with increasing basicity, and shows the expected decrease in the entropy of activation due to steric hindrance. Malonanilic acid, however, again shows an *increase* in enthalpy of activation with increasing basicity and does not appear to suffer any steric hindrance in the solvent 8-methylquinoline.

Data are not available for the reaction of malonic acid in the glycols. However, studies have been reported on the decarboxylation of β -resorcylic acid in the glycols and other polar solvents,¹¹ in which it has been established that β -resorcylic acid behaves like an electrophilic agent, similar to malonic acid. A comparison of the activation parameters for the decarboxylation of malonanilic acid and β -resorcylic acid in the three glycols used in this research is illuminating (see Table III).

It will be seen in Table III that the enthalpy of activation for the decarboxylation of β -resorcylic acid decreases in the order 1,4-butanediol, 2,3-butanediol,

Table III: Activation Parameters for the Decarboxylation of Malonanilic Acid^a and β -Resorcylic Acid^b in Several Glycols

Solvent	—Malonanilic acid—		— β -Resorcylic acid—	
	ΔH^* , kcal./mole	ΔS^* , e.u./mole	ΔH^* , kcal./mole	ΔS^* , e.u./mole
1,4-Butanediol	23.7	-12.7	36.26	+11.7
2,3-Butanediol	28.1	-1.5	24.9	-17.1
1,3-Butanediol	32.6	+10.4	19.76	-27.8

^a Source of malonanilic acid data: this research. (See Table II). ^b Source of β -resorcylic acid data: see ref. 11.

and 1,3-butanediol, whereas for malonanilic acid it *increases* in this order.

The mechanism of the decarboxylation of malonanilic acid in polar solvents is thus apparently *not* the same as that for the decarboxylation of malonic acid and other electrophilic acids. It would appear, on the basis of these results, that malonanilic acid functions as a nucleophilic agent.

A plot of ΔH^* vs. ΔS^* for the decarboxylation of malonanilic acid in the aniline series is linear (see Fig. 2), the equation for the straight line, as determined by the method of least squares, being

$$\Delta H^* = 370\Delta S^* + 28,170$$

The slope of this line is thus 370°K., which is 97°. This is the so-called isokinetic temperature, that is, the

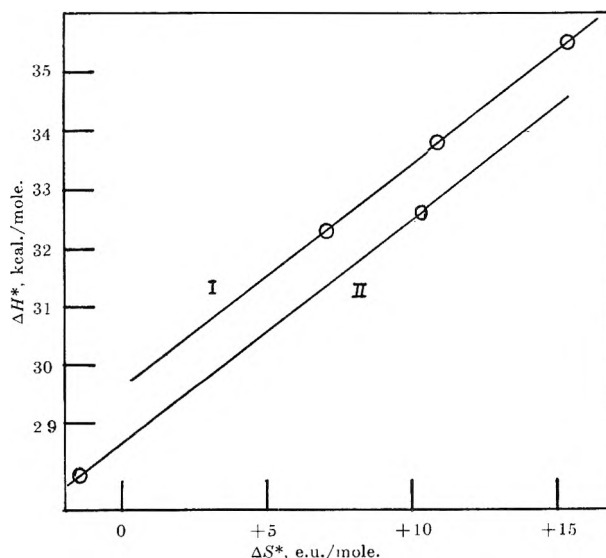


Figure 2. Enthalpy-entropy plot for the decarboxylation of malonanilic acid in cresols (line I) and glycols (line II).

(11) L. W. Clark, *J. Phys. Chem.*, **67**, 2831 (1963).

temperature at which the rate of reaction is the same for all the solvents conforming to the line.¹²

Acknowledgment. Acknowledgment is made to the donor of The Petroleum Research Fund, administered

by the American Chemical Society, for support of this research.

(12) J. E. Leffler and E. Grunwald, "Rates and Equilibria of Organic Reactions," John Wiley and Sons, Inc., New York, N. Y., 1963, p. 129.

X-Ray Studies of Hydrogen–Silver–Palladium Electrodes

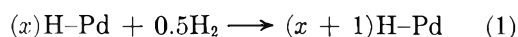
by S. D. Axelrod and A. C. Makrides

Tyco Laboratories, Inc., Waltham, Massachusetts (Received February 1, 1964)

The potential of Ag–Pd alloys decreases, during absorption of hydrogen from aqueous solutions, to a value characteristic of the alloy, and after a time at this value, it drops gradually to zero. X-Ray studies of Ag–Pd alloys charged with hydrogen show that the potential plateau corresponds to an α – β transformation similar to that found with the H–Pd system. Alloys containing 30% or more silver do not show a potential plateau during the absorption of hydrogen, and the X-ray studies indicate that a continuous expansion of the lattice occurs in this case. The lattice parameter–potential diagrams for H–Ag–Pd alloys of varying silver content essentially coincide once the β -phase is formed although the concentration of dissolved hydrogen is substantially different for each alloy. These results are discussed in terms of a model according to which dissolved hydrogen exists as protons with the corresponding electrons going into the d-band of the alloy.

I. Introduction

During absorption of hydrogen from aqueous solution, the potential of palladium decreases at first to 49.5 mv. vs. a H⁺/H₂ electrode in the same solution and, after several hours at this value, drops gradually to zero.^{1–3} Although there is some disagreement about the interpretation of the time–potential curves,^{2,3} recent work^{4,5} has shown that the potential plateau corresponds to the α – β transformation in the H–Pd system. The potential-determining reaction during adsorption of hydrogen is



where $(x)\text{H-Pd}$ represents hydrogen dissolved in palladium to an atomic ratio x . The potential plateau corresponds to the horizontal portion of the H–Pd isotherm where gaseous hydrogen dissolves at a constant pressure to yield the β -phase.^{6,7}

Palladium alloys behave similarly to palladium, except that the total amount of dissolved hydrogen at saturation generally becomes less as the ratio of the second element to palladium is increased. Of particular interest are Ag–Pd alloys which are used widely for

(1) A. Frumkin and N. Alačjalova, *Acta Physicochim. URSS*, **19**, 1 (1944); N. Hitzler and C. A. Knorr, *Z. Elektrochem.*, **53**, 233 (1949).

(2) J. P. Hoare and S. Schuldiner, *J. Electrochem. Soc.*, **102**, 485 (1955); **104**, 564 (1957); S. Schuldiner, G. W. Castellan, and J. P. Hoare, *J. Chem. Phys.*, **28**, 16, 20, 22 (1958).

(3) T. B. Flanagan and F. A. Lewis, *ibid.*, **29**, 1417 (1959).

(4) T. B. Flanagan and F. A. Lewis, *Trans. Faraday Soc.*, **55**, 1400, 1409 (1959).

(5) P. C. Aben and W. G. Burgers, *ibid.*, **58**, 1989 (1962).

(6) A. Sieverts, *Z. physik. Chem.*, **88**, 451 (1914); H. Bruning and A. Sieverts, *ibid.*, **A163**, 409 (1932); A. Sieverts and H. Hagen, *ibid.*, **A174**, 247 (1935); A. Sieverts and G. Zapf, *ibid.*, **A174**, 359 (1935).

(7) L. J. Gillespie and F. P. Hall, *J. Am. Chem. Soc.*, **48**, 1207 (1926); L. J. Gillespie and L. S. Galstaum, *ibid.*, **58**, 2565 (1936).

purification of hydrogen.^{8,9} It has been found that the hydrogen solubility in these alloys at $P_{H_2} = 1$ atm. decreases uniformly with silver content to essentially zero at about 60–70% silver.¹⁰ However, it has also been reported^{11,12} that the plateau potential at which the α - β transformation presumably takes place increases with silver content to a maximum at about 26 atom % silver and then decreases again at greater silver contents. This last finding is in doubt since time-potential data for this system are discrepant.^{11–13}

X-Ray studies of the H-Ag-Pd system are also in disagreement. Krüger and Gehm¹⁴ report that an α - β transformation occurs during absorption of hydrogen by Ag-Pd alloys up to 60% silver. On the other hand, Rosenhall¹⁵ finds that the α - β transformation does not take place above about 24% silver. In view of these conflicting results, and because of different interpretations of the nature of the transformation associated with the potential plateau,^{2,3} an attempt was made here to correlate the potential of Ag-Pd alloys during absorption of hydrogen with the structure of the alloy as determined by X-ray diffraction. It was found that the potential plateau observed with alloys containing up to about 25 atom % silver arises from an α - β transformation in the H-Ag-Pd system. A potential plateau was not observed with an alloy containing 30.5 atom % silver, and the X-ray studies showed that a continuous expansion of the lattice of this alloy occurred as hydrogen was absorbed.

II. Experimental

A series of Pd-Ag alloys was prepared by melting commercially pure palladium and spectrographically pure silver (Johnson-Matthey) in zircon-lined carbon crucibles in an induction heating unit. The charge was melted in a protective atmosphere of high purity nitrogen and cast into a previously outgassed carbon mold held at 750°. The charge was superheated to increase the fluidity of the melt and to allow for a temperature decrease during casting. The resulting ingots were sealed in an evacuated quartz tube and homogenized for 48 hr. at 800°.

The lattice parameters of the alloys were determined by X-ray diffraction and are given in Table I. These data compare well with other reported results.^{16,17} Electrodes were made by drawing alloys into 15-mil wire followed by annealing at 950° for 0.5 hr. Metallographic examination of electrodes so prepared showed that they consisted of single phase equiaxed grains with an average grain diameter, measured by a linear technique, of approximately 0.05 mm. Although the corresponding grain density, roughly 10^7 grains/cm.³, is somewhat low, continuous halos were obtained in the

X-ray work which permitted accurate measurements of the lattice spacing. The composition of each alloy was determined by chemical analysis. In addition to the above alloys, a commercially available Pd-Ag alloy containing 23.8% silver was studied.

Table I: Lattice Parameters of H-Ag-Pd Alloys

Atom % Ag	Å.			Charged to $P_{H_2} =$ 1 atm., $E = 0$	$E,$ mv., at 30°
	$\alpha_{\text{un-}}$ charged alloy	α_{max}	β_{min}		
0	3.890	3.893	4.025	4.040	49.5
10.4	3.908	3.922	4.003	4.033	65.5
20.0	3.923	3.945	3.993	4.027	82.5
23.8	3.931	(3.991)	(3.996)	4.027	87.5
30.5	3.942	4.026	(99 ?)

The wire electrodes were spot-welded to platinum and then sealed in Pyrex holders. The wire-glass junction was coated with a small amount of a fluorocarbon (Kelf polymer wax) so that only the alloy was exposed to solution. An all-Pyrex electrolytic cell was used for charging the electrodes with hydrogen. The cell and its components were cleaned in a concentrated chromic-sulfuric acid solution (cleaning solution) and rinsed with hot, triply distilled water. Potentials were measured against a platinized platinum electrode with a Sargent chart recorder, which was periodically calibrated against a Leeds and Northrup K-2 potentiometer. The current drain in the potential measuring circuit was less than 10^{-7} amp./cm.².

2 N HClO₄ solutions were prepared from conductivity water and 70% A.R. grade Mallinckrodt perchloric acid. Electrolytic hydrogen was purified by diffusion through a Ag-Pd alloy at 425°. The solution was saturated with hydrogen before a sample was introduced into the cell and a continuous flow of gas was

(8) A. S. Darling, *Platinum Metals Rev.*, **2**, 16 (1958); J. B. Hunter, *ibid.*, **4**, 130 (1960).

(9) H. Connor, *ibid.*, **6**, 130 (1962).

(10) Z. L. Vert and I. P. Tverdovskii, *Zh. Fiz. Khim.*, **28**, 317 (1954).

(11) F. A. Lewis and W. H. Schurter, *Naturwissenschaften*, **47**, 177 (1960).

(12) F. A. Lewis, *Platinum Metals Rev.*, **5**, 21 (1961).

(13) J. P. Hoare, C. W. Castellon, and S. Schuldiner, *J. Phys. Chem.*, **62**, 1141 (1958).

(14) F. Krüger and G. Gehm, *Ann. Physik.*, (5) **16**, 190 (1933).

(15) G. Rosenhall, *ibid.*, (5) **24**, 297 (1935).

(16) V. G. Kuznetsov, *Izv. Zekt. Platinij, Akad. Nauk SSSR*, No. **20**, 5 (1946).

(17) B. R. Coles, *J. Inst. Met.*, **84**, 346 (1956).

maintained through the solution during each run. The cell was thermostated at $30 \pm 0.1^\circ$.

The electrode potential of an alloy decreases as it absorbs hydrogen from solution. Electrodes were withdrawn at various potentials and immediately coated with a wax in order to avoid loss of hydrogen. Various coatings were tried, *e.g.*, collodion, Duco cement, styrene, polystyrene, high-vacuum grease, and glyptal, with only limited success. A satisfactory coat was produced by Apiezon wax dissolved in trichloroethylene. The criterion used to determine the effectiveness of a particular type of coating was whether the X-ray patterns of samples changed with time after the application of the coat. Samples coated with Apiezon wax consistently gave time-independent X-ray patterns.

The coated sample was accurately positioned in a Debye-Scherrer powder pattern camera (114.6-mm. diameter) and was continuously rotated in a Cu $K\alpha_{1,2}$ X-ray beam of 20 ma. at 35 kv. The exposure time was 3.5 hr.

Different samples gave rise to different potential-time curves. This was probably due to the fact that the geometric position of the electrode in the cell and the flow conditions (stirring by gas) were not reproduced from run to run. However, in spite of these differences, the lattice parameter was shown to have a fixed relation to the potential; several samples having different potential-time curves had the same lattice parameter when withdrawn at the same potential. This observation allows a composite lattice parameter *vs.* potential curve to be constructed with the assurance that individual samples will fit on the same general curve.

III. Results

The change in potential with time during the absorption of hydrogen from a $2 N HClO_4$ solution by a 10.4 atom % Ag-Pd alloy is shown in Fig. 1. This plot is typical of all alloys with 24 atom % or less silver. In Fig. 2 are shown optical density tracings of X-ray patterns of samples removed at the various potentials indicated in Fig. 1. The resulting lattice parameter-potential curve is shown in Fig. 3.

There is a continuous increase of the lattice parameter up to the plateau potential (see Fig. 1-3), at which point a new phase appears. The simultaneous presence of the α - and β -phases is shown by the two sets of lines in Fig. 2c. As additional hydrogen is absorbed, the lines corresponding to the α -phase disappear and are replaced by the β -phase lines. Both the α - and the β -phases are face-centered cubic, but the β -phase has a more expanded structure. The lattice parameter of

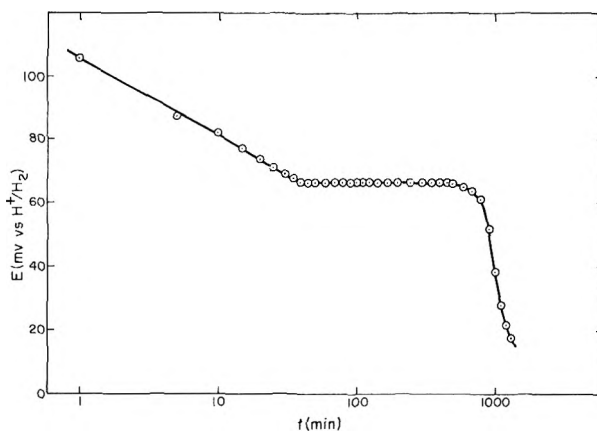


Figure 1. A time-potential curve for a 10.4 atom % silver alloy during absorption of hydrogen from $2 N HClO_4$ at 30° .

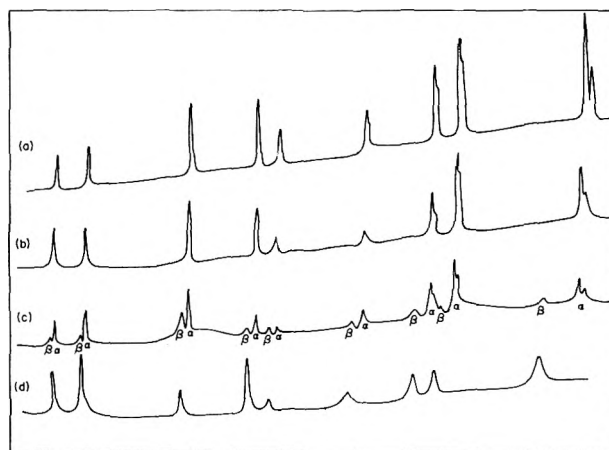


Figure 2. Intensity profiles for a 10.4 atom % silver alloy: (a) uncharged; (b) charged with hydrogen to a potential of 70 mv.; (c) charged to the plateau potential (65.5 mv.); (d) charged to a potential of 17 mv.

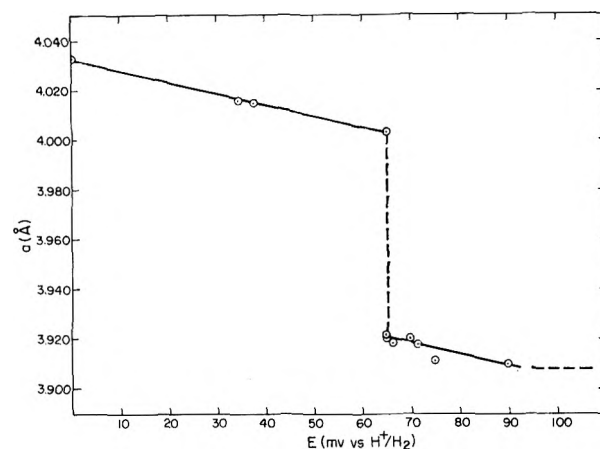


Figure 3. Lattice parameter *vs.* potential plot for 10.4 atom % Ag-Pd alloy ($2 N HClO_4$ at 30°).

the β -phase increases continuously as the potential at which the sample is removed becomes less positive (Fig. 3).

The X-ray pattern of the uncharged sample, shown in Fig. 2a, has sharp, completely resolved back reflection $K\alpha_1\alpha_2$ doublets indicating a well-annealed, fine-grained structure. When hydrogen is absorbed, the back reflection doublets become diffuse, suggesting that the lattice becomes distorted as hydrogen is dissolved in the alloy.

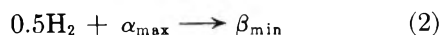
Similar results were obtained with a 20.0 atom % silver alloy and are shown in Table I and Fig. 4. A 23.8 atom % silver alloy also shows a potential plateau, but of much shorter duration. If the lattice parameter-potential plot has a discontinuity at the plateau potential, it must be very small (Fig. 4). Also, it did not prove possible to find two phases (*i.e.*, two sets of lines) with samples removed at the potential plateau.

A 30.5 atom % silver alloy electrode does not show a potential plateau during absorption of hydrogen. There is, however, a definite change in the rate at which the potential changes with time, which occurs at a reproducible potential of 99 ± 3 mv. The lattice parameter-potential curve does not show a discontinuity, the lattice parameter being a smooth function of potential (Fig. 5).

A limited amount of work was also carried out with pure palladium. An annealed, palladium wire charged with hydrogen to a potential of 0.049 v. showed both the α - and the β -phases with lattice parameters of 3.893 and 4.025 Å., respectively, which are in good agreement with the results given in ref. 5 (3.894 and 4.025 Å.).

IV. Discussion

The essential result of the X-ray work with the 10.4 and 20.0 atom % silver alloys is the correspondence of the potential plateau to the region of co-existence of the α - and β -phases of the H-Ag-Pd system. In addition, the X-ray diffraction patterns show that the surface layer of these alloys consists of only the α - or β -phases at, respectively, potentials above and below the plateau potential. It may be concluded that the plateau potential arises from the α - β transformation and corresponds to the process



where α_{max} is the saturated α -phase and β_{min} the β -phase containing no additional dissolved hydrogen. Therefore, the potential behavior of these alloys is entirely equivalent to that of pure palladium.⁴

The plateau potential is essentially a thermodynamic potential although the system is not, strictly speaking,

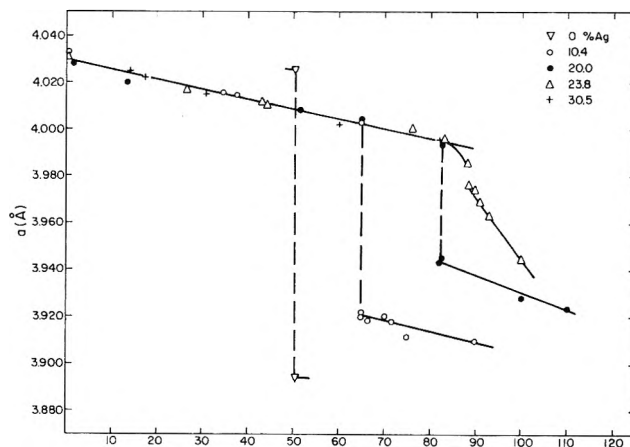


Figure 4. Lattice parameter vs. potential for Ag-Pd alloys and for pure palladium.

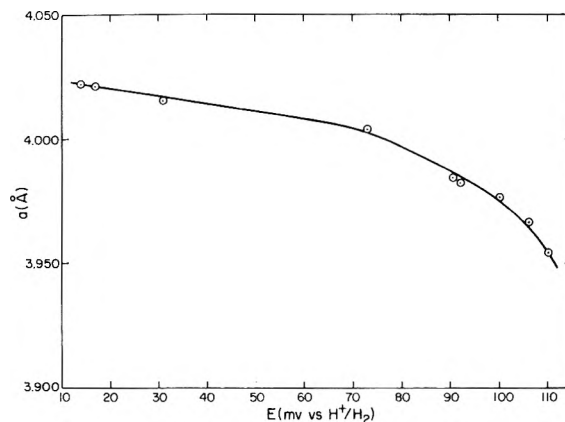
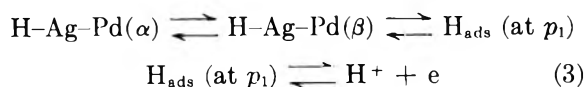
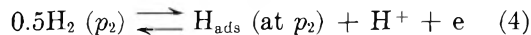


Figure 5. Lattice parameter vs. potential for a 30.5 atom % Ag-Pd alloy (2 N HClO₄ at 30°).

at equilibrium. The over-all process of hydrogen absorption may be split into a sequence of steps involving transport of molecular hydrogen to the metal-electrolyte interface, dissociative adsorption of hydrogen, and solution of hydrogen into the metal. If the rate at which hydrogen is transported to the interface is much smaller than the rate at which hydrogen is absorbed, the surface concentration of hydrogen is determined by the concentration of hydrogen in the metal. Therefore, the potential of the alloy at any time, t_1 , corresponds to that of a hydrogen electrode at an equivalent pressure, p_1 , less than 1 atm. In particular, the plateau potential at the α - β transformation vs. a H^+ - H_2 electrode is given by



At the platinized platinum electrode



where p_1 is the hydrogen pressure corresponding to the α - β transformation and p_2 is the pressure of hydrogen in the solution (here, 1 atm.). It is obvious from (3) and (4) that the plateau potential *vs.* a standard hydrogen electrode (s.h.e.) is independent of the total pressure of hydrogen in solution and is given by

$$E_p = \frac{-RT}{2F} \ln p_1 \text{ (vs. s.h.e.)} \quad (5)$$

The increasingly positive value of E_p with increasing silver content of the alloy shows that the equilibrium hydrogen pressure, p_1 , at which the α - β transformation takes place decreases at higher silver concentrations. The pressures calculated from eq. 5 decrease from 17.0 mm. for pure palladium to 0.92 mm. for the 23.8 atom % Ag-Pd alloy.

The above interpretation of the plateau potential of palladium and Ag-Pd alloys can be extended to other potentials by making the same assumptions about the relative rates of the various steps during hydrogen absorption. In particular, it may be used to explain the dip of the potential immediately before the plateau potential is established (Fig. 6). This slight fall of potential below E_p , which is also observed with palladium,⁴ is probably associated with the supersaturation of the α -phase necessary for nucleating the β -phase.^{4,5} The activation energy for nucleation is probably not negligible even at the surface since the volume expansion accompanying the formation of the β -phase is considerable (about 8%).¹⁸

The α - β Transformation. A more detailed discussion of the H-Ag-Pd system will be postponed to a later communication in which the thermodynamic properties

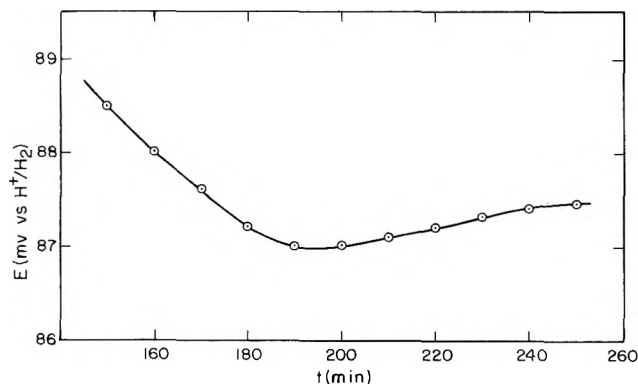


Figure 6. Time-potential curve for a 20.0 atom % Ag-Pd alloy showing a dip of potential immediately before the plateau potential is established. The potential dip is probably associated with a supersaturation of the α -phase prior to nucleation of the β -phase.

of the system are described. However, some general features which are evident from the present X-ray and potential measurements are reviewed briefly here.

Hydrogen dissolved in palladium probably exists as protons, with the electrons going into the d-band of the metal, which becomes full when about 0.6 electron per palladium atom is supplied by hydrogen.^{19,20} The α - β transition in the Pd-H system probably arises from a net attractive potential between dissolved protons, most likely due to attractive interactions between the electrons which provide Fermi screening for the protons. At any rate, this transition can be treated as a phase transition in a regular assembly with good agreement with experiment.^{20,21}

The effect of silver on the absorption of hydrogen is twofold. First, when a nontransition metal is added to palladium the magnetic susceptibility falls as if the valency electrons of the added metal entered states in a d-band or d-states of palladium atoms.²² The decrease in susceptibility may arise either because electrons are donated to a d-band which becomes eventually full or because the increase in the average distance between palladium atoms and the random substitution of silver for palladium atoms does not permit a full development of a d-band. It seems probable that a common collective band is formed in palladium-rich alloys although in silver-rich alloys the d-band picture may not be applicable.²³ In any case, the addition of silver decreases the number of unoccupied d-states and, therefore, decreases the total amount of hydrogen which can be dissolved in the metal. In addition to this effect, silver atoms apparently interact attractively with dissolved hydrogen, the interaction being basically similar to that between dissolved protons. Consequently, the free energy of solution of hydrogen into the metal becomes more negative as the silver content increases, and this is reflected in a larger solubility of hydrogen at low pressures and in a decrease of the equilibrium pressure (or increase of the potential) at which the α - β transition takes place.

An important result which bears on the above qualitative discussion is the coincidence, at any given po-

(18) U. Dehlinger in "The Physical Chemistry of Metallic Solutions and Intermetallic Compounds," Vol. II, Chemical Publishing Co., New York, N. Y., 1960, p. 24.

(19) D. P. Smith, "Hydrogen in Metals," University of Chicago Press, Chicago, Ill., 1948, p. 128.

(20) R. H. Fowler and E. A. Guggenheim, "Statistical Thermodynamics," Cambridge University Press, London, 1960, p. 560.

(21) J. R. Lacher, *Proc. Roy. Soc. (London)*, **A161**, 525 (1937).

(22) F. E. Hoare, J. C. Matthews, and J. C. Walling, *ibid.*, **A216**, 502 (1953).

(23) W. Hume-Rothery and B. R. Coles, *Advan. Phys.*, **3**, 149 (1954).

tential below the transition potential, of the lattice parameters of all the H-Ag-Pd alloys studied. It should be noted that the hydrogen content is substantially different for each alloy, and indeed a plot of lattice parameter *vs.* hydrogen content would not reveal this striking regularity. This result suggests that the electronic structure of H-Ag-Pd alloys containing 10–30% silver is equivalent once the β -phase is formed. Figure 4 shows that the free energy, or, to a good approximation, the energy of solution of hydrogen, is a function of the electronic structure of this alloy, but is independent of the hydrogen concentration once the β -

phase H-Ag-Pd alloy is formed. Thus, the formation of the β -phase can be described as a phase transition brought about by attractive interactions between dissolved protons which is accompanied by an expansion of the lattice due to the filling of the d-band by electrons donated by hydrogen atoms.

Acknowledgment. The authors gratefully acknowledge the skillful experimental assistance of Mr. R. D. McNeill. This work was supported by the Harry Diamond Laboratory, U. S. Army, under contract DA-49-186-ORD-982.

Absorption of Hydrogen by Silver-Palladium Alloys

by A. C. Makrides

Tyco Laboratories, Inc., Waltham, Massachusetts (Received February 1, 1964)

Time-potential curves were obtained during the absorption of hydrogen from aqueous solution by Ag-Pd electrodes and the extent of absorption was determined by potentiostatic techniques. Silver has the following effects on the absorption isotherms: (a) the pressure, p_0 , of the α - β transition decreases with silver content up to about 25 atom % silver; (b) the α - β transition does not occur above 30 atom % silver; (c) the solubility of hydrogen at low pressures ($p \leq p_0$) increases with silver content; (d) the heat of solution at p_0 increases with silver content; (e) the maximum solubility ($p \gg p_0$) decreases with silver content. The above results are discussed in terms of a model, frequently proposed for H-Pd, in which hydrogen is assumed to dissolve as protons with the electrons occupying d-states in the conduction band. It is suggested that interactions between electrons which provide Fermi screening for the protons are responsible for an attractive hydrogen-hydrogen interaction leading to a phase transition in the isotherm. A similar interaction between silver and hydrogen is postulated to account for the changes of p_0 observed with the alloys. The decrease of the maximum solubility (approximated by the solubility at $P_{H_2} = 1$ atm.) is attributed to a decrease in the number of available electron states in the d-band. The elimination of the phase transition with alloys of 30 atom % or more silver is attributed to the decrease of the maximum solubility of hydrogen below a calculated critical value.

Introduction

Transition metals absorb hydrogen extensively to form nonstoichiometric compounds whose composition varies over wide limits. In some cases, the structure of the metal lattice is changed when hydrogen is absorbed, suggesting that the hydrides should be considered as definite chemical compounds rather than as interstitial solid solutions.¹ However, in other cases, most prominently in absorption of hydrogen by palladium, there is considerable doubt whether a chemical compound is formed.² Two hypotheses have been advanced to account for the Pd-H system. In one model, hydrogen is assumed to be present interstitially either as atoms or as protons. In a second model, a hydride phase is postulated and it is assumed that this phase deviates from stoichiometry because of hydrogen vacancies. According to this view, dissolved hydrogen has a helium-like configuration of electrons in much the same way as in the alkali hydrides.³

Theoretical calculations of the energy states of hydrogen in metals generally predict that hydrogen

should ionize to H^+ .^{4,5} Friedel⁵ has shown that an occupied bound level may or may not exist for solutes with an excess charge of unity dissolved in monovalent metals. The existence of a bound level depends on the relative magnitudes of the energies corresponding to the bottom of the conduction band and to the ionization potential of the solute element. The former can be estimated from the energy of sublimation, the first potential of ionization, and the Fermi energy of the metal. A detailed calculation for hydrogen in copper shows that a bound electron state probably does not exist, but rather that the proton is screened by Fermi electrons near the bottom of the conduction band.

(1) G. G. Libowitz in "Nonstoichiometric Compounds," *Advances in Chemistry Series*, American Chemical Society, 1963, p. 74.

(2) T. R. P. Gibb in ref. 1, p. 99.

(3) G. G. Libowitz and T. R. P. Gibb, *J. Phys. Chem.*, **60**, 510 (1956); T. R. P. Gibb and D. P. Schumacher, *ibid.*, **64**, 1407 (1960); T. R. P. Gibb, *J. Inorg. Nucl. Chem.*, **24**, 349 (1962).

(4) I. Isenberg, *Phys. Rev.*, **79**, 736 (1950).

(5) J. Friedel, *Phil. Mag.*, [7] **43**, 153 (1952); *Advan. Phys.*, **3**, 446 (1954).

Applying this same criterion to hydrogen in palladium (palladium behaves as if it were zerovalent), it is found that the bottom of the conduction band lies below the ionization potential of hydrogen; consequently, it is likely that no bound level exists and that screening of the proton charge is provided by a shift of the conduction electrons. However, this is only a tentative conclusion since the band structure of palladium is considerably more complex than that of the monovalent metals.

Although the experimental observations on the Pd-H system can be accounted for by either the solid solution or the hydride models, the solid-solution model appears to yield a more consistent description. The main experimental findings are that about 0.7 H/Pd is taken up at 30° and 1 atm. of H₂⁶; that a transition (the α - β transformation) takes place at 19 mm., the H/Pd ratio increasing from about 0.03 (α -phase) to about 0.55 (β -phase)⁶⁻⁸; and that a decrease of magnetic susceptibility accompanies hydrogen absorption, the susceptibility decreasing to essentially zero at 0.65 H/Pd.⁹

The H-Pd isotherms can be described by assuming either an attractive interaction between interstitial hydrogen¹⁰ or an attractive interaction between hydrogen vacancies.¹¹ In both cases, a transition pressure is predicted, provided the temperature is below a critical value related to the interaction energy.^{10,11} However, in order to secure agreement between the experimental isotherm and the one calculated on the basis of interaction between vacancies in a stoichiometric phase of hydride, it is necessary to assume that the maximum hydrogen to metal ratio is well below unity, *i.e.*, that a stoichiometric compound (PdH) is not attained.¹¹

The change in magnetic susceptibility can be explained by either model. If an interstitial solid solution is postulated, the change in susceptibility is attributed to the transfer of electrons from hydrogen to the palladium d-band which is expected to become full at about 0.6 H/Pd.¹² This result is in agreement with changes produced by monovalent metals (silver, gold) which form substitutional solid solutions with palladium.^{13,14} The hydride model also predicts a decrease in magnetic susceptibility as hydrogen is absorbed: each Pd-H bond removes an electron, presumably from the d-band; the redistribution of the remaining electrons is expected to decrease the number of unpaired electrons in the metal lattice, resulting in a decrease in susceptibility. However, it is not evident from this model that there should be any simple relation between the number of d-band holes in pure palladium and the saturation uptake of hydrogen. An

alternative hypothesis is that the increased separation of the palladium atoms in the β -phase (the lattice parameter increases by about 3.5%) prevents the formation of a collective d-band in the hydride.¹⁵

The mobility of hydrogen in palladium at low temperatures¹⁶ suggests strongly that hydrogen exists as screened protons rather than as firmly-bound hydride ions. This conclusion is supported by the observed electromigration of hydrogen to the negative end of a biased filament¹⁷ and by n.m.r. studies of PdH_{0.66}.¹⁸

One approach to the characterization of the Pd-H interactions is through the investigation of hydrogen absorption by palladium alloys. Silver-palladium alloys are particularly interesting in this respect because a complete series of solid solutions (f.c.c.) is formed with lattice parameters which deviate but little from a simple additive function of the lattice constants of the parent elements. Hydrogen absorption by Ag-Pd alloys has been studied previously,¹⁹⁻²² but the results are in many respects contradictory. One possible cause of discrepancies is the difficulty of attaining equilibrium at low temperatures, probably because the surface reactions (adsorption, dissociation) are slow. Although the kinetics of the surface processes are more favorable when hydrogen is absorbed from an aqueous electrolyte, even in this case the experimental results are at variance, indicating that an equilibrium state was not always achieved.

In the present study, the Ag-Pd alloy electrodes were "activated" by deposition of a thin coat of palladium black and were charged with hydrogen electrolytically

- (6) L. J. Gillespie and F. P. Hall, *J. Am. Chem. Soc.*, **48**, 1207 (1926); L. J. Gillespie and L. S. Galstaum, *ibid.*, **58**, 2565 (1936).
- (7) T. B. Flanagan and F. A. Lewis, *J. Chem. Phys.*, **29**, 1417 (1959).
- (8) T. B. Flanagan and F. A. Lewis, *Trans. Faraday Soc.*, **55**, 1409, 1417 (1959).
- (9) A. E. Oxley, *Proc. Roy. Soc. (London)*, **A101**, 264 (1922); B. Svensson, *Ann. Physik*, **18**, 299 (1933).
- (10) J. R. Lacher, *Proc. Roy. Soc. (London)*, **A161**, 525 (1937).
- (11) C. G. Libowitz, *J. Appl. Phys.*, **33**, 399 (1962).
- (12) N. F. Mott and H. Jones, "Metals and Alloys," Dover Publications, Inc., 1958, pp. 170-174, 198-200.
- (13) E. Vogt, *Ann. Physik*, **14**, 1 (1932).
- (14) B. Svensson, *ibid.*, **14**, 699 (1932).
- (15) A. Michel and M. Gallissot, *Compt. rend.*, **208**, 434 (1939); **221**, 551 (1945).
- (16) R. Ash and M. Barrer, *J. Phys. Chem. Solids*, **16**, 246 (1960).
- (17) A. Coehn and W. Specht, *Z. Physik*, **62**, 1 (1930); A. Coehn and H. Jurgens, *ibid.*, **71**, 179 (1931).
- (18) R. E. Norberg, *Phys. Rev.*, **86**, 745 (1952).
- (19) F. Kruger and G. Gehm, *Ann. Physik*, [5] **16**, 190 (1933).
- (20) G. Rosenhall, *ibid.*, [5] **24**, 297 (1935).
- (21) Z. L. Vert and I. P. Tverdovskii, *Zh. Fiz. Khim.*, **28**, 317 (1954).
- (22) F. A. Lewis and W. H. Schurter, *Naturwissenschaften*, **47**, 177 (1960).

using a potentiostatic technique. These procedures ensured equilibrium and yielded reproducible and consistent results. The two most distinct effects of alloying with silver are the decrease in the equilibrium pressure at which α - β transition occurs and the decrease of the hydrogen solubility at pressures above that corresponding to the α - β transformation. The present study was primarily concerned with these two effects.

Experimental

The preparation of the Ag-Pd alloys was described previously.²³ The alloy electrodes were either in the form of wire (0.0375-cm. diameter) or of plates (area ~ 0.25 cm.², thickness 0.0025–0.025 cm.) and were in all cases annealed at 950° for 30 min. The wire electrodes were spot-welded to platinum and then sealed in Pyrex holders. The wire-glass junction was coated with a small amount of a fluorocarbon (Kelf polymer wax) so that only the alloy was exposed to solution. These electrodes were used mainly in studies of the potential-time relation during absorption of molecular hydrogen dissolved in the electrolyte. The electrolyte cell and potential measuring circuit were described previously.²³

The electrolyte was a 2 *N* HClO₄ aqueous solution prepared from conductivity water (triply distilled, one stage from dilute KMnO₄) and 70% A.R. grade Mallinckrodt perchloric acid. Hydrogen was purified by diffusion through a Ag-Pd alloy at 425°. High purity argon was used for providing an inert atmosphere.

The amount of dissolved hydrogen at any potential was determined by potentiostatically discharging at 600 mv. (*vs.* H⁺-H₂ in the same solution) electrodes equilibrated with hydrogen at various potentials. The three-compartment cell with a Luggin capillary used in this work was similar to cells generally employed in studies of electrode kinetics.²⁴ A fast-rise Wenking potentiostat (rise time $\sim 10^{-6}$ sec.) was used.

The major experimental difficulty encountered was in controlling the potential at the high rates at which hydrogen ionizes at positive potentials. The iR drop between the tip of the Luggin-Haber capillary and the electrode surface, which is normally negligible, amounted here to a hundred or more millivolts depending on the particular current density. Since the potential drop sensed by the potentiostat includes this potential, a large iR contribution means that the potential across the electrode-electrolyte interface is less than the measured (or set) value.

The problem was circumvented by matching the potential drop from capillary to electrode by an

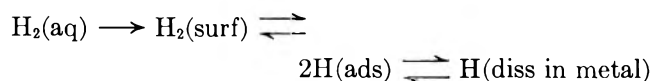
external resistance, R_2 , and feeding the potential developed across this resistance when a current I was flowing in the circuit back into the potentiostat. The feedback was through a 1:1 amplifier which inverted and isolated the potential from ground. Thus, by adding the output signal of the amplifier to the set potential on the potentiostat, the iR drop from capillary to electrode was automatically compensated and the potential across the electrode-electrolyte interface was maintained constant and independent of the current.

The resistance of the solution between capillary tip and electrode was determined by measuring the current-potential characteristics for hydrogen ion discharge on palladium at high current densities. It has been shown that the activation overpotential (*i.e.*, the potential drop across the metal-solution interface) for hydrogen discharge on palladium is constant at current densities above 10 ma./cm.².²⁴ The total cathodic overpotential measured on palladium (using a probe in the conventional way) consists of an iR term plus a constant activation term independent of the current. The current-potential curve on palladium is linear above 10 ma./cm.² and has a slope proportional to the resistance between probe and electrode surface. Generally, R ranged from 0.2 to 0.5 ohm depending on the distance between the electrode and the tip of the capillary probe.

In certain cases (see below), the electrode was coated with a thin layer of palladium black deposited electrolytically from a 2% PdCl₂ solution.

Results

Electrode Potentials. The potential of Ag-Pd alloys decreases, during absorption of molecular hydrogen dissolved in the electrolyte, in the way illustrated previously.²³ Just as with palladium,^{8,26} the potential can be related to the thermodynamic functions for hydrogen absorption by the alloy. Although these systems are not obviously at equilibrium since the potential is not invariant with time, the kinetics of absorption are such that the electrode potential reflects the activity of hydrogen dissolved in the metal. In the series of steps involved in absorption of molecular hydrogen

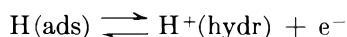


(23) S. D. Axelrod and A. C. Makrides, *J. Phys. Chem.*, **68**, 2154 (1964); A. C. Makrides, *J. Electrochem. Soc.*, **109**, 977 (1962).

(24) R. Clamroth and C. A. Knorr, *Z. Elektrochem.*, **57**, 399 (1953); C. A. Knorr, *ibid.*, **57**, 599 (1953).

(25) R. J. Ratchford and G. W. Castellan, *J. Phys. Chem.*, **62**, 1123 (1958).

and



all but the first step are essentially at equilibrium. Thus, over most of the potential-time curve, the activity of molecular hydrogen at the immediate vicinity of the electrode is essentially that corresponding to the amount of hydrogen dissolved in the metal. Therefore, the system (Ag-Pd)-H₂-H⁺-H₂(1 atm.)-Pt is equivalent to a hydrogen concentration cell with the pressure of hydrogen at the Ag-Pd electrode determined by the activity of hydrogen in the alloy.

These observations imply that hydrogen is absorbed as fast as it diffuses to the electrode surface. The maximum rate of diffusion depends on the rate of stirring, on the viscosity and density of the solution, and on the geometry of the electrode. It is not possible to fix precisely this maximum rate, but a reasonable estimate is about 2×10^{-5} cc./cm.²/sec. or 2×10^{-4} amp./cm.². The total time required to charge an electrode with hydrogen to a potential of zero vs. the H⁺-H₂ electrode under these conditions can be calculated from the dimensions of the specimen (~ 2 cm. \times 0.038-cm. diameter) and from the solubility of hydrogen in the alloy (8-15 coulombs). This time is, approximately, 15 hr., which is of the order found experimentally (10-20 hr.). The precise time depended on the flow conditions in the immediate vicinity of the electrode and these varied from electrode to electrode and from run to run. Because of these variations, the total time for the decrease of the potential to zero varied with any given electrode by as much as a factor of 5.

The potential arrest observed during absorption of molecular hydrogen from solution (Fig. 1) is reproducible and characteristic of each alloy. It corresponds to the α - β transformation, as was shown by the X-ray work reported previously.²³ Therefore, this arrest is entirely similar to the potential plateau observed during absorption of hydrogen by electrodes of pure palladium.

Perhaps the most interesting observation in connection with the time-potential measurements during hydrogen absorption is the existence on palladized Ag-Pd alloys of two potential arrests, one corresponding to the α - β transition for the alloy and the other to the α - β transition in the palladium coating (Fig. 1). The potentials at which these two transformations occur are the same, within experimental error, with the corresponding potentials for the unpalladized alloy and for bulk palladium. This implies that the alloy and the coating of palladium black deposited on its surface are in equilibrium with respect to hydrogen, *i.e.*, that

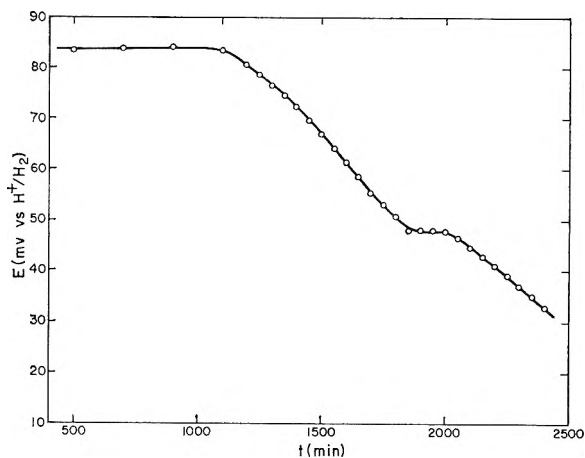


Figure 1. Potential-time trace for a palladized 20.0 atom % Ag-Pd alloy during absorption of hydrogen from a 2 *N* HClO₄ solution. Note the potential plateau at 84 mv. (85 mv. for untreated Ag-Pd alloys) and the second, short arrest at 48 mv. which coincides with the potential of the H-Pd plateau.

$\mu_{\text{H}}^{\text{Pd}} = \mu_{\text{H}}^{\text{Ag-Pd}}$, where μ_{H} is the chemical potential of hydrogen in the indicated phases. Ordinarily, the requirement for equilibrium at a metal to metal contact is $\bar{\mu}_e^{\text{A}} = \bar{\mu}_e^{\text{B}}$, where $\bar{\mu}_e$ is the electrochemical potential for electrons in the metal. If metal A is not exposed to the solution and metal B is, the electrode potential of B is entirely independent of the nature of A since $\bar{\mu}_e^{\text{A}}$ cancels out in the over-all expression for the potential. If both A and B are exposed to the solution, the potential is generally a mixed potential and falls somewhere between the reversible potentials of A and B. If both A and B are inert indicator electrodes, the potential is determined by some oxidation-reduction couple in solution, *e.g.*, H⁺-H₂, and is, of course, the same for both A and B.

The behavior of the Pd-(Ag-Pd) system does not correspond to any of these cases. This is to be expected if the additional condition for equilibrium given by $\mu_{\text{H}}^{\text{Pd}} = \mu_{\text{H}}^{\text{Ag-Pd}}$ is satisfied at the Pd-(Ag-Pd) interface. This condition can be written as

$$\bar{\mu}_{\text{H}^+}^{\text{Pd}} + \bar{\mu}_e^{\text{Pd}} = \bar{\mu}_{\text{H}^+}^{\text{Ag-Pd}} + \bar{\mu}_e^{\text{Ag-Pd}}$$

so that, taking into account the equilibrium for electrons, we have

$$\bar{\mu}_{\text{H}^+}^{\text{Pd}} = \bar{\mu}_{\text{H}^+}^{\text{Ag-Pd}}$$

Thus, the electrode system Pd-(Ag-Pd) is unusual in that equilibrium across the interface of two metals involves not only electrons but also hydrogen ions.

Potential-time curves for a series of Ag-Pd alloys (not palladized) were determined and the plateau potentials are given in Fig. 2. The plateau potential

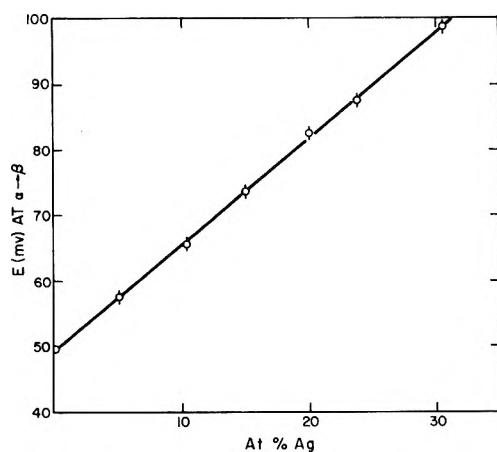


Figure 2. Plateau potentials as a function of silver content. The value shown for the 30.5 atom % silver alloy is the potential at which a change in the derivative of the potential-time curve is observed.

becomes increasingly positive as the silver content is increased, the relation between potential and silver content being linear. At the same time, the duration of the plateau potential decreases as the silver content increases. At 30 atom % silver, the potential plateau has virtually disappeared; instead, a change in the rate at which the potential decreases with time occurs at a reproducible value of 99 ± 3 mv. The potential of a 40 atom % silver alloy decreased continuously from positive potentials (>100 mv.) to zero without any arrest.

The Solubility of Hydrogen in Ag-Pd Alloys. The amount of dissolved hydrogen was determined for 10.4, 23.8, and 30.5 atom % Ag-Pd alloys at a series of potentials between zero and 120 mv. vs. $H^- - H_2$ in the same solution. In each case, the palladized alloy was charged potentiostatically at 0 mv. vs. $H^+ - H_2$ until the current dropped to zero. The potential was then adjusted to a desired value within the range given above and the current was followed with time until it again decayed to zero; the electrode was then discharged at 600 mv. vs. $H^+ - H_2$. The current-time curves were integrated to obtain the total amount of hydrogen oxidized between zero and the selected potential, and between the selected potential and 600 mv. The sum of these two integrals was constant and was equal to the value obtained by discharging directly, at 600 mv., electrodes which had been charged with hydrogen at 0 mv. vs. $H^+ - H_2$. The results are presented in Fig. 3 and in Table I.

Figure 3 gives essentially isotherms for the solution of hydrogen in these alloys, the potential scale corresponding to a logarithmic scale for the pressure of

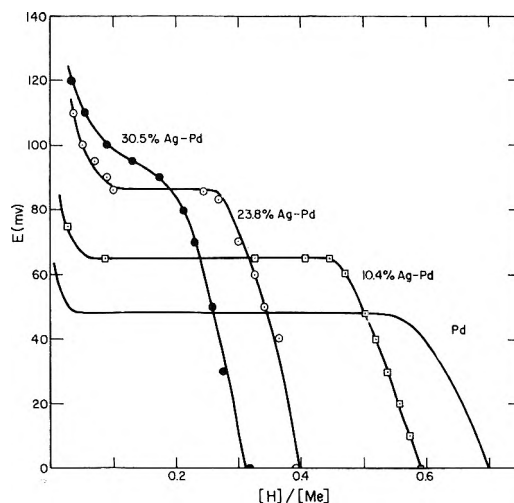


Figure 3. The amount of dissolved hydrogen, as determined from potentiostatic discharge at 600 mv., at various potentials for a series of Ag-Pd alloys. These curves are equivalent to isotherms with $E = 0.030 \log p$, where $p = 1$ atm. hydrogen (see text).

Table I: Hydrogen Solubility at $P_{H_2} = 1$ atm. at 30°

Atom % silver	H/Me	H/Me ^a	H/Pd
0	0.70	0.69	0.70
10	...	0.57	0.63
10.4	0.582	...	0.64
20.0	0.49	0.45	0.61
23.8	0.384	...	0.50
26	...	0.36	0.49
30.5	0.340	...	0.49
40.0	...	0.24	0.40
50	...	0.15	0.30

^a Lewis and Schurter, ref. 22.

hydrogen ($E = -RT/2F \ln P_{H_2}$). In general, the isotherms for the Ag-Pd alloys resemble those of palladium with two modifications: the α - β transformation, indicated by the horizontal portion of the isotherm, occurs at progressively more positive potentials (lower equivalent hydrogen pressures), while the hydrogen solubility (at an equivalent $P_{H_2} = 1$ atm.) decreases uniformly as the silver content increases.

Temperature coefficients at the α - β transformation were obtained from the temperature dependence of the potential plateau. Heats calculated from these results are plotted as a function of silver content in Fig. 4.

Discussion

The isotherms presented in Fig. 3 and the potentials corresponding to the α - β transformation are in general

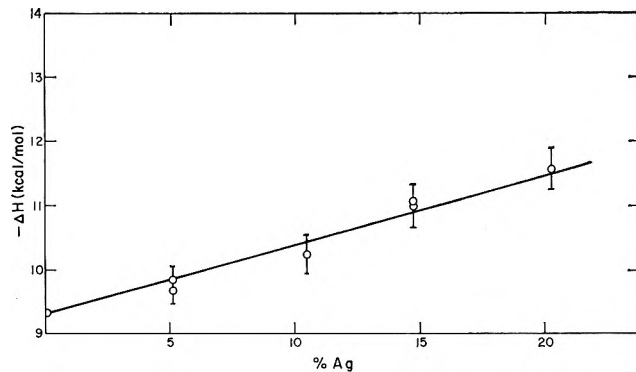


Figure 4. Energies of solution, per mole of hydrogen, calculated from the temperature coefficient of the plateau potential, as a function of silver content.

agreement with other results reported for this system.¹⁹⁻²² There are, however, some differences, particularly in relation to the α - β transformation observed with the alloys. Vert and Tverdovskii²¹ determined isotherms for the absorption of hydrogen by Ag-Pd alloys from galvanostatic charging curves. They interpreted their results as showing an α - β transformation up to about 50 atom % silver. The present study and the X-ray results reported previously²³ show that the α - β transition does not occur at or above 30 atom % Ag. Lewis and Schurter²² obtained time-potential curves for a series of alloys up to 50 atom % Ag. They found that the potential plateau becomes more positive with increasing silver content up to about 26 atom % silver, and subsequently decreases rapidly (3 mv. at 40 atom % silver). Our results show that the potential plateau disappears at about 30 atom % silver; it is certainly not observed at 40 atom % silver. Therefore, it is likely that the potential arrests observed by Lewis and Schurter²² at a few (3-6 mv.) millivolts for the 30 and 40 atom % silver alloys are due to some other cause peculiar to their experimental system and not to an α - β transformation.

The amount of dissolved hydrogen determined by potentiostatic discharge at $P_{H_2} = 1$ atm. ($E = 0.000$ v.) is in good agreement with the results of Lewis and Schurter,²² who measured the solubility by vacuum degassing of electrodes which had attained a potential of zero volts vs. the H_2 -Pt electrode. However, these solubilities are uniformly higher than the values determined by Vert and Tverdovskii²¹ by galvanostatic charging. A possible cause for the lower values reported in ref. 21 is failure to attain equilibrium at any given potential during galvanostatic charging.

The Absorption Isotherms. The Pd-H isotherms can be described either by assuming an attractive inter-

action between interstitial hydrogen¹⁰ or an attractive interaction (clustering) between vacancies (see above).¹¹ The equations derived from these models are essentially the same, but the interpretation of the terms differs

Hydrogen interaction

$$\ln p = \ln p_0 + 2 \ln \frac{\theta}{1 - \theta} + \frac{z_i E_{ii}}{kT} (1 - 2\theta) \quad (1)$$

Vacancy interaction

$$\ln p = \ln p_0 + 2 \ln \frac{n}{s - n} + \frac{z_v E_{vv}}{skT} (s - 2n) \quad (2)$$

In eq. 1, p_0 is the pressure of the transition, θ is the fraction of available sites occupied by hydrogen, z_i is the number of nearest neighbors for each interstitial hydrogen, and E_{ii} is the interaction energy for each pair of interstitials ($E_{ii} > 0$ for attractive interaction). In eq. 2, s is the stoichiometric hydrogen to metal ratio, n is the H/M ratio at p , and E_{vv} is the energy of interaction of a pair of hydrogen vacancies. In the case of the Pd-H system, eq. 2 does not fit the experimental results if a stoichiometric Pd-H is assumed; a reasonably good fit (however, see below) is obtained only if s is set equal to the maximum solubility observed experimentally ($s = H/Pd = 0.70$ at 25° and 0.61 at 290°). With this assumption, eq. 2 is reduced to exactly the same equation as (1). In the following discussion, the terminology of eq. 1 is used.

We adopt as a working hypothesis the suggestion¹² that hydrogen dissolved in palladium exists essentially as protons which are screened by Fermi electrons. This hypothesis explains in a simple way most of the known facts about the system and is in accord with the admittedly approximate theoretical conclusions about the state of dissolved hydrogen.

The interactions between dissolved protons which give rise to the flat portion of the isotherm are probably a result of interactions between the electrons which provide screening. It is known^{26,27} that there occur, around a solute (impurity) atom, changes of electronic density which oscillate with distance and which are fairly long range. These long-range fluctuations of electronic charge are responsible, for example, for the magnetic coupling of nuclei *via* the conduction electrons²⁸ and for changes of the Knight shift caused by solute atoms.^{26,27} It is suggested here that an interaction exists between the "tails" of the electron density

(26) T. J. Rowland, *Phys. Rev.*, **119**, 900 (1960); **125**, 459 (1962).

(27) A. Blandin, E. Daniel, and J. Friedel, *Phil. Mag.*, **4**, 180 (1959); A. Blandin and E. Daniel, *J. Phys. Chem. Solids*, **10**, 126 (1959).

(28) N. Bloembergen and T. J. Rowland, *Phys. Rev.*, **97**, 1679 (1955).

distributions around dissolved protons, which is attractive in character.

Hydrogen in the palladium metal lattice probably occupies interstitial octahedral positions to form a rock-salt type structure.²⁹ The distance between the centers of hydrogen atoms in such a structure is about 2.8 Å. and the number of nearest neighbors is 12. The attractive interaction postulated here involves relatively small energies, *i.e.*, about 0.4 kcal. per hydrogen pair. Of the total energy of solution (~ 57 kcal./mole hydrogen), the contribution of a hydrogen interaction with the lattice is by far the largest term, and is about 55 kcal./mole hydrogen. This energy corresponds to introducing a hydrogen ion interstitially in the palladium lattice and an electron in the conduction band. In screening by Fermi electrons, the solute atom merely displaces states in the zone of the conduction band without creating new ones. Thus, one more state is occupied for every attracted electronic charge. Therefore, the solubility is expected to correspond approximately to the number of available states with low-lying energies and these, in the case of palladium, are essentially d-states amounting to about 0.6 per palladium atom.^{12,30}

There are two observations which we might make in connection with this model. First, although the model predicts a "limiting" solubility, it is clear that a sharp cut-off point is not expected but rather a gradual decrease in the amount of hydrogen dissolved per unit increment of pressure, once a composition of approximately 0.6 H/Pd is reached. Second, the heat of solution, E_i , is probably not constant but actually decreases with the hydrogen concentration. This change is unrelated to the solute-solute interactions given by E_{ii} and is due to the distribution of the available empty states in the d-band over an energy range of approximately 0.1–0.15 e.v.³⁰

These two effects are probably responsible for the deviation of the isotherms from what is predicted by eq. 1. According to this equation, the isotherms should be symmetrical about $\theta = 0.5$.¹³ In fact (see Fig. 5), the Pd-H isotherms are not symmetrical about this point, the solubility at high pressures decreasing considerably more gradually than expected from eq. 1. It may be argued that this deviation from the predicted isotherm arises from the approximation made in deriving eq. 1, specifically, from the assumption of random distribution of hydrogen (Bragg-Williams approximation³¹). However, the next approximation (the quasi-chemical approximation) also predicts isotherms which are symmetrical about $\theta = 0.5$.³¹ Other corrections^{32,33} to the basic eq. 1, *e.g.*, Rushbrooke's treatment³² which includes a dependence of the internal

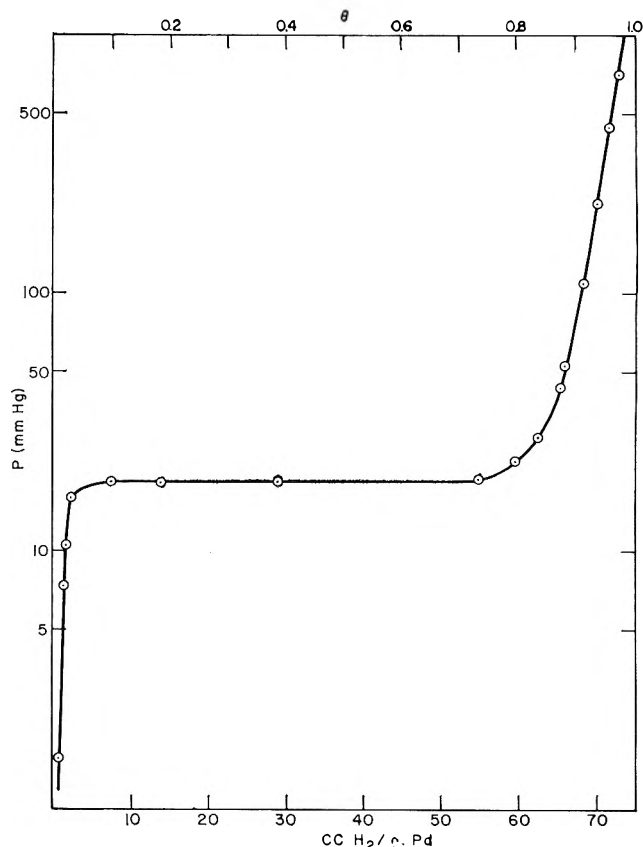


Figure 5. The H-Pd isotherm at 30.0° from data of Gillespie and Hall.⁶ The midpoint of the transition falls considerably below $\theta = 0.5$ so that the isotherm is not symmetrical. Instead, there is an extended "tail" on the high pressure side indicating that the solubility approaches a limiting value more slowly than predicted by eq. 1. The isotherms for the Ag-Pd alloys (see Fig. 3) have the same characteristic.

partition function in the absorbed state on θ , yield isotherms which are symmetrical about $\theta > 0.5$, whereas the midpoint of the transition for the hydrogen isotherms occurs at $\theta < 0.5$. Thus, it is likely that the basic assumptions on which eq. 1 is based, namely, a fixed number of available sites and a constant E_i , are only approximately true for the Pd-H system.

The Ag-Pd-H Isotherms. There are three basic changes in the absorption isotherms produced by alloy-

(29) J. E. Worsham, M. K. Wilkinson, and C. G. Shull, *J. Phys. Chem. Solids*, **3**, 303 (1957).

(30) F. E. Hoare, J. C. Matthews, and J. C. Walling, *Proc. Roy. Soc. (London)*, **A216**, 502 (1953).

(31) R. Fowler and E. A. Guggenheim, "Statistical Thermodynamics," Cambridge University Press, London, 1960, pp. 429-443, 558-563.

(32) G. H. Rushbrooke, *Proc. Cambridge Phil. Soc.*, **34**, 424 (1938).

(33) B. B. Fisher and W. G. McMillan, *J. Chem. Phys.*, **28**, 555 (1958).

ing palladium with silver. First, the transition pressure is shifted to smaller values (Fig. 3) and, at sufficiently high silver content (≥ 30 atom %), the transition no longer occurs. Second, the heat of solution of hydrogen, E_i , in the alloy increases with silver content, the increase being approximately proportional to X_{Ag} . Third, the solubility at $P_{H_2} = 1$ atm. decreases approximately linearly with silver content (see Fig. 6).

The isotherms with the Ag-Pd alloys show that p_0 decreases with silver content according to

$$-\log p_0 = \frac{2F}{2.30RT}E = 1.63 + 6.0X_{Ag} \quad (3)$$

where X_{Ag} is the atom fraction of silver in the uncharged alloy. The pressure for this transformation is related to the energy of absorption by

$$\log p_0 = \log K(T) -$$

$$\frac{2}{2.30kT} \left[E_i - \frac{D_0}{2} + \frac{z_i}{2} E_{ii} \right] \quad (4)$$

where $\ln K(T)$ varies only slowly with temperature. Consequently, to a very good approximation

$$\frac{\partial \log p_0}{\partial(1/T)} = \frac{-2}{2.30k} \left[E_i - \frac{D_0}{2} + \frac{z_i}{2} E_{ii} \right] \quad (5)$$

where E_i is the heat of solution of hydrogen at an interstitial site where all the neighboring sites are unoccupied and D_0 is the heat of dissociation of hydrogen. Figure 4 shows that the right-hand side of eq. 5 increases from about 4.8 kcal./g.-atom of hydrogen (9.5 kcal./mole of H_2) for pure palladium to 5.8 kcal./g. atom of hydrogen for the 20.4 atom % silver alloy.

The solubility of hydrogen in the alloys at $P_{H_2} = 1$ atm. ($E = 0$) decreases as silver is introduced in the lattice. Table I shows that the H/Pd ratio also decreases from about 0.70 for pure palladium to 0.30 for the 50 atom % silver alloy. It is clear that silver produces two distinct effects: an increase of solubility at low pressures but, also, a decrease of the limiting solubility (here approximated by the solubility at $P_{H_2} = 1$ atm.). These effects probably have a different origin; the first is likely a result of an interaction between an interstitial hydrogen and a silver ion, while the second is probably caused by changes of the electronic structure of the solid which accompany the introduction of silver atoms in the lattice.

The increase of the right-hand side of eq. 5 with silver content may be due to a change of either E_i or of E_{ii} . The isotherms suggest that E_{ii} remains unaltered as silver is introduced in the lattice. The value of θ at the end of the transition can be used to estimate $z_i E_{ii}$ from eq. 1. The calculation is imprecise and the

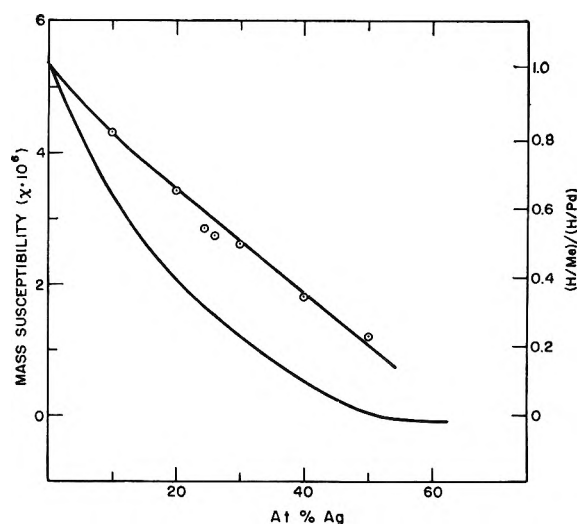


Figure 6. The mass susceptibility³⁰ and the hydrogen solubility as a function of silver content. The solubility in the alloys is given in terms of the hydrogen solubility in palladium.

estimate is not very good as judged from results with pure palladium. This is probably because the isotherms do not follow eq. 1 rigorously for the reasons given above. However, this calculation still shows that E_{ii} for the alloys is probably the same as for pure palladium. Thus, the increase of the r.h.s. of eq. 5 with silver content is probably due to an increase in the energy of solution of hydrogen at an isolated interstitial site and not an increase of the energy of interaction between dissolved hydrogen.

The above discussion suggests that the shift of p_0 to smaller values (and the increase of E_i) is due to an attractive interaction between silver and hydrogen. This interaction is probably similar to that between interstitial hydrogens, *viz.*, it arises from exchange interactions between the electrons which provide screening for protons and for silver ions. It is not possible to state in advance whether this effect should be attractive or repulsive. In view of its small magnitude ($\sim 2-3$ kcal. or 0.1 e.v./hydrogen), it is doubtful whether even a detailed calculation would show whether an attractive or repulsive effect is to be expected.

If such an attractive interaction exists, and if it is treated as an additive pair interaction, then it is clear that there must be differences in the heat of absorption of hydrogen at different sites in Ag-Pd alloys, *i.e.*, the heat will be larger for sites with a greater number of nearest neighbor silver atoms. Since the Ag-Pd solid solutions are random, the various sites will be randomly distributed. It is not immediately obvious that the adsorption isotherm for such a system will

show an α - β transition as it does for pure palladium. A detailed treatment of this problem will be presented elsewhere; suffice it to state here that, if the Ag-H interaction energy is small, the main features of the isotherm are not altered and an α - β transition is still expected in agreement with the experimental observations for the palladium-rich alloys. The pressure, p_0 , of the transition is expected to decrease, as is found experimentally. Therefore, it is permissible to assume that the addition of silver essentially increases E_i and that the shift of the transition to lower pressures is due to the increase of E_i .

If the above assumptions are correct, the shift of p_0 with X_{Ag} should correspond to the increase of the heat of solution. Using the experimental data of Fig. 4 and relations 4 and 5, we calculate at 303°K.

$$\frac{\partial \log p_0}{\partial X_{Ag}} = -7.5 \quad (6)$$

which is in fair agreement with eq. 3.

The solubility of hydrogen at $P_{H_2} = 1$ atm. ($\gg p_0$) decreases linearly with silver content (Fig. 6). Using the model discussed above for absorption by pure palladium, the decrease of solubility is attributed to a decrease in the number of unoccupied d-states when silver is introduced in the lattice. The number of d-band holes may be taken to be proportional to the magnetic susceptibility of the alloys³⁰ according to the well-known account given by Mott and Jones.¹² A comparison of the decrease in magnetic susceptibility and hydrogen solubility is given in Fig. 6. Although both quantities decrease more or less linearly with silver content, the magnetic susceptibility drops much faster than the solubility. Furthermore, the susceptibility drops to zero at somewhat lower Ag content (~ 50 atom % silver) than the extrapolated value for zero hydrogen solubility (~ 65 atom % silver).

An effect, which is not included in the above description and which may account for these discrepancies, is the attractive interaction between silver and hydrogen which increases the energy of solution, and hence the solubility of hydrogen. This interaction in effect makes it possible to utilize electronic energy states lying above the d-states and still maintain a net negative free energy of solution for hydrogen.

It should be pointed out that attempts to describe the H-Ag-Pd system in terms of a compound between palladium and hydrogen have been made. The main difficulty in such analysis is the continuously decreasing H/Pd ratio (Table I and ref. 21) which changes from about 0.7 for pure palladium to about 0.15 at 65 atom % silver. A suggestion that the H/Pd ratio remains constant if only the amount involved in the

α - β transition is considered²¹ has no theoretical justification and cannot be correct since the α - β transformation itself does not exist above 30 atom % Ag.

The decrease of the maximum solubility, irrespective of its origin, accounts for the suppression of the α - β transformation at about 30 atom % silver. The simplest way of showing this is to refer to the derivation of eq. 1 or 2 (see ref. 11 and 31). If it is assumed that there are N_s sites available in pure palladium and each site has z_i neighbors, then the number of pairs of neighboring occupied sites, assuming a completely random distribution of adsorbed hydrogen (Bragg-Williams approximation), is given by

$$\bar{N}_{HH} = \frac{1}{2} z_i N_H^2 / N_s \quad (7)$$

This formula is derived (ref. 31, p. 431) by assuming that each site has a probability N_A/N_s of being occupied. In the case of the alloys, the maximum solubility ($P_{H_2} \gg p_0$) is less than N_s , the absorption being reduced because E_i decreases sharply when the d-band holes are all filled. In these cases, therefore, the probability of a site being occupied is $(N_A/N_s)(S(\text{alloy})/S(\text{Pd}))$, where S is the maximum solubility of hydrogen. Using this result, we find that the relation between p and θ is modified for the alloys to read

$$\ln p = \text{constant} + 2 \ln \frac{\theta}{1 - \theta} + \frac{2}{kT} (1 - 2\theta) z_i E_{ii} \frac{S(\text{alloy})}{S(\text{Pd})} \quad (8)$$

where θ is now calculated with reference to pure palladium. According to eq. 8, there are two values of θ for each value of p over a range of θ -values, provided

$$z_i E_{ii} \frac{S(\text{alloy})}{S(\text{Pd})} > 4kT \quad (9)$$

For pure palladium, $z_i E_{ii}$ can be calculated from the critical temperature as 4.6 kcal. (ref. 31) or from a detailed analysis of the isotherms as a 4.2 kcal. (ref. 11). Taking a mean of about 4.4 kcal., we find that at $(S(\text{alloy})/S(\text{Pd})) = 0.5$ the inequality (9) is no longer satisfied at room temperature. Consequently, the isotherm is expected to be continuous and a two-phase region should not be observed. The above ratio of solubilities corresponds to the 30 atom % silver alloy (see Fig. 3) for which an α - β transition is, in fact, not observed.

In summary, the H-Ag-Pd system can be described in terms of an extension of the model which has been suggested for the H-Pd system. The main effects of

silver are a decrease of the hydrogen pressure corresponding to the α - β transition (and an eventual elimination of this transition at about 30 atom % silver) and a decrease of the solubility at $P_{H_2} = 1$ atm. The first effect can be described by an attractive interaction

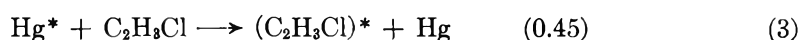
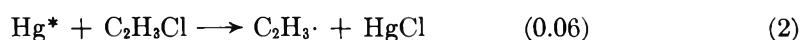
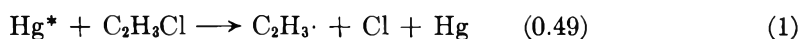
between silver and hydrogen, which is similar to that between dissolved hydrogens. The second can be attributed to a decrease in the unoccupied electron states in the d-band of the alloy resulting from the random substitution of silver for palladium.

The Reaction of Hg 6(³P₁) Atoms with Vinyl Chloride

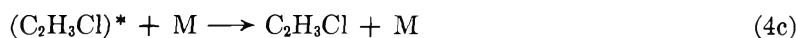
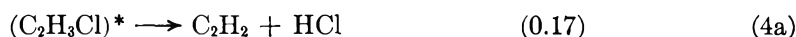
by M. G. Bellas, J. K. S. Wan, W. F. Allen, O. P. Strausz, and H. E. Gunning

Department of Chemistry, University of Alberta, Edmonton, Alberta, Canada (Received February 7, 1964)

The reaction has been studied both by ²⁰²Hg-monoisotopic and natural mercury sensitization techniques. Principal primary products are 1,3-butadiene, acetylene, hydrogen chloride, calomel, and polymer. Above 200° the three isomeric chlorobutadienes appear. Three primary steps have been established



followed by



where the numbers in parentheses give the quantum yield values at zero pressure. It is shown that quenching at the chlorine atom leads largely to (1) and (2) and quenching at the π -bond to (3). The heavy chlorine atom promotes intersystem crossing or more probably phosphorescence in the excited triplet molecule, $\text{C}_2\text{H}_3\text{Cl}^*$, thereby shortening its lifetime as compared to the corresponding C_2H_4 species. Butadiene and chlorobutadienes arise from displacement-type reactions of $\text{C}_2\text{H}_3\cdot$ and $\text{C}_2\text{H}_2\text{Cl}\cdot$ radicals, respectively, with $\text{C}_2\text{H}_3\text{Cl}$. Radical-radical reactions are unimportant even at 10 mm. substrate pressure. Above 200° chlorine atoms abstract hydrogen atoms from $\text{C}_2\text{H}_3\text{Cl}$ initiating a chain process. An approximate value of 16.0 kcal./mole was found for the activation energy of this abstraction reaction.

Introduction

The mercury-photosensitized reactions of the simple olefins have been studied extensively, including ethylene^{1,2} various deuterated ethylenes,^{1,3} propylene,¹ the butenes,¹ 1-pentene,¹ cyclopentene,⁴ cyclohexene,⁵ allene,¹ butadienes,¹ allyl,⁶ and cyclooctatetraene.¹ In each case the primary step appears to yield vibrationally-excited triplet biradicals which undergo collectively a variety of reactions, including unimolecular isomerization, molecular and free-radical elimination, and collisional deactivation to the ground electronic state. Tetrafluoroethylene⁷ excepted, only one study has been reported on the reactions of halogen-substituted olefins. Koizumi and Nakatsuka,⁸ from an in-

vestigation of the photopolymerization of vinyl chloride, concluded that the reaction was photosensitized by mercury atoms, the effective light being 1849 Å.

(1) R. J. Cvetanović in "Recent Advances in Reaction Kinetics," G. Porter, Ed., in press.

(2) J. P. Chesick, *J. Am. Chem. Soc.*, **85**, 3718 (1963).

(3) D. W. Setser, B. S. Rabinovitch, and D. W. Placzek, *ibid.*, **85**, 862 (1963).

(4) W. A. Gibbons, W. F. Allen, and H. E. Gunning, *Can. J. Chem.*, **40**, 568 (1962).

(5) G. DeMaré and H. E. Gunning, 46th Chemical Institute of Canada Conference, Toronto, June, 1963.

(6) R. Srinivasan, *J. Phys. Chem.*, **67**, 1367 (1963).

(7) B. Atkinson, *J. Chem. Soc.*, 2684 (1952).

(8) M. Koizumi and K. Nakatsuka, *J. Chem. Soc. Japan*, **72**, 431 (1951); **75**, 205 (1954).

Now halogen atom substitution should alter the important features of the olefinic reaction in a number of ways, and the investigation of such systems could provide valuable information on the chemistry of triplet states and the mechanism of energy transfer processes. The details of the vinyl chloride study follow.

Experimental

^{202}Hg -Monoisotopic Sensitization. The technique of monoisotopic photosensitization wherein a specific isotopic species (^1Hg) is uniquely excited in natural mercury vapor (^NHg) to the 3P_1 state for reaction with the substrate has recently been detailed in a review article from this laboratory.⁹ The experiments were performed in a single-pass system, using a helical quartz reaction cell, wound from tubing 15 mm. in i.d. and 60 cm. in length. The light source was a quartz electrodeless discharge tube containing mercury, 98.3 atom % in ^{202}Hg , axially mounted in the spiral cell with the discharge maintained by a 2450-Mc. oscillator (Baird Associates). The lamp temperature was kept constant at 18°. The experimental orientations of the cell-lamp-microwave antenna assembly and that of the rotating sector used here (*vide infra*) are shown in Fig. 5 and 6 of ref. 9.

Further experimental details have been given elsewhere.¹⁰ Lamp intensities were measured by propane actinometry.^{11,12}

Natural Mercury Sensitization. The reaction was investigated in a circulating system (300 cc. in volume) comprised of a cylindrical quartz reaction cell, 5 cm. in diameter and 6 cm. in length, a gas circulating pump, a stripper, and a mercury saturator. The gas circulating pump was specially constructed to have essentially no "dead" volume. The rotor blades were of stainless steel with the rotor mounted on Rulon bearings. Coupling for the external magnetic drive was provided by a glass-encased iron bar affixed to the top of the rotor. The stripper was a simple straight-tube condenser through which water, thermostated at $20.5 \pm 0.1^\circ$, was circulated. For the saturator a U-tube was used containing ca. 1 cc. of mercury maintained at $25.1 \pm 0.1^\circ$ by a constant temperature bath. In each cycle the gases were driven sequentially to the stripper, the saturator, the reaction cell, and back to the pump. Thereby a constant mercury vapor pressure in the cell was maintained regardless of the cell temperature. In the high temperature runs the stripper served to cool the hot gases emerging from the reaction cell and thus prevented a rise in the surface temperature of the mercury in the saturator. Tests showed that the efficient circulation provided by the

pump effected a complete replenishment of mercury vapor in the reaction zone in spite of its consumption in the reaction through calomel formation.

The cell was housed in a large aluminum block furnace, the temperature of which did not fluctuate at 300° by more than $\pm 1^\circ$.

For the light source a Hanovia SC-2537 mercury resonance lamp, thermostated at 25.5° , was used. A Vycor 7910 filter was employed to remove radiation below 2000 Å.

The absorbed light intensity at 2537 Å. was determined with propane as actinometer^{11,12} (taking ϕ_H , for this reaction as 0.50 at room temperature) as well as with *n*-butane-nitrous oxide mixtures,¹³ assuming unit efficiency for nitrogen formation. The two determinations showed excellent agreement.

The gases used were obtained from Matheson of Canada. The vinyl chloride (99.9% min.) was further purified by low temperature distillation. Gas chromatography (g.c.) on two different columns, a 6.5-m. dimethyl sulfolane column (I) and a 8.3-m. dibutyl maleate column, both operated at 0° revealed no detectable impurities. Repeated low temperature distillations of the sulfur hexafluoride (98.0% min.) resulted in 99.5% purity as indicated by mass spectrometric analysis. Nitric oxide (99.0% min.) was triply distilled through liquid oxygen prior to use. Mass spectrometric analysis showed it to be at least 99.9% pure.

The gases were circulated for 5 min. prior to irradiation to allow for proper equilibration. At the end of each run the fraction, noncondensable at -159.5° , was collected and measured in a gas buret and subsequently analyzed by g.c. on column I. Ethylene and acetylene were easily separated and directly measured. What remained, *i.e.*, the difference between the total fraction and the amount of $\text{C}_2\text{H}_4 + \text{C}_2\text{H}_2$ as determined from peak areas, was shown to be HCl in separate experiments by reaction with AgNO_3 . The material condensable at -159.5° was divided into two parts, one of which was analyzed on column I, and consisted of a trace of acetylene, the 1,3-butadiene

(9) H. E. Gunning and O. P. Strausz in "Advances in Photochemistry," Vol. I, W. A. Noyes, Jr., G. S. Hammond, and J. N. Pitts, Jr., Ed., Interscience Publishers, New York, N. Y., 1963.

(10) J. K. S. Wan, O. P. Strausz, W. F. Allen, and H. E. Gunning, to be published.

(11) S. Bywater and E. W. R. Steacie, *J. Chem. Phys.*, **19**, 319 (1951).

(12) Y. Rousseau and H. E. Gunning, unpublished results.

(13) R. J. Cvetanović, *J. Chem. Phys.*, **23**, 1208 (1955); R. J. Cvetanović, W. E. Falconer, and K. R. Jennings, *ibid.*, **35**, 1225 (1961); Y. Rousseau and H. E. Gunning, *Can. J. Chem.*, **41**, 465 (1963).

product, and unreacted vinyl chloride. The remainder was also analyzed on column I in the low temperature runs ($<200^\circ$), but on a 1.8-m. dimethyl sulfolane column in the high temperature runs ($>200^\circ$). The three isomeric monochlorobutadienes, *i.e.*, 2-chloro-1,3-butadiene, *cis*-1-chloro-1,3-butadiene, and *trans*-1-chloro-1,3-butadiene, could be resolved on the 1.8-m. column. The sensitivities for all the products (except for *cis*- and *trans*-1-chloro-1,3-butadiene which were assumed to have the same relative response as the 2-chloro-1,3-butadiene) were obtained from calibration curves of sample size *vs.* peak area. Product identifications were carried out by mass spectrometric analysis of products isolated from the chromatographic effluent. The predominant chlorobutadiene product was concluded to be the 2-chloro isomer, from the mass spectrometric cracking pattern, as well as from the fact that the predominant g.c. peak was separated by almost 4 min. in retention time from the two minor ones, which exhibited partial overlap, suggesting the *cis* and *trans* isomers.

Results

I. ^{202}Hg -Monoisotopic Photosensitization. Preliminary experiments carried out in a static system showed the major reaction to be the polymerization of vinyl chloride. This was indicated by the formation of a yellowish solid deposit, accompanied by a gradual drop in pressure, which increased to a limiting value with increasing substrate pressure. The pressure drop was measured at 25° at constant irradiation times of 120 min. but using different initial pressures (P_i). The following values were found: 0.2 mm. at $P_i = 5.0$ mm., 0.8 mm. at $P_i = 17.5$ mm., 2.5 mm. at $P_i = 45$ mm., and 3.0 mm. at $P_i = 71, 98,$ and 102 mm. The polymer contained embedded calomel which was extracted by solution in EDTA. From this solution the mercury was recovered and isotopically analyzed.

A study of the isotopic composition of the mercury in the calomel product was made as a function of flow rate and substrate pressure in the flow system, using the ^{202}Hg electrodeless discharge lamp. The abundance of ^{202}Hg was found to rise rapidly with increasing flow rates of vinyl chloride, maximizing at *ca.* 44% at flow rates exceeding 3.5 mM/min. The effect of substrate pressure manifested itself in a flat maximum of *ca.* 44% abundance at $P \simeq 14$ mm. The isotopes other than ^{202}Hg were present in proportion to their natural abundances, even at the highest pressure used, 78 mm., indicating the absence of any complications associated with pressure broadening of the hyperfine absorption contours or source broadening of

the emission line. At a $\text{C}_2\text{H}_3\text{Cl}$ flow of 4.5 mM/min. $\phi_{(\text{HgCl})}$ was 0.15 and did not vary in the pressure range 7–78 mm.

Steady illumination does not necessarily provide a true picture of isotopic mercury distribution in the mercury-containing product in monoisotopic sensitization. Even under fast flow conditions a localized isotopic mercury depletion may occur. The use of a rotating sector eliminates this difficulty.⁹

Both the quantum yield of calomel formation and the abundance of ^{202}Hg increased under sector conditions as compared to the values obtained under steady illumination. The highest abundance of ^{202}Hg in the calomel product under optimum conditions (at $P = 20$ mm., $\text{C}_2\text{H}_3\text{Cl}$ flows over 3.0 mM/min., sector slit width of 2 mm. at 300 r.p.m.) was found to be 51.8%, while $\phi_{(\text{HgCl})}$ here was 0.19 in the pressure range 4–50 mm. With these data the quantum yield for $^{202}\text{HgCl}$ formation may be computed

$$\phi_{(^{202}\text{HgCl})} = 0.19 \times \frac{(51.8 - 29.8)}{(100 - 29.8)} =$$

$$0.06 \text{ mole/einstein;}$$

where 29.8 = mole % of ^{202}Hg in $^{\text{N}}\text{Hg}$.

II. Photosensitization by $^{\text{N}}\text{Hg}(^3P_1)$ Atoms at Low Temperature. The only products found at temperatures from 40 to 200° were polymer, 1,3-butadiene, calomel, acetylene, hydrogen chloride, and ethylene. Hydrogen, trichloroethanes, and dichlorobutenes were specifically sought and found absent.

Owing to the volatility of calomel at elevated temperatures, its deposition in the reaction cell could be conveniently prevented at 120° and above simply by efficient circulation of the reactant gas. Moreover, since preliminary studies had shown the reaction to have no significant temperature coefficient between 40 and 120° , detailed studies were performed only at and above temperatures of 120° .

Plots of quantum yields of product formation *vs.* pressure at 120° appear in Fig. 1. The yield of butadiene rises to a maximum at 75 mm. and then decreases slowly with further increase in pressure, whereas acetylene exhibits a much less pronounced pressure dependence. Hydrogen chloride and ethylene, both less important products, decrease rapidly with pressure.

The material balance, disregarding polymer formation, is poor. The relations $\phi_{(\text{HgCl})} = 2\phi_{(\text{C}_2\text{H}_4)} + \phi_{(\text{C}_2\text{H}_2)}$ and $\phi_{(\text{HCl})} = \phi_{(\text{C}_2\text{H}_2)} - \phi_{(\text{C}_2\text{H}_4)}$ should hold. Plots of calculated values for these quantities *vs.* substrate pressure are given in Fig. 2. The points represent measured values. The chlorine deficiency thus disclosed is attributable to the scavenging of

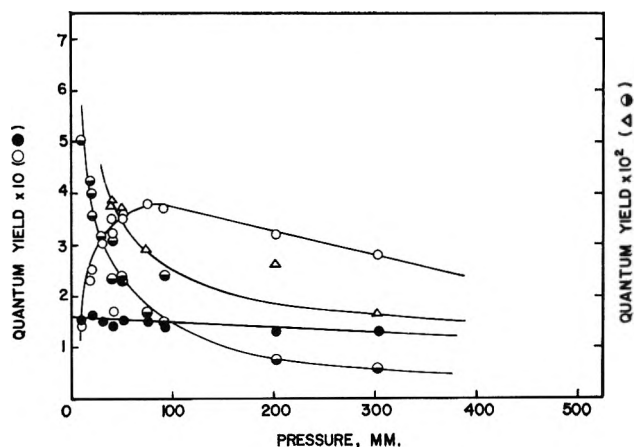


Figure 1. Quantum yields *vs.* substrate pressure for 10-min. exposures for an absorbed light intensity of 0.585 μ einstein/min. and a cell temperature of 120°: ●, acetylene; ○, 1,3-butadiene; Δ , hydrogen chloride; \odot , ethylene.

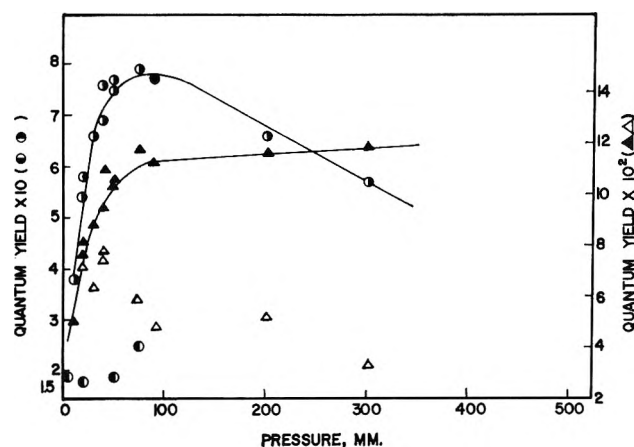


Figure 2. Quantum yields *vs.* pressure for 10-min. exposures at an absorbed intensity of 0.585 μ einstein/min. and cell temperature of 120°: \odot , HgCl calculated; \circ , HgCl measured; \blacktriangle , HCl calculated; Δ , HCl measured.

chlorine atoms by substrate molecules with concomitant polymer formation.¹⁴

That C₂H₂ is formed in a molecular process was shown in a run performed using 75 mm. substrate pressure with 15 mole % NO at 118°. Butadiene formation was completely suppressed whereas the yield of C₂H₂ was only slightly affected (owing to competitive quenching by NO).

The effect of inert gas on the reaction was checked in a separate experiment. The addition of 129 mm. of SF₆ to 75 mm. of C₂H₃Cl at 120° resulted in a slight lowering of the product yields. More significant was the fact that the yields of C₄H₆ and C₂H₂ were the same as those obtained in a run with pure substrate at a

pressure of 75 + 129 = 204 mm. Thus, C₂H₃Cl and SF₆ appear to be equally efficient in reducing the formation of C₄H₆ and C₂H₂.

A detailed time study, the results of which are plotted in Fig. 3, revealed the presence of secondary reactions. Ethylene formation diminishes at shorter exposure times, whereas the yields of C₂H₂, HCl, and C₄H₆ increase more or less rapidly, depending on the substrate pressure used. Hence, C₂H₄ appears to be a secondary product, whereas C₂H₂, HCl, and C₄H₆ (as well as calomel) are primary products of the reaction. At both pressures employed, 10 and 75 mm., the corresponding quantum yields appear to extrapolate to the same limiting values, namely $\phi_{(C_2H_2)} = 0.17$ and $\phi_{(C_4H_6)} = 0.51$. The extrapolation of $\phi_{(C_4H_6)}$ is more certain at 75 mm. pressure, where a suppressing effect on $\phi_{(C_4H_6)}$ is already apparent. By extrapolating the high pressure part of the $\phi_{(C_4H_6)}$ plot in Fig. 1 to zero pressure this suppression is found to be 7% of the quantum yield. If a correction for this is applied, the value of $\phi_{(C_4H_6)}$ at zero reaction time and zero pressure is found to be 0.55.

III. Photosensitization by ^NHg (³P₁) Atoms at High Temperature. Between 200 and 325° the reaction is characterized by a sudden increase in $\phi_{(HCl)}$, more rapid polymerization, and the appearance of additional

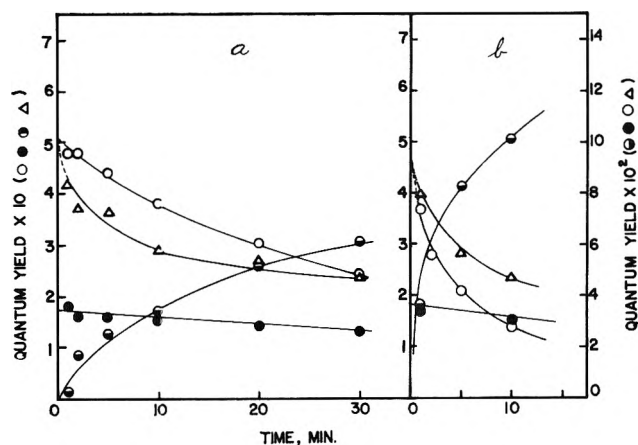


Figure 3. (a) Quantum yields *vs.* time at a substrate pressure of 75 mm. and a cell temperature of 120° with an absorbed light intensity of 0.585 μ einstein/min.: ○, 1,3-butadiene; ●, acetylene; \odot , ethylene; Δ , hydrogen chloride. (b) Quantum yields *vs.* time at a substrate pressure of 10.5 mm. and a cell temperature of 120° with an absorbed light intensity of 0.585 μ einstein/min.: \odot , ethylene; ●, acetylene; Δ , hydrogen chloride; ○, 1,3-butadiene.

(14) H. Schmitz and H. J. Schumacher, *Z. physik. Chem.*, B52, 72, (1942); F. S. Dainton, D. A. Lomax, and M. Weston, *Trans. Faraday Soc.*, 58, 308 (1962); P. B. Ayscough, A. J. Cocker, F. S. Dainton, and S. Hirs, *ibid.*, 58, 318 (1962).

products: 2-chloro-1,3-butadiene and *cis*- and *trans*-1-chloro-1,3-butadiene. At 300° the heavy polymer deposition on the incident window of the cell seriously reduced reproducibility (decrease in I_a is ca. 15–20% in a 10-min. run).

The effect of temperature on product yields is shown in Fig. 4. The yields of HCl and the chlorobutadienes increase rapidly with temperature in contrast to those of butadiene and acetylene which rise only very moderately. Above 270°, $\phi_{(\text{HCl})}$ exceeds unity; above 290°, the combined quantum yields of C_4H_6 , $\text{C}_4\text{H}_5\text{Cl}$, C_2H_2 , and C_2H_4 also exceed unity.

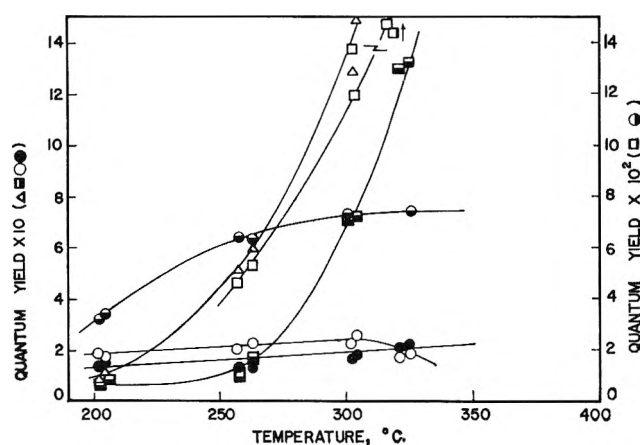


Figure 4. Quantum yields vs. temperature for 10-min. exposures at a substrate pressure of 75 mm.: ●, ethylene; ●, acetylene; □, *cis*- and *trans*-1-chloro-1,3-butadiene; ■, 2-chloro-1,3-butadiene; △, hydrogen chloride; ○, 1,3-butadiene.

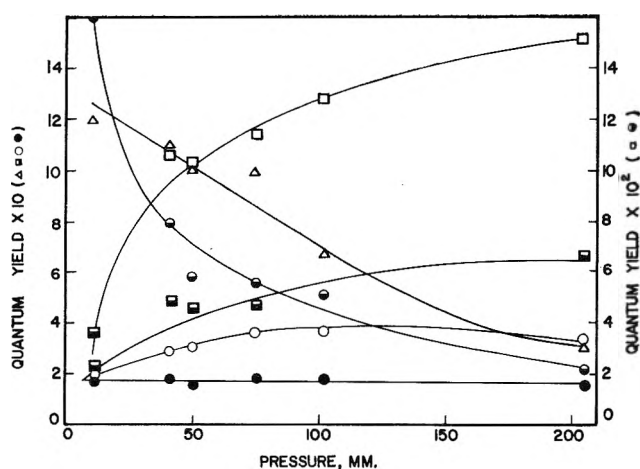


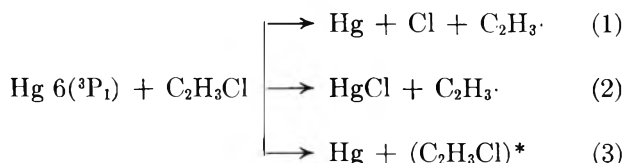
Figure 5. Quantum yield vs. pressure for 10-min. exposures at an absorbed light intensity of 0.214 μ einstein/min. and cell temperature of 265°: ●, ethylene; ●, acetylene; □, *cis*- and *trans*-1-chloro-1,3-butadiene; ○, 1,3-butadiene; ■, 2-chloro-1,3-butadiene; △, hydrogen chloride.

The results of a pressure study carried out at 265° are presented in Fig. 5. The trend for C_4H_6 , C_2H_2 , and HCl formation here is similar to that at 120°, with the basic difference being the much larger quantum yield of the HCl product, with a value above unity at low pressures. The chlorobutadienes rise gradually at a decreasing rate with increasing pressure up to 200 mm., the highest pressure studied.

The effect of nitric oxide at higher temperatures is identical with that found at 120°. Thus, at 300° 20 mole % of NO completely suppressed the formation of butadiene and the chlorobutadienes but left unaltered the acetylene yield.

Discussion

The presence of two quenching sites within the vinyl chloride molecule, *i.e.*, the π -bond and the chlorine atom, suggests the possibility of a plurality of primary processes in the mercury-photosensitized decomposition of this molecule. Indeed, the data presented in the previous section require the inclusion of three primary steps



with quantum efficiencies of 0.49, 0.06, and 0.45 mole/einstein, respectively.

Now, it is instructive to attempt to relate the total quenching efficiency of the vinyl chloride molecule, as well as the relative quantum yields of the two primary radical-forming steps 1 and 2 and the excited molecule-forming step 3, to the relative quenching efficiencies of the olefinic π -bond and the chlorine atom in the vinyl chloride molecule. Assuming that the quenching cross section (σ_Q^2) of the π -bond is the same in vinyl chloride as in ethylene (20.2 \AA^2) and that $\sigma_Q^2(\text{Cl})$ is the same as in hydrogen chloride (24.8 \AA^2) or methyl chloride (24.6 \AA^2),¹⁵ a value of 29.2 \AA^2 can be derived for $\sigma_Q^2(\text{C}_2\text{H}_3\text{Cl})$ from the simple model shown in Fig. 6. This is in good agreement with the experimental value of 29.3 \AA^2 .¹⁵ Furthermore, making the assumption that quenching at the chlorine atom leads to (1) and (2) and that quenching at the π -bond results in (3), from the model we obtain 56:44 for the ratio $(\phi_{(1)} + \phi_{(2)})/\phi_{(3)}$ which compares favorably with the experimental value of 55:45. These findings thus indicate that interaction of $\text{Hg } 6(^3\text{P}_1)$

(15) Y. Rousseau, M. G. Bellas, O. P. Strausz, and H. E. Gunning, to be published.

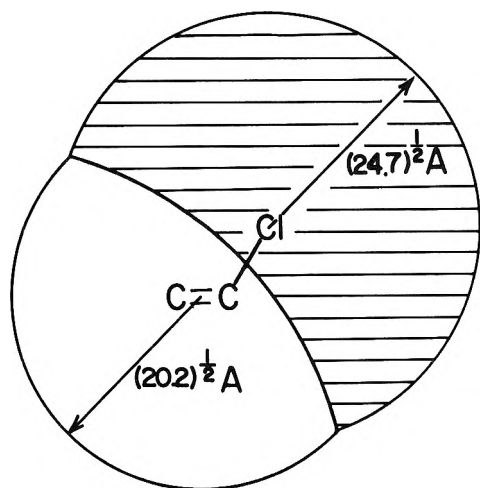
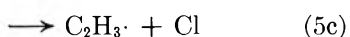
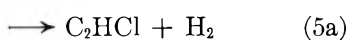
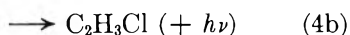
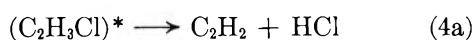


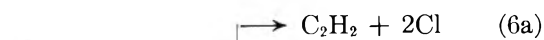
Figure 6. Graphical estimation of the quenching cross section of vinyl chloride and the relative quenching efficiencies of the π -bond and chloride atom. The structural parameters were taken as follows: the $C=C-Cl$ bond angle as 122° , the $C=C$ and $C-Cl$ bond lengths as 1.33 and 1.73 Å., respectively.¹⁶ Quenching at the chlorine atom site is assumed to extend to the midpoint of the $C-Cl$ bond.

atoms at the chlorine atom site results in the vinyl scission, and that excited C_2H_3Cl formation is associated with quenching at the π -bond, *i.e.*, process 3.

By analogy with studies on olefinic hydrocarbons¹ the energy-rich molecule formed in step 3 is probably a vibrationally excited triplet with the following possible fates



Now, since neither hydrogen nor chlorobutadiene (which should form if chlorovinyl radicals were present, as will be shown later) could be detected among the reaction products below 200° , steps 5a and 5b can be eliminated from this sequence. The importance of (5c) cannot be evaluated from the present study. However, by analogy with the photolysis of *cis*-1,2-dichloroethylene, where it is postulated¹⁶ that the two modes of decomposition



originate from different upper electronic levels, step 6b arising from the lower lying and step 6a from the higher one, it appears likely that (5c) has no significance in Hg $6(3P_1)$ photosensitization. Evidence for the occurrence of (4a) is fairly unambiguous. The quantum yields at zero pressure for steps 4a and 4b are 0.17 and 0.28 mole/einstein, respectively, and are only slightly affected by temperature between 120 and 325° or by pressure in the range 10–200 mm.

This slight pressure effect should be contrasted with the very marked pressure dependence over the same range for reactions of unsubstituted olefins with Hg $6(3P_1)$ atoms. From the small pressure dependence of (4a) an approximate value of 1.4×10^{-11} sec. can be estimated for the lifetime of $(C_2H_3Cl)^*$. The much shorter lifetime of this species as compared to the lifetimes for the various excited states of olefinic hydrocarbons¹⁷ formed in Hg $6(3P_1)$ photosensitization can be ascribed to enhanced intersystem crossing or more probably phosphorescence brought about by spin-orbital coupling. These transitions have been shown to be very sensitive to internal as well as external heavy-atom perturbations.^{18,19} The rate constant for this process is 1.72×10^{10} sec.⁻¹, whereas in the case of olefinic hydrocarbons it is at most 10^8 sec.⁻¹ but quite probably much lower. The rate constant for step 4a is 1.05×10^{10} sec.⁻¹ which is one order of magnitude larger than that for olefins. The molecular elimination of HCl is energetically more favorable than that of H_2 from either C_2H_4 or C_2H_3Cl .²⁰ Another contributing factor may be the larger size and higher polarizability of the chlorine atom compared to the hydrogen atom.

The above interpretation concerning primary processes implies perfect quantum efficiency for processes 1 and 2 in agreement with work on methyl chloride,¹⁰ the only other organic chloride thoroughly investigated. The low relative yield for calomel formation *via* the isotopically specific route (2), *i.e.*, $\phi_{(2)}/(\phi_{(1)} + \phi_{(2)}) = 0.11$, indicates that vinyl radicals behave in the same way as other mono- α -hydrogenated radicals

(16) M. H. J. Wijnen, *J. Am. Chem. Soc.*, **83**, 4109 (1961).

(17) The averaged value for the excited states of C_2H_4 is given by Cvetanović as 4×10^{-9} sec. Rabinovitch has calculated values of 1.5×10^{-9} and 3.3×10^{-10} sec. for the two excited states of *trans*-1,2-dideuterioethylene.³ The values¹ for 1-butene are 6.3×10^{-9} and 19×10^{-9} sec. and for deuterio-1-butene 16×10^{-9} and 87×10^{-9} sec.

(18) M. A. El-Sayed and T. Pavlopoulos, *J. Chem. Phys.*, **39**, 1899 (1963).

(19) S. P. McGlynn, J. Daigre, and F. J. Smith, *ibid.*, **39**, 675 (1963).

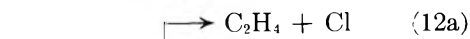
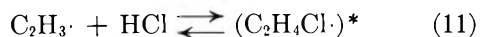
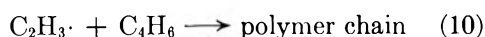
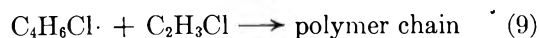
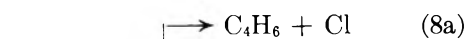
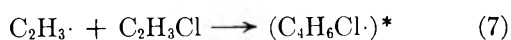
(20) From heats of formation: [H = 52, Cl = 29, C_2H_4 = 12.5, and C_2H_3Cl = 7.5 kcal./mole (P. Goldfinger and G. Martens, *Trans. Faraday Soc.*, **57**, 2220 (1961))] $D(C_2H_3-H) - D(C_2H_3-Cl) = 18$ kcal./mole.

with respect to their ability to stabilize the initially formed HgCl through the absorption of excess energy in the quenching complex.⁹

The occurrence of $C_2H_3 + C_2H_3$ reactions, which would yield C_2H_4 and C_2H_2 *via* disproportionation and C_4H_6 *via* recombination, is ruled out by a number of experimental facts. The time study (Fig. 3) demonstrates conclusively the secondary nature of the reaction giving rise to ethylene. Furthermore, if butadiene were formed *via* recombination of vinyl radicals arising from the primary reaction, the calculated primary quantum yield for vinyl chloride disappearance would exceed unity: *i.e.*, $2\phi_{(C_4H_6)} + \phi_{(C_2H_2)} = 2 \times 0.55 + 0.17 = 1.27$. Butadiene and acetylene cannot arise from the same source since NO completely suppresses the formation of the former but has no effect on the latter. Finally, the striking difference in the dependence of their yields upon pressure (*cf.* Fig. 1) dismisses as unimportant their formation *via* vinyl radical recombination-disproportionation reactions.

For 10-min. exposures, $\phi_{(C_4H_6)}$ increases more than twofold between 10 and 75 mm. (*cf.* Fig. 1). But for both pressures $\phi_{(C_4H_6)} = 0.51$ within the uncertainty of the extrapolation to zero time (Fig. 3). Thus, the primary step for vinyl radical formation is pressure independent (above 10 mm.) and the pressure trend exhibited by the butadiene product is due to secondary reactions.

In the light of these arguments the following sequence of reactions is proposed

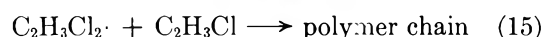


According to this scheme the sole source of C_4H_6 is the displacement-type reaction of vinyl radicals with vinyl chloride shown in steps 7 and 8.²¹ The chlorine split in (8a) is facilitated by the resonance energy of conjugation in the butadiene product, as evidenced by the fact that the saturated radicals ($C_2H_3Cl_2 \cdot$, $C_2H_4Cl \cdot$), although abundantly present in the system, do not react *via* (8a). It is through the competition be-

tween reactions 7 and 10 that $\phi_{(C_4H_6)}$ does not attain its maximum value until a pressure of 75 mm. is reached (Fig. 1). At still higher pressures $\phi_{(C_4H_6)}$ decreases slowly, due to collisional deactivation of the "hot" chlorobutenyl radicals (step 8b), their ultimate fate being polymer formation *via* reaction 9. From the linearly descending slope of the $\phi_{(C_4H_6)}$ *vs.* pressure curve (Fig. 1) the approximate lifetime of $(C_4H_6Cl \cdot)^*$ was estimated to be *ca.* 6.0×10^{-11} sec. It can be shown that a simplified kinetic treatment of steps 1, 2, and 7-10 yields a rate expression for C_4H_6 formation which is in qualitative agreement with the experimental plot in Fig. 1. However, it is not of a form suitable for the evaluation of individual rate constants. Also, it should be pointed out that reaction 10 would probably occur with any other radical present in the system.

Reactions 11 and 12 adequately explain not only C_2H_4 formation *via* a secondary route but also the strong suppressing effect of pressure upon the yields of C_2H_4 and HCl. The role of "hot" chloroethyl radicals in photochlorinations has been pointed out recently by Dainton, *et al.*,^{14,22a} and by Huybrechts, *et al.*^{22b} The activation energy for reaction 11 must be very small and is probably less than that for abstraction by methyl radicals, *i.e.*, 2.1 kcal./mole.²³

Up to this point the fate of the chlorine atoms formed in reactions 1, 8a, and 12a has been neglected. Undoubtedly the main route for chlorine atom disappearance is addition to vinyl chloride, followed by polymerization of the substrate



This is apparent from the rapid pressure decrease in the system and the appearance of the solid polymeric material upon prolonged irradiation.

Assuming additional calomel formation *via* the secondary reaction



the ratio of the rates for reaction 14 and 16 can be expressed in the form

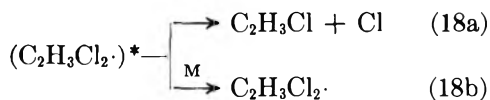
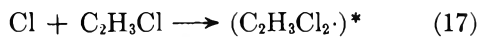
(21) Pertinently, Sherwood and Gunning have recently demonstrated the occurrence of a similar reaction with ethynyl radicals: $C_2H + C_2HCl \rightarrow C_4H_2 + Cl$ [A. G. Sherwood and H. E. Gunning, *J. Am. Chem. Soc.*, **85**, 3506 (1963)].

(22) (a) P. B. Ayscough, A. J. Cocker, and F. S. Dainton, *Trans. Faraday Soc.*, **58**, 284 (1962); (b) G. Huybrechts, L. Meyers, and G. Verbeke, *ibid.*, **58**, 1128 (1962).

(23) R. J. Cvetanovic and E. W. R. Steacie, *Can. J. Chem.*, **31**, 158 (1953).

$$\frac{R_{(14)}}{R_{(16)}} = \frac{k_{(17)}k_{(18b)}P}{(k_{(18a)} + k_{(18b)}M)k_{(16)}(\text{Hg})}$$

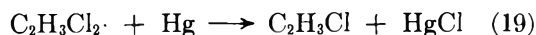
where P is the vinyl chloride pressure, M is the total pressure in the system, and the rate constants refer to the reactions



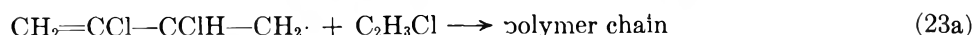
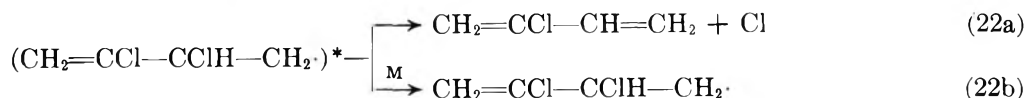
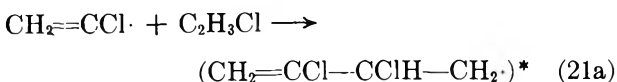
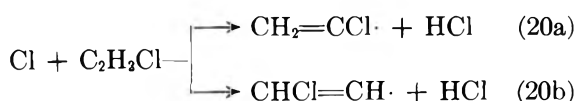
This expression predicts a strong pressure effect on the rate ratio,²⁴ $R_{(14)}/R_{(16)}$, at the low pressures used in the investigation. Yet, the measured values of $\phi_{(\text{HgCl})}$ are constant over the pressure range 4–78 mm. In addition, if the quantum yields measured are correct, the experimental value of

$$R_{(14)}/R_{(16)} \approx (2\phi_{(1)} + \phi_{(2)})/(\phi_{(\text{HgCl})} - \phi_{(2)}) \approx 5-8$$

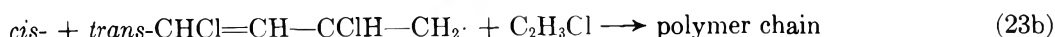
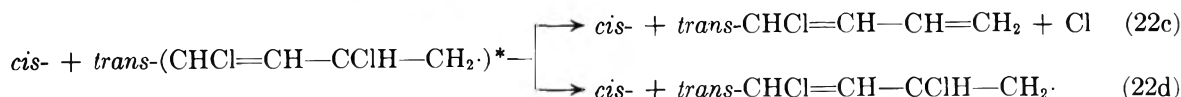
appears to be too low.²⁵ On these grounds the main source of isotopically nonspecific calomel is not (16), but rather the slightly exothermic reaction



At temperatures of 200° and above, the data indicate the occurrence of chain processes. The striking increase in $\phi_{(\text{HCl})}$, as well as the formation and rapid increase in importance of the chlorobutadienes, with temperature requires the inclusion of the following reactions in addition to those already proposed for the low-temperature region

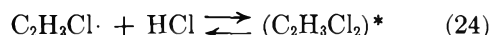


and



The abstraction reactions by chlorine atoms, (20a) and (20b), commence at temperatures around 200° where the quantum yield for chlorobutadiene formation is 0.008 mole/einstein. Both the 1-chlorovinyl and the 2-chlorovinyl radicals are formed in reaction 20 as shown by the appearance of three isomeric chlorobutadiene products: the *cis*- and *trans*-1-chlorobutadienes arising from the 2-chlorovinyl radical and the 2-chlorobutadiene from the 1-chlorovinyl radical. The predominance of one of the isomers is indicated from the data of Fig. 4 for the reaction at 303.5°, where the three isomers were in the approximate ratio of 12:1:1 and at 320.5°, where the ratio is 16:1:1.

The strong pressure dependence of HCl formation at higher temperatures (*cf.*, Fig. 6) is explained in the same manner as above with the added participation of reaction 24



followed by subsequent reactions similar to (18a) and (18b).

According to the mechanism postulated, $\phi_{(\text{C}_2\text{H}_3\text{Cl}_2\cdot)^*}$ should be nearly equal to $\phi_{(\text{HCl})}$, whereas it was always found to be less. Presumably the yield of the chlorobutadienes is reduced by secondary reactions similar to those postulated for C₄H₆. Now activation energies for radical addition reactions have been shown to be smaller for conjugated diolefins than monoolefins.²⁶

(24) The (C₂H₂Cl₂·)* radical formed in reactions analogous to (17) has been assigned a lifetime of 10⁻⁸ sec. before dissociating²¹ and the lifetime of the (C₂H₃Cl₂·)* radical should be nearly the same.

(25) The Arrhenius parameters for (17) are log $A = 9.5$ (l. mole sec.) and $E = 1.0$ kcal./mole [F. S. Dainton, private communication, 1962].

(26) Thus, Mandelcorn and Steacie [L. Mandelcorn and E. W. R. Steacie, *Can. J. Chem.*, **32**, 474 (1954)] obtained a value of 2.5 kcal./mole for the activation energy of methyl radical addition to 1,3-butadiene and 7.0 ± 1.5 kcal./mole for the addition to ethylene. In a more recent study Rajbenback and Szwarc [A. Rajbenback and M. Szwarc, *Proc. Roy. Soc. (London)*, **A251**, 394 (1959)] have shown that the activation energy for methyl radical addition to ethylene is 2.85 kcal./mole higher than for the addition to 1,3-butadiene.

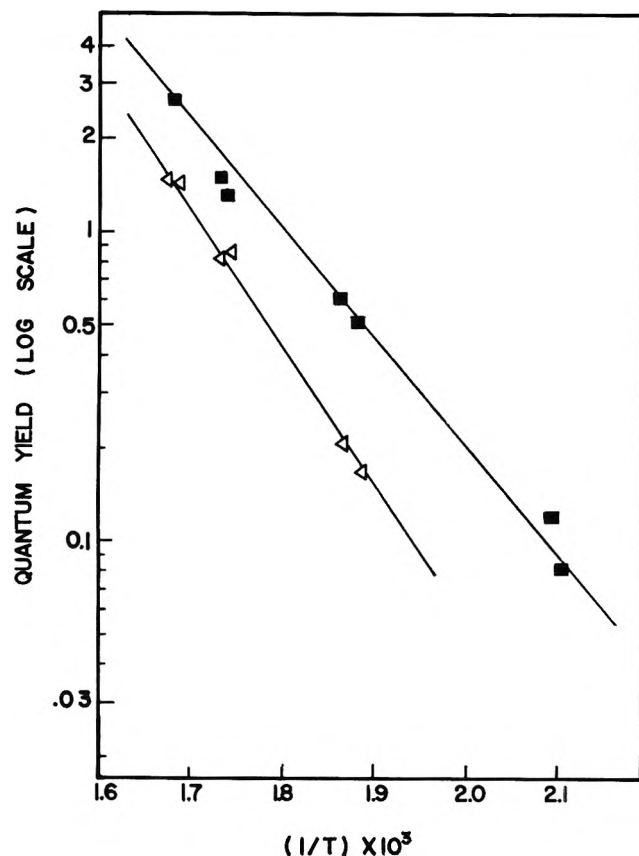


Figure 7. Logarithm of the quantum yield vs. $(1/T) \times 10^3$: ■, the combined chlorobutadienes; Δ, hydrogen chloride.

Consequently, the chlorobutadienes, although present in low concentrations, can compete favorably with vinyl chloride at moderately high temperatures. At still higher temperatures this difference in reactivity should gradually diminish leading to an increase in the $\phi_{(C_4H_6Cl)}/\phi_{(HCl)}$ ratio. This was indeed found to be the case.

$t, ^\circ C.$	204	263	303.5	320.5
$\phi_{(C_4H_6Cl)}/\phi_{(HCl)}$	0.09	0.34	0.56	0.56

The complexity of the system is further borne out by the differences in the activation energies for the formation of the chlorobutadienes and the hydrogen chloride. From the Arrhenius plots in Fig. 7, using the method of least squares, the following activation energies were obtained

$$E_{(HCl)} = 15.0 \text{ and } E_{(C_4H_6Cl)} = 20.8 \text{ kcal./mole}$$

$E_{(C_4H_6Cl)}$ is a complex quantity including the activation energies not only for the formation but also for the destruction of the chlorobutadienes in secondary reactions; and since these latter become less important at higher temperatures, $E_{(C_4H_6Cl)}$ will be greater than $E_{(HCl)}$. On the other hand it can be shown by a steady-state treatment of a simplified mechanism comprising steps 1, 2, 14, 20, 22a, and 22c that $E_{(HCl)}$ is related to the activation energies of the elementary steps 20 and 14 by

$$E_{(HCl)} = E_{(20)} - E_{(14)}$$

Whence, taking the value of $E_{(14)} = 1.0$ kcal./mole, as given by Dainton, *et al.*,²⁵ a value of 16.0 kcal./mole is obtained for reaction 20. The high activation energy for the abstraction of a hydrogen atom from vinyl chloride is consistent with this reaction occurring only at temperatures exceeding 200° , in agreement with the work of Rust and Vaughan²⁷ on the thermal chlorination of C_2H_4 , where it was observed that addition was the only important reaction at 235° . It appears that $E_{(20)} = 16.0$ kcal./mole is the first value published for the activation energy for the abstraction of a hydrogen atom from an olefinic carbon atom.

Acknowledgment. The partial support of the National Research Council of Canada under Grant No. T-162 is gratefully acknowledged.

(27) F. F. Rust and W. E. Vaughan, *J. Org. Chem.*, **5**, 472 (1940).

Isotopic Fractionation of Hydrogen between Water and the Aqueous Hydroxide Ion¹

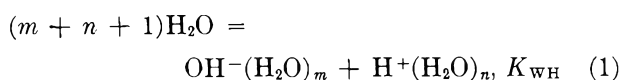
by Karl Heinzinger and Ralph E. Weston, Jr.

Department of Chemistry, Brookhaven National Laboratory, Upton, New York 11973 (Received February 17, 1964)

The fractionation of hydrogen isotopes between aqueous solutions of sodium hydroxide and potassium hydroxide and the vapor phase in equilibrium with the solutions has been measured at 13.5°. The separation factor thus obtained has been used to calculate a value of 4.2 for the equilibrium constant, K_H , of the isotope exchange equilibrium $\text{H}_2\text{O} + \text{OD}^- = \text{HDO} + \text{OH}^-$. This value is in reasonable agreement with that obtained from spectroscopic data, and from other equilibria, including the ratio of ionization constants for light and heavy water. A comparison of values from different types of experiment enables one to reach some conclusions concerning the hydration of the hydroxide ion.

Introduction

The ratio of the ionization constants of light and heavy water, $K_{\text{WH}}/K_{\text{WD}}$, is related to a combination of the isotopic fractionation factor between water and hydronium ion and between water and hydroxide ion. If we write the equation for the dissociation process of water without specifying the extent of ionic solvation, we obtain



and a similar equation can be written for heavy water. Then

$$\begin{aligned} \frac{K_{\text{WH}}}{K_{\text{WD}}} &= \frac{[\text{D}_2\text{O}]^{m+n+1}[\text{OH}^-(\text{H}_2\text{O})_m][\text{H}^+(\text{H}_2\text{O})_n]}{[\text{H}_2\text{O}]^{m+n+1}[\text{OD}^-(\text{D}_2\text{O})_m][\text{D}^+(\text{D}_2\text{O})_n]} \\ &= \frac{[\text{OH}^-(\text{H}_2\text{O})_m][\text{D}_2\text{O}]^{m+1/2}}{[\text{OD}^-(\text{D}_2\text{O})_m][\text{H}_2\text{O}]^{m+1/2}} \times \\ &\quad \frac{[\text{H}^+(\text{H}_2\text{O})_n][\text{D}_2\text{O}]^{n+1/2}}{[\text{D}^+(\text{D}_2\text{O})_n][\text{H}_2\text{O}]^{n+1/2}} \quad (2) \end{aligned}$$

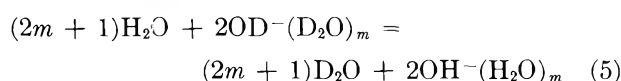
The rule of the geometric mean can then be used to relate the two factors of eq. 2 to the measured fractionation factors. In our previous paper,² we showed that the second factor is just

$$\lambda^{1/2} = \left(\frac{2n + 1}{2} \kappa_L \right)^{2n+1} \quad (3)$$

where κ_L is the equilibrium constant for the reaction



The first factor, which may be designated as $\lambda_H^{1/2}$, is the square root of the equilibrium constant for the exchange reaction



and is related to κ_H , which is defined as the equilibrium constant for



by

$$\lambda_H^{1/2} = \left[\frac{2m + 1}{2} \kappa_H \right]^{2m+1} \quad (7)$$

From the combination of these, we obtain

$$\frac{K_{\text{WH}}}{K_{\text{WD}}} = \left[\frac{2m + 1}{2} \kappa_H \right]^{2m+1} \left[\frac{2n + 1}{2} \kappa_L \right]^{2n+1} \quad (8)$$

In our previous paper² we reported measurements of κ_L , and in this paper we give results for κ_H .

(1) Research performed under the auspices of the U. S. Atomic Energy Commission.

(2) K. Heinzinger and R. E. Weston, Jr., *J. Phys. Chem.*, **68**, 744 (1964).

Table I: Experimental Results

Concn., moles/l.	r	α_B/α_W	$\left \frac{\Delta \alpha_B}{\alpha_W} \right $	$\frac{r(1+r/2)}{\left(\frac{\alpha_B}{\alpha_W}(1+r/2) - 1 \right)^2}$	K_H	$ \Delta K_H $
NaOH						
7.84	0.1476	0.9638	0.0017	130	4.23	0.22
10.20	0.1983	0.9567	0.0009	82	3.85	0.08
12.12	0.2435	0.9472	0.0015	70	3.90	0.11
KOH						
6.99	0.1396	0.9626	0.0007	168	4.69	0.12
10.30	0.2228	0.9456	0.0008	96	4.37	0.08

Principle of the Measurement

In the same way as in the previous paper² we can relate the separation factor between liquid and vapor of a hydroxide solution to the equilibrium constant of eq. 6. With the assumption that the alkali hydroxide is completely dissociated, this leads to

$$\kappa_H = \frac{r}{(\alpha_B/\alpha_W)(1+r/2) - 1 + mr} \quad (9)$$

or, with a more obvious dependence on m

$$1/\kappa_H = m + [(\alpha_B/\alpha_W)(1+r/2) - 1]/r \quad (10)$$

In these equations, α_B and α_W are the separation factors for the hydroxide solution and the pure water, respectively, and are defined by $(D/H)_{\text{liquid}}/(D/H)_{\text{vapor}}$, while r is given by

$$r = \frac{N_{\text{OH}-(\text{H}_2\text{O})_m} + N_{\text{XOH}}}{N_{\text{H}_2\text{O}} + mN_{\text{OH}-(\text{H}_2\text{O})_m}} \quad (11)$$

$$= N_{\text{XOH}}^0/N_{\text{H}_2\text{O}}^0$$

The superscript zero refers to the "formal" concentration, and the N values are mole fractions.

The same method has been used by Green and Taube to determine the analogous oxygen isotope fractionation between water and hydroxide ion.³

Experimental

Since the experiments were done in the same way as those described in the previous paper,² it is not necessary to repeat the description. The temperature was again $13.5 \pm 0.5^\circ$.

Sodium hydroxide (Mallinckrodt Chemical Works) and potassium hydroxide (Baker's Analyzed) pellets were dissolved in triply distilled water, which was taken from a large supply. For the determination of the D/H ratio of the liquid, the hydroxide solutions were neutralized by adding gaseous CO_2 (Matheson

"Bone Dry") from a cylinder. After neutralization, the water was removed from the resulting solution of carbonate by distillation *in vacuo* into a trap at -78° . The removal was completed by heating the remaining solid to 300° for 0.5 hr., and the trap (at -78°) was then evacuated to remove carbon dioxide. The water thus collected was reduced to hydrogen with uranium, as was the water from the vapor samples.

Results and Discussion of Errors

In Table I, the results of our measurements and their associated errors are given for the specific case where m is zero. For this special case, we shall designate κ_H by K_H . The values of α_B/α_W are based on the following numbers of independent experiments, with the same solution for each of the concentrations: 7.84 M NaOH, 6; 10.20 M NaOH, 5; 12.12 M NaOH, 6; 6.99 M KOH, 3; 10.30 M KOH, 4. The error $|\Delta(\alpha_B/\alpha_W)|$ is the average deviation at each concentration. The error in K_H is obtained by taking the partial derivatives with respect to r and α_B/α_W

$$\pm \Delta K_H = \frac{[r(1+r/2)|\Delta(\alpha_B/\alpha_W)| + |(\alpha_B/\alpha_W) - 1||\Delta r|]}{[(\alpha_B/\alpha_W)(1+r/2) - 1]^2} \quad (12)$$

In the table only the error caused by $\Delta(\alpha_B/\alpha_W)$ is listed, because the first term in the numerator of eq. 12 is large compared with the second term. Again, the error is calculated for $m = 0$. For $m \geq 1$ the error is smaller.

Table I seems to indicate a slight dependence on the concentration of hydroxide and on the cation, but this effect is within or barely outside the limits of error. For comparison with other measurements we therefore use an average value of 4.21. This gives us an average deviation of ± 0.27 . This error is still reasonable com-

(3) M. Green and H. Taube, *J. Phys. Chem.*, **67**, 1565 (1963).

pared with the different values in the literature for the ratio of the dissociation constants of light and heavy water.

Table II gives the values of κ_H as a function of m , from eq. 9.

Unfortunately, the error in these measurements increases rapidly as r decreases, which makes it impractical to work at lower concentrations of alkali hydroxide. Because ion-pair association may occur in solutions as concentrated as those we have used,⁴ the equilibrium constant for isotopic fractionation is not necessarily independent of concentration. This depends on the difference in isotopic fractionation between water and the hydroxide ion as a free ion or as the anion of an ion pair. Alternatively, this effect may be ascribed to changes in activity with concentration. The value of K_H for dilute solutions may, therefore, be slightly different from the value calculated here.

Table II: Dependence of κ_H on m

	0	1	2	3	4
κ_H	4.21	0.81	0.45	0.31	0.24
$\left(\frac{2m+1}{2}\kappa_H\right)^{2m+1}$	2.11	1.82	1.84	1.83	2.00
K_{WH}/K_{WD}^a	6.31	5.44	5.50	5.47	5.98

^a Calculated according to eq. 8 with $[(2n+1)\kappa_L/2]^{2n+1} = 2.99$.²

Comparison of K_H with Values Obtained by Other Methods

Table III compares the results of the present experiments with values derived from other types of experiments and from statistical mechanical calculations. These are discussed in this section.

Table III: K_H Obtained by Various Methods

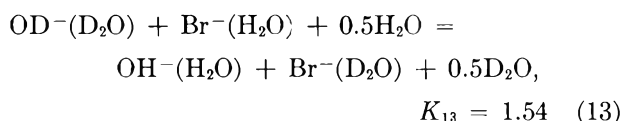
Method	K_H , 13.5°
This work	4.21
Spectroscopic data, free rotation assumed	3.45
Spectroscopic data, hindered rotation	2.72
Reactions 13-15	5.2
Reactions 14, 16-19	4.4
Reaction 20	2.2

1. K_H Calculated from Spectroscopic Data. From the single vibrational frequency of the hydroxide ion, one can calculate the reduced partition function ratio

$f(\text{OD}^-/\text{OH}^-)$. The best value for this frequency is probably that for $\text{LiOH}\cdot\text{H}_2\text{O}$ measured by Jones,⁵ who gives the following data: $\text{LiOH}\cdot\text{H}_2\text{O}$, $\omega_e = 3735$, $\omega_e X_e = 80.5$ (assumed by analogy with LiOH); $\text{LiOD}\cdot\text{D}_2\text{O}$, $\omega_e = 2720$, $\omega_e X_e = 44.0$ (again assumed). The calculated value of ν_{OH} is in good agreement with the band at 3600 cm^{-1} observed in aqueous hydroxide solutions by Busing and Hornig.⁶

The value of $f(\text{OD}^-/\text{OH}^-)$ is combined with $f(\text{HDO}/\text{H}_2\text{O})^2$ and the separation factor of pure water to give the tabulated value of K_H . The above calculation is probably oversimplified because it has treated the aqueous hydroxide ion as an isolated ion. Swain and Bader⁷ argue that the two rotational degrees of freedom have become librational degrees of freedom with a single (doubly-degenerate) frequency of 475 cm^{-1} for OH^- , and $475/\sqrt{2}\text{ cm}^{-1}$ for OD^- . This treatment leads to a smaller value of K_H , as shown in Table III, and even poorer agreement with the experimental value. Swain and Bader calculated a value of 3.58 from spectroscopic data which is not explicitly given in their paper.

2. K_H from Other Equilibria Involving the Hydroxide Ion. Kingerley and La Mer⁸ have measured the equilibrium constant for the reaction



The temperature dependence of this equilibrium constant is small and will be neglected. This differs from the equilibrium we have studied because it involves the transfer of a hydroxide ion and of a bromide ion from light to heavy water. There is evidence (some of which is summarized in ref. 6) that hydroxide ion has little effect on the structure of water, and we shall assume, therefore, that the free energy of transfer of this ion from light to heavy water is zero. For the bromide ion, a value for the transfer energy has been calculated by Swain and Bader, with the assumption of a particular model for solvated ions. This gives

(4) The n.m.r. shift of OH^- in an aqueous solution of KOH is linear with the atom fraction of protons in the ion up to a concentration of $\sim 15\text{ M}$ [H. S. Gutowsky and A. Saika, *J. Chem. Phys.*, **21**, 1688 (1953)]. However, the shift for an NaOH solution is only two-thirds as great at this concentration. This has been attributed to ion-pair formation.

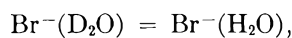
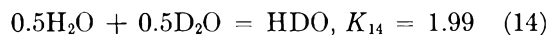
(5) L. H. Jones, *ibid.*, **22**, 217 (1954).

(6) W. R. Busing and C. F. Hornig, *J. Phys. Chem.*, **65**, 284 (1961).

(7) C. G. Swain and R. F. W. Bader, *Tetrahedron*, **10**, 182 (1960).

(8) R. W. Kingerley and V. K. La Mer, *J. Am. Chem. Soc.*, **63**, 3256 (1941).

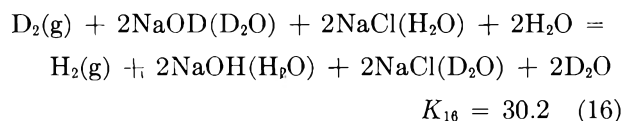
eq. 15,⁷ which can be combined with eq. 13 and 14⁹ in order to obtain K_H .



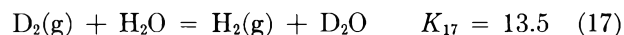
$$K_{16} = 1.67 \text{ (at } 13.5^\circ) \quad (15)$$

The uncertainty in this method is in the value of K_{16} .

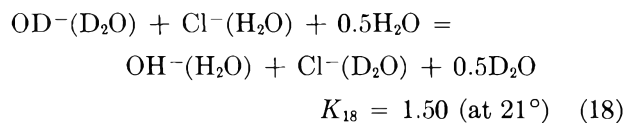
A similar reaction, differing only in the anion which is transferred, can be obtained from measurements with the hydrogen and deuterium gas electrodes in alkaline solutions. The measurements of Abel, Bratu, and Redlich¹⁰ give the equilibrium constant (at 21°) for the reaction



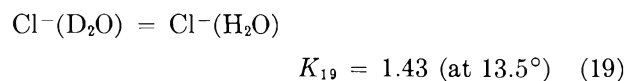
Subtracting (17)⁹ from (16)



and taking one-half of the difference, we obtain

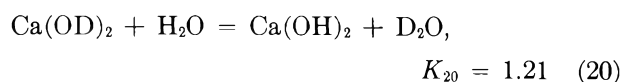


Equation 18 differs from eq. 13 by the substitution of a chloride ion for a bromide ion; if one can again assume no temperature dependence, the values of K_{13} and K_{18} agree within experimental error. However, according to Swain and Bader, K_{19} , the equilibrium constant for the reaction



is somewhat smaller than K_{16} , and this will introduce a corresponding factor into the value of K_H . Evidently there is an inconsistency in these two sets of data.

Kingerley and La Mer⁸ have determined the equilibrium constant for the hydrogen isotope exchange between calcium hydroxide and water, by dissolving calcium oxide in a mixture of light and heavy water and measuring the change in isotopic composition of the solvent. In this way, they obtained a value of 1.21 for the equilibrium constant corresponding to the reaction



When this is combined with K_{14} , it gives a very low value of 2.2 for K_H . It seems likely that equilibrium

was not attained in the system studied by Kingerley and La Mer.

3. K_H from the Ionization Constants of Light and Heavy Water. Several values of the dissociation constant ratio may be found in the literature,^{8,10-14} and these are given in Table IV. The values are derived from e.m.f. measurements with different types of cells, except for that by Kingerley and La Mer⁸ which comes from the combination of the equilibrium constant of reaction 13 with several other equilibrium constants. The resulting value actually differs from $K_{\text{WH}}/K_{\text{WD}}$ by the ratio of equilibrium constants for the transfer from light to heavy water of a chloride ion compared with a bromide ion. It should be corrected by the ratio K_{15}/K_{19} .

Table IV: Ratio of the Dissociation Constants of H_2O and D_2O and Values of K_H Derived Therefrom

$t, ^\circ\text{C.}$	$K_{\text{WH}}/K_{\text{WD}},$ $t, ^\circ\text{C.}$	$K_{\text{WH}}/K_{\text{WD}},$ 13.5°	K_H^a	Ref.
25	5.1	5.4	3.6	12
20	5.42	5.63	3.8	11
21	6.27	6.5	4.4	10
25	6.45	6.69	4.5	14
25	6.54	6.99	4.7	8
25	7.50	8.01	5.4	^b
25	7.2	7.8	5.2	13

^a Calculated with the assumption that $m = 0$ and $n = 1$.

^b The preceding value corrected for ion transfer as described in the text.

To make comparisons with our value of K_H , it is necessary to know the temperature dependence of $K_{\text{WH}}/K_{\text{WD}}$. The only direct measurement is by Wynne-Jones,¹² who found $\Delta\Delta H = 970 \pm 50$ cal./mole. A similar value can be obtained from the combination of reactions used by Kingerley and La Mer. The value obtained by Wynne-Jones has been used to obtain the $K_{\text{WH}}/K_{\text{WD}}$ ratio at 13.5°; the error in making this temperature correction is estimated to be 1-2%.

It is evident from eq. 8 that the value of κ_H derived from the dissociation constant ratio depends on both the number of equivalent hydrogen atoms in the sol-

(9) H. C. Urey, *J. Chem. Soc.*, 562 (1947).

(10) E. Abel, E. Bratu, and O. Redlich, *Z. physik. Chem.*, **A173**, 353 (1935).

(11) G. Schwarzenbach, A. Epprecht, and H. Erlenmeyer, *Helv. Chim. Acta*, **19**, 1292 (1936).

(12) W. F. K. Wynne-Jones, *Trans. Faraday Soc.*, **32**, 1397 (1936).

(13) V. Gold and B. M. Lowe, *Proc. Chem. Soc.*, 140 (1963).

(14) P. Salomaa, L. L. Schaleger, and F. A. Long, *J. Am. Chem. Soc.*, **86**, 1 (1964).

vated proton and in the solvated hydroxide ion. If we assume values of 3 and 1 for these quantities, respectively, the values of K_H thus obtained are shown in Table IV. The value of κ_L used in this calculation was that of our earlier experiments.² The experimental value of K_H obtained here lies somewhere in the middle of the rather large range encompassed by the values obtained from different K_{WH}/K_{WD} experiments.

This method of obtaining K_H appears to have first been used by Brescia.¹⁵ From measurements of the rate of hydrolysis of ethyl orthoformate in mixtures of light and heavy water, he derived a value of K_L ,¹⁶ using essentially the same procedure as that used subsequently by Purlee.¹⁷ This was then combined with the ratio K_{WH}/K_{WD} to give 4.5 for K_H , which is within the range of values we have derived in the same way.

Hydration of the Hydroxide Ion

As in the case of the proton in solution, it is probable that strong hydrogen bonds are formed between the solute ion and solvent molecules. A possible model, with three solvent molecules in the inner solvation sphere of the hydroxide ion, has been proposed by Ackermann,¹⁸ on the basis of heat capacity and activity coefficient data.

The values of K_H derived above from spectroscopic data and from other equilibria are independent of any assumed value for m . Our experimental value agrees with these only if m is assumed to be zero. However, as is shown in Table II, this conclusion is not reached from a consideration of K_{WH}/K_{WD} obtained from our data. The fact that the other data agree only with a model in which $m = 0$ is not necessarily in conflict with Ackermann's model. The water molecules which behave as if strongly bonded to the hydroxide ion from the standpoint of heat capacity or activity coefficient measurements may still be bonded weakly enough so that their contribution to isotopic fractionation with the solvent is negligible.

Acknowledgments. We wish to thank Mr. A. P. Irsa for his invaluable assistance with the mass spectrometric analyses, and Dr. R. W. Stoenner and his analytical group for analyses of solutions.

(15) F. Brescia, *J. Chem. Phys.*, **7**, 310 (1939).

(16) F. Brescia, *J. Am. Chem. Soc.*, **60**, 2811 (1938).

(17) E. L. Purlee, *ibid.*, **81**, 263 (1959).

(18) Th. Ackermann, *Discussions Faraday Soc.*, **24**, 180 (1957); cf. also A. M. Azzam, *Z. physik. Chem. (Frankfurt)*, **32**, 309 (1962), for a dissenting opinion.

Radiolysis of Solid Solutions of Acrylamide and Propionamide¹

by G. Adler, D. Ballantine, R. Ranganathan,

Brookhaven National Laboratory, Upton, New York

and T. Davis

Chemistry Department, New York University, New York, New York (Received February 21, 1964)

A wide range of solid solutions of acrylamide and propionamide were irradiated to various doses and the gaseous decomposition products measured. G -values for H_2 , CO , and CH_4 were determined at several temperatures. The results indicate that either energy transfer reactions or hydrogen atom scavenging are important in determining relative yields. The G -value for CO as a function of composition is unusual and may be influenced by lattice structure. Finally, the hydrogen yield has been found to be primarily the result of a bimolecular reaction.

Introduction

Pure acrylamide has been shown to polymerize in the solid state both during and after exposure to ionizing radiation to yield polymers of molecular weight in excess of 50,000.^{2,3a} Morawetz^{3b} demonstrated that in solid solution with the isomorphous but nonpolymerizable propionamide the reaction occurred at equivalent rates but molecular weights were reduced. This behavior was attributed to a classical chain transfer reaction, but later work by Adler⁴ was suggestive of the fact that some other process may be involved. Since Burton⁵ and co-workers demonstrated that the radiolysis of liquid organic mixtures may involve complex transfer processes, it was felt that detailed radiolysis of acrylamide-propionamide mixtures might help clarify the previous studies. Recent reports by Dainton⁶ demonstrate that such energy transfer reactions in solid organic solutions can indeed occur and are greatly affected by crystallinity factors.

Experimental

Materials. Eastman Kodak pure grade propionamide was recrystallized twice from acetone and was dried for several days in a vacuum desiccator. The observed melting point was 80.0–81.0°.

The acrylamide, obtained from American Cyanamide, was recrystallized from acetone and was dried in the same manner as propionamide. The observed melting point was 83.0–83.5°.

Labeled propionamide- d_7 was obtained from Volk Radiochemical Co., Skokie, Ill., with an isotopic content, specified by the supplier, of 98.14 atom % deuterium.

Sample Preparation and Irradiation. The solid solutions were prepared by weighing the two components in the required proportions, melting them together in a 90° bath and then cooling the melt quickly in a liquid nitrogen bath. It was previously shown^{3b} by X-ray diffraction that mixtures prepared in this fashion formed true solid solutions over the complete composition range.

All samples were degassed on a vacuum manifold for 48 hr. at 10^{-5} mm. and the irradiations performed in the Co^{60} γ -pool at Brookhaven National Laboratory. Irradiation dosimetry was done with Fricke dosimeters.

Analysis. Total gas analyses were made using a modified Saunders-Taylor apparatus and a conven-

(1) (a) This work was performed under contract for the U.S.A.E.C.; (b) This paper is based on a thesis submitted to New York University by R. Ranganathan in partial fulfillment of the requirements for a Ph.D. degree.

(2) B. Baysal, G. Adler, D. Ballantine, and A. Glines, *Polymer Letters*, **1**, 257 (1962).

(3) (a) T. Fadner, I. Rubin, and H. Morawetz, *J. Polymer Sci.*, **37**, 549 (1959); (b) T. Fadner and H. Morawetz, *ibid.*, **45**, 475 (1960).

(4) G. Adler, *ibid.*, in press.

(5) (a) J. P. Manion and M. Burton, *J. Phys. Chem.*, **56**, 560 (1952); (b) M. Burton and W. N. Patrick, *ibid.*, **58**, 421 (1954); (c) M. Burton and S. Lipsky, *ibid.*, **61**, 1461 (1957).

(6) F. Dainton, *et al.*, *Discussions Faraday Soc.*, **36**, 153 (1963).

tional gas-measuring vacuum manifold. The gases which were noncondensable at -196° were collected immediately after opening the irradiated sample to the gas-measuring system. The sample was then melted to ensure removal of any trapped gases and a collection of the noncondensable gases at -196° repeated. Only these -196° noncondensable gases were analyzed completely and were composed mainly of hydrogen, methane, and carbon monoxide.

The sample was then warmed to room temperature and again noncondensable gases were collected.

Gas analysis on the separated fractions was done using a Consolidated mass spectrometer and/or by gas chromatography using a Perkin-Elmer gas chromatograph with a modified silica packing (Perkin-Elmer Column S).

Experimental Results. The yields of hydrogen and carbon monoxide *vs.* dose for 100% propionamide are given in Fig. 1 where it is seen that the yields of both gases are linear over the entire dose range. The yield of hydrogen from 100% acrylamide is also linear in Fig. 2,

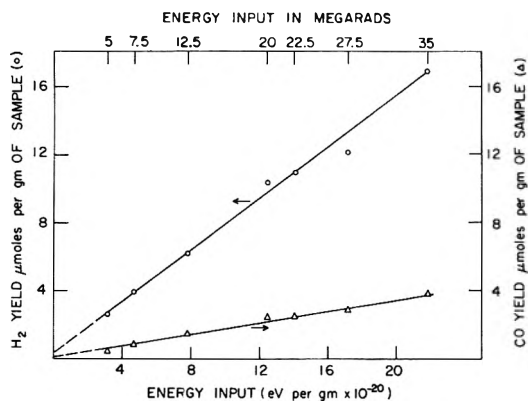


Figure 1. Product yields as a function of total energy input from γ -irradiation of pure propionamide.

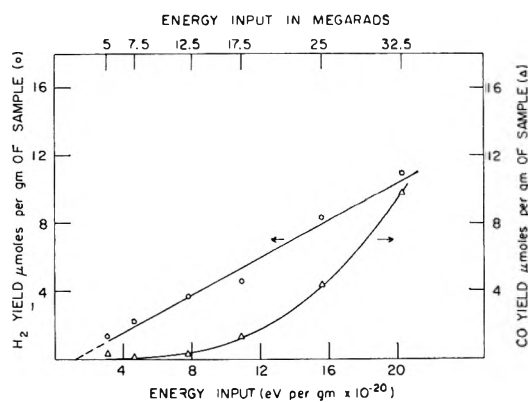


Figure 2. Product yields as a function of total energy input from γ -irradiation of solid solution of composition 50% propionamide, 50% acrylamide.

but the yield is an order of magnitude lower. The carbon monoxide observed in the radiolysis of pure acrylamide was very low, G_{CO} 0.001. For intermediate solid solution composition the yield of hydrogen was always linear with dose, and the slope decreased with increasing acrylamide content.

The yield for CO *vs.* dose was not linear for a solid solution containing greater than 25% acrylamide as seen in Fig. 3 for a 50-50 mole % composition. One can only determine then differential G or an overall G -value for CO. The yields of CO at several doses over a range of composition are shown in Fig. 3.

The data on G -value for H₂, CO, and CH₄ for pure propionamide and acrylamide as a function of temperature are shown in Fig. 4 and 5. It is readily seen that G for H₂ and CH₄ from pure propionamide is independent of temperature from -176° to about 60° while

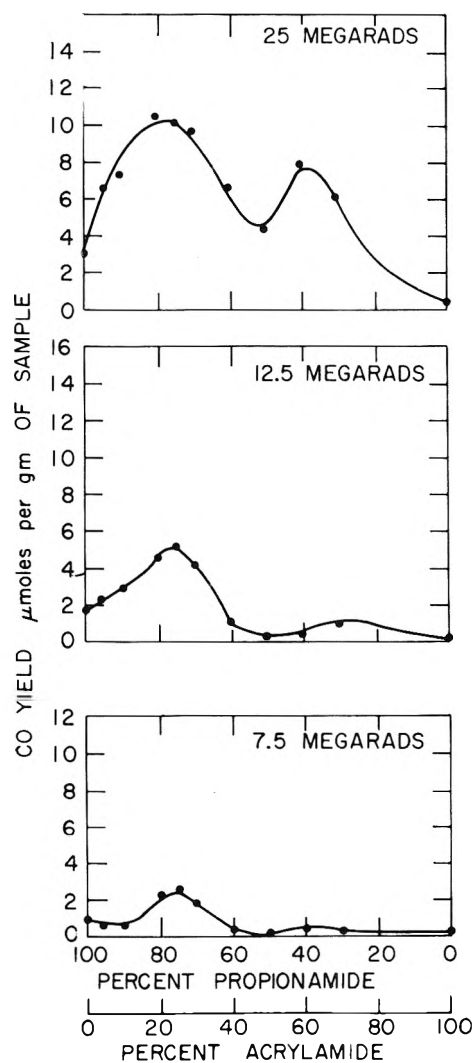


Figure 3. Comparison of CO yields as a function of composition of solid solution.

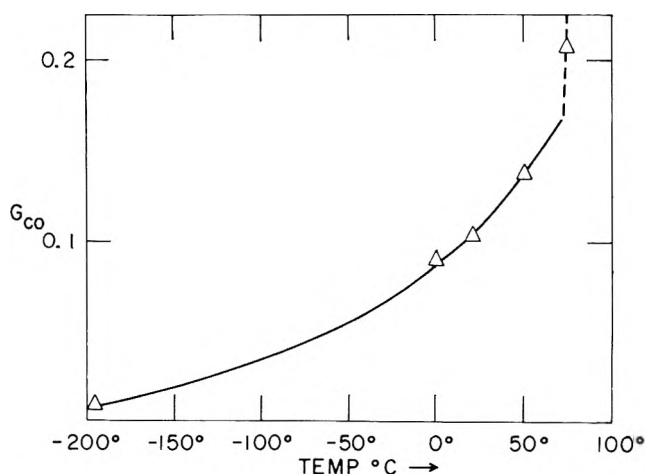
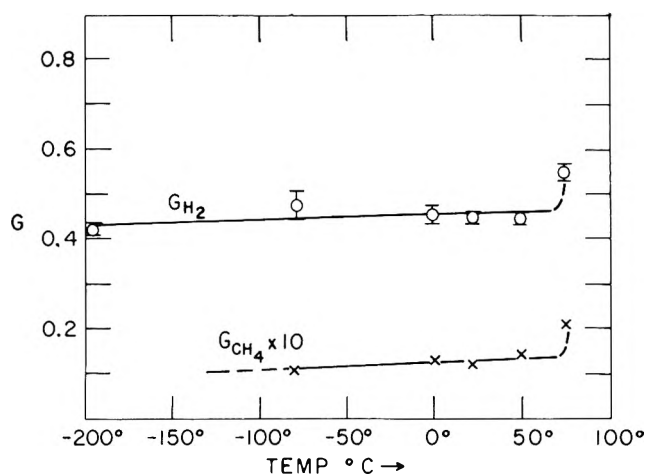


Figure 4. Top: product yields as a function of irradiation temperature of propionamide. Bottom: carbon monoxide yield as a function of irradiation temperature of propionamide.

G_{CO} shows an activation energy which is about 2 kcal./mole based on an Arrhenius plot of the available data.

The data from irradiation of mixtures of propionamide- d_7 and propionamide are given in Table I. Using the argument of Dyne⁷ to differentiate a unimolecular from a bimolecular reaction leading to hydrogen formation the data in Table I were plotted in Fig. 6. The intercept gives the $G_{D_2}(\text{uni})$ and in this instance is equal to about 0.02. A conservative estimate of $G_{H_2}(\text{uni})$ would appear to be $G_{H_2}(\text{uni}) = 0.08$. Comparison of $G_{H_2}(\text{uni}) = 0.08$ with the observed $G_{H_2}(\text{total})$ for propionamide of $G = 0.44$ indicates that the hydrogen is formed principally by a bimolecular process.

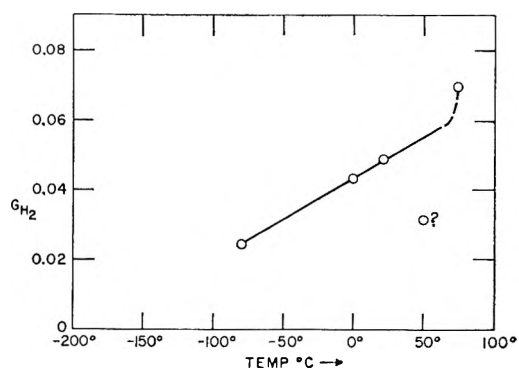


Figure 5. Hydrogen yield as a function of irradiation temperature of acrylamide.

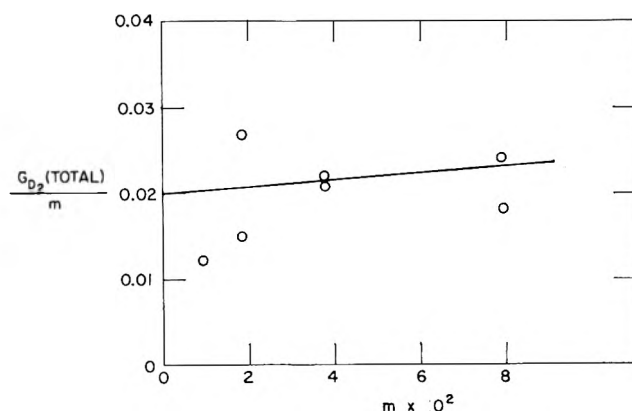


Figure 6. Plot of data in Table I.

Discussion

Any explanation of the yields of the various products should take into account conditions peculiar to the solid state. Factors of molecular size of products and lattice dimensions may affect diffusion and recombination reactions in a manner different from the liquid or gaseous state. The small size of the hydrogen molecule will cause it to be least affected and so it will be considered first.

Figure 7 shows the variation of G_{H_2} with composition at two temperatures, 22 and -78° . It is at once apparent that for intermediate compositions of propionamide and acrylamide G_{H_2} is not a simple average value given by the mixture rule for two components A and B and represented by the solid straight line in Fig. 7.

$$G_{H_2}(\text{mixture}) = G_{H_2}(A) \times \text{electron fraction of A} + G_{H_2}(B) \times \text{electron fraction of B}$$

Curve B gives the results at -73° and is typical of observations made in many two-component liquid systems. The acrylamide component is providing a

(7) P. J. Dyne and W. M. Jenkins, *Can. J. Chem.*, **38**, 539 (1960).

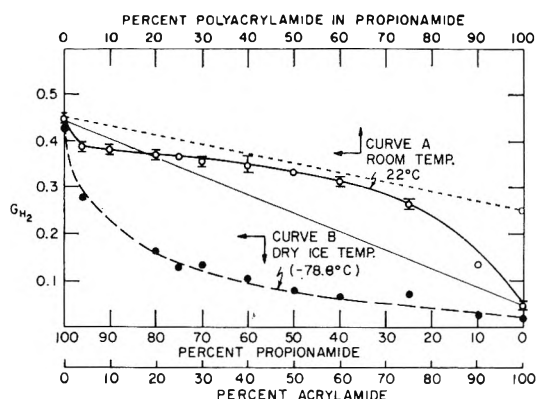


Figure 7. Hydrogen yield as a function of composition of solid solution of propionamide-acrylamide.

Table I: Analysis of Total Hydrogen Yield from the Solid Solutions of Propionamide- d_7 and Propionamide, γ -Irradiation (22°) at 12.5 Mrads

Concentration of propionamide- d_7 , wt. %	Mole %		
	H ₂	HD	D ₂
1	99.06	0.88	0.06
	99.21	0.77	0.02
2	98.46	1.44	0.10
	98.60	1.35	0.05
4	97.17	2.66	0.17
	97.15	2.70	0.15
8	94.49	5.19	0.32
	94.37	5.27	0.36

Mole % RD	$m \times 10^3$	G_{H_2}	% D ₂	$G_{D_2} \times 10^3$	G_{D_2}/m
0.913	0.921	0.63	0.06	0.378	0.041 ^a
		0.54	0.02	0.108	0.012
1.83	1.86	0.495	0.10	0.495	0.027
		0.557	0.05	0.279	0.015
3.66	3.80	0.490	0.17	0.833	0.022
		0.523	0.15	0.785	0.021
7.35	7.93	0.44	0.32	1.41	0.018
		0.523	0.36	1.88	0.024

^a Not included in Fig. 6 since the basis of collection of gas in this instance was different from the rest.

protective effect and such behavior can be explained by a mechanism in which hydrogen is scavenged by an unsaturated component, in this case acrylamide.

Curve B can also be explained by what is generally called energy transfer. This transfer may involve either a transfer of ionization or excitation energy to

acrylamide which has the ability to dissipate the energy without generation of hydrogen.

Curve A which gives the variation of G_{H_2} at room temperature is much more complex and difficult to interpret. At room temperature it is necessary to include consideration of G_{H_2} from polyacrylamide since acrylamide can be converted to a polymer under the conditions employed. It has been shown that at this temperature polymerization of the acrylamide approaches completion at doses below 5 Mrads at all compositions containing greater than 10% acrylamide.

The G_{H_2} (polyacrylamide) can be determined in two ways and the value obtained depends on the method employed. It has been noted earlier that the yield from acrylamide is linear to a dose of 25 Mrads. Since it has been shown under similar irradiation temperatures that acrylamide is "essentially completely" polymerized at less than 3 Mrads, one could conclude that G_{H_2} (polyacrylamide) is the same as G_{H_2} (acrylamide), namely $G_{H_2} = 0.047$. This would account for the linear relationship of yield of H₂ vs. dose which was determined experimentally. Alternatively, the G_{H_2} polyacrylamide was determined by irradiation of polymer which had been separated from irradiated acrylamide samples by a selective solvent technique. The G_{H_2} from polyacrylamide prepared in this fashion was 0.24 or almost five times greater than that obtained from unseparated polymer.

It is believed that in the situation where acrylamide crystals are irradiated continuously beyond the point where polymerization approaches completion a trace amount of monomer becomes trapped among growing polymer molecules and remains unreacted. It is possible that these isolated molecules can act as efficient energy transfer agents or scavengers. Effectively, then, the remaining trace of acrylamide acts as a protective agent for the polyacrylamide which is formed. Such an explanation also would account for the higher G_{H_2} from polymer which has been washed with a solvent that can dissolve monomer.

Curve A is best considered in comparison to a calculated G_{H_2} curve based on G_{H_2} from pure propionamide and G_{H_2} from precipitated polyacrylamide. Such a calculated curve appears as the dashed line in Fig. 7. All deviations from this calculated line are negative and can be interpreted at all compositions in terms of an energy transfer from either propionamide or polyacrylamide to acrylamide molecules or by hydrogen scavenging by acrylamide.

The temperature dependence of G_{H_2} from pure propionamide and acrylamide is shown in Fig. 4 and 5. The temperature dependence is small for acrylamide, an activation energy of ~ 1 kcal./mole and zero for

propionamide. The absence of any appreciable temperature effect is often cited as evidence for hot hydrogen atoms as the reactive intermediates.

However, if hot atoms are involved in the formation of hydrogen it is difficult to invoke an efficient hydrogen scavenging by acrylamide to account for reduced G_{H} in the mixed solutions. This result considered alone would tend to favor energy transfer as the reaction which is responsible for the protective role of acrylamide.

The interpretation of the data for the other radiolysis products which were identified is more complex. These products, CH_4 , C_2H_6 , and CO , are of greater physical size and their ability to diffuse through the cage formed by the lattice is less than that of hydrogen. Reactions involving them would be expected to be influenced to a greater degree by the physical domain in which they originate.

If one considers the formation of methane, two facts are observed. As the data in Fig. 4 indicate, the formation of methane from propionamide is one of low yield and also uninfluenced by temperature from -78° to temperatures close to the melting point. The other fact is that in compositions containing greater than 40% acrylamide no methane is found while below 30% acrylamide the G_{CH_4} is relatively constant.

The reason for the abrupt change in G_{CH_4} with composition may lie in difference in lattice dimensions. In propionamide, acrylamide, and their solid solutions the molecules are bound together as sheets by hydrogen bonding through the amide groups. These sheets have the hydrocarbon part of the molecules outermost. The sheets are stacked to form the crystal structure.

Other than chemical saturation the principal difference between acrylamide and propionamide crystals is that the distance between sheets is 11% greater in the propionamide.⁸ In solid solutions, of course, the average distance is intermediate. It is believed that the larger intersheet distance of propionamide permits freer diffusion along the planes formed by the hydrocarbon portion of the molecules.

In the event of bond rupture to produce a CH_3 radical the cage in the case of pure propionamide would thus be significantly looser and any prompt recombination reaction would be reduced. In combinations containing greater than 40% acrylamide the mobility of methyl radicals appears to be so reduced because of a sufficiently tight cage that the formation of methane is prevented almost completely.

This difference in the intermolecular distances of acrylamide and propionamide has also been used to explain⁸ the inhibition by oxygen of polymerization of acrylamide in mixed crystals containing greater

than 60% propionamide. Here it is suggested that oxygen could not inhibit polymerization in pure acrylamide crystals because of its inability to diffuse into the lattice. However, introduction of propionamide sufficiently increased the intermolecular space to permit oxygen diffusion and hence inhibition. Analogous effects of oxygen on e.s.r. signals decays were observed in the acrylamide-propionamide system for similar reasons.

If one considers the change of G_{CH} with composition, it follows a different behavior from G_{H} , and the behavior is difficult to reconcile with an energy transfer process. If energy is indeed transferred from propionamide to acrylamide, the G_{CH} should be expected to follow a pattern similar to that of G_{H} .

When one considers the G_{CO} yields vs. composition the picture becomes very confused. At compositions of greater than 75% propionamide the yield of CO vs. dose is linear but with compositions of less than 75% propionamide the yield vs. dose is nonlinear. With pure acrylamide the CO yield is linear but the G_{CO} is only 0.001.

In Fig. 3 the CO yield for various compositions is shown at several dose levels and a strange result is observed. There are found two distinct maximums in these curves at concentrations of about 75 and 40% propionamide. It is difficult to relate this to any energy transfer process. In fact, at this point no good explanation exists although in very vague terms it is believed to be related to some critical changes in the average distance between hydrocarbon chains in the lattice.

Little is known about the $G_{\text{C}_2\text{H}_6}$ at this time except that in pure propionamide the $G_{\text{C}_2\text{H}_6}$ can be as great as 0.3. The fact that this is more than an order of magnitude greater than the G_{CH} , indicates that the carbon-carbon bond α to the amide group is preferentially scissioned. This result is analogous to those early studies of Breger⁹ on fatty acids and work on the photolysis of amides.¹⁰

Allen and Rao¹¹ found acetonitrile in reasonably high yield in studies of the radiolysis of acetamidol. No nitriles were found in this work but the analytical techniques were not sufficiently extensive or complete to rule out their formation.

(8) G. Adler, Proceedings of the International Symposium of the Radiation Industry, Polymerization and Graft Copolymerization, TID 7643, 127 (1962).

(9) I. A. Breger and V. L. Burton, *J. Am. Chem. Soc.*, **68**, 1629 (1946).

(10) G. H. Booth and R. G. Norrish, *J. Chem. Soc.*, 188 (1952).

(11) A. O. Allen and K. N. Rao, BNL Annual Report 40, July 1, 1960.

The radiolysis of solid solutions of acrylamide and propionamide yields gaseous products which are mainly H₂, CO, CH₄, and C₂H₆. The yields of hydrogen can be interpreted on the basis of efficient energy transfer from propionamide to acrylamide or by a protective scavenging of hydrogen atoms by the acrylamide

double bonds. At any rate, a protective effect similar to that shown in many liquid mixtures can exist in truly crystalline solids. The yields of the other gaseous products are not explainable by energy transfer or scavenging alone and differences in lattice dimensions are believed to play a significant role.

Radiolysis of Cyclohexane. V.

Purified Liquid Cyclohexane and Solutions of Additives¹

by S. K. Ho and G. R. Freeman

Department of Chemistry, University of Alberta, Edmonton, Alberta, Canada
(Received February 29, 1964)

The initial product yields (G values) in the γ -radiolysis of highly purified liquid cyclohexane have been found to be: hydrogen 5.6 ± 0.1 ; cyclohexene 3.2 ± 0.2 ; 1-hexene 0.40 ± 0.05 ; n -hexane 0.08 ± 0.02 ; methylcyclopentane 0.15 ± 0.01 ; ethylcyclohexane ~ 0.04 ; dicyclohexyl 1.76 ± 0.05 ; cyclohexylhexene 0.12 ± 0.02 ; unidentified C₁₂ ~ 0.05 . Cyclohexylcyclohexene was a secondary product. Both oxygen and p -benzoquinone reduced the major liquid product yields to the same limiting values: cyclohexene 1.5 ± 0.1 ; 1-hexene 0.27 ± 0.03 ; dicyclohexyl 0.29 ± 0.03 . From the reduction in the yields of these products, and on the assumption that free radicals were being scavenged by the additives, a lower limit of 1.1 ± 0.3 was obtained for the ratio of the rate constants $k_{\text{disproportionation}}/k_{\text{combination}}$ for cyclohexyl radicals in liquid cyclohexane.

Introduction

In the radiolysis of liquid cyclohexane, there is as yet no general agreement on the initial yields of the various products,^{2a-6} and reports on the nature and yields of some of the minor products are in conflict.^{2,4-7} Only Dyne and Stone⁴ have reported a good balance between hydrogen and hydrogen-deficient products.

As the first part of an investigation of track reactions in liquid cyclohexane by the study of the effect of L.E.T. on the distribution of products in solutions of various additives, the present work deals with the product yields of γ -radiolysis with oxygen and p -benzoquinone as scavengers. Because of the conflicting results reported for oxygen^{2a,8} and the different behavior of

benzoquinone as a scavenger as compared with that of oxygen,⁶ re-examination of these systems should be useful. In view of the discrepancy of results in the literature, the system of pure cyclohexane has also been

(1) The research for this paper was supported in part by The Defence Research Board of Canada, Grant No. 1601-17.

(2) (a) H. A. Dewhurst, *J. Phys. Chem.*, **63**, 813 (1959); (b) G. R. Freeman, *J. Chem. Phys.*, **33**, 71 (1960).

(3) T. D. Nevitt and L. P. Remsberg, *J. Phys. Chem.*, **64**, 969 (1960).

(4) P. J. Dyne and J. A. Stone, *Can. J. Chem.*, **39**, 2381 (1961).

(5) J. W. Falconer and M. Burton, *J. Phys. Chem.*, **67**, 1743 (1963).

(6) E. S. Waight and P. Walker, *J. Chem. Soc.*, 2225 (1960).

(7) A. C. Nixon and R. E. Thorpe, *J. Chem. Phys.*, **28**, 1004 (1958).

(8) G. Dobson and G. Hughes, *Proc. Chem. Soc.*, 109 (1963).

reinvestigated. It was suspected that the disagreement in yields might have been due to impurities present in the cyclohexane used by various workers, although cyclohexane of three different grades have been reported to give the same product yields at relatively high doses.^{2a} Special attention has therefore been paid to the purification of cyclohexane. Highly purified cyclohexane was also required in the determination of the yields of the minor products, which otherwise would have been masked by the impurities.

Experimental

Cyclohexane. Phillips Research Grade cyclohexane contained traces of cyclohexene and benzene (totaling about 0.07%), as well as other impurities which appeared as three small peaks before the cyclohexane peak on a 2.5-m. 40% (w./w.) tricresyl phosphate (TCP) column, and gave a lower hydrogen yield than did a purified sample (see later). Prolonged shaking with concentrated sulfuric acid removed only cyclohexene. The cyclohexane was therefore purified as follows: it was shaken with a 1 : 20 mixture of fuming sulfuric acid and concentrated sulfuric acid, which reacted with both cyclohexene and benzene, for 30 hr. with renewal of the acid mixture every 5 hr.; it was then washed with dilute sodium hydroxide and then with water; it was dried over several batches of magnesium sulfate then fractionally distilled. The remaining impurities, apparently saturated hydrocarbons, did not affect the major product yields but interfered with the gas chromatographic analysis of the minor C₆ products. The cyclohexane was therefore further purified by gas chromatography, using a 6-m. column of 40% TCP on firebrick. The collected cyclohexane was dried and fractionally distilled as before. The distillate contained less than 10⁻⁶ mole fraction of any impurity and was used in most of the experiments. In some experiments, the gas chromatographic purification was omitted.

Other Materials. The following were used as additives: oxygen (Canadian Liquid Air) and *p*-benzoquinone (Fisher Reagent Resublimed Grade, which was sublimed before use).

The following were used as gas chromatographic standards: Phillips Research Grade *n*-hexane, methylcyclopentane, and 1-hexene: Aldrich dicyclohexyl; Frinton cyclohexylcyclohexene. Phillips Research Grade cyclohexene contained up to 20% nonvolatile residue, depending on the length of exposure of the sample to air; thus, it was fractionally distilled in a stream of nitrogen immediately before use. After treatment with anhydrous calcium chloride to remove cyclohexanol, cyclohexanone (Matheson Coleman and

Bell) was distilled at reduced pressure in nitrogen immediately before use. After shaking with sodium hydroxide solution to remove phenol, cyclohexanol (Fisher Reagent Grade) was extracted from the hydroxide solution with ether and was distilled at reduced pressure in nitrogen.

Irradiation. Two-milliliter samples, degassed by the freeze-pump-thaw technique and sealed in 4-ml. Pyrex tubes equipped with break-seals, were irradiated at 23 ± 2° with Co⁶⁰ γ -rays. The dose rates, determined with the Fricke dosimeter and using $G(\text{Fe}^{3+}) = 15.6$ and $\epsilon(\text{Fe}^{3+}, 304 \text{ m}\mu, 25^\circ) = 2201$,⁹ were in the region of 5×10^{18} e.v./hr. per ml. of cyclohexane.

Product Analysis. The gaseous products that were volatile at -196° were collected in a calibrated McLeod-Toepler apparatus and their composition analyzed gas chromatographically with a charcoal column on a Burrell Kromo-Tog K7 with a hydrogen flame detector.¹⁰ Other gaseous products were not analyzed.

The liquid products were analyzed on a Burrell Kromo-Tog K2 with a thermal conductivity detector. The following 2.5-m. U-shaped columns were used, with 30/60 mesh firebrick as support where necessary. Burrell medium activity silica gel, 40% TCP, 10% silicone oil DC-710, 5% silicone grease, and 10% Ucon 75H-1400. All columns were temperature programmed except the TCP, which was used at 100°. The C₆ products were analyzed on the TCP and silica gel columns, C₁₂ products on all the columns except TCP, and oxygenated products on the Ucon column. A 10% Carbowax 4000 column was also used for identification purposes. Whenever possible, more than one column was used for the analysis of each product. Calibration curves from standard samples were determined with each series of analyses. These changed only slightly from one series to another. Dicyclohexyl was used as the standard for all the C₁₂ products, since cyclohexylcyclohexene was not available and the cyclohexylcyclohexene, being not sufficiently pure, could only serve for identification purposes.

Total peroxides found in the cyclohexane-oxygen system were analyzed by the arsenious oxide-iodine method.¹¹ This involved reacting the peroxides on a steam bath with a definite, excess volume of standard arsenious oxide solution, sufficient ethyl alcohol being added to give one homogeneous phase. When most of the alcohol had evaporated, water was added and the solution was again boiled. This was repeated four

(9) A. O. Allen, "The Radiation Chemistry of Water and Aqueous Solutions," D. Van Nostrand Co., Toronto, 1961.

(10) The authors were indebted to Mr. W. J. Holtzlander for this analysis.

(11) S. Siggia, *Ind. Eng. Chem., Anal. Ed.*, 19, 872 (1947).

times to expel all the alcohol and volatile organic matter. After acidification with dilute sulfuric acid and addition of about 0.5 g. of sodium bicarbonate, the excess arsenious oxide in the cold solution was titrated with standardized iodine solution. The "dead stop" method,¹² being more sensitive than starch, was used for location of the end point. Blanks were determined and found to be negligible.

The ferrous thiocyanate method¹³ for the determination of peroxides was found to be unsatisfactory in that it gave very high results, even with a sample of hydrogen peroxide.

Results

Pure Cyclohexane. The gaseous products that were volatile at -196° consisted of hydrogen with about 0.1% of methane. Figure 1 shows the variation of the G value (number of molecules formed per 100 e.v. absorbed by the system) of hydrogen with dose, for highly purified cyclohexane. Extrapolation to zero dose gives an initial value, G_i , of 5.6 ± 0.1 . The reported uncertainty of $\pm 0.1 G$ unit attempts to take into consideration all sources of experimental error. Results obtained with less pure cyclohexane are also shown in Fig. 1. Unpurified Eastman Spectrograde cyclohexane, which contained at least three impurities (total 0.5%) but no detectable cyclohexene or benzene, gave essentially the same hydrogen yield as the highly purified cyclohexane. Unpurified Phillips Research Grade cyclohexane and the purified material to which

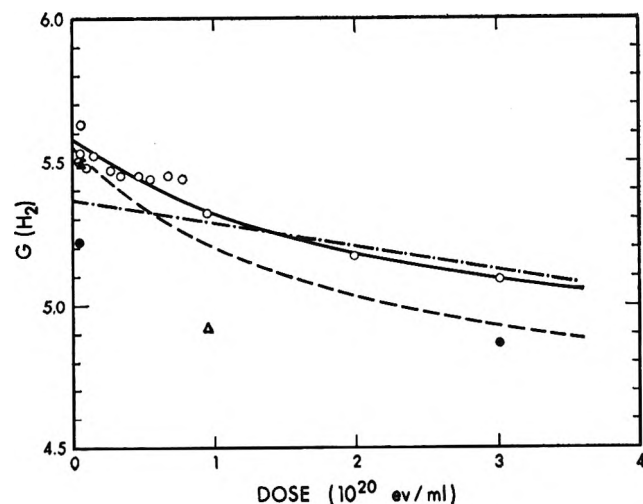


Figure 1. The variation of $G(\text{H}_2)$ with dose: \circ , Phillips Research Grade cyclohexane, highly purified; \bullet , Phillips Research Grade cyclohexane, unpurified; \blacktriangle , Eastman Spectrograde cyclohexane, unpurified; \triangle , Phillips Research Grade cyclohexane, highly purified with 0.1% cyclohexene added; - - -, results of Dyne and Stone⁴; - · -, results of Freeman.^{2b}

0.1% of cyclohexene had been added gave lower yields. The value of $G(\text{CH}_4)$ from the highly purified cyclohexane was about 0.006.

The dose dependences of the yields of cyclohexene and dicyclohexyl, as obtained with different analytical columns, are shown in Fig. 2. Each point on the cyclohexene curve represents the average of the values obtained from the TCP and silica gel columns, because the results from these two columns were in agreement with each other. The initial G value for cyclohexene is 3.2 ± 0.2 . The listed uncertainty attempts to take into consideration all sources of experimental error.

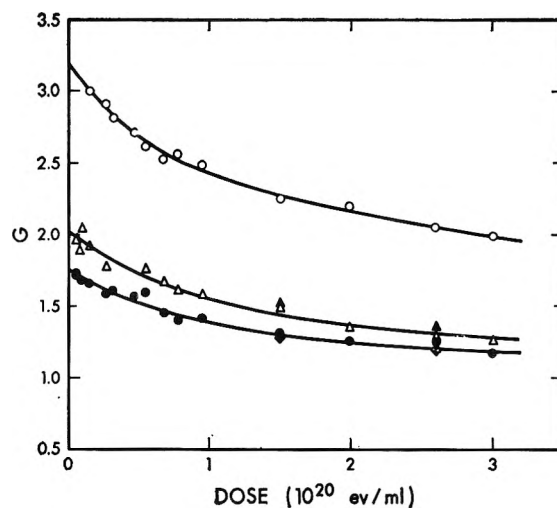


Figure 2. The variation of $G(\text{cyclohexene})$ and $G(\text{dicyclohexyl})$ with dose: cyclohexene, \circ ; dicyclohexyl, columns: \bullet , silicone oil; Δ , silica gel; \blacklozenge , Ucon; \blacktriangle , silicone grease.

While the chromatograms of the products in the C_{12} region show two peaks on both the silical gel (only one measurable peak at doses smaller than 2×10^{20} e.v. ml^{-1}) and silicone grease columns, those on the silicone oil and Ucon columns show three and four measurable peaks, respectively (two of the Ucon peaks are not well resolved). Thus, there are at least four C_{12} products, dicyclohexyl, cyclohexylhexene (identified by Dyne and Stone⁴), cyclohexylcyclohexene, and the other remains unidentified. It appears that the main C_{12} peak on both the silicone oil and Ucon columns measures dicyclohexyl only. But the peak on the silica gel column is the sum of dicyclohexyl, cyclohexylhexene, and possibly the unidentified C_{12} , and the peak on the silicone grease column is the sum of dicyclohexyl,

(12) C. W. Foulk and A. T. Bawden, *J. Am. Chem. Soc.*, **48**, 2045 (1926).

(13) C. D. Wagner, H. L. Clever, and E. D. Peters, *Ind. Eng. Chem., Anal. Ed.*, **19**, 980 (1947).

Table I: Initial Product Yields from Pure Cyclohexane

Product	This work	Reference			
		5	4 <i>G</i>	2b	2a
Hydrogen	5.6 ± 0.1	5.6	5.55	5.37	5.5
<i>n</i> -Hexane	0.08 ± 0.02
1-Hexene	0.40 ± 0.05	~0.2
Methylcyclopentane	0.15 ± 0.01	~0.3
Cyclohexene	3.2 ± 0.2	3.02	3.27	2.28	2.5
Ethylcyclohexane	~0.04
Cyclohexylhexene	0.12 ± 0.02	...	0.27	0.23	...
Dicyclohexyl	1.76 ± 0.05	1.67	1.95	1.24	2.0
Cyclohexylcyclohexene	0	~0.07	0	0.1-0.2?	...
Unidentified C ₁₂	~0.05	~0.2
Other	...	~0.3	...	~0.1 ^a	~0.3 ^b
Dose rate (10 ¹⁸ e.v./ml. hr.)	5	23	29	0.7	4 × 10 ⁴
Minimum dose (10 ¹⁹ e.v./ml.) for liquid analysis	1	1	1	4	100

^a C₉. ^b Intermediate cyclohexanes.

Table II: Limiting Yields in the Presence of Oxygen (*G* Values)

Product	This work	Reference			
		8	2a	16	21
<i>n</i> -Hexane	<0.01
1-Hexene	0.26 ± 0.02
Methylcyclopentane	~0.03
Cyclohexene	1.49 ± 0.10	0.38	0.7	...	1.14
Ethylcyclohexane	<0.01
Cyclohexylhexene	~0.03
Dicyclohexyl	0.29 ± 0.03	...	<0.1	...	0.3
Cyclohexylcyclohexene	~0.01
Cyclohexanone	2.63	2.1	3.5	0.6 ^a	2.28
Cyclohexanol	3.17	...	3.7	...	2.40
Peroxides	0.61	1.2 ^b	1.1
				1.0 ^c	
				0.2 ^d	
Other	0.2 ^e	0 ^e
				1.8 ^f	
Dose rate (10 ¹⁸ e.v./ml. hr.)	5	?	4 × 10 ⁴	360	>10 ⁶
Approximate minimum dose (10 ¹⁹ e.v./ml.)	2	?	100	20	200

^a Carbonyl. ^b Total peroxide. ^c Hydroperoxide. ^d Dialkyl peroxide. ^e Acid. ^f Water.

cyclohexylcyclohexene, and possibly the unidentified C₁₂. The *G* values calculated for the different C₁₂ products seem to agree with this deduction. The initial *G* value for the composite C₁₂ peak on silica gel is 2.0 ± 0.1, whereas that for dicyclohexyl on the silicone oil column is 1.76 ± 0.05.

Figure 3 gives the yields of the minor products. All the C₆ hydrocarbons, as determined with the TCP column, appear to be primary products. The yield of

1-hexene tends to decrease with increasing dose. The results for cyclohexylhexene obtained from three different columns appear again in two sets, with the yield derived from the silicone oil column being approximately the sum of the two unresolved Ucon peaks, one of which was assigned to cyclohexylhexene. By the arguments above, the lower value of 0.12 was taken for *G*(cyclohexylhexene). It is clear from its dependence on dose that cyclohexylcyclohexene is a secondary

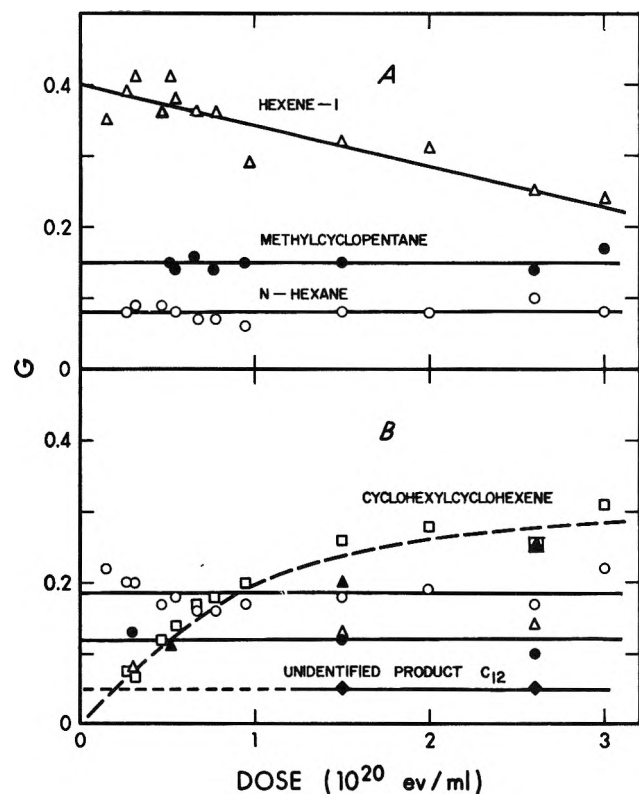


Figure 3. Yields of minor products as a function of dose. (A) C_6 : *n*-hexane, O; methylcyclopentane, ●; 1-hexene, Δ. (B) C_{12} : cyclohexylhexene, columns: O, silicone oil; ●, Ucon; Δ, silicone grease. Cyclohexylcyclohexene, columns: □, silicone oil; ▲, Ucon. Unidentified product (Ucon), ◆.

product. This is supported by the fact that the yield was greatly increased by adding 0.1% of cyclohexene to the cyclohexane before irradiation.

Ethylcyclohexane was detectable on all the columns except TCP, with a yield of approximately 0.04, apparently not much affected by dose. The product yields are summarized in Table I.

Solutions of Additives. The effect of oxygen on the liquid product yields is shown in Fig. 4. These appeared to be independent of oxygen pressures greater than about 100 mm. and are listed in Table II. Dose appears to have very little effect on the yields of the four main products (Fig. 5).

No hydrogen peroxide could be detected in the irradiated solutions with titanium reagent,¹⁴ and tests for hydroperoxides¹⁵ were inconclusive. The yield of total peroxide was independent of oxygen pressures greater than about 100 mm., and the concentration of peroxide increased linearly with dose (Fig. 6). The peroxide plot, however, does not pass through the origin, even though doses down to 1.5×10^{17} e.v. ml.⁻¹ were used. When calculated from the slope of the line,

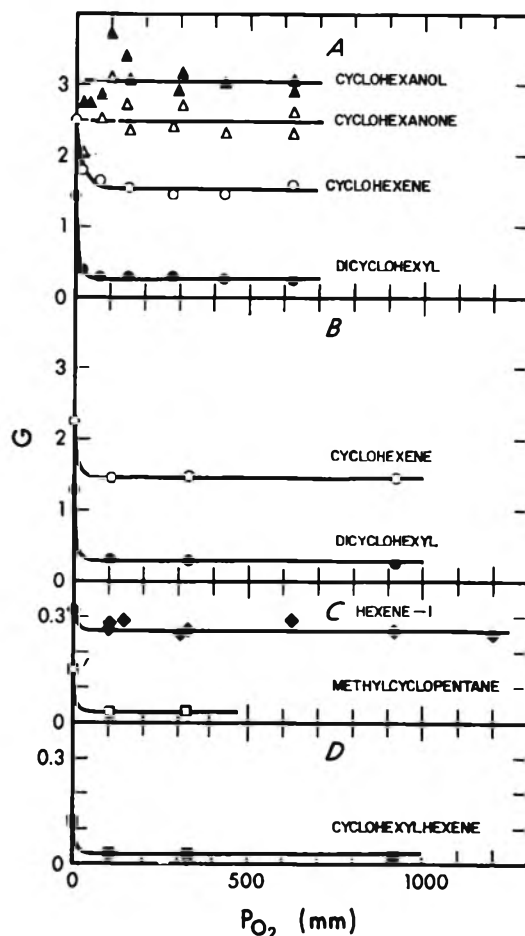


Figure 4. Effect of oxygen on product yields. (A) Dose = 9.5×10^{19} e.v. ml.⁻¹. (B, C, D) Dose = 1.50×10^{20} e.v. ml.⁻¹: ▲, cyclohexanol; Δ, cyclohexanone; O, cyclohexene; ●, dicyclohexyl; ◆, 1-hexene; □, methylcyclopentane; ■, cyclohexylhexene.

by the method of least squares, $G(\text{peroxides})$ equals 0.61. It may be mentioned in this connection that linear extrapolation (least squares) of the data of Bakh^{16a} also shows a similar positive intercept (Fig. 6).

Benzoquinone solutions produce, on irradiation, a green precipitate identified as quinhydrone.⁶ The effects of benzoquinone on the product yields are shown in Fig. 7. The cyclohexane product yields were reduced, with yields of liquid products apparently reaching a limit at a benzoquinone concentration of about 1×10^{-2} M. Table III gives the limiting yields of those products that were detectable.

(14) H. Pobiner, *Anal. Chem.*, **33**, 1423 (1961).

(15) W. C. Wolfe, *ibid.*, **34**, 1329 (1962).

(16) (a) N. A. Bakh, "Arbeiten über Strahlenchemie," Akademie-Verlag, Berlin, 1960, p. 167; (b) N. A. Bakh and N. I. Popow, *ibid.*, p. 180.

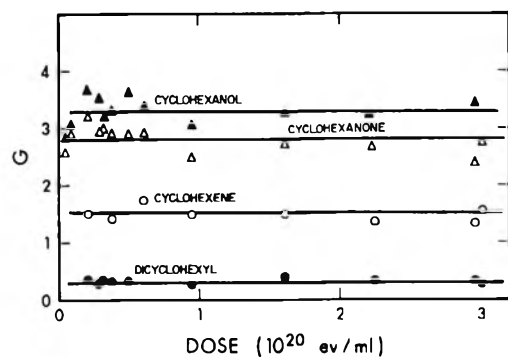


Figure 5. Product yields as a function of dose. Pressure of oxygen, approximately 140 mm. O, Cyclohexene; ●, dicyclohexyl; Δ, cyclohexanone; ▲, cyclohexanol.

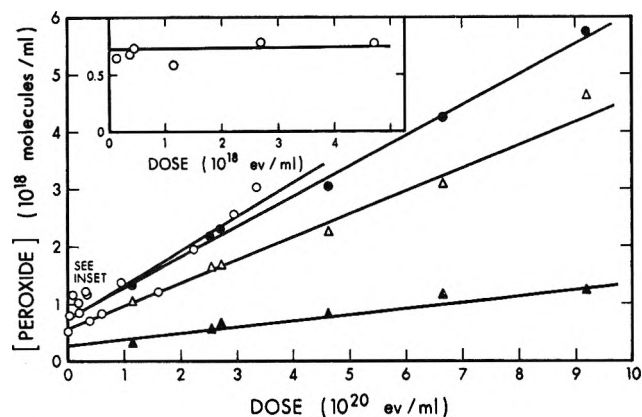


Figure 6. Formation of peroxides as a function of dose: O, total peroxide (present work); ●, total peroxide (Bakh^{16a}); Δ, alkyl hydroperoxide (Bakh^{16a}); ▲, dialkyl peroxide (Bakh^{16a}).

Table III: Limiting Yields in *p*-Benzoquinone Solutions (*G* Values)

Product	Reference	
	This work	6
1-Hexene	0.28 ± 0.02	...
Cyclohexene	1.54 ± 0.04	2.4
Dicyclohexyl	0.29 ± 0.02	~0.4
Dose rate (10 ¹⁶ e.v./ml. hr.)	5	3
Dose (10 ¹⁹ e.v./ml.)	10	60

Discussion

Product Yields in Pure Cyclohexane. Table I shows, in addition to the results of the present investigation, some reported initial yields in the radiolysis of pure cyclohexane. Two additional reported hydrogen yields are 5.27¹⁷ and 5.85.¹⁸ In attempting to account for such discrepancies, the results of the present work are compared with those of Dyne and Stone⁴ and of Free-

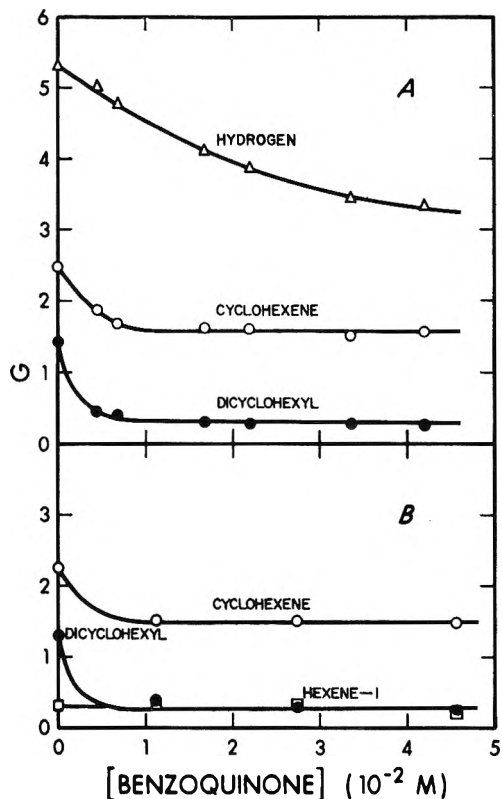


Figure 7. Effect of *p*-benzoquinone on product yields. (A) Dose = 9.5×10^{19} e.v. ml.⁻¹. (B) Dose = 1.50×10^{20} e.v. ml.⁻¹. Δ, Hydrogen; O, cyclohexene; ●, dicyclohexyl; □, 1-hexene.

man^{2b} (Fig. 1). The present results and those of Dyne and Stone show nearly equal initial *G* values. There is, however, discrepancy between the present results and those of Freeman at low doses, although good agreement is found at higher doses. At least two sources of error can be contemplated in the earlier work.^{2b} First, from the sharp increase in $G(\text{H}_2)$ with decreasing dose, it is obvious that a linear extrapolation is not justified, and a correct initial *G* value is obtainable only by working at low conversions. Secondly, there might have been an error in the calibration of the small volumes of the McLeod-Toepler combination. An investigation has shown that, for a 0.2-cc. volume, the error due to neglect of the "dead space" of the mercury meniscus could be as large as 2%. The amount of grease on a stopcock can also cause an error. Great care is therefore needed to be certain that the calibration and yield measurements involve exactly the same volumes.

(17) G. E. Adams, J. H. Baxendale, and R. D. Sedgwick, *J. Phys. Chem.*, **63**, 854 (1959).

(18) M. Burton, J. Chang, S. Lipsky, and M. P. Reddy, *Radiation Res.*, **8**, 203 (1958).

Stringent purification of cyclohexane has reduced $G(\text{CH}_4)$ from about 0.02^{2b} to about 0.006.

Agreement in the initial value of $G(\text{cyclohexene})$ among the more recent investigations is quite good. The reported low values of others are likely due to erroneous extrapolation to zero dose from results obtained at high doses. Possible dose rate effects cannot be ruled out at present.

As indicated in the Experimental section, different chromatographic columns give different results for C_{12} products. Our values of 1.76 and 0.12 for dicyclohexyl and cyclohexylhexene, respectively, are both lower than the values of 1.96 and 0.27 obtained by Dyne and Stone who used an Apiezon L grease column. We note that yields obtained by the silicone grease column appear to be composite and a similar situation might exist with the Apiezon L grease column.

Although the yields of cyclohexene and dicyclohexyl both decrease with dose to the extent of 30–40% over the range investigated, the ratio of their yields shows only a very slight decrease (about 6%) with dose (Fig. 8). This might suggest that most of the reduction in yields of cyclohexene and dicyclohexyl as radiolysis proceeds involves a precursor common to both products.

Cyclohexylcyclohexene has been described as a primary product^{5,6} and as a secondary product.^{4,19} We observed it as a secondary product, arising from the cyclohexene formed in the radiolysis.

From the initial yields of the liquid products, Dyne and Stone⁴ have calculated the hydrogen equivalent of 5.49 as compared with their $G_i(\text{H}_2)$ of 5.55. Our results, even on the assumption that the unidentified C_{12} product has a hydrogen equivalent of one unit per molecule, give only 5.03 (with limits of about ± 0.29), as compared with $G_i(\text{H}_2) = 5.6$. It seems almost certain that some other products, possibly with molecular weights higher than dicyclohexyl, have been missed. Recently, Roberts and Hamill reported $G(\text{HI}) \approx 0.4$ for the post-irradiation addition of iodine to cyclohexane, which indicates that some product has not yet been identified.²⁰

Product Yields in Solutions of Additives. The diversity of reported yields in the cyclohexane–oxygen system is evident from Table II. Our finding supports Dewhurst's observation^{2a} that $G(\text{cyclohexene})$ is independent of dose, but his yield of 0.7, determined both by infrared spectroscopy and gas chromatography, is to be contrasted with the value of 1.49 obtained in this work, which is also much greater than the value of 0.38 reported by Dobson and Hughes.⁸ The value of 1.14 obtained from pulse radiolysis²¹ also appears to be low. Any effect due to dose rate should give a bigger rather

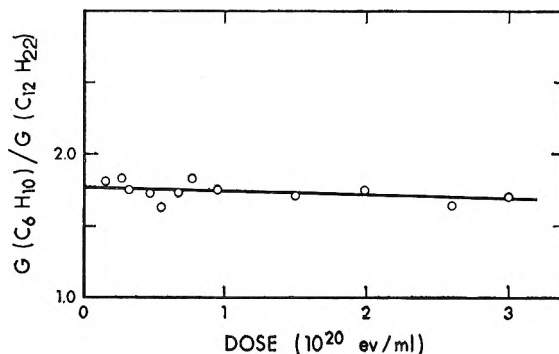


Figure 8. The variation of $G(\text{cyclohexene})/G(\text{dicyclohexyl})$ with dose, for pure cyclohexane.

than a smaller cyclohexene yield. However, if the irradiation set-up were such that an appreciable amount of ozone formed in the oxygen gas above the cyclohexane, the ozone would be absorbed by the solution and would react with the cyclohexene.

Our value of 0.3 for $G(\text{dicyclohexyl})$, also apparently independent of dose, agrees well with the value obtained by McCarthy and MacLachlan.²¹ The same yield has been reported for solutions saturated with iodine.^{2a}

The negligible yields, in the presence of oxygen, of the other hydrocarbon products, with the exception of 1-hexene, suggest their formation predominantly by free radical processes. 1-Hexene, on the other hand, appears to come largely from a non-scavengeable process such as an intramolecular isomerization.^{22,23}

The reported yields of cyclohexanol and cyclohexanone vary over quite a range, $G(\text{cyclohexanol})$ being usually found to be slightly greater than $G(\text{cyclohexanone})$.²⁴ The differences in the reported yields are probably due to differences in analytical techniques and to differences in conditions of irradiation. The method of analysis used in the present work was direct (cyclohexanone and cyclohexanol were separated gas chromatographically and pure standards were used to calibrate each compound) and low irradiation doses were used to minimize the occurrence of secondary reactions.

Bakh^{16a} obtained the G values shown in Table II for the various peroxides by drawing tangents at the origin of the product concentration *vs.* dose curves (the

(19) G. R. Freeman, *Can. J. Chem.*, **38**, 1043 (1960).

(20) J. Roberts and W. H. Hamill, *J. Phys. Chem.*, **67**, 2446 (1963).

(21) R. L. McCarthy and A. MacLachlan, *Trans. Faraday Soc.*, **57**, 1107 (1961).

(22) G. R. Freeman, *J. Chem. Phys.*, **36**, 1534 (1962).

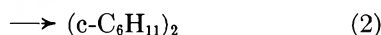
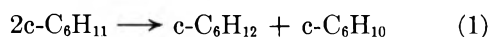
(23) A. Singh and G. R. Freeman, to be published.

(24) Dobson and Hughes have reported the contrary, ref. 8.

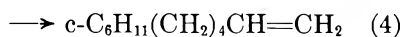
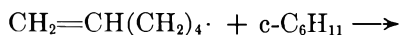
respective data are reproduced in Fig. 6). There is a close correspondence between Bakh's and the present results for total peroxide, with peroxide concentration increasing more or less linearly with dose. But clearly the lines do not pass through the origin, for reasons yet unknown. By taking the slopes of the lines, the data of Bakh would yield the following values: $G(\text{total peroxide}) = 0.53$, which is in good agreement with our value of 0.61; $G(\text{ROOH}) = 0.42$ and $G(\text{ROOR}') = 0.11$. Analyzing the peroxides by the acetic acid-potassium iodide method, McCarthy and MacLachlan²¹ have obtained a value of 1.1. This method was not used in this work because of the interference not only by cyclohexene²⁵ but also by reactions that occurred even in blanks.

Practically the same limiting yields of 1-hexene, cyclohexene, and dicyclohexyl were obtained with benzoquinone as with oxygen (Fig. 4 and 7). On the other hand, using vacuum ultraviolet spectroscopy, Waight and Walker⁶ found that the yield of cyclohexene was hardly affected by benzoquinone, while $G(\text{dicyclohexyl})$ was reduced. We are unable to account for the discrepancy, but it appears from our results that, on the whole, the effects of benzoquinone closely parallel those of oxygen.

$k_{\text{disproportionation}}/k_{\text{combination}}$ for Cyclohexyl Radicals. It has often been suggested that much of the cyclohexene and dicyclohexyl formed during the radiolysis of cyclohexane result from the reactions (where c denotes a cyclic compound)



To account for the formation of cyclohexylhexene, it has been suggested^{2b} that excited cyclohexyl radicals undergo C-C cleavage to form hexenyl radicals, which then react as follows



The disproportionation reaction alternative to (3), to form 1,5-hexadiene and cyclohexane, did not occur to an appreciable extent because 1,5-hexadiene was not observed in the reaction products.

The fact that the decrease in the yields of the liquid products caused by oxygen is nearly balanced by the production of alcohol, ketone, and peroxide suggests that the action of oxygen is to scavenge alkyl radicals. Since benzoquinone and oxygen reduce the yields of 1-hexene, cyclohexene, and dicyclohexyl to the same limit-

ing values, benzoquinone also apparently scavenges alkyl radicals.

If the reactions that are inhibited by the additives are reactions 1-4, then, from the decrease in the respective product yields, one can obtain an estimate of the value of the ratio k_1/k_2 . This would be given by

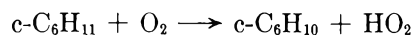
$$\frac{k_1}{k_2} = \frac{G_1(c\text{-C}_6\text{H}_{10})}{G_2((c\text{-C}_6\text{H}_{11})_2)} = \frac{[G_i - G_3 - G_s](c\text{-C}_6\text{H}_{10})}{[G_i - G_s]((c\text{-C}_6\text{H}_{11})_2)}$$

where G_i is the initial yield, G_s is the limiting yield in the presence of scavenger, and G_1 , G_2 , and G_3 refer to the yields of the products in reactions 1, 2, and 3, respectively.

Reaction 3 produces both 1-hexene and cyclohexene, so that the decrease in cyclohexene yield due to inhibition of reaction 3 is equal to the decrease in the 1-hexene yield. Thus

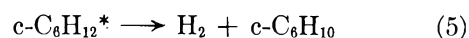
$$G_3(c\text{-C}_6\text{H}_{10}) = [G_i - G_s](1\text{-hexene})$$

Therefore, $k_1/k_2 = 1.1$, with uncertainty limits of ± 0.3 . This value represents a lower limit because the calculation assumed that disproportionation between the radical and scavenger, *e.g.*

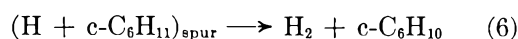


did not occur to an appreciable extent. When compared with the values 1.31²⁶ and 1.47⁵ obtained for k_1/k_2 from mercury photosensitization experiments, the present result is consistent with the suggestion that the free radical reactions are indeed scavenged as assumed above. Although the possibility that the additives react with a precursor of the radicals cannot be ruled out, the formation of the alcohol, ketone, and peroxide in the oxygen solutions would be more difficult to explain in this case.

The preceding discussion referred to reactions in the bulk medium. It is not known if this value of k_1/k_2 would also apply to reactions in the spurs because the initial relative orientations of the radicals in a spur might not be completely random and some of the radicals might still possess excess energy at the time of reaction. Cyclohexene might also be generated in other reactions, such as²⁷



and



(25) K. Nozaki, *Ind. Eng. Chem., Anal. Ed.*, **18**, 583 (1946).

(26) C. E. Klots and R. H. Johnsen, *Can. J. Chem.*, **41**, 2702 (1963).

(27) For example, (a) P. J. Dyne and J. Denhartog, *ibid.*, **41**, 1794 (1963); (b) ref. 5.

For these reasons it is not yet possible to clearly interpret the high value of the ratio of the residual yields of cyclohexene and dicyclohexyl, $G_8(c-C_6H_{10})/G_8((c-C_6-$

$H_{11})_2) = 5.1$. It is hoped that the investigation of the α -radiolysis of cyclohexane solutions will help to elucidate the problem.

Investigation of the Vanadium-Hydrogen System by X-Ray Diffraction Techniques^{1,2}

by Arnulf J. Maeland

Contribution No. 302 from the Department of Chemistry, Tufts University, Medford 55, Massachusetts (Received February 29, 1964)

X-Ray diffraction techniques were used to establish a partial constitutional diagram for the vanadium-hydrogen system. At room temperature the primary solid solution (b.c.c.) extends to $VH_{0.05}$. A body-centered tetragonal hydride phase was found between compositions $VH_{0.46}$ and $VH_{0.90}$ with axial ratio (c/a) increasing from 1.100 to 1.126. A two-phase field exists at intermediate compositions. A second two-phase region extends from $VH_{0.90}$ to the maximum hydrogen content studied, *i.e.*, $VH_{1.80}$. Additional studies at higher temperatures (up to 320°) show the variation in lattice parameters with temperature and hydrogen content.

Introduction

Metal-hydrogen systems have been the subject of numerous investigations in recent years.³ Comparatively little information has, however, been published on the vanadium-hydrogen system, a factor which prompted the present study.

Early attempts by Hägg⁴ to elucidate the system by X-ray diffraction techniques were inconclusive. Hägg observed no shift in the vanadium diffraction lines with hydrogen absorption, but new lines appeared in the diffraction patterns indicating the existence of another phase. Interpretation of the patterns was not possible because the lines were too weak and diffuse to measure.

Roberts⁵ examined vanadium deuteride, $VD_{0.75}$, by X-ray and neutron diffraction methods. At room temperature his sample gave an X-ray pattern which was interpreted as a swollen b.c.c. arrangement of vanadium atoms with $a_0 = 3.148 \text{ \AA}$. Neutron diffraction revealed only one large peak at the 110 position

and a very diffuse background. An order-disorder transition occurred at $207 \pm 10^\circ K$.

Trzeciack, *et al.*,⁶ reported $VH_{0.94}$ to be single phase tetragonal with $a_0 = 3.02$ and $c_0 = 3.36 \text{ \AA}$.

Rostoker⁷ gave 3.019 for a_0 and 3.359 \AA for c_0 for a vanadium hydride of the same composition. X-Ray

(1) A preliminary report of this investigation was presented as part of a paper "Non-Stoichiometric Hydrides" at the Symposium on Non-Stoichiometric Compounds, 141st National Meeting of the American Chemical Society, Washington, D. C., March, 1962.

(2) This research was supported by the U. S. Atomic Energy Commission.

(3) For a recent review see T. R. P. Gibb, Jr., "Primary Solid Hydrides," in "Progress in Inorganic Chemistry," Vol. 3, Interscience Publishers, New York, N. Y., 1962.

(4) G. Hägg, *Z. physik. Chem.*, **B11**, 433 (1931).

(5) B. W. Roberts, *Phys. Rev.*, **100**, 1257 (1955).

(6) M. J. Trzeciack, D. F. Dilthey, and M. W. Mallett, BMI-1112 (1956).

(7) W. Rostoker, "The Metallurgy of Vanadium," John Wiley and Sons, Inc., New York, N. Y., 1958.

diffraction studies by other authors⁸⁻¹⁰ confirm the existence of a tetragonal hydride phase in the system.

The preparation of a nonstoichiometric dihydride of vanadium has been reported.¹¹ It has an f.c.c. arrangement of vanadium atoms with $a_0 = 4.271 \pm 0.002 \text{ \AA}$. The hydrogen atoms presumably occupy tetrahedral sites resulting in a fluorite, C-1, type structure at VH_2 . This structure has not been demonstrated, but is inferred from the estimated radius of hydrogen.

Experimental

Apparatus. The vacuum system used for degassing and hydriding is of all-glass construction with the exception of the reaction tube which is made of quartz. Pressures lower than 10^{-6} mm., as indicated on a NRC Equipment Corp. ionization gage, can readily be obtained. The high pressure system used for the preparation of vanadium dihydride has been described previously.¹¹

Materials. Two types of iodide vanadium were used. Granular vanadium of 99.8% minimum purity was obtained from Oregon Metallurgical Corp., and crystal bar vanadium of 99.92% purity was furnished by Dr. F. H. Spedding, Ames Laboratory. The combined nitrogen, oxygen, and hydrogen content of the granular material was less than 0.1% according to the supplier. Supplier's analysis for crystal bar vanadium: C, 95 p.p.m.; O, 200 p.p.m.; N, <10 p.p.m.; Fe, 150 p.p.m.; Cr, 200 p.p.m.; others, <200 p.p.m. Pure hydrogen was obtained from the thermal decomposition of uranium hydride.

Preparation of Hydrides. Samples of 0.1-0.6 mole of vanadium metal were etched in an aqueous solution of 5% HF-45% HNO_3 , followed by two rinses each in water, isopropyl alcohol, and anhydrous ether. The samples were hydrided according to the following procedure: the metal, contained in a stainless steel boat, was placed in a quartz combustion tube and outgassed under vacuum (10^{-6} mm.) with slow increase in temperature to 700° . After partial cooling to about 400° purified hydrogen at 1 atm. was allowed to enter the reaction tube. Slow cooling to room temperature followed. The resulting hydride was transferred to the drybox and crushed into 325-mesh powder under a protective atmosphere of argon. The powdered hydride was then dissociated and degassed as before at 700° and 10^{-6} mm. The metallic powder prepared in this manner without exposure to air was found to be very reactive. Hydrides of various compositions ($\text{VH}_{0.05}$ - $\text{VH}_{0.82}$) were prepared from the powder by reaction at room temperature with a known amount of hydrogen. (The reaction is exothermic, however, and is consequently accompanied by a rise in sample tem-

perature.) The hydrides were finally homogenized by heating to 300° for 2-5 hr. with agitation (by vibrating the quartz tube). A few samples were analyzed by thermal decomposition and measurement of the evolved hydrogen. The values obtained by analysis and those calculated from absorption gave good agreement ($\text{H/V} = n \pm 0.03$). Preparation of the dihydride has been described elsewhere.¹¹

X-Ray Diffraction Procedure. Diffraction patterns were obtained with a Straumanis-type G.E. powder camera using nickel-filtered copper radiation. Samples for high temperature X-ray examination were sealed under argon (hydrogen in the case of the high hydrogen content samples studied) in 0.3-mm. Pyrex capillaries which were heated by a thermostated hot-air jet. Identical X-ray patterns at room temperature before and after high temperature runs showed that no irreversible changes in structure or composition had occurred. Specimen temperature was measured with an accuracy of $\pm 2^\circ$. Samples for room temperature examination were also protected from the atmosphere by sealing the capillaries under argon in the drybox. Lattice parameters for the cubic phases were determined from plots of a vs. the Nelson-Riley function¹² using all reflections. The method of least squares was employed in calculating a_0 and c_0 for the tetragonal phase using the same error function (and all diffraction lines). The high temperature patterns of the b.c.c. phase showed fair resolution in the back reflection region and these parameters are accurate to $\pm 0.003 \text{ \AA}$. Except in a few instances, the body-centered tetragonal patterns displayed broad unresolved lines in the back reflection region, and the accuracy for a_0 and c_0 is therefore much less, only $\pm 0.01 \text{ \AA}$.

Results and Discussion

Room Temperature Experiments. Results of room temperature observations on the vanadium-hydrogen system are summarized in Fig. 1. The primary solid solution (b.c.c. α -phase) extends to $\text{VH}_{0.05}$ and is accompanied by a distension of the vanadium lattice from 3.027 to 3.037 \AA . At $\text{VH}_{0.05}$ the body-centered tetragonal β -phase appears with a decrease in the a axis to 3.002 \AA . and an expansion in the c direction to

(8) M. M. Antonova and G. V. Samsonov, *Zh. Prikl. Khim.*, **33**, 1407 (1960).

(9) Z. Bieganski and B. Stalinski, *Bull. Acad. Polon. Sci., Ser. Sci. Chim.*, **9**, 367 (1961).

(10) R. L. Zanowick and W. E. Wallace, *J. Chem. Phys.*, **36**, 2059 (1962).

(11) A. J. Maeland, T. R. P. Gibb, Jr., and D. P. Schumacher, *J. Am. Chem. Soc.*, **83**, 3728 (1961).

(12) J. B. Nelson and D. P. Riley, *Proc. Phys. Soc. (London)*, **57**, 160 (1945).

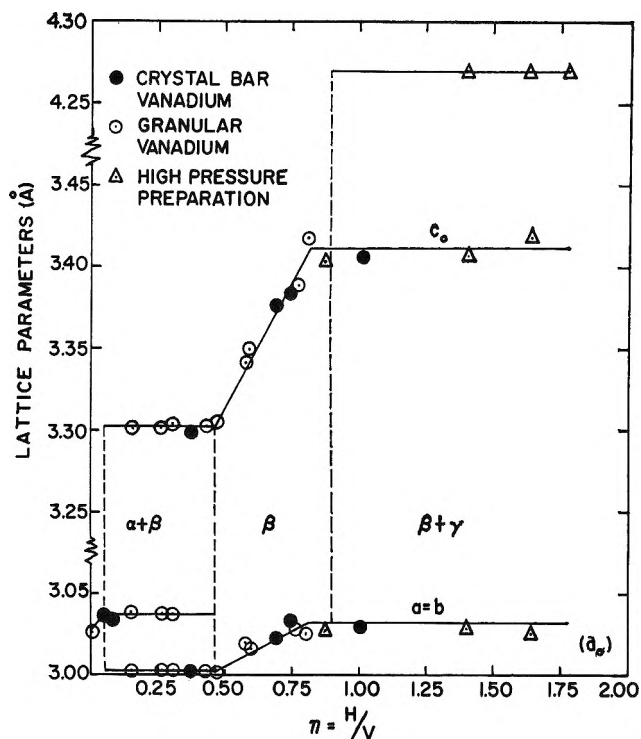


Figure 1. The variation of lattice parameters with hydrogen content at room temperature. Phase boundaries are indicated by dotted lines.

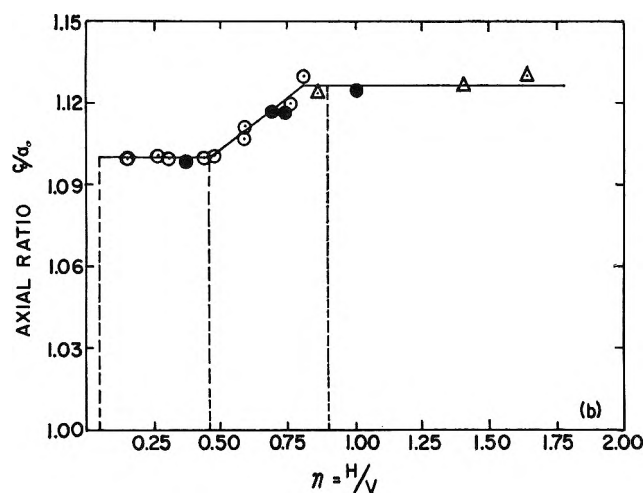


Figure 2. Variation in axial ratio with hydrogen content at room temperature.

3.302 Å. A two-phase region extends to $VH_{0.46}$ at which composition the α -phase disappears. A linear expansion of a_0 and c_0 is observed as the hydrogen content of the β -phase increases. This expansion amounts to 1 and 3% in a_0 and c_0 , respectively, when the composition reaches $VH_{0.80}$. Further increase in the hydrogen content causes no change in the X-ray

patterns until the f.c.c. γ -phase appears at $VH_{0.90}$. This second two-phase region was found to extend to the maximum hydrogen content studied, *i.e.*, $VH_{1.80}$. It is presumably followed by another single phase region (γ) as indicated by the gradual decrease in intensities of the β -phase reflections with increasing hydrogen content.

It should be pointed out that the $\beta/\beta + \gamma$ phase boundary is somewhat uncertain. This phase boundary was determined from the observation that the 111, 311, 331 reflections of the f.c.c. phase were present, but weak, in samples prepared under high pressure and having a composition of $VH_{0.90}$ and disappeared when the hydrogen content was decreased below this value. A crystal bar sample of vanadium, however, was hydrided under 1 atm. of hydrogen and reached a composition of $VH_{1.01}$, but the X-ray pattern showed no indication of an f.c.c. phase. The change in axial ratio of the β -phase, shown in Fig. 2, is in agreement with the trend suggested by Zanowick and Wallace.¹⁰ Our values for a_0 and c_0 , however, are substantially larger in each case than those obtained by these authors. The difference may be due to the different methods used in arriving at a value for a_0 and c_0 .

High Temperature Experiments. A number of high temperature isocompositional studies were made to determine and locate phase boundaries. The results are presented in Fig. 3. Line AB marks the $\alpha/\alpha + \beta$ phase boundary and was determined by cooling runs on samples with hydrogen content less than $VH_{0.37}$. In these runs the sample, contained in a sealed Pyrex capillary, was first heated to approximately 300° for 1-2 hr. to ensure complete transformation to the α -phase. It was then cooled from 300° to the de-

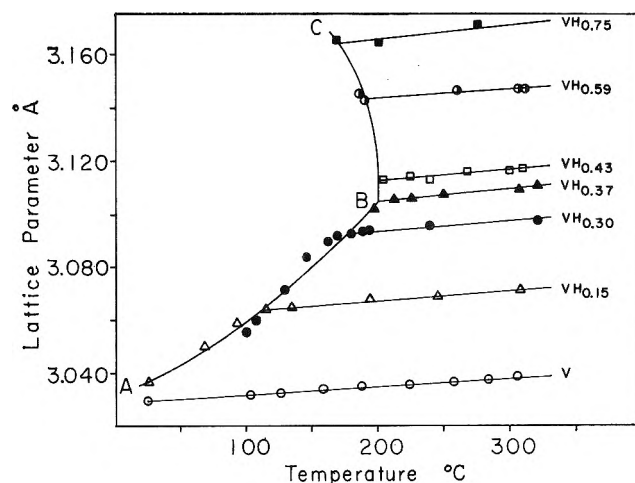


Figure 3. Lattice parameters of various vanadium-hydrogen alloys as functions of temperature.

sired temperature and held a minimum of 1 hr. before making the X-ray exposure. The isocompositional lattice parameters were found to be linear functions of temperature in the α -field as indicated in the figure. When the samples were cooled past the $\alpha/\alpha + \beta$ phase boundary, some β -phase was formed with a resulting decrease in the hydrogen content of the α -phase and a sudden decrease in lattice parameter. By decreasing the temperature, further depleting the α -phase of hydrogen, the line AB was traced. Cooling runs, according to the procedure outlined above, were extended to samples which at room temperature existed as single phase body-centered tetragonal alloys. The behavior can be illustrated by considering the results obtained from cooling runs made with $\text{VH}_{0.59}$. This alloy remained single phase b.c.c. from 300° down to 189° and transformed completely to β -phase at 180° . At the intermediate temperature, 185° , the X-ray pattern indicated about equal amounts of b.c.c. α -phase and body-centered tetragonal β -phase. Similar behavior was observed with $\text{VH}_{0.69}$ and $\text{VH}_{0.75}$. Line BC in Fig. 3 shows the position of this $\alpha/\alpha + \beta$ phase boundary. Attempts were made to extend the study to higher hydrogen contents, but dissociation and loss of hydrogen became a serious problem when the temperature was increased to 300° . This was evidenced by an abnormally low lattice constant for the b.c.c. phase. Room temperature patterns before and after heating also indicated clearly that hydrogen loss had occurred in the heating process. In the case of $\text{VH}_{0.75}$ (the maximum composition studied at these higher temperatures) hydrogen loss was evident at 300° . It was found, however, that the sample could be heated to 260° with complete transformation to α -phase, then cooled to the desired temperature without loss of hydrogen. This latter procedure was therefore followed for the cooling runs for $\text{VH}_{0.75}$. From Fig. 3 coefficients of expansion for pure vanadium (crystal bar sample) and hydrides of various compositions can be calculated. The value obtained for vanadium was $10.6 \times 10^{-6} \text{ deg.}^{-1}$ which is in good agreement with reported values.^{13,14} For $\text{VH}_{0.15}$ and $\text{VH}_{0.37}$ the values are $13.1 \times 10^{-6} \text{ deg.}^{-1}$ and $13.5 \times 10^{-6} \text{ deg.}^{-1}$, respectively.

The curves in Fig. 3 were extrapolated to room temperature and a value for $a_{R.T.}$ for each composition was obtained. These values were then used to calculate the vanadium unit cell volume ($a_{R.T.}^3$), which would result if the vanadium lattice remained b.c.c. throughout the composition range ($\text{V}-\text{VH}_{0.75}$). Comparing the calculated volume with the observed tetragonal unit cell volume, a^2c , it is found that the observed

volume is smaller than the calculated volume. In other words in β -phase formation the tetragonal distortion, which we believe to be a result of the ordering of the interstitial hydrogens, is associated with a relative contraction in the vanadium unit cell volume.

The data in Fig. 1 and 3 were used to construct a partial phase diagram for the vanadium-hydrogen system. The $\alpha/\alpha + \beta$ phase boundary represented by AB and BC in Fig. 4 was taken directly from Fig. 3. Line BG representing the $\beta/\beta + \alpha$ boundary was obtained from cooling runs on samples of compositions $\text{VH}_{0.59}$, $\text{VH}_{0.69}$, and $\text{VH}_{0.75}$, whereas BE is based on the room temperature observation and the disappearance of the α -phase from $\text{VH}_{0.43}$ ($\alpha + \beta$) on heating. Suggested phase boundaries in the right-hand side of Fig. 4 have been dotted in; further work is obviously required to clarify this region of the vanadium-hydrogen phase diagram.

X-Ray and neutron diffraction studies of vanadium-deuterium alloys both at high and low temperature have recently been completed and will be reported in a subsequent publication.¹⁵

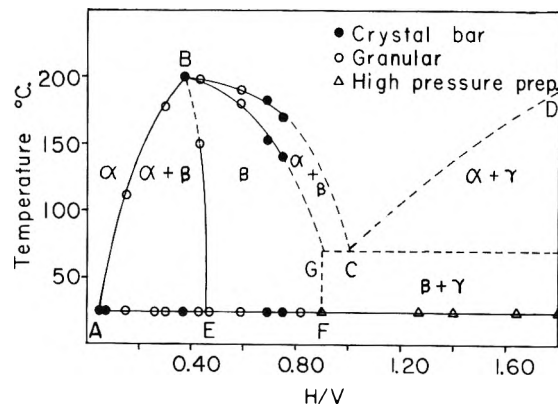


Figure 4. Tentative phase diagram for the vanadium-hydrogen system.

Acknowledgment. The author is indebted to Dr. D. P. Schumacher for the high-pressure preparations, to Dr. K. Hardcastle and to Dr. T. R. P. Gibb, Jr., for frequent discussions during the course of this investigation. Mrs. Judy Knudsen Canonico assisted materially in connection with her senior thesis.

(13) W. J. James and M. E. Straumanis, *Z. physik. Chem. (Frankfurt)*, **29**, 134 (1961).

(14) A. U. Seybolt, "Rare Metals Handbook," C. A. Hampel, Ed., Reinhold Publishing Corp., New York, N. Y., 1954, p. 593.

(15) K. Hardcastle, to be published.

Electrodialytic Polarization of Ion-Exchange Membrane Systems

by H. P. Gregor and Marvin A. Peterson¹

Department of Chemistry, Polytechnic Institute of Brooklyn, Brooklyn, New York
(Received February 29, 1964)

The extent of electro-dialytic polarization at a cation-exchange membrane in potassium chloride solutions of different concentration (0.0005–0.05 *M*) and stirred such that the boundary layer thickness varied from 4 to 30 μ was determined by measuring the (equal) rates of production of hydrogen and hydroxide ions as a function of the current density. The hydrogen ion flux across the film rose quite steeply as a critical current density was obtained, above which the transport number of hydrogen ions across the membrane reached 0.4–0.7. At currents below the critical value, the hydrogen ion flux was calculated by assuming that its migration alone was operative, employing its ambient solution concentration (pH 7) and the potential gradient at the solution–membrane interface, the latter being derived from a solution of the Nernst–Planck equation applied to potassium chloride alone. At currents above the critical value, the hydrogen ion flux and transport number were calculated by assuming that in this region the potassium ion was transported by diffusion alone. Reasonable agreement between theory and experiment was obtained.

During the passage of a direct current across most porous membranes interposed between neutral electrolytic solutions, changes in the pH of these solutions have been observed. Bethe and Toropoff² noted that during electroosmosis through a collodion parchment or a gelatin membrane the anolyte became alkaline and the catholyte acidic, the reverse of what occurs under ordinary electrolysis of neutral solutions between platinum electrodes. Using material balance considerations, they correlated the transport numbers of the cation and anion of the salt, and also those of hydrogen and hydroxide ions, postulating that the effect arose because the membrane was more permeable to either cationic or anionic species.

With ion-exchange membranes, this pH shift is considerably more marked than is observed with presumably uncharged porous membranes under the same experimental conditions. For example, at low current densities and with neutral salt solutions and cation-exchange membranes, the hydrogen ion transport number across the membrane is virtually zero; it rises markedly with increasing current density, and when a critical current density is reached the hydrogen ion flux across the membrane becomes a substantial fraction of the total current. A parallel effect occurs with anion-permeable membranes and hydroxide ion

transport. The effect depends upon the degree of stirring of the ambient solutions, the concentration of salts, the properties of the membrane, and the nature of the electrolyte present. Peers³ measured polarization by examining current–voltage curves, as did Rosenberg and Tirrell⁴ and Cowan and Brown⁵; Uchino, *et al.*,⁶ measured the extent of the pH disturbance. These polarization effects have been commonly observed in practical electro-dialytic processes, as evidenced by an increase in the operating voltage and the formation of acid in compartments being demineralized.

This contribution describes polarization phenomena in cation-exchange membrane systems and presents a theoretical interpretation of these effects.

(1) Taken in part from the dissertation of Marvin A. Peterson, submitted in partial fulfillment of the requirements for the degree of Doctor of Philosophy in Chemistry, Polytechnic Institute of Brooklyn, Brooklyn, N. Y., June, 1960.

(2) A. Bethe and T. Toropoff, *Z. physik. Chem.*, **88**, 686 (1914); **89**, 597 (1915).

(3) A. M. Peers, *Discussions Faraday Soc.*, **21**, 124 (1956).

(4) N. W. Rosenberg and C. E. Tirrell, *Ind. Eng. Chem.*, **49**, 780 (1957).

(5) D. A. Cowan and J. H. Brown, *ibid.*, **51**, 1445 (1959).

(6) T. Uchino, S. Nakaoka, H. Hani, and T. Yawataya, *J. Electrochem. Soc. Japan*, **26**, 366 (1958).

Experimental

Membranes selected for this study were of the homogeneous interpolymers type manufactured by the Nalco Chemical Co. and designated Nalfilm 1. The preparation of similar materials has been described by Gregor, *et al.*,⁷ while preparation of the same or similar materials is described in two patents.⁸ The properties of the particular cation-permeable membranes selected were summarized by Peterson and Gregor.⁹ The membranes had a thickness of 96 μ and a water content of 23.5% (by weight). Their resistance in 0.1 *M* potassium chloride solution was 16.5 ohm-cm.² and 28.0 ohm-cm.² in 0.001 *M* solution. The concentration of sulfonic acid groups in the membrane phase was 2.86 *m*, 8.5×10^{-3} mequiv. (milliequivalents) cm.⁻² or 0.88 *M*. In 0.1 *M* potassium chloride solution the diffusible electrolyte or co-ion content of the membrane was 0.027 *m*. In 0.001 *M* KCl solution the diffusion coefficient of potassium ions was 1.09×10^{-7} cm.² sec.⁻¹, rising to 1.71×10^{-7} cm.² sec.⁻¹ in 0.1 *M* solution. Other studies by Heymann and O'Donnell¹⁰ and by Jacobsen¹¹ have shown that the diffusion coefficients of hydrogen and potassium ions in the membrane phase are approximately proportional to their limiting diffusion coefficients in aqueous solution. The transport number of the potassium ion in the membrane phase in 0.001 *M* potassium chloride solution was 1.000 and 0.983 in 0.1 *M* solution, as determined both by diffusion coefficient and by diffusion potential measurements. Drawing an analogy between these membranes and comparable sulfonated ion-exchange resins, the selectivity coefficient for potassium-hydrogen exchange is taken to be approximately 2.0.

The experimental determination of the rates of transport across the membrane under the influence of an applied electric field was accomplished in a modified version of the cell used earlier.⁹ The cell was modified by enlarging the opening between the electrode and stirrer compartments to provide for good stirring in the electrode compartments which contained silver-silver chloride electrodes in the form of plated silver screens. Both half-cells were stirred as before in a well-defined manner, and isothermal cooling coils maintained the system at a constant temperature (25.0°). The membrane area common to both solutions was 3.42 cm.².

With 0.05 *M* potassium chloride solution in the cell, its resistance was 280 ohms and at the 0.005 *M* concentration level the resistance was 26 megohms.

The boundary layer thickness δ had been determined previously from exchange-diffusion experiments em-

ploying potassium and ammonium ions and using Fick's law⁹; it varied from 1.2 to 30.4 μ at different rates of stirring. Since these values were derived from transport experiments, they are functionally correct for the polarization experiments described herein.

The performance of a specific experiment was as follows: the membrane specimens were equilibrated in the solution for at least 24 hr. Then each half-cell compartment (115 ml.) was filled and stirring initiated. Then current was passed for 90 sec. (the duration of each run) during which time the exact setting of the power supply for the desired current density was made. The solutions were replaced and each run repeated until the amount of hydrogen and hydroxide ions found in the ambient solutions was constant. This was necessary because the membrane had to be transformed from its original potassium state into the appropriate potassium-hydrogen state. The duration of each run was 90 sec. with intermittent sampling at 45 sec. The lapsed time was always less than 10% of that required to deplete the left-hand compartment, assuming that only potassium and chloride ions carried the current. At current densities well below the critical current density, the capacity of the membrane was large compared to the amount of acid generated, but at and above the critical current, the membrane capacity was small compared to the acid generated. Typical data are shown in Table I, one set for a dilute solution and a high rate of stirring, and another for a relatively concentrated one at a lower rate of stirring. The amount of hydrogen and hydroxide ions formed was computed from differences in the initial and final pH values and assuming that the mean activity coefficient of the acid or base was equal to that of the potassium chloride present. Figures 1-4 show plots of a flux for hydrogen ions across the membrane as a function of the current density. The theoretical curves will be discussed in a subsequent section. Also shown is the total current across the membrane.

Table I shows that under most conditions the solutions were neutral during only the early part of the process. As will be shown later, it is the total electrolyte concentration which is important here; the nature of the ions present plays a secondary role.

(7) H. P. Gregor, H. Jacobson, R. C. Shair, and D. M. Wetstone, *J. Phys. Chem.*, **61**, 141 (1957); H. P. Gregor and D. M. Wetstone, *ibid.*, **61**, 151 (1957); **62**, 3, 274 (1958).

(8) H. P. Gregor and H. I. Pazelt, U. S. Patents 3,004,909 (October 17, 1961), and 3,004,904 (October 17, 1961).

(9) M. A. Peterson and H. P. Gregor, *J. Electrochem. Soc.*, **106**, 1051 (1959).

(10) E. Heymann and I. J. O'Donnell, *J. Colloid Sci.*, **4**, 405 (1949).

(11) H. Jacobsen, Dissertation, Polytechnic Institute of Brooklyn; 1959.

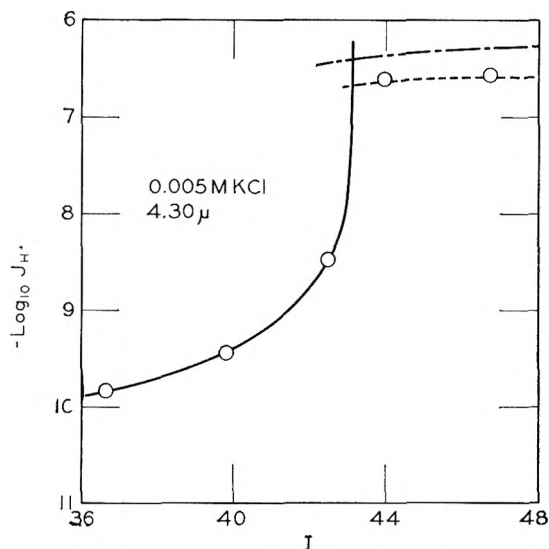


Figure 1. Flux of hydrogen ions (in equiv. $\text{cm.}^{-1} \text{sec.}^{-2}$) as a function of current (in ma. cm.^{-2}) across a cation-permeable membrane in 0.005 M potassium chloride, with the rate of stirring adjusted to give a boundary layer of 4.3μ . Curve (—) computed from $\bar{J}_{\text{H}^+} = c_{\text{H}^+}^{\alpha} D_{\text{H}^+} (d\Phi/dx)^{\beta}$; curve (---) computed from $\bar{J}_{\text{H}^+} = I - c_{\text{K}^+}^{\alpha} D_{\text{K}^+} / \delta$; curve (- · -) is the total ionic flux or I .

Table I: Measured pH Changes

Current density, ma. cm.^{-2}	Anolyte or catholyte	pH		
		0 sec.	45 sec.	90 sec.
0.0005 M KCl, $\delta = 4.3 \mu$				
1.46	A	6.04	6.43	6.63
	C	6.05	6.04	6.03
3.22	A	6.05	6.97	7.25
	C	6.05	6.02	6.00
4.10	A	6.04	7.87	8.17
	C	6.04	5.79	5.63
4.54	A	6.05	9.48	9.78
	C	6.05	4.49	4.20
5.85	A	6.06	9.68	9.97
	C	6.05	4.30	4.00
0.05 M KCl, $\delta = 30.4 \mu$				
29.2	A	6.69	6.72	6.76
	C	6.68	6.67	6.66
45.0	A	6.67	6.81	6.92
	C	6.68	6.65	6.61
57.0	A	6.69	7.29	7.53
	C	6.67	6.45	6.30
58.5	A	6.68	10.64	10.83
	C	6.67	3.34	3.14

Theoretical

For a single membrane interposed between two solutions, the notation employed will designate each region as



where α and ϵ are the two stirred regions whose composition is known, the β and γ regions are the two boundary layers of thickness δ and λ , respectively, and the superscript bar refers to the membrane phase of thickness L . The distance x is zero at the α - β boundary. The membrane-solution interfaces are design-

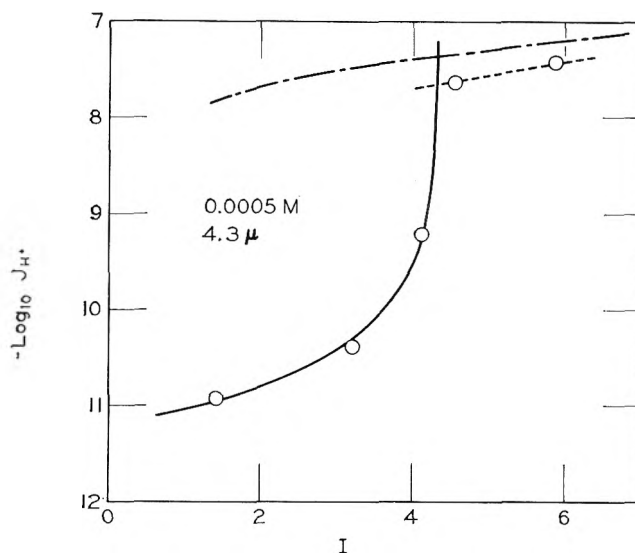


Figure 2.

nated by the prime and double-prime symbols. Concentrations of the K^+ , Cl^- , H^+ , and OH^- ions are designated as c_1 , c_2 , c_3 , and c_4 , all in moles cm.^{-3} . Thus, the designation c_1^{β} refers to the potassium ion concentration in the β region ($0 < x < \delta$), $c_1^{\beta'}$ is its concentration in β adjacent to the solution-membrane interface, \bar{c}_1' its concentration at the same interface, but in the membrane phase, etc.

Consider potassium chloride as being the sole component in the β region. Then, if I is the current (in equiv. $\text{cm.}^{-2} \text{sec.}^{-1}$)

$$J_1 = -D_1 \frac{dc_1}{dx} - \frac{Z_1 \bar{\gamma} D_1 c_1}{RT} \frac{d\psi}{dx}$$

where D is the diffusion coefficient, $\bar{\gamma}$ the faraday, Z the valence (always positive), J the flux density in moles $\text{cm.}^{-2} \text{sec.}^{-1}$ (for univalent species), and ψ the potential. Setting $\Phi = Z \bar{\gamma} \psi / RT$

$$-\frac{J_1}{D_1} = \frac{dc_1}{dx} + c_1 \frac{d\Phi}{dx} \quad (1)$$

Also

$$-\frac{J_2}{D_2} = \frac{dc_2}{dx} - c_2 \frac{d\Phi}{dx} \quad (2)$$

With an ideally selective cation-permeable membrane, $J_2 = 0$ at $x = \delta$ and in the steady state, $J_2^\beta = 0$. D_1 can be set equal to D_2 because for potassium chloride $t_1 = 0.49$ in the solution phase. Also c_1 would equal

$$\begin{aligned} d\Phi/dx &= -I/2D(c^\alpha - Ix/2D) \\ (d\Phi/dx)^{\beta'} &= -I/(2Dc^\alpha - I\delta) \end{aligned}$$

It is evident that the potential gradient in region β is nonlinear, and that as $I \rightarrow 2Dc^\alpha/\delta$, the field goes to infinity. This is defined as the critical current density I^* .

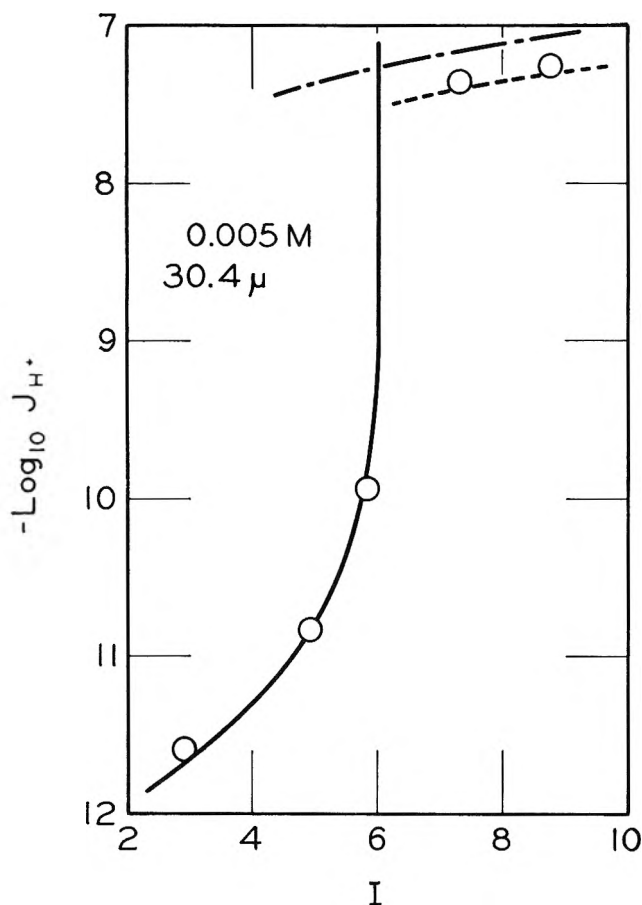


Figure 3.

c_2 by the ordinary conditions of electroneutrality. However, since the field $d\Phi/dx$ is not uniform in the β region, there is a finite space charge, proportional to $c_1 - c_2$. For the time being, we will neglect this space charge and set $c_1 = c_2$. Then

$$-\frac{J_1}{D} = 2c \frac{d\Phi}{dx} = 2 \frac{dc}{dx} = -\frac{I}{D}$$

or the concentration gradient is linear and

$$c^\alpha - c^\beta = \frac{Ix}{2D}; \quad c^\alpha - c^{\beta'} = \frac{I\delta}{2D}$$

The potential gradient is

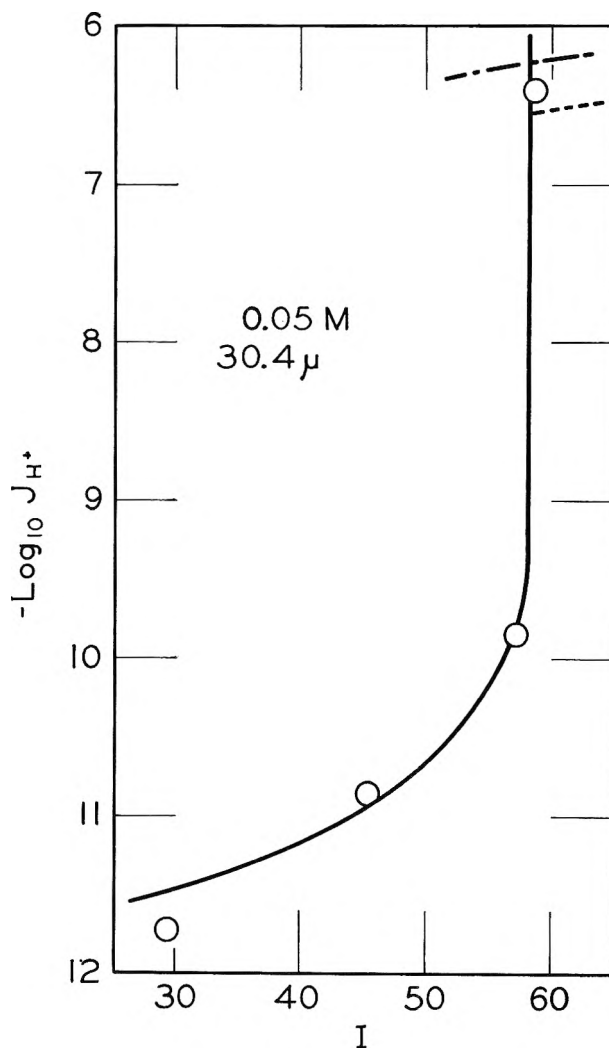


Figure 4.

As a first approximation it may be assumed that the concentrations of H^+ and OH^- ions are not changed by concentration polarization in the β -region, and that the hydrogen ion flux across the membrane is equal to its concentration at the β -membrane boundary times the field at that point, or

$$J_3^\beta = J_3^{\beta'} = c_3^\alpha D_3 (d\Phi/dx)^{\beta'} = \bar{J}_3$$

Figures 1-4 show values of \bar{J}_3 computed on this basis.

Based on the previous simplifications, \bar{J}_3 becomes infinite at $I \geq I^*$. To compute \bar{J}_3 values under these conditions, we assume that the potassium ion is carried by *diffusive processes only*, and that migration plays no significant part. Then

$$J_1^\beta = \bar{J}_1 = c_1^\alpha D_1 / \delta$$

and

$$\bar{J}_3 = I - c_1^\alpha D_1 / \delta$$

These curves were also computed and are shown in Fig. 1-4. It is evident that however gross these two approximations, the theoretical and experimental curves fit quite well.

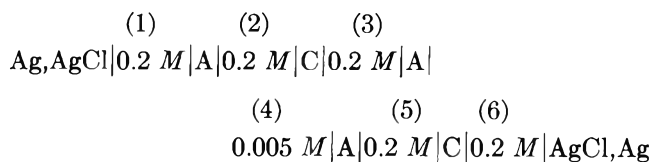
Discussion

An examination of Fig. 1-4 shows that over a wide range of experimental conditions, the simplified expressions developed here describe the experimental results rather well. Table I shows also that the flux of hydrogen and hydroxide ions was quite constant over the 90-sec. interval, although the pH of solution α was changing from about 7 to 10 or as high as 10.8. Thus, although the composition of the solution phase changed from $5 \times 10^{-4} M$ potassium chloride to one with the same salt content but $10^{-4} M$ in potassium hydroxide, the rate of acid and base production was unchanged. This suggests that the generation process occurs rather independently of the ionic composition of the solution.

To fix the site of generation, a cell was constructed wherein the surface of the membrane could be viewed directly.¹² The large silver-silver chloride anode in $0.5 M$ potassium chloride was separated from the α -phase by an anion-permeable membrane. The α -region was unstirred and contained $0.001 M$ salt, while the ϵ -region contained $0.5 M$ salt and the silver-silver chloride cathode. The indicator brom thymol blue was in the α -solution, and on the passage of current it was observed that the membrane surface became strongly alkaline, with hydroxide ions migrating away from it into the solution. This result definitely verifies the existence of the generation process and its location at the solution-membrane interface.

Another cell was designed to help clarify the site of

generation and also the effect of the solution composition. It was a modification of that of Oda¹³ and consisted of the following chain¹⁴



where A and C refer to anion- and cation-permeable membranes, and where the salt was potassium chloride, unless otherwise noted. The solution volumes were small (150 ml.) except in cell 4 through which a large volume was passed to drain (or for analysis). With this cell, it was observed that the flux of hydroxide ions into (3) was equal to the flux of hydrogen ions into (4), with no significant pH change being observed in cell 5. Further, when the solution in (4) was $0.005 M$ potassium chloride, $0.004 M$ salt, and $0.001 M$ hydrochloric acid or $0.004 M$ salt and $0.001 M$ potassium hydroxide, approximately the same generation of acid and base (within a factor of 2) was observed. These observations fix the site of the generation process at the depleted solution-membrane boundary and verify the assumptions as to the concentration profile, namely that the generation process is influenced primarily by the total electrolyte concentration and only secondarily by its composition.

A theoretical treatment of this system, one which does not make the simplifying assumptions described earlier but solves the Nernst-Planck equation for all four species, has been made.¹⁵ It includes terms for the generation process and considers also the change in the rate of the dissociation of water with the electric field (Wien effect). The expressions thus obtained were not susceptible to analysis, but solvable by numerical methods employing a computer.

Acknowledgment. The authors wish to thank the National Science Foundation and the Office of Saline Water for their support of this study.

(12) H. P. Gregor and P. C. Wu, to be published.

(13) Y. Oda, private communication.

(14) M. Espelosin and H. P. Gregor, to be published.

(15) H. P. Gregor and I. F. Miller, to be published.

The Adsorption of Aromatic Vapors on Water Surfaces^{1a}

by M. Blank^{1b}

Department of Physiology, College of Physicians and Surgeons, Columbia University, New York, New York

and R. H. Ottewill

Department of Physical Chemistry, University of Bristol, England (Received March 2, 1964)

The adsorption of benzene, toluene, *o*-xylene, and chlorobenzene on the surface of a 0.1 *M* sodium chloride solution was studied as a function of the partial vapor pressure. The surface tensions were measured by the dipping plate method and the surface potentials were measured with a Radium 226 air electrode and an electrometer. (The surface potentials of adsorbed films of cumene were also examined.) By applying Gibbs' adsorption equation to the surface pressure–vapor pressure data, the adsorption isotherms were calculated. The dependence of the surface pressure on the molecular area indicates that the monolayers are gaseous. The free energies, enthalpies, and entropies of adsorption were calculated from measurements at different temperatures, and the entropies were consistent with the loss of one degree of translational freedom on adsorption. The surface potentials for all adsorbates correlated with the surface tensions and indicated that at low surface coverages the surface potential depended largely upon the interaction between the water and the phenyl ring. Near saturation pressure, when the film molecules were close packed and oriented, the surface potential also depended upon the permanent dipole moment of the adsorbed vapor.

Introduction

Since the surfaces of liquids are homogeneous, they are ideally suited for studying adsorption. In recent years, the adsorption of a number of vapors on water surfaces has been studied by measuring the variations in surface tension with partial pressure of organic vapor.^{2–7} The surface pressure–area characteristics of several adsorbed films and the changes in the thermodynamic functions upon adsorption have been determined. The related problem of the adsorption of vapors on insoluble monolayers (on water) has also received attention, largely because of the dependence of monolayer properties on the spreading solvent.^{8–10} These studies have found that the interaction of vapors with monolayers depends upon the monolayer concentration as well as the vapor pressure. Another liquid surface that has been used to study the adsorption of vapors is mercury^{11,12}; and in this case, the surface potential changes have been measured. Surface potentials indicate changes in the orientation of dipoles at the surface and therefore provide additional information about the adsorption process. In the present work, the

change in surface potential (as well as the surface pressure) was investigated as a function of the vapor pressure for benzene and several substituted benzenes. The

(1) (a) An account of this work was presented before the Division of Colloid and Surface Chemistry at the 144th National Meeting of the American Chemical Society, Los Angeles, Calif., April, 1963; (b) Supported by a Research Career Development Award (GM-K3-8158) and a Research Grant (GM-10101) from the U. S. Public Health Service.

(2) (a) L. I. A. Micheli, *Phil. Mag.*, **3**, 895 (1927); (b) H. Cassel and F. Formstecher, *Kolloid-Z.*, **61**, 18 (1932).

(3) R. H. Ottewill and D. C. Jones, *Nature*, **166**, 687 (1950).

(4) C. L. Cutting and D. C. Jones, *J. Chem. Soc.*, 4067 (1955).

(5) D. C. Jones and R. H. Ottewill, *ibid.*, 4076 (1955).

(6) D. C. Jones, R. H. Ottewill, and A. P. J. Chater, Proceedings of the Second International Congress of Surface Activity, Vol. 1, Butterworth and Co. Ltd., London, 1957, p. 188.

(7) R. H. Ottewill, Ph.D. Thesis, Queen Mary College, London, 1951.

(8) K. E. Hayes and R. B. Dean, *J. Phys. Chem.*, **57**, 80 (1953).

(9) H. D. Cook and H. E. Ries, Jr., *ibid.*, **60**, 1533 (1956).

(10) M. L. Robbins and V. K. La Mer, *J. Colloid Sci.*, **15**, 123 (1960).

(11) C. Kemball and E. K. Rideal, *Proc. Roy. Soc. (London)*, **A187**, 53 (1946).

(12) C. Kemball, *ibid.*, **A201**, 377 (1950).

study of this group of related compounds has enabled further information to be obtained about the nature of the adsorbed film and about the interaction between the adsorbate and the water surface.

Experimental

Materials. Water was doubly distilled from an all-glass apparatus. A 0.1 *M* sodium chloride solution was made up using this water and reagent grade NaCl which had been roasted for 5 hr. at 700°.

The vapors were formed by bubbling water pumped nitrogen through the pure liquids of reagent grade or better (purchased from Matheson, Coleman and Bell). The boiling ranges of the liquids were: benzene 80.0–80.3°, *o*-xylene (1,2-dimethylbenzene) 14.3–144.5°, cumene (isopropylbenzene) 151–153°, and chlorobenzene 130–132°. The toluene, which was used to standardize the technique (gas flow rate, electrode position, etc.), was a Chromatoquality Reagent 99+ mole %. Liquids of reagent grade (from British Drug Houses, Ltd.) with similar specifications were used for the work done in England.

Vapor Pressures. Vapor pressures of benzene and toluene were calculated from the formula

$$\log p_{\text{mm}} = -\frac{0.05223}{T} A + B \quad (1)$$

For benzene $A = 44,222$ and $B = 9.846$ and for toluene $A = 34,172$ and $B = 7.966$. The vapor pressures of *o*-xylene were interpolated from data given in the International Critical Tables. For cumene, the vapor pressures were calculated from a formula, similar to eq. 1, given in the A.P.I. Research Project 44 of the National Bureau of Standards. The vapor pressures of chlorobenzene were calculated from an equation (containing five constants) given by Mündel.¹³

Measurement of Adsorption and Surface Potential. The apparatus was essentially the same as that used by Jones and Ottewill.⁵ The adsorption vessel, however, has a deeper inner trough and the nitrogen-vapor mixture splits into two streams which enter the cell in two tangential jets. This achieves good mixing with a minimum of disturbance to the surface. A 0.1 *M* sodium chloride solution was used in the trough.

Surface pressure measurements were made using a torsion balance in conjunction with a roughened mica (or platinum) plate. The surface potential measurements were made using a sealed Radium 226 air electrode (purchased from U. S. Radium Corp.) in the air just above the trough and a silver-silver chloride electrode in the sodium chloride solution. The air electrode was connected to a Keithley electrometer (Model 610A). The best position for the electrode appeared

to be about 2–5 mm. above the surface near the center of the trough. The potential readings were quite stable but it was found helpful to surround the electrode with a grounded cage.

The surface in the trough was cleaned by overflowing and the potential of the clean surface read off (V_0). At the same time, the scale reading obtained with the mica plate in the surface was taken as corresponding to the surface tension of the clean surface (γ_0). Nitrogen-organic vapor mixture was then admitted to the cell at a rate of 650 cc./min.; this corresponded to a complete change of atmosphere in the cell every half minute. Readings were usually constant after about 2 min., and were normally recorded after 5 min. From the reading of the potential (V), the surface potential was calculated as $\Delta V = V_0 - V$. The surface pressure, $\pi = \gamma_0 - \gamma$, the difference between the surface tension of pure water (γ_0) and a film-covered surface (γ). The partial vapor pressure, p , of the organic liquid was increased gradually until the saturation pressure, p_0 , was reached. Experiments were carried out at 15° unless otherwise indicated.

Results and Discussion

The curves of ΔV and π vs. partial pressure of vapor, p , for benzene, toluene, *o*-xylene, and chlorobenzene are presented in Fig. 1 and 2. The ΔV vs. p curve for cumene is given in Fig. 3.

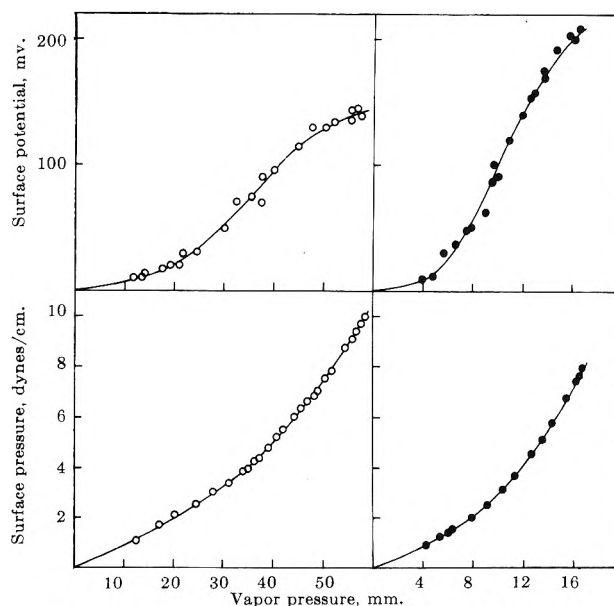


Figure 1. Surface pressure vs. vapor pressure and surface potential vs. vapor pressure curves for the adsorption of benzene and toluene on water at 15°: —○—, benzene; —●—, toluene.

(13) C. F. Mündel, *Z. physik. Chem.*, **85**, 435 (1913).

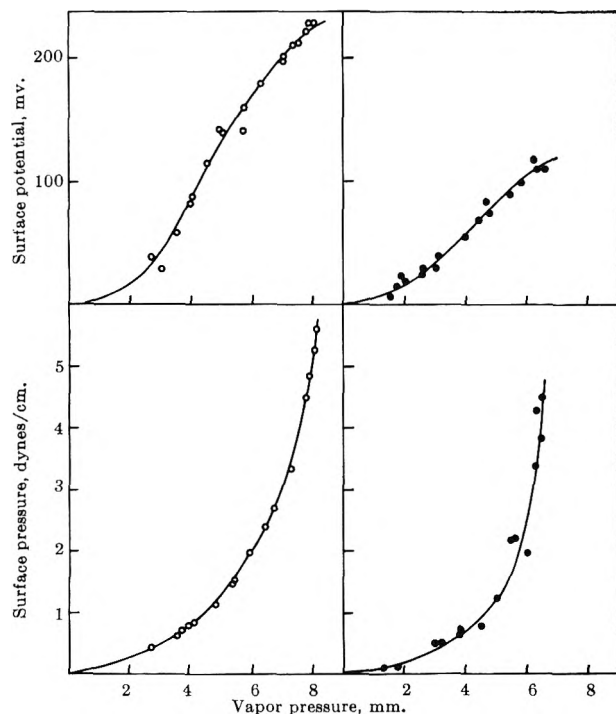


Figure 2. Surface pressure *vs.* vapor pressure and surface potential *vs.* vapor pressure for the adsorption of *o*-xylene and chlorobenzene on water at 15°: —○—, *o*-xylene; —●—, chlorobenzene.

The π *vs.* p curves are similar to those obtained in earlier work with aliphatic hydrocarbons, anisole, phenetole, carbon tetrachloride, fluorobenzene, and chloroform.^{3,6} The ΔV *vs.* p curves have the same general form for all the materials investigated in the present work. In the low vapor pressure region ΔV changes very little, then at the point where π starts to increase rapidly ΔV also starts to increase rapidly. As saturation pressure is approached, ΔV appears to level off.

The adsorption excess of the organic vapor at the interface, with the adsorption of water taken as zero, was derived from the π *vs.* p curves using Gibbs' adsorption equation

$$\Gamma = \frac{1}{RT} \frac{\partial \pi}{\partial \ln p} \quad (2)$$

The curves of Γ *vs.* p were all of the same general form and obeyed the general relationship

$$\Gamma = \frac{ap}{1 - bp} \quad (3)$$

where a and b are constants. A typical example, the curve for benzene at 15°, is given in Fig. 4. Comparison of the adsorption isotherm with the ΔV *vs.* p curve

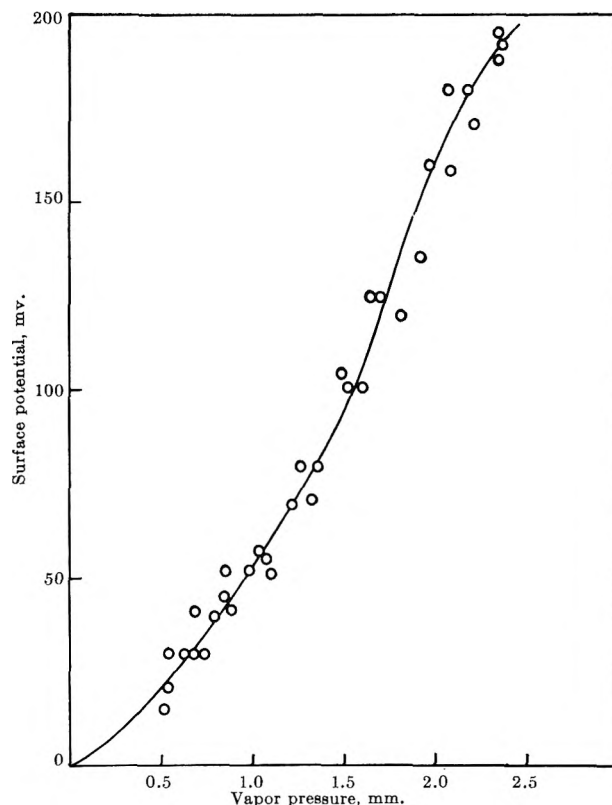


Figure 3. Surface potential *vs.* vapor pressure for the adsorption of cumene on water at 15°.

shows that both ΔV and π start to change rapidly in the same p region, *i.e.*, $p > 30$ mm.

The surface area per molecule can readily be derived from the surface excess using the relationship

$$A = \frac{1}{\Gamma N} \quad (4)$$

where N = Avogadro's number. The π *vs.* A and ΔV *vs.* A curves for benzene at 15° are shown in Fig. 5. It is clear from the π *vs.* A curves that the films are gaseous. From plots of πA *vs.* π , it appears that the attractive term predominates and that the πA values fall increasingly below the ideal value as π increases.

Adsorption Measurements. The Gibbs' free energy of adsorption, $-\Delta G$, can be calculated⁵ from the intercept at $\pi = 0$ on a plot of $\log \pi/p$ *vs.* π . The values calculated from the data presented here and from some earlier work of Ottewill⁷ are given in Table I. The enthalpies and entropies of adsorption were also calculated, where possible, from the variation of the free energy of adsorption with temperature using the Gibbs-Helmholtz equation

$$\Delta G - \Delta H = T(\partial \Delta G / \partial T) = -T\Delta S \quad (5)$$

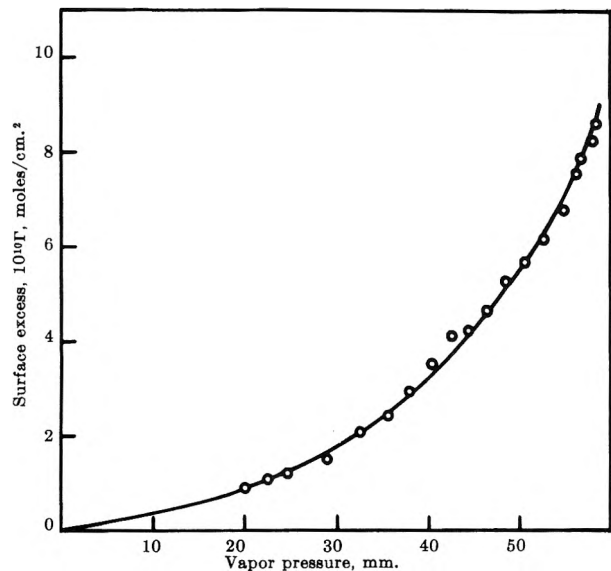


Figure 4. The surface excess of vapor vs. vapor pressure curve for the adsorption of benzene on water at 15°.

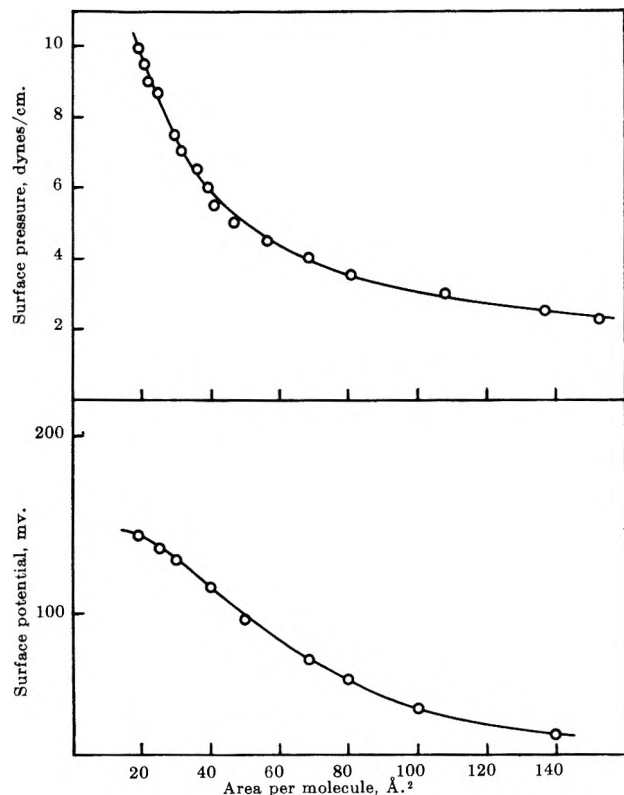


Figure 5. The surface pressure and surface potential vs. the area occupied per molecule for the adsorption of benzene on water at 15°.

Table I: Free Energy, Enthalpy, and Entropy of Adsorption on Water

Material	Temp., °C.	ΔG, cal.	ΔH, cal.	ΔS, e.u.
Benzene	0.0	4037		
	7.5	4022		
	15.0	3968	6174	7.2
Toluene	5.0	4569		
	15.0	4467	7681	10.2
<i>o</i> -Xylene	15.0	4452		

The translational entropy of a molecule which has three-dimensional freedom is given by the Sackur-Tetrode equation

$${}_3S_{trans} = 2.303R \log (M^{3/2}T^{5/2}) - 2.30 \quad (6)$$

where *M* is the molecular weight and the entropy is in cal. deg.⁻¹ for a pressure of 1 atm. An expression for the two-dimensional translational entropy has been given by Kemball¹¹ as

$${}_2S_{trans} = 2.303R \log (MTa) + 65.80 \quad (7)$$

where *a* is the area per molecule, defined in the standard state as equal to (22.53*T*) Å.² If it assumed that adsorption involves only the loss of one degree of translational freedom, the entropy of adsorption, Δ*S*, is given by eq. 6 minus eq. 7. In Table II a comparison

Table II: Theoretical and Observed Entropy Changes

Material	{}_3S_{trans}	{}_2S_{trans}	{}_3S_{trans} - {}_2S_{trans}	Δ <i>S</i> _{exp} ± 20%
Benzene	38.83	29.95	8.88	7.2
Toluene	39.33	30.28	9.05	10.2

is made between the values calculated theoretically and those obtained experimentally for benzene and toluene. The agreement, allowing for experimental error, is sufficiently close to suggest that adsorption involves essentially only the loss of one translational degree of freedom. Therefore, the adsorbed film must be a mobile one.

The curves of Γ vs. *p* show a continuous increase of Γ up to *p*₀. Calculations of the percentage monolayer, *d* = 100Γ/Γ_m, where Γ_m = the surface excess for a vertically oriented monolayer, indicate that in some cases multilayers were formed. Since water has a homogeneous surface, multilayer formation cannot occur as a consequence of capillary condensation but can be accounted for by the concept of a disjoining

The values of Δ*H* and Δ*S* are also given in Table I. The Δ*H* of adsorption is comparable to the Δ*H* of vaporization. The Δ*S* values are discussed below.

pressure. In the case of condensation on glass, Derjaguin and Zorin¹⁴ found that multilayers were usually formed when p/p_0 was between 0.95 and 1.0. In the case of the benzene–water system, the surface tension of benzene against air at 15° is 29.4 dynes/cm. and the interfacial tension of water–benzene is 34.5 dynes/cm., a total of 63.9 dynes/cm. From the present work, the surface tension of water in equilibrium with benzene vapor was found to be 63.6 dynes/cm. or 0.3 dyne/cm. lower. As pointed out by Kitchener,¹⁵ the surface free energy in the adsorbed layer of benzene must increase with the thickness of the layer. This is equivalent to a negative disjoining pressure in the multilayer. In the case of benzene, on the basis of vertically oriented molecules the monolayer was completed at a p/p_0 of about 0.96. This would be consistent with a small negative disjoining pressure in the multilayer.

Surface Potential Measurements. There is a difficulty in interpreting changes in surface potential since adsorption inevitably occurs on the electrode as well as on the surface. To assess the importance of adsorption on the air electrode two water surfaces were used; one was kept clean while toluene vapor, at various p 's, was circulated over the other. The radium electrode was then passed many times between the two surfaces and the ΔV readings, obtained from 15 to 20 sec. after transfer, were as if adsorption had not occurred on the electrode surface. In another test, three different air electrodes were used to measure the ΔV due to an adsorbed film of toluene and the values agreed to within the experimental error, even though the absolute potential values differed by over 100 mv. The ΔV obtained with an electrode that has been immersed in water is the same during the several days it takes for the absolute potential to return to its original value. Therefore, it appears safe to conclude that adsorption on the air electrode did not affect the general nature of the results.

The change in the potential across an interface, ΔV , caused by the adsorption of a molecule may be written as

$$\Delta V = 4\pi n\mu + \psi_0 \quad (8)$$

where μ = the surface dipole moment, n = the number of dipoles per cm.,² and ψ_0 = the potential drop due to the formation of an electrical double layer at the interface. (In the present work all the adsorbates were non-ionic and $\psi_0 = 0$.) Although μ is usually ascribed to the dipole moment of the adsorbed molecule, it also includes the effects of the reorientation of water dipoles in the surface.

Table III gives a summary of the maximum values of p , Π , and ΔV for the various vapors. (The value for

Table III: Properties of Vapors and Adsorbed Films

Substance	Vapor		Adsorbed film	
	Pressure, mm., 15°	Dipole moment, e.s.u.	Maximum surface pressure, dynes/cm.	Maximum surface potential, mv.
Benzene	58.5	0	9.9	142
Toluene	16.8	+0.36	9.1	210
<i>o</i> -Xylene	8.10	+0.62	5.7	232
Cumene	2.40	+0.79	4.9 est.	194
Chlorobenzene	6.70	-1.70	5.8	116

the maximum surface pressure of cumene was estimated using a lens of cumene on a 0.1 *M* NaCl solution at 15°, a technique that gives the correct value for toluene.) There appears to be no relation between ΔV and the parameters of the adsorption, p_0 or Π . However, ΔV appears to be related to a molecular parameter, the dipole moment (μ), also given in the table. In Fig. 6 the surface potential values at p_0 are plotted against the dipole moment of the adsorbate in the vapor phase. The values also have been corrected for the different areas of the adsorbate molecules using: (1) the projections of vertically oriented molecular models onto a surface, (2) the limiting surface areas on surface pressure–area curves (where available), and (3)

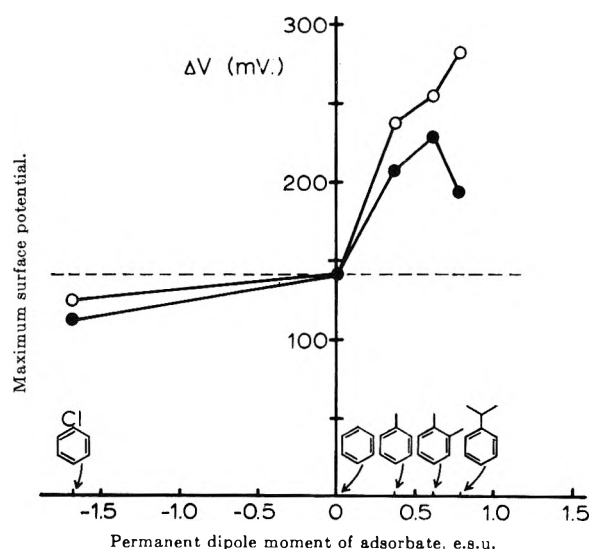


Figure 6. The maximum surface potential vs. the dipole moment of the aromatic adsorbate in the vapor phase: —●—, measured values; —○—, corrected for the different areas per molecule.

(14) B. V. Derjaguin and Z. M. Zorin, Proceedings of the 2nd International Congress of Surface Activity, Vol. 2, Butterworth and Co. Ltd., London, 1957, p. 145.

(15) J. A. Kitchener, *Endeavour*, 22, 118 (1953).

the molar volumes. This procedure corrects the ΔV readings to the same concentration of adsorbed dipoles as that of benzene.

Although benzene does not have a dipole moment, a ΔV of 142 mv. was found. This must arise from the interaction between the phenyl ring and the water dipoles at the surface. The interaction varies as a function of p , as in Fig. 1, presumably because of variations in the concentration and orientation of phenyl rings on the surface. Since a phenyl group was common to all the vapors examined, it is reasonable to assume that deviations from the value of ΔV obtained for benzene (deviations from the dashed horizontal line of Fig. 6) arise from the additional interactions due to the permanent dipole moments of the molecules. This suggestion is supported by the fact that the deviations from the ΔV for benzene vary with the sign and the magnitude of the dipole moments.

In studying the adsorption of toluene on mercury, Kemball¹² found a sharp change in ΔV corresponding to the reorientation of the toluene molecules from the horizontal to the vertical. Although the surface isotherms as well as the ΔV changes indicate that the toluene molecules reoriented at higher p , the observed variation of ΔV was gradual. This is probably due to the additional interaction of toluene with the water dipoles. [It may be no coincidence that when this interaction is subtracted (as in Fig. 6), the ΔV for toluene on water (68 mv.) agrees approximately with Kemball's value of 55 mv. on mercury.]

The initial orientation of water dipoles at a water-air interface can be inferred from the magnitudes of ΔV for the different vapors. The data indicate that toluene causes a much greater ΔV than chlorobenzene, even though it has the smaller dipole moment. This suggests that the toluene molecule adsorbs without causing as great a rearrangement of the surface water dipoles. Therefore, the water dipoles must have the same orientation as the permanent dipole of the adsorbed toluene molecules, namely, with the hydrogens directed toward the vapor phase. In the adsorption of chlorobenzene, where the dipole moment is of opposite sign, there is considerable rearrangement of the water dipoles and the effect of the permanent dipole moment of the adsorbate on ΔV is obscured. The orientation of the water dipoles with their hydrogen atoms pointing toward the gas phase is in agreement with the findings of other workers¹⁶

Acknowledgments. Some of the work reported in this paper was done in the Department of Colloid Science, Cambridge, England. We wish to thank the U. S. Public Health Service for supporting M. B. for a visit to the Department of Colloid Science during September to December, 1961. We also wish to thank Dr. D. C. Jones for discussions during the earlier parts of this work.

(16) D. A. Haydon, *Kolloid-Z.*, **185**, 148 (1962).

Exchange and Diffusion of Ions in Glass

by R. H. Doremus

General Electric Research Laboratory, Schenectady, New York (Received March 2, 1964)

Relations between various parameters involved in the interdiffusion of two ions in glass are derived and the assumptions in these derivations exposed. The exchange and diffusion of silver ions in soda-lime glass at 374° were examined. The self-diffusion coefficient of sodium was about 12 times that of silver. The Einstein equation relating the self-diffusion coefficient of sodium to the electrical conductivity of the glass was obeyed without correction for correlations, in contrast to earlier results on sodium silicate glasses. The profile of silver diffusing into the glass from a melt of silver chloride was measured, and this interdiffusion was also followed by the change of weight and of electrical resistance of the glass. These interdiffusion measurements were consistent with equations used by Helfferich, assuming that the self-diffusion coefficients of silver and sodium in the glass were constant. The ratio of self-diffusion coefficients calculated from these equations agreed with that found in tracer diffusion experiments. The result of constant self-diffusion coefficients in the glass is discussed in terms of the theory for ionic diffusion by defects. The implications of the present results to the mechanism of operation of glass electrodes are also considered.

Introduction

When a common soft glass is placed into a melt or solution containing monovalent ions, these ions exchange with the sodium ions in the glass. This process is analogous to the exchange of ions in a resin exchanger, since the negative oxygen ions in the glass are rigidly held in a silicate network. The rate at which this exchange proceeds is controlled by the diffusion of the ions in the glass.^{1,2} A study of this exchange and diffusion can therefore provide insight into mechanisms of ionic transport in glass, which in turn may help in the understanding of the structure of the glass.

The operation of glass electrodes depends upon the exchange of ions in the glass with the ions in the solution whose concentration is being measured. It is not clear whether this exchange leads to development of an electrical potential in the glass itself, or if only its surface becomes charged. Better knowledge of the exchange process can perhaps elucidate this problem.

In this study the exchange and diffusion of silver ions into a soft glass containing sodium were examined in detail.

Relations between Transport Parameters

Systems without bulk flow of material are considered. The flux J of a species flowing per unit area and time is given by

$$J = cv \quad (1)$$

where c is the concentration of the species and v is its average molecular velocity. The driving force for transport in the x direction is the negative of the gradient in total chemical potential μ (sometimes called "electrochemical potential")

$$\frac{\partial \mu}{\partial x} = \frac{RT}{c} \frac{\partial c}{\partial x} \frac{\partial \ln a}{\partial \ln c} + ZFE \quad (2)$$

in which a is the thermodynamic activity, Z the ionic charge, F the faraday, E the electrical potential gradient, R the gas constant, and T the temperature. A generalized mobility u can be defined as the average

(1) G. Schulze, *Ann. Physik*, **40**, 335 (1913).

(2) R. H. Doremus, "Diffusion in Noncrystalline Silicates," in Vol. II of "Modern Aspects of the Vitreous State," Butterworth and Co., Ltd., London, 1962, p. 1.

ionic velocity per unit driving force. Then the mobility u^* for self-diffusion is given by

$$u^* = \frac{-v}{\frac{RT}{c} \frac{\partial c}{\partial x}} = \frac{-J}{RT \frac{\partial c}{\partial x}} = \frac{D}{RT} \quad (3)$$

in which D is the self-diffusion coefficient. The electrical mobility u_e in an experiment in which the electrical conductivity σ is measured is given by

$$u_e = \frac{-v}{ZEF} = \frac{\sigma}{Z^2 F^2 c} \quad (4)$$

To derive the Einstein equation, which relates the self-diffusion coefficient of an ion to the electrical conductivity of a system in which the current is carried only by this ion, the mobilities as defined above are assumed to be equal. Then

$$\sigma = \frac{Z^2 F^2 D c}{RT} \quad (5)$$

In other derivations of this equation^{3,4} thermodynamic expressions for a system in equilibrium are used, but these expressions are unsatisfactory, since in a transport experiment the system is not in equilibrium. Deviations from the Einstein equation in solids because of correlations and in aqueous solutions because of the distortion of the electric field around a moving ion demonstrate this deficiency. The present derivation is based upon a simple physical assumption, and a deviation from the Einstein equation shows when this assumption is not valid.

In glasses eq. 5 is often not exact; to give equality σ must be multiplied by a factor f between 0.25 and 0.65. It has been suggested that the f factor for glasses can be explained because of correlations in a defect mechanism of diffusion^{5,6}; such a mechanism has been proposed by Charles⁷ to explain electrical conductivity and dielectric relaxation of glasses, but f has not been calculated from this model.

Equations relating the results of self-diffusion experiments and those involving diffusion of several different ions under a concentration gradient can also be derived by assuming that the mobilities of a species i in the two types of experiments are equal. Then

$$\frac{D_i}{RT} = \frac{-v_i}{\frac{RT}{c_i} \frac{\partial c_i}{\partial x} \frac{\partial \ln a_i}{\partial \ln c_i} + Z_i F E} \quad (6)$$

or

$$J_i = -D_i \left[\frac{\partial c_i}{\partial x} \frac{\partial \ln a_i}{\partial \ln c_i} + \frac{Z_i c_i E F}{RT} \right] \quad (7)$$

These flux equations are sometimes called the Nernst-Planck equations. Deviations from eq. 6 and 7 can be taken into account by dividing D_i by a factor f_i in the same way as in eq. 5.

From the conditions of electrical neutrality for two diffusing ions and eq. 7 the potential gradient is

$$E = \frac{RT}{F} \frac{\partial c_1}{\partial x} \left[\frac{Z_1(D_2 - D_1)}{Z_1^2 c_1 D_1 + Z_2^2 c_2 D_2} \right] \frac{\partial \ln a_1}{\partial \ln c_1} \quad (8)$$

To develop this electrical potential small deviations in electrical neutrality must occur in the ionic system. However, the number of ions involved in these deviations is negligible compared to the total ionic concentrations.

When eq. 8 is put into eq. 7, the flux is given by

$$J_1 = -D_1 \left[\frac{Z_1^2 c_1 D_2 + Z_2^2 c_2 D_2}{Z_1^2 c_1 D_1 + Z_2^2 c_2 D_2} \right] \frac{\partial \ln a_1}{\partial \ln c_1} \frac{\partial c_1}{\partial x} \quad (9)$$

with a similar equation for J_2 . The coefficients of the concentration gradient are the same for both species; for 1:1 electrolytes with constant activity coefficients this "inter-diffusion coefficient" is

$$\bar{D} = \frac{D_1 D_2}{N_1 D_1 + N_2 D_2} \quad (10)$$

in which $N_i = c_i / (c_1 + c_2)$.

Recently Karreman and Eisenman⁸ assumed the relation $a = c^n$, with n a constant, for ions in silicate glasses. Then $\partial \ln a / \partial \ln c = n$, and a constant factor of n appears on the right-hand side of eq. 8, 9, and 10.

Equation 9 has been solved numerically for various geometries by Helfferich and Plesset⁹ and Helfferich¹⁰ with the assumption that the self-diffusion coefficients D_1 and D_2 are constant with concentration (N_1 and N_2). In this paper their calculated profiles are compared with experiments on glass to see if the assumptions of equal mobilities in self and gradient diffusion and of constant self-diffusion coefficients are obeyed.

(3) A. Einstein, *Ann. Phys.*, **77**, 549 (1905).

(4) N. F. Mott and R. W. Gurney, "Electronic Processes in Ionic Crystals," Oxford University Press, London, 1948, p. 63.

(5) A. B. Lidiard in "Handbuch der Physik," Vol. 20, Electrical Conductivity II, Springer-Verlag, Berlin, 1957, p. 246.

(6) Y. Haven and J. M. Stevels in "Travaux du IV Congrès Intern. du Verre," Imprimerie Chaix, Paris, 1957, p. 343.

(7) R. J. Charles, *J. Appl. Phys.*, **32**, 1115 (1961).

(8) G. Karreman and G. Eisenman, *Bull. Math. Biophys.*, **24**, 413 (1962).

(9) F. Helfferich and M. S. Plesset, *J. Chem. Phys.*, **28**, 418 (1958).

(10) F. Helfferich, *J. Phys. Chem.*, **66**, 39 (1962).

Experimental Methods

The composition of the glass as found by chemical analysis is given in Table I. Glass tubes of 1.36-cm. o.d. and 0.12-cm. wall thickness were annealed at about 550° and then cooled very slowly (1–2°/min.) to room temperature.

Table I: Composition of Glass in Weight %

SiO ₂	72.6	B ₂ O ₃	0.8
Na ₂ O	15.2	Sb ₂ O ₃	0.655
CaO	4.6	SO ₃	0.27
MgO	3.6	Fe ₂ O ₃	0.06
Al ₂ O ₃	1.7	BaO	0.01
K ₂ O	0.7		

The tracer-diffusion coefficient of an ion in the glass was measured by placing an open-ended tube of the glass in molten sodium nitrate containing a radioactive isotope (silver-110 or sodium-22) of the ion being followed. After remaining in the melt for a period the glass was removed, the excess sodium nitrate washed off, and layers of the glass were successively etched off with 4% hydrofluoric acid. As the etching proceeded, a few pits appeared on the glass surface; but otherwise the surface appeared smooth and uniform. These acid solutions were counted in a plastic counting cell with a conventional Gieger-Müller counting tube and a scaler. The thickness of the etched layer was calculated from the change in weight after etching and the density of the glass (2.48 g./cm.³). The diffusion coefficient D was calculated by comparing the profile with the equation

$$c = c_0 \operatorname{erfc}(x/2Dt) \quad (11)$$

in which erfc is the conjugate error function, t is the diffusion time, c is the concentration of tracer at the distance x from the melt-glass interface, and $c = c_0$ when $x = 0$.

The diffusion coefficient measured in this way is the self-diffusion coefficient for sodium ions if isotope effects are negligible. However, for silver this method actually measures the interdiffusion coefficient at very small silver concentration. Equation 10 shows that this interdiffusion coefficient is equal to the self-diffusion coefficient of the dilute species if the gradient of the activity coefficient is negligible.

In the interdiffusion experiments a tube with one end closed off was placed into molten silver nitrate. Sodium nitrate was inside the tube, and platinum electrodes in the two melts were used to make electrical contact. The progress of the diffusion was traced in

several different ways, described in the following paragraphs. In the following equations subscript 1 refers to the ion initially in the glass (sodium) and subscript 2 to the ion diffusing into the glass (silver).

The electrical resistance R of the glass was followed as diffusion progressed. This resistance is given by

$$R = \frac{1}{A} \int_0^L \frac{dx}{\sigma}$$

in which A is the surface area exposed to the melt containing the foreign ion, L is the thickness of the glass, and σ is the specific electrical conductivity of the glass at a distance x from the glass-melt interface. If $y = x\sqrt{D_1t}$, where D_1 is the self-diffusion coefficient of sodium in the initial glass, then

$$R - R_1 = \frac{\sqrt{D_1t}R_1}{L} \int_0^{L/\sqrt{D_1t}} \frac{(\sigma_1 - \sigma)dy}{\sigma} \quad (12)$$

in which R_1 and σ_1 are the initial resistance and conductivity, respectively, when the glass contains only sodium ions, and $R_1 = L/\sigma_1A$. Since σ is a function of ionic concentration only, which in turn is a function of y only, the integral is a constant as long as $L \gg \sqrt{D_1t}$ and the concentration profile has a constant shape as diffusion proceeds. Under these conditions the change in resistance $R - R_1$ is proportional to the square root of time, and the proportionality constant gives information about the concentration profile. The resistance of the glass was measured with a Shedlovsky (Wheatstone) bridge, using alternating current of 1000 c.p.s.

Interdiffusion was also followed by weighing to find the total amount m_2 , in moles, of silver that had diffused into the glass for a time t

$$m_2 = A \int_0^t J_2^0 dt = -2A \sqrt{\bar{D}^0t} \left(\frac{\partial c_2}{\partial z} \right)_{z=0} \quad (13)$$

where $z = x/\sqrt{\bar{D}^0t}$, J_2^0 is the flux of silver when $x = 0$, and \bar{D}^0 is the interdiffusion coefficient when $x = 0$. Thus, m_2 is also proportional to the square root of diffusion time, since the differential is constant for a constant profile. The total change in weight ΔW of a tube was found after diffusion; then

$$m_2 = \frac{\Delta W}{M_2 - M_1}$$

where M_i is the molecular weight of i .

The profile of diffusing material was measured by etching off successive layers of the glass with 4% HF and analyzing the resulting solutions for silver with radioactive silver tracer; in this case the tracer was used simply to analyze for the silver, not to measure

a self-diffusion coefficient. To prevent adsorption of silver from the etching solutions by containing vessels and to extract all silver from the substances etched from the glass, the HF solution was neutralized with ammonia after etching and some 0.2 *N* sodium cyanide solution added to complex the silver ions and keep them in solution. The thickness *d* of the etched layers was calculated from the change in weight ΔW after etching and the following formula

$$d = \frac{\Delta W - m_{Ag}(M_{Ag} - M_{Na})}{\rho_0 A}$$

in which m_{Ag} is the total number of moles of silver in the layer, M is the molecular weight, and ρ_0 is the density of the glass before diffusion.

Results

The profile of sodium tracer diffusing into the glass from a sodium nitrate melt at 374° is shown in Fig. 1; the diffusion coefficient calculated from this profile and eq. 11 is 1.02×10^{-9} cm.²/sec.

The profile of silver tracer diffusing into the glass from a sodium nitrate melt is also shown in Fig. 1. Silver is partitioned preferentially into the glass; the partition coefficient is about 200, in agreement with the results of Schulze on a glass of similar composition.¹ Thus, even though the diffusion coefficient of silver in the melt was much higher than in the glass, there was probably an appreciable concentration gradient of silver tracer in the melt near the glass surface. However, this gradient does not change the form of the diffusion profile in the glass, since the concentration of silver in the glass at its surface remains constant throughout the diffusion, as shown by Crank.¹¹ This conclusion was checked by measuring the profile for ratios of melt volume to glass surface area varying by a factor of ten; the same profile was found in every case. The same profile shape (that of eq. 11) was also found for different times of diffusion. The average diffusion coefficient of silver tracer from three different experiments was 8.5×10^{-11} cm.²/sec.

In Fig. 2 the experimentally determined profile of silver diffusing into the glass from a silver nitrate melt at 378° is compared to solutions of eq. 9 and 10 with the assumption that the self-diffusion coefficients D_1 and D_2 are constant. Unpublished computer solutions for semi-infinite geometry and various ratios of D_1/D_2 were supplied to the author by F. Helfferich. Solutions of this type may also be derived from Fig. 12.12, p. 273, of Crank,¹¹ or the equations of Fujita (ref. 11, p. 167). The curve drawn in the figure is for $D_1/D_2 = 10$, where D_1 is the self-diffusion coefficient of the species initially in the glass (sodium) and D_2 for that

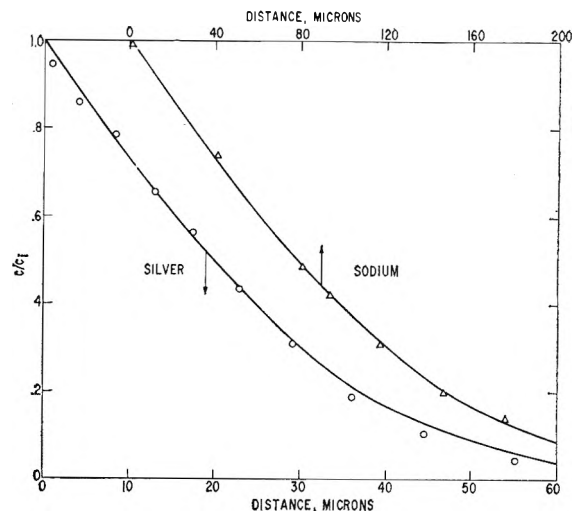


Figure 1. Concentration profiles of sodium and silver tracer diffusing from a sodium nitrate melt into a soda-lime glass at 374°. Times of diffusion 1135 min. for sodium, 1024 min. for silver. Lines drawn from eq. 11.

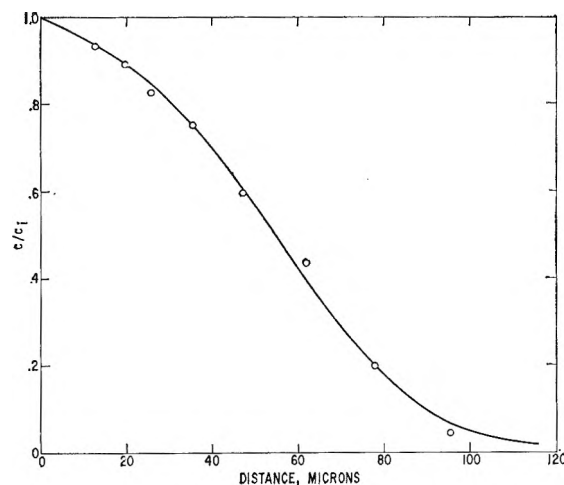


Figure 2. Concentration profile of silver that had diffused from a silver nitrate melt into a soda-lime glass for 1097 min. at 378°. Line drawn from Helfferich's solution of eq. 10 with $D_1/D_2 = 10$.

initially in the melt (silver). The derived value of this ratio is not very precise because the shape of the curve does not change much as the ratio changes; however, one can readily say that it is closer to 10 than 5 or 20. The value of D_1 calculated from this curve is 1.1×10^{-9} cm.²/sec. at 378°, or about 1.0×10^{-9} cm.²/sec. at 374°, assuming² an activation energy of 20 kcal./mole. This result is in good agreement with the value found in the tracer diffusion experiment with sodium

(11) J. Crank, "The Mathematics of Diffusion," Oxford University Press, London, 1956, p. 38.

ions. The ratio between the experimental values of the sodium and silver tracer diffusion coefficients is 12, which agrees with the interdiffusion value of D_1/D_2 within the error of determining it from the profile.

The electrical resistance of the glass as silver diffused into it from a silver nitrate melt at 378° is shown in Fig. 3. The resistance of the glass changed linearly with the square root of diffusion time after temperature equilibrium was established, as required by eq. 12. From several different experiments in which silver diffused into the glass from a silver nitrate melt the average value of the ratio $m_2/A\sqrt{t}$ was found to be 2.76×10^{-7} mole/cm.² sec.^{1/2} by weighing the glass after diffusion for a time t . From the slope of the line in Fig. 3 and this result, the ratio D_1/D_2 and the absolute values of these coefficients can be calculated as follows if the assumption of constant self-diffusion coefficients with concentration is made.

The electrical conductivity σ at a point x is

$$\sigma = \sigma_1 N_1 + \sigma_2 N_2$$

where σ_1 is the conductivity of the glass when it contains only species i and $N_i = c_i/(c_1 + c_2)$ as before. It is now assumed that the ratio $\sigma_1/\sigma_2 = D_1/D_2$. This assumption is valid if the ions in the sodium and silver forms of the glass follow eq. 5 with the same factor f to account for deviations from this equation. Then from eq. 12

$$R - R_1 = \frac{-\sqrt{D_1 t} R_1}{L} \int_0^L \frac{N_2 (D_2/D_1 - 1) dy}{1 + N_2 (D_2/D_1 - 1)} \quad (14)$$

For any particular ratio D_1/D_2 the integral in eq. 14

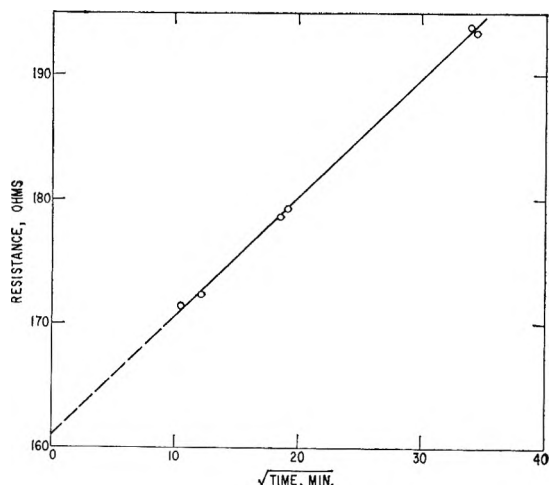


Figure 3. The change of electrical resistance of a soda-lime glass as silver diffused into it from a silver nitrate melt at 378° .

is constant with time when $L \gg \sqrt{D_1 t}$, as pointed out previously. Results of numerical integration of this integral for certain values of D_1/D_2 are shown in Table II. If the activity coefficients of the ions are constant throughout the glass $\partial \ln a/\partial \ln c = 1$, so that \bar{D}^0 , the interdiffusion coefficient at $x = 0$, equals D_1 from eq. 10. In this case $y = z$. Values of $(\partial c/\partial y) = (\partial c/\partial z)$ at $y = z = 0$, as calculated from Fujita's equations (ref. 11, p. 169), are also shown in Table II. With the two parameters given in Table II as functions of D_1/D_2 , the value of this ratio and also of D_1 can be calculated from eq. 13 and 14 and the experimental results of resistance and weight change during diffusion. From the data mentioned in the last paragraph D_1 (sodium) and D_2 (silver) are about 1.2×10^{-9} and 1.0×10^{-10} , respectively, corrected to 374° , in reasonable agreement with the results of the tracer diffusion measurements.

Table II: Parameters Calculated for Eq. 13 and 14 for Various Values of D_1/D_2

$\frac{D_1}{D_2}$	$\frac{1}{c_2} \left(\frac{\partial c_2}{\partial y} \right)_{y=0}$	$\int_0^L \frac{D_1 t}{1 + N_2 (D_2/D_1 - 1)} dy$
0	0.565	
2	.501	
4	.425	1.46
10	.327	2.44
20	.264	3.46
91.7	.147	
358	.0885	
4900	.0288	34.4

The interdiffusion was followed in yet another way. A glass tube was placed in molten silver nitrate at 376° for 265 min., and then into molten silver nitrate containing silver tracer for 258 min. at 376° . The resultant profile of radioactive silver in the glass is shown in Fig. 4. Also shown in Fig. 4 is the profile of total silver concentration, calculated from the profile in Fig. 2. The penetration of radioactive silver is much greater than would be expected from the tracer diffusion of silver into the sodium form of the glass because of the electric field set up by the initial interdiffusion of silver and sodium.

Discussion

The good agreement between results derived from the resistance change, weight change, and profiles in interdiffusion experiments and the tracer diffusion measurements appears to confirm the various assumptions made to derive relations between these experimental

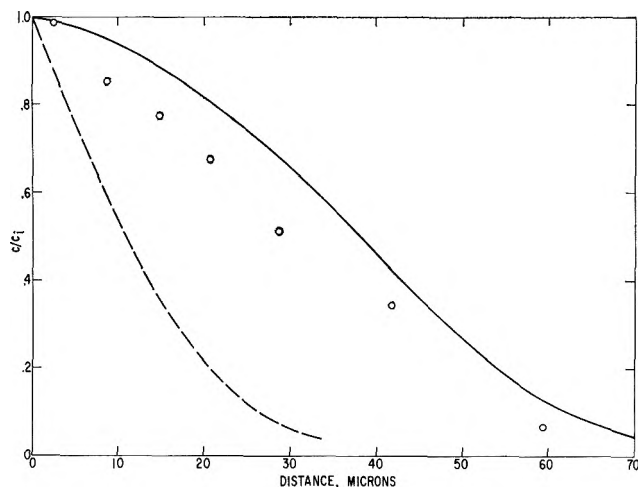


Figure 4. Diffusion of silver tracer from a silver nitrate melt into a soda-lime glass for 265 min. after diffusion of nontracer silver into the glass from a silver nitrate melt for 258 min. at 376°. Solid line, total concentration of silver; points, concentration profile of silver tracer; dashed line, expected diffusion of silver tracer into a uniform glass.

parameters. The assumption of equal mobilities in self- and interdiffusion experiments, used to derive eq. 6 and 7, can be tested at least partially with eq. 5. In the present glass eq. 5 was satisfied within the experimental error of about $\pm 10\%$ in D_1 at 374°. This result is in surprising contrast to the results of other investigators^{2,12,13} who have measured f factors for sodium in silicate glasses from 0.4 to 0.65, but not higher. A possible reason for these differences is that the present study was made in a commercial glass with many constituents, whereas the other investigations were made with simple sodium silicate and sodium calcium silicate glasses melted in the laboratory.

To obtain eq. 10 it was assumed that the activity coefficients of the sodium and silver ions were constant in the glass. If a relation of the form $a = c^n$ between the activity and concentration of ions in the glass is valid, the present results show that within experimental error $n = 1$ since the interdiffusion coefficient of eq. 10 is about equal to D_1 when $N_1 = 0$. The data of Schulze¹ on the partitioning of silver ion between melts of sodium and silver nitrate and a soda-lime glass can be used to derive a value of n by plotting the log of the ratio of ionic concentrations in the melt as a function of the log of this ratio in the glass. The result at 354° is an n of about 1.1, which is within experimental error of the present findings.

The result of constant self-diffusion coefficients with ionic concentration can be examined with theories of ionic diffusion in silicate glasses. Charles⁷ proposed

that ionic transport in glass occurs by a defect mechanism, in which the defect consists of two ions in different sites around one oxygen ion. In any defect mechanism the diffusion coefficient D can be described by the equation^{2,5}

$$D = N\nu \exp(\Delta S/R) \exp(-\Delta H/RT) \quad (15)$$

in which N is the concentration of defects, ν is the vibration frequency of the diffusing ion, and ΔS and ΔH are the entropy and enthalpy of "activation." Apparently the sodium and silver ions are completely exchangeable, reside in similar sites, and diffuse by the same mechanism. Then the constancy of each self-diffusion coefficient with ionic ratio rules out any change in N , the defect concentration, with changing ionic ratio, so that the difference in self-diffusion coefficients must result from different transition frequencies of the two ions. From the results of Schulze¹ it appears that the activation energies for sodium self-diffusion, deduced from the electrical resistivity, and for silver self-diffusion, as deduced from the interdiffusion experiments as a function of temperature, were very nearly the same.² Therefore, the values of ΔH for the two ions must be nearly the same, and the only explanation for different self-diffusion coefficients can be different values of ΔS . This entropy of activation can arise from elastic distortions of the silicate network in the vicinity of the jumping ion.¹⁴ It is not surprising, therefore, that ΔS is very sensitive to the size of the ion. Charles¹⁵ found that quite large amounts of strain or pressure had little effect on the activation energy for conduction, but that the absolute value of the conductivity was changed substantially by strain or pressure, presumably because of changes in ΔS . A more complete description of the ratios of self-diffusion coefficients in different silicate glasses awaits more detailed knowledge of the diffusion mechanism in these glasses.

The present results can be compared with Schulze's measurements of the diffusion of silver ions into a soda-lime glass. Schulze concluded that the silver ion was more mobile than the sodium ion in the glass. In view of the present results, this conclusion seems unlikely. Schulze's evidence for this conclusion involved measurements of the electrical resistance and profile of silver in the glass after introduction of silver with an electric field at 297°. It seems likely

(12) J. V. Fitzgerald, *J. Am. Ceram. Soc.*, **34**, 314 (1951).

(13) K. K. Evstrop'ev in "The Structure of Glass," Vol. II, Consultants Bureau, New York, N. Y., 1960, p. 237.

(14) C. Wert and C. Zener, *Phys. Rev.*, **76**, 1169 (1949).

(15) R. J. Charles, *J. Am. Ceram. Soc.*, **45**, 105 (1962).

that misleading results were caused by the large strain introduced into the glass by the rapid increase of the silver concentration at a low temperature. In this work glass treated in this way cracked into pieces upon standing overnight, whereas after the interdiffusion without external electric field the glass was as strong as before introduction of silver. It seems reasonable, therefore, to interpret the results of Schulze with the assumption of constant self-diffusion coefficients. The concentration profile of Schulze for silver diffusion at 354° fits the profile calculated for $D_1/D_2 = 4$, as shown in Fig. 5, with $D_1 = 3.7 \times 10^{-10}$ cm.²/sec. The value of D_1 calculated from the weight change *vs.*

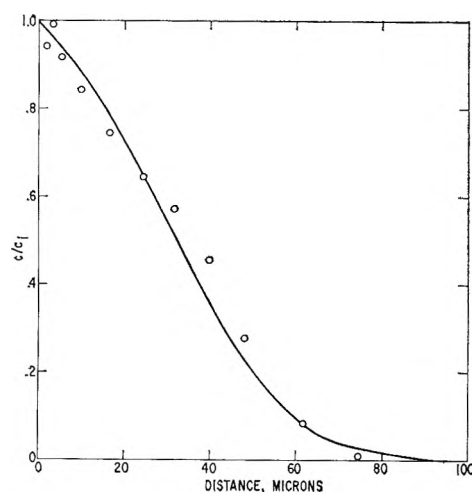


Figure 5. Concentration profile of silver that had diffused from a silver nitrate melt into a soda-lime glass for 720 min. at 354° , as found by Schulze.¹⁰ Line drawn from Helfferich's solution of eq. 10 with $D_1/D_2 = 4$.

\sqrt{t} relationship found by Schulze is 4.3×10^{-10} cm.²/sec. if $D_1/D_2 = 4$. The value of D_1 calculated from the electrical resistivity of the glass without silver is 2.4×10^{-10} , which is somewhat low. Schulze measured the weight change as a function of time for different surface concentrations of silver; these results agree with those calculated from eq. 10 and 13 with $D_1/D_2 = 4$ within the rather large scatter of the experimental data. Therefore, the results of Schulze appear to be consistent with the assumption of constant self-diffusion coefficients and a ratio $D_1/D_2 = 4$. The difference between this ratio and that of 12 found in this study is surprising, since the glass in the two studies had a similar composition, the only significant differences being somewhat more potassium and aluminum in Schulze's glass.

The results of this study indicate that a potential gradient, given by eq. 8, is set up in the glass when silver diffuses into it. The total potential drop V across the glass resulting from this diffusion potential is given by

$$V = \int_0^L E dx = \frac{RT}{F} \int_{c_0}^{c_L} \frac{(1 - D_1/D_2) dc_1}{c_1(D_1/D_2) + c_2} = \frac{RT}{F} \ln \frac{1 + N_L(D_1/D_2 - 1)}{1 + N_0(D_1/D_2 - 1)} \quad (16)$$

where N_L and N_0 are the mole fractions of component 1 in the glass at the two respective surfaces. The integration can be performed in this way only if D_1/D_2 is constant with changing N_1 . This potential depends only upon the ionic ratios at the two glass surfaces and upon the ratio D_1/D_2 . It is not influenced by the shape of the diffusion profile, the time of diffusion, or the absolute values of ionic concentrations of diffusion coefficients.

The present results have some pertinence to the origin of potentials in glass electrodes. These electrodes are sensitive to the concentrations of different ions in solution, depending upon the composition of the glass. The ion to which the electrode is sensitive exchanges with the ions already in the glass, and a potential difference between the glass and the solution is set up because of a difference of the activity of the ion in the solution and the glass. From the present work one would expect that a potential is also set up in the glass if the exchanging ions have different self-diffusion coefficients in the glass. Thus, in the common soda-lime glass electrode used to measure hydrogen ion concentration the interdiffusion of hydrogen and sodium ions should give rise to an internal potential in the glass. On the other hand when a sodium aluminosilicate glass is used to measure sodium ion concentration no internal potential is expected because the exchanging ions are the same. From eq. 16 the total potential becomes constant as soon as ionic equilibrium is reached at the surface, and the internal potential depends only upon the ratio of the ionic self-diffusion coefficients for a constant surface concentration of exchanging ions. Thus, the stability and reproducibility of potentials measured by glass electrodes is understandable.

Acknowledgments. The author is grateful to F. Helfferich for helpful discussions and to W. C. Hagel and R. E. Hoffman for critical reviews of the manuscript.

Self-Diffusion in Tin at High Pressure

by C. Coston and N. H. Nachtrieb

Department of Chemistry and Institute for the Study of Metals, the University of Chicago, Chicago, Illinois 60637
(Received March 5, 1964)

Measurements are reported for *a*-axis and *c*-axis self-diffusion in tin from 0 to 10 kbars and for temperatures in the range 160–228°. At zero pressure, $D_a = 10.7 \exp(-25,100 \pm 800)/RT$ and $D_c = 7.7 \exp(-25,600 \pm 1000)/RT$. The activation volume is 5.3 ± 0.3 cm.³ g.-atom⁻¹ (33% of the g.-atomic volume) for both principal directions and appears to be independent of temperature. The data are most simply interpreted in terms of a vacancy mechanism, in which two distinct kinds of jumps occur.

Introduction

Activation energies ΔH determined from the temperature dependence of the diffusion rate in single crystals of the elementary metals are most satisfactorily correlated with theoretically calculated activation energies for a vacancy diffusion mechanism.¹ Recent work on the pressure dependence, which leads to the activation volume ΔV , has supported this mechanism.² The work of Simmons and Balluffi³ provides near-conclusive evidence for the existence of high concentrations of vacancies in the noble metals and aluminum near their melting points. Hence, a vacancy diffusion mechanism is reasonable in these and similar metals.

Solid-state diffusion has been considered an activated process, with a Gibbs free energy of activation ΔG . For the vacancy mechanism, it is natural to distinguish between contributions to ΔG from the formation of sessile vacancies at equilibrium in the lattice, ΔG_t , and from the additional free energy ΔG_m necessary to move the vacancy from the equilibrium position to the midpoint of the diffusive jump. The activation enthalpy and volume have analogous components; diffusion studies yield only their sum. For close-packed hard spheres, ΔV_t should be 1 molar volume, and ΔV_m should be of this order.² Other crystal structures will have smaller motional contributions. Measured values of ΔV range from about 25% of an atomic volume (lithium) to 90% (silver), and are greater than 50% for close-packed structures.²

Rice and co-workers^{4–6} have developed a dynamical theory of diffusion which, while formally equivalent to activated state theory, avoids the least tenable assumptions of the activated state, and which identi-

fies the important microscopic contributions to the diffusive process. The activation energy is replaced by

$$\Delta H = U_0 + \sum_j U_j + \sum_{k>l} H_{kl} + \Delta H_t \quad (1)$$

where U_0 is the translational energy a diffusing atom must obtain to successfully effect the jump, $\sum_j U_j$ is the excess energy over the thermal average for any atoms hindering the motion of the diffusing atom to move sufficiently aside for that atom to pass, and $\sum_{k>l} H_{kl}$ accounts for adjustments of the surrounding atoms not specifically included in the jump process. ΔH_t is the formation enthalpy of a vacancy.

Using this approach, Rice and Nachtrieb⁵ conclude that a correspondence between diffusion and melting should exist in the form

$$\left[\frac{\partial \ln (D/\gamma a^2 \nu)}{\partial T_m/T} \right]_{T_m} = \text{constant} \quad (2)$$

and that

(1) D. Lazarus, "Advances in Solid State Physics," Vol. 10, F. Seitz and D. Turnbull, Ed., Academic Press, Inc., New York, N. Y., 1960, p. 71.

(2) D. Lazarus and N. H. Nachtrieb, "Solids Under Pressure," W. Paul and D. M. Warschauer, Ed., McGraw-Hill Book Co., Inc., New York, N. Y., 1963, p. 43.

(3) R. O. Simmons and R. W. Balluffi, *Phys. Rev.*, **117**, 52 (1960); **119**, 600 (1960); **125**, 862 (1962); **129**, 1533 (1963).

(4) S. A. Rice, *ibid.*, **112**, 804 (1958).

(5) S. A. Rice and N. H. Nachtrieb, *J. Chem. Phys.*, **31**, 139 (1959).

(6) A. W. Lawson, S. A. Rice, R. D. Corneliussen, and N. H. Nachtrieb, *ibid.*, **32**, 447 (1960).

$$\Delta H = \frac{\Delta H_m}{\Delta V_m} \Delta V \quad (3)$$

where the subscript m refers to fusion. While (2) and (3) hold remarkably well for a large number of metals to 10 kbars⁷ Hudson and Hoffman⁸ have found large deviations for lead at higher pressure. The correspondence between diffusion and melting probably exists only in the limit of zero pressure.

From the foregoing it is evident that vacancy diffusion occurs in metals which crystallize in close-packed structures in which the void volume is a minimum. Anisotropic structures typically have larger void volumes; and if interstitial self-diffusion occurs in metals, those with anisotropic structures should be relatively favored. Since no theoretical calculations for activation energies have been made for such systems, it is necessary to determine the activation volumes, as well as activation energies, to form reliable conclusions about the diffusion mechanism. White tin is anisotropic, with a void volume at 25° of 46.5%, and is thus a favorable metal. Self-diffusion studies in tin at zero pressure have been reported by Fensham⁹ and by Meakin and Klokhholm.¹⁰ The results of Fensham are anomalous, giving activation energies which disagree with results for similar metals. Meakin and Klokhholm found close agreement with other low melting metals, but could show only that a vacancy mechanism was consistent with their results, not that it was required. This study was undertaken to determine unequivocally the diffusion mechanism in tin.

It is perhaps desirable to ask at this point what is the significance of the quantity $(\partial \ln D / \partial P)_T$ in an anisotropic system. Girifalco and Grimes¹¹ have analyzed the effect of strain on the diffusion relations as developed by Vineyard.¹² Their results are generalized to anisotropic systems in the Appendix, and it is clear that the measured quantity is indeed a volume, related to the usual activation volume in isotropic systems. This result adds confidence in the conclusions drawn from this study.

Experimental

Large single crystals were grown from 99.999% tin¹³ by a modified Bridgman technique. Crystal quality was checked with a modified Laue back-reflection technique, in which the only collimation of the X-ray beam was a 0.10-in. diameter pinhole. This gave a beam which struck about 1 cm.² of the crystal surface. Any crystal defects in this area appeared as irregularities in the X-ray film spots. Only crystals which gave nearly perfect spots were accepted for diffusion studies.

The large crystals were oriented by the usual Laue back-reflection technique. Cubes approximately 1 cm. on an edge and with their faces oriented close to perpendicular to the (100) or (001) axis, principle axes for diffusion, were cut out with a Servomet spark cutter. These cubes were again checked for quality with large-spot X-rays. No difference in quality of faces perpendicular or parallel to the tetragonal (001) axis was detected. Once again only the best crystals were retained. Two faces of each cube were oriented on a small goniometer head by X-rays so that the desired crystal axis and the goniometer axis were parallel to 0.5° of arc. The goniometer head was then aligned optically in a microtome to cut the crystal face perpendicular to the desired axis. Microtoming gave a plane basal surface flat to within 2 μ. The crystal was annealed for 24 hr. to remove the slight cold work introduced by the microtome.

Sn¹¹³ in carrier metal was vapor deposited on the diffusion faces at pressures less than 10⁻⁵ mm. Typically, films less than 1 μ thick and having an activity of close to 10⁵ counts per min. were achieved.

The crystal was sealed in a Pyrex ampoule under vacuum and placed in a wire-wound resistance furnace at the desired temperature for the zero pressure anneals. Temperature was measured with a carefully calibrated iron-constantan thermocouple positioned near the ampoule at the center of an aluminum bronze block which minimized temperature gradients around the ampoule. Temperature was measured to 0.15° and absolute temperature at the crystal was probably correct to within 1°. Correction for finite warm-up rate was applied, in no case being greater than 0.5% of the anneal time. No cooling correction was needed.

High pressure was generated by a liquid hydraulic system of the Bridgman type.¹⁴ Pressure was transmitted by Dow-Corning 200 silicone fluid and measured with a manganin wire coil calibrated against the freezing point of mercury (7640 kg./cm.² at 0°). Automatic pressure control, plus a continuous pressure record, was obtained by monitoring the imbalance of a Wheatstone bridge with a recording potentiometer. Pressure was maintained to within 10 kg./cm.² of the mean

- (7) R. A. Hultsch and R. G. Barnes, *Phys. Rev.*, **125**, 1832 (1962).
- (8) J. B. Hudson and R. E. Hoffman, *Trans. AIME*, **221**, 761 (1961).
- (9) P. J. Fensham, *Australian J. Sci. Res.*, **3A**, 91 (1950); **4**, 229 (1951).
- (10) J. D. Meakin and E. Klokhholm, *Trans. AIME*, **218**, 463 (1960).
- (11) L. A. Girifalco and H. H. Grimes, *Phys. Rev.*, **121**, 982 (1961).
- (12) G. H. Vineyard, *J. Phys. Chem. Solids*, **3**, 121 (1957).
- (13) Purchased from Vulcan De-Tinning Company.
- (14) P. W. Bridgman, "The Physics of High Pressure," G. Bell and Sons, London, 1958.

Table I: Thermal Expansion^a and Linear Compression Coefficients^b for Tin

$\alpha_c, \text{deg.}^{-1}$	$\kappa_c, \text{atm.}^{-1}$	$\Delta\kappa_c, \text{deg.}^{-1} \text{atm.}^{-1c}$	$\delta_c^{2b}, \text{atm.}^{-2}$	$\Delta\delta_c, \text{deg.}^{-1} \text{atm.}^{-2d}$
36.4×10^{-6}	6.693×10^{-7}	0.0053×10^{-7}	4.09×10^{-12}	-0.0037×10^{-12}
$\alpha_a, \text{deg.}^{-1}$	$\kappa_a, \text{atm.}^{-1}$	$\Delta\kappa_a, \text{deg.}^{-1} \text{atm.}^{-1c}$	$\delta_a^{2b}, \text{atm.}^{-2}$	$\Delta\delta_a, \text{deg.}^{-1} \text{atm.}^{-2d}$
16.7×10^{-6}	6.008×10^{-7}	0.0027×10^{-7}	4.19×10^{-12}	0.0013×10^{-12}

^a S. Lee and W. Raynor, *Proc. Phys. Soc.*, **B67**, 739 (1954). ^b Ref. 14, p. 169; $\Delta l/l_0 = \kappa P - \delta P^2$. ^c $\Delta\kappa = d\kappa/dT$. ^d $\Delta\delta = d\delta/dT$

pressure. The bomb was immersed in a Dow-Corning 500 silicone oil bath at the desired temperature. Crystal temperature was measured on a carefully calibrated chromel-alumel thermocouple near the crystal in the bomb. Temperature was measured to 0.25° , but variable temperature gradients prevented knowing the temperature at the crystal to better than within about 2° . Corrections were applied for finite warming and cooling rates. These were always less than 2%.

After the anneal, each nonactive face was microtomed to eliminate surface diffusion effects. The common edge between the two diffusion faces was also removed. Radioactive slices 2μ thick were grouped in threes; each group was weighed to $\pm 10 \mu\text{g.}$, then counted in a methane flow proportional counter operating in the plateau region. Ten thousand counts above background were collected from each sample. Approximate penetration profiles were determined as shown in Fig. 1. Slice thickness and face misalignment corrections were applied to the diffusion coefficient calculations.¹⁵ The relative error in the diffusion coefficients is close to $\pm 5\%$.

Experimental Results

From the thermal expansion and compressibility data given in Table I, the diffusion coefficients were corrected for the effects of thermal expansion and linear compression. This effect is small, never much greater than 1%. At the highest pressures it was occasionally negative or zero. The corrected diffusion coefficients, as well as other pertinent quantities, are given in Table II.

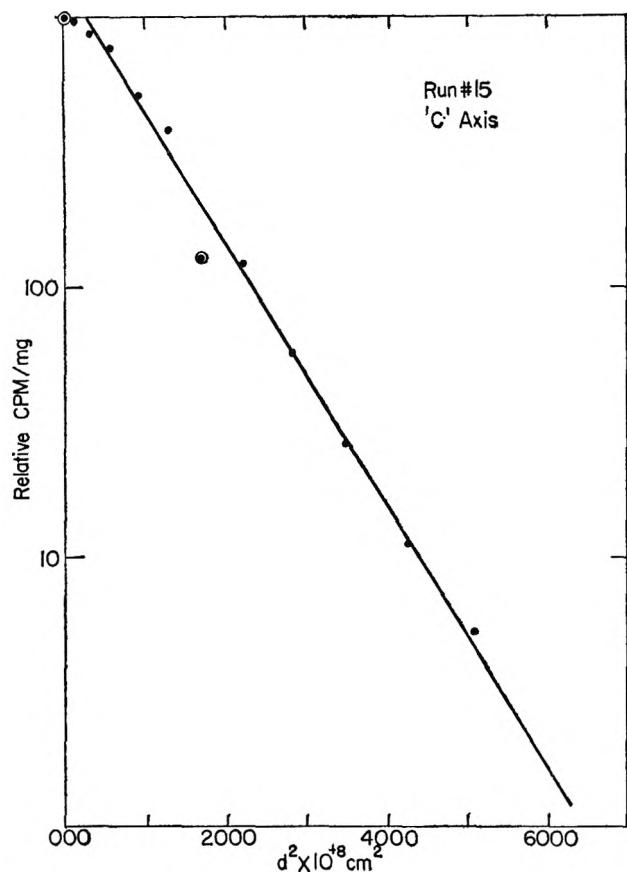
Isobars. A temporary value of $(\partial \ln D/\partial P)_T$ was taken from a plot of the data as approximate isobars, and this value was used to correct each diffusion coefficient to the nominal (*i.e.*, 000, 2000, etc.) pressure of the run. Corrections were never greater than 3%, so that a more accurate correction procedure is unnecessary. The corrected isobars for *a*- and *c*-axis diffusion are shown in Fig. 2 and 3. The lines shown are not least-squares lines, but are instead intuitive lines which show more clearly the trends in the data.

Table II: Diffusion Data

$P,$ kg./cm. ²	$T, ^\circ\text{C.}$	$D_a \times 10^{11},$ cm. ² /sec.	$D_c \times 10^{11},$ cm. ² /sec.	$\frac{D_a}{D_c}$
000	160.4	0.2113
000	162.6	0.249
000	160.8	...	0.0986	...
000	176.3	0.557	0.255	2.184
000	191.7	1.400	0.563	2.487
000	207.7	3.583	1.558	2.300
000	225.8	10.09	4.82	2.093
2158	189.6	0.918	0.471	1.949
1640	207.9	2.893	1.360	2.127
1992	225.6	7.363	3.403	2.164
1932	228.8	7.892	4.378	1.803
4116	190.1	0.800
3988	192.0	...	0.360	...
3907	211.3	2.748	1.293	2.125
4007	225.1	5.124	2.876	1.782
3977	235.9	10.029	4.866	2.062
6089	190.0	0.5495
6035	192.6	0.679	0.272	2.496
6017	208.1	1.557	0.701	2.221
6104	224.6	4.883	2.300	2.123
6020	239.8	10.769	4.196	2.567
7999	191.9	0.400	0.1834	2.181
7909	207.8	...	0.471	...
7959	208.8	1.389	0.664	2.092
7970	224.8	3.642	1.507	2.417
8079	239.8	7.691	3.100	2.451
10090	192.0	0.3467	0.159	2.181
10120	207.6	0.9839	0.422	2.331
10105	225.3	2.910	1.368	2.127
10134	244.8	7.765	2.727	2.847

This is justified since four points are inadequate for a meaningful least-squares treatment, particularly in view of the scatter in the data. Activation energies and D_0 values derived from these isobars are given in Table III. A reasonable mean value of the standard deviations for the activation energies is 1.25 kcal., or 5%, while the relative error of the D_0 values is close to 10%.

(15) G. A. Shirn, E. S. Wajda, and H. B. Huntington, *Acta Met.*, **1**, 514 (1953).

Figure 1. Typical *c*-axis penetration profile.Table III: Activation Energies and D_0 Values

	Pressure, kg./cm. ²					
	000	2000	4000	6000	8000	10,100
ΔH_a , kcal./mole	25.12	25.57	25.61	26.33	27.24	27.90
ΔH_c , kcal./mole	25.55	25.81	26.70	27.48	28.06	28.48
D_0^a , cm. ² /sec.	9.06	10.7	9.40	15.2	29.9	42.1
D_0^c , cm. ² /sec.	6.23	7.16	13.4	21.7	28.8	35.2

The trend toward higher ΔH values with increased pressure implies an activation volume greater than zero since thermodynamics gives

$$\left(\frac{\partial \Delta H}{\partial P}\right)_T = T \left(\frac{\partial \Delta S}{\partial P}\right)_T + \Delta V \quad (4)$$

From the development of ΔS by Keyes¹⁶ (neglecting the pressure variation of thermal expansion, α) we have

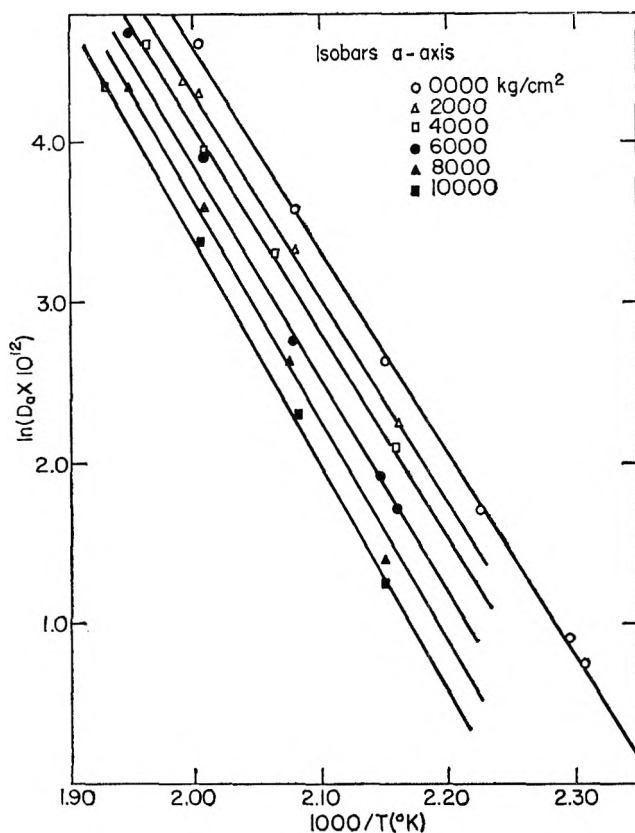
$$\left(\frac{\partial \Delta S}{\partial P}\right)_T = 2 \left(\gamma - \frac{1}{3}\right) \alpha \Delta V \quad (5)$$

where γ is the Gruneisen constant. Combining (4) and (5)

$$\Delta V = \left[1 + 2 \left(\gamma - \frac{1}{3}\right) \alpha T\right]^{-1} \left(\frac{\partial \Delta H}{\partial P}\right)_T \quad (6)$$

Thus, a positive change in ΔH with pressure assures that ΔV is greater than zero. This is consistent with previous high pressure diffusion studies.²

An approximate value of $(\partial \Delta H / \partial P)_T = 12.5$ cm.³/mole leads to the value $\Delta V = 12.0$ cm.³. This result does not agree with the value obtained from the usual method of determining ΔV and undoubtedly reflects the uncertainty in higher pressure isobar slopes (Fig. 2 and 3).

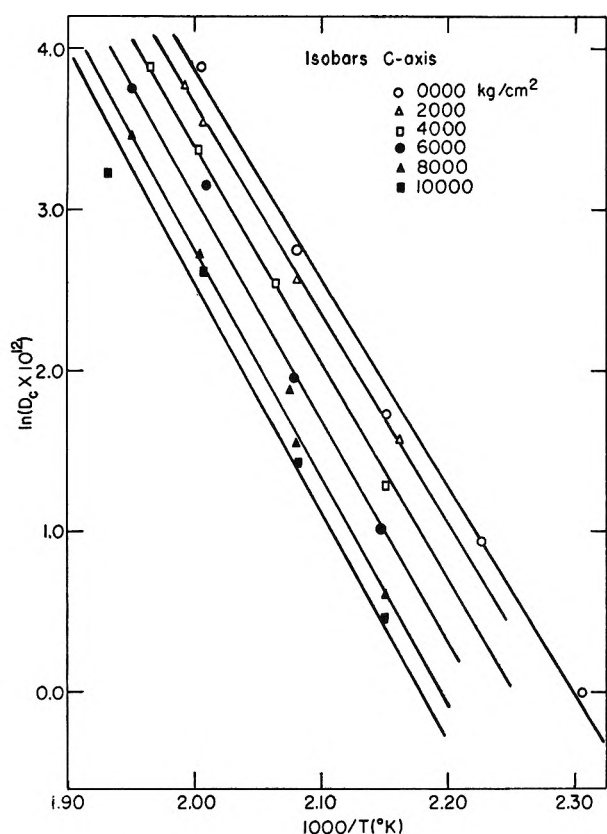
Figure 2. *a*-Axis diffusion isobars.

The most striking feature of the data in Table III is that the activation energies for both *a*- and *c*-axis diffusion are the same to well within experimental error. This is surprising, in view of the definite anisotropy in thermal expansion and compressibility shown in Table I. More important, Meakin and Klokholm¹⁰ observed considerable diffusion anisotropy in their work on tin. This discrepancy is discussed more fully in a later section. The similarity of activa-

(16) R. W. Keyes, "Solids Under Pressure," W. Paul and D. M. Warschauer, Eds., McGraw-Hill Book Co., Inc., New York, N. Y., 1963, p. 71.

Table IV: Activation Volumes

$T, ^\circ\text{C}.$	a axis			c axis		
	225.6	208.8	192.0	225.6	208.8	192.0
$\Delta V, \text{cm}^3$	4.96 ± 0.38	5.20 ± 0.25	5.91 ± 0.50	5.31 ± 0.38	5.23 ± 0.30	5.36 ± 0.30


 Figure 3. c -Axis diffusion isobars.

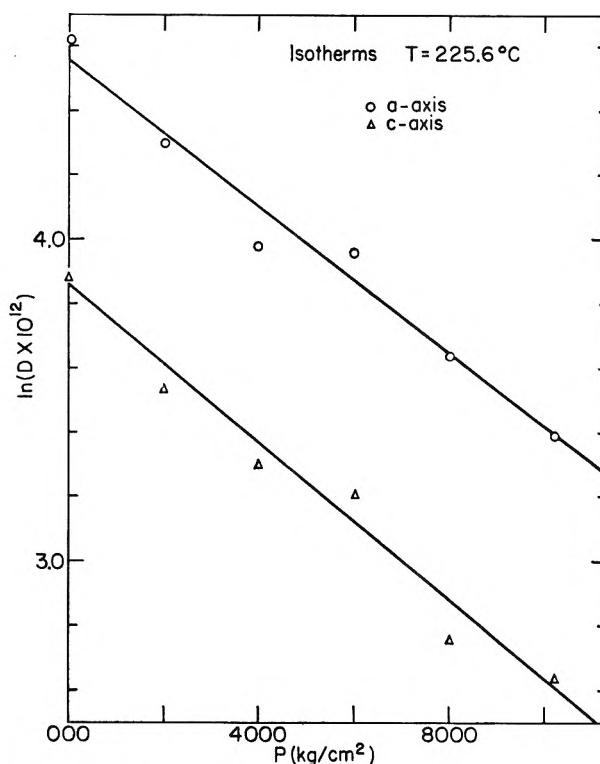
tion energies for diffusion in intrinsically different directions plays an important role in the discussion of possible diffusion mechanisms in tin.

Isotherms. Values of $(\partial \ln D / \partial T)_P$ from the isobars were used to correct the data to the appropriate nominal temperatures (225.6, 208.8, 192.0°). Corrections were generally less than 5%. The least-squares isotherm at 225.6° is shown in Fig. 4. Activation volumes derived from these isotherms *via* the usual formula²

$$\left(\frac{\partial \ln (D / \gamma a^2 \nu)}{\partial P} \right)_T = -\Delta V / RT \quad (7)$$

are given in Table IV, along with their standard deviations.

As for ΔH values, the activation volumes are essentially equal for both a - and c -diffusion directions. The apparent variation in a -axis ΔV values may or may not


 Figure 4. Diffusion isotherms (225.6°) for a and c axes.

be real since it is just outside the limits of experimental error. For the purposes of this discussion, ΔV can be considered constant, equal to 5.3 cm^3/mole for both a - and c -axis diffusion. This result is central in the discussion of possible diffusion mechanisms.

Corresponding States Test. The isobar data and the change in melting temperature of tin with pressure are sufficient to test the corresponding states relation (2) of Rice and Nachtrieb.⁵ The most accurate determination of the melting curve to 10 kbars has been made by Babb.¹⁷ From his results, T_m/T was found for each value of D . Figure 5 is a plot of $\ln D$ against T_m/T for diffusion along each axis. The lines shown are least-squares lines for the respective axis. Apparently the corresponding states relation is quite closely satisfied.

It is interesting to compare a - and c -axis values of

(17) S. E. Babb, *J. Chem. Phys.*, 37, 922 (1962).

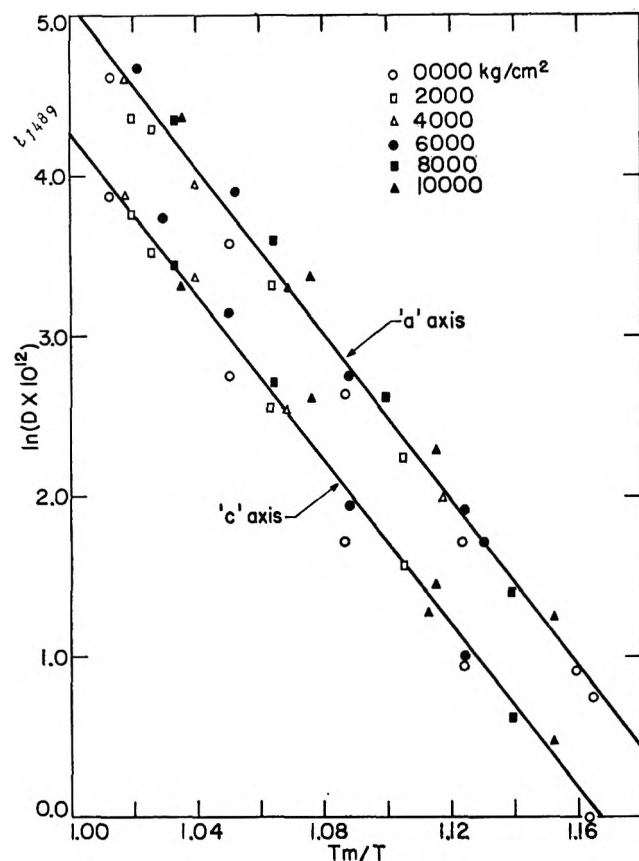


Figure 5. *a*- and *c*-axis diffusion coefficients as a function of reciprocal reduced temperature.

several quantities derived from the data in Fig. 5. Since T_m is a function of pressure, eq. 2 may be written

$$\left(\frac{\partial \ln(D/\gamma a^2 \nu)}{\partial T_m/T} \right)_{T_m} = \frac{1}{T_m} \left(\frac{\partial \ln(D/\gamma a^2 \nu)}{\partial 1/T} \right)_P = - \frac{\Delta H}{RT_m} \quad (8)$$

or

$$\Delta H = -RT_m(\text{constant}) \quad (9)$$

Hence, if the corresponding states law holds, the activation enthalpy should vary linearly with T_m . Slopes of the T_m/T curves and representative values of ΔH at three pressures from eq. 9 are given in Table V. Comparison with similar ΔH values from Table III supports the conclusion that the slopes of the isobars as drawn in Fig. 2 and 3 are probably too steep at higher pressures.

The increase in ΔH with pressure, taken from Table V, may be used in eq. 6 to calculate a mean activation volume of 6.1 cm.³, in satisfactory agreement with the value of 5.3 cm.³ derived more directly from the isotherms. Since the latter give ΔV more directly, the lower value is considered more reliable.

Table V: Quantities Derived from Corresponding States Test

Quantity	<i>a</i> axis	<i>c</i> axis
Slope	-25.686	-25.413
Standard deviation ^a	0.142	0.148
ΔH ($P = 0$) ^b	25,780 cal.	25,500 cal.
ΔH ($P = 5000$) ^b	26,570 cal.	26,290 cal.
ΔH ($P = 10,100$) ^b	27,350 cal.	27,060 cal.
ΔV	6.1 cm. ³	6.1 cm. ³

^a This corresponds to a difference in D values of $\sim 15\%$.
^b P is in kg./cm.².

The corresponding states relation (3) may be tested using the values $\Delta H = 25.3$ kcal. and $\Delta V = 5.3$ cm.³ (derived from this study), $\Delta H_m = 1690$ cal.,¹⁸ and $\Delta V_m = 0.454$ cm.³.¹⁹ The right-hand side of (3) predicts that $\Delta H = 19.75$ kcal., only 80% of the observed 25.3 kcal. The discrepancy is outside of the accumulated experimental error, and hence this relation does not seem to hold well for tin. This is surprising in view of the agreement observed for a large number of other metals.⁷

D_a/D_c Ratio. Examining the isotherms (Fig. 4) more closely shows that the isotherm points tend to deviate in pairs from their "best" positions, being both high or both low at each pressure. This variation is probably the result of uncertainty in temperature at the position of the crystal, as mentioned previously. Figure 5 shows that *a*- and *c*-axis diffusion coefficients differ by only a constant factor close to 2.2 over the entire temperature and pressure range, and that no significant difference in ΔH exists for the two directions. Table V gives the spread in the data for this plot. Deviations from this plot, too, are pairwise, and the most meaningful comparison between *a*- and *c*-axis diffusion rates is not found here. Instead, the D_a/D_c ratios given in Table II for those runs in which both quantities were determined successfully have been used to calculate a mean value $\langle D_a/D_c \rangle_{av} = 2.20 \pm 0.15$. The ratio of diffusion rates in fundamentally different crystal directions evidently varies little over the temperature and pressure range used in this study. This is truly a remarkable result. Furthermore, the large spot X-rays used to determine crystal quality are indistinguishable in terms of crystal perfection for either axis. The explanation of the remarkable sameness then must lie in the nature of the fundamental diffusion process in tin.

(18) U. S. National Bureau of Standards Circular 500, F. Rossini, Ed., U. S. Government Printing Office, Washington, D. C., 1952, p. 649.

(19) S. G. Kubaschewski, *Trans. Faraday Soc.*, 45, 931 (1949).

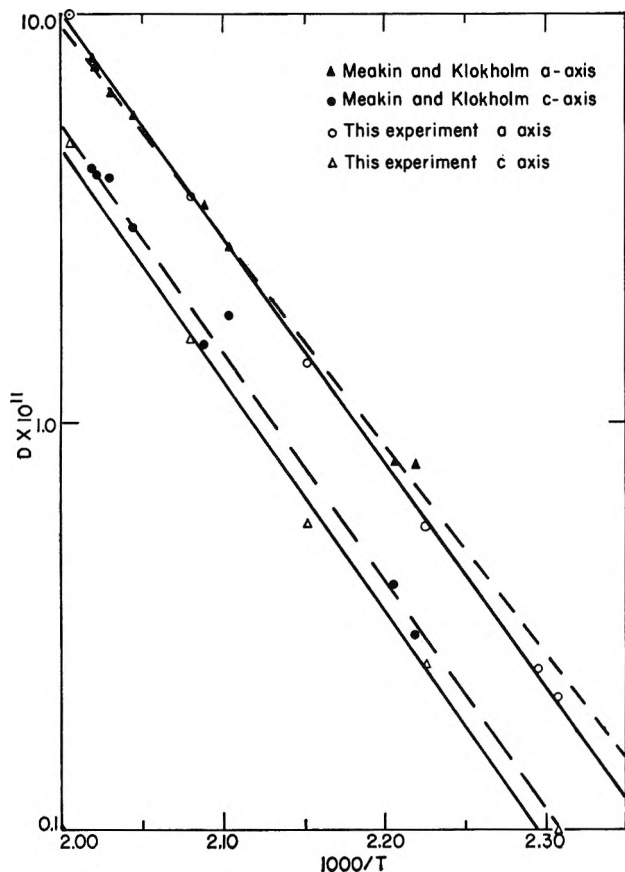


Figure 6. Comparison of *a*- and *c*-axis diffusion coefficients with data of Meakin and Klokhholm.

Discussion

The zero pressure results of this experiment are compared with the previous results of Meakin and Klokhholm in Fig. 6. Evidently, the absolute values of *D* agree very well between the two studies, though the *D* values of the present experiment are generally slightly smaller, particularly at lower temperatures for *a*-axis values. ΔH and D_0 values derived from each study are given in Table VI.

Table VI: Comparison of Zero Pressure Results

	—Meakin and Klokhholm—		—This study—	
	<i>a</i> axis	<i>c</i> axis	<i>a</i> axis	<i>c</i> axis
$D_0, \text{cm.}^2/\text{sec.}$	1.4 ± 0.5	8.2 ± 0.6	10.7 ± 1	7.7 ± 3
$\Delta H, \text{kcal./mole}$	23.3 ± 0.5	25.6 ± 0.8	25.2 ± 1.0	25.6 ± 1.2

The differences in ΔH and D_0 values in Table VI seem outside experimental error. In view of the con-

stant D_a/D_c ratio found in this study, the present authors cannot but feel that their *a*-axis results are more closely correct than the earlier values. The greater temperature range of this experiment increases the accuracy of the isobar slope, and hence ΔH , which supports this conclusion.

Lack of agreement between the *a*-axis results of the two studies is puzzling, particularly in view of the excellent *c*-axis fit. The only significant divergence of the experimental techniques involved cutting out the diffusion specimen. Meakin and Klokhholm used a fine jeweler's saw, while a spark cutter was employed in this study. Greater long-range crystal damage results from sawing than spark erosion, which might account for the lower *D* values for most of this study. The crossover for *a*-axis diffusion is not explained on this basis.

The conclusion that bulk diffusion is observed rests primarily on the linearity of the penetration profiles obtained (Fig. 1) over more than an order of magnitude change in activity. Assuming that this conclusion is valid, we inquire into the nature of the diffusive process.

In close-packed metals, activation volumes on the order of half the molar volume are assumed to indicate vacancy diffusion.² A smaller $\Delta V/V$ ($=26\%$) in the nonclose-packed metal lithium has led to speculation that interstitial diffusion might be operating in that metal.⁷ The present study has observed a relative activation volume of very similar size (33%), hence interstitial diffusion should be considered. That it is not likely may be seen by considering the quench-resistance studies of vacancies in gold. From the rate of annealing under pressure of quenched-in resistivity, Emrick²⁰ concluded that the motional activation volume of vacancies in gold was only 15% of the atomic volume. The resistivity quenched into gold at high pressures by Heubener and Homan²¹ indicates that the formation volume of vacancies is 53% of an atomic volume. It is difficult to see how in tin a larger relative volume would be needed for motion than in the close-packed gold structure. Hence, an upper limit of $\Delta V_{\text{mob}}/V = 0.15$ implies a lower limit of $\Delta V_{\text{form}}/V = 0.18$, and this positive formation volume implies a vacancy diffusion mechanism. A similar analysis leads to vacancy diffusion for lithium.

A more complete description of the white tin structure is necessary before discussing the proposed jump mechanism. Two interpenetrating body-centered tetragonal lattices give a unit cell with atoms at

(20) R. M. Emrick, *Phys. Rev.*, **122**, 1720 (1961).

(21) R. P. Heubener and C. G. Homan, *ibid.*, **129**, 1162 (1963).

(000), $(\frac{1}{2} 0 \frac{1}{4})$, $(\frac{1}{2} \frac{1}{2} \frac{1}{2})$, and $(0 \frac{1}{2} \frac{3}{4})$ with unit cell dimensions at 25° of $a = 5.820 \text{ \AA}$, $c = 3.175 \text{ \AA}$, so that $c/a = 0.5456$. Each atom has four nearest neighbors at a distance of 3.016 \AA , directed $\sim 15^\circ$ out of the a -axis plane, and two next nearest neighbors along the c -axis at 3.175 \AA .

In this structure two distinct kinds of jump are possible for bulk diffusion *via* vacancies. If in Fig. 7a the vacancy is at the site labeled 1, it may exchange with either of four nearest neighbors labeled 2 or two next-nearest neighbors labeled 3. Only these jumps are considered; other jumps are essentially blocked by the atoms neighboring the vacancy. For convenience, a vacancy jump from site 1 to site 2 shall be called an "a" jump, not exactly in the a -axis direction, and a "c" jump will be the vacancy jump from site 1 to site 3. Note that the "a" jump contains a component in the c -axis direction which contributes to c -axis diffusion, while "c" jumps do not contribute to a -axis diffusion.

In view of the essentially identical energies and volumes associated with diffusion along the different axes, it is attractive to postulate that only one jump, the "a" type, might satisfactorily account for the results of this study. We check this possibility by forming the ratio

$$\frac{D_c}{D_a} = \frac{\gamma_c' c^2 \nu_c' e^{+\Delta S_c'/R} e^{-\Delta H_c'/RT}}{\gamma_a a^2 \nu_a e^{+\Delta S_a/R} e^{-\Delta H_a/RT}} \quad (10)$$

where all terms have their usual meaning. If only "a" jumps are assumed then $\Delta H_a = \Delta H_c'$, $\Delta S_a = \Delta S_c'$, and $\nu_a = \nu_c'$, and (10) becomes

$$\frac{D_c}{D_a} = \frac{\gamma_c' c^2}{\gamma_a a^2} \quad (11)$$

The component of an "a" jump in the a -axis direction is one-half the length of an edge of the unit cell. There are four possible jumps of this type, only two of which contribute to diffusion along a given a -axis, so $\gamma_a a^2 = \frac{1}{2}(2)(a/2)^2 = a^2/4$. All a jumps contain components in the c -axis direction of magnitude $c/4$, so $\gamma_c' c^2 = \frac{1}{2}(4)(c/4)^2 = c^2/8$. The factor $\frac{1}{2}$ in front of each product arises from the definition of the γ -values.²² Since $D_a/D_c = 2.20$, we have

$$\begin{aligned} 1/2.20 &= 0.454 \neq (1/8)c^2/(1/4)a^2 = \\ & (1/2)(c^2/a^2) = 0.15 \quad (12) \end{aligned}$$

since the ratio (c^2/a^2) is 0.298. Hence, the observed rate of c -axis diffusion is a factor of three too high to be explained by only "a" jumps. The missing two-thirds of the observed rate must be assigned to "c"-type jumps, so that c -axis diffusion is a combination of both elementary jumps.

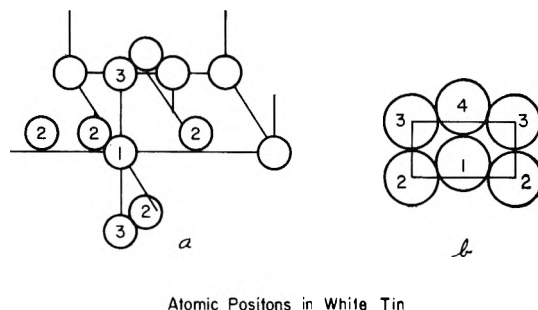


Figure 7. Atomic positions in tin.

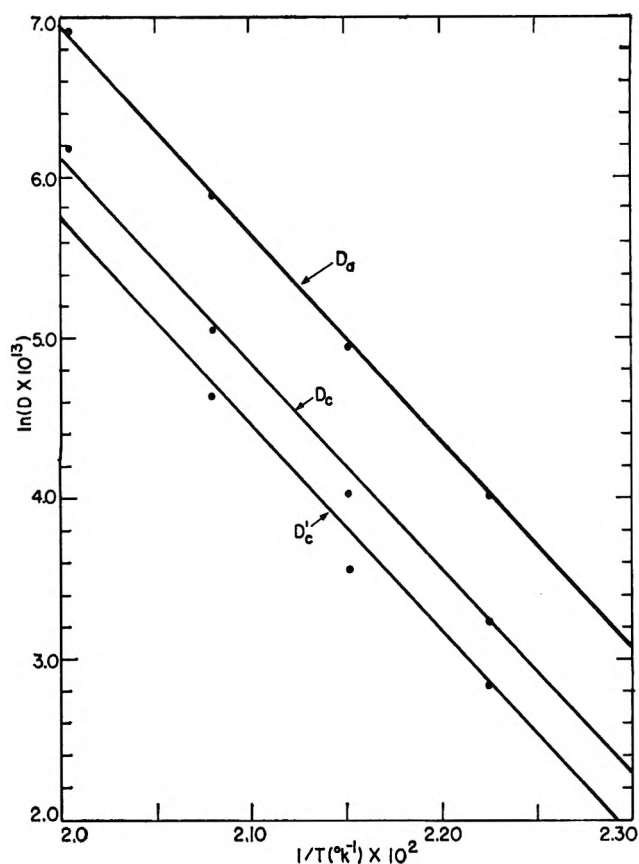


Figure 8. Contributions of a - and c -type jumps.

Similar to Meakin and Klokholm,¹⁰ we compare the diffusion coefficients for "a" and "c" jumps separately by subtracting $0.15D_a$ from each D_c value at the same temperature. This removes the "a"-jump contribution to c -axis diffusion. Figure 8 shows the zero-pressure isobars for D_a , D_c , and D_c' , where $D_c' = D_c - 0.15D_a$. Least squares gives $D_0' = 4.64 \text{ cm}^2/\text{sec}$. and $\Delta H_c' = 25.6 \text{ kcal}$., essentially unchanged in

(22) C. Zener, *J. Appl. Phys.*, **22**, 372 (1952).

ΔH and somewhat lower $\ln D_0$ than the uncorrected isobar results.

Since the isobars in Fig. 8 are essentially parallel, we can determine the relative jump frequencies, defined⁴ as $\Gamma_i = \nu_i e^{\Delta S_i/R} e^{-\Delta H_i/RT}$ for the i th jump type, by substituting $\gamma_a a^2 = 1/4 a^2$, $\gamma_c c^2 = 1/2(2)(c)^2 = c^2$, and $D_c/D_a = 0.306$ into eq. 10. Thus

$$0.306 = \frac{c^2}{1/4 a^2} \frac{\Gamma_c}{\Gamma_a} = 1.19 \frac{\Gamma_c}{\Gamma_a} \quad (13)$$

or

$$\Gamma_c = 0.257 \Gamma_a \quad (14)$$

Hence, the jump frequency for direct vacancy motion along the c -axis is only roughly 25% of the frequency of "a" jumps. This result provides considerable information about the details of the jump mechanism in tin.

Rice and co-workers⁴⁻⁶ have analyzed the conditions for a diffusive jump. Briefly, the atom must have a critical amplitude in the direction of the vacancy, and simultaneously, and also most restrictively, all blocking atoms must move aside with a breathing mode of sufficient amplitude to allow the diffusing atom to pass. These criteria may be visualized for tin in terms of Fig. 7a and 7b. Figure 7b is a view of the a - c plane looking along the a -direction in the tin crystal. Suppose that in Fig. 7b the site labeled 1 is vacant. If a "c" jump is to occur (exchange with the site labeled 3), then both atoms labeled 4, plus the two body-centered atoms not shown, must move aside. Thus, both the conditions of sufficient amplitude of the diffusing atom and a suitable breathing mode of the four blocking atoms must be satisfied. But from Fig. 7a it is evident that any one of the atoms labeled 2 may move into the vacancy at 1 without interference from blocking atoms. Hence, the only condition for "a" jumps is that the diffusing atom have sufficient amplitude to effect the jump. Relaxation of the atoms toward the vacancy will modify this picture only slightly, since now a breathing motion is required for the other atoms labeled 2 in Fig. 7a if one of these is to jump. But the required amplitude is small, and should be easily achieved. Thus, "a" jumps are greatly favored, since the frequency of occurrence of the necessary breathing mode in both pairs of blocking atoms involved in "c" jumps is expected to be much lower than the frequency with which the amplitude conditions are fulfilled for either jump. This agrees with (14).

But the activation energies should be different for these jumps, since the jump conditions are different. We use eq. 1 to compare the relative importance of various contributions to ΔH . ΔH_i is the same for each jump type, since all vacancies are presumed equiv-

alent. The sums $\sum_{k>l} \Delta H_{kl}$ should be very nearly the same for both jump types. The terms U_0 will be close to equal for each jump type, though perhaps slightly larger for "c" jumps. At first the energy contributions from $\sum_j U_j$ appear quite anisotropic, since the sum is zero for "a" jumps, but finite for "c" jumps into an unrelaxed vacancy. Relaxation should increase this contribution nearly equally for each type. To determine the anisotropy in ΔH , it is necessary to form some estimate of $\sum_j U_j$ for "c" jumps.

The dynamical theory, as developed by Manley,²³ identifies as the critical variable for each atom j the difference Δq_j between the maximum attainable amplitude, $q_{j\max}$, and the necessary amplitude to just permit the jump, $q_{j\min}$. In tin the geometry is such that $q_{j\min}$ is 0.106 Å. at 25°, and it decreases slightly with temperature. But from Mössbauer measurements in tin²⁴ the root mean squared vibrational amplitudes of atoms in the $\langle 100 \rangle$ direction at 300°K. is ~ 0.150 Å. and increases to 0.178 Å. at 400°K. and to 0.204 Å. at 500°K. Apparently, at the diffusion temperatures the root mean squared amplitudes are nearly a factor of two larger than $q_{j\min}$, and the atoms j do not need to acquire extra energy for a diffusive jump. Obviously, they must still satisfy the breathing mode requirement, and this will limit the jump rate. But anisotropy in ΔH due to different contributions from $\sum_j U_j$ will be small, since both jump types require little or no increase over the mean thermal energies for the interfering atoms.

It can still be argued that the activation energies could be quite unequal if the admittedly nonidentical factors U_0 and $\sum_j U_j$ of (1) were dominant. It has been estimated⁶ that the various terms for a simple model have the approximate weights $\Delta H_i = 20$ -40%, $U_0 = 30$ -60%, $U_j = 15$ -25%, and $\sum_{k>l} \Delta H_{kl} = 5$ -10%.

Recent results of quenching measurements and lattice dilatation studies in Ag,²⁵ Au,²⁶ and Cu³ show that a more probable weight for ΔH_i for the noble metals is close to 60%. While tin is far from a noble metal, it seems likely that the formation enthalpy is still close to 50% of the total effect. Thus, anisotropy in the activation energies must be small as observed.

Entropy. The activation entropy, ΔS , was calculated from the usual relation¹

(23) O. P. Manley, *J. Phys. Chem. Solids*, **13**, 244 (1960).

(24) A. J. F. Boyle, D. St. P. Bunbury, C. Edwards, and H. E. Hall, *Proc. Phys. Soc. (London)*, **A77**, 129 (1961).

(25) M. Doyama and J. S. Koehler, *Phys. Rev.*, **127**, 21 (1962).

(26) J. E. Bauerle and J. S. Koehler, *ibid.*, **107**, 1493 (1957).

$$\Delta S = R \ln (D_0/\gamma a^2 \nu) \quad (15)$$

The choice of ν is difficult and has been related to a normal mode analysis of lattice vibrations by several authors.^{4,12} In practice, the Debye frequency is used as the best available estimate. In this experiment the jump rates differing by a factor of 4 can only be the result of differences in ΔS and ν , and the uncertainty in ν is compounded further. Consider three cases: $\nu_a = \nu_c$ and the D_0 differences are reflected in ΔS ; $\nu_a = 4\nu_c$, the jump rate difference being almost entirely due to ν differences; $\nu_a = 2\nu_c$, an intermediate case. These cases are presented in Table VII, with calculations based on $\nu_a = \nu_\theta$, where $\theta_D = 142^\circ\text{K}$.²⁷ It is interesting that $\Delta S_a = \Delta S_c$ if $\nu_a = 2\nu_c$. The ΔS values do not agree well with Meakin and Klokholm, who apparently used a much different Debye temperature.

Table VII: Activation Entropies

Case	ΔS_a , e.u.	ΔS_c , e.u.	Relationships
1	16.6	17.8	$\nu_a = 4\nu_c$
2	16.6	15.1	$\nu_a = \nu_c$
3	16.6	16.4	$\nu_a = 2\nu_c$

Keyes¹⁶ has used continuum theory to write

$$\Delta S = 2(\gamma - 1/3)\alpha\Delta G \quad (16)$$

where α and γ are the thermal expansion coefficient and the Grüneisen constant. To a first approximation, this study gives $\Delta G \simeq \Delta H = 25.3$ kcal. and $\Delta S = 5.2$ e.u. From this estimate $\Delta G = \Delta H - T\Delta S = 23.0$ kcal., and $\Delta S = 4.75$ e.u. This is much lower than the observed ΔS values and seems to cast doubt on the applicability of the theory.

Volume. It is interesting to note that DeVries, Baker, and Gibbs,²⁸ in a preliminary report, have found an activation volume for creep in tin of about 30% of the molar volume, in close agreement with the 33% observed in this study. Their results have not been fully published to date so further comment is difficult.

Keyes¹⁶ has also developed the relation

$$\Delta V = 2 \left(\gamma - \frac{1}{3} \right) \kappa \Delta G \quad (17)$$

where κ is the compressibility. Using $\Delta G = 23.0$ kcal., we have $\Delta V = 5.1$ cm.³, in excellent agreement with the observed 5.3 cm.³. Hence, the strain energy approach gives quite good agreement for ΔV , though the predicted ΔS is not good.

We can get some indication as to why no anisotropy in ΔV was observed in this study from considering eq.

12a in the Appendix. The S_i are sums of elastic constants, the same for all k directions, so anisotropy comes only from the M_i^k (the $\gamma RT s_{ij} \delta_{ik}$ term is small, so anisotropy from this source is negligible). But the M_i^k are defined by eq. 8a in terms of a formation and a motion contribution, w_i and m_i^k ; only the latter can be anisotropic. But we have seen that in gold this term is only 22% of the total activation volume, and in general $w_i \geq m_i^k$ is probably valid. Therefore, any anisotropy in m_i^k for different k is largely masked by the isotropic w_i contribution.

Probably the largest contribution to anisotropy in ΔV_{mob} arises because the blocking atoms must assume a breathing mode before the diffusing atom may exchange with the vacancy. But the previous comments about vibration amplitudes in tin show that this effect will be small at best, since little or no "excess" volume is required. Hence, ΔV_a should be almost equal to ΔV_o .

From eq. 10a we can get some idea of the magnitude of the M_i^k . The tin elastic moduli were taken from Mason and Bommel.²⁹ For the a -axis isotherm at 225.6° we have

$$4.82 \text{ cm.}^3 = (M_1^1 + M_2^1)(10.3 \times 10^{-13}) + M_3^1(7.8 \times 10^{-13}) \quad (18)$$

so that an upper limit for M_i^k is $\sim 5 \times 10^{12}$ ergs = 10^3 kcal. The work of Liu and Drickamer³⁰ on the effect of uniaxial compression on diffusion in zinc can be used in a consistent way³¹ to evaluate some individual M_i^k values. From the elastic data for zinc of Hearmon,³² we find that $M_1^3 = 35 \times 10^3$ kcal. and $M_3^3 = 190 \times 10^3$ kcal. These values are up to two orders of magnitude greater than the upper bounds found for tin and also exceed similar upper limits determined from the hydrostatic pressure results for zinc by the same margins. Two possible explanations of this difficulty are: (1) the effect of pressure is not adequately accounted for by a sum over the individual stress components of the form of eq. 10a; (2) some gross difficulty exists in the experiments. Neither alternative is favored; indeed both may be partially correct.

(27) R. E. DeWames, T. Wolfram, and G. W. Lehman, *Phys. Rev.*, **131**, 529 (1963).

(28) K. L. DeVries, G. S. Baker, and P. Gibbs, *Bull. Am. Phys. Soc.*, [II] **6**, 169 (1961).

(29) W. P. Mason and W. E. Bommel, *J. Acoust. Soc. Am.*, **28**, 930 (1956).

(30) T. Liu and H. G. Drickamer, *J. Chem. Phys.*, **22**, 312 (1954).

(31) See A. W. Lawson, *ibid.*, **22**, 1948 (1954). However, if the stress range is great enough, $\partial \ln D_i / \partial P_i$ may be evaluated using only uniaxial stress data. This avoids the inconsistency.

(32) R. F. S. Hearmon, *Rev. Mod. Phys.*, **18**, 409 (1946).

Acknowledgments. The authors wish to express their thanks to the Air Force Office of Scientific Research for partial support of this work under Grant AFOSR 62-231. The general support of the Advanced Research Projects Agency and the U. S. Atomic Energy Commission is also gratefully acknowledged.

Appendix

The jump frequency has been developed very generally by Vineyard¹² as

$$\Gamma = \left(\frac{KT}{2\pi m}\right)^{1/2} \int_{\sigma} e^{-\varphi/RT} d\sigma / \int_A e^{-\varphi/RT} dA \quad (1a)$$

where φ is the potential energy for all the atoms in the crystal, A is an appropriate phase space volume taken at an atom neighboring a vacancy, and σ is an appropriate hypersurface taken at the saddle configuration of the jump. To a first approximation, A is the same for different jump directions in anisotropic systems; hence anisotropy must arise mostly from different σ_k for different jump types k . Thus (1a) becomes

$$\Gamma_k = \left(\frac{KT}{2\pi m}\right)^{1/2} \int_{\sigma_k} e^{-\varphi/RT} d\sigma_k / \int_A e^{-\varphi/RT} dA \quad (2a)$$

Following Girifalco and Grimes,¹¹ expand φ in terms of the strains, ϵ_i , to first order, and define

$$m_i^k = \left\langle \frac{\partial \varphi}{\partial \epsilon_i} \right\rangle_A - \left\langle \frac{\partial \varphi}{\partial \epsilon_i} \right\rangle_{\sigma_k} \quad (3a)$$

where $\langle \rangle$ denotes the usual statistical averages over A or σ_k . Now (2a) becomes

$$\Gamma_k(\epsilon) = \Gamma_k(0) \exp \left[\frac{1}{RT} \sum_i m_i^k \epsilon_i \right] \quad (4a)$$

The vacancy concentration may be written analogously as

$$n_v(\epsilon) = n_v(0) \exp \left[\frac{1}{RT} \sum_i w_i \epsilon_i \right] \quad (5a)$$

where

$$w_i = \left\langle \frac{\partial \varphi_0}{\partial \epsilon_i} \right\rangle - \left\langle \frac{\partial \varphi_v}{\partial \epsilon_i} \right\rangle \quad (6a)$$

Here φ_0 and φ_v are the potential energies of the crystal

without and with a vacancy, respectively. Note that w_i is independent of direction k .

From the zero strain expression $D_k(0) = \gamma_k a_k^2 n_v \cdot (0) \Gamma_k(0)$, the diffusion coefficient of the strained crystal is

$$D_k(\epsilon) = D_k(0) (1 + \epsilon_k)^2 \exp \left[\frac{1}{RT} \sum_i M_i^k \epsilon_i \right] \quad (7a)$$

where

$$M_i^k = m_i^k + w_i \quad (8a)$$

The only unknown quantities in (7a) are the M_i^k . These may be found from

$$\frac{\partial \ln D_k(\epsilon)}{\partial \epsilon_i} - \frac{2 \partial \ln (1 + \epsilon_k)}{\partial \epsilon_i} = \frac{M_i^k}{RT} \quad (9a)$$

From elasticity theory we write $\epsilon_i = \sum_j s_{ij} P_j$, where the stress, P_j , is a force per unit area (pressure), and the s_{ij} are constants. Then (9a) becomes

$$\sum_j \frac{\partial \ln D_k(P)}{\partial P_j} - 2 \sum_j s_{kj} / 1 + \sum_j s_{kj} P_j = \sum_{i,j} \frac{M_i^k s_{ij}}{RT} \quad (10a)$$

From the Zener formalism²² we have

$$\frac{\partial \ln D_k(P)}{\partial P} - 2 \sum_j s_{kj} = \frac{1}{RT} \sum_{i,j} \Delta V_{ij}^* - \sum_j s_{ij} \quad (11a)$$

so that

$$\sum_{i,j} \Delta V_{ij}^* = \sum_i (M_i^k + \gamma RT \delta_{ik}) s_i \quad (12a)$$

where δ_{ik} is the Kronacker delta, and we have set $1 + \sum_j s_{ij} P_j$ equal to unity, and where $\sum_j s_{ij} = S_i$. Summing (12a) over j gives ΔV^k in terms of strain components, ΔV_i^k , while a sum over i gives the stress components ΔV_j^k . Hydrostatic pressure measurements give only their sums so neither set is more significant.

The M_i^k will have the same relations as the s_{ij} . For example, for nonshear stresses, the x and y axes of tetragonal crystals are indistinguishable so that only five independent M_i^k remain, for instance, M_1^1 , M_2^1 , M_3^1 , M_1^3 , and M_3^3 . Hence, five uniaxial and/or hydrostatic diffusion experiments are required to determine fully the M_i^k in this case.

Anion Exchange of Metal Complexes. XIV.¹ The Effect of Acidity on the Sorption of Lanthanides from Lithium Nitrate Solutions²

by Y. Marcus and M. Givon

Radiochemistry Department, Soreq Research Establishment, Israel Atomic Energy Commission, Yavne, Israel (Received March 6, 1964)

Activity coefficients of small concentrations of nitric acid in 1–8 *m* lithium nitrate have been determined potentiometrically, using quinhydrone and glass electrodes. The invasion of a Dowex 1 resin by nitric acid and lithium nitrate from a 3.90 *m* total nitrate solution has been measured. Activity coefficients of nitric acid in the resin were calculated. The acidity dependence of the distribution of La, Eu, Yb, and Am between resin and a lithium nitrate solution was measured. Sorption of the species $M(\text{NO}_3)_6^{-2}$, for $M = \text{Eu, Yb}$, and possibly Am, and $\text{La}(\text{NO}_3)_7^{-4}$ was found to be consistent with the experimental data.

Introduction

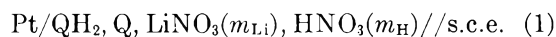
It has been noted³ that the concentration of nitric acid has an appreciable effect on the sorption of a number of lanthanides on an anion exchanger from lithium nitrate solutions. Such an effect has also been observed for the sorption of americium¹ and other ions.⁴ It is generally observed that an increase of the concentration of nitric acid at constant total nitrate concentration causes a decrease of the distribution coefficient.

In order to give a quantitative interpretation of this effect, additional information is required. This includes the activity of the nitric acid in the lithium nitrate solution and in the resin. These data were obtained from series of experiments, in which the potentials of quinhydrone and glass electrodes were measured as a function of the acidity at constant nitrate concentration, with and without resin present.

Experimental

Materials. Reagent grade chemicals were used throughout. The resin was Dowex 1-X 8 for the acid and americium sorption experiments and Dowex 1-X 10 for the experiments involving sorption of the lanthanides. Quinhydrone was once recrystallized from water. The americium was a sample of nominally Am^{241} , obtained from Oak Ridge National Laboratories.

Methods. Potentiometric measurements were carried out at 30° using the cells



where QH_2 , Q denotes saturated quinhydrone, // s.c.e. the saturated calomel electrode with a liquid junction, and GE a glass electrode. The instrument used was a Radiometer 22 pH meter, provided with a GK 2021 combined glass-calomel electrode. Solutions were stirred magnetically. An attempt to use a platinum-black-hydrogen electrode resulted in unsteady potentials in nitrate solutions, contrary to its behavior in chloride solutions.⁵ Acid was added to a lithium nitrate solution from a microburet.

Resin in nitrate form was prepared by treating the chloride form in a column with a large excess of lithium nitrate solution. The water content of the wet resin was determined by the centrifugation method, that of air-dry resin by heating in a vacuum oven at 60°. Imbibed nitrate was determined by elution with water and spectrophotometric measurement at 300 $m\mu$ (ϵ 7.15). The capacity (2.95 mequiv./g. of dry resin) was deter-

(1) Previous paper in series: Y. Marcus, M. Givon, and G. R. Choppin, *J. Inorg. Nucl. Chem.*, **25**, 1457 (1953).

(2) Presented in part at the 1st Meeting of the Israel Chemical Society, Beer Sheva, December, 1963; *Israel J. Chem.*, **1**, 255 (1963).

(3) Y. Marcus and F. Nelson, *J. Phys. Chem.*, **63**, 77 (1959).

(4) F. Nelson and K. A. Kraus, *J. Am. Chem. Soc.*, **76**, 5916 (1954); R. F. Buchanan and J. P. Faris, Conf. Use Radioisotopes Phys. Sci. Ind., Copenhagen, 1960, paper RICC/173.

(5) R. G. Bates, "Electrometric pH Determination," John Wiley and Sons, New York, N. Y., 1954.

mined for the chloride form by elution with nitrate and potentiometric titration with AgNO_3 .

The distribution of the lanthanides was measured at 25 and 78° by the column technique, as reported previously³; that of americium was measured at ca. 25° by the batch method, analyzing the solutions both spectrophotometrically and radiometrically.

Results and Discussion

A. Nitric Acid Activities in Lithium Nitrate Solutions. The e.m.f. values of cell 1 were measured for $m_{\text{Li}} = 1.00$ *m*, 1.99 *m*, 3.98 *m*, 5.55 *m*, and 8.00 *m* for various acid concentrations, ranging from about 10^{-5} *m* to 10^{-1} *m*. (The acid concentration is very small as compared with the lithium nitrate concentration, which is therefore practically equivalent with the total nitrate concentration.) The e.m.f. values were corrected for the liquid junction potential and salt effect on the quinhydrone electrode according to the equation

$$E_{\text{true}} = E_{\text{meas}} - |\Delta E_j| - |\Delta E_{\text{salt}}| \quad (3)$$

The liquid junction correction ΔE_j between lithium nitrate and saturated potassium chloride was calculated from the Henderson⁶ equation, using equivalent conductances from standard compilations.⁷ The salt effect correction ΔE_{salt} was calculated according to Stonehill.⁸ The value for lithium nitrate was obtained from a linear combination of the values for potassium nitrate and chloride and lithium chloride. The correction was found to be $\Delta E_{\text{salt}} = 3.8C_{\text{Li}}$ mv., and the appropriate molal values were calculated from the equation⁹

$$C_{\text{Li}} = m_{\text{Li}}(0.997 - 0.031m_{\text{Li}} + 0.0008m_{\text{Li}}^2) \quad (4)$$

The total corrections were 7, 14, 25, 33, and 45 mv., respectively, in increasing order of the lithium nitrate concentrations used.

From the e.m.f. data (in mv.) pH values (pH_Q) were calculated as a function of m_{H}

$$\text{pH}_Q = \frac{(E_Q^\circ - E_{\text{see}}^\circ) - E_{\text{true}}}{60.15} \quad (5)$$

where $(E_Q^\circ - E_{\text{see}}^\circ) = 454.0$ mv. at 30° was taken from Bates.⁵ The results are shown in Table I.

Mean molal activity coefficients of nitric acid in lithium nitrate solutions ($\gamma_{\pm \text{HNO}_3}$ (in LiNO_3), designated in short γ_{H} in the following) were calculated from the pH_Q data as a function of the total nitrate concentration. They, too, are shown in Table I. It can be seen that γ_{H} does not vary appreciably with the acid concentration. The average values of γ_{H} are plotted in Fig. 1 as a function of the lithium nitrate concentration, together with values of the mean ac-

Table I: Some Values of pH_Q , pH_{GE} , and γ_{H} at Various LiNO_3 Molalities

	$m_{\text{HNO}_3} \times 10^3$	pH_Q	ΔpH	γ_{H}
$m_{\text{Li}} = 1.00$	1.12	2.73	0.02	1.66
	2.23	2.50	0.02	1.41
	4.46	2.23	0.02	1.33
	8.35	1.95	0.05	1.34
	16.7	1.68	0.03	1.24
	33.4	1.38	0.02	1.24
	55.7	1.18	0.00	1.19
	112	0.90	-0.01	1.13
	$\gamma_{\text{H}} = 1.33^a$			
	$m_{\text{Li}} = 3.98$	1.22	2.34	0.16
2.42		2.14	0.19	2.99
4.84		1.81	0.19	3.20
9.67		1.51	0.19	3.20
18.2		1.21	0.24	3.40
36.2		0.90	0.22	3.47
60.4		0.68	0.24	3.47
122		0.40	0.25	3.29
$\gamma_{\text{H}} = 3.31^a$				
$m_{\text{Li}} = 8.00$		1.32	1.53	0.31
	2.64	1.15	0.35	18.4
	5.28	0.87	0.36	17.7
	9.90	0.60	0.38	17.5
	19.9	0.29	0.40	17.8
	39.6	0.00	0.41	17.3
	66.0	-0.18	0.40	15.8
	132	-0.44	...	14.4
	$\gamma_{\text{H}} = 17.7^a$			

^a Mean value of γ_{H} (including data not shown in the table).

tivity coefficient of lithium nitrate¹⁰ and of the ionic part of nitric acid.¹¹ The activity coefficients of nitric acid in lithium nitrate are seen to be much higher than both $\gamma_{\pm \text{LiNO}_3}$ in lithium nitrate and $\sqrt{\gamma_{\text{H}} \cdot \gamma_{\text{NO}_3^-}}$. A similar high result which is also shown in Fig. 1 was obtained by Rosenthal and Dwyer¹² for nitric acid at low concentration in 6 *M* (about 7.5 *m*) sodium nitrate.

The data of Fig. 1 lead to values of α_{H} for Harned's¹³ rule

- (6) P. Henderson, *Z. physik. Chem.*, **59**, 118 (1907).
- (7) B. E. Conway, "Electrochemical Data," Elsevier Publishing Co., Amsterdam, 1952; R. Parsons, "Handbook of Electrochemical Constants," Butterworth and Co., Ltd., London, 1959.
- (8) H. I. Stonehill, *Trans. Faraday Soc.*, **39**, 67 (1943).
- (9) Y. Marcus and I. Abrahamer, *J. Inorg. Nucl. Chem.*, **22**, 141 (1961).
- (10) R. A. Robinson and R. H. Stokes, "Electrolyte Solutions," Butterworth and Co., Ltd., London, 1959.
- (11) H. A. C. McKay, *Trans. Faraday Soc.*, **52**, 1568 (1956).
- (12) D. Rosenthal and J. S. Dwyer, *J. Phys. Chem.*, **66**, 2687 (1962).
- (13) H. S. Harned, *J. Am. Chem. Soc.*, **48**, 326 (1926).

$$\log \gamma_H = \log \gamma_{\pm \text{HNO}_3}(m_{\text{Li}}) - \alpha_H m_{\text{Li}} \quad (6)$$

which range from -0.26 at $1 m$ to -0.12 at $8 m$ lithium nitrate, *i.e.*, very high values. If Guggenheim's treatment¹⁴ were applicable, $\alpha_H + \alpha_{\text{Li}}$ should be zero, and

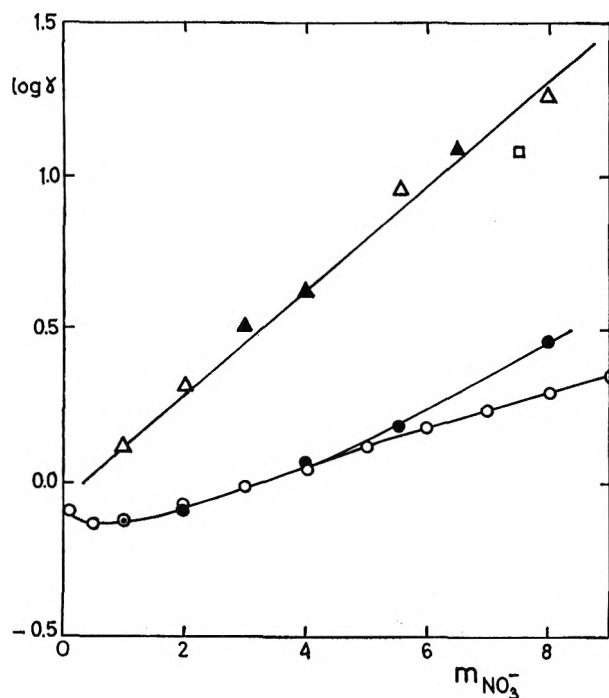


Figure 1. Mean molal activity coefficients in nitrate solutions: \circ , $\gamma_{\pm \text{LiNO}_3}$ in lithium nitrate¹⁰; \bullet , $\sqrt{\gamma_{\text{H}^+} \gamma_{\text{NO}_3^-}}$ for nitric acid in nitric acid¹¹; Δ , $\gamma_{\pm \text{HNO}_3}$ in lithium nitrate, this work, from pH_Q ; \blacktriangle , $\gamma_{\pm \text{HNO}_3}$ in lithium nitrate from pH_{GE} and eq. 7; \square , $\gamma_{\pm \text{HNO}_3}$ in sodium nitrate.¹²

$\alpha_H - \alpha_{\text{Li}} = 2(\varphi_{\text{HNO}_3} - \varphi_{\text{LiNO}_3})/2.303m_{\text{Li}}$ where the φ -values are the osmotic coefficients for the pure components of total molality m_{Li} . Values of α_H calculated by this method, using φ_{LiNO_3} from ref. 10 and φ_{HNO_3} calculated from the water activities,¹⁵ yielded values about eight times smaller than the observed values. This means that the hydrogen ions are influenced not only by the nitrate but also by the lithium ions.¹⁴

Parallel determinations of the pH values were made for 1.0, 2.0, 3.0, 4.0, 5.5, 6.5, and 8.0 m lithium nitrate solutions with a glass electrode calibrated against two standard buffers of nominal pH 4 and 7. The data (pH_{GE}) are given in Table I. It can be seen that for each lithium nitrate concentration the differences $\Delta \text{pH} = \text{pH}_{\text{GE}} - \text{pH}_Q$ vary only slightly with the acid concentration and are a linear function of the total nitrate concentration.

$$\Delta \text{pH} = 0.048m_{\text{Li}} \quad (7)$$

This difference in pH is probably due to the lithium ion effect on the glass electrode. The functions pH_{GE} vs. acidity were used as empirical means for determining the actual acid concentration from glass electrode measurements.

B. Nitric Acid Activity in the Resin Phase. Two series of experiments were made in which small known amounts of 4.04 m nitric acid were added to a known quantity of 3.90 m lithium nitrate solution containing a weighed amount of anion-exchange resin, and the pH was measured with a glass electrode after attainment of equilibrium. The acidity range in solution was 3×10^{-4} to $10^{-1} m$. The results were corrected for dilution and it was assumed that the pH values which in this instance were measured at 25° could be used with the empirical curves which were determined at 30° .

From these measurements the equilibrium acidities in solution were calculated and from the difference between initial and equilibrium acidity the invasion into the resin was estimated as molality of nitric acid in the resin \bar{m}_H . For this purpose values of the equilibrium water content of the resin are required. These were determined by the centrifugation method for resin in equilibrium with a practically neutral lithium nitrate solution and for the resin at the end of each run. Water contents of (410 mg./g. of dry resin) did not vary appreciably with acidity. The invaded electrolyte was eluted from the resin at the end of one run and the acid and total nitrate concentration determined directly. Values of \bar{m}_H vs. m_H are shown in Fig. 2. The point for the directly determined acidity falls neatly on the plot of \bar{m}_H vs. m_H which is linear with a slope of 19.5 ± 1.5 .

The total concentration of the invading nitrate in the resin was 4.96 m , of which 1.72 m was nitric acid and 3.24 m lithium nitrate. The latter value agrees well with the value interpolated from Danon's¹⁶ data, which shows that it is independent of the acidity. The molality of exchange sites is the ratio of the capacity to the water content, 7.25 m , and the total nitrate molality in the resin is 12.2 m .

From these molalities the ratios of the mean activity coefficients in the two phases, $\Gamma_{\text{Li}} = \bar{\gamma}_{\text{Li}}/\gamma_{\text{Li}}$ and $\Gamma_{\text{H}} = \bar{\gamma}_{\text{H}}/\gamma_{\text{H}}$ (where $\bar{\gamma}_M$ and γ_M designate in short $\gamma_{\pm \text{MNO}_3}$ in the resin and solution phases, respectively) are calculated from the relations

$$\Gamma_{\text{Li}}^2 = m_{\text{Li}}m_{\text{NO}_3}/\bar{m}_{\text{Li}}(\bar{m}_{\text{Li}} + \bar{m}_H + \bar{m}_R) \quad (8a)$$

and

$$\Gamma_{\text{H}}^2 = m_{\text{H}}m_{\text{NO}_3}/\bar{m}_{\text{H}}(\bar{m}_{\text{Li}} + \bar{m}_H + \bar{m}_R) \quad (8b)$$

(14) E. A. Guggenheim, *Phil. Mag.*, 19, 588 (1935).

(15) E. Högföldt and B. Bolander, *Arkiv Kemi.*, 21, 161 (1963).

(16) J. Danon, *J. Phys. Chem.*, 65, 2039 (1961).

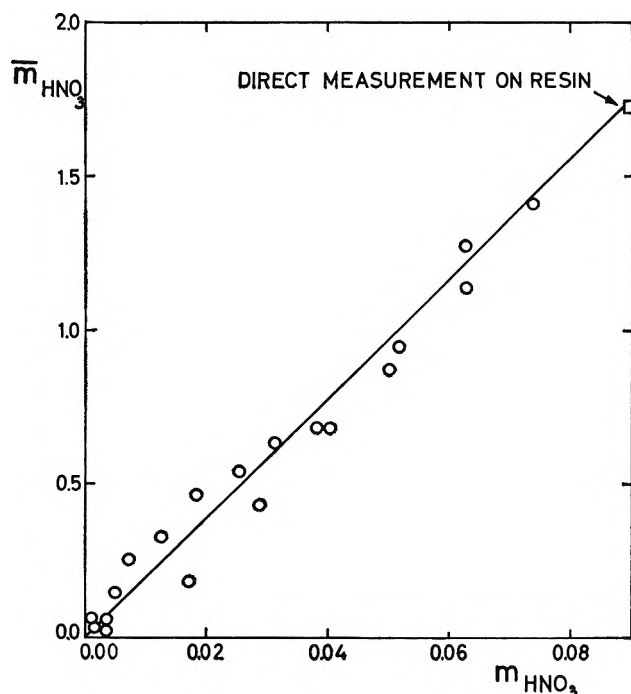


Figure 2. Nitric acid invasion into Dowex 1-X 8 from 3.90 *m* lithium nitrate as a function of the acidity: O, from pH_{GE} ; □, direct determination.

The results are shown in Table II. It can be seen that Γ_{Li} decreases from 0.67 to 0.62 as the acidity of the solution increases from 3×10^{-4} to 9×10^{-2} *m*. The value at low acidity is consistent with the value of 0.68 interpolated from Danon's¹⁶ data. The value of Γ_{H} is

Table II: Values of Γ_{H} and Γ_{Li} for Dowex 1-X 8 at 3.90 *m* Nitrate Ion Concentration, $\bar{m}_{\text{Li}} = 3.24$, $\bar{m}_{\text{R}} = 7.22$

m_{H}	\bar{m}_{H}	m_{Li}	$(\bar{m}_{\text{H}} + \bar{m}_{\text{Li}} + \bar{m}_{\text{R}})$	Γ_{H}	Γ_{Li}
0.00028	0.014	3.90	10.47	0.086	0.670
0.0047	0.152	3.89	10.61	0.106	0.665
0.0063	0.250	3.89	10.71	0.096	0.660
0.0089	0.340	3.88	10.80	0.097	0.655
0.0123	0.330	3.88	10.79	0.116	0.655
0.0180	0.470	3.87	10.93	0.117	0.655
0.0250	0.540	3.86	11.00	0.129	0.655
0.0315	0.630	3.86	11.09	0.132	0.650
0.0385	0.670	3.85	11.13	0.141	0.650
0.0405	0.670	3.85	11.13	0.144	0.645
0.0510	0.870	3.84	11.33	0.140	0.640
0.0520	0.940	3.84	11.40	0.135	0.635
0.0625	1.270	3.84	11.73	0.125	0.635
0.0630	1.120	3.84	11.58	0.135	0.630
0.0740	1.400	3.83	11.86	0.129	0.630
0.0840	1.170	3.82	11.63	0.151	0.625
0.0910	1.290	3.81	11.75	0.150	0.625

approximately 0.13, as compared with 0.36 for resin in equilibrium with pure 3.9 *m* nitric acid.¹⁶ It is seen that high concentrations of lithium nitrate decrease Γ_{H} considerably. Since T_{H} is a measure of the relative acid strength in the resin and the solution, it is clear that the invading excess lithium nitrate causes a decrease in the acid strength.

This result may be compared with the data of Nelson and Kraus¹⁷ for hydrochloric acid in lithium chloride at a total molality of 9.9. Hydrochloric acid was found to be rather weak in the presence of high concentrations of lithium chloride, $T_{\text{H}} = 0.14$, compared with $T_{\text{H}} = 0.60$ for pure 9.9 *m* hydrochloric acid. Again T_{Li} changes only little; it increases (contrary to the nitrate case where it decreases) from 0.77 to 1.09 as the acid concentration increases.

The decrease in acid strength in the resin may be explained by the hypothesis of the formation of the binitrate ion $\text{H}(\text{NO}_3)_2^-$. Such an ion could be formed by ion-dipole interaction in low acid-high nitrate solutions. The low effective dielectric constant of the resin phase could favor its formation. In a medium of still lower dielectric constant, such as toluene¹⁸ or a solution of a trialkylamine in a hydrocarbon,¹⁹ the dimerization of nitric acid has been found. For the corresponding chloride system a species HCl_2^- has been proposed.²⁰⁻²² Formation of this $\text{H}(\text{NO}_3)_2^-$ species in the resin will cause a decrease in the concentration of free nitrate ions as the nitric acid concentration in the resin increases. If all the acid is in this form, then

$$\bar{m}_{\text{NO}_3} = \bar{m}_{\text{R}} + \bar{m}_{\text{Li}} - \bar{m}_{\text{H}} \quad (9)$$

C. Distribution of Lanthanides and Americium as a Function of Acid Concentration. Results for lanthanum, europium, and ytterbium obtained previously² in 4.6 *m* lithium nitrate and values for americium in 4.0 *m* lithium nitrate are shown in Fig. 3. The curves are normalized against the distribution coefficient at very low acidity, D_0 . Some experiments for lanthanum and europium were carried out at both 25 and 78°, but no significant differences between the results were found. The figure shows that above about 0.01 *m* nitric acid the distribution coefficients begin to be affected by the acidity.

(17) F. Nelson and K. A. Kraus, *J. Am. Chem. Soc.*, **80**, 4154 (1958).

(18) C. J. Hardy, B. F. Greenfield, and D. Scargill, *J. Chem. Soc.*, 60 (1961).

(19) E. Högfeltdt and F. Fredlund, private communication.

(20) S. Lindenbaum and G. E. Boyd, U.S.A.E.C. Report ORNL-3320, 1962, p. 75.

(21) J. R. Beatty and G. J. Leigh, *J. Chem. Soc.*, 4726 (1962).

(22) G. Duyckaerts, J. Fuger, and W. Müller, Euratom Report No. 426.f, 1963.

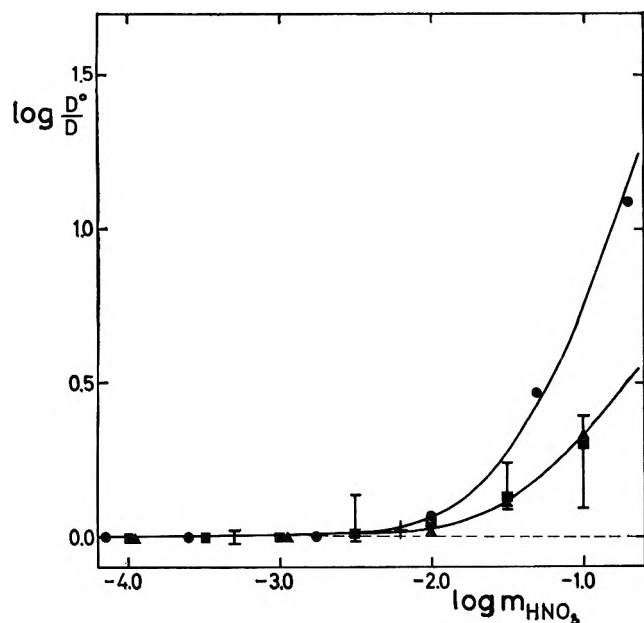
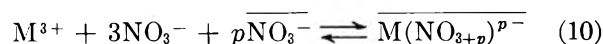


Figure 3. Acidity effect on the distribution of (●) La, (■) Eu, (▲) Yb, and (I) Am between lithium nitrate and anion-exchange resin. The curves are calculated from eq. 12 with $p = 2$ (lower) and $p = 4$ (upper).

The following argument can be used to interpret the data. It is assumed that the metal ions distribute between the resin and the solution according to the reaction



It has been shown²³ that the distribution coefficient is proportional to the p th power of the effective nitrate activity in the resin. This latter quantity is the product of the free nitrate ion concentration and the effective activity coefficient of the nitrate ion²³ which is assumed to vary linearly between $\tilde{\gamma}_{Li}$ and $\tilde{\gamma}_H$ according to the fractions of salt and acid invading the resin

$$\tilde{\gamma}_{NO_3 \text{ eff}} = \frac{\tilde{m}_H}{\tilde{m}_H + \tilde{m}_{Li}} \tilde{\gamma}_H + \frac{\tilde{m}_{Li}}{\tilde{m}_H + \tilde{m}_{Li}} \tilde{\gamma}_{Li} \quad (11)$$

Since in the absence of acid the effective ligand activity would be $(\tilde{m}_{Li} + \tilde{m}_R)\tilde{\gamma}_{Li}$, the ratio of the distribution coefficients in absence and in presence of acid will be

$$\begin{aligned} \log \frac{D_0}{D} &= p \log (\tilde{m}_R + \tilde{m}_{Li})\tilde{\gamma}_{Li} - \\ & p \log (\tilde{m}_{NO_3^- \text{ free}})\tilde{\gamma}_{NO_3 \text{ eff}} = p \log (\tilde{m}_R + \tilde{m}_{Li})\tilde{\gamma}_{Li} - \\ & p \log (\tilde{m}_R + \tilde{m}_{Li} - \tilde{m}_H) \times \\ & \left[\frac{\tilde{m}_H}{\tilde{m}_H + \tilde{m}_{Li}} \tilde{\gamma}_H + \frac{\tilde{m}_{Li}}{\tilde{m}_H + \tilde{m}_{Li}} \tilde{\gamma}_{Li} \right] = pF_H \quad (12) \end{aligned}$$

where F_H is a correction function. Values of F_H for 3.9 *m* lithium nitrate were calculated from the data obtained in parts A and B above. The various random errors in the quantities entering the calculations and systematic errors such as the difference in temperature between the data in parts A and B and in concentration between the data in parts B and C were estimated to yield a relative error of $\pm 20\%$ in F_H at the 95% confidence limit. Within this error limits, eq. 12 is seen to fit the results for the lanthanides (Fig. 3) with $p = 2$ for europium and ytterbium and $p = 4$ for lanthanum. Application of eq. 12 with $p = 3$ does not fit the data. The data for americium are not sufficiently precise for a good fit.

If it is accepted that the fit in Fig. 3 is evidence for the operation of the acid effect according to eq. 12, and absorption on the resin according to eq. 10, then the values $p = 2$ and $p = 4$ indicate the formation of $Eu(NO_3)_5^{2-}$, $Yb(NO_3)_5^{2-}$, and $La(NO_3)_7^{4-}$. High coordination numbers for the lanthanides, up to 8 or 9, have been variously reported,²⁴ so that the high values of the ligand number do not seem to be improbable, provided the nitrate is a monodentate ligand. Species with five nitrate ions per lanthanide have been shown to form in long-chain amine extraction.⁹ A species $Nd(NO_3)_5^{2-}$ has been found in a spectrophotometric study of $Nd(NO_3)_3$ in ethanol.²⁵

Acknowledgment. Thanks are due to Messrs. A. Gafni and M. Compan and Mrs. N. Bauman for help in carrying out the experiments.

(23) Y. Marcus and C. D. Coryell, *Bull. Res. Council Israel*, **8A**, 1 (1959).

(24) *E.g.*, $Nd(HCO_3)_6^{3-}$ and $Eu(HCO_3)_7^{4-}$, J. A. Marinsky and H. S. Sherry, *Inorg. Chem.*, **3**, 334 (1964); *cf.* also G. Vincentini, *J. Inorg. Nucl. Chem.*, **24**, 1351 (1962); P. W. Selwood, "Magnetochemistry," Interscience Publishers, Inc., New York, N. Y., 1956, pp. 152-153.

(25) I. Abrahamer and Y. Marcus, Israel AEC Semi-annual Report, June-December, 1963, IA-920 (in press).

The Critical Temperature and Coexistence Curve for Bismuth Chloride¹

by J. W. Johnson and Daniel Cubicciotti

Stanford Research Institute, Menlo Park, California 94026 (Received March 12, 1964)

The critical temperature of BiCl_3 has been found to be $1178 \pm 5^\circ\text{K}$. and the critical density to be 1.210 ± 0.006 g./cc. The coexistence curve for liquid and vapor has been fitted by the equations: $\rho = 1.210 + 1.268((1178 - T)/1178) \pm 2.347((1178 - T)^{1/3}/1178)$ (+ for liquid phase; - for vapor phase). These equations are of the same form as those developed by Guggenheim for argon, nitrogen, oxygen, methane, and carbon monoxide. It is concluded that bismuth chloride behaves very much like a molecular fluid at least with respect to the critical parameters.

Introduction

The critical parameters of many metallic halides which do not exhibit ionic conductance have been determined.^{2a} The liquid densities of sodium and potassium chlorides from the melting point to the normal boiling point have been reported, and estimates of the critical constants of the alkali halides have been made.^{2b} Recently the electrical conductivity of molten bismuth chloride has been measured³ to 625° and has been found to exhibit a maximum in the specific conductance curve near the normal boiling point of 441° . A knowledge of the orthobaric densities and critical temperature of bismuth chloride permits a determination of the applicability of various relationships developed for the critical parameters of molecular liquids to a molten, ionically conducting salt.

Experimental

A visual method was used in the determination of the critical temperature and orthobaric densities of bismuth chloride. The salt was contained in sealed clear fused-quartz tubes which were heated in a furnace containing two vertical slits for illumination and observation of the samples at temperature.

Bismuth chloride, prepurified by distillation under an atmosphere of hydrogen chloride, was distilled into quartz tubes of various dimensions in an atmosphere of dry hydrogen chloride and inert gas. The tubes were then evacuated to remove residual gas and sealed off under vacuum.

Those tubes intended for use in the critical temperature determinations were constructed of quartz tubing, 2-mm. bore \times 8-mm. o.d. and 6 cm. long. These

were filled to approximately one-third the total internal volume with molten bismuth chloride at 300° . The tubes used in the determinations of liquid and vapor volumes were 3-mm. bore \times 6-mm. o.d. and 6 cm. long. The amount of BiCl_3 introduced at 300° was governed by the requirement that the salt completely fill the tube as a liquid or vapor at the desired temperature. Additional liquid density measurements were made by using quartz "floats" of known densities constructed by sealing tungsten wire of various lengths into evacuated quartz tubes, 2-mm. bore \times 4-mm. o.d. and 2 cm. long. These "floats" were sealed into quartz tubes, 5-mm. bore \times 7.4-mm. o.d. and 6 cm. long, containing enough bismuth chloride so that the "float" would float in the liquid phase.

A nickel cylinder 115 cm. long and 4.8 cm. in diameter with a central hole of 1.6 cm. diameter drilled to within 1 cm. of the bottom was used to hold the quartz ampoules in the furnace. This block had two 3-mm. diameter holes drilled parallel to the central hole for the insertion of thermocouples. The block was mounted on a rotating ceramic cylinder in the center of the furnace and could be turned so that the sample tube could be observed through the observation slit in the furnace shell with a telescope mounted on a stand outside the furnace. When observations were

(1) This work was made possible by the support of the Research Division of the U. S. Atomic Energy Commission under Contract No. AT(04-3)-106.

(2) (a) K. A. Kobe and R. E. Lynn, Jr., *Chem. Rev.*, **52**, 117 (1953); (b) A. D. Kirshenbaum, J. A. Cahill, P. J. McGonigal, and A. V. Grosse, *J. Inorg. Nucl. Chem.*, **24**, 1287 (1962).

(3) L. F. Grantham and S. J. Yosim, *J. Phys. Chem.*, **67**, 2506 (1963).

not being made, the block could be rotated to shield the sample from view.

The furnace used in this work was 350 cm. long and 200 cm. in diameter with a Mullite center tube having a bore of 5 cm. Radial illumination and observation slits 6 mm. wide and 7.6 cm. long at an angle of 60° were cut through the furnace insulation and central tube. These slits were covered with 6-mm. thick Pyrex plate-glass mounted on the outside of the furnace to reduce heat loss through convection. The windings of 20-gauge Nichrome wire were arranged parallel to the longitudinal axis of the central tube and insulated with an 8-cm. layer of firebrick.

In operation a piece of clear, fused quartz tubing was inserted in the nickel block and the quartz sample tube placed on a ceramic insulator inside this tube. The nickel block was inserted in the furnace and adjusted so that the sample was clearly visible through the slit when illuminated with a tungsten lamp. A control thermocouple and a measuring thermocouple were inserted into the thermocouple wells in the nickel block and then a ceramic cylinder 10 cm. long and 5 cm. in diameter was placed on top of the nickel block for insulation. After the assembly was complete the furnace temperature was slowly raised and periodic observations of the sample tube were made by turning on the tungsten lamp and rotating the nickel block until the sample tube and contents were visible in the telescope whose objective was mounted 30 cm. from the center of the furnace.

The density determinations were carried out either (a) by observing the temperature at which the liquid just filled the tube (and then quickly reducing the furnace temperature to avoid breaking the tube), or (b) by observing the temperature at which the last trace of liquid disappeared in the case of the vapor densities. With practice these temperatures could be determined with a reproducibility of $\pm 3^\circ$ or less. After the temperature was determined, the tube was cooled to room temperature, cleaned, scratched with a file, and its weight in air and water was determined. The tube was then broken at the file mark; the bismuth chloride was dissolved in 3 *N* HNO₃; the pieces of empty tube were rinsed in distilled water and were dried. The tube fragments were again weighed in air and water. From these weighings the amount of bismuth chloride and the internal volume of the tube (approximately 0.4 cm.³) could be found and the density of liquid or vapor at the recorded temperature calculated. Additional liquid density measurements were made by using quartz "floats" whose density was determined by weighing in air and water. In these cases the temperature at which the float sank and the temperature at

which it rose again agreed, in some cases, within 2° although in general the spread was about 4°.

Determination of the critical temperature required continuous observation of the sample over long periods of time, and this exposure of the sample through the open slits set up temperature gradients in the tube. A correction for this error was made by determining the temperature indicated by a thermocouple placed inside an open sample tube compared to the block temperature. This correction varied depending on the vertical position along the slit and amounted to 4–8° at the critical temperature.

Results and Discussion

In the determination of the critical temperature of bismuth chloride, the liquid–vapor interface was observed through the telescope as the sample was heated. The meniscus became flat and then disappeared as the critical temperature was approached and exceeded. As the critical temperature was approached from above, a dark band about 2 mm. wide appeared in the tube out of which the meniscus emerged. The temperatures of disappearance and reappearance of the liquid–vapor interface were observed three times for each of four sample tubes. As mentioned earlier, a correction of 4–8° had to be applied to each observed temperature, the individual correction being dependent on the position of the interface in the tube. The corrected temperatures are listed in Table I. In view of the magnitude of the correction and the effect of the temperature gradient on the liquid–vapor interface, the critical temperature was taken as $905 \pm 5^\circ$.

Table I: Critical Temperature of Bismuth Chloride

Tube no.	Temp., °C., meniscus	
	Disappearance	Appearance
1	906.2	904.1
	905.9	904.0
	906.1	904.4
2	903.6	901.7
	903.9	901.7
	903.1	901.9
3	904.6	902.3
	904.9	902.0
	905.0	902.6
4	907.1	904.9
	905.9	905.1
	906.1	905.0
Average	905.2	904.3
Accepted value	905 \pm 5°	

The experimental densities of bismuth chloride liquid and vapor at various temperatures are presented in Table II and the coexistence curve is shown in Fig. 1. The first column in Table II indicates the method used to determine the liquid density. The vapor densities were all determined by volume. An uncertainty of $\pm 3^\circ$ is assigned to all temperatures listed in Table II.

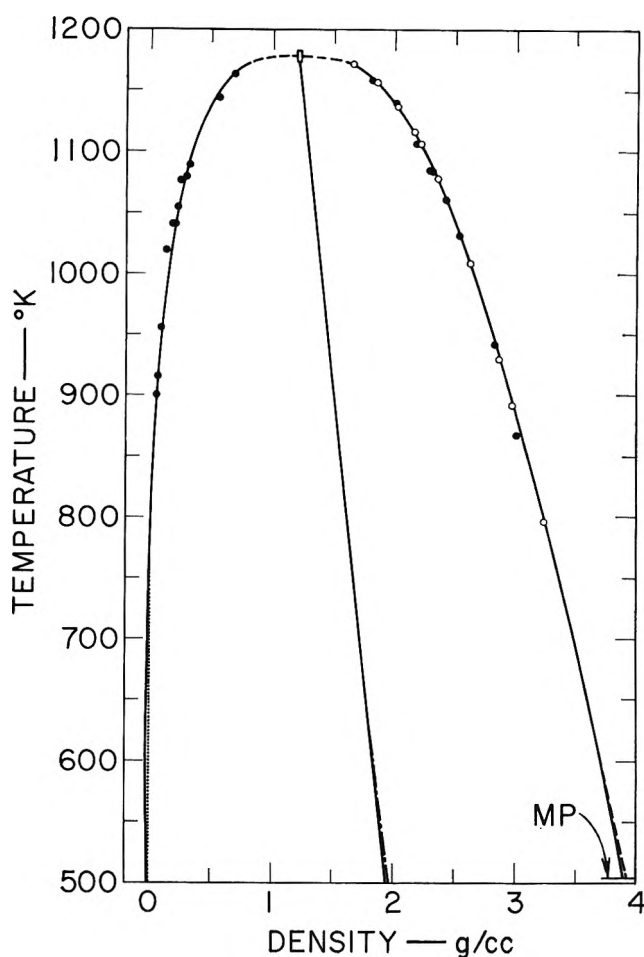


Figure 1. Bismuth chloride coexistence curve: O, float measurements; ●, volume measurements; —, calculated from eq. 3; —, experimental liquid density, ref. 5; experimental gas density (zero); - · -, average of experimental liquid and gas densities.

Guggenheim⁴ has developed empirical equations for the coexistence curves of the inert gases, oxygen, nitrogen, methane, and carbon monoxide, having the form

$$\rho_{\text{liq}}/\rho_{\text{crit}} = 1 + 0.75\left(\frac{T_c - T}{T_c}\right) + 1.75\left(\frac{T_c - T}{T_c}\right)^{1/2} \quad (1a)$$

$$\rho_{\text{vap}}/\rho_{\text{crit}} = 1 + 0.75\left(\frac{T_c - T}{T_c}\right) - 1.75\left(\frac{T_c - T}{T_c}\right)^{1/2} \quad (1b)$$

These equations were rearranged and the coefficients of the temperature terms generalized to the form

$$\rho = \rho_{\text{crit}} + a\left(\frac{T_c - T}{T_c}\right) \pm b\left(\frac{T_c - T}{T_c}\right)^{1/2} \quad (2)$$

where T is the temperature and T_c the critical temperature. The experimentally determined densities given in Table II and the critical temperature of 1178°K . were used to determine the values of a , b , and ρ_{crit} which gave the best fit to both liquid and vapor densities. The equations derived are

$$\rho_{\text{liq}} = 1.210 + 1.268\left(\frac{1178 - T}{1178}\right) + 2.347\left(\frac{1178 - T}{1178}\right)^{1/2} \quad (3a)$$

$$\rho_{\text{vap}} = 1.210 + 1.268\left(\frac{1178 - T}{1178}\right) - 2.347\left(\frac{1178 - T}{1178}\right)^{1/2} \quad (3b)$$

These relations reproduce the experimental data quite well as may be seen in Table II and Fig. 1 where the coexistence curve was calculated from these equations. Below about 800°K ., eq. 3 does not fit experience very well. For the vapor eq. 3b gives negative densities. The actual values are essentially zero (5.4×10^{-3} at the boiling point— 714°K .)—and smaller at lower temperatures). Guggenheim's equation in general gives negative vapor densities below $0.55T_c$. For the liquid eq. 3a gives values that are also too small.

It is of interest to compare the average density line derived from the addition of (3a) and (3b) and dividing by 2

$$\frac{\rho_{\text{liq}} + \rho_{\text{vap}}}{2} = 1.210 + 1.268\left(\frac{1178 - T}{1178}\right) = 1.210 + 1.072 \times 10^{-3}(1178 - T) \quad (4)$$

with that derived from the density equation given by Keneshea and Cubicciotti⁵ for their measurements of the density of bismuth chloride between the melting point and the normal boiling point. Their data are fitted by

$$\rho_{\text{liq}} = 4.417 - 2.2 \times 10^{-3}t \quad (250-450^\circ) \quad (5)$$

(4) E. A. Guggenheim, *J. Chem. Phys.*, **13**, 253 (1945).

(5) F. J. Keneshea and D. Cubicciotti, *J. Phys. Chem.*, **62**, 843 (1958).

Table II: Orthobaric Density Data for Bismuth Chloride

Method	Temp., °K.	Liquid phase			Vapor phase			
		Obsd.	Calcd.	Calcd. - Obsd.	Temp., °K.	Obsd.	Calcd.	Calcd. - Obsd.
Float	797	3.239	3.231	-0.008	901	0.059	0.059	0
Volume	868	3.012	3.048	+0.036	916	0.074	0.070	-0.004
Float	892	2.974	2.971	-0.003	956	0.095	0.103	+0.008
Float	930	2.864	2.873	+0.009	1020	0.138	0.179	+0.041
Volume	942	2.834	2.837	+0.003	1041	0.189	0.211	+0.022
Float	1009	2.630	2.621	-0.009	1041	0.210	0.211	+0.001
Volume	1032	2.536	2.537	+0.001	1055	0.233	0.237	+0.004
Volume	1061	2.428	2.423	-0.005	1075	0.270	0.279	+0.009
Float	1079	2.360	2.344	-0.016	1080	0.299	0.290	-0.009
Volume	1085	2.303	2.317	+0.014	1089	0.328	0.314	-0.014
Volume	1085	2.287	2.317	+0.030	1144	0.562	0.527	-0.035
Float	1107	2.221	2.206	-0.015	1163	0.690	0.678	-0.012
Volume	1107	2.188	2.206	+0.018				
Float	1117	2.164	2.151	-0.013				
Float	1138	2.022	2.031	+0.009				
Volume	1140	2.017	1.999	-0.018				
Float	1157	1.855	1.846	-0.009				
Volume	1158	1.804	1.835	+0.031				
Float	1171	1.648	1.645	-0.003				
							Av. dev.	0.013
				Av. dev.				0.013

Rearranging eq. 5 into a form similar to eq. 4 and dividing by 2, since the vapor may be assumed to have a negligible density in this temperature range, gives

$$\rho_{\text{liq}}/2 = (\rho_{\text{liq}} + \rho_{\text{vap}})/2 = 1.213 + 1.1 \times 10^{-3}(1178 - T) \quad (6)$$

where T is expressed in °K. This comparison can be seen in Fig 1. The excellent agreement between eq. 4 and 6 is to a certain extent fortuitous since the critical temperature has an uncertainty of $\pm 5^\circ$ and the critical density an estimated uncertainty of ± 0.006 g./cc. However, the agreement does suggest the average density line for bismuth chloride is a linear function of the temperature from the melting point to the critical point.

The applicability of Guggenheim's relation for molecular fluids to bismuth chloride prompted a comparison of the experimental critical temperature and density with values that would be predicted for a "normal" fluid. Accordingly, the graphical method of Riedel, as revised by Pitzer⁶ and co-workers, was applied to bismuth chloride. The parameters used were the normal boiling point (713°K.⁷), the 100-mm. boiling point (616°K.⁷), and the liquid density (3.713 g./cc. at 603°K.⁵). Applying the method outlined by Pitzer, we found it predicted a critical temperature of 1170°K. at a pressure of 98 atm. and critical volume of 261 cc./mole (and an acentric factor of 0.31). The

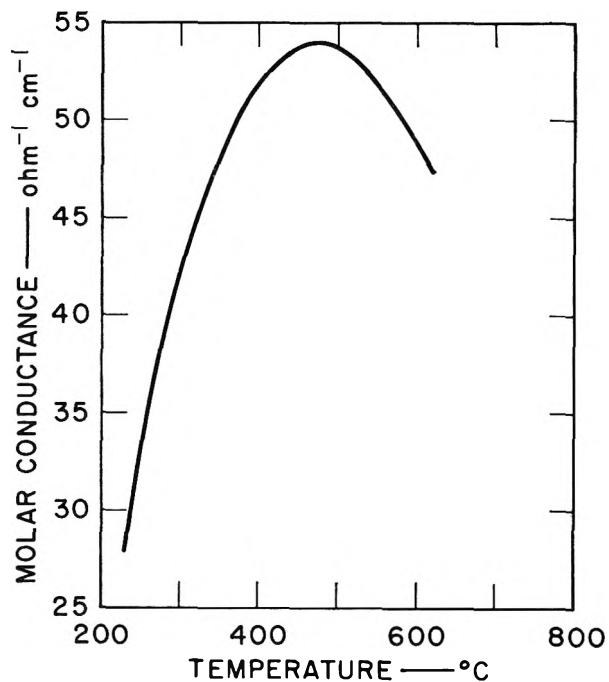


Figure 2. Molar conductance of liquid bismuth chloride. Curve calculated from ref. 3 and present data.

(6) See: Lewis and Randall, "Thermodynamics," revised by Pitzer and Brewer, McGraw-Hill Book Co., New York, N. Y., 1961, Appendix 1.

(7) D. Cubicciotti, C. M. Kelley, and F. J. Keneshea, *J. Phys. Chem.*, 62, 463 (1958).

measured values reported above are $1178 \pm 5^\circ\text{K}$. and 261 ± 1 cc./mole; so the critical temperature and density are essentially those predicted for a *normal* fluid.

Pitzer points out that a more sensitive test for a normal fluid is found in the surface tension. From Pitzer's eq.⁶ A1-20 we calculated the hypothetical surface tension at 0°K . to be 161 dynes/cm. and from his eq. A1-19 the surface tension at 272° becomes 75 dynes/cm. This value can be compared with the experimental one reported by Bradhurst and Buchanan⁸ of 66.1 dynes/cm. at 272° . The experimental value is about 12% below that predicted for a normal fluid indicating that significant deviations from the behavior of normal fluids might be expected.

Grantham and Yosim³ have measured the specific electrical conductivity of molten bismuth chloride up to 625° . The molar conductance obtained from the product of the specific conductance (ref. 3) and the molar volume (present data) is shown in Fig. 2. The shape of the curve is essentially the same as that for specific conductance since the molar volume changes relatively slowly with temperature; however, the maximum in the molar conductance appears at about 475° , instead of about 425° as in the specific conductance.

The interesting aspect of the curve, as Grantham and

Yosim have already indicated, is the decrease of conductance above about 475° . This decrease may well be due to a decrease in ionization of the bismuth chloride. A continuation of the trend of the molar conductance as a function of temperature above 475° in Fig. 2 would indicate a conductivity near zero at the critical temperature. This is in agreement with the view that liquid bismuth chloride acts as a molecular liquid near the critical point. The magnitude and temperature coefficient of the molar conductance below the maximum, while not so large as those of the molten alkali halides, are still comparable to ionic salts, such as YCl_3 , and about half of the values of LaCl_3 . Thus, from the melting point to the boiling point bismuth chloride can be considered to be ionic; and yet the vaporization properties of this liquid (boiling points at 760 mm. and 100 mm. and liquid density) seem to be typical of molecular fluids since they correctly predict the critical temperature and density when compared with the same properties of normal fluids.

Acknowledgments. Mr. G. Withers and Mr. W. Silva performed some of the experimental work.

(8) D. H. Bradhurst and A. S. Buchanan, *Australian J. Chem.*, **14**, 409 (1961).

A Zeroth-Order Approximation for Bond Energies, Hybridization States, and Bond Ionicities. I. Diatomic Molecules and A^I-B^I Crystals^{1a}

by Ricardo Ferreira^{1b}

Chemistry Department, Indiana University, Bloomington, Indiana (Received March 13, 1964)

In the first part of the paper bond energies and ionicities of 33 diatomic molecules and crystals of the type A^I-B^I are calculated by writing the bond energy $D(A-B)$ as a function of the ionicity x and maximizing $D(A-B)$ with respect to x . This is made possible by partitioning the bond energy into a sum of a homopolar term (a decreasing function of x) and a heteropolar term (the sum of an electrostatic term and a charge-transfer term). It is found that crystals are more ionic than the corresponding diatomic molecules, and also that lithium halides are more ionic than the corresponding sodium and potassium halides. In the second part of the paper, the bond energy is expressed as a function of two variables, the ionicity and the degree of s-character (α^2) of the more electronegative atom. $D(A-B)$, x , and α^2 for ten binary compounds are calculated by maximizing $D(A-B)$ with respect to x and α . It is shown that the fluorine atom has a higher degree of s-character than the other halogens in corresponding compounds.

Introduction

A zeroth-order approximation in quantum chemistry can be defined as one in which the molecular properties of interest to the chemist (bond energies, force constants, ionicities, etc.) are calculated from data of the corresponding isolated atoms (ionization potentials, electron affinities, etc.).² Considering on one hand the great difficulties inherent in *ab initio* calculations of fair sized molecules and, on the other hand, the fact that many of the so-called electron correlation effects are implicitly included in the free atom data, it is possible that zeroth-order calculations will remain useful for some time to come.

The most general physical principle operative in the chemical bonding is that the bond energy must correspond to a minimum in the total energy of the system with respect to the separated atoms. The bond energy³ of a heteroatomic molecule, $D(A-B)$, can be given by the sum of a *homopolar* term and a *heteropolar* term. The latter is given by the sum of an electrostatic term plus the energy variation due to the process of charge transfer from the less electronegative atom to the more electronegative one.⁴ As pointed out by Lindqvist,⁵ in this partitioning of the bond energy the heteropolar term includes only the energy connected

with charge transfer; the classical Coulomb interaction between atoms, without electron transfer, is part of the homopolar bond energy. Lindqvist⁵ also noted that as we increase the ionicity of a bond, the energy due to the heteropolarity increases but simultaneously the homopolar energy decreases.

We have done some work along these lines^{4b} based on the *principle of electronegativity equalization*.⁶ We realize now, however, that this generalization in its original form is not strictly valid (except if the bonded atoms are separated by an infinite distance!) and this led us to the decision of making a more detailed study of this subject.

(1) (a) This work was supported by grants from the U.S.A.F. Office of Scientific Research and the National Science Foundation; (b) on leave of absence from the University of Brasilia, Brasil.

(2) We also make use of the experimental dissociation energies of homopolar molecules.

(3) Since the energy minimum calculated from quantum mechanics includes the zero-point energy we will use, whenever it is possible, *bond energies*, D_e , and not *bond dissociation energies*, D_0 . These two quantities are related by the expression $D_e = D_0 + 1/2h\nu_0$.

(4) (a) R. P. Iczkowski and J. L. Margrave, *J. Am. Chem. Soc.*, **83**, 3547 (1961); (b) R. Ferreira, *Trans. Faraday Soc.*, **59**, 1064, 1075 (1963).

(5) I. Lindqvist, *Nova Acta Reg. Soc. Sci. Uppsala*, **17**, No. 11 (1960).

(6) R. T. Sanderson, *Science*, **114**, 670 (1951).

The One-Parameter Treatment

Shull⁷ has pointed out the difficulties that one encounters when trying to define the *ionic character*, or *ionicity*, of a chemical bond. In this paper we will define ionicity in the following way: consider a localized two-center bonding MO in a diatomic molecule AB

$$\Psi_M = c_A\psi_A + c_B\psi_B \quad (1)$$

The MO is normalized, hence $c_A^2 + c_B^2 + 2c_Ac_B S_{AB} = 1$. We will further assume that $S_{AB} = 0$, so that the normalization condition reduces to $c_A^2 + c_B^2 = 1$. If $X_A(0)$ and $X_B(0)$ are the electronegativities of the neutral atoms A and B and if $X_A(0) > X_B(0)$, we can write $1 \geq |c_A| \geq |c_B|$. We define the ionicity of a bond as

$$x = c_A^2 - c_B^2 \quad (0 \leq x \leq 1) \quad (2)$$

Considering the two extreme values, if $c_B = 0$, $x = 1$, $\psi_M = \psi_A$; we can say in this case that the bond is an *ionic bond*. If $c_B = c_A = (1/2)^{1/2}$, then $x = 0$, $\psi_M = 1/\sqrt{2}(\psi_A + \psi_B)$, and we can say that the bond A-B is a *normal covalent bond*.

This definition, of course, does not remove the difficulties discussed by Shull⁷ in relation to the VB treatment since ψ_A and ψ_B are not orthogonal. It has the advantage, however, that it leads to a simple formulation of the function $\mu(x)$ (see below) in terms of the concept of bond order.⁸

In this first approximation we will consider the variation of bond energy with the single parameter x . In a second treatment (two-parameter treatment) we will discuss how the bond energy varies with both the ionicity and the hybridization state of the bonded atoms.

For two atoms at the internuclear equilibrium distance (r_e) we can write in a general way

$$D(A-B) = D(A-B)_0\mu(x) + \Phi(x) + \delta(x) \quad (3)$$

where $D(A-B)_0$ is the normal covalent bond energy,⁹ $\mu(x)$ is a decreasing function of x , $\Phi(x)$ represents the electrostatic energy, and $\delta(x)$ is another function of x that gives the variation in energy due to the charge transfer. If one knows the forms of the functions $\mu(x)$, $\Phi(x)$, and $\delta(x)$, and the value of $D(A-B)_0$, we can maximize¹⁰ $D(A-B)$ with respect to x

$$d(D(A-B))/dx = 0 \quad (4)$$

and thus calculate x and, by substituting in (3), obtain $D(A-B)$.

The Normal Covalent Bond Energy, $D(A-B)_0$. At the present time there is apparently no rigorous way of calculating the energy of a normal covalent bond

between two different atoms and, in fact, the concept of a normal covalent bond itself breaks down at a more sophisticated level. Pauling and Yost⁹ first proposed an arithmetic mean rule

$$D(A-B)_0 = 1/2(D(A-A) + D(B-B)) \quad (5)$$

This equation gives meaningless results when applied to the alkali metal hydrides¹¹ and Pauling and Sherman¹² later suggested a geometrical mean rule

$$D(A-B)_0 = (D(A-A) \cdot D(B-B))^{1/2} \quad (6)$$

The theoretical basis for eq. 6 is the criterion of bond strength defined as the product of the angular parts of the bond orbitals (Slater atomic orbitals) along the bond direction. There is now sufficient evidence showing that this criterion of bond strength is less satisfactory than the one based on the numerical value of the overlap integral.¹³⁻¹⁶ On the other hand, a somewhat rough MO calculation¹⁷ favors the arithmetic mean rule. Thus, it was possible to show that

$$\beta_{AB} = 1/2(\beta_{AA} + \beta_{BB}) \quad (7)$$

where $\beta_{AB} = \int \psi_A^* H \psi_B d\tau - 1/2[\int \psi_A^* H \psi_A d\tau + \int \psi_B^* H \psi_B d\tau] S_{AB}$. Since¹⁸ $D(A-B)_0 = -2\beta_{AB}$, it is reasonable to suppose that eq. 5 holds within the limits of validity of eq. 7. In this report we will consistently use the arithmetic mean rule to calculate $D(A-B)_0$.

Two words of caution: first, as Mulliken¹⁷ pointed out, the arithmetic mean rule, or the more fundamental eq. 7, does not show the dependence of $D(A-B)_0$ on the bond distance. As is always the case in this type of approximation, we will consider the atoms at their equilibrium distance, r_e . Second, the arithmetic mean rule implies that the hybridization states of atoms A and B are the same in the homoatomic molecules A_2

(7) H. Shull, *J. Appl. Phys.*, **33**, 290 (1962).

(8) C. A. Coulson, *Proc. Roy. Soc. (London)*, **A169**, 419 (1939).

(9) L. Pauling and D. M. Yost, *Proc. Natl. Acad. Sci.*, **18**, 414 (1932).

(10) The maximum value of $D(A-B)$, considered as a positive quantity, corresponds to the minimum in the energy of the molecule as compared with the separated atoms.

(11) It seems that in the alkali metal hydrides the concept of electron-pair bonds begins to break down even at this level.

(12) L. Pauling and J. Sherman, *J. Am. Chem. Soc.*, **59**, 1450 (1937).

(13) A. Maccoll, *Trans. Faraday Soc.*, **46**, 369 (1950).

(14) R. S. Mulliken, *J. Phys. Chem.*, **56**, 295 (1952).

(15) C. A. Coulson, "Valence," Oxford University Press, London, 1953, pp. 198-201.

(16) F. A. Cotton, *J. Chem. Phys.*, **35**, 228 (1961).

(17) R. S. Mulliken, *J. Chim. Phys.*, **46**, 535 (1949).

(18) The equality $D(A-B)_0 = -2\beta_{AB}$ has a reasonable MO justification. The same cannot be said for the relation $D(A-B) = -2\beta_{AB}$, since the ionic contribution to the total bond energy depends on the difference of the diagonal matrix elements.

and B_2 and in the heteroatomic system AB. We will discuss the limitations of this point in detail later (in the two-parameter treatment).

The Function $\mu(x)$. By a simple extension of the concept of bond order,⁸ it is possible to define what may be called a *covalent bond order*. In Coulson's treatment the mobile bond order between two atoms is given by

$$p_{AB} = \sum_j n_j c_{A_j} c_{B_j} \quad (8)$$

where n_j is the number of electrons in the j th orbital. Since we are considering a single localized σ -MO with two electrons, the covalent bond order is simply $2c_A c_B$. From eq. 2 it is easily seen that

$$p_{AB} = 2c_A c_B = (1 - x^2)^{1/2} = \mu(x) \quad (9)$$

The homopolar bond energy is given by

$$D(A-B)_0 \mu(x) = \frac{1}{2}[D(A-A) + D(B-B)](1 - x^2)^{1/2} \quad (10)$$

If $c_A = c_B = (1/2)^{1/2}$, $\mu(x) = 1$ and the covalent bond order is equal to 1. In this case the homopolar bond energy is equal to $D(A-B)_0$. The homopolar bond energy decreases with increasing values of x and if $x = 1$ it goes to zero.¹⁹ It should be pointed out again that the function $\mu(x) = p_{AB}$ is, strictly speaking, dependent on the bond length, but in this treatment we will consider only the equilibrium distance.

The Electrostatic Function, $\Phi(x)$. Although many potential functions have been proposed for the essentially ionic compounds,^{20a} it is not a straightforward matter to calculate the electrostatic energy in molecules like HCl, BrF, etc. Wall^{20b} used the original Born-Landé function

$$\Phi = Ax^2 \frac{e^2}{r_e} \frac{(n-1)}{n} \quad (11)$$

where A is the Madelung constant (for diatomic molecules, $A = 1$) and n is a repulsive coefficient.²¹ In crystals n is determined from compressibility data but for the gaseous compounds only reasonable guesses can be made. Wall attributed to n values ranging from 2 to 6 in HF, 3 to 7 in HCl, 3.5 to 7.5 in HBr, and 4.5 to 8.5 in HI. His results, however, are not strictly valid because he was gauging them by a comparison, unwarranted as we know now, between the experimental dipole moments and the primary dipole moments. Warhurst²² in his treatment of the hydrogen halides used a Born-Mayer potential²³ with $1/\rho = 3.00$. For the alkali metal halides, Born and Mayer had shown that the best value of $1/\rho$ is 2.90. Warhurst's value was thus chosen because the repulsive

term in the hydrogen halide molecules is smaller than the one in the alkali metal halides.

Since for the extremely ionic compounds the Born-Landé function²⁴ gives results within $\pm 5\%$ of the experimental values and since for the essentially covalent compounds, where the Born-Landé function is probably a poorer approximation, the term $\Phi(x)$ is relatively unimportant, we will use eq. 11 in the calculation of the electrostatic energy. With the exception of the hydrogen halides we will use the repulsive coefficients given by Sherman.²⁵ For the hydrogen halides we will make two sets of calculations, the first one with Sherman's coefficients for the halogen anions and $n = 5$ for hydrogen, the second one with $n = 9$ for the four hydrogen halides. The value $n = 9$ was chosen to take into account the smaller repulsive terms in these molecules.

The Function $\delta(x)$. We will assume^{4a, 26-28} that the energy of an electron in an atomic orbital is a *continuous* and *differentiable* function of the charge in the atom, x , in the interval $+1 \geq x \geq -1$. Furthermore, this function $\epsilon(x)$ is *single-valued* for each valence state. This simple electrostatic approach is justified because in one given orbital the electrons must have opposite spins and the exchange integral vanishes. From the experimental values of $\epsilon(x)$ for the three integral values of x , $+1$, 0 , -1 (corresponding, respectively, to I_{VS} , 0 , and $-E_{VS}$), an infinite number of curves can be drawn. The function adopted is the simplest one, namely, the parabola²⁹

$$\epsilon(x) = \frac{1}{2}(I_{VS} + E_{VS})x + \frac{1}{2}(I_{VS} - E_{VS})x^2 \quad (12)$$

(19) The concept of covalent bond order was firstly discussed by Professor Mulliken at the Shelter Island Conference on Valence Theory (Conference Report, 1951, p. 67). It would also be possible to use the generalized bond order definition of Chirgwin and Coulson [*Proc. Roy. Soc. (London)*, **A201**, 196 (195C)], but the inclusion of overlap would change little the numerical results.

(20) (a) See the complete analysis of P.-O. Löwdin, *Phil. Mag. Suppl.*, **5**, No. 17 (1956); (b) F. T. Wall, *J. Am. Chem. Soc.*, **61**, 1051 (1939).

(21) In this paper x is a pure number (*cf.* eq. 2) which measures the fractional (excess or decrement) electron content of the bonded atoms.

(22) E. Warhurst, Victor Henri Memorial Volume, Liege, Desoer, 1948, p. 57.

(23) M. Born and J. E. Mayer, *Z. Physik*, **75**, 1 (1932).

(24) M. Born and A. Landé, *Verhandel. Devt. Physik. Ges.*, **20**, 120 (1918).

(25) J. Sherman, *Chem. Rev.*, **11**, 93 (1932).

(26) H. O. Pritchard and F. H. Sumner, *Proc. Roy. Soc. (London)*, **A235**, 136 (1956).

(27) C. K. Jørgensen, "Orbitals in Atoms and Molecules," Academic Press, New York, N. Y., 1962, p. 80.

(28) J. Hinze, M. A. Whitehead, and H. H. Jaffé, *J. Am. Chem. Soc.*, **85**, 148 (1963).

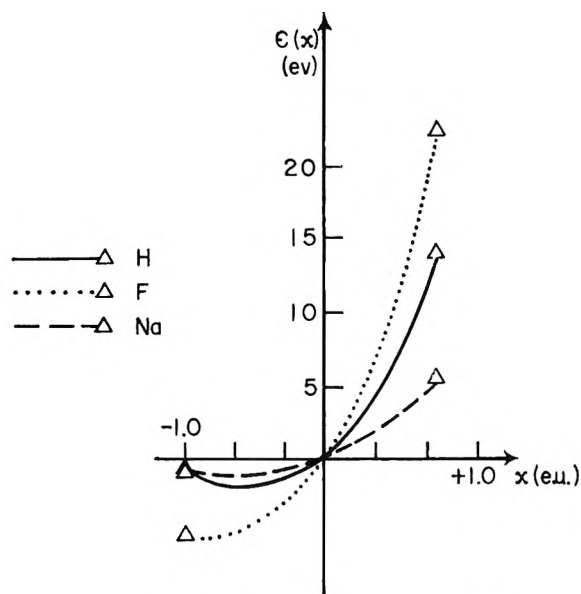


Figure 1. Parabolic functions between energy and charge.

Figure 1 shows the curves for three distinct elements, H, F, and Na.

We define the electronegativity of an atom A as the derivative of $\epsilon_A(x)$ with respect to x , that is, electronegativity is the potential acting on the atomic orbital ψ_A .^{4a,26-28} Thus

$$X_A(x) = d\epsilon_A(x)/dx \quad (13)$$

For a neutral atom ($x = 0$)

$$X_A(0) = d\epsilon_A(0)/dx \quad (14)$$

It can be immediately seen that the electronegativity of a neutral atom defined by eq. 14 is identical with Mulliken's definition.³⁰ From eq. 12 and 13 we obtain

$$X_A(x) = 1/2(I_A + E_A) + (I_A - E_A)x \quad (15)$$

and

$$X_A(0) = 1/2(I_A + E_A) \quad (16)$$

In the same way we can write for B

$$X_B(x) = 1/2(I_B + E_B) + (I_B - E_B)x \quad (17)$$

and

$$X_B(0) = 1/2(I_B + E_B) \quad (18)$$

It must be pointed out that since $X_A(0) > X_B(0)$ we have $x < 0$ in eq. 15 and $x > 0$ in eq. 17. In other words, the sense of the bond polarity is determined by the difference $X_A(0) - X_B(0)$. The energy variation corresponding to the transfer of a partial charge x is given by

$$\delta(x) = (1/2(I_A + E_A)x - 1/2(I_A - E_A)x^2) - (1/2(I_B + E_B)x + 1/2(I_B - E_B)x^2) \quad (19)$$

If we want to introduce the concept of electronegativity as defined above, then eq. 19 can be written

$$\delta(x) = X_A(0)x - 1/2(I_A - E_A)x^2 - X_B(0)x - 1/2(I_B - E_B)x^2 \quad (20)$$

Since $X_A(0) > X_B(0)$, for small values of x , the function $\delta(x)$ is a positive quantity and contributes to the stability of the molecule AB.

The Complete Bond Energy Function. Equation 3 can now be written

$$D(A-B) = 1/2(D(A-A) + D(B-B))(1 - x^2)^{1/2} + (Ax^2/r_e)(n - 1)/n + X_A(0)x - 1/2(I_A - E_A)x^2 - X_B(0)x - 1/2(I_B - E_B)x^2 \quad (21)$$

This is the fundamental equation of the present treatment. In the two limiting cases, $x = 0$ and $x = 1$, eq. 21 gives the normal covalent bond energy and the ionic bond energy, that is

$$D(A-B) = 1/2(D(A-A) + D(B-B)) \quad (x = 0) \quad (22)$$

$$D(A-B) = (A/r_e)(n - 1)/n + E_A - I_B \quad (x = 1) \quad (23)$$

Assuming that r_e is a constant and differentiating $D(A-B)$ with respect to x

$$dD(A-B)/dx = -D(A-B)_0x(1 - x^2)^{-1/2} + (2Ax/r_e)(n - 1)/n + X_A(0) - (I_A - E_A)x - X_B(0) - (I_B - E_B)x \quad (24)$$

Making $(dD(A-B)/dx) = 0$, one obtains

$$x = \frac{X_A(0) - X_B(0)}{D(A-B)_0(1 - x^2)^{-1/2} + (I_A - E_A) + (I_B - E_B) - \frac{2A}{r_e} \frac{(n - 1)}{n}} \quad (25)$$

Equation 25 permits one to calculate the ionicity x by successive approximations.

So far we have considered only diatomic molecules but the treatment can be extended to ionic crystals of the type A^I-B^I . In these cases the Madelung

(29) Recently, G. Klopman [*J. Am. Chem. Soc.*, **86**, 1463 (1964)] has discussed the theoretical basis of the empirical parabolic relation. He has shown that this relation is as valid as the general expression for the energy of an atomic configuration (eq. 11 of his paper). Klopman (private communication) has now extended his calculations to heteroatomic systems and his results compare well with ours.

(30) R. S. Mulliken, *J. Chem. Phys.*, **2**, 782 (1934).

constant is greater than 1. The proper choice of $D(A-B)$ in a solid, however, is not as clear-cut as for a diatomic molecule, since there are too few electrons to make bonds between all neighbor atoms. In our calculations we use the same value for the covalent bond energy in molecules and the corresponding crystals but the results for the latter are probably less reliable.

Criticism of the Principle of Electronegativity Equalization. Before proceeding with the actual calculations, it will be interesting to examine the limits of validity of the principle of electronegativity equalization.⁶ This generalization states that the electronegativities of bonded atoms at their equilibrium positions are equal. It can be shown that this principle is valid only if there are no interactions between the atoms.

Suppose that two atoms A and B are at an infinite distance apart so that there is no overlapping between the bonding orbitals of each atom nor electrostatic forces between the atoms. In this case, as the charge x is transferred from B to A the condition for minimum energy is $(d\delta(x)/dx) = 0$. From eq. 20

$$X_A(0) - (I_A - E_A)x - X_B(0) - (I_B - E_B)x = 0 \quad (26)$$

Hence

$$X_A(0) - (I_A - E_A)x = X_B(0) + (I_B - E_B)x \quad (27)$$

We can see that in this particular case we can say that electronegativity equalization is attained, that is, $X_A(-x) = X_B(+x)$. However, this is no longer true if we consider actual cases in which the atoms are bonded by covalent and electrostatic terms. As the charge is transferred from one atom to another we must also take into account the simultaneous decrease in the covalent energy and increase in the heteropolar energy. This was also pointed out by Jørgensen,²⁷ who stated that the principle of equilibrated electronegativity must be corrected for the Madelung energy (our $\Phi(x)$) and the covalent bond energy. As noted by Pearson and Gray³¹ the only general principle to be used as a criterion to calculate the ionicity is that the total energy of the system must be at a minimum, and this corresponds to $dD(A-B)/dx = 0$, not $d\delta(x) = 0$.

It cannot be denied, however, that Sanderson's generalization has some appeal to chemists, and it has been used with varying degrees of success by Sanderson himself³² and other investigators.^{4b,28} For some molecules at least the increase in the ionic term is approximately balanced by the decrease in the homopolar term and equalization of electronegativities is roughly achieved. It can be shown, however, that in general

the equilibrated electronegativities method gives ionicity values that are too low. From eq. 27 one obtains

$$x = (X_A(0) - X_B(0))/((I_A - E_A) + (I_B - E_B)) \quad (28)$$

This is eq. 3 of the paper by Hinze, Whitehead, and Jaffé.²⁸ If we compare (28) with (25) it is seen that since $(2A/r_e)(n - 1)$ is in general larger than $D(A-B)_0(1 - x^2)^{-1/2}$ the ionicities calculated by eq. 28 are smaller than the ones calculated by (25).³³

Results and Discussion

We have calculated the ionicities and bond energies of 22 diatomic molecules [(LiF(g), LiCl(g), LiBr(g), LiI(g), NaF(g), NaCl(g), NaBr(g), NaI(g), KF(g), KCl(g), KBr(g), KI(g), HF(g), HCl(g), HBr(g), HI(g), ClF(g), BrF(g), IF(g), BrCl(g), ICl(g), and IBr(g)] and 11 ionic crystals (LiF(c), [LiCl(c), LiI(c), NaCl(c), NaBr(c), NaI(c), KF(c), KCl(c), KBr(c), and KI(c)]. All these crystals are of the sodium chloride type ($A = 1.7476$). NaF(c) was not included because no data for the bond distance of this crystal were found in the literature.

Ionicities and bond energies were calculated by an iterative procedure with the IBM 709 computer of the C.R.C. of Indiana University. We have collected all the pertinent atomic and molecular (or crystal) data in Tables I, II, and III.

Table I: Ionization Potentials and Electron Affinities^a

Element	Ionization potential, e.v.		Electron affinity, e.v.	
	$I(p)$	$I(s)$	$E(p)$	$E(s)$
H		13.595		0.747
F	20.98	38.24 ^b	3.48 ^c	24.37 ^b
Cl	15.09	24.02 ^b	3.63 ^d	14.45 ^b
Br	13.72	22.07 ^e	3.38 ^d	14.50 ^e
I	12.61	18.00 ^e	3.08 ^d	13.38 ^e
Li		5.39		0.82 ^f
Na		5.14		0.47 ^f
K		4.35		0.69 ^g

^a Data from H. O. Pritchard and H. A. Skinner, *Chem. Rev.*, **55**, 745 (1955). ^b See ref. 43. ^c D. Cubicciotti, *J. Chem. Phys.*, **31**, 1646 (1959). ^d R. S. Berry, C. W. Reimann, and G. N. Spokes, *ibid.*, **37**, 2278 (1962). ^e J. Hinze and H. H. Jaffé, *J. Phys. Chem.*, **67**, 1501 (1963). ^f R. Edlen, *J. Chem. Phys.*, **33**, 98 (1960). ^g H. O. Pritchard, *Chem. Rev.*, **52**, 529 (1953).

(31) R. G. Pearson and H. B. Gray, *Inorg. Chem.*, **2**, 358 (1963); see also G. Klopman, *J. Am. Chem. Soc.*, **86**, 1463 (1964).

(32) R. T. Sanderson, "Chemical Periodicity," Reinhold Publishing Co., New York, N. Y., 1960.

(33) The principle of electronegativity equalization may possibly be preserved by introducing a generalized definition of effective electronegativity.

Table II: Bond Distances^a

Compound	Bond distance, Å.	Compound	Bond distance, Å.
LiF(g)	1.564	NaCl(c)	2.814
LiCl(g)	2.00	NaBr(c)	2.980
LiBr(g)	2.17	NaI(c)	3.231
LiI(g)	2.392	KF(c)	2.664
NaF(g)	2.10 ^b	KCl(c)	3.138
NaCl(g)	2.361	KBr(c)	3.285
NaBr(g)	2.502	KI(c)	3.525
NaI(g)	2.712	HF(g)	0.917
KF(g)	2.55	HCl(g)	1.275
KCl(g)	2.666	HBr(g)	1.414
KBr(g)	2.821	HI(g)	1.604
KI(g)	3.048	ClF(g)	1.628
LiF(c)	2.009	BrF(g)	1.756
LiCl(c)	2.566	IF(g)	1.985
LiBr(c)	2.747	BrCl(g)	2.138
LiI(c)	3.002	ICl(g)	2.321
		IBr(g)	(2.5)

^a Data from "Tables of Interatomic Distances and Configuration in Molecules and Crystals," L. Sutton, Ed., Special Publication No. 11, The Chemical Society, London, 1958. ^b H. J. Zieger and D. I. Bolef, *Phys. Rev.*, **85**, 788 (1952).

Table III: Bond Energies of the Homoatomic Molecules^a

Molecule	Bond energies, D_e , kcal. mole ⁻¹
H ₂	109.46
F ₂	37.3
Cl ₂	57.88
Br ₂	45.92
I ₂	35.68
Li ₂	25.5
Na ₂	17.5
K ₂	11.9

^a Data from ref. 36 and 37.

Bond Ionicities. Table IV shows the calculated ionicities for the 33 compounds and it also shows the values of the product (xer_e) for the diatomic molecules only. This product is the *primary dipole moment*, and, as expected, it is always larger than the experimental values for the gaseous dipole moments, shown in column 4 of Table IV. The result expressed by the inequality

$$x > \frac{\mu_{\text{exp}}}{er_e} \quad (29)$$

is due to the fact that the total electric moment is given by the vector sum of the primary, overlap, and

Table IV: Ionicities and Dipole Moments

Compound	x , e.u.	xer_e , D.	μ_{exp} , D.
LiF(g)	0.909	6.83	6.28
LiCl(g)	0.862	8.26	5.9
LiBr(g)	0.852		
LiI(g)	0.817		
NaF(g)	0.766		
NaCl(g)	0.800	9.07	8.5
NaBr(g)	0.801		
NaI(g)	0.772	10.02	4.9
KF(g)	0.752	9.18	7.33
KCl(g)	0.831	10.6	10.5
KBr(g)	0.839	11.4	10.4
KI(g)	0.823	12.0	11.1
LiF(c)	0.986		
LiCl(c)	0.968		
LiBr(c)	0.972		
LiI(c)	0.971		
NaCl(c)	0.966		
NaBr(c)	0.971		
NaI(c)	0.972		
KF(c)	0.979		
KCl(c)	0.969		
KBr(c)	0.977		
KI(c)	0.979		
HF(g)	0.615 (0.718) ^a	2.71 (3.16) ^a	1.74-1.91
HCl(g)	0.251 (0.273) ^a	1.53 (1.67) ^a	1.08
HBr(g)	0.153 (0.162) ^a	1.02 (1.10) ^a	0.80
HI(g)	0.069 (0.070) ^a	0.53 (0.54) ^a	0.42
ClF(g)	0.184	1.44	0.88
BrF(g)	0.241	2.02	1.29
IF(g)	0.278		
BrCl(g)	0.067	0.69	0.57
ICl(g)	0.128	1.43	0.65
IBr(g)	0.063		

^a These values are calculated with $n = 9$ in the Born-Landé function.

hybridization moments. Two general conclusions, however, should be pointed out.

1. Crystals are more ionic than the corresponding diatomic molecules. This results from the fact that the larger Madelung constant makes the electrostatic terms more important in the case of the crystals. This is also expected from the classical (polarizability) models, since the polarization of the anion by the cation is larger for diatomic molecules.

2. Lithium compounds are more ionic than the corresponding sodium compounds and, in most cases, than the corresponding potassium compounds. This effect, experimentally found by Dailey and Townes,³⁴ is due to the large Coulomb energy connected with the short interatomic distances in the lithium compounds.

(34) B. P. Dailey and C. H. Townes, *J. Chem. Phys.*, **23**, 118 (1955).

Bond Energies. The bond energies calculated from eq. 21 are shown in Table V. The experimental values for $D(A-B)$ are given in the second column of this table; they were obtained in the following way: for the gaseous alkali metal halides the values shown are the dissociation enthalpies³⁵ (ΔH°_{298}). Values given for the hydrogen halides and interhalogen compounds are bond energies, D_e , obtained from the bond dissociation energies and zero-point frequencies.^{36,37} For the ionic crystals, the experimental bond energies are atomization energies calculated from the relation

$$D(A-B) = U_{AB} + E_A - I_B \quad (30)$$

where U_{AB} is the lattice energy obtained from the Born-Haber cycle. For comparison, the last column of Table V shows the values of $D(A-B)$ calculated from the classical Born-Landé function.

Table V: Calculated and Experimental Bond Energies^c

Compound	$D(A-B)$ (exptl.)	$D(A-B)$ (calcd.)	$D(A-B)$ (Born-Landé)
LiF(g)	137.5	140.0	
LiCl(g)	111.9	113.7	
LiBr(g)	100.2	96.7	
LiI(g)	84.6	80.3	
NaF(g)	114.0	113.5	
NaCl(g)	97.5	103.1	
NaBr(g)	86.7	88.9	
NaI(g)	72.7	74.3	
KF(g)	117.6	111.0	
KCl(g)	101.3	106.5	
KBr(g)	90.9	92.8	
KI(g)	76.8	78.4	
LiF(c)	201.5	199.2	197.6
LiCl(c)	163.9	158.3	154.3
LiBr(c)	148.2	140.7	139.1
LiI(c)	128.3	120.9	119.4
NaCl(c)	151.9	150.4	147.2
NaBr(c)	138.5	134.7	133.5
NaI(c)	120.5	116.2	115.3
KF(c)	174.5	173.0	171.9
KCl(c)	154.5	152.2	149.4
KBr(c)	141.9	138.6	138.8
KI(c)	125.4	122.0	121.7
HF(g)	139.9	111.4 (120.1) ^b	
HCl(g)	106.5	90.2 (90.7) ^b	
HBr(g)	90.3	80.2 (80.3) ^b	
HI(g)	73.8	72.7 (72.7) ^b	
ClF(g)	61.6	53.7	
BrF(g)	(55.9)	51.9	
IF(g)	(46)	50.6	
BrCl(g)	52.7	52.5	
ICl(g)	50.1	49.0	
IBr(g)	42.3	41.4	

^a Bond energies in kcal. mole⁻¹. ^b Values calculated with $n = 9$ in the Born-Landé function.

It is seen that the agreement between calculated and experimental values is reasonably good for the extremely ionic and extremely covalent compounds but poorer for the molecules of an intermediate character (HF, HCl, ClF, etc.). For the 23 essentially ionic compounds the average over-all accuracy is $\pm 3\%$. It should be pointed out that for the ionic crystals, the calculated bond energies tend to be lower than the experimental values; this probably is due to the choice of the Born-Landé function, since this classical model gives still lower values. It is possible that our results could be improved by the use of a better potential function $\Phi(x)$ like the Born-Mayer function,²³ but we do not think this is worthwhile considering the approximate character of this treatment. We will show next that the larger discrepancies found for HF, HCl, etc., are in part due to our neglect of the hybridization of the bonding orbitals.

The Two-Parameter Treatment

Thus far we have considered the bond energy as a function of a single parameter, the ionicity x . A more complete treatment, however, should include as a second variable the hybridization state of the bonded atoms.

Mulliken's well-known saying that "a little hybridization goes a long way" reminds us of the dangers of many arbitrary assignments of hybrid wave functions. For example, there is now sufficient evidence, both from SCF-MO and VB calculations,^{38,39} showing that in the halogen molecules the bonded atoms use almost pure p-orbitals. We hope to show, nevertheless, that in *heteroatomic molecules* the more electronegative atom uses s, p hybrid orbitals, because in this case the s-p promotion energy is compensated not only by an increase in the overlap integral but also by an augmented electrostatic term $\Phi(x)$, due to an increase in $X_A(0)$. This analysis indicates also that we can safely neglect s-p hybridization of the less electronegative atom, a fact that has been recognized for some time now.⁴⁰

Let us assume that atom A ($X_A(0) > X_B(0)$) uses a normalized hybrid σ -AO of the form

$$\psi_A = \alpha\psi_s + (1 - \alpha^2)^{1/2}\psi_p \quad (31)$$

(35) L. Brewer and E. Brackett, *Chem. Rev.*, **61**, 425 (1961).

(36) T. L. Cottrell, "The Strengths of the Chemical Bond," 2nd Ed., Butterworths, London, 1958.

(37) G. Herzberg, "Spectra of Diatomic Molecules," 2nd Ed., D. Van Nostrand, New York, N. Y., 1950.

(38) B. J. Ransill, *Rev. Mod. Phys.*, **32**, 245 (1960).

(39) G. L. Caldow and C. A. Coulson, *Trans. Faraday Soc.*, **58**, 633 (1962).

(40) H. A. Bent, *J. Chem. Phys.*, **33**, 304, 1259 (1960).

All the energy terms of this AO are linear functions of the amount of s-character, α^2 . For instance

$$I_A(\alpha^2) = \alpha^2 I_A(s) + (1 - \alpha^2) I_A(p) = I_A(p) + \alpha^2 (I_A(s) - I_A(p)) \quad (32)$$

In the same way we can write

$$E_A(\alpha^2) = E_A(p) + \alpha^2 (E_A(s) - E_A(p)) \quad (33)$$

$$X_A(\alpha^2) = X_A(p) + \alpha^2 (X_A(s) - X_A(p)) \quad (34)$$

The promotion energy is also a linear function of the amount of s-character, that is, $P_A(\alpha^2) = \alpha^2 P_A$.

Mulliken, *et al.*,⁴¹ have shown that hybrid AO overlap integrals are given by the linear combination of non-hybrid overlap integrals. Since we have assumed that only atom A hybridizes, eq. 77 of the article by Mulliken, *et al.*, reduces to

$$S(\alpha) = \alpha S(1) + (1 - \alpha^2)^{1/2} S(0) \quad (35)$$

where $S(0)$ is the overlap integral if atom A uses a pure p-orbital and $S(1)$ is the overlap integral if atom A uses a pure s-orbital. Assuming that the normal covalent bond energy is directly proportional to the overlap integral, eq. 36 applies.

$$x = \frac{[X_A(p) + \alpha^2 (X_A(s) - X_A(p))] - X_B}{D(A-B)_0 (1 - x^2)^{-1/2} [(S(1)/S(0))\alpha + (1 - \alpha^2)^{1/2}] + [(I_A(p) - E_A(p)) + (I_B - E_B) - (2A(n - 1))/r_e n] + [(I_A(s) - I_A(p)) - (E_A(s) - E_A(p))]\alpha^2} \quad (41)$$

$$\alpha = \frac{D(A-B)_0 (1 - x^2)^{1/2} (S(1)/S(0))}{D(A-B)_0 (1 - \alpha^2)^{-1/2} (1 - x^2)^{1/2} - 2(X_A(s) - X_A(p))x + [(I_A(s) - I_A(p)) - (E_A(s) - E_A(p))]\alpha^2 + 2P_A} \quad (42)$$

$$D(A-B)_{0,\alpha} = \underline{D(A-B)_0} (S(\alpha)/S(0)) \quad (36)$$

Hence

$$D(A-B)_{0,\alpha} = D(A-B)_0 [\alpha (S(1)/S(0)) + (1 - \alpha^2)^{1/2}] \quad (37)$$

It is known that the length of a bond A-B will vary with the hybridization state of the bonded atoms. However, for the small amount of s-character we will discuss in this paper, it can be assumed that r_e is independent of the hybridization state of A and we can now write

$$D(A-B) = D(A-B)_0 (1 - x^2)^{1/2} [\alpha (S(1)/S(0)) + (1 - \alpha^2)^{1/2}] + \frac{Ax^2 (n - 1)}{r_e n} + [X_A(p) + \alpha^2 (X_A(s) - X_A(p))]x - 1/2 [(I_A(p) + \alpha^2 (I_A(s) - I_A(p))) - [E_A(p) + \alpha^2 (E_A(s) - E_A(p))]]x^2 - X_B x - 1/2 (I_B - E_B)x^2 - \alpha^2 P_A \quad (38)$$

Equation 38 is the two-variable counterpart of eq. 21; it is easily seen that when $\alpha^2 = 0$, (38) reduces to (21).

Calculation of Bond Energies, Ionicities, and Degrees of s-Character. Assuming that $D(A-B)$ as given in eq. 38 is a continuous and differentiable function of x and α in the intervals $0 \leq x \leq 1$ and $0 \leq \alpha \leq 1$, the necessary conditions for $D(A-B)$ to be a maximum⁴² are that $(\partial D(A-B)/\partial x)_\alpha = 0$ and $(\partial D(A-B)/\partial \alpha)_x = 0$. Hence

$$(\partial D(A-B)/\partial x)_\alpha = -D(A-B)_0 x (1 - x^2)^{-1/2} [\alpha (S(1)/S(0)) + (1 - \alpha^2)^{1/2}] + \left[\frac{2A(n - 1)}{nr_e} \right] x + [X_A(p) + \alpha^2 (X_A(s) - X_A(p))] - [(I_A(p) + \alpha^2 (I_A(s) - I_A(p))) - [E_A(p) + \alpha^2 (E_A(s) - E_A(p))]]x - X_B - (I_B - E_B)x = 0 \quad (39)$$

and

$$(\partial D(A-B)/\partial \alpha)_x = D(A-B)_0 (1 - x^2)^{1/2} [(S(1)/S(0)) - \alpha (1 - \alpha^2)^{-1/2}] + 2(X_A(s) - X_A(p))x\alpha - [(I_A(s) - I_A(p)) - (E_A(s) - E_A(p))]\alpha^2 x^2 - 2\alpha P_A = 0 \quad (40)$$

This system of simultaneous equations, eq. 39 and 40, can be solved by an iterative method to give x and α , and by substitution in (38) we can calculate $D(A-B)$. From (39) we obtain (41), and likewise from (40) we get (42). It is easily seen that if $\alpha = 0$, (41) reduces to (25). Let us call x_0 the value of x calculated from (25). We can now substitute x_0 in (42) and obtain a value of α that we will call α_1 . Substituting α_1 in (41) we obtain a value x_1 ; this value is substituted in (42) and we obtain α_2 , and so on by iteration until self-consistency is obtained in both x and α . Substituting the self-consistent x and α in eq. 38 we calculate the bond energy, $D(A-B)$.

Results and Discussion

We have made the calculations for LiF(g), LiCl(g), NaF(g), LiF(c), LiCl(c), HF(g), HCl(g), HBr(g),

(41) R. S. Mulliken, C. A. Rieke, D. Orloff, and H. Orloff, *J. Chem. Phys.*, **17**, 1248 (1949).

(42) The sufficient condition $(\partial^2 f/\partial x^2)(\partial^2 f/\partial \alpha^2) - \partial^2 f/\partial x \partial \alpha > 0$ is also shown by the function $D(A-B) = f$.

Table VI: Ionicities, Hybridization States, and Bond Energies

Compound	Ionicity	α	% s-character	$D(A-B)$ (calcd.), kcal. mole ⁻¹	$D(A-B)$ (exptl.), kcal. mole ⁻¹
LiF(g)	0.910	0.121	1.48	140.8	137.5
LiCl(g)	0.860	0.226	5.09	116.1	111.9
NaF(g)	0.768	0.068	0.47	114.0	114.0
LiF(c)	0.985	0.250	6.23	200.0	201.5
LiCl(c)	0.965	0.388	15.1	160.4	163.9
HF(g)	0.623 (0.724) ^a	0.210 (0.242) ^a	4.4 (5.8) ^a	120.8 (129.9) ^a	139.9
HCl(g)	0.274 (0.297) ^a	0.200 (0.203) ^a	4.0 (4.1) ^a	99.1 (99.7) ^a	106.5
HBr(g)	0.171 (0.180) ^a	0.155 (0.156) ^a	2.4 (2.4) ^a	86.2 (86.3) ^a	90.3
HI(g)	0.079 (0.080) ^a	0.124 (0.124) ^a	1.5 (1.5) ^a	76.6 (76.6) ^a	73.8
ClF(g)	0.187	0.062	0.38	55.3	61.6

^a These values are calculated with $n = 9$ in the Born-Landé function.

HI(g), and ClF(g). With the exception of hydrogen bromide, these are the systems for which numerical values for the overlap integrals are reported in Mulliken's tables.⁴¹ The overlap integrals for HBr(g) were obtained by interpolation.

The s-p promotion energies for the halogen atoms are⁴³: F, 20.89 e.v.; Cl, 10.76 e.v.; Br, 10.95 e.v.; I, 10.17 e.v. All the other necessary data are shown in Tables I, II, and III. The calculations were made with the IBM 709 computer of the R.C.C. of Indiana University. The results are shown in Table VI.

It is seen that for the extremely ionic compounds the calculated ionicities and bond energies did not change appreciably from the values calculated by the simpler treatment. There was, however, a definite improvement in the results for the hydrogen halides and ClF (for the hydrogen halides the value $n = 9$ gave better results, particularly in the case of HF).

It is interesting to note that the amount of s-character of the halogen atoms in the hydrogen halides is small and that it is largest for fluorine (4.4% or, alternatively, 5.8%), decreasing monotonically to iodine (1.5%). This trend is observed in spite of the considerably larger s-p promotion energy of fluorine compared with the other halogens, and it is due to the great increase of the term $(X_F(s) - X_F(p))$ in eq. 38. Now,

it is well known that the bond angle data in homologous series of molecules like H₂O, H₂S, H₂Se, and H₂Te, or, NH₃, PH₃, AsH₃, and SbH₃, when analyzed within the assumption that the orthogonality condition applies to the localized bonding orbitals of these molecules, indicate that the amount of s-character is a maximum for the second period atoms (O, N, etc.). Because the lighter atoms have in general larger s-p promotion energies than their higher homologs the resulting apparent contradiction has been held against the assumption of strict orthogonality, or against the criterion of bond angle data as a measurement of hybridization state. Our analysis, however, shows that α^2 is indeed maximum for the second period atoms and the stabilization factor is the gain in ionic energy brought by the increased electronegativity of the more electronegative atom.

Acknowledgments. We are greatly indebted to Dr. Keith Howell, Mr. Gene Barnett, and Mr. Hollace Cox for their collaboration in the numerical calculations, and to Professor Harrison Shull for his comments and hospitality. Thanks are also due to Dr. G. Klopman for many helpful discussions and to Professor Coulson for the benefit of correspondence.

(43) J. Hinze and H. H. Jaffé, *J. Am. Chem. Soc.*, **84**, 540 (1962); *J. Phys. Chem.*, **67**, 1501 (1963).

Voltammetric Study of the Volmer Reaction on Platinum in Sulfuric Acid Solution. I. Dependence of the Exchange Current Density upon the Hydrogen Coverage at 30°

by M. W. Breiter

General Electric Research Laboratory, Schenectady, New York (Received March 13, 1964)

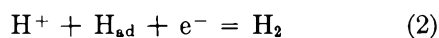
The discharge resistance of the Volmer reaction was determined as a function of potential and hydrogen coverage from the frequency dependence of the capacity in an equivalent parallel circuit for the interfacial impedance by voltammetry with superimposed alternating current. The reciprocal discharge resistance as a function of potential reflects the same specific heterogeneity of the platinum surface with two types of sites for hydrogen adsorption in 1 *N* H₂SO₄ as equilibrium measurements of the hydrogen coverage. It has two maxima which appear at about half coverage of the strongly bonded hydrogen and of the weakly bonded hydrogen. The coverage dependence of the anodic and cathodic partial currents is computed approximately and discussed.

Introduction

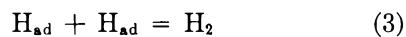
It was demonstrated by Dolin and Ershler¹ that the kinetics of the Volmer reaction



can be studied on platinum by impedance measurements at anodic potentials $U > 0.06$ v. The contribution of the Heyrovsky reaction



and of the Tafel reaction



to the impedance becomes negligible with increasing anodic potential since their exchange current densities are proportional to certain powers of the hydrogen pressure p_{H} , at the surface and since p_{H} , decreases rapidly with potential. Dolin and Ershler derived the following frequency dependence of the impedance in an equivalent parallel circuit of a capacitance C_{P} and a resistance R_{P} .

$$C_{\text{P}} = C_{\text{D}} + \frac{C_2}{1 + w^2 r^2 C_2^2} \quad (4)$$

$$1/R_{\text{P}} = \frac{w^2 r C_2^2}{1 + w^2 r^2 C_2^2} \quad (5)$$

Here w = frequency, C_{D} = double layer capacity, $C_2 = -F\Gamma(d\theta/dU)$ = pseudo-capacity of adsorbed hydrogen atoms, $F\Gamma$ = charge equivalent of a monolayer of hydrogen atoms, θ = hydrogen coverage, $r = (\partial U/\partial I)_{\theta, \text{CH}^+}$ = discharge resistance, U = electrode potential, and I = faradaic current. It was shown¹ that eq. 4 and 5 predict the frequency dependence correctly at large frequencies. The observed deviations at intermediate and small frequencies were attributed to the heterogeneity of the surface. Eucken and Weblus² obtained the predicted frequency dependence of C_{P} at low frequencies on pretreated electrodes. Finally the frequency dependence of C_{P} and $1/R_{\text{P}}$ according to eq. 4 and 5 could be established³ on electrodes which were pretreated anodically before each measurement to produce a comparable surface state of high "activity." Obviously the impedance depends strongly upon the pretreatment of the electrode. The correctness of eq. 4 was substantiated^{3,4} by obtaining the same

(1) P. Dolin and B. Ershler, *Acta Phys. Chim. URSS*, **13**, 747 (1940).

(2) A. Eucken and B. Weblus, *Z. Elektrochem.*, **55**, 114 (1951).

adsorption isotherm from the graphical integration of the C_2-U curve and from anodic charging curves.

It was found¹⁻³ that r is relatively small in the studied potential range. The equilibrium of eq. 1 can be considered practically established for charging curves or voltammetric current-potential curves if the condition $I \ll I_0(U)$ is fulfilled. Here I_0 represents the exchange current density of reaction 1 at the potential U

$$I_0(U) = \frac{RT}{F} \frac{1}{r(U)} \quad (6)$$

Thus, the equilibrium properties of the layer of adsorbed hydrogen atoms can be easily studied.⁵

The properties of the platinum surface are revealed better by C_2-U curves or voltammetric $I-U$ curves than by charging curves since the first two types of curves represent the first derivative of the latter. The C_2-U curves^{2,3} and voltammetric $I-U$ curves⁶ consist of two or more overlapping parts depending upon the electrolyte composition. Hydrogen atoms are bonded^{2,7} in these regions with different free energy of adsorption. The energy of adsorption is nearly independent of coverage inside each region. It was suggested⁸ that these regions are reflected by the $1/r$ curve. However, the limited number of data points in the previous investigations^{1-3,9,10} was not sufficient evidence. A comprehensive review was given by Frumkin⁵ recently.

Voltammetry with superimposed alternating current was used in the present investigation to clarify the above question. A periodic potential of triangular shape was applied potentiostatically to the test electrode between 0.05 and 1.5 v., measured against a hydrogen electrode in the same electrolyte (1 N H₂SO₄). The sweep speed was 30 mv./sec. for all the measurements. The quasistationary $I-U$ curves are reproducible within 5% after the initial five cycles. This is due to the intermediate formation and reduction of an oxygen layer. Impurities which are still on the surface after an initial cleansing of the electrode by washing it in hot chromic acid and then in double-distilled water are removed by the repeated surface oxidation during the first cycles. The concentration of impurities which are dissolved in the electrolyte during the cleaning process is so small that the impurities do not diffuse to the electrode during the time of half a cycle. The superimposed alternating current serves to measure the ohmic and capacitive component of the impedance as a function of potential at a given frequency. The reproducibility of the a.c. measurements was $\pm 5\%$. A sufficient number of data points is easily obtained with this technique.

Experimental

The measurements were made in a Pyrex vessel of conventional design, thermostated at $30 \pm 0.5^\circ$. The test electrode, a bright platinum wire of purity 99.99%, was in the axis of a cylindrical spiral made of platinum wire. The electrolyte was stirred with purified helium before each run. Then the stirring was interrupted, and all the data were taken in quiescent solution. The reference electrode, a reversible hydrogen electrode, was in a compartment separated by a porous disk from the compartment of the test electrode.

The following pre-electrolysis procedure proved successful to remove traces of organic impurities from the solution. Hydrogen and oxygen were simultaneously evolved at 1a for 1 hr. at 70° in the test vessel. A large bright platinum cylinder served as the anode, a platinum wire as the cathode. Hydrogen peroxide was formed to some extent during this process. Afterward the electrolyte was stirred with purified hydrogen for 1 hr. at 70° in the presence of the large platinum cylinder. This time was sufficient for the complete decomposition of H₂O₂. Molecular hydrogen was removed from the electrolyte by helium stirring. The presence of traces of organic impurities is easily recognized by small oxidation waves in the $I-U$ curves at about 0.7 and 1.2 v. during the anodic cycle at elevated temperatures (above 50°).

The technique of the impedance measurements was described in detail elsewhere.¹¹ It allows was to record the ohmic (R_s) and capacitive ($1/wC_s$) component of the impedance in a series circuit directly as a function of potential at a given frequency. The sensitivity of the arrangement was increased by using a Varian F80 X-Y recorder. Figure 1 represents as an example a part of the $I-U$ curve, part of the R_s-U curve, and part of the $1/wC_s-U$ curve at 10 kc.p.s. The curves are reproductions of the original traces. Arrows indicate the direction of the sweep. The contribution of the electrolytic resistance to P_s is eliminated.¹¹

(3) M. Breiter, H. Kammermaier, and C. A. Knorr, *Z. Elektrochem.*, **60**, 37 (1956).

(4) M. Breiter, C. A. Knorr, and W. Völkl, *ibid.*, **59**, 681 (1955).

(5) A. N. Frumkin in "Advances in Electrochemistry and Electrochemical Engineering," Vol. 3, John Wiley and Sons, Inc., New York, N. Y., 1963, p. 287.

(6) F. G. Will and C. A. Knorr, *Z. Elektrochem.*, **64**, 258 (1960).

(7) M. Breiter, *Electrochim. Acta*, **7**, 25 (1962); *Ann. N. Y. Acad. Sci.*, **101**, 709 (1963).

(8) M. Breiter in "Transactions of the Symposium on Electrode Processes," John Wiley and Sons, Inc., New York, N. Y., 1961, p. 307.

(9) T. Birtintseva and B. Kabanov, *Zh. Fiz. Khim.*, **33**, 844 (1959).

(10) G. Klein, Thesis, Technische Universität, Berlin, 1961.

(11) M. Breiter, *Electroanal. Chem.*, **7**, 38 (1964).

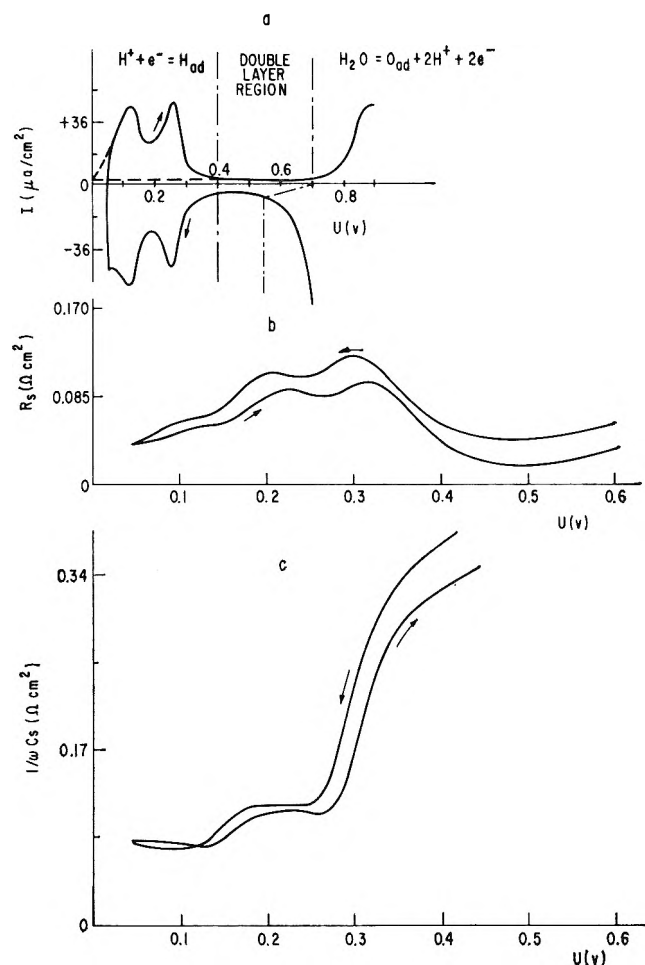


Figure 1. (a) Voltammetric I - U curve with 30 mv./sec. on platinum in 1 N H_2SO_4 . (b) Ohmic component of the impedance at 10 kc.p.s. in an equivalent series circuit. (c) Capacitive component at 10 kc.p.s.

The three characteristic regions (hydrogen region, double layer region, oxygen region) are marked for the I - U curve.

The results obtained during the anodic sweep were analyzed only. This is due to the fact that the integration of the I - U curves yields reliable adsorption isotherms⁶ for the anodic sweep while the small contribution of H_2 evolution at the low sweep speed between 0.15 and 0.05 v. during the cathodic sweep is difficult to correct for (see the slightly larger value of the peak current at about 0.1 v. during the cathodic sweep in Fig. 1a). The integration was carried out stepwise for intervals of 10 mv., starting at 0.45 v. ($\theta = 0$). A small correction for the double layer charging was applied graphically (see the dashed line parallel to the abscissa during the anodic sweep in Fig. 1a). It corresponds to an average value of 100 $\mu\text{f}/\text{cm}^2$ for C_D in the hydrogen region. An extrapolation was made

for the current between 0.05 and 0 v. as shown in Fig. 1a. Since hydrogen is evolved in this potential region, a measurement of the coverage is not feasible at the low sweep speed. In agreement with previous results^{3,4} θ was put equal to 1 at $U = 0$. The impedance measurements were made at 0.2, 0.5, 1, 2.5, 5, and 10 kc.p.s. $R_P(U, w)$ and $C_P(U, w)$ were computed in the usual way at intervals of 20 mv. from the measured values $R_s(U, w)$ and $1/\omega C_s(U, w)$. A testing of eq. 4 requires the knowledge of C_D . The double layer capacity which is dependent upon frequency on solid electrodes was taken as the minimal value of C_P in the double layer region at each frequency. This is a reasonable approximation since traces of adsorbed hydrogen on the one side of the double layer region and traces of the oxygen coverage on the other side have the effect of increasing the measured value of the capacity.

The integration and most of the numerical computations were carried out with suitable programs by the G.E. 225 computer.

Results

The discharge resistance r can be obtained either by choosing a suitable r to fit the C_P data according to eq. 4 or from $1/R_P$ at large frequencies according to eq. 5. In this paper the first method was preferred for two reasons: (a) C_P is obtained by computation from R_s and $1/\omega C_s$ and is not very sensitive to slight errors in R_s which can be introduced by the elimination of the electrolytic resistance since the capacitive component is usually larger than the ohmic one. (b) If r is very small the frequency of 10 kc.p.s. may not be sufficiently large that $r \approx R_P$. Since $C_2 = C_P(200 \text{ c.p.s.}) - C_D(200 \text{ c.p.s.})$ has an average value of 10^{-3} f./cm^2 between 0.05 and 0.25 v. at 30° , r should be larger than 0.16 ohm cm^2 so that the condition $wrC_2 \geq 10$ is fulfilled. In practice r turned out to be smaller than 0.16 ohm cm^2 . The applicability of eq. 4 was checked for different potentials. Table I shows the relative deviation between the experimental C_P and the computed one for the studied frequency range at different potentials. Obviously eq. 4 can be considered fulfilled within the experimental error. This error may be as large as 10% since the reproducibility is 5% for both $R_s(U, w)$ and $1/\omega C_s(U, w)$.

The reciprocal value of the discharge resistance is plotted as a function of potential and of coverage in Fig. 2a and 2b. The reciprocal value was taken because it is proportional to the exchange current density of reaction 1 at 0.06 v. $< U < 0.4$ v. Arrows in Fig. 2a mark the location of the two peak currents obtained from the I - U curve (see Fig. 1).

Table I: Relative Deviation $|(C_{\text{measd}} - C_{\text{calcd}})/C_{\text{measd}}| \cdot 100$ between the Measured C_p and the Computed One at Different Potentials

w , kc.p.s.	0.1 v.	0.14 v.	0.20 v.	0.24 v.	0.30 v.	0.34 v.
0.2	0	0	0	0	0	0
0.5	2	2	2	7	5	5
1.0	4	2	4	14	1	4
2.5	2	0	8	16	0	6
5.0	0	0	0	0	0	0
10.0	10	12	5	3	14	15

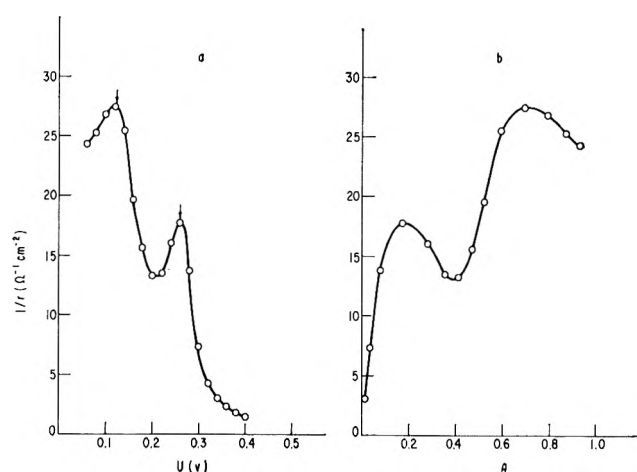


Figure 2. Reciprocal discharge resistance of the Volmer reaction as a function of potential (a) and hydrogen coverage (b).

Discussion

The $I-U$ curve in Fig. 1a has a characteristic shape with two maxima in the hydrogen region. The two types of sites for hydrogen adsorption are clearly distinguishable.^{6,7} Hydrogen adsorbed in the vicinity of the more anodic peak is called strongly bonded. Hydrogen adsorbed in the vicinity of the more cathodic peak is designated as weakly bonded. The R_s-U curve and the $1/wC_s-U$ curve exhibit maxima and minima for the anodic and cathodic sweep. The hydrogen region as defined by the $I-U$ curve is clearly recognizable in these curves. The shape of the R_s-U curve at 10 kc.p.s. suggests that the exchange current density of the Volmer reaction as a function of potential reflects the same surface heterogeneity as the $I-U$ curves. However, the discharge resistance r had to be determined as a function of potential and hydrogen coverage to obtain a satisfactory correlation.

Figure 2a demonstrates that the $1/r-U$ curve has a shape which is similar to that of the $I-U$ curve in Fig. 1a. The exchange current density of the Volmer reaction has maxima which coincide practically with the

peaks of the $I-U$ curve. The two regions for hydrogen adsorption can be clearly distinguished in the $1/r-U$ curve and the $1/r-\theta$ curve. The maxima of $1/r$ are located close to half coverage of the strongly bonded hydrogen and of the weakly bonded one. In terms of total coverage the strongly bonded hydrogen corresponds roughly to $\theta \leq 0.4$ and the weakly bonded hydrogen to $\theta \geq 0.4$. The overlapping makes a better separation difficult. The exchange current density is smaller for the strongly bonded hydrogen ($0.18 \leq U \leq 0.45$ v.) than for the weakly bonded hydrogen ($0 \leq U \leq 0.18$ v.) in the present study. It is obvious from Fig. 2a and 2b that $1/r$ is not independent of coverage at medium coverages as it is required by Temkin's kinetic expressions^{5,12} for the Volmer reaction. The values of $1/r$ in the present study compare well with those of previous measurements on activated electrodes in 8 N H_2SO_4 ³ and 1 N H_2SO_4 .⁹

The Volmer reaction itself is a net reaction which includes^{1,5} surface diffusion as one of the single steps. The experimental result that equilibrium studies ($I-U$ curve) and kinetic results ($1/r-U$ curve) show the same type of dependence upon hydrogen coverage is in agreement with the assumption of a rapid surface diffusion of hydrogen atoms at 30°. However, this assumption is not necessary for the interpretation in the present case. It follows from a simple estimate that the rate of collision of H^+ ions with the surface in A/cm^2 is considerably larger than the exchange current density.

The coverage dependence of the exchange current density of the Volmer reaction can be expressed in a general way.¹³

$$I_0(U) = k_1 a_1(\theta) \exp \frac{\alpha F(U - \psi)}{RT} = k_2 a_2(\theta) {}_0c_{\text{H}^+} \exp \frac{-(1 - \alpha)F(U - \psi) - F\psi}{RT} \quad (7)$$

Here k_1 and k_2 are rate constants, a_1 and a_2 express the dependence upon coverage, ${}_0c_{\text{H}^+}$ is the H^+ ion concentration in the bulk, ψ is the inner potential at the inner Helmholtz plane of the double layer, and α is the transfer coefficient. The functions $k_1 a_1(\theta)$ and $k_2 a_2(\theta) {}_0c_{\text{H}^+}$ can be computed.

$$k_1 a_1(\theta) = I_0(U) \exp \frac{-\alpha UF}{RT} \exp \frac{\alpha \psi F}{RT} \quad (8)$$

$$k_2 a_2(\theta) {}_0c_{\text{H}^+} = I_0(U) \exp \frac{(1 - \alpha)UF}{RT} \exp \frac{\alpha \psi F}{RT} \quad (9)$$

(12) M. Temkin, *Zh. Fiz. Khim.*, 15, 296 (1941).

(13) M. Breiter and R. Clamroth, *Z. Elektrochem.*, 58, 493 (1954).

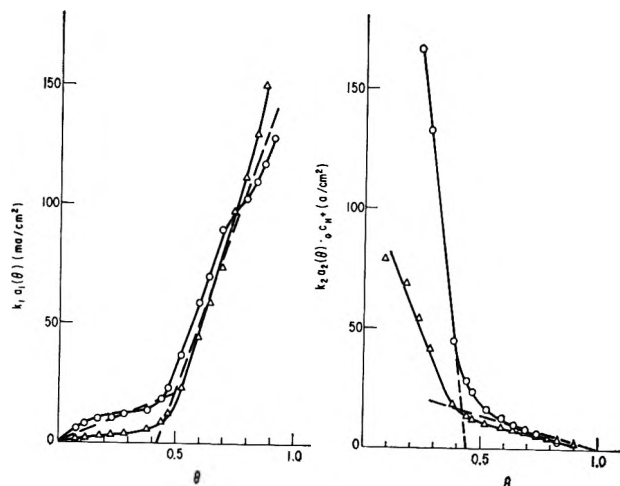


Figure 3. Coverage dependence of the anodic (a) and cathodic (b) partial current density of the Volmer reaction with (O) and without (Δ) correction for the ψ -potential.

The computation requires the knowledge of α and $\psi(U)$. While the transfer coefficient α is known to be close to 0.5 from previous investigations^{4,10,14-16} on platinum the ψ -potential can only be computed approximately by applying Stern's theory¹⁷ and using 0.11 v. as point of zero charge from the data of Slygin, Frumkin, and Medvedovsky¹⁸ in sulfate solution and $C_D(10 \text{ kc.p.s.})$ as the integral capacity in the hydrogen region.

The results of the outlined computation are plotted in Fig. 3a and 3b. To show the effect of the ψ -potential the computation was also made for $\psi = 0$. As

to be expected from the location of the point of zero charge the ψ -effect is small for the potential region of the weakly bonded hydrogen while it has to be considered (factor 2 to 4) in the region of the strongly bonded hydrogen. The two regions are clearly distinguishable in Fig. 3a and 3b. It is indicated by dotted lines in Fig. 3a and 3b that the coverage dependence can be expressed in a crude approximation by equations of the Langmuir type with different values of k_1 and k_2 for the two regions of hydrogen adsorption as suggested by Eucken and Weblus.²

$$a_2(\theta') = \theta' \quad (10)$$

$$a_2(\theta') = 1 - \theta' \quad (11)$$

Here θ' is either the coverage of the weakly or of the strongly bonded hydrogen. The values of k_1 and k_2 can be determined in this approximation from Fig. 3a and 3b.

Acknowledgment. The author acknowledges gratefully the advice of Dr. B. McCarroll, General Electric Research Laboratory, in the writing of the computer programs.

(14) K. Rosenthal, P. Dolin, and B. Ershler, *Acta Phys. Chim. URSS*, 21, 214 (1946).

(15) C. Salkind and B. Ershler, *Zh. Fiz. Khim.*, 25, 565 (1951).

(16) L. N. Nekrassov, *Vestn. Mosk. Univ., Ser. II, Khim.*, 15, 19 (1960).

(17) See detailed discussion by R. Parsons in "Modern Aspects of Electrochemistry," Vol. 1, Butterworth and Co., Ltd., London, 1954, p. 103.

(18) A. Slygin, A. Frumkin, and V. Medvedovsky, *Acta Phys. Chim. URSS*, 4, 911 (1936).

Voltammetric Study of the Volmer Reaction on Platinum in Sulfuric Acid Solution. II. Temperature Dependence and Heat of Activation

by M. W. Breiter

General Electric Research Laboratory, Schenectady, New York (Received March 13, 1964)

The discharge resistance of the Volmer reaction was determined on smooth platinum as a function of potential or hydrogen coverage in the potential region of hydrogen adsorption between 0 and 60° in 1 *N* H₂SO₄ by voltammetry with superimposed alternating current. The reciprocal discharge resistance as a function of potential demonstrates that the exchange current density depends in a similar way upon the partial coverage in the potential region of the strongly and of the weakly bonded hydrogen. The separation of the two regions becomes better pronounced with increasing temperature. The enthalpy change of the Volmer reaction at constant coverage θ is about 5 kcal./mole and independent of coverage for $\theta \leq 0.7$. It decreases then with increasing coverage. An estimate of the pre-exponential factor of the exchange current density is made at low coverage of the strongly bonded hydrogen.

Introduction

It was demonstrated in the preceding paper that voltammetry with superimposed alternating current is a useful technique for the determination of the discharge resistance of the Volmer reaction at room temperature as a function of anodic potential or hydrogen coverage in the potential region $0.4 \geq U > 0.06$ where hydrogen atoms are adsorbed. The measurements were made at comparable surface states. In this paper the same technique was applied to study the temperature dependence of the discharge resistance of the Volmer reaction and to determine the heat of activation as a function of coverage. A systematic investigation of this type has not yet been published. Parsons' measurements¹ of the discharge resistance on platinum in 0.5 *N* HCl between 0 and 45° were made at the potential of the hydrogen electrode ($U = 0$) only. In order to avoid² a contribution of the Heyrovsky reaction or of the Tafel reaction to the impedance the measurements were carried out at potentials $U \geq 0.06$ in the region of hydrogen adsorption between 0 and 60° in 1 *N* H₂SO₄.

Experimental

The vessel, the procedure of pre-electrolysis, and the technique were as described in the preceding paper.

The temperature was maintained at $\pm 0.5^\circ$. The electrode potential refers to a hydrogen electrode at the same temperature and in the same electrolyte as the test electrode. The frequency range was 200 c.p.s. to 10 kc.p.s. The rate of the linear potential change was 30 mv./sec.

The correctness of the elimination of the ohmic potential drop which is caused by the electrolytic resistance R_{E1} between test and reference electrode in the a.c. measurements is important. It was checked. The curves in Fig. 1a and 1b are typical for a measurement without compensation of the electrolytic resistance at 40°. The ohmic component of the interfacial impedance in an equivalent series circuit of resistance R_s and capacitance C_s is nearly independent of potential for $U > 0.4$ v. while the capacitive component allows a clear distinction between the hydrogen region, the double region, and the oxygen region. The independence of potential suggests that the measured R_s at 10 kc.p.s. is equal to R_{E1} for $U > 0.4$ v. This conclusion was verified in the following way. The conductivity of the electrolyte was determined as a function of temperature in a conductivity cell at

(1) R. Parsons, *Trans. Faraday Soc.*, **56**, 1340 (1960).

(2) M. Breiter, *Electrochim. Acta*, **7**, 25 (1962).

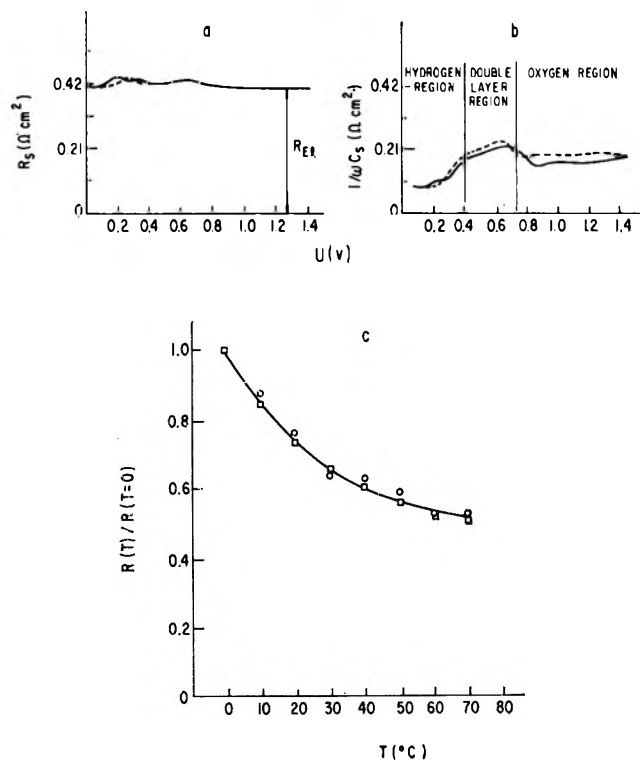


Figure 1. (a) Ohmic component of the impedance in a series circuit at 10 kc.p.s. as a function of potential without compensation of the electrolytic resistance at 40°. (b) Capacitive component at 10 kc.p.s. as a function of potential. (c) \square , ratio of the conductivity of 1 N H_2SO_4 at temperature T to that at $T = 0$; \circ , ratio of R_{E1} at temperature T to that at $T = 0$.

10 kc.p.s. The ratio of the conductivity at the temperature T to that at $T = 0^{\circ}$ is plotted in Fig. 1c as a function of temperature. Since the cell constant is independent of temperature the ratio of the measured resistances R at T and at $T = 0^{\circ}$ is equal to that of the respective conductivities. The points (\square) of the conductivity measurements are connected with a solid line. Then the same ratio was formed with $R_{E1}(T)$ and $R_{E1}(T = 0)$. Figure 1c shows that the agreement is satisfactory.

The large number of numerical calculations and integrations were made by the G.E. 225 computer with suitable programs.

Results

The discharge resistance r of the Volmer reaction was obtained from the frequency dependence of the capacity C_P of the interfacial impedance in an equivalent parallel circuit as in the preceding paper. It was checked if the respective formula (eq. 4 in the preceding paper) is in agreement with the experimental C_P values after choosing a suitable r as the only pa-

rameter at a given potential. The relative deviation between the measured and the computed C_P was calculated. Table I represents the results at 0.14 v. as a typical example. Obviously the formula can be considered fulfilled within the experimental error at $T \geq 10^{\circ}$. The reason for the large deviation at $T = 0$ is not yet known.

Table I: $[(C_{\text{measd}} - C_{\text{calcd}})/C_{\text{measd}}] \times 100$ as a Function of Temperature and Frequency at 0.14 v.

Frequency, c.p.s.	0°	10°	20°	30°	40°	50°	60°
200	3	1	0	0	0	0	0
500	7	16	2	2	9	10	5
1000	40	8	4	1	11	20	4
2500	58	9	3	0	4	17	10
5000	0	0	0	0	0	0	20
10000	25	24	24	12	13	4	0

The reciprocal value of r is plotted in Fig. 2 as a function of potential at different temperatures between 0

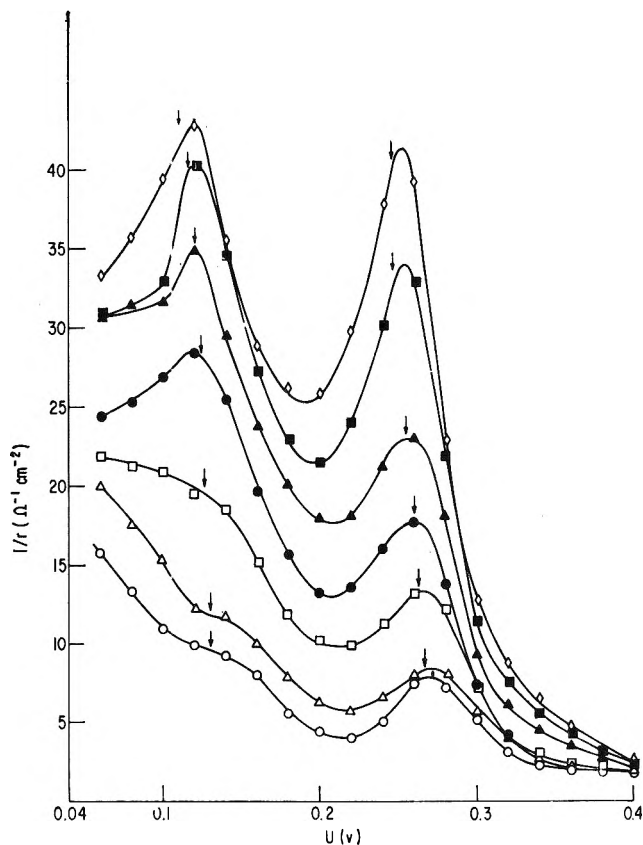


Figure 2. Reciprocal discharge resistance as a function of potential: \circ , 0°; Δ , 10°; \square , 20°; \bullet , 30°; \blacktriangle , 40°; \blacksquare , 50°; \blacklozenge , 60°.

and 60°. Although the error in the r values at 0° will be large, they were included for reasons of comparison.

The net enthalpy change of the Volmer reaction depends upon the coverage, the free energies of activation for the forward and reverse reaction, respectively, and the ψ -potential. Parsons published^{1,3} detailed derivations and demonstrated that the experimental enthalpy change ΔH at constant coverage

$$\Delta H = (1 - \alpha)\Delta h_1 + \alpha\Delta h_2 \quad (1)$$

can be obtained from the temperature dependence of r . Here Δh_1 and Δh_2 are the enthalpy changes for the anodic and cathodic partial current, respectively. The net current consists of the two partial currents. Taking into account the ψ -potential, $\ln 1/r + \alpha\psi F/RT$ was plotted vs. $1/T$ at different θ -values in Fig. 3 between 0 and 50°. The term $\alpha\psi F/RT$ was computed for $\alpha = 0.5$ according to Stern's theory, and the integration of the I - U curve yielded the coverage as a function of potential. Details of both procedures are described in the preceding paper. For $\theta < 0.8$ the experimental points in Fig. 3 scatter around straight lines whose slopes are proportional to ΔH . The straight lines at different θ are parallel within the experimental error. They do not cover the whole temperature range at $\theta = 0.8$ and $\theta = 0.9$. The points at 0° which include a larger error than the other data (see Table I) deviate the most from the straight lines.

Discussion

The discharge resistance r decreases at a given potential with T (see Fig. 2). The same specific heterogeneity of the platinum surface which is observed by equilibrium measurements of the hydrogen coverage is reflected by the $1/r$ - U curves. It is pronounced more strongly with increasing temperature above 20°. The two arrows at each $1/r$ - U curve in Fig. 2 mark the position of the two peaks of the I - U curve at the same temperature. Evidently the peaks of the I - U curves coincide practically with the maxima of the respective $1/r$ - U curves. The discussion of the dependence of $1/r$ upon θ at 30° in the preceding paper can be transferred to the results in Fig. 2 for $T > 10^\circ$. The $1/r$ - U curves at 0 and 10° in Fig. 2 show an additional effect between 0.1 and 0.06 v. whose origin is not yet known. Otherwise the reasoning of the preceding paper applies to them too.

In Fig. 4 three different enthalpy changes are plotted as a function of θ . The upper curve represents the free enthalpy change of the Tafel reaction. It was determined from the experimental isotherms of hydrogen adsorption (integrated I - U curves) on the platinum electrode in the usual way.⁴ This enthalpy

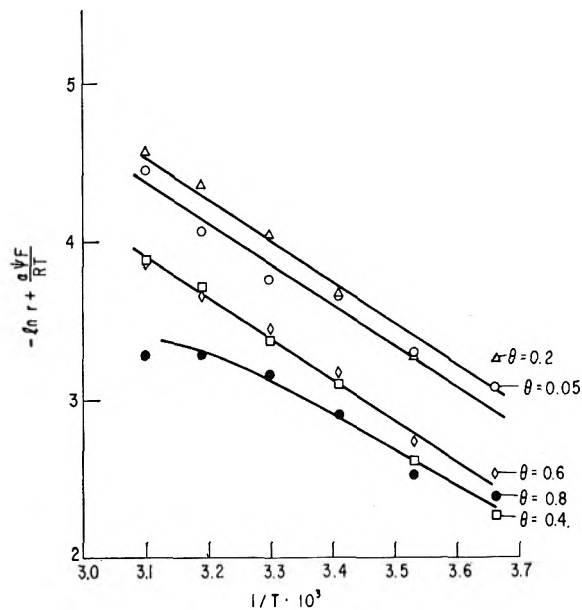


Figure 3. Plot of $(-\ln r + \alpha\psi F/RT)$ vs. $1/T$ at different coverage.

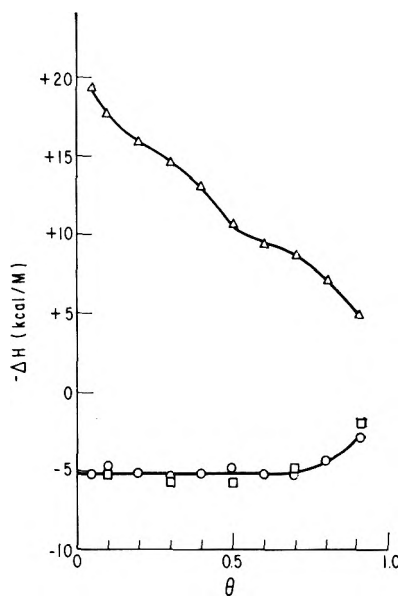


Figure 4. Free enthalpy changes as functions of coverage: Δ , Tafel reaction; \circ , Volmer reaction under consideration of the ψ -potential; \square , Volmer reaction under neglect of the ψ -potential.

change decreases rapidly with coverage in the initial part ($\theta < 0.1$). Then the two regions which correspond to the two hydrogen waves of the I - U curves are clearly distinguishable. Hydrogen atoms were called

(3) R. Parsons, *Trans. Faraday Soc.*, **54**, 1053 (1958).

(4) W. Böld and M. Breiter, *Z. Elektrochem.*, **64**, 897 (1960).

strongly bonded for $\theta < 0.5$ and weakly bonded for $\theta \geq 0.5$.

In contrast, the ΔH value of the Volmer reaction as defined by eq. 1 is practically independent of coverage for $\theta < 0.8$. (see lower curve) It has an average value of 5 kcal./M. For $\theta \geq 0.8$ it decreases with θ . It can be demonstrated that this result is not caused to a large extent by the term $a\psi F/RT$. A plot of $\ln 1/r$ vs. $1/T$ under the assumption $\psi = 0$ yields straight lines, similarly as in Fig. 3. The ΔH values which were determined from the slope of these lines are also plotted in Fig. 4. They do not differ much from the ΔH values obtained under consideration of the ψ -potential.

The pre-exponential factor of the exchange current density can be estimated on the basis of the results in Fig. 2 and 4 for small coverage of the strongly bonded hydrogen. This factor reflects¹ the entropy change ΔS of the Volmer reaction

$$\Delta S = (1 - \alpha)\Delta S_1 + \alpha\Delta S_2 \quad (2)$$

Here ΔS_1 is the entropy change of the anodic partial current and ΔS_2 that of the cathodic one. The slope in the linear part of a plot of $I_0(\theta) \exp(\alpha\psi F/RT)$ vs. $\theta^{1/2}$ yields the experimental free energy change

$$\Delta G = (1 - \alpha)\Delta g_1 + \alpha\Delta g_2 \quad (3)$$

Since ΔH is known, the entropy term can be computed. An average value of 2×10^4 amp./cm.² was found for the pre-exponential factor for $T > 20^\circ$. This value is roughly one-hundredth the theoretical estimate¹⁶ of the pre-exponential factor, which is defined in a slightly different way there¹ than here.

Acknowledgment. The author acknowledges gratefully the assistance of Dr. B. McCarroll in the programming.

(5) M. Temkin, *Tr. Soveschsh. Elektrochim. Akad. Nauk SSSR, Otd. Khim. Nauk* (Moscow), 181 (1953).

The Measurement of Molecular Weight Distribution in Polymers by Cross Linking-Solubility Methods^{1a}

by William W. Graessley^{1b}

Department of Chemical and Metallurgical Engineering, University of Michigan, Ann Arbor, Michigan (Received March 13, 1964)

The relationship between molecular weight distribution in linear polymers and their subsequent cross linking-solubility behavior has been studied, using samples of polystyrene of different average molecular weights and molecular weight distribution. Films of the polymers were cross linked by γ -radiation, and gel fraction as a function of radiation dose was determined by solvent extraction. The properties of the solubility curves obtained for each sample were sufficient to provide two independent characterizations of the distribution, $\overline{DP_w}/\overline{DP_n}$ and $\overline{DP_z}/\overline{DP_w}$, as well as two radiation parameters, the radiation dose at gelation in the absence of chain scission, and the chain scission parameter.

Introduction

This paper describes an investigation to determine whether useful information on molecular weight distribution can be obtained from the effects of cross linking on the solubility properties of polymers. It is well known that the introduction of random cross links between the chains in a solid polymer alters its solubility properties to the extent that, beyond a minimum cross-linking density, a three-dimensional network is formed, and a uniform solution is no longer formed when the polymer is placed in a suitable solvent. With increasing cross-link density, the amount of the gel phase increases at the expense of sol, and the relative proportion of gel (the "insoluble" fraction) can be determined by solvent extraction.

If cross linking alone occurs, the solubility curve depends only on the initial distribution of molecular weights. Equation 1 or its equivalent has been derived by a number of investigators^{2,3} for primary chains with large numbers of mers per chain

$$1 - x = \int_0^{\infty} W(n)e^{-\alpha xn} dn \quad (1)$$

where α is the cross-link density, the fractional number of mers in the system participating in cross links, $(1 - x)$ = weight fraction of the polymer which is soluble, and $W(n)$ is the initial molecular weight distribution, the fractional weight of polymer with degree of polymerization n in the uncross-linked polymer.

The number-, weight-, and z -average degrees of polymerization are defined in terms of $W(n)$ in the usual way

$$\overline{DP_n} = \left[\int_0^{\infty} \frac{W(n)}{n} dn \right]^{-1};$$

$$\overline{DP_w} = \int_0^{\infty} nW(n) dn; \quad \overline{DP_z} = \frac{\int_0^{\infty} n^2W(n) dn}{\int_0^{\infty} nW(n) dn}$$

High energy radiation is a convenient cross-linking agent for many polymers since it produces cross links in direct proportion to the total radiation dose ($\alpha = kR$). However, main chain scission occurs as well, also in direct proportion to the total dose. Most polymers therefore require two parameters to describe their radiation behavior: one, the proportionality constant k , relating α and R ; the other, a chain scission parameter β , measuring the number of main chain fractures produced per cross-linked unit formed. These param-

(1) (a) Based on a doctoral dissertation submitted to the University of Michigan (1959), and presented in part at the 138th National Meeting of the American Chemical Society, New York, N. Y., 1960; (b) Department of Chemical Engineering, Technological Institute, Northwestern University, Evanston, Ill.

(2) (a) P. J. Flory, *J. Am. Chem. Soc.*, **69**, 30 (1947); (b) A. Charlesby, *Proc. Roy. Soc. (London)*, **A222**, 542 (1954).

(3) A. C. Baskett, *Intern. Symp. Macromol. Chem.*, Milan and Turin, 1954; *Ricerca Sci. Suppl.*, **A379** (1955).

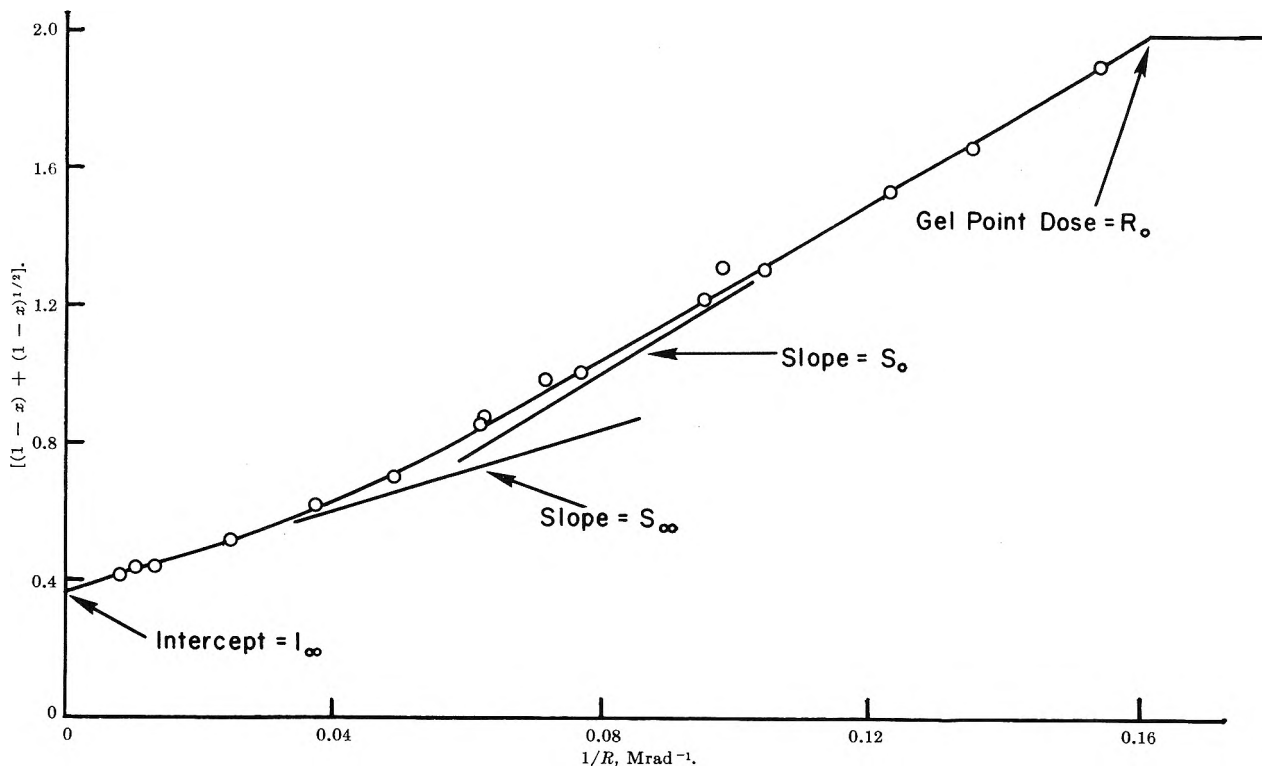


Figure 1. Gel curve for narrow distribution sample N-1.

eters are presumed to be characteristic constants for a polymer and independent of molecular weight and distribution.

The simultaneous occurrence of chain scission changes the solubility behavior by continuously altering the primary molecular weight distribution during cross linking. The modified solubility equation for linear primary chains is^{4,5}

$$1 - x = \frac{x^2 w(s) + \beta^2 + 2x\beta \int_0^s w(\lambda) d\lambda}{(x + \beta)^2} \quad (2)$$

where $w(s) = \int_0^{\infty} W(n)e^{-sn} dn$; $s = \alpha(x + \beta)$. This equation has been used to calculate theoretical gel curves for a special class of initial distributions and for various values of the chain scission parameter.⁵

The solubility curve as given by either eq. 1 or 2 is dependent primarily on the moments of the initial distribution and only indirectly on the detailed shape of the distribution curve. Thus, solubility measurements offer some promise of furnishing average molecular weights (actually ratios of average molecular weights such as $\overline{DP_w}/\overline{DP_n}$ and $\overline{DP_z}/\overline{DP_w}$) for cross-linkable polymers of unknown distribution, even though a complete determination of the distribution curve cannot be

made because of the excessive accuracy required of the experimental data to invert eq. 2 or even eq. 1.

Calculations of Distribution Parameters from the Solubility Curve. Charlesby and Pinner⁶ have pointed out that a particularly useful way to analyze the solubility-cross-linking data is to plot [soluble fraction + (soluble fraction)^{1/2}] vs. (radiation dose)⁻¹. Figure 1 shows the main features of a typical curve. Below a critical dosage the polymer remains completely soluble, but beyond the gel point dosage R_0 , the solubility decreases with a slope S_0 . For large R the solubility (as $(1 - x) + (1 - x)^{1/2}$) approaches a limiting value I_{∞} with a limiting slope S_{∞} .

The behavior of the gel curve in this latter region of high cross-linking density may be obtained directly from eq. 2, assuming only that α is linear in R

$$I_{\infty} = \lim_{R \rightarrow \infty} [(1 - x) + (1 - x)^{1/2}] = \beta \quad (3)$$

$$S_{\infty} = \lim_{R \rightarrow \infty} \left[\frac{d}{d(1/R)} \left\{ (1 - x) + (1 - x)^{1/2} \right\} \right] = \frac{\overline{DP_w}}{\overline{DP_n}} \rho \quad (4)$$

(4) P. A. Small, *J. Polymer Sci.*, **18**, 431 (1955).

(5) M. Inokuti, *J. Chem. Phys.*, **38**, 2999 (1963).

(6) A. Charlesby and S. H. Pinner, *Proc. Roy. Soc. (London)*, **A249**, 367 (1959).

\overline{DP}_w and \overline{DP}_n refer to the initial (unirradiated) polymer, and ρ is a "virtual" gel-point dosage, the radiation dose at which gelation would have occurred in the absence of chain scission.^{7a} In the presence of chain scission the observed gel-point dose R_0 is greater than ρ ; moreover, ρ is related to the initial \overline{DP}_w of the sample by the relation^{7b}: $\alpha(\text{gel point}) = 1/\overline{DP}_w$.

Thus

$$\rho = \frac{1}{k\overline{DP}_w} \quad (5)$$

Although ρ is not directly measurable, it can be calculated approximately from the properties of the gel curve in the vicinity of the gel point. At the gel point, $x = 0$ and eq. 2 becomes

$$1 - \beta/2 = \frac{1}{\alpha\beta} \int_0^{\alpha\beta} w(\lambda) d\lambda \quad (6)$$

Likewise, the rate of increase of gel with cross-link density at the gel point may be evaluated from eq. 2

$$\left(\frac{dx}{d\alpha}\right)_{x=0} = \frac{2\alpha(1 - \beta/2) - w(\alpha\beta)}{3\beta w(\alpha\beta) + (\beta - 1)} \quad (7)$$

If β is small and the primary distribution not too broad, $w(\alpha\beta)$ may be expanded in powers of β in eq. 6 and 7. The coefficients of the series will depend on the moments of the primary distribution, and these can be expressed as the various \overline{DP} 's of the system. After simplifying and discarding terms of order β^2 and higher

$$\frac{1}{\rho} = \frac{1}{R_0} + \frac{\beta}{S_0} \quad (8)$$

$$\left(\frac{S_0}{3\rho}\right) \frac{\overline{DP}_z}{\overline{DP}_w} = 1 + \beta \frac{R_0}{S_0} \left[\frac{3}{2} \frac{\overline{DP}_{z+1}}{\overline{DP}_z} - 2 \right] \quad (9)$$

in which

$$S_0 = \left[\frac{d}{d(1/R)} \{ (1-x) + (1-x)^{1/2} \} \right]_{x=0}$$

These last two equations reduce to exact expressions when $\beta = 0$, and they are also exact for any β in samples conforming to the "most probable" distribution: $W(n) = a^2 n e^{-an}$, $\overline{DP}_w/\overline{DP}_n = 2$, $\overline{DP}_z/\overline{DP}_w = 3/2$, $\overline{DP}_{z+1}/\overline{DP}_z = 4/3$. Equations 8 and 9 may thus be regarded as first-order corrections near the gel point for small amounts of chain scission when the initial distribution deviates from the most probable distribution. Comparison with theoretical gel data calculated for model distributions using eq. 2 indicates they are substantially correct, for moderate values of β , over a range of dis-

tribution breadths from essentially monodisperse to somewhat broader than the most probable distribution.

Thus, the four equations (eq. 3, 4, 8, and 9) provide a method for calculating two radiation parameters, ρ and β , and two distribution parameters, $\overline{DP}_w/\overline{DP}_n$ and $\overline{DP}_z/\overline{DP}_w$, from the four gel curve properties, R_0 , S_0 , I_∞ , and S_∞ . Strictly speaking, eq. 9 requires a foreknowledge of $\overline{DP}_{z+1}/\overline{DP}_z$ for computing $\overline{DP}_z/\overline{DP}_w$, but since the term containing $\overline{DP}_{z+1}/\overline{DP}_z$ is small for small β , an approximate value, consistent with the apparent trend in $\overline{DP}_w/\overline{DP}_n$ and $\overline{DP}_z/\overline{DP}_w$, should be adequate for obtaining a firm value of $\overline{DP}_z/\overline{DP}_w$.

Experimental Procedure

Polystyrene was chosen for the study because it is easy to prepare and characterize as a linear polymer, and it is cross linked by radiation with few side reactions. One series of samples was prepared by thermal polymerization in bulk to low conversion (<15%) at various temperatures. Polymers of this type generally conform fairly closely to the most probable distribution and are designated MPD in the tables. A group of samples with narrow distribution (designated N in the tables) were prepared by precipitation-fractionation of one of the bulk polymerized samples. Broad distribution samples (designated B) were prepared by blending two samples with widely different average molecular weights: B-1 was an equal weight mixture of two MPD samples, and B-2 was the same for two N samples.

Molecular weight was measured for all samples by conventional light scattering methods in a Brice-Phoenix light scattering photometer. The scattering intensity of dilute solutions in benzene was recorded as a function of concentration and scattering angle, and \overline{DP}_w was obtained by the usual Zimm method. \overline{DP}_w and the distribution curves for the N samples were measured by Dr. H. W. McCormick of the Dow Chemical Co. using sedimentation techniques described elsewhere.⁸ The polymerization and molecular weight data are collected in Table I. The distribution parameters are in Table IV.

The polymers were cross linked in a cobalt-60 γ -radiation source. All irradiations took place in the central cavity of the source where the dose rate was approximately 0.8×10^6 rads/hr.; very precise relative

(7) (a) Charlesby and Pinner⁷ arrived at the equivalent of eq. 3 and 4 by another argument showing that they are generally true even for initially nonlinear chains. They chose to express their result as $S_\infty = 1/k\overline{DP}_n$ (obtained here by substitution of eq. 5 into eq. 4) thereby allowing a calculation for k for samples of known \overline{DP}_n .
(b) W. H. Stockmayer, *J. Chem. Phys.*, **12**, 125 (1944).

(8) H. W. McCormick, *J. Polymer Sci.*, **36**, 341 (1959).

Table I: Polymerization and Molecular Weight Data for Samples

Sample	Preparation	$\bar{M}_w \times 10^{-4}$	
		Light scattering	Sedimentation
MPD-1	Room temperature (thermal)	4.93	...
MPD-2	53° (thermal poly.)	2.05	...
MPD-3	60° (thermal poly.)	1.75	...
MPD-4	25° (photo poly.)	1.52	...
MPD-5	65° (thermal poly.)	1.44	...
MPD-6	75° (thermal poly.)	1.19	...
N-1	Fractionation of MPD-3	3.36	3.68
N-2	Fractionation of MPD-3	2.69	...
N-3	Fractionation of MPD-3	2.42	2.40
N-4	Fractionation of MPD-3	1.82	1.77
N-5	Fractionation of MPD-3	1.77	1.87
N-6	Obtained from Dow Chemical Co.	0.226	0.248
B-1	Mixture of MPD-1, MPD-6	3.04	...
B-2	Mixture of N-2 and N-6	1.46	...

doses were obtained by always placing the samples at the same location in the cavity. (One series of experiments at an intensity of 0.08×10^6 rads/hr. showed that dose rate had no effect on the results.)

Films of the polymers, 2-8 mils thick, were cast from benzene solution and evacuated at elevated temperatures for 1 week or more in an effort to eliminate traces of solvent and dissolved oxygen. Under these conditions sample thickness was found to have no effect on the results.

The films were irradiated *in vacuo* to various total doses, set aside for about 1 week, and then extracted exhaustively in benzene at 35°. (Immediate extraction produced erratic solubilities, while delayed extraction gave constant and highly reproducible results.) Other extraction solvents were tried: toluene and cyclohexane gave the same solubilities as benzene, but methyl ethyl ketone appeared to cause a slow, selective rupture of cross links, and equilibrium solubilities were not attainable.

Charlesby-Pinner plots of the resulting solubility data are shown in Fig. 1-4.

Results and Discussion

The solubility data for all MPD samples gave linear graphs as shown in Fig. 2, which is consistent with eq. 2 requiring that distributions of the form $W(n) = a^2 ne^{-an}$ have solubility curves of the form

$$(1-x) + (1-x)^{1/2} = 2\rho\left(\frac{1}{R}\right) + \beta \quad (10)$$

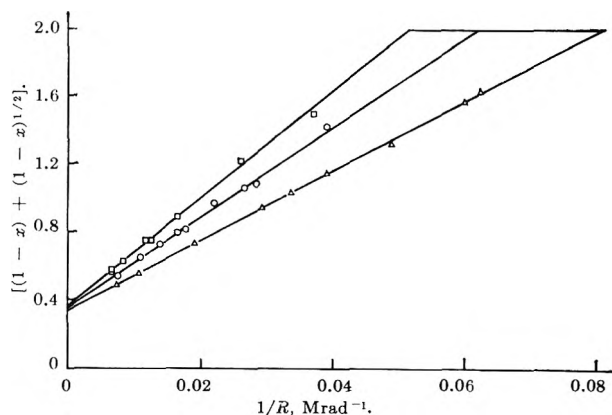


Figure 2. Gel curves for several samples having the most probable distribution: Δ , MPD-2; \circ , MPD-4; \square , MPD-6.

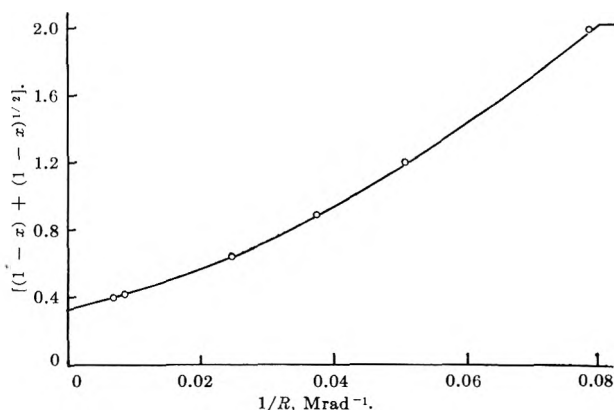


Figure 3. Gel curve for narrow distribution sample N-5.

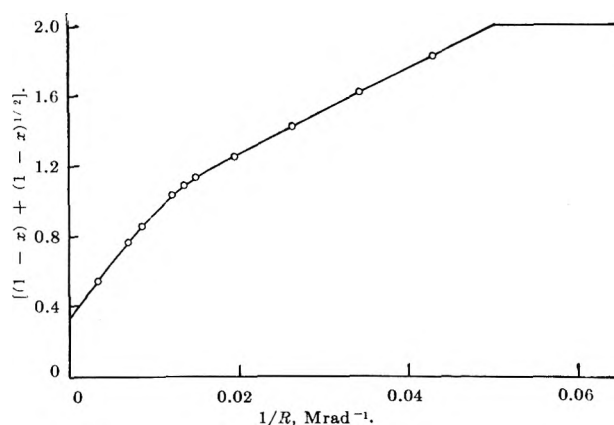


Figure 4. Gel curve for broad distribution sample B-2.

Thus ρ and β are immediately obtained from the slope and intercept of the solubility curve, and its linear form confirms the expected distribution.

Gel curves for the N samples (narrow distribution) and the B samples (broad distribution) were not linear,

and in fact they were distinguishable by their qualitative behavior: the solubility curves of the former show a positive (upward) curvature, while the latter show a negative curvature. The solubility parameters required to determine $\overline{DP_w}/\overline{DP_n}$ and $\overline{DP_z}/\overline{DP_w}$ for these samples are shown in Table II.

Table II: Measured Gel Curve Constants for the Narrow and Broad Distributive Samples

Sample	R_0 , Mrads	S_0 , Mrads	I_∞	S_∞ , Mrads
N-1	6.19	12.2	0.37	6.00
N-3	9.00	19.5	0.35	9.55
N-4	12.3	29.3	0.34	11.5
N-5	13.4	27.6	0.34	17.0
B-1	7.73	9.74	0.37	21.9
B-2	19.7	23.9	0.34	60.7

Before proceeding with the calculation of $\overline{DP_w}/\overline{DP_n}$ and $\overline{DP_z}/\overline{DP_w}$, it is worthwhile to examine the assumption that k and β are true constants of the polymer: that cross linking and chain scission are both proportional to radiation dose and independent of average molecular weight and molecular weight distribution. Table III shows values of ρ , β , and k , calculated from

Table III: Calculated Radiation Parameters for Polystyrene

Sample	β	ρ , Mrads	k , rad ⁻¹ × 10 ¹¹
MPD-1	(0.49)	3.85	0.55
MPD-2	0.34	10.3	0.49
MPD-3	0.38	11.0	0.54
MPD-4	0.35	13.5	0.51
MPD-5	0.36	13.7	0.53
MPD-6	0.35	16.3	0.54
N-1	0.37	5.20	0.59
N-3	0.35	7.75	0.55
N-4	0.34	11.5	0.50
N-5	0.34	10.8	0.54
B-1	0.37	6.0	0.57
B-2	0.34	15.4	0.46

the data. The average value of the chain scission parameter (excluding MPD-1), $\beta = 0.35 \pm 0.015$, is the same as measured by Schulz⁹ for polystyrene using high energy electrons. However, the cross-linking constant, $k = (0.53 \pm 0.04) \times 10^{-11}$ rad⁻¹, is at some variance to the value of 1.23×10^{-11} , calculated from the Schulz data, and 1.1×10^{-11} from Wall's data.¹⁰ Swelling measurements were made on the gels to obtain an

independent estimate of k , and a value of $(0.55 \pm 0.2) \times 10^{-11}$ was found, agreeing with our other results. The source of our disagreement with the other workers is not known.

Except for β in MPD-1 the variations in the radiation parameters from polymer to polymer are small and quite consistent with the experimental errors in the measurements. The slight trend in both β and k with molecular weight appears to be real, but is not large enough to affect the results materially.

The distribution results for the N and B samples are shown in Table IV together with a comparison of values

Table IV: Comparison of Distribution Parameters from the Gel Curves with Those from Sedimentation Measurements

Sample	$\overline{DP_w}/\overline{DP_n}$		$\overline{DP_z}/\overline{DP_w}$		$\overline{DP_{z+1}}/\overline{DP_z}$
	Sedimentation	Gel curve	Sedimentation	Gel curve	
N-1	1.08	1.15	1.06	1.19	1.1
N-3	1.12	1.24	1.09	1.12	1.1
N-4	1.15	1.48	1.11	1.18	1.1
N-5	1.06	1.07	1.05	1.04	1.0
B-1	3.26	3.66	2.05	1.99	1.5
B-2	3.72	3.94	2.15	1.89	1.3

^a Values in eq. 9 to compute $\overline{DP_z}/\overline{DP_w}$.

of $\overline{DP_w}/\overline{DP_n}$ and $\overline{DP_z}/\overline{DP_w}$ from the ultracentrifuge (N samples) or from the known composition of the mixtures (B samples). Also shown are the approximate values selected for $\overline{DP_{z+1}}/\overline{DP_z}$ to compute firm values of $\overline{DP_z}/\overline{DP_w}$ in eq. 9. In practice, it is quite easy to select reasonable numbers since a series of molecular weight ratios such as $\overline{DP_w}/\overline{DP_n}$, $\overline{DP_z}/\overline{DP_w}$, $\overline{DP_{z+1}}/\overline{DP_z}$... generally takes on a smooth and systematic series of values. For example, N-4 has a firm (calculated) value of $\overline{DP_w}/\overline{DP_n} = 1.48$. An approximate value for $\overline{DP_z}/\overline{DP_w}$ can be obtained by neglecting the term containing $\overline{DP_{z+1}}/\overline{DP_z}$ in eq. 9.

$$\frac{\overline{DP_z}}{\overline{DP_w}} \approx \frac{3\rho}{S_0} = \frac{(3)(11.5)}{(27.6)} = 1.25$$

The rate of decrease in the series $\overline{DP_w}/\overline{DP_n} = 1.48$, $\overline{DP_z}/\overline{DP_w} \approx 1.25$ suggest that the next term, $\overline{DP_{z+1}}/\overline{DP_z}$, should be about 1.1 assuming the series is smoothly approaching 1.0. When this value is substituted in eq. 9 the new result is $\overline{DP_z}/\overline{DP_w} = 1.18$, and since

(9) A. R. Schulz, P. I. Roth, and G. V. Rathmann, *J. Polymer Sci.*, **22**, 495 (1956).

(10) L. A. Wall and D. W. Brown, *J. Phys. Chem.*, **61**, 129 (1957).

$\overline{DP}_{z+1}/\overline{DP}_z = 1.1$ is still consistent, 1.18 is the firm value for $\overline{DP}_z/\overline{DP}_w$. The relatively minor effect of various values for $\overline{DP}_{z+1}/\overline{DP}_z$ on $\overline{DP}_z/\overline{DP}_w$ is shown by the comparison for sample N-50 shown in Table V.

Table V

Assumed $\overline{DP}_{z+1}/\overline{DP}_z$	Resulting $\overline{DP}_z/\overline{DP}_w$ (eq. 9)
1.3	1.24
1.2	1.21
1.1	1.18
1.0	1.15

Conclusions

The comparisons in Table IV show that information on the molecular weight distribution of a linear polymer can be obtained from an analysis of its cross linking-solubility behavior without assumptions as to the particular form of the distribution, if the chain scission pa-

rameter is small. Apparently, there is some tendency toward overestimation of $\overline{DP}_w/\overline{DP}_n$ for narrow distributions and underestimation for broad distributions. This may reflect some systematic error in measuring S_∞ because of curvature, or more likely, it may mean that the simple, first-approximation equations are unable to compensate completely for the effect of chain scission. However, the discrepancy is generally small and the numerical agreement quite satisfactory. It should be noted also that $\overline{DP}_w/\overline{DP}_n$ and $\overline{DP}_z/\overline{DP}_w$ are obtained from quite different portions of the gel curve and thus constitute independent tests of the data.

Acknowledgments. The author is grateful to the National Science Foundation for predoctoral fellowship support during 1956-1959. Thanks are due also to Dr. R. E. Skochdopole and Dr. H. W. McCormick of the Dow Chemical Company, to Professor Brymer Williams and Professor D. W. McCready for their many helpful suggestions through the work, and to Dr. L. M. Hobbs and Dr. J. A. Manson whose interest originally led to the study.

The Continuous Absorption Spectra of Chlorine, Bromine, Bromine Chloride, Iodine Chloride, and Iodine Bromide

by Daniel J. Seery and Doyle Britton

Department of Chemistry, University of Minnesota, Minneapolis 14, Minnesota (Received March 16, 1964)

The continuous absorption spectra for gaseous Cl_2 , Br_2 , BrCl , ICl , and IBr between 220 and 600 $m\mu$ are reported. The experimental data have been fitted to theoretical curves of the type suggested by Sulzer and Wieland. The parameters for these curves are given.

Introduction

In the course of shock tube studies of the interhalogen compounds and the dissociation of the halogens, we have found it necessary to know the extinction coefficients for ICl , BrCl , Br_2 , and Cl_2 in the visible and

near-ultraviolet. Since the literature values for ICl and BrCl are incomplete or appear to be incorrect, we have determined the continuous absorption spectra of these compounds, as well as IBr , between 220 and 600 $m\mu$. Br_2 and Cl_2 have been redetermined in order to

calculate consistent values for BrCl, which only exists in equilibrium with its elements. The earlier work will be described in the Discussion.

The decadic extinction coefficient, ϵ , is defined by $\log(i_0/i) = \epsilon cl$, where i_0/i is the ratio of the incident light intensity to the intensity transmitted through l cm. of c moles/l. of the compound in question. With Cl_2 and Br_2 this is unambiguous; with the interhalogens the possibility of disproportionation to the elements must be considered and allowed for.

Experimental

Chemicals. Matheson Coleman and Bell Co. Cl_2 stated to be 99.5% pure had been earlier found to contain excessive CO_2 (up to 10%) and was purified by liquefying the Cl_2 and repeatedly pumping off the CO_2 rich vapors above the liquid until the infrared absorption at 2350 cm.^{-1} indicated less than 1% CO_2 . Allied Chemical Co. Br_2 was used without further purification. Mallinckrodt analytical reagent grade I_2 was used without further purification. Fisher "pure" IBr was used without purification. BrCl was prepared by mixing various proportions of Cl_2 and Br_2 and allowing the mixture to equilibrate. ICl was prepared by the method of Cornog and Karges.¹ The freezing point was found to be 26.76° compared to the literature value of 27.19° , but it was very sharp.

Measurements. All measurements were made on a Cary Model 11 recording spectrophotometer using 10-cm. quartz cells. A stopcock and ground glass connector was cemented to the cell with Apiezon W for the Br_2 and Cl_2 experiments. This was found to be too reactive with the interhalogens and Kel-F grease was substituted. The ground glass parts had been well ground before being used and a minimum of wax or grease was necessary. Reaction with the grease or wax was shown to be negligible in the arrangements used by the constancy of the spectra over several hours. Pressures were measured on a Pyrex spiral manometer.² All measurements were made at room temperature, $25 \pm 2^\circ$.

Chlorine. Four measurements of the spectrum of Cl_2 , at concentrations of 1.47×10^{-3} to $4.57 \times 10^{-3} M$, were made. The weighted averages of these measurements are reported in Table I.

Bromine. Three measurements of the spectrum of Br_2 , at concentrations of 0.86×10^{-3} to $1.32 \times 10^{-3} M$, were made. The weighted averages are reported in Table I.

Bromine Chloride. Nine measurements were made of the spectrum of BrCl. To each of the Br_2 samples mentioned above was added approximately half, once, and twice the amount of Cl_2 as Br_2 originally present.

Table I: Extinction Coefficients vs. Wave Length

Wave length, $m\mu$	Extinction coefficients, ^a mole ⁻¹ l. cm. ⁻¹				
	Cl_2	Br_2	BrCl	ICl	IBr
220	17.5	55.8	9.4
230	18.8	92.5	14.9
240	0.2	...	16.3	115.1	26.7
250	0.3	...	11.5	113.3	43.7
260	0.6	...	7.7	92.2	56.1
270	2.3	...	4.2	63.7	60.4
280	7.0	...	2.5	40.3	55.2
290	17.0	...	1.4	24.6	44.0
300	31.4	...	1.3	15.9	32.5
310	48.3	...	3.9	12.0	20.8
320	61.8	0.2	10.0	10.5	14.1
330	67.0	0.8	23.6	9.6	8.8
340	61.8	2.9	45.4	8.6	5.6
350	49.6	10.0	71.4	8.1	3.8
360	34.4	23.3	94.9	9.2	4.0
370	21.8	47.6	107.4	13.9	6.2
380	12.9	81.4	106.3	23.0	10.9
390	8.6	119.0	93.7	36.3	18.2
400	5.0	148.9	76.6	49.6	31.5
410	3.5	165.0	60.0	64.5	53.5
420	2.6	165.5	47.9	75.5	83.0
430	1.9	155.5	39.6	83.9	117.1
440	1.4	140.8	34.3	92.7	153.5
450	0.9	127.4	30.2	101.6	188.1
460	...	117.1	26.8	109.0	222.8
470	...	108.4	23.0	111.4	257.6
480	...	101.5	18.6	107.0	290.6
490	...	93.2	14.2	95.0	313.5
500	...	82.9	10.5	77.0	318.2
510	...	70.7	7.4	59.6	303.2
520	...	46.2 ^b	...	42.9	269.6
530	...	33.5	...	30.0	224.5
540	...	26.3	...	20.9	176.6
550	...	20.7	...	14.9	136.9
560	...	16.1	...	11.3	95.8
570	...	11.9	...	9.0	71.2
580	...	8.8	...	7.4	52.0
590	...	6.1	...	5.5	38.1
600	4.6	29.6

^a The uncertainty in the values given is about 0.5 except for IBr where it is ~ 2.5 . ^b Discrete absorption of Br_2 begins at $512 m\mu$ and causes an increased uncertainty in the values for Br_2 and BrCl at longer wave lengths.

In each of these mixtures the BrCl concentration was calculated using the equilibrium constant³ of 8.01 for the reaction $\text{Br}_2 + \text{Cl}_2 = 2\text{BrCl}$. About 40 min. was allowed for equilibrium to be attained. Judging from

- (1) J. Cornog and R. A. Karges, *J. Am. Chem. Soc.*, **54**, 1882 (1932).
- (2) J. D. Ray, *Rev. Sci. Instr.*, **32**, 600 (1961).
- (3) W. H. Evans, T. R. Munson, and D. D. Wagman, *J. Res. Natl. Bur. Std.*, **55**, 147 (1955).

the reproducibility of the spectra after the mixing period this was sufficient time. The observed optical density was assumed to be given by

$$\log(i_0/i) = l(\epsilon_{\text{Br}_2}c_{\text{Br}_2} + \epsilon_{\text{Cl}_2}c_{\text{Cl}_2} + \epsilon_{\text{BrCl}}c_{\text{BrCl}})$$

and the value of ϵ_{BrCl} calculated therefrom. The good agreement among the various samples would indicate that the equilibrium constant used is correct. The actual BrCl concentration ranged from 0.62×10^{-3} to 2.33×10^{-3} M. The weighted averages of the extinction coefficients are given in Table I.

Iodine Chloride. Three measurements were made of the spectrum of ICl at concentrations between 0.97×10^{-3} and 1.74×10^{-3} M. The reported value, 3.41×10^{-6} , of the disproportionation constant³ for the reaction $2\text{ICl} = \text{I}_2 + \text{Cl}_2$ would indicate that no correction need be made for I_2 and Cl_2 concentrations, that this reaction could be ignored. This was checked by three more runs in which Cl_2 was added to the ICl and the observed optical density assumed to be

$$\log(i_0/i) = l(\epsilon_{\text{ICl}}c_{\text{ICl}} + \epsilon_{\text{Cl}_2}c_{\text{Cl}_2})$$

The agreement ($\pm 1\%$ or less) between the values of ϵ_{ICl} determined in the presence and absence of Cl_2 showed that the disproportionation was, indeed, negligible, and also that there is no significant formation of ICl_3 . The weighted averages of ϵ_{ICl} for the runs using pure ICl are listed in Table I.

Iodine Bromide. Four measurements were made of the spectrum of IBr at concentrations between 0.17×10^{-3} and 0.25×10^{-3} M. As with ICl the disproportionation equilibrium constant,³ 2.08×10^{-3} , was small enough to be ignored. This was confirmed by four runs with added Br_2 , which gave the same ($\pm 1\%$ or less) values for ϵ_{IBr} . The lower concentrations used here (limited by the lower vapor pressure of IBr) makes the accuracy of these measurements less. The weighted averages of the runs using pure IBr are listed in Table I.

Results

The measured extinction coefficients are presented in Table I. The curve for Cl_2 has been determined previously by Gibson and Bayliss.⁴ Our results are in close agreement with theirs. The curve for Br_2 has been determined twice previously. We agree reasonably well with the results of Gray and Style,⁵ but our results are consistently higher than those of Acton, Aicken, and Bayliss⁶ (approximately 10% higher at the maximum). The curve for BrCl has only been determined previously between 240 and 270 $\text{m}\mu$.⁵ Our results agree with this work. The curve for ICl has been determined previously by Binder⁷ in the ultra-

violet and by Gibson and Ramsberger⁸ in the visible. We agree with the former, but are consistently much higher than the latter (approximately 35% at the maximum). No previous work on IBr has been reported.

All of the preceding references are to measurements in the gas phase. Gilliam and Morton⁹ have measured all of these compounds in solution in CCl_4 , and if the BrCl results are corrected for the disproportionation of BrCl, the maxima in solution are roughly 50% higher than the corresponding maxima in the gas phase. Buckles and Mills¹⁰ have measured the extinction coefficients of Br_2 , I_2 , and IBr in solutions in acetic acid, carbon tetrachloride, and trifluoroacetic acid. The intensity of the absorption for a given compound varies depending upon the solvent used; for all three solutes the spectra in trifluoroacetic acid were roughly identical with the gas phase spectra. In view of the variation of the intensity depending upon the solvent and phase, it would be of interest to re-examine the claim of Bayliss and Rees,¹¹ denied by Evans,¹² that the extinction coefficient of gaseous Br_2 changes with the pressure in the presence of inert gases.

Our interest in these data has been to use them to predict high temperature values of the extinction coefficients. Sulzer and Wieland¹³ have developed a simple theory for the continuous absorption spectra of diatomic molecules which says that the spectrum can be resolved into Gaussian peaks and that each peak can be described by

$$\begin{aligned}\epsilon(\omega, T) &= \epsilon_m(T) \exp\{-[(\omega - \omega_0)/\Delta\omega(T)]^2\} \\ \epsilon_m(T) &= \epsilon_{m0} [\tanh(hc\omega_v/2kT)]^{1/2} \\ \Delta\omega(T) &= \Delta\omega_0 [\tanh(hc\omega_v/2kT)]^{-1/2}\end{aligned}$$

where $\epsilon(\omega, T)$ is the extinction coefficient at ω cm^{-1} and $T^\circ\text{K}$, ω_v is the vibrational frequency of the molecule, and ϵ_{m0} , ω_0 , and $\Delta\omega_0$ are the maximum, position, and half the mean width of the Gaussian peak at 0°K . Values

- (4) G. E. Gibson and N. S. Bayliss, *Phys. Rev.*, **44**, 188 (1933).
- (5) L. T. M. Gray and D. W. G. Style, *Proc. Roy. Soc. (London)*, **A126**, 603 (1930).
- (6) A. P. Acton, R. G. Aicken, and N. S. Bayliss, *J. Chem. Phys.*, **4**, 474 (1936).
- (7) J. L. Binder, *Phys. Rev.*, **54**, 114 (1938).
- (8) G. E. Gibson and H. C. Ramsberger, *Phys. Rev.*, **30**, 598 (1927).
- (9) A. E. Gilliam and R. A. Morton, *Proc. Roy. Soc. (London)*, **A124**, 604 (1929).
- (10) R. F. Buckles and J. F. Mills, *J. Am. Chem. Soc.*, **76**, 6021 (1954).
- (11) N. S. Bayliss and A. L. G. Rees, *Trans. Faraday Soc.*, **35**, 792 (1939).
- (12) D. F. Evans, *J. Chem. Phys.*, **23**, 1425 (1955).
- (13) P. Sulzer and K. Wieland, *Helv. Phys. Acta*, **25**, 653 (1952).

Table II: Parameters for Gaussian Peaks at 0°K.
Fit from the Data of Table I

Gas	ϵ_{m_0}	ω_0	$\Delta\omega_0$
Cl ₂	71.6 ± 0.7	30456 ± 24	3085 ± 31
Br ₂	90.1 ± 2.9	20452 ± 59	1582 ± 51
	204.2 ± 1.4	24159 ± 42	2102 ± 32
BrCl	25.1 ± 0.5	21952 ± 59	1945 ± 64
	121.2 ± 0.4	26768 ± 17	2537 ± 19
ICl	21.3 ± 0.2	43898 ± 64	5023 ± 75
	50.7 ± 1.1	20818 ± 15	1229 ± 24
	100.3 ± 0.9	22598 ± 23	2804 ± 13
	9.4 ^a ± 0.3	30775 ± 69	2407 ± 92
IBr	137.8 ± 0.4	40986 ± 15	4332 ± 27
	169.8 ± 7.1	19715 ± 20	1132 ± 30
	288.0 ± 6.5	20951 ± 34	2211 ± 16
	78.9 ± 1.4	37289 ± 74	3848 ± 77

^a The weak peak in ICl was found by fitting the strong peaks on either side to Gaussian curves and then taking the differences between observed and calculated values and treating these differences as observed data.

of ω_v are known from spectroscopic measurements and are¹⁴: Cl₂, 561.1 cm.⁻¹; Br₂, 323.2; BrCl, 443.1; ICl,

382.2; IBr, 267.4. The other parameters are determined from the experimental curves. We have determined these parameters for all of the experimentally observed peaks in our spectra. The fit has been made by least-squares calculations for one or two peaks at a time, depending on whether the peaks are overlapped or not. These calculations were made using a FORTRAN program on the Control Data 1604 computer of the Numerical Analysis Center of the University of Minnesota. The results are shown in Table II together with estimated standard deviations for the parameters. It should be emphasized that the peak heights listed here are for 0°K. and will not correspond to the experimental values at room temperature.

Acknowledgments. We wish to thank the U. S. Army Research Office (Durham) for their support of this work. We also wish to thank Mr. E. G. Saettler for making preliminary measurements of some of these spectra.

(14) "JANAF Thermochemical Tables," The Dow Chemical Co., Midland, Mich., June, 1960.

Isolated Helical Macromolecules

by Arthur V. Tobolsky

Department of Chemistry, Princeton University, Princeton, New Jersey (Received March 19, 1964)

There is at present no convincing theory explaining why isolated extended helical macromolecules exist, nor why they should be confined mainly to polypeptides, proteins, and polynucleotides. Thermodynamic reasoning suggests that even among these latter classes, the isolated extended single strand helix, unstabilized by electric charges, may be a relatively rare phenomenon. On the other hand there are reasons for suspecting that in dilute solution many crystallizable macromolecules may fold up into single molecule "lattices" or associate laterally into small micelles. These states may exist for a long time even if they are metastable with respect to eventual precipitation of a gross crystalline phase.

The extended double strand helix was postulated as the basic structure of DNA in 1953¹; unpairing of the double strand helix and the existence of an ordered, extended single strand helix was also postulated as a basic step in the transmission of hereditary information. Isolated synthetic polypeptide molecules existing in an extended helical conformation in dilute solution were reported shortly thereafter.² A similar result was reported for the natural protein, tropomyosin.³ The existence of isolated, extended, single and double strand helices in solution seems to be a cornerstone of the science of molecular biology. The term extended helix is used herein as meaning a rod-like non-folded structure as opposed to a highly folded structure (such as a polyethylene single crystal) or highly coiled structure (such as a globular protein).

By contrast the older science of polymer chemistry has produced no such phenomenon as yet. Crystallizable synthetic polymers such as nylon, polyethylene, and polyvinylidene chloride of symmetrical structure have been known for more than 25 years. Since 1955 stereospecific polymers such as isotactic polypropylene and isotactic polystyrene have been known and widely available⁴; these too are highly crystallizable.

However, nylon, polyethylene, polyvinylidene chloride, isotactic polystyrene, isotactic polypropylene, etc., are crystalline (or semicrystalline) only in the bulk state or as very small polymer single crystals. In the bulk state there exist amorphous regions where portions of the molecule are in random coil configurations and also crystalline regions where the polymer molecules are associated together (or folded upon them-

selves) within a three-dimensional lattice. In solution the isolated macromolecules of these polymers are in random coil configurations, *i.e.*, the totality of conformations available to the macromolecule by virtue of its restricted internal rotation.

Polypeptides, proteins, and polynucleotides (DNA, RNA, Poly A, Poly U, etc.) certainly are semicrystalline in the bulk state, even if somewhat swollen by water. In this state there may be amorphous regions (depending on how the polymer is handled) but there certainly are regions of three-dimensional lattice order. The surprising situation is that these polymers are reputed to dissolve (under certain conditions) as *isolated extended* helical macromolecules (one-dimensional crystals). Wherefore the great difference between these contrasting classes of macromolecules: proteins, polypeptides, and polynucleotides *vs.* all the rest? (Amylose is helical but not fully extended in solution.⁵ Other examples may soon be forthcoming.⁶)

The first task is to dispel any magical qualities associated with the word helix or helical. If we regard the planar zigzag conformation of crystalline polyethylene as a degenerate helix, as indeed we must, then

- (1) J. D. Watson and F. H. C. Crick, *Nature*, **171**, 737, 964 (1953).
- (2) P. M. Doty, A. M. Holtzer, J. H. Bradbury, and E. R. Blout, *J. Am. Chem. Soc.*, **76**, 4493 (1954); P. M. Doty, J. H. Bradbury, and A. M. Holtzer, *ibid.*, **78**, 947 (1956); P. M. Doty and J. T. Yang, *ibid.*, **78**, 498 (1956).
- (3) C. M. Kay and K. Bailey, *Biochim. Biophys. Acta*, **40**, 149 (1960); and references cited therein.
- (4) G. Natta, *Angew. Chem.*, **68**, 393 (1956).
- (5) V. S. R. Rao and J. F. Foster, *Biopolymers*, **1**, 527 (1963).
- (6) H. G. Elias and G. Adank, *Makromol. Chem.*, **69**, 241 (1963).

the conformations assumed by *all* crystallizable macromolecules in their crystalline unit cells are indeed helical. This is inherent for a repeating sequence of units in a linear macromolecule. The word helical will be used here as meaning an ordered conformation of the macromolecule, with a translational repeat vector along the chain axis.

We shall first discuss some of the crystal structures found in the solid state. In the case of linear polyethylene (polymethylene) the X-ray interpretation of the crystal structure indicates a parallel array of extended planar zigzag chains with a very high degree of lateral order as well as order in the direction parallel to their length. In other words we are here dealing with an essentially perfect three-dimensional space lattice.

Atactic polyvinyl alcohol is also crystalline, and the basic crystal structure is the same as that of polyethylene. On every alternate carbon atom one hydrogen atom has been replaced by an hydroxyl group, but this replacement is random as regards the *d* or *l* configuration. Although a great deal of disorder has thereby been introduced into the structure, the basic crystal lattice remains unaltered because the hydroxyl group is sufficiently small to replace isomorphously the hydrogen atom.

Random copolymers of ethylene and propylene with up to 20 mole % of propylene still retain a certain amount of crystallinity. Small sequences of polymethylene can crystallize with each other, and also a certain small amount of isomorphous replacement of hydrogen atoms by methyl groups is tolerated within the polyethylene lattice. However, atactic polypropylene is amorphous as are copolymers of ethylene and propylene near the 1:1 mole ratio.

The X-ray data obtained from solid films of synthetic polypeptides or from natural proteins such as keratin fibers in many cases indicate a crystal lattice based on the α -helix. This is a particular conformation of the polypeptide chain first proposed by Pauling in which 3.7 polypeptide residues occur per turn and in which the conformation is stabilized by intramolecular hydrogen bonding.⁷ The polymer molecules within the crystallites, while remaining parallel, appear to have some degree of disorder in a direction parallel to their length.

Synthetic polypeptides are nevertheless truly crystalline; they even show well-developed spherulites under appropriate conditions. Despite some disorder parallel to the length of the chain, the crystalline regions are also crystalline in a thermodynamic sense; they would be expected to have a latent heat of fusion, a discontinuous change of volume during melting, etc. Unfortunately none of the homopolymers melts below

the temperature of decomposition (300°), so these quantities have not been measured.

The structures of some simple homopolymeric polypeptides such as α -poly-L-alanine have been studied in great detail.⁸ However it is very worthy of note that presumably random copolymers such as the 1:1 copolymer of DL-phenylalanine and L-leucine also give crystalline polymers. These too are based on the α -helix conformation. The X-ray diagrams suggest that the helices, while remaining parallel and retaining their lateral periodicity, tend to be disordered along their length.⁸

It would appear that isomorphous replacement with a quite drastic variation of the side group on the amino acid is tolerated by the crystal lattices based on the α -helix. Also some disorder parallel to the length of the helices is tolerated without destroying the crystal lattice.

The possibility of isomorphous replacement of the amino acids without destroying the three-dimensional lattice structure means that in the crystalline regions of natural proteins, such as keratin, there need not be a matching of identical amino acid sequences in adjacent α -helices. A crystalline "lattice" can exist without such matching, at least in certain regions of the polymer. These crystalline regions in which the α -helix conformation of the individual macromolecules are preserved are stabilized by intermolecular lattice energy, just in the same way that the planar zigzag conformation in atactic polyvinyl alcohol is stabilized by intermolecular lattice energy.

In order to explain the existence of isolated helical macromolecules in solution, several theoretical questions must be raised. First, it may be conceded that for an isolated macromolecule in solution, the completely ordered and extended helical conformation, *i.e.*, the planar zigzag conformation of polyethylene or the α -helix conformation of a polypeptide, may be the one of lowest energy at 0°K. However, as the temperature is raised, why does not a *very diffuse* disordering of the helical conformation occur as the temperature is raised? For polymethylene there is only a small energy difference between alternative configurations of successive chain atoms. This is about 600 cal./mole of CH₂ units for the energy difference between the *trans* (planar zigzag) and *gauche* (skewed) configurations which the successive C-C links in polymethylene can alternatively adopt. Ignoring steric exclusions, for a polymethylene chain of *n* C-C links there are 3^{*n*-2}

(7) L. Pauling, R. B. Corey, and H. R. Branson, *Proc. Natl. Acad. Sci. U.S.A.*, **37**, 205 (1951).

(8) C. H. Bamford, A. Elliott, and W. E. Hanby, "Synthetic Polypeptides," Academic Press, New York, N. Y., 1956, Chapters VII and VIII.

allowed conformations with an essentially continuous distribution of conformational energies. This would lead to a *very* gradual disordering of the planar zigzag conformation. By contrast the reported helix-coil transition in polypeptides or globular proteins generally occur over an interval of 10° or less, which is diffuse compared to the melting of three-dimensional solids. However, this is a quite sharp transition compared to the *theoretical* disordering of the planar zigzag conformation of an isolated polymethylene molecule, if the theory is based only on the energy difference between *trans* and *gauche* configurations.

In order to "explain" the unexpectedly sharp transition from helix to random coil several theories have been forwarded, of which the Zimm-Bragg theory is representative.⁹ The basic postulate is that it is thermodynamically *very* unfavorable to create a boundary region between a disordered random coil region of the macromolecule and an ordered helical portion of the macromolecule. The statistical weight of the first turn of the α -helix of a polypeptide has been denoted as σs by Zimm and Bragg compared to the statistical weight unity for a peptide segment within a random coil region and the weight s for a segment of a helix not in the first turn. At the melting temperature s equals unity. If σ were zero, the transition between the completely ordered helical macromolecule and the completely random coil macromolecule would be infinitely sharp. In order to explain the slightly diffuse transition reported for synthetic polypeptides, σ must be given a value of about 10^{-4} . With this value one can fit the data for per cent crystallinity (or helicity) *vs.* temperature. If σ were unity, the disordering would be so diffuse that no transition could be observed or defined.

It is the author's opinion that the Zimm-Bragg treatment of the helix-coil transition for extended helical macromolecules does not really *predict* that the isolated helical macromolecule should exist or that it should undergo a phase transition. The existence of distinct perfectly ordered helical regions, random coil regions, and boundary regions with different partition functions is preassumed by the theory. When σ equals zero the theory is precisely like the very elementary cell model frequently used to describe melting of a solid. The assembly of n atoms is supposed to be allowed only two configurations corresponding to the solid and the liquid. The partition function of a solid cell is f_s , the partition function of a liquid cell is f_L . The partition function of the assembly of n atoms is therefore $f_s^n + f_L^n$. This shows a sharp transition at the temperature at which f_s equals f_L . Although this is a model for melting, it is not a theory based on first principles.

The Zimm-Bragg theory is actually a very fine mathe-

matical *model* (as opposed to an *a priori* theory) to describe diffuse melting provided that one presupposes a crystalline phase, an amorphous phase, and a boundary phase. It seems to be applicable for diffuse melting in a three-dimensional lattice.¹⁰ However, it gives no convincing *a priori* reason why σ should be as small as 10^{-4} for an isolated polypeptide. The theory could be used to fit the data for a helix-coil transition in any isolated macromolecule, *provided* such a transition was found. For other macromolecules, many of which have very complicated helical structures in their crystalline unit cells, it would be expected that σ might be small also. There is no convincing reason why σ should be smaller and hence the helix-coil transition in polypeptides should be much sharper than for all other macromolecules. Although we should perhaps not expect σ to be very small for simple structures such as polyethylene, it would be just as easy to accept a small value of σ for the complicated helical structures of many isotactic and syndiotactic polymers, as it is for the α -helix. All that one would have to do is demonstrate a helix-coil transition: a σ -value would be immediately calculated and universally accepted as "explaining" the phenomenon. Some of the helical crystal structures of isotactic polyolefins are so complex that the crystal density is lower than the density of the amorphous melt. Certainly one would think that the σ -value in these cases should be small.

To explain why relatively sharp helix-coil transitions are reported only for certain classes of macromolecules we have to look beyond the Zimm-Bragg theory and related theories. Let us therefore consider the value of the melting temperature for this transition.

The melting point T_f' for the helix-coil transition in an isolated macromolecule is given by

$$T_f' = \Delta H_f' / \Delta S_f' \quad (1)$$

where $\Delta H_f'$ and $\Delta S_f'$ are the enthalpy change and entropy change for the transition per mole of segments. It is to be expected that $\Delta S_f'$ would be of the order of magnitude R per mole of segments (repeat units), and this would be more or less the same for all macromolecules. (For linear polyethylene the repeat unit CH_2 has *one* possible configuration in the helical (planar zigzag) conformation, and *three* possible configurations in the random coil state; the value of $\Delta S_f'$ should be approximately $R \ln 3$.)

It might be argued that $\Delta H_f'$ may be larger for a polypeptide than for other macromolecules because the

(9) B. H. Zimm and J. K. Bragg, *J. Chem. Phys.*, **33**, 1349 (1960).

(10) A. V. Tobolsky, *ibid.*, **37**, 1139 (1962); *J. Polymer Sci.*, **A1**, 301 (1963); *J. Chem. Phys.*, in press. (Lambda point transitions in solids are treated here.)

α -helix is stabilized by internal hydrogen bonding. If this is so, then it merely means that T_f' for other synthetic macromolecules would be lower and the isolated helical macromolecule would be stable only at low temperatures and perhaps overlooked in the experimental work reported to date. However, even in polyethylene (polymethylene), the energy difference between the completely ordered planar zigzag conformation and the completely disordered random coil is about 600 cal./mole of repeating CH_2 units. In other words $\Delta H_f' \approx 600$, $\Delta S_f' \approx 2$, and therefore $T_f' \approx 300^\circ\text{K.}$, which is obviously not an experimentally inaccessible temperature.

If the expected value of σ or the expected value of T_f' do not give completely convincing reasons why the helix-coil transition in isolated or paired macromolecules has been reported *only* in proteins, polypeptides, and polynucleotides, let us turn to other reasons and other difficulties. From an *a priori* point of view it would appear that there would be a tremendous tendency for a supposedly isolated helical macromolecule to either fold up into a three-dimensional "lattice" or else to associate with other helical macromolecules into a three-dimensional lattice. In the latter case, it could either precipitate as a gross bulk phase or remain dispersed as small micelles.

In the former case, the isolated macromolecule could fold into a polymer single crystal possibly somewhat swollen by solvent. This could conceivably occur in an extremely dilute solution of very high molecular weight polymethylene. Or it could coil up into a complex coiled structure which maintains the conformational stability of the favored helix but also gains energetic stability from an intermolecular "lattice" interaction. In this case too the "lattice" may be somewhat swollen by solvent. We use the word "lattice" in quotation marks here because although in an isolated globular protein molecule we have a nearly completely ordered *three-dimensional* structure, which may have a "lattice" energy, there may be no repeating unit cell within a single molecule. However, when globular proteins are brought into the solid state by careful procedures, one can often obtain true three-dimensional space lattices in which the unit cell may involve more than one molecule.¹¹

We have emphasized the importance of lattice energy or "lattice" energy in stabilizing an ordered helical conformation and shall now present some thermodynamic reasons for this emphasis. To investigate this matter we shall first consider the melting of bulk phase crystalline macromolecules into a molten state where the molecules are in the random coil state. This is the type of melting actually observed in crystalline polymers like

polyethylene, isotactic polypropylene, nylon, etc. The melting point T_f'' is given by

$$T_f'' = \Delta H_f'' / \Delta S_f'' \quad (2)$$

where $\Delta H_f''$ is the heat of fusion per mole of segments (repeat units) and $\Delta S_f''$ is the entropy of fusion per mole of segments and is of order of magnitude R cal./mole deg. These quantities have been tabulated for many polymers.¹² Explicitly, $\Delta H_f''$ is 785 cal./mole per CH_2 unit in polyethylene (more accurately designated as polymethylene), $\Delta S_f''$ is 1.90 cal./mole per CH_2 unit in this same polymer, and T_f'' is therefore 410°K. or 137° .

Part of the 785 cal./mole for the $\Delta H_f''$ of the CH_2 units (perhaps 600 cal./mole) may be assigned to the breaking up of the intramolecular energy of stabilization of the perfectly ordered planar zigzag conformation. However, we would expect *at least* 100 cal./mole CH_2 units to be assignable to intermolecular attractive energy (a gross underestimate to make my calculations as unfavorable as possible for my cause). For comparison, the heat of fusion of methane is 225 cal./mole.

We can now consider another (probably hypothetical) phase transition: the fusion of the bulk phase crystalline polymer into a melt in which the individual macromolecules retain their completely ordered extended helical conformation.

Once again

$$T_f''' = \Delta H_f''' / \Delta S_f''' \quad (3)$$

For this phase transition we shall consider $\Delta H_f'''$ and $\Delta S_f'''$ per mole of macromolecules rather than per mole of segments. $\Delta S_f'''$ is of the order of magnitude of R cal./deg. mole since the macromolecules gain only communal entropy or translational entropy but *not* conformational entropy in the melting process. On the other hand $\Delta H_f'''$ is proportional to the number of segments in the macromolecule. For explicitness let us suppose that the number of segments (repeating units) in the macromolecule is 100; further suppose that the intermolecular latent heat of melting *per segment* was 100 cal./mole, which as we have seen is a low estimate. Then $\Delta H_f''' \approx 10,000$ cal./mole of macromolecules, $\Delta S_f''' \approx 2$ cal./deg. mole of macromolecules, and $T_f''' \approx 5000^\circ\text{K.}$, a temperature at which no organic macromolecules would be stable.

The high temperature of melting indicates very low solubility of the molten species, *i.e.*, the helical macromolecules. To justify this statement, let us examine

(11) F. H. C. Crick and J. C. Kendrew, *Advan. Protein Chem.*, 12, 133 (1957).

(12) L. Mandelkern, *Chem. Rev.*, 56, 903 (1956).

the formula for the depression of melting point produced by a solvent¹³

$$-\ln a_1 = \frac{\Delta H_f''' T_f''' - T}{R T_f''' T} \quad (4)$$

In eq. 4, a_1 is the activity of the polymer in the solution. The standard state is the pure molten polymer, for which a_1 equals unity. Equation 4 of course indicates that the pure molten polymer is at equilibrium with the solid at temperature T_f''' . Equation 4 makes the approximation that $\Delta H_f'''$ is independent of temperature.

For an ideal solution a_1 is of course equal to x_1 , the mole fraction of species (1) in the solution at equilibrium with pure solid (1) at temperature T , *i.e.*, x_1 is the solubility of species (1) at temperature T expressed as a mole fraction. We can readily compute that for an ideal solution for which $\Delta H_f''' = 10,000$; $T_f''' = 5000$, the solubility at $T = 300^\circ\text{K}$. is $x_1 = 1.4 \times 10^{-7}$. This is so small a solubility that it is practically out of the experimental range.

Although the ideal solution law would certainly not hold for helical macromolecules dissolved in most conceivable solvents, the above calculation nevertheless indicates that the solubility of helical macromolecules would tend to be very low. This consideration would make it appear that the possibility of observing an isolated, extended (nonfolded) helical macromolecule in solution is strongly obviated by the tendency of these molecules to associate into disperse solid phase, or at least fold up upon themselves to form a three-dimensional lattice or "lattice." In cases where the isolated extended helical macromolecule can be *definitively* established, we must expect that the intermolecular attraction between these molecules in the bulk phase must be exceptionally low or the solvent effect very unusual.

Consider the following artificial case: a *single* very high molecular weight polymethylene molecule is formed in solution in its extended planar zigzag form. According to our thermodynamic considerations it would probably either "melt" into the random coil configuration or else it would tend to fold up into a crystalline micelle since in this way it would be stabilized by lattice energy. Energy considerations would suggest that the gross structure of this folded single crystal would be such as to present a minimum surface to volume ratio.

The isolated extended helical macromolecule of polymethylene can exist only in a good solvent, where solvent-polymer interactions are more favorable than polymer-polymer interactions which promote the tendency to fold into a crystalline micelle. Yet it is precisely these good solvents which would probably tend to counter

the energy difference between ordered helical conformations and disordered random coil conformations and to promote the tendency of the helical macromolecule to "melt." Although this statement is only a qualitative one, it is nevertheless true that isolated extended helical macromolecules such as polybenzyl glutamate have been reported only in poor solvents.² The relative importance of hydrogen bonding *vs.* hydrophobic bonding in the formation of helical structures is one important aspect of the unusual solvent requirements.^{14,15}

Exactly the same considerations would apply to a *single* molecule of atactic polyvinyl alcohol, except that the folded crystalline micelle would be a quite disordered "lattice" compared to the folded micelle of polymethylene.

To the author's knowledge it has never been demonstrated that synthetic macromolecules such as polymethylene or polyvinyl alcohol will in extremely dilute solutions form single molecule "lattices." However, there is a distinct possibility that solutions of this type will eventually be found. These may be metastable with respect to eventual precipitation of a gross crystalline phase.

In the case of a synthetic polypeptide homopolymer the same arguments would apply as in the case of polymethylene, except that the folded crystalline micelle would again be a more disordered "lattice" than that of polymethylene. This would be even more true for a synthetic polypeptide copolymer.

In order to preserve an isolated extended helical polypeptide molecule we require a good solvent that will solvate the polymer segments and prevent them from folding into a "lattice" or associating with other molecules. Nevertheless, this good solvent must not solvate the intramolecular hydrogen bond favoring the α -helix conformation. This is a quite restrictive requirement.

In the case of natural proteins the fact that globular proteins are so common seems consistent with the idea that the conformational stability of the α -helix (or other favored helices) must be stabilized by "lattice" energy in order for a particular conformation to be preserved in an isolated macromolecule. The ordered sequence of amino acids in globular proteins means that each isolated molecule is exactly like all the rest (in contrast to synthetic polypeptide copolymers). This unusual feature makes it possible for globular proteins

(13) J. H. Hildebrand and R. L. Scott, "Solubility," Reinhold Publishing Corp., New York, N. Y., 1950, Chapters I and II.

(14) W. Kauzmann *Advan. Protein Chem.*, **14**, 1 (1959).

(15) B. H. Zimm, P. Doty, and K. Iso, *Proc. Natl. Acad. Sci. U.S.A.*, **45**, 1601 (1959).

to crystallize into a true three-dimensional lattice in the solid phase.

More detailed discussion regarding the forces which make for the ordered structure of globular proteins has been reviewed by Kauzmann.¹⁴ This discussion is quite consistent with the viewpoint presented here.

Globular proteins, polynucleotides, and certain synthetic polypeptides are polyelectrolytes when dissolved in water. The electrostatic effects certainly play an important role in stabilizing certain conformations and in affecting the interactions between polymer segments in the same molecule or in different molecules. These effects are too complex to assess in this discussion. They may be a vital factor in explaining the existence of isolated extended helical macromolecules in certain cases. However, rod-like isolated helical macromolecules have been reported for polybenzyl glutamate, which is not a polyelectrolyte.

Certain conclusions seem to follow: there is at present no convincing theory explaining why isolated extended helical macromolecules exist or why they should be confined to proteins, polypeptides, and polynucleotides. A more penetrating theory would be very desirable. It may also be that even for biological macromolecules or synthetic polypeptides the isolated extended helix is a rare and unusual phenomenon if considered as a thermodynamically stable phase.

It would appear that a careful scrutiny of the experimental facts concerning postulated isolated extended helical macromolecules should be made. Their existence is so convenient for many purposes of the biochemist that one wonders whether the distinctions between isolated extended helical macromolecules, folded helical molecules (into lattices or "lattices"), and associated helical molecules (a disperse, perhaps swollen, crystalline phase) are always carefully made. The distinctions between these are not trivial; X-ray scattering from these three types of "solutions" should be very different. One would expect a powder diagram (sharp rings) from the last two but not from the first. Biological mechanisms in or on dispersed crystalline solid phases or "lattices" may also be quite different from mechanisms involving isolated extended helical macromolecules.

Acknowledgments. The author wishes to extend his especial thanks to Professors W. J. Kauzmann and J. R. Fresco. The thoughts in this manuscript were hammered out in discussions with them, based upon initial skepticism concerning the ubiquitous invocation of isolated extended helical macromolecules in the science of molecular biology. However, the author assumes full responsibility for the conclusions, which are not necessarily shared by his colleagues at the present time.

The Filtration of Amorphous and Sized Crystalline Silica Suspensions Flocculated by High Polymers

by Jacqueline C. Kane, Victor K. La Mer, and Henry B. Linford

Department of Chemical Engineering, Columbia University,
New York, New York (Received March 19, 1964)

Further investigations were conducted into the filtration behavior of crystalline and amorphous silica dispersions flocculated by high polymers. Four new cationic and anionic flocculants were tested for filtration improvement with amorphous silica suspensions and found to be effective. In all cases, the relationship between the optimum polymer concentration and the solid content remained linear. The effect of changing the chemical nature of the polyelectrolytes as well as the surface area and crystalline structure of the silica was probed using suspensions of sized crystalline silica with Superfloc 16 (weakly anionic), ET-494 (cationic), and PAM 3 (weakly anionic) as flocculating agents. The relationships between the optimum polymer concentration and the solid content appeared to be dependent upon the size of silica particles in suspension.

Introduction

Previously published results from this laboratory^{1,2} have shown that silica dispersions of various solids content are flocculated readily by high molecular weight polymers. Originally, this research program was undertaken to verify the eighth-power filtration relationship discovered by Smellie and La Mer³ for suspended solid materials different from those tested previously.^{3,4} A second objective of this research is to ascertain what changes in the eighth-power law occur if the solid content is decreased toward the low values encountered in industrial water purification processes. A natural corollary to the above program involves an investigation of the effect of the particle size of suspended material on this same filtration law. This paper presents the results of the second research objective.

Smellie and La Mer proposed that if the final concentration of polymer flocculant in solution was P , and the initial concentration was P_0 , then the amount adsorbed could be represented by $k_{SL}W\theta$.³ Here k_{SL} has units of g. of polymer/g. of solid and is proportional to the surface area of solid and hence dependent upon the fineness of grinding. W is the solid content in g. of solid/100 g. of water and θ is the dimensionless fraction of solid surface covered by adsorbed polymer. Accordingly, $k_{SL}W$ must be a measure of total surface area. Thus

$$P = P_0 - k_{SL}W\theta \quad (1)$$

Omitting the details of the theoretical development for which the reader should consult the original reference,³ it can be shown that if the refiltration rate (the rate of passing clear filtrate back through the formed filter cake) improvement $Q - Q_0$ is expressed in terms of θ , the following equation results.

$$Q - Q_0 = \frac{Q_0}{R_0^2} K^2 W^4 \theta^4 (1 - \theta)^4 \quad (2)$$

Here Q and Q_0 are the refiltration rates with and without polymer, respectively, R is the radius of the average floc, and K is a constant; W and θ are defined above. The quantity $\theta^4(1 - \theta)^4$ results theoretically from the model of polymer bridging suggested by La Mer and Smellie, where the extent of polymer adsorption will be a function of both the fraction of solid surface covered and the fraction of the surface still available for additional adsorption.^{3,5} Equations 1 and 2 can be com-

(1) J. C. Kane, V. K. La Mer, and H. B. Linford, *J. Phys. Chem.*, **67**, 1977 (1963).

(2) J. C. Kane, V. K. La Mer, and H. B. Linford, presented at the 147th National Meeting of the American Chemical Society, Philadelphia, Pa., April, 1964.

(3) R. H. Smellie and V. K. La Mer, *J. Colloid Sci.*, **13**, 589 (1958).

(4) T. W. Healy and V. K. La Mer, *J. Phys. Chem.*, **66**, 1835 (1962).

(5) V. K. La Mer and T. W. Healy, *ibid.*, **67**, 2417 (1963).

bined, together with the assumption of a Langmuir-type adsorption, to yield an expression relating the refiltration rates, Q and Q_0 , to the initial polymer concentration, P_0 . This equation is independent of the equilibrium polymer concentration, P . Hence

$$Q - Q_0 = \frac{k'P_0^4}{\left(\frac{1 + bk_{SL}W}{b} + \frac{P_0}{1 + bk_{SL}W}\right)} \quad (3)$$

where

$$k' = \frac{\left(\frac{Q_0}{R_0^2}\right) K^2 W^4 (1 + bk_{SL}W)^4}{b^4} \quad (4A)$$

Here b is a function of the rate constants for the adsorption and desorption processes and the conditions of agitation.

The behavior exhibited by a variety of slimes and flocculating agents has shown that a plot of the refiltration rate *vs.* P_0 gives a curve which passes through a maximum. The value of P_0 at which the refiltration rate is maximized is denoted by P_m , the optimum polymer concentration.

Differentiating eq. 3 and setting the derivative equal to zero to yield the optimum gives an expression for P_m in terms of the solid content and hence the surface area of solid, *i.e.*

$$P_0 (\text{optimum}) = P_m = \frac{1}{b} + 2k_{SL}W + bk_{SL}^2W^2 \quad (4)$$

Rearranging eq. 3 and combining constants yields

$$P_0^{1/2}/((Q - Q_0) \times 10^3)^{1/8} = A + BP_0 \quad (5)$$

where A and B are constants whose ratio A/B has been shown to be equal to P_m (ref. 3). Taking logarithms and substituting for A in eq. 5 gives

$$\ln \left(\frac{P_0^4}{(Q - Q_0) \times 10^3} \right) = 8 \ln (P_0 + P_m) + 8 \ln B \quad (6)$$

A plot of $\ln [P_0^4/((Q - Q_0) \times 10^3)]$ *vs.* $\ln (P_0 + P_m)$ should be linear with a slope of 8.0, and the calculated value of the ratio of A/B should check the value of P_m obtained directly from experiment.

Experimental

The experimental procedure has been explained in detail elsewhere.¹ (As in previous work, the pH was held constant at a value between 5.5 and 6.0.) The sample of amorphous silica was supplied by Whittaker, Clark, and Daniels, New York, N. Y. (No. 19, 99% less than 43 μ).

The samples of crystalline silica were supplied by Pennsylvania Glass Sand Corporation, Pittsburgh, Pa., under their trade name MIN-U-SIL. A typical chemical analysis supplied by the manufacturer in data sheet No. 201 shows 99.90% silicon dioxide and traces of iron, aluminum, titanium, calcium, and magnesium oxides. The important data of the four grades used are outlined below with surface area being indicated by SA and average particle size (surface mean) being indicated by PS. In all four cases the logarithmic cumulative size distribution function was reasonably linear with the values of the extremes shown below.

1. MIN-U-SIL 5: SA, 20,600 cm.²/g.; PS, 1.1 μ ; 98% finer than 5 μ , 60% finer than 1.5 μ .
2. MIN-U-SIL 10: SA, 11,000 cm.²/g.; PS, 2.06 μ ; 98% finer than 10 μ , 40% finer than 2.5 μ .
3. MIN-U-SIL 15: SA, 8400 cm.²/g.; PS, 2.7 μ ; 98.5% finer than 15 μ , 32% finer than 3 μ .
4. MIN-U-SIL 30: SA, 5400 cm.²/g.; PS, 4.19 μ ; 98% finer than 30 μ , 27% finer than 5 μ .

For additional information, the reader should consult the data sheet mentioned above.

The effective new polymer flocculants for the amorphous silica were

1. PAM 2: American Cyanamid; a polyacrylamide of molecular weight 3–5 million, 3% COOH.⁶
2. Primaflor C-3: Rohm and Haas; a polyalkylamine-type polyelectrolyte of molecular weight > 10,000.
3. Primaflor C-5: Rohm and Haas; a polyalkylamine-type polyelectrolyte of molecular weight > 10,000.
4. UCAR resin C-149: Union Carbide; a cationic polymer with a molecular weight of several hundred thousand.

Results

Amorphous Silica. Figures 1 and 2 summarize the results of refiltration experiments for the different polymer–solid content systems using the sample of amorphous silica. These figures should be compared with Fig. 5 and 6 of ref. 1. In Fig. 1, P_m is expressed in p.p.m., while in Fig. 2, P_m has the units of g. of polymer/g. of silica. Typical plots of eq. 5 and 6 are of the elongated S-shaped type with the linear portion centrally located as described previously.¹ Also, good agreement with the expected (logarithmic) slope of 8.0

(6) The optimum polymer concentration of PAM 2 indicated by settling rate and final sediment volume measurements did not improve the refiltration rate. Subsequently, however, investigations at lower concentrations of polymer revealed that PAM 2 could be an effective flocculating agent.

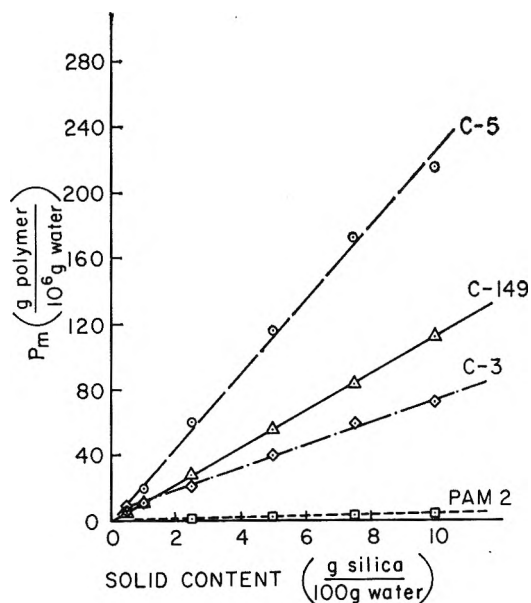


Figure 1. Plot of optimum polymer concentration expressed as g./10⁶ g. of water vs. solid content for four new polymers effective in flocculating amorphous silica.

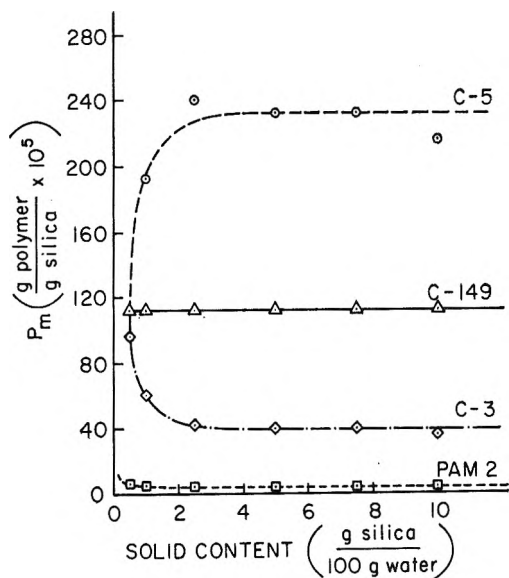


Figure 2. Plot of optimum polymer concentration expressed as g./g. of silica vs. solid content for four new polymers effective in flocculating amorphous silica.

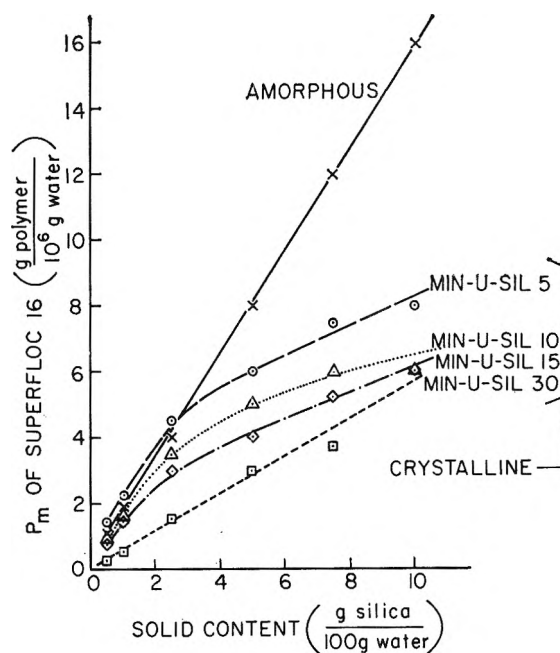


Figure 3. Plot of the optimum concentration of Superfloc 16 expressed as g./10⁶ g. of water vs. solid content for four crystalline silica suspensions.

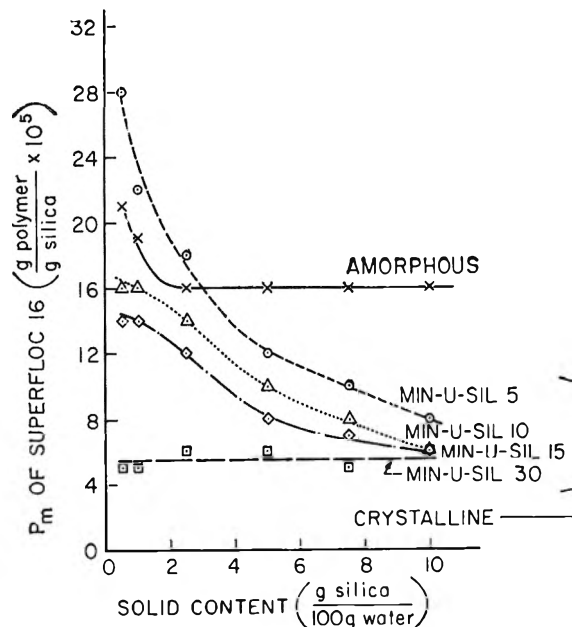


Figure 4. Plot of the optimum concentration of Superfloc 16 expressed as g./g. of silica vs. solid content for four crystalline silica suspensions.

$\pm 5\%$ is obtained, while the experimental and calculated values of $P_m = A/B$ give a satisfactory check. For a typical set of results, see Table I.

Crystalline Silica. Figures 3 and 4 summarize the results obtained from filtration experiments on crystalline silica suspensions flocculated by Superfloc 16, a polyacrylamide from American Cyanamid. In each figure, the curve obtained with the sample of amor-

phous silica and the same flocculant (see Fig. 5, ref. 1) is included for a comparison. Here again, agreement with the predicted (logarithmic) slope of $8.0 \pm 5\%$ is good, while the values of P_m obtained by the graphi-

Table I: Typical Results from Filtration Experiments^a

Solid content, g./100 g. of water	P_m		Slope of best straight line through central points
	Exptl., p.p.m.	Calcd., p.p.m.	
10.0	72	69.6	8.19
5.0	40	43.7	7.85
2.5	21	21.3	8.11
1.0	12	11.7	8.10
0.5	9.6	8.7	8.44

^a Data are for amorphous silica flocculated by C-3.

cal and analytical methods are in accord. For a typical set of results, see Table II.

Table II: Typical Results from Filtration Experiments^a

Solid content, g./100 g. of water	P_m		Slope of best straight line through central points
	Exptl., p.p.m.	Calcd., p.p.m.	
10.0	6.0	7.4	7.49
5.0	4.0	2.5	7.88
2.5	3.0	3.0	7.95
1.0	1.4	1.3	8.28
0.5	0.7	0.66	8.30

^a Data are for crystalline MIN-U-SIL 15 flocculated by Superfloc 16.

Figures 5 and 6 summarize the results obtained by flocculating MIN-U-SIL 5 and MIN-U-SIL 30 samples with ET-494, a cationic polyethylenimine from Dow Chemical Co., and with PAM 3, a high molecular weight anionic polyacrylamide from American Cyanamid Co. Results from Superfloc 16 are repeated for comparison.

Discussion of Results—Summary

Amorphous Silica. Figure 1 shows that for all the new polymers tested, the relationship between the optimum polymer concentration, P_m , and the solid content, W , is linear. This is exactly the result obtained with silica using four other polymeric flocculating agents.¹ Qualitatively, this relationship has been explained by assuming that for the systems exhibiting this behavior, the $bk_{SL}^2W^2$ term of eq. 4 is negligible compared to the term in W to the first power.

Figure 2 shows the relationship between the optimum polymer concentration requirement in grams per gram of silica and the dilution. The behavior of PAM 2 and C-3 parallel that of Superfloc 16; C-5 corresponds to PAM 3; and C-149 acts like ET-494 and Jaguar +.¹ These results give additional supporting evidence to

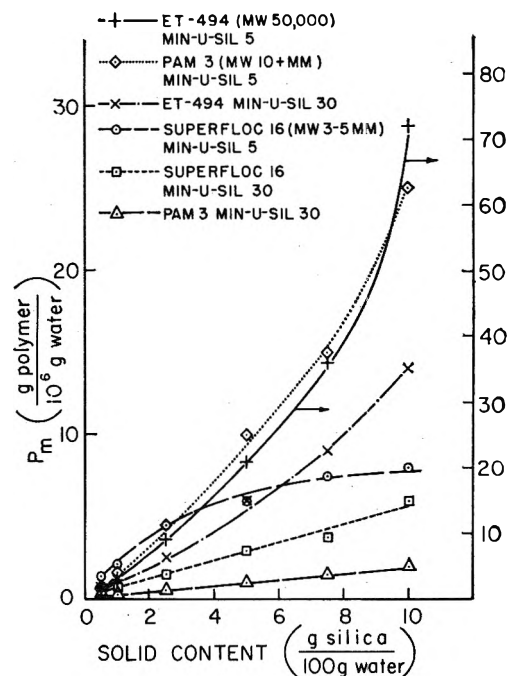


Figure 5. Plot of optimum polymer concentration expressed as g./10⁶ g. of water vs. solid content for flocculated MIN-U-SIL 5 and MIN-U-SIL 30 suspensions.

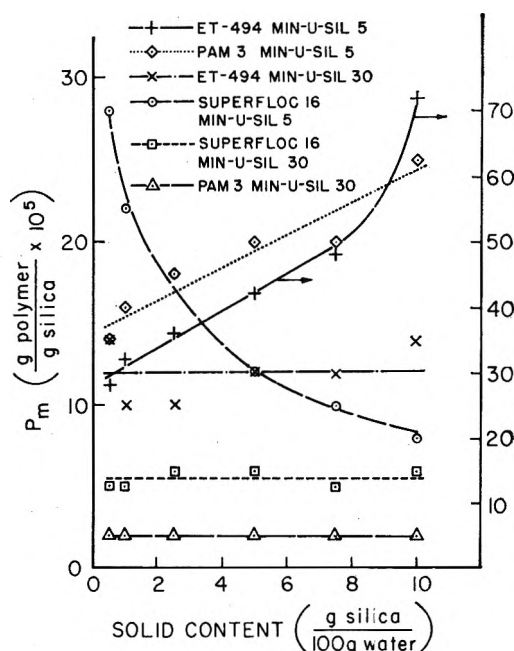


Figure 6. Plot of optimum polymer concentration expressed as g./g. of silica vs. solid content for flocculated MIN-U-SIL 5 and MIN-U-SIL 30 suspensions.

the theory previously advanced by these authors to explain the variation of P_m at decreasing solid contents²; thus PAM 2 is of intermediate molecular weight (3-5

million) and has an increasing requirement for P_m with increasing dilution, and C-149 is a low molecular weight polymer whose requirement for P_m is independent of dilution. Nothing definite can be said about C-3 and C-5 because no molecular weight data were supplied by the manufacturer. However, based on the above-mentioned theory, it is surmised that C-3 has a molecular weight between 1 and 5 million, while C-5 has a molecular weight greater than 5 million.

Crystalline Silica. The behavior exhibited by the suspension of crystalline silica flocculated by Superfloc 16 is unexpected and differs markedly from the results obtained previously with either phosphate slimes⁷ or amorphous silica dispersions.¹ The general shapes of the curves suggest a *square root relationship* between the optimum polymer concentration, P_m , and the solid content, W (see Fig. 3). Furthermore, MIN-U-SIL 30 seems to represent the limiting solid particle size of crystalline silica above which the relationship returns to the linear form previously reported for other systems such as amorphous silica polymer¹ and AgBr polyelectrolyte⁸ suspensions. No explanation of this critical particle size is immediately apparent.

Although these results were unexpected, they nevertheless proved to be self-consistent. For example, at any given solid content, the optimum concentration of polymer increased with decreasing average particle size and increasing area as expected from eq. 4 and the results obtained with clays.⁹ In addition, Fig. 4 shows that for all the systems except MIN-U-SIL 30, P_m increased with dilution, thus exhibiting the same behavior as with amorphous silica. This plot focuses vividly on the effects of varying both the crystalline nature and particle size of the suspended material. It should also be noted in passing, that except for MIN-U-SIL 5 in the range of low solids content, considerably more polymer was necessary to reach the optimum in the amorphous system than in the crystalline one despite the larger particle size of the former. Although displaced vertically, the amorphous silica curve exhibited behavior intermediate between the MIN-U-SIL 15 and MIN-U-SIL 30 crystalline samples.

Figure 5 shows that the cationic polymer, ET-494, and the almost nonionic polymer, PAM 3, flocculating MIN-U-SIL 5 exhibit a behavior typical of the phosphate slimes studied by La Mer and Smellie, *i.e.*, P_m varying with W^2 (ref. 5). For these two polymers, as with Superfloc 16, MIN-U-SIL 30 appears to represent the limiting particle size of crystalline material above which P_m varies linearly with W .

P_m decreases with increasing molecular weight of polymer for a given solid and solid content except in the

case of the Superfloc 16 with MIN-U-SIL 5. Superfloc 16 seems to be particularly effective in flocculating MIN-U-SIL 5 even at concentrations of $1/3$ to $1/9$ those of PAM 3 and ET-494.

Examination of Fig. 6 and comparison with Fig. 6 of ref. 1 reveals the extreme sensitivity of flocculated systems to: (1) changes in the polymer flocculant, (2) changes in the crystalline nature of the suspended material, and (3) changes in the average particle size or total surface area of the suspended solid.

The theory postulated originally by Kane, La Mer, and Linford² describes the functionality of the optimum polymer concentration with varying solid content in terms of the number of polymer segments adsorbed per polymer molecule, β ; β remains constant with dilution when MIN-U-SIL 30 is the suspended solid, but behaves in a fashion analogous to the amorphous silica when MIN-U-SIL 5 is flocculated by PAM 3 and Superfloc 16 (ref. 2). Again, it is worth noting that, in the case of both polymers, the behavior with amorphous silica was intermediate between that of MIN-U-SIL 5 and MIN-U-SIL 30. Obviously, β must be a function of the particle size of the suspended material as well as the polymeric flocculating agent. While an explanation of the anomalous results obtained with ET-494 is not immediately apparent, the relative sizes of the polymer chain and the particle may be another variable of the system which has not been considered sufficiently, but may cause a change in β with increasing dilution.

It should be emphasized that the bonding between particle and polymer and hence the effectiveness of bridging need not be a function of only the specific chemical interactions occurring and the particle size or total solid surface area, but may also involve the microscopic physical characteristics of the solid surface itself. In any event, the data presented herein strengthen our contention that the specific nature of the short-range chemical interactions are extremely important in flocculated systems.

Acknowledgment. The authors acknowledge the valuable assistance of Theodore Bielen and Robert Power whose measurements supplied many of the data for this publication. We thank the American Cyanamid Company, Rohm and Haas, and Union Carbide Chemicals Company for the polymer samples which they so kindly supplied. The work was conducted under U.S.P.H.S. Grant WP 00240-02.

(7) V. K. La Mer, R. H. Smellie, and P. K. Lee, *J. Colloid Sci.*, **12**, 566 (1957).

(8) S. Kratochvil, B. Tezak, and J. P. Kratochvil, *ibid.*, **19**, 373 (1964).

(9) W. F. Langelier, H. F. Ludwig, and R. G. Ludwig, *Proc. Am. Soc. Civ. Engrs.*, **78**, Separate No. 118 (Feb., 1952).

Molecule-Wall Collisions in Porous Media at Low Gas Pressure

by William S. Horton

*Advanced Technology Laboratories, General Electric Company, Schenectady 5, New York
(Received March 20, 1964)*

It is shown by applying the cosine law of molecular reflection derived by Knudsen that the expected number of wall collisions experienced by a gaseous molecule chemically produced within a double open-ended pore at low pressure is given approximately for a zero-order reaction by $1/6(L/r)^2$, where L is the length of the pore and r the radius. Corresponding results for partially utilized pores, pores closed at one end, and for first-order surface reactions in pores open at both ends are $(f(3-f)/12)(L/r)^2$, $(2/3)(L/r)^2$, and $(1/2) \cdot (L/r)^2(h \cosh(h) - \sinh(h))/h^2 \sinh(h)$, respectively, where f is the fraction of the pore utilized, h is the dimensionless quantity $L\sqrt{k/2rD}$, k is the intrinsic first-order surface reaction rate constant, and D is the gaseous diffusion constant within the pores.

Introduction

The physicochemical influence of catalysts has an extensive literature, and reference is particularly appropriate to Wheeler,¹ who has treated the effect of pores extensively, following some initial work of Thiele.² Wheeler's results have been applied to the direct, ostensibly uncatalyzed, reaction between oxygen and porous graphite.³ These investigators have shown that the apparent order of a chemical reaction will be changed from the true order by slow diffusion of reactant into the pores. When such diffusion is significant, a surface-gas reaction truly j th order with respect to concentration of the gaseous reactant exhibits an apparent order of $(j+1)/2$ to the observer.⁴ Also, the effective diffusion coefficient for a gas at low pressure within a pore is independent of the pressure, to a first order of approximation. This arises because, as shown by Knudsen,⁵ the simple law $D = \lambda\bar{c}/3$ which applies to ordinary pressures must now be replaced by $D = 2r\bar{c}/3$; where D is the diffusion coefficient, λ is the "mean free path," \bar{c} is the mean molecular velocity, and r is the radius of the pore. At sufficiently low pressures, the mean free path becomes equal to the diameter of the pore. Knudsen observed this result and derived it theoretically by assuming that molecules colliding with the pore walls undergo diffuse, rather than specular, reflection. Regardless of the angle of incidence, the probability that reflection will occur at an angle θ is proportional solely to \cos

θ , where θ is the angle between the reflected path and the normal to the surface at the point of contact.

Although the effects mentioned above have been extensively treated, apparently the influence on the number of molecule-wall collisions within the pores has not. Obviously this is of importance in understanding the mechanisms of heterogeneous chemical reactions because the "primary product" may be altered by secondary reactions if many such collisions occur before the product molecules leave the pores; particularly since after collision a molecule is thought to "rest" at the site before leaving.⁵ In what follows approximate expressions for the average number of molecule-wall collisions undergone by a product molecule as a function of the pore dimensions and surface reaction rates are derived.

Statement of the Problem

Consider a porous material undergoing chemical reaction with a gaseous species. Only those reaction rate magnitudes are assumed here such that gaseous diffusion within the pores is a significant kinetic step

(1) A. Wheeler, "Advances in Catalysis," Vol. III, Academic Press, Inc., New York, N. Y., 1951, pp. 249-327.

(2) E. W. Thiele, *Ind. Eng. Chem.*, **31**, 916 (1939).

(3) G. Blyholder and H. Eyring, *J. Phys. Chem.*, **61**, 682 (1957); **63**, 1004 (1959).

(4) Reference 1, p. 282.

(5) M. Knudsen, *Ann. Physik*, **28**, 75 (1909).

in the mechanism. Consider that primary product molecules are produced as a result of reaction over the interior surface of a right circular cylinder open at both ends. (Pore geometry is specified at this point for simplicity of exposition only.) A typical molecule may follow the path shown in Fig. 1. In general,

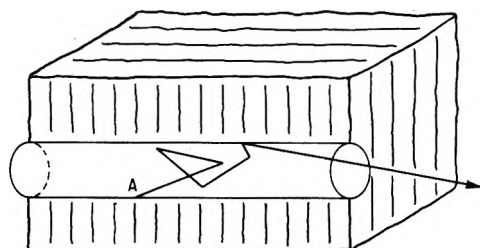


Figure 1.

let n be the number of collisions for an escaping molecule. Assume there is no interference between molecule trajectories, reasonable for low pressures where the mean free path is quite long. Then given an assembly of product molecules, the number of wall collisions prior to escape for each molecule is an independent realization of the random variable n . The variable, n , ranges from zero to infinity with the probability of n collisions given by $\text{Prob}(n)$ and with

$$\sum_{n=0}^{\infty} \text{Prob}(n) = 1$$

This last statement assumes that a molecule is sure to escape once produced. It is desired to calculate the expected (mean) value of n , or

$$\mu = \sum_{n=0}^{\infty} n \text{Prob}(n)$$

In principle if an expression can be obtained for $\text{Prob}(n)$ the required computation is trivial. However, note that within a pore for any given product molecule the probability of escape is dependent upon its nascent position within the pores (signified as x , the distance from one end) and an angle ϕ which the trajectory plane makes with the cylindrical pore axis. (The trajectory plane is defined as that plane passing through both the normal to the surface at the point of production and through the trajectory.)

For example, consider Fig. 2 with respect to determining $\text{Prob}(0)$, the probability that molecules produced in the surface element dS leave the pore without further contact. Without loss of generality the pore has been rotated about the cylinder axis so that the normal AC to the element of surface at A , dS (not shown), is

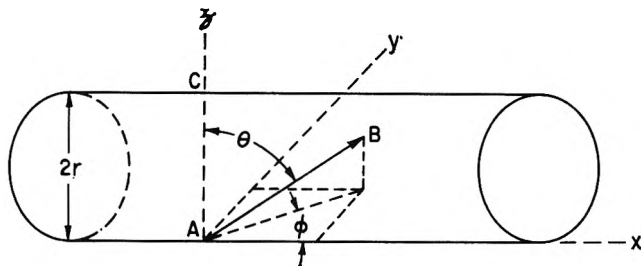


Figure 2.

normal to the z -axis. For molecules produced on dS , the probability of escape without wall collision is proportional to $\cos \theta d\theta$ and this is a function of x and $L - x$ (for escape from the left-hand opening) for a pore of length L . It is also obvious that the probability of escape is a function of the angle ϕ .

General Solution

At a given distance, x , from the mouth of the pore $\text{Prob}(n, x)$ represents the combined probability that the molecule was produced at point x and experienced n wall collisions before leaving the pore. $\text{Prob}(n/x)$ represents the probability that if the molecule were produced at x , n is the wall-collision number. $\text{Prob}(x)$ is the probability that the molecule was produced at x . By a fundamental rule of combinatorial probabilities, then

$$\text{Prob}(n, x) = \text{Prob}(n/x) \times \text{Prob}(x) \quad (1)$$

Equation 1 applies to the two-dimensional sample space consisting of the integers $0 \leq n \leq \infty$, and the continuous variable $0 < x < L$. The expected value of n is to be computed within this sample space. Because of eq. 1 this can be obtained from

$$\mu = \frac{\int_0^L \left[\sum_0^{\infty} n \text{Prob}(n/x) \right] \text{Prob}(x) dx}{\int_0^L \left[\sum_0^{\infty} \text{Prob}(n/x) \right] \text{Prob}(x) dx} = \frac{\int_0^L \left[\sum_0^{\infty} n \text{Prob}(n/x) \right] \text{Prob}(x) dx}{\int_0^L \text{Prob}(x) dx} \quad (2)$$

where the second equality follows as long as the normalizing condition

$$\sum_0^{\infty} \text{Prob}(n/x) = 1, 0 < x < L \quad (3)$$

is assured. Equations 2 and 3 supply a general solution to the stated problem insofar as neither geometry of pores nor order of reaction has been specified. Geometry of pores will enter an evaluation of $\text{Prob}(n/x)$

and $\text{Prob}(x)$. Mathematical description of the chemical reaction kinetics will enter an evaluation of $\text{Prob}(x)$. In what follows, a few simple cases are treated from the approximate viewpoint of the mean forward step within the pore.

That eq. 2 is difficult to evaluate arises, of course, because the summation includes the factor $\text{Prob}(n/x)$. $\text{Prob}(x)$ involves the pore surface distribution of created molecules which is determined by the chemical kinetics, but $\text{Prob}(n/x)$ involves also the pore surface distribution of wall collision sites. $\text{Prob}(0/x)$ may be expressed analytically, but expressing $\text{Prob}(n/x)$ becomes progressively more difficult as n increases. Since even elementary argument shows that μ is large, prohibitively many contributions to the summation are required. The view is taken here that a mean forward step within the pore can be assigned to the molecule, and that this represents the expected value of the distance traveled toward a pore mouth between successive collisions irrespective of whether this is toward the right or toward the left. This concept is related to that used to derive the diffusion constant for low pressure gas within a pore.⁵ Thus, in the figure, AB represents an actual trajectory. The mean forward step is defined as the expected value of the projection of AB on the x axis, and its magnitude is represented by l . A is a reaction (or collision) site. B is the first (or next) collision site. Although a circular cylindrical pore has been pictured, the remarks to this point apply to any pore geometry.

The actual series of wall collisions which lead to exit from the pore is now replaced by a stepwise process whereby after creation on the pore surface, or arrival by collision, the molecule moves either to the left or to the right one step of magnitude l and with equal probability for the two directions. This is a reasonable and useful picture of the process because (a) since μ is large very many steps are generally involved and use of an "average" length of steps is a good approximation and (b) any application of the results to chemical reactions in porous media will involve more serious approximations arising from attempts to ascribe a particular geometry to the system of pores. As a result of this process replacement, the problem of evaluating $\sum n \text{Prob}(n/x)$ becomes the classic random walk in one dimension. Feller⁶ has treated the "gambler's ruin" variation of linear random walk by the use of difference equations, calling D_z the duration of the game. If we normalize variables by the transformations

$$z = x/l, a = L/l \quad (4)$$

Then $\sum n \text{Prob}(n/z)$ equals D_z and eq. 2 becomes

$$\mu = \frac{\int_0^a D_z \text{Prob}(z) dz}{\int_0^a \text{Prob}(z) dz} \quad (5)$$

Further progress toward a solution now depends upon pore geometry and the detailed nature of the chemical reaction. One further step can be added, however, which particularizes only some of the pore geometry.

Assume a perfectly straight pore and consider the cases: (I) open at both ends and (II) closed at one end; then expressions for D_z may be inserted in (5). The solution of the "gambler's ruin" by Feller is given by case I. The equation to solve is

$$D_z = (1/2)D_{z+1} + (1/2)D_{z-1} + 1 \quad (6)$$

with the boundary conditions⁷

$$\text{case I: } D_0 = D_a = 0 \quad (7)$$

$$\left. \begin{array}{l} \text{case II: } D_0 = D_1 + 1 \\ D_a = 0 \end{array} \right\} \quad (8)$$

Feller's solution⁶ for case I and the easily demonstrated solution for case II are

$$\text{case I: } D_z = z(a - z) \quad (9)$$

$$\text{case II: } D_z = a^2 - z^2 \quad (10)$$

Zero-Order Reactions

These chemical reactions proceed at constant rate on the surface of the pore as long as some reactant gas molecules are available

$$\text{Prob}(z) = kdz \quad (11)$$

Equation 5 may now be evaluated using eq. 9, 10, and 11 to give

$$\text{case I (open pores): } \mu = (1/6)a^2 = (1/6)(L/l)^2 \quad (12)$$

$$\text{case II (one end closed): } \mu = (2/3)a^2 = (2/3)(L/l)^2$$

There are a variety of methods for computing L , and in the example given later one will be illustrated. The mean forward step within a pore depends upon geometry but estimates are available. Application of elementary theory by Knudsen long ago suggested the value $l = 2r$, where r is the pore radius for right circular cylindrical geometry and where the gas pressure

(6) W. Feller, "An Introduction to Probability Theory and Its Applications," Vol. I, 2nd Ed., John Wiley and Sons, Inc., New York, N. Y., 1957, pp. 317, 318.

(7) Feller's solution is general only for the points 0, 1, etc. Generality for a continuous z requires trigonometric factors of period one: cf. W. E. Milne, "Numerical Calculus," Princeton University Press, Princeton, N. J., 1949, p. 326. However, for case I the physical requirements $D_z = D_{a-z}$ for $0 < z < a$, $D_{a/2}' = 0$, and $D_{a/2}'' < 0$ for all a eliminates these factors. For case II, the corresponding requirements which also eliminate the trigonometric factors are: $D_{-z} = D_z$ for all $0 < z < a$, $D_z'' < 0$ for all $0 < z < a$.

is sufficiently low to give a free space mean free path $\gg 2r$. The value $2r$ follows from an argument based on diffusion and the net transport of molecules across a plane normal to the cylinder axis. Because we are not concerned with net transport but with collision numbers for which molecules going in opposite directions have no influence upon one another a direct evaluation of l according to definition is preferable.

The cosine law of molecular reflection is invoked again. For the case of chemical reaction one assumes either that the newly created product molecule obeys the same law for its first trajectory, or that the first trajectory contributes insignificantly to the over-all result. By referring to Fig. 2, using spherical coordinates with the collision site as origin and inserting $\sin \theta$ to integrate the solid angle, one obtains

$$l = \frac{\int \int (\rho \sin \theta \cos \phi) \sin \theta \cos \theta \, d\theta d\phi}{\int \int \sin \theta \cos \theta \, d\theta d\phi} = r \quad (13)$$

where the limits of integration are 0 and $\pi/2$ for both angles. The term, $(\rho \sin \theta \cos \phi)$, represents the trajectory projection in the x direction and ρ is eliminated by virtue of the equation for the cylinder: $\rho^2 \sin^2 \theta \sin^2 \phi + \rho^2 \cos^2 \theta - 2r\rho \cos \theta = 0$. It may be noted in passing that applying the same procedure in only two dimensions does yield the result $2r$.

Fractional Pore Utilization

Since, as Wheeler¹ has shown, even zero-order reactions may not completely utilize the pore it is of interest to see the effect this may have on the molecule-wall collision number. Incomplete use of the surface for purpose of reaction does not preclude the unreacting surface from providing collision sites for product molecules, so the random walk part of the treatment remains unchanged. For doubly open pores the only change is in the limits of integration for eq. 2 and its analog (5). Since both D_z and $\text{Prob}(z)$ are symmetric about $z = (a/2)$, the limits for eq. 5 may be $0 \leq z \leq fa/2$ where f is the fraction of the pore utilized by reaction. Then with eq. 9 one obtains the result

$$\mu = \frac{f(3-f)}{12} a^2 = \frac{f(3-f)}{12} \left(\frac{L}{l}\right)^2 \quad (14)$$

which reduces to eq. 12 for $f = 1$. The extension to pores closed at one end is obvious.

First-Order Reactions

The general treatment is now clear and is here extended with a minimum of comment to first-order reactions in pores open at both ends. A different chemical kinetic situation changes $\text{Prob}(z)$. From Wheeler,¹ with transformed variables

$$\text{Prob}(z) = K \cosh [h(1-2)z/a] \quad (15)$$

where K is a normalizing constant, h is the dimensionless quantity $L\sqrt{k/2rD}$, k is the specific first-order surface velocity constant, and D is the gaseous diffusion coefficient. Substitution of eq. 9 and 12 into eq. 15 leads to

$$\mu = \frac{1}{2} \left(\frac{L}{l}\right)^2 \frac{h \cosh(h) - \sinh(h)}{h^2 \sinh(h)} \quad (16)$$

Further extension of the approach is obvious, although it should be emphasized that the expression for $\text{Prob}(z)$ depends upon the detailed chemical kinetics.

Example

A calculation may be made of the expected number of collisions which a product molecule, produced within the pores of graphite, would make before leaving the pore from the data of Blyholder and Eyring.³ In order to choose the appropriate case among those derived above we consider that (a) the reaction order on the surface is zero, (b) the pores are open at both ends, and (c) the interior pore surface may or may not be utilized completely. The authors³ assumed incomplete utilization for the specimens upon which a decision was based about the CO/CO_2 ratio. For the given data (ref. 3, Table III) one can show that only the last two runs utilize less than the complete surface and that for these $f = 0.82$ and 0.90 , respectively. For the smaller of these, using the fractional pore formula merely decreases the collision by about 11%.

From the reaction rate data showing change-over from one-half- to zero-order reaction as a function of specimen thickness L is estimated to be greater than 10^{-3} cm. A more direct method for the specimens used in the deciding runs utilizes the formula $L = \sqrt{2} V_p/S_x$ (ref. 1, p. 259) where V_p/S_x is the geometric volume to surface ratio. For the half-cylindrical shell shapes used this becomes essentially $L = t/\sqrt{2}$ where t is the shell thickness, 0.1 cm. Therefore $L \simeq 7.07 \times 10^{-2}$ cm., and $(L/r) \simeq 7.07 \times 10^{-2} \div 3.7 \times 10^{-5} \simeq 2000$. Since the three-dimensional result for l is equal to r , $\mu \simeq (1/6)(L/r)^2 \simeq 7 \times 10^5$.

The Differential Thermal Analysis of Perchlorates. VI. Transient

Perchlorate Formation during the Pyrolysis of the Alkali Metal Chlorates¹

by Meyer M. Markowitz, Daniel A. Boryta, and Harvey Stewart, Jr.

Footle Mineral Company, Research and Engineering Center, Exton, Pennsylvania
(Received April 2, 1964)

The initial chemical changes in the pyrolysis of the five alkali metal (M) chlorates under a slowly rising temperature program involve the reactions: (a) $MClO_3 \rightarrow MCl + 1.5O_2$, and (b) $MClO_3 \rightarrow 0.75MClO_4 + 0.25MCl$; subsequent phenomena are associated with the decompositions of the more thermally stable perchlorates, (c) $MClO_4 \rightarrow MCl + 2O_2$. The extent of conversion of $MClO_3$ per reaction b increases in the order Li (40%) < Na (67%) < K, Rb, Cs (87%) at the expense of reaction a. The increasing order of thermal stabilities of these metal chlorates follows the decreasing polarizing powers of M^+ though the stability differences among $KClO_3$, $RbClO_3$, and $CsClO_3$ are rather small. Each of the $MClO_3$ compounds appears to possess a congruent melting point in contrast to the corresponding $MClO_4$ salts which, except for $LiClO_4$, undergo simultaneous fusion and rapid decomposition. The catalytic effects of MnO_2 additions to $MClO_3$ salts result primarily in the acceleration of reaction a. The general trends in thermal stability among compounds of the type $MClO_x$ ($x = 1, 2, 3, 4$) as a function of M and x are discussed briefly.

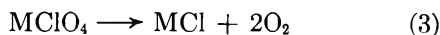
Introduction

Though the alkali metal (M) perchlorates have been extensively studied by application of differential thermal analysis (d.t.a.)^{2,3} and of thermogravimetric analysis (t.g.a.),^{3,4} the corresponding chlorates appear not to have received such systematic treatment. In the present investigation, therefore, the pyrolysis relationships among the five $MClO_3$ compounds as revealed by d.t.a. and t.g.a. are presented.

Of interest is the observation that for each $MClO_3$ salt only the initial portion of the thermal decomposition sequence involves the chlorate anion which disappears by virtue of the reactions



Thus, the succeeding pyrolytic processes refer primarily to the breakdown of $MClO_4$ as per



The extent of reaction 1 was found to increase with decreasing atomic weight of M in the order Li > Na > K, Rb, Cs; the converse being true for reaction 2.

As a group, the $MClO_3$ compounds were found to exhibit long temperature intervals between liquefaction and measurable rates of decomposition. Consequently, these chlorates, unlike the corresponding $MClO_4$ analogs with the exception of $LiClO_4$,⁵⁻⁷ effectively possess congruent melting points.

Experimental

Equipment and Procedures. D.t.a. experiments to about 800° were performed using equipment previously described⁸ in conjunction with calibrated chromel-alumel thermocouples shielded in concentric close-fitting quartz tubes. Where visual observation

(1) Presented at the 147th National Meeting of the American Chemical Society, Philadelphia, Pa., April 5-10, 1964.

(2) S. Gordon and C. Campbell, *Anal. Chem.*, **27**, 1102 (1955).

(3) M. M. Markowitz, D. A. Boryta, and R. F. Harris, *J. Phys. Chem.*, **65**, 261 (1961).

(4) G. G. Marvin and L. B. Woolaver, *Ind. Eng. Chem., Anal. Ed.*, **17**, 474 (1945).

(5) M. M. Markowitz, *J. Phys. Chem.*, **61**, 505 (1957).

(6) M. M. Markowitz, *ibid.*, **62**, 827 (1958).

(7) A. E. Simchen, *ibid.*, **65**, 1093 (1961).

(8) M. M. Markowitz, D. A. Boryta, and H. Stewart, Jr., *Inorg. Chem.*, **2**, 768 (1963).

of the test sample was desired at temperatures up to about 350°, both sample and alumina reference, contained in test tubes, were heated in a stirred silicone-fluid bath (550 Fluid, Dow Corning Corp., Midland, Mich.) in accordance with a d.t.a. method detailed earlier.⁶

Complementary t.g.a. runs to about 700° were made by procedures developed in other studies.^{9,10} In order to avoid interpreting small weight losses due to volatile impurities as indicative of the onset of sample decomposition, the t.g.a. reaction temperatures reported here correspond to the loss of 2% of the total observed weight loss, *i.e.*, the 2% decomposition temperature.

Each d.t.a. and t.g.a. experiment was performed with a 1-g. sample under a dry, flowing argon atmosphere at a linear heating rate of 4°/min.¹¹

Materials. LiClO₃ was prepared by double decomposition of Li₂SO₄ and Ba(ClO₃)₂ in aqueous media¹²; after filtration of the precipitated BaSO₄ and evaporation of water from the filtrate, the solid product obtained was dried for 2 days at 100° and 1 μ pressure. Because of the extremely hygroscopic nature of the anhydrous material, it was stored over P₂O₅ and only handled in a drybox under a dry inert atmosphere. NaClO₃ and KClO₃ were used as the commercially available reagent grade compounds after drying at 110°. RbClO₃ and CsClO₃ were made from the respective chlorides by reaction with equivalent quantities of NaClO₃ in water solution; the initial crops of sparingly soluble RbClO₃ and CsClO₃ crystals were washed, recrystallized once from water, and dried at 110°. All the chlorates were analyzed for Cl⁻ contents gravimetrically by precipitation as AgCl and for ClO₃⁻ contents as additional Cl⁻ after reduction with aqueous SO₂. *Anal.*: Calcd. for LiClO₃: ClO₃⁻, 92.3. Found: ClO₃⁻, 92.0; Cl⁻, 0.02. Calcd. for NaClO₃: ClO₃⁻, 78.4. Found: ClO₃⁻, 78.4; Cl⁻, 0.00. Calcd. for KClO₃: ClO₃⁻, 68.1. Found: ClO₃⁻, 68.1; Cl⁻, 0.00. Calcd. for RbClO₃: ClO₃⁻, 49.4. Found: ClO₃⁻, 49.4; Cl⁻, 0.00. Calcd. for CsClO₃: ClO₃⁻, 38.6. Found: ClO₃⁻, 38.6; Cl⁻, 0.00. All materials were ground to pass through a 325-mesh sieve.

Reagent grade MnO₂, of 0.72 m.²/g. specific surface area, was dried at 110°, was analyzed for total manganese by the bismuthate method and for active oxygen by oxidation of H₂C₂O₄, and was back-titrated with 0.1 N KMnO₄. *Anal.* Calcd.: Mn, 63.2; active O, 18.40. Found: Mn, 62.9; active O, 18.44.

The densities of RbClO₃ and CsClO₃ as determined by a gas pycnometer method were found to be 3.184 and 3.626 g./cc., respectively, at room temperature.

Experimental Results

D.t.a. Experiments with Pure Chlorates. The d.t.a. curves obtained for the pure MClO₃ salts are presented in Fig. 1. The pertinent data derived from these thermograms are summarized in Table I.

Table I: D.t.a. Temperatures for MClO₃ Compounds

MClO ₃	Cryst. trans., °C.	M.p., °C., T _f , MClO ₃	Onset of rapid decompn., °C., T _d , MClO ₃	ΔT = T _d - T _f	M.p., °C., MCl
LiClO ₃	111	129	367	138	607
NaClO ₃	...	263	465	202	800
KClO ₃	...	357	472	115	768
RbClO ₃	323	342	480	138	721
CsClO ₃	305	388	483	95	644

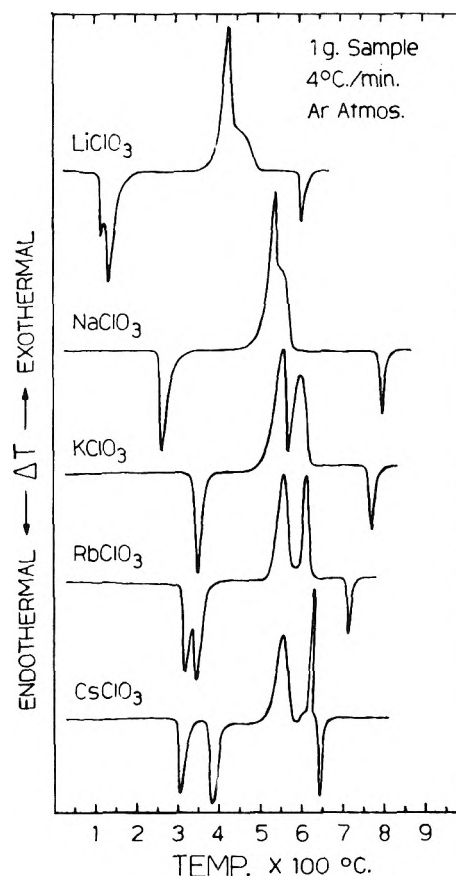


Figure 1. D.t.a. curves for pure alkali metal chlorates.

(9) M. M. Markowitz and D. A. Boryta, *Anal. Chem.*, **32**, 1588 (1960).

(10) M. M. Markowitz and D. A. Boryta, *J. Chem. Eng. Data*, **7**, 586 (1962).

(11) M. M. Markowitz, D. A. Boryta, and G. Capriola, *J. Chem. Educ.*, **38**, 96 (1961).

(12) A. Potilitzin, *J. Russ. Phys. Chem. Soc.*, **16**, 840 (1883).

(13) J. W. Retgers, *Z. physik. Chem.*, **5**, 449 (1890).

The crystallographic transition and fusion phenomena (except for the melting of CsClO_3) were also observed visually as the d.t.a. traces were recorded, thereby permitting identification of the processes relating to these endothermic breaks. Each of these phase changes was found to be reversible on three sequentially repeated heating and cooling cycles with no change in the determined invariant temperatures, thus suggesting constancy of composition despite the exposure of the chlorates to temperatures slightly above their melting points. The ($\beta \rightarrow \alpha$) polymorphism found for LiClO_3 at 111° has been reported previously¹⁴⁻¹⁶ and tends to substantiate the nonexistence^{14,15} of another transition ($\gamma \rightarrow \beta$) said to occur at 44° .¹⁶ The ($\beta \rightarrow \alpha$) phase changes determined for RbClO_3 (323°) and for CsClO_3 (305°) apparently have not been reported in the literature heretofore.

It is of interest to note that the d.t.a. curves of Fig. 1 show that the decomposition region of each of the MClO_3 salts consists of a pair of exotherms. In the instances of KClO_3 , RbClO_3 , and CsClO_3 good temperature separation is found between the two successive breaks, whereas for LiClO_3 and NaClO_3 , there is clearly some overlap of the processes giving rise to these thermal effects.¹⁷ Resolution of the nature of these pairs of exotherms will be made subsequently in this paper.

The residues from the d.t.a. runs with LiClO_3 were found to be alkaline to phenolphthalein; the reaction products from the other chlorates were neutral to this indicator. Thus, it seems likely that a portion of the LiClO_3 decomposes as per



However, in all instances, the final endotherms correspond closely to the reported melting points for the respective metal chlorides, thereby establishing reaction 1 as the ultimate, preponderant decomposition state for the pure chlorates.

Constant Temperature Experiments with Pure Chlorates. The d.t.a. curves of Fig. 1 show long temperature intervals between MClO_3 fusion and the onset of rapid chlorate decomposition as indicated by the start of the first exotherm (cf. Table I, column 5). This behavior would therefore suggest that for all practical purposes the chlorates are kinetically stable at their melting points and probably to some temperature beyond before appreciable rates of thermal decomposition are achieved. Accordingly, 4-5-g. samples of these materials were heated for 2 days under dry, flowing argon at temperatures slightly above their respective melting points. The effluent gas stream was bubbled through KI solution to ascertain

any release of chlorine; no chlorine was found to be evolved from any of the chlorate melts at the temperatures indicated in Table II. The cooled, solidified residues were pulverized and analyzed, yielding the data of Table II. Clearly, these compounds show a considerable degree of stability in the liquid phase near their melting points. This behavior is in marked contrast to the heavier MClO_4 salts where fusion and rapid thermal decomposition are concomitant occurrences.³ Thus, congruent melting points can be ascribed to each of the pure chlorates of Table II. It is to be anticipated that phase studies of anhydrous salt systems, akin to those performed with LiClO_4 , are entirely feasible with MClO_3 compounds as components.^{3,5,18,19}

Table II: Analyses of Residues of MClO_3 Salts Heated for 2 days Above Melting Point under Flowing Argon

MClO_3	M.p., MClO_3 , $^\circ\text{C}$.	Temp. of heating, $^\circ\text{C}$.	% MClO_3^a	% MCl^a	% MClO_4 , by diff. ^a
LiClO_3	129	135	99.54	0.06	0.40
NaClO_3	263	300	99.49	0.02	0.49
KClO_3	357	370	99.56	0.38	0.06
RbClO_3	342	370	98.83	0.38	0.80
CsClO_3	388	400	85.12	4.11	10.77

^a Weight %.

The partial decomposition of MClO_3 to MClO_4 (reaction 2) shown in Table II is in accord with the known behavior of MClO_3 compounds.²⁰⁻²²

Interrupted D.t.a. Runs for Pure Chlorates. The chemical reactions taking place during the thermal decompositions of the chlorates were determined by performing d.t.a. runs to the peak temperatures of

(14) A. N. Campbell and J. E. Griffiths, *Can. J. Chem.*, **34**, 1647 (1956).

(15) L. Berg, *Z. anorg. allgem. Chem.*, **155**, 311 (1926); **166**, 231 (1927); **181**, 131 (1929).

(16) C. A. Kraus and W. M. Burgess, *J. Am. Chem. Soc.*, **49**, 1225 (1927).

(17) M. M. Markowitz, D. A. Boryta, and H. Stewart, Jr., *J. Chem. Eng. Data*, in press.

(18) M. M. Markowitz and R. F. Harris, *J. Phys. Chem.*, **63**, 1519 (1959).

(19) M. M. Markowitz and D. A. Boryta, *ibid.*, **65**, 1419 (1961).

(20) T. W. Clapper, W. A. Gale, and J. C. Schumacher, "Perchlorates: Their Properties, Manufacture, and Uses," J. C. Schumacher, Ed., Reinhold Publishing Corp., New York, N. Y., 1960, pp. 71-100.

(21) C. C. Addison, "Supplement to Mellor's Comprehensive Treatise on Inorganic and Theoretical Chemistry," Supplement II, Longmans, Green and Co., London, 1956, Part I, pp. 538-539.

(22) C. E. Otto and H. S. Fry, *J. Am. Chem. Soc.*, **46**, 269 (1924).

the first exotherms of Fig. 1, quenching the sample holders in ice water, and then analyzing the final solids. The results obtained from these experiments are given in Table III. From these data it may be seen that in each instance the first break is a composite of the two simultaneously occurring reactions represented by eq. 1 and 2; and for the cases of LiClO_3 and NaClO_3 , the overlapping of the first and second exothermic breaks also indicates the occurrence of appreciable perchlorate decomposition (reaction 3) within the temperature ranges covered by the first exotherms. However, the extent of overlap cannot be estimated from these d.t.a. experiments although some quantitative measure can be estimated from the t.g.a. runs to be discussed subsequently. Nevertheless, it is clear that the second exothermic breaks in the d.t.a. patterns of Fig. 1 refer primarily to the pyrolysis of the initially formed MClO_4 compounds. It is pertinent to note from Table III that about 87% of the KClO_3 , RbClO_3 , and CsClO_3 engage in reaction 2. The extents of decomposition as per reaction 1 based on the chemical analyses contained in Table III are in good agreement with the weight loss data, as are the chlorine balances. These results would thus support the absence of any appreciable quantities of hypochlorites or chlorites as intermediates in the chlorate decompositions. However, independent weight loss and chlorine balance checks after the d.t.a. runs were not possible with LiClO_3 due to considerable sample splattering.

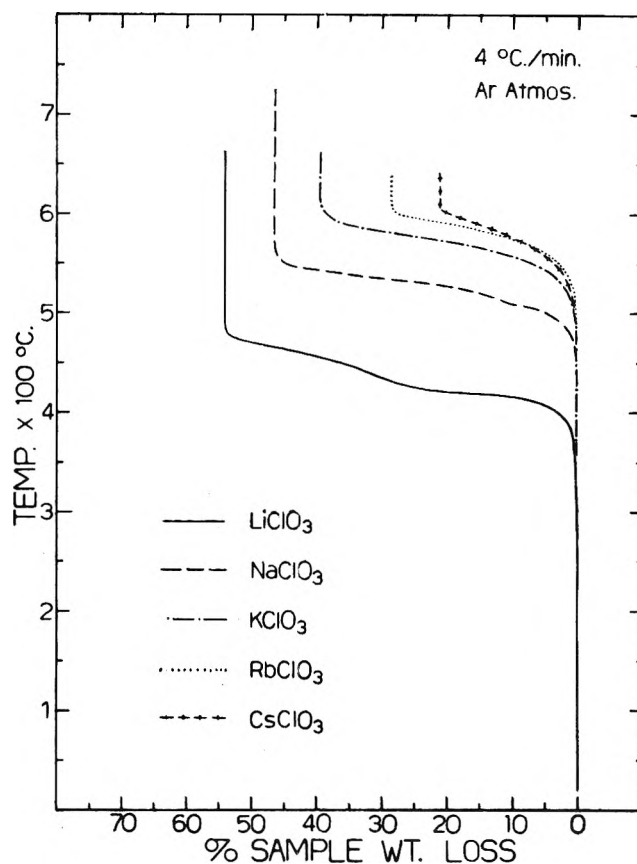


Figure 2. T.g.a. curves for pure alkali metal chlorates.

picture of the events taking place than does the t.g.a. approach.

T.g.a. Experiments with Pure Chlorates. The t.g.a. patterns obtained for the pure MClO_3 salts are presented in Fig. 2. The initial weight losses must be due to reaction 1, whereas the succeeding decrements characterize MClO_4 pyrolysis (reaction 3). The pertinent t.g.a. data are summarized in Table IV.

Table III: MClO_3 Salts Heated to Peak Temperatures of First Exotherms on D.t.a. Curves, 4°/Min. Heating Rate from Ambient

	Residue composition, mole %			% MClO_3 decomposing to $\text{MCl} + 1.5\text{O}_2$	% MClO_3 decomposing to $0.25\text{MCl} + 0.75\text{MClO}_4$	Peak temp., °C.
	% MClO_3	% MCl	% MClO_4^a			
LiClO_3^b	0.9	68.2	30.3	57.8	40.2	425
NaClO_3	2.6	47.3	50.1	30.5	66.9	542
KClO_3	0.9	33.9	65.2	12.1	87.0	566
RbClO_3	1.6	32.9	65.5	11.0	87.4	563
CsClO_3	1.3	34.0	64.7	12.4	86.3	560

^a By difference. ^b Also contains 0.6 mole % Li_2O .

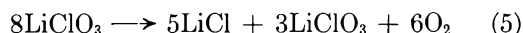
Because the formation of MClO_4 in MClO_3 melts is not accompanied by any change in sample weight but still represents a mode of MClO_3 decomposition, the d.t.a. technique tends to give a more complete

Table IV: T.g.a. Results for Pure MClO_3 Compounds

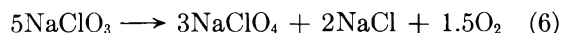
MClO_3	% of weight loss based on conversion to MCl	Temp., °C. of 2% of total weight loss
LiClO_3	102.5	384
NaClO_3	100.8	474
KClO_3	100.9	502
RbClO_3	100.7	513
CsClO_3	100.7	489

Inspection of the t.g.a. curves for LiClO_3 and NaClO_3 shows marked decreases in rates of weight loss at about

430 and 512°, respectively, corresponding to aggregate weight losses of 51.2 and 24.1% of the total final weight losses. In the case of LiClO_3 , it was shown by isothermal decomposition experiments¹⁷ and by chemical analyses of residues from interrupted t.g.a. runs of LiClO_3 ¹⁷ that the initial steps in the pyrolysis sequence of LiClO_3 can be closely represented by the over-all equation



Reaction 5 is characterized by 50% of the weight loss corresponding to complete conversion of the LiClO_3 to LiCl (reaction 1). This is then consistent with the observed t.g.a. behavior for LiClO_3 (Fig. 2) which indicates that above 430°, the resulting weight loss is due to the decomposition of LiClO_4 (reaction 3). By analogy it is felt that the decrease in rate of weight loss found for NaClO_3 is due to the slower decomposition of the more thermally stable NaClO_4 formed earlier in the temperature program by the composite reaction



It is doubtful if eq. 5 and 6 have exact stoichiometric significance in representing the chemical changes occurring during the initial heating of these chlorates; rather, such equations appear to be reflections of the relative average rates of the direct chlorate decomposition route (eq. 1) and of the disproportionation path (eq. 2). On this basis, it may be seen that for LiClO_3 the ratio, average rate reaction 1/average rate reaction 2, is approximately 1, for NaClO_3 , it is $1/4$, and for K, Rb, and CsClO_3 , it is $1/9$. Assuming that these rate ratios hold, then it can be computed that for LiClO_3 , the pair of exotherms in Fig. 2 overlap such that about 18% of the LiClO_4 originally formed decomposes by time the peak temperature is reached; for NaClO_3 , about 19% of the NaClO_4 formed decomposes in the region of decomposition overlap. Alternations in slope are not evident in the intermediate stages of decomposition in the t.g.a. curves for K, Rb, and CsClO_3 due to the occurrence of reaction 1 to only a rather small degree in a region of rapidly increasing reaction rate.

The data of Table IV show quantitatively that MCl is the major reaction product from the pyrolysis of a chlorate. However, the high weight loss found for LiClO_3 also betokens the occurrence of reaction 4 to the extent of 3.8%. Direct determination of the chlorine gas evolved from decomposing LiClO_3 showed reaction 4 to occur to the extent of 4.5%. While NaClO_3 evolved a slight trace of chlorine, the other

MClO_3 salts gave only chlorine-free oxygen upon decomposition.

Thermal Behavior of 90 Mole % MClO_3 -10 Mole % MnO_2 Mixtures. In every instance the effect of additions of MnO_2 to MClO_3 is an appreciable lowering of the thermal stability of the MClO_3 compound. Except for LiClO_3 - MnO_2 , the d.t.a. patterns of these mixtures (Fig. 3) show decomposition to become rapid soon after following a transition temperature (*viz.*, RbClO_3 - MnO_2 and CsClO_3 - MnO_2) or a fusion temperature (*viz.*, NaClO_3 - MnO_2 and KClO_3 - MnO_2). Such behavior would indicate that for the heavier MClO_3 salts, those processes resulting in enhanced freedom of movement of the ionic lattice units facilitate catalytic decomposition by MnO_2 . The t.g.a. results (Fig. 4) demonstrate slow decomposition to start for each of the MClO_3 - MnO_2 mixtures, again with the exception of the LiClO_3 - MnO_2 sample, at some temperature below the transition or melting points. It appears likely then that the observed fusion temperatures in the presence of MnO_2 refer to mixtures of MClO_3 with the decomposition products formed up to that point. How-

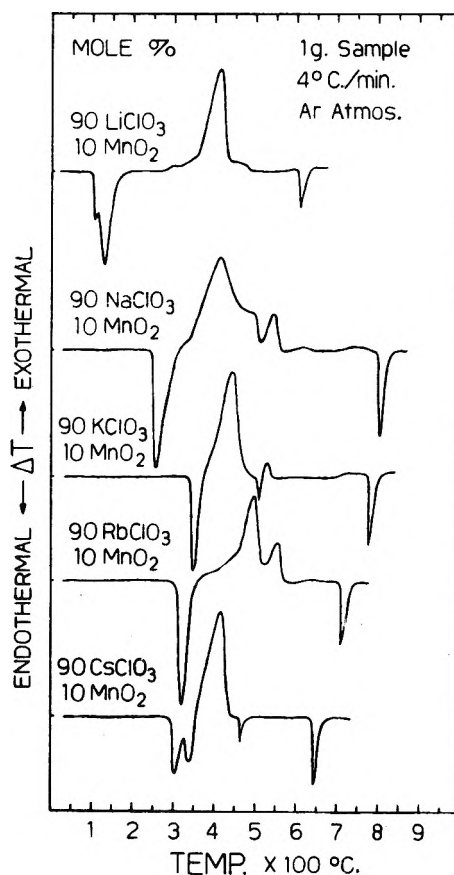


Figure 3. D.t.a. curves for 90 mole % MClO_3 -10 mole % MnO_2 mixtures.

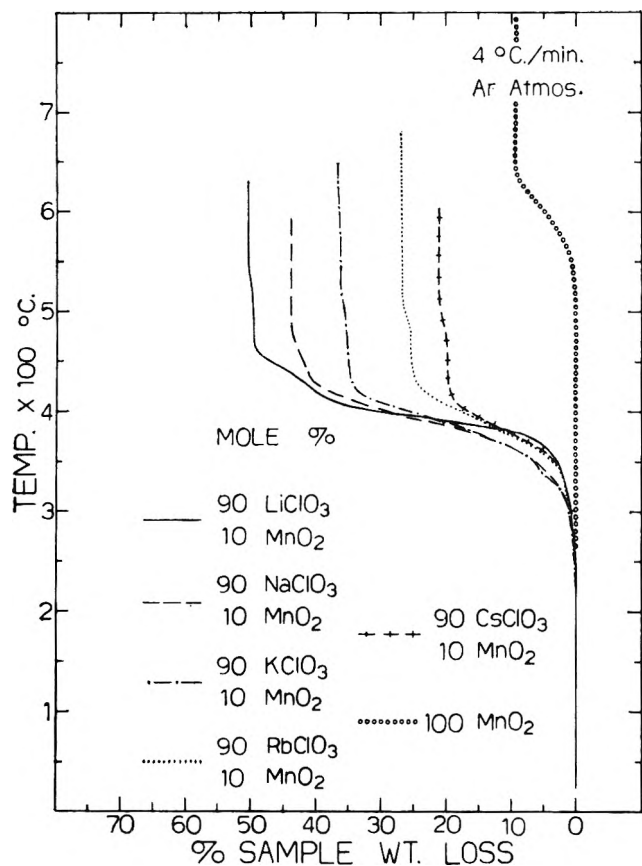


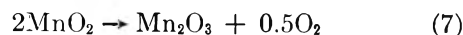
Figure 4. T.g.a. curves for 90 mole % $MClO_3$ -10 mole % MnO_2 mixtures.

ever, the d.t.a. curves of Fig. 3 show that this effect is small, probably because of the considerably higher melting points of the chlorides and perchlorates compared with the chlorates (Table I). From the t.g.a. patterns of Fig. 4 it may be seen that the catalysis by MnO_2 has resulted in a leveling of the thermal stabilities of these mixtures to very similar aspects with the consequence, for example, that for each mixture, the 2% decomposition temperature is about 300°.

Inspection of Fig. 3 and 4 suggests that the primary catalytic action of the MnO_2 is to increase the rate of reaction 1 with a resultant diminution in the extent to which reaction 2 occurs. Thus, in the d.t.a. curves for each mixture except $CsClO_3$ - MnO_2 , only small exotherms attributable to $MClO_4$ decomposition are found following the large primary decomposition exotherms. For the $CsClO_3$ - MnO_2 mixture the small endotherm at about 465° following the large exotherm is characteristic of a reversible crystallographic transition for $CsCl$.^{23,24} However, this endotherm could be a composite of exothermic $CsClO_4$ decomposition and the endothermic $CsCl$ phase change. The t.g.a. curve for $LiClO_3$ - MnO_2 manifests a decrease in rate

of weight loss at about 406° and an aggregate weight loss corresponding to about 25% conversion of $LiClO_3$ to $LiClO_4$, rather than 50% as found for pure $LiClO_3$ (Fig. 2). Comparison of the t.g.a. curves for $MClO_3$ - MnO_2 samples with those obtained for 90 mole % $MClO_4$ -10 mole % MnO_2 mixtures under similar heating conditions²⁵ shows the latter generally to have 2% decomposition temperatures about 150° higher than the former. This observation again tends to emphasize the greater thermal stabilities of $MClO_4$ salts over the corresponding $MClO_3$ compounds.

The weight loss stemming from the heating of pure MnO_2 (Fig. 4) in combination with X-ray powder patterns and active oxygen content of the residual product show the decomposition reaction to yield Mn_2O_3 as per the reaction^{26,27}



Faint traces of chlorine gas were determined in the gases evolved from the $NaClO_3$ - MnO_2 and $KClO_3$ - MnO_2 mixtures²⁸⁻³⁰; none from the $RbClO_3$ - MnO_2 and $CsClO_3$ - MnO_2 samples. The $LiClO_3$ - MnO_2 sample indicated 4.3% decomposition of $LiClO_3$ to Li_2O (reaction 4) based on chlorine release. Each of the total weight losses determined by t.g.a. for the $MClO_3$ - MnO_2 mixtures, except for $LiClO_3$ - MnO_2 , could be accounted for by reactions 1 and 7. Apparently reaction 4 does not appear to be appreciably affected by the presence of MnO_2 .

Discussion of Results

Because the disproportionation of $MClO_3$ compounds to perchlorates (reaction 2) does not involve any change in weight of the sample, the d.t.a. method is more suitable to gauging the thermal stabilities of the chlorates than is the t.g.a. method which initially at least is principally a measure of reaction 1. As evidenced by many other oxyanion salts of the alkali metals,³¹⁻³³ the thermal stabilities of the $MClO_3$

(23) C. D. West, *Z. Krist.*, **88**, 94 (1934).

(24) G. Wagner and L. Lippert, *Z. physik. Chem.*, **31B**, 273 (1936).

(25) M. M. Markowitz, D. A. Boryta, and H. Stewart, Jr., unpublished results.

(26) A. D. Mah, "Thermodynamic Properties of Manganese and Its Compounds," U. S. Bureau of Mines Report of Investigations 5600, 1960.

(27) T. E. Moore, M. Ellis, and P. W. Selwood, *J. Am. Chem. Soc.*, **72**, 856 (1950).

(28) J. M. Geidis and E. G. Rochow, *J. Chem. Educ.*, **40**, 78 (1963).

(29) O. Bostrup, K. Demandt, and K. O. Hansen, *ibid.*, **39**, 573 (1962).

(30) J. W. Mellor, "Comprehensive Treatise on Inorganic and Theoretical Chemistry," Vol. I, Longmans, Green and Co., London, 1922, p. 360.

(31) R. K. Osterheld and M. M. Markowitz, *J. Phys. Chem.*, **60**, 863 (1956).

salts are seen from the d.t.a. data presented in Table I to follow the order $\text{Li} < \text{Na} < \text{K} < \text{Rb} < \text{Cs}$. Nevertheless, as found for MClO_4 compounds,^{3,34} the range of thermal decomposition temperatures for rapid pyrolysis is quite small despite the large range of cation sizes in proceeding from Li^+ to Cs^+ (empirical ionic crystal radii in Å.³⁵: Li^+ , 0.78; Na^+ , 0.98; K^+ , 1.33; Rb^+ , 1.49; Cs^+ , 1.65). The sequence found for the MClO_4 salts at a higher heating rate and with larger sample sizes³ is $\text{Li} < \text{Na} < \text{Cs} < \text{K} < \text{Rb}$, which corresponds to the order of fusion temperatures of these materials under the prevailing heating conditions. A reflection of this fusion effect in accelerating the pyrolyses of perchlorates is readily seen in the instance of KClO_4 .^{36,37} Thus, the first-order liquid phase decomposition of KClO_4 is about 50 times faster than the corresponding first-order solid phase decomposition. It appears likely that the decompositions of all the perchlorates formed during the heating of the MClO_3 salts (Fig. 1) stem from the liquid phase due to the formation of low melting MClO_4 - MCl compositions. The observed order of thermal stabilities of the relatively low melting MClO_3 salts may be most conveniently related to the decreasing polarizing powers of ionic potentials of the cations in passing from Li^+ to Cs^+ .³⁸

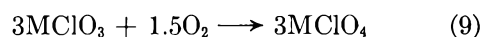
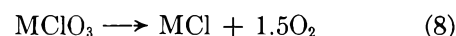
The fact that large quantities of MClO_4 are transiently formed as each MClO_3 salt is heated substantiates the greater thermal stabilities of the perchlorates in comparison to the corresponding chlorates. This, of course, can also be judged by comparing the t.g.a. and d.t.a. results previously obtained³ for pure MClO_4 compounds with the present results for the MClO_3 salts. High cation polarizing power appears to favor direct MClO_3 decomposition to MCl (reaction 1) as gauged from Table III for LiClO_3 and NaClO_3 ; with the other MClO_3 compounds, there is virtually complete participation (87%) in the disproportionation reaction (eq. 2) which leads to perchlorate formation. The temperatures at which these intermediate MClO_4 - MCl mixtures decompose rapidly correspond fairly closely to newly determined d.t.a. decomposition temperatures for the pure MClO_4 under the same conditions of sample size and heating rate used in the present study.²⁵

Addition of MnO_2 to MClO_3 results in a leveling effect relative to the observed thermal stabilities such that differences in stability previously related to polarizing effects seem to be virtually eliminated. Consequently, the t.g.a. curves (Fig. 4) for each of the MClO_3 - MnO_2 mixtures are quite similar. The d.t.a. curves for these heterogeneous samples (Fig. 3) indicate that the MnO_2 brings about acceleration of re-

action 1 at the expense of MClO_4 formation. For both the pure MClO_3 salts and the MClO_3 - MnO_2 mixtures, MCl is the ultimate primary product of thermal decomposition as would be anticipated from the greater thermodynamic stabilities of the MCl salts as compared with the equivalent oxides.^{17,34} The d.t.a. patterns of Fig. 3 emphasize the trend that processes giving rise to increased anion mobility tend to facilitate decomposition. Thus, the MClO_3 - MnO_2 mixtures are seen to decompose rapidly for each of the MClO_3 salts, except LiClO_3 , virtually immediately following or concurrent with a crystallographic transition (*i.e.*, "Hedvall effect"³⁹) or a liquefaction phenomenon.

The exothermic natures found for reactions 1, 2, and 3 are consistent with estimates made for the enthalpy changes characterizing these reactions.^{3,17}

The disproportionation reactions of the lower oxyanions of chlorine (MClO_x) to the higher oxyanions (MClO_y , where $y = 3, x = 1, 2$; $y = 4, x = 3$) may be looked upon as internal oxygenation processes. Thus, for the conversion of MClO_3 to MClO_4 , the oxygenation can be represented by the sum of the individual reactions



It can be seen from the present studies that the extent of occurrence of step 9 appears to be dependent on the nature of M . The results obtained here suggest the degree of internal oxygenation to decrease with increasing polarizing power of M so as to favor O_2 release (reaction 8). The oxygenation of MClO_x compounds to the MClO_y state seems to be a more likely occurrence than the oxygenation of MCl to MClO_y .^{40,41}

(32) W. E. Van Arkel, "Molecules and Crystals in Inorganic Chemistry," 1st Ed., Interscience Publishers, Inc., New York, N. Y., p. 118.

(33) R. T. Sanderson, "Chemical Periodicity," Reinhold Publishing Corp., New York, N. Y., 1960, pp. 162-166.

(34) M. M. Markowitz, *J. Inorg. Nucl. Chem.*, **25**, 407 (1963).

(35) J. R. Partington, "An Advanced Treatise on Physical Chemistry: The Properties of Solids," Vol. 3, Longmans, Green and Co., London, 1952, p. 137.

(36) A. E. Harvey, M. T. Edmison, E. D. Jones, R. A. Seybert, and K. A. Catto, *J. Am. Chem. Soc.*, **76**, 3270 (1954).

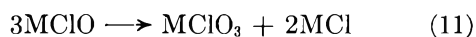
(37) A. E. Harvey, C. J. Wassink, T. A. Rodgers, and K. H. Stern, *Ann. N. Y. Acad. Sci.*, **79**, 971 (1960).

(38) G. H. Cartledge, *J. Am. Chem. Soc.*, **50**, 2855, 2863 (1928); **52**, 3076 (1930).

(39) K. Hauffe, "Reaktionen In und An Festen Stoffen," Springer-Verlag, Berlin, 1955, pp. 583, 594, 629.

(40) A. V. Bosch and A. H. W. Aten, *J. Am. Chem. Soc.*, **75**, 3835 (1953).

It is instructive to attempt to delineate the trends in thermal stability among compounds of the general type $MClO_x$ ($x = 1, 2, 3, 4$) as a function of both M and x . In the present study, the conversion of $MClO_3$ to $MClO_4$ in the course of thermal decomposition was demonstrated to occur for each $MClO_3$ salt. $MClO_2$ and $MClO$ salts are known to form appreciable amounts of $MClO_3$ at elevated temperatures as per the over-all reactions^{21,42}



Accordingly, it seems clear that for a given M , the order of thermal stability for $MClO_x$ compounds is $MClO_4 > MClO_3 > (MClO_2, MClO)$. Significantly, this is also similar to the order of extent of π -bonding for these oxyanions of chlorine, *i.e.*, $ClO_4^- > ClO_3^- > ClO_2^- > ClO^- = 0$.⁴³⁻⁴⁵ Though little information is available relative to the entire families of $MClO_2$

and $MClO$ compounds, it appears reasonable that, other factors being equal, for a given value of x , the thermal stabilities of the compounds $MClO_x$ will be principally determined by the degree of anion polarization and will therefore be in the sequence $LiClO_x > NaClO_x > KClO_x > RbClO_x > CsClO_x$. However, as seen in the instances of the chlorates and perchlorates, the differences in thermal stabilities manifested by the K , Rb , and Cs salts of the same anion are rather small, thereby suggesting a limit in the effect of the diminution of cation polarizing power toward these anions below the ionic potential of K^+ .

(41) A. Glasner and L. Weidenfeld, *J. Am. Chem. Soc.*, **74**, 2464 (1952).

(42) R. B. Heslop and P. L. Robinson, "Inorganic Chemistry," Elsevier Publishing Co., New York, N. Y., 1960, pp. 380-384.

(43) E. L. Wagner, *J. Chem. Phys.*, **37**, 751 (1962).

(44) E. Cartmell and G. W. A. Fowles, "Valency and Molecular Structure," Academic Press, Inc., New York, N. Y., 1956, pp. 179, 180.

(45) H. G. Palmer, "Valency: Classical and Modern," 2nd Ed., Oxford University Press, London, 1959, p. 154.

A Mass Spectrometric Study of Some Alkyl-Substituted Phosphines¹

by Yasuo Wada and Robert W. Kiser

Department of Chemistry, Kansas State University, Manhattan, Kansas (Received April 2, 1964)

The appearance potentials of positive ions in the mass spectra of trimethylphosphine, triethylphosphine, monomethylphosphine, and monoethylphosphine are reported. Assignments of the probable processes of ionization and dissociation made are consistent with the observed energetics from the electron impact data. The molecular ionization potentials of trimethylphosphine, triethylphosphine, monomethylphosphine, and monoethylphosphine were determined to be 8.60, 8.27, 9.72, and 9.61 e.v., respectively. The molecular ionization potentials of these compounds were in good agreement with those calculated using the group orbital method (8.35 e.v. for triethylphosphine, 9.53 e.v. for monomethylphosphine, and 9.40 e.v. for monoethylphosphine). The ionization potential of methinophosphide, HCP, is derived to be 13.0 ± 0.6 e.v.

Introduction

We have studied previously the phosphorus hydrides phosphine and diphosphine by using mass spectrometric methods.² In the course of further investigation of phosphorus compounds, we have extended our studies to the alkyl-substituted phosphines, trimethyl-, triethyl-, monomethyl-, and monoethylphosphine.

In this paper we report the information obtained on the above compounds, including the mass spectral cracking patterns and appearance potentials for the principal positive ions. From the measured appearance potentials, probable processes are postulated for the formation of the various positive ions consistent with the energetic data.

Experimental

The experimental data reported here were obtained using a Bendix time-of-flight mass spectrometer. The instrumentation has been described previously.³ The mass spectra were obtained at a nominal electron energy of 70 e.v. Appearance potentials were determined by the extrapolated voltage difference method.⁴ The technique of Lossing, Tickner, and Bryce⁵ and the energy compensation method⁶ also were used. Calibration of the voltage scale in the determination of ionization and appearance potentials was accomplished by mixing xenon with the compound being investigated.

The samples of trimethylphosphine and triethyl-

phosphine were prepared similar to the method described by Hibbert.⁷ The prepared trialkylphosphines were finally separated from the reaction mixture as the silver iodide complex.⁸ This complex is very stable and provided significant aid in the necessary handling processes. The samples of pure trialkylphosphines were prepared by the simple thermal decomposition of the trialkylphosphine-silver iodide complex in a vacuum system followed by fractional distillation steps using liquid nitrogen as the refrigerant.

The samples of monomethylphosphine and monoethylphosphine were prepared both in a similar manner⁹ and by the same method.¹⁰ A slight modification,

(1) This work was supported in part by the U. S. Atomic Energy Commission under Contract No. AT(11-1)-751 with Kansas State University. Portion of a dissertation submitted by Y. Wada to the Graduate School of Kansas State University in partial fulfillment of the requirements for the degree of Doctor of Philosophy.

(2) Y. Wada and R. W. Kiser, *Inorg. Chem.*, **3**, 174 (1964).

(3) E. J. Gallegos and R. W. Kiser, *J. Am. Chem. Soc.*, **83**, 773 (1961).

(4) J. W. Warren, *Nature*, **165**, 810 (1950).

(5) F. P. Lossing, A. W. Tickner, and W. A. Bryce, *J. Chem. Phys.*, **19**, 1254 (1951).

(6) R. W. Kiser and E. J. Gallegos, *J. Phys. Chem.*, **66**, 947 (1962).

(7) H. Hibbert, *Ber.*, **39**, 160 (1906).

(8) F. G. Mann, A. F. Wells, and D. Purdie, *J. Chem. Soc.*, 1828 (1937); F. G. Mann and A. F. Wells, *ibid.*, 708 (1938).

(9) N. Davidson and H. C. Brown, *J. Am. Chem. Soc.*, **64**, 719 (1942).

(10) R. I. Wagner and A. B. Burg, *ibid.*, **75**, 3869 (1953).

using an inert atmosphere of nitrogen, was made so as to conduct the reaction under atmospheric pressure rather than in a vacuum system. The prepared samples were then fractionally distilled until reasonably pure samples were obtained.

Results

The partial mass spectral cracking patterns and the clastograms which were obtained are given in Fig. 1-4. Experimentally determined mass spectra and appearance potentials for the principal positive ions formed from the compounds investigated are given in columns 2 and 3 of Tables I-IV. Peaks at $m/e = 14, 16, 28,$ and 32 have been omitted because of unknown contributions from nitrogen and oxygen. The probable processes for the formation of the various ions and the heats of formation consistent with the proposed processes are presented in columns 4 and 5 of Tables I-IV.

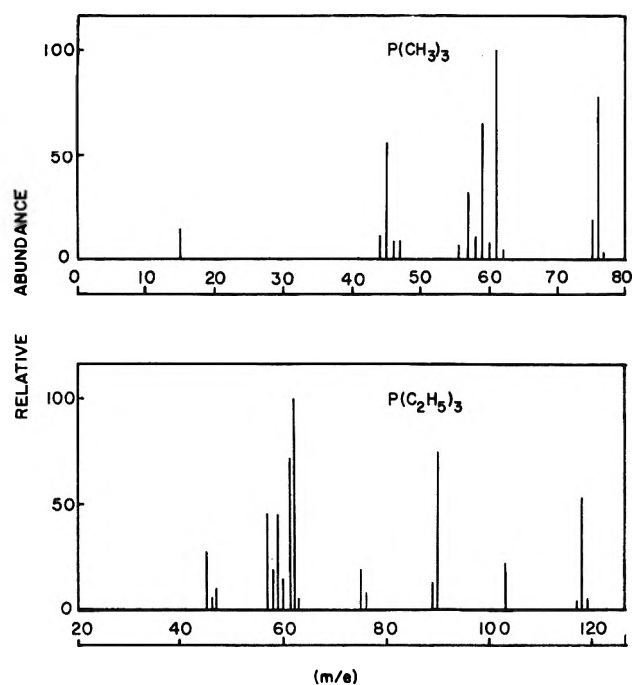


Figure 1. 70-e.v. mass spectra of trimethyl- and triethylphosphine.

The heat of formation of trimethylphosphine in the gas phase is -23.2 kcal./mole.¹¹ Since the heats of formation of triethyl-, monomethyl-, and monoethylphosphine were not available in the literature, we deduced the values from the known values for trimethylphosphine and phosphine (1.3 kcal./mole¹²) to be -38 kcal./mole, -7 kcal./mole, and -12 kcal./mole, respectively, using the method of Franklin.¹³ Other

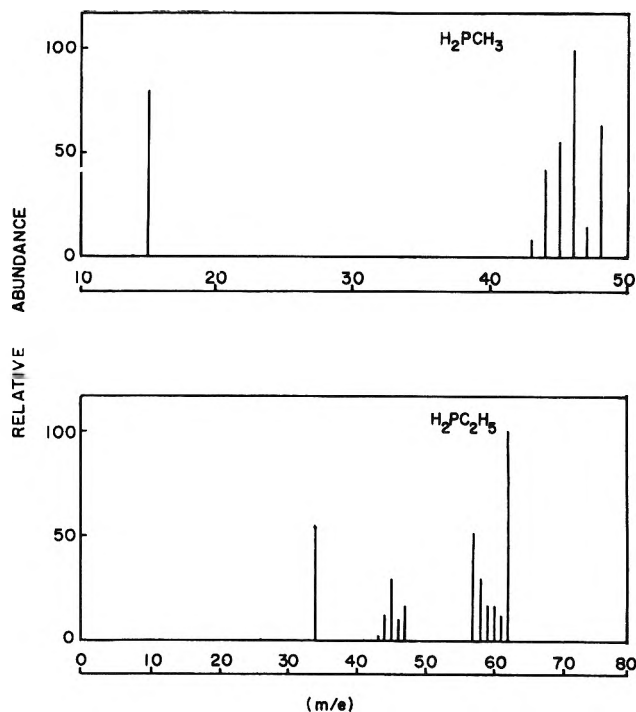


Figure 2. 70-e.v. mass spectra of monomethyl- and monoethylphosphine.

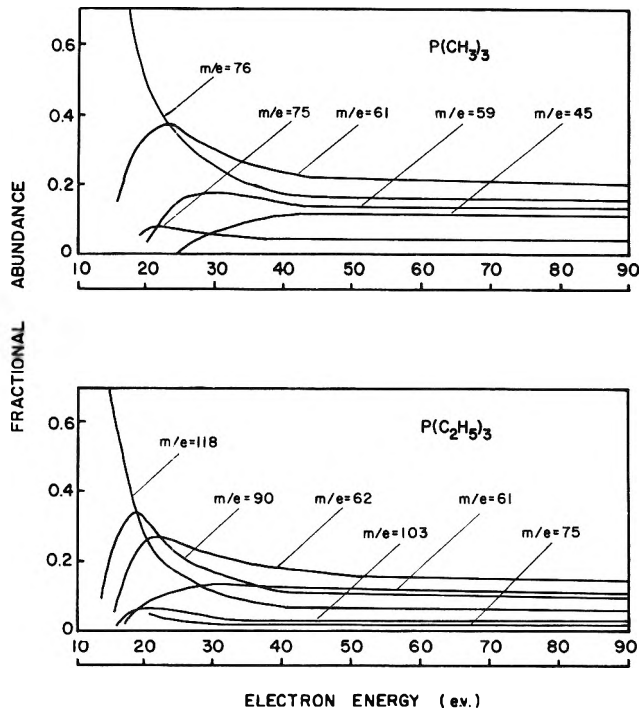


Figure 3.—Clastograms for trimethyl- and triethylphosphine.

(11) L. H. Long and J. F. Sackman, *Trans. Faraday Soc.*, **53**, 1606 (1957).

(12) S. R. Gunn and L. G. Green, *J. Phys. Chem.*, **65**, 779 (1961); S. R. Gunn, *ibid.*, **68**, 949 (1964).

(13) J. L. Franklin, *Ind. Eng. Chem.*, **41**, 1070 (1949).

Table I: Appearance Potentials and Heats of Formation of the Principal Ions from Trimethylphosphine

<i>m/e</i>	Relative abundance	Appearance potential, e.v.	Probable process	ΔH_f (ion), kcal./mole
15	15.2		$P(CH_3)_3 \rightarrow CH_3^+ + (?)$	
34	0.8			
35	0.7	14.2 ± 0.2	$\rightarrow PH_4^+ + CH_3 + C_2H_2$	218
43	1.1	13.2 ± 0.3	$\rightarrow PC^+ + CH_3 + H_2 + CH_4$	267
44	12.1	18.4 ± 0.2	$\rightarrow PCH^+ + 2CH_3 + H_2$	337
45	56.4	16.1 ± 0.4	$\rightarrow PCH_2^+ + 2CH_3 + H$	232
46	10.3	14.0 ± 0.3	$\rightarrow PCH_3^+ + C_2H_4 + H_2$	287
47	11.4	14.7 ± 0.2	$\rightarrow HPCH_3^+ + CH_3 + CH_2$	216
57	32.8	16.7 ± 0.2	$\rightarrow PC_2H_2^+ + CH_3 + 2H_2$	330
58	11.8			
59	66.2	14.0 ± 0.2	$\rightarrow P(CH_2)_2^+ + CH_3 + H_2$	268
60	9.4			
61	100.0	11.7 ± 0.2	$\rightarrow P(CH_3)_2^+ + CH_3$	215
62	4.1			
75	20.0	10.2 ± 0.5	$\rightarrow (H_3C)_2PCH_2^+ + H$	160
76	78.2	$8.6_0 \pm 0.2$	$\rightarrow P(CH_3)_3^+$	175
77	3.0			

Table II: Appearance Potentials and Heats of Formation of the Principal Ions from Triethylphosphine

<i>m/e</i>	Relative abundance	Appearance potential, e.v.	Probable process	ΔH_f (ion), kcal./mole
34	6.6	14.7 ± 0.2	$PC_6H_{16} \rightarrow PH_3^+ + 3C_2H_4$	264
35	1.1	14.7 ± 0.3	$\rightarrow PH_4^+ + C_2H_3 + 2C_2H_4$	212
45	29.0	19.1 ± 0.5	$\rightarrow PC^+ + 2C_2H_6 + CH_3$	295
46	4.7	17.9 ± 0.5	$\rightarrow PCH_3^+ + C_2H_5 + C_2H_4 + CH_3$	313
47	9.8	15.8 ± 0.2	$\rightarrow HPCH_3^+ + C_2H_5 + C_2H_4 + CH_2$	224
57	46.9	16.5 ± 0.3	$\rightarrow PC_2H_2^+ + C_2H_5 + C_2H_4 + 2H_2$	309
58	20.7	16.7 ± 0.2	$\rightarrow PC_2H_3^+ + 2C_2H_5 + H_2$	303
59	45.7	16.0 ± 0.2	$\rightarrow PC_2H_4^+ + 2C_2H_5 + H$	235
60	14.5	13.4 ± 0.5	$\rightarrow PC_2H_5^+ + C_2H_4 + C_2H_6$	279
61	73.0	14.0 ± 0.2	$\rightarrow HPC_2H_5^+ + C_2H_5 + C_2H_2 + H_2$	209
62	100.0	12.7 ± 0.2	$\rightarrow H_2PC_2H_5^+ + 2C_2H_4$	230
63	5.0			
75	19.5	13.8 ± 0.5	$\rightarrow (H_3C)_2PCH_3^+ + C_2H_5 + CH_2$	190
76	8.1			
89	14.1	11.4 ± 0.3	$\rightarrow P(C_2H_5)_2^+ + C_2H_5$	203
90	75.6	10.7 ± 0.3	$\rightarrow HP(C_2H_5)_2^+ + C_2H_4$	196
103	22.8	12.0 ± 0.2	$\rightarrow (H_3C)_2PCH_2^+ + CH_3$	207
118	52.7	8.27 ± 0.24	$\rightarrow P(C_2H_5)_3^+$	153

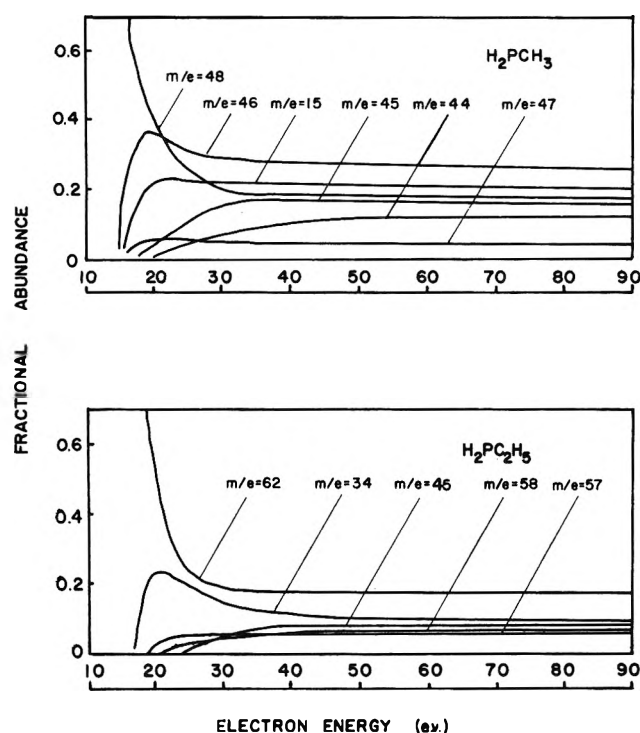
Table III: Appearance Potentials and Heats of Formation of the Principal Ions from Monomethylphosphine^a

<i>m/e</i>	Relative abundance	Appearance potential, e.v.	Probable process	ΔH_f (ion), kcal./mole
15	79.7	14.8 ± 0.2	$H_2PCH_3 \rightarrow CH_3^+ + PH_2$	309
43	8.3	14.5 ± 0.3	$\rightarrow PC^+ + H + 2H_2$	275
44	42.6	14.7 ± 0.3	$\rightarrow PCH^+ + 2H_2$	332
45	56.6	14.7 ± 0.2	$\rightarrow PCH_2^+ + H + H_2$	280
46	100.0	12.2 ± 0.2	$\rightarrow PCH_3^+ + H_2$	274
47	15.8	11.6 ± 0.12	$\rightarrow HPCH_3^+ + H$	208
48	63.7	9.72 ± 0.15	$\rightarrow H_2PCH_3^+$	217

^a Peaks of *m/e* = 31, 32, 33, and 34, due to PH₃ impurities, have been omitted.

Table IV: Appearance Potentials and Heats of Formation of the Principal Ions from Monoethylphosphine

m/e	Relative abundance	Appearance potential, e.v.	Probable process	ΔH_f (ion), kcal./mole
34	53.2	11.2 ± 0.2	$\text{PC}_2\text{H}_2 \rightarrow \text{PH}_3^+ + \text{C}_2\text{H}_4$	234
43	25.3	12.0 ± 0.3	$\rightarrow \text{PC}^+ + \text{CH}_3 + 2\text{H}_2$	233
44	14.4	13.1 ± 0.5	$\rightarrow \text{PCH}^+ + \text{CH}_4 + \text{H}_2$	308
45	35.2	12.7 ± 0.4	$\rightarrow \text{PCH}_2^+ + \text{CH}_3 + \text{H}_2$	249
46	10.9	12.0 ± 0.2	$\rightarrow \text{PCH}_3^+ + \text{CH}_4$	283
47	19.7	12.2 ± 0.2	$\rightarrow \text{HPCH}_3^+ + \text{CH}_3$	238
57	50.7	15.8 ± 0.3	$\rightarrow \text{PC}_2\text{H}_2^+ + 2\text{H}_2 + \text{H}$	300
58	35.2	12.9 ± 0.4	$\rightarrow \text{PC}_2\text{H}_3^+ + 2\text{H}_2$	291
59	19.4	12.9 ± 0.3	$\rightarrow \text{PC}_2\text{H}_4^+ + \text{H} + \text{H}_2$	238
60	18.7	12.0 ± 0.2	$\rightarrow \text{PC}_2\text{H}_5^+ + \text{H}_2$	265
61	13.2	12.0 ± 0.3	$\rightarrow \text{HPC}_2\text{H}_5^+ + \text{H}$	213
62	100.0	9.47 ± 0.5	$\rightarrow \text{H}_2\text{PC}_2\text{H}_5^+$	206

**Figure 4.** Clastograms for monomethyl- and monoethylphosphine.

heats of formation employed in our thermochemical calculations were those tabulated by Gallegos.¹⁴

The molecular ionization potentials of the alkyl-substituted phosphines investigated are summarized in Table V and compared with the calculated values using the group orbital method.^{15,16} It is seen that the ionization potentials determined experimentally are in good agreement with the calculated values.

Discussion

$m/e = 34$. This ion can only be PH_3^+ and is observed from both triethylphosphine and monoethyl-

Table V: Molecular Ionization Potentials of the Alkyl-Substituted Phosphines

Molecule	Ionization potential, e.v.	
	Calculated	Measured
$m = I(\text{CH}_4)$	12.99 ^a	
$p = I(\text{PH}_3)$	10.20 ^b	
$b = \text{C-C parameter}$	1.55 ^a	
$\phi = \text{P-C parameter}$	1.53 ^c	
$\text{P}(\text{CH}_3)_3$	(8.60)	8.60, ^c 9.2 ^d
$\text{P}(\text{C}_2\text{H}_5)_3$	8.35	8.27 ^c
$\text{HP}(\text{CH}_3)_2$	9.02	9.7 ^d
$\text{HP}(\text{C}_2\text{H}_5)_2$	8.87	
H_2PCH_3	9.53	9.72 ^c
$\text{H}_2\text{PC}_2\text{H}_5$	9.40	9.61 ^c

^a These parameters are given by Franklin, ref. 15, and Price, *et al.*, ref. 16. ^b See ref. 2. ^c This work. ^d See ref. 17.

phosphine. It is not significant in the mass spectrum of either of the methyl-substituted phosphines. Assuming that the neutral fragments are as listed in Tables II and IV, the heat of formation of this ion is calculated to be 264 kcal./mole in the triethylphosphine study and 234 kcal./mole in the monoethylphosphine study. $\Delta H_f(\text{PH}_3^+)$ from PH_3 is 237 kcal./mole.^{2,17}

$m/e = 35$. The ion must be PH_4^+ in trimethyl- and triethylphosphines. The appearance potentials of this interesting ion are determined to be 14.2 e.v. from trimethylphosphine and 14.7 e.v. from triethylphosphine. Assuming the neutral fragments are $\text{C}_2\text{H}_2 + \text{CH}_3$, and $\text{C}_2\text{H}_3 + 2\text{C}_2\text{H}_4$, respectively, $\Delta H_f(\text{PH}_4^+)$

(14) E. J. Gallegos, "Mass Spectrometric Investigation of Saturated Heterocyclics," Doctoral Dissertation, Kansas State University, Manhattan, Kan., January, 1962.

(15) J. L. Franklin, *J. Chem. Phys.*, **22**, 1304 (1954).

(16) W. C. Price, R. Bralsford, P. V. Harris, and R. G. Ridley, *Spectrochim. Acta*, **14**, 45 (1959).

(17) J. Fischler and M. Halmann, *J. Chem. Soc.*, 31 (1964).

is calculated to be 218 kcal./mole and 212 kcal./mole. Taking the average value of $\Delta H_f(\text{PH}_4^+) = 215 \pm 3$ kcal./mole, the proton affinity of PH_3 is determined to be 153 kcal./mole. Wendlandt¹⁸ has reported a value of 207 ± 10 kcal./mole for the proton affinity of PH_3 . Vetchinkin, *et al.*,¹⁹ have reported 194 ± 7 kcal./mole for the proton affinity of NH_3 , whereas 227 kcal./mole is given for the proton affinity of NH_3 by Wendlandt.¹⁸ Lampe, Franklin, and Field²⁰ have reported 167 kcal./mole as the lower limit for the proton affinity of H_2O . From the fact that PH_3 is a weaker base than NH_3 , the proton affinity of PH_3 is expected to be a little lower than 167 kcal./mole.

$m/e = 43$. This ion may be PC^+ in all cases. $\Delta H_f(\text{PC}^+)$ is calculated to be 267 kcal./mole from $\text{P}(\text{CH}_3)_3$, and 275 kcal./mole in the H_2PCH_3 case, assuming that the neutral fragments are as shown in Tables I-V. The value of 275 kcal./mole of H_2PCH_3 is likely too high. Note that this ion is analogous to CN^+ .

$m/e = 44$. This ion is PCH^+ . From the appearance potentials obtained, $\Delta H_f(\text{PCH}^+)$ is determined to be 337 kcal./mole in $\text{P}(\text{CH}_3)_3$, 332 kcal./mole in H_2PCH_3 , and 308 kcal./mole in $\text{H}_2\text{PC}_2\text{H}_5$. This ion, the analog of HCN^+ , is discussed separately below.

$m/e = 45$. This ion, PCH_2^+ , is observed in all compounds with rather high relative abundance. The $\Delta H_f(\text{PCH}_2^+)$ is calculated to be 232 kcal./mole for $\text{P}(\text{CH}_3)_3$, 280 kcal./mole for H_2PCH_3 , and 249 kcal./mole for $\text{H}_2\text{PC}_2\text{H}_5$. The values of $\Delta H_f(\text{PCH}_2^+)$ are rather poorly spread from 232 to 280 kcal./mole. The ion formation processes may be quite different in each case.

$m/e = 46$. The ion corresponding to this m/e value can only be PCH_3^+ . The appearance potentials for this ion are determined in all compounds. $\Delta H_f(\text{PCH}_3^+)$ is calculated to be 287 kcal./mole from $\text{P}(\text{CH}_3)_3$, 313 kcal./mole from $\text{P}(\text{C}_2\text{H}_5)_3$, 274 kcal./mole from H_2PCH_3 , and 283 kcal./mole from $\text{H}_2\text{PC}_2\text{H}_5$. A "best value" is probably 280 kcal./mole.

$m/e = 47$. $\Delta H_f(\text{HPCH}_3^+)$ values calculated from the data obtained are 208-238 kcal./mole. However, $\Delta H_f(\text{HPCH}_3^+)$ values from PR_3 are close to each other and average 220 kcal./mole.

$m/e = 48$. From among the four molecules studied, this ion is produced only from H_2PCH_3 . The process of formation is ionization without dissociation. From the thermochemical data and determined appearance potential, $\Delta H_f(\text{H}_2\text{PCH}_3^+) = 217$ kcal./mole.

$m/e = 55$. The ion is probably PC_2^+ and is only observed in the case of the ethyl-substituted phosphines. From the appearance potential data, $\Delta H_f(\text{PC}_2^+)$ is calculated to be 254 kcal./mole (from $\text{H}_2\text{PC}_2\text{H}_5$).

$m/e = 56$. The appearance potentials of this ion were determined only in the ethyl-substituted phosphines. The ion is probably HPC_2^+ . $\Delta H_f(\text{HPC}_2^+)$ is calculated to be 309 kcal./mole (from $\text{H}_2\text{PC}_2\text{H}_5$).

$m/e = 57$. Values of the heats of formation of this ion are in the range 300-330 kcal./mole. The ion is fairly intense in each mass spectrum. Thus, the processes of formation of the ions might be quite unique for each case.

$m/e = 58$. The ion corresponding to $m/e = 58$, was studied only in the ethyl-substituted phosphines. This ion is PC_2H_3^+ . Assuming that the neutral fragments are as shown in Tables I-V, $\Delta H_f(\text{PC}_2\text{H}_3^+)$ is calculated to be 303 kcal./mole (from $\text{P}(\text{C}_2\text{H}_5)_3$) and 291 kcal./mole (from $\text{H}_2\text{PC}_2\text{H}_5$).

$m/e = 59$. This ion is observed in $\text{P}(\text{CH}_3)_3$, $\text{P}(\text{C}_2\text{H}_5)_3$, and $\text{H}_2\text{PC}_2\text{H}_5$. However, where $\text{P}(\text{CH}_2)_2^+$ may be the ion from $\text{P}(\text{CH}_3)_3$, the ion, PC_2H_4^+ , may be formed from the ethyl-substituted cases. The heats of formation calculated show this reasoning clearly; $\Delta H_f[\text{P}(\text{CH}_2)_2^+] = 268$ kcal./mole, while $\Delta H_f(\text{PC}_2\text{H}_4^+)$ is 235 kcal./mole in the $\text{P}(\text{C}_2\text{H}_5)_3$ case and 238 kcal./mole in the $\text{H}_2\text{PC}_2\text{H}_5$ case.

$m/e = 60$. The ion observed in the ethyl-substituted phosphine spectra is PC_2H_5^+ . $\Delta H_f(\text{PC}_2\text{H}_5^+)$ is calculated to be 279 kcal./mole for $\text{P}(\text{C}_2\text{H}_5)_3$, assuming that the neutral fragments are $\text{C}_2\text{H}_5 + \text{C}_2\text{H}_5$, and 265 kcal./mole for $\text{H}_2\text{PC}_2\text{H}_5$.

$m/e = 61$. The ion corresponding to $m/e = 61$ formed in $\text{P}(\text{CH}_3)_3$ may be $\text{P}(\text{CH}_3)_2^+$, which is the most dominant ion in the spectrum, while in $\text{P}(\text{C}_2\text{H}_5)_3$ and $\text{H}_2\text{PC}_2\text{H}_5$ it is possibly HPC_2H_5^+ . If a CH_3 is the only neutral fragment in $\text{P}(\text{CH}_3)_3$, $\Delta H_f[\text{P}(\text{CH}_3)_2^+]$ is calculated to be 215 kcal./mole. $\Delta H_f(\text{HPC}_2\text{H}_5^+)$ is calculated to be 209 kcal./mole from the $\text{P}(\text{C}_2\text{H}_5)_3$ study and 213 kcal./mole from the $\text{H}_2\text{PC}_2\text{H}_5$ study.

$m/e = 62$. Appearance potentials were determined for the ion of this m/e only in $\text{P}(\text{C}_2\text{H}_5)_3$ and $\text{H}_2\text{PC}_2\text{H}_5$. The ion is probably $\text{H}_2\text{PC}_2\text{H}_5^+$. This ion results from the simple ionization process in $\text{H}_2\text{PC}_2\text{H}_5$. $\Delta H_f(\text{H}_2\text{PC}_2\text{H}_5^+)$ calculated is 230 kcal./mole from the $\text{P}(\text{C}_2\text{H}_5)_3$ study and 206 kcal./mole from the $\text{H}_2\text{PC}_2\text{H}_5$ study. The lower value is believed to be more nearly correct.

$m/e = 75$. The ion must be $(\text{H}_3\text{C})_2\text{PCH}_2^+$ from $\text{P}(\text{CH}_3)_3$, and $\text{H}_5\text{C}_2\text{PCH}_3^+$ from $\text{P}(\text{C}_2\text{H}_5)_3$. $\Delta H_f[(\text{H}_3-$

(18) W. Wendlandt, *Science*, **122**, 831 (1955).

(19) S. I. Vetchinkin, E. A. Pshenichnov, and N. D. Sokolov, *Zh. Fiz. Khim.*, **33**, 1269 (1959).

(20) F. W. Lampe, J. L. Franklin, and F. H. Field, "Kinetics of the Reactions of Ions with Molecules," in "Progress in Reaction Kinetics," Pergamon Press, New York, N. Y., 1961.

$C_2PCH_2^+$] is 160 kcal./mole and $\Delta H_f(H_5C_2PCH_3^+)$ is determined to be 190 kcal./mole.

$m/e = 76$. This ion is only produced upon ionization of $P(CH_3)_3$. The ionization potential determined leads to the calculation of $\Delta H_f[P(CH_3)_3^+] = 175$ kcal./mole. This ion is quite abundant in the mass spectrum of trimethylphosphine, in opposition to the findings of Cullen and Frost.²¹

$m/e = 89$. The ion is $P(C_2H_5)_2^+$. Assuming that C_2H_5 is the neutral fragment, $\Delta H_f[P(C_2H_5)_2^+]$ is calculated to be 203 kcal./mole.

$m/e = 90$. The ion must be $HP(C_2H_5)_2^+$. It has a very high abundance. From the determined appearance potential, $\Delta H_f[HP(C_2H_5)_2^+] = 196$ kcal./mole is calculated, providing that the neutral fragment is C_2H_4 . Using an estimated heat of formation for $HP(C_2H_5)_2 = -25$ kcal./mole, $I[HP(C_2H_5)_2]$ is found to be 9.6 e.v.. This value is higher than the theoretical value of 8.87 e.v. (see Table V).

$m/e = 103$. $\Delta H_f[(H_5C_2)PCH_2^+] = 207$ kcal./mole is calculated, assuming that the neutral fragment is CH_3 .

$m/e = 118$. $P(C_2H_5)_3^+$ is the ion of $m/e = 118$. From the ionization potential determined, $\Delta H_f[P(C_2H_5)_3^+]$ is calculated to be 153 kcal./mole.

Ionization Potential of Methinophosphide. Gier first prepared the very reactive, pyrophoric methinophosphide (HCP) in 1961.²² Apparently this is the only known compound containing a $C\equiv P$ bond.²² Gier reported the mass spectrum for this molecule and, although the mass spectrum did not aid in distinguishing between the HCP and HPC structures, the structure of HCP was established by means of infrared studies of HCP. Recently Tyler²³ used microwave techniques with both HCP and DCP to verify the structure of HCP and to determine bond lengths and rotational constants. Although the mass spectrum was reported by Gier, no appearance potentials were given. In an attempt to add to our knowledge of the properties of this interesting molecule, we have derived a value for the ionization potential of methinophosphide using our appearance potential data for the HCP^+ ion de-

termined by electron impact in each of the studied alkylphosphines.

Estimating by analogy from nitrogen-containing organic compounds to phosphorus-containing organic compounds, and using Franklin's approach,¹³ a value of $\Delta H_f(HCP) \simeq 27$ kcal./mole is obtained. Coupling this estimate with the average value of $\Delta H_f(HCP^+) = 326 \pm 13$ kcal./mole, the ionization potential of methinophosphide is calculated to be 13.0 ± 0.6 e.v. It is interesting to compare this derived value for $I(HCP)$ to experimental values ranging from 13.7 to 13.9 e.v.²⁴⁻²⁸ for $I(HCN)$.

Using this estimated $\Delta H_f(HCP)$ and taking $D(H-CP) = D(H-CN) = 114$ kcal./mole,²⁹ a value of $\Delta H_f(CP) \simeq 89$ kcal./mole is calculated, which in turn leads to a value of $D(C\equiv P) = 158$ kcal./mole. This last result is nearly the same as the value of $D_0(C\equiv P) = 6.9$ e.v. given by Herzberg.³⁰ Taking the average value of $\Delta H_f(CP^+) = 268 \pm 22$ kcal./mole and using $\Delta H_f(CP) = 89$ kcal./mole, the ionization potential of CP is calculated to be 7.8 ± 1 e.v. This value may be compared to $I(CN) = 14.2-14.6$ e.v.³¹⁻³³. It is seen that a direct electron impact study of methinophosphide is desirable.

(21) W. R. Cullen and D. C. Frost, *Can. J. Chem.*, **40**, 390 (1962).

(22) T. E. Gier, *J. Am. Chem. Soc.*, **83**, 1769 (1961).

(23) J. K. Tyler, *J. Chem. Phys.*, **40**, 1170 (1964).

(24) T. N. Jewett, *Phys. Rev.*, **46**, 616 (1934).

(25) J. D. Morrison and A. J. C. Nicholson, *J. Chem. Phys.*, **20**, 1021 (1952).

(26) B. C. Cox, Ph.D. Thesis, University of Liverpool, 1953 (reported by J. D. Craggs and H. S. W. Massey, *Handbuch Physik*, (I) **37**, 314 (1959)).

(27) C. J. Varsel, F. A. Morrell, F. E. Resnik, and W. A. Powell, *Anal. Chem.*, **32**, 182 (1960).

(28) K. Watanabe, T. Nakayama, and J. R. Mottl, *J. Quant. Spectry. Radiative Transfer*, **2**, 369 (1962).

(29) T. L. Cottrell, "The Strengths of Chemical Bonds," 2nd Ed., Butterworth and Co. Ltd. London, 1958, p. 271.

(30) G. Herzberg, "Molecular Spectra and Molecular Structure. I. Spectra of Diatomic Molecules," 2nd Ed., D. Van Nostrand Co., Inc., New York, N. Y., 1950, p. 523.

(31) D. P. Stevenson, *J. Chem. Phys.*, **18**, 1347 (1950).

(32) J. T. Herron and V. H. Dibeler, *J. Am. Chem. Soc.*, **82**, 1555 (1960).

(33) J. Berkowitz, *J. Chem. Phys.*, **36**, 2533 (1962).

Enthalpy Changes in the Reaction of Hydrogen(I), Nickel(II), and Copper(II) Ions with Some α -Amineoximes

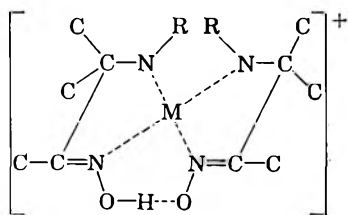
by James C. Wang,¹ John E. Bauman, Jr., and R. Kent Murmann²

Department of Chemistry, University of Missouri, Columbia, Missouri (Received April 3, 1964)

The heats of protonation of several α -alkylamineoximes are reported. Using the previously reported acid-association constants, the entropy changes for the association have been calculated and are discussed in terms of the hydrophobic changes in the protonated amines. The heats of formation of nickel(II) and copper(II) complexes of these ligands are reported and entropy changes involved in complexation calculated. These are discussed in terms of the hydrophobic nature of the ligand, steric effects, and the strength of the hydrogen bond.

Introduction

Aliphatic α -amineoximes have coordinating properties intermediate between α -diamines and α -dioximes (*i.e.*, ethylenediamine and dimethylglyoxime). The solubility and stability characteristics of the α -amineoxime complexes make them more suitable for study than those formed with the other ligands. The structure of these complexes has previously been inferred from their chemical and physical behavior³ and their formation constants are known⁴ with a reasonable degree of accuracy. The structure of the complexes in the solid state has been shown to be⁵



and with nickel(II) at least, the evidence strongly suggests that this structure persists in aqueous solution. A determination of the enthalpy and entropy changes involved in coordination was begun in order to answer questions about the nature of the hydrogen bond, the structural differences between nickel(II) and copper(II) complexes, and the steric effect in complexes of forced *cis* configuration.

This paper reports the enthalpy and entropy changes involved in the protonation and in the association of

copper(II) and nickel(II) with α -N-alkylamineoximes (AO).⁶

Experimental

Materials. The ligands were prepared according to the method previously described.³ They were recrystallized from benzene-petroleum ether mixtures and dried under vacuum. Those not previously synthesized⁷ (MeAO, EtAO, allyl-AO) gave correct equivalent weights $\pm 1\%$ when titrated with HCl solutions. With the exception of allyl-AO, which has not been analyzed, the carbon, hydrogen, nitrogen analyses agree with those calculated. These analyses have either been^{3,4} or will be reported⁸ in the near future.

(1) This report is based on portions of a doctoral dissertation to be submitted by James C. Wang to the graduate school of the University of Missouri in partial fulfillment of the requirements for the degree of Doctor of Philosophy. The work has been supported by Grant NSF-GP-585 from The National Science Foundation and by Grants A-3006 and GM-10353 from The National Institutes of Health.

(2) Person to whom correspondence should be addressed.

(3) R. K. Murmann, *J. Am. Chem. Soc.*, **79**, 521 (1957); D. L. Lewis and R. K. Murmann, *J. Inorg. Nucl. Chem.*, **20**, 1431 (1963).

(4) R. K. Murmann, *J. Am. Chem. Soc.*, **80**, 4174 (1958).

(5) The designation -H in the formula type $[\text{Ni}(\text{AO})_2\text{-H}]^+$ is meant to imply the essentially complete ionization of a H^+ from one of the ligands with the resulting formation of a hydrogen bond.

(6) The symbolism used here is AO = 2-amino-2-methyl-3-butanone oxime, MeAO = 2-methylamino-2-methyl-3-butanone oxime; and EtAO, *n*-PrAO, *i*-PrAO, *n*-BuAO, and allyl-AO represent the same ligand with the appropriate N-alkyl group.

(7) We are indebted to Mr. David L. Lewis for the preparation and analysis of these ligands and their complexes.

Likewise, the complexes were prepared according to the published procedure. They gave the same infrared spectra as earlier analyzed samples. The newer compounds of MeAO and EtAO gave correct analyses for C, H, N, Ni, ClO_4^- according to the formula $[\text{Ni}(\text{MeAO})_2\text{-H}]\text{ClO}_4$. The Ni-EtAO complex contained 1.0 H_2O .

Only the AO and MeAO complexes of copper(II) could be studied since the α -N-alkylamineoximes containing higher alkyl groups form a binuclear species of the type $[\text{Cu}_2(\text{R-AO})_2(\text{OH})_2\text{-H}]^+$.

Methylamine, dimethylamine, and *n*-butylmethylamine were obtained from Eastman Kodak Co. The latter compound was distilled and the middle one-third fraction used. The simple amines were not pure and probably were contaminated with other amines to the extent of 2% or less. All other substances were of reagent grade.

Calorimetry. Enthalpy changes for the reactions $\text{AO}_{\text{aq}} + \text{H}_{\text{aq}}^+ \xrightarrow{\Delta H_p} \text{AOH}_{\text{aq}}^+$ and $[\text{Ni}(\text{AO})_2\text{-H}]_{\text{aq}}^+ + 3\text{H}_{\text{aq}}^+ \xrightarrow{\Delta H_T} \text{Ni}_{\text{aq}}^{2+} + 2\text{AOH}_{\text{aq}}^+$ were measured by a thermometric titration-type calorimeter identical in design with the one previously reported.⁹ The calorimeter was calibrated by measuring the heat of neutralization of 0.03 *M* NaOH with 0.03 *M* HCl. ΔH for this reaction is known to be -13.50 ± 0.05 kcal./mole.¹⁰ The temperature difference between the titrant and the calorimeter was measured $\pm 0.005^\circ$ and correction made for the heat effect due to this difference. The heat capacity of the final solution was determined in each run by quantitative electrical heating. The sensitivity of the thermister bridge circuit was $3 \times 10^{-6}^\circ$.

The heats of protonation of the amines and α -amineoximes (ΔH_p) were measured by adding standardized HClO_4 (0.0595 *M*) in 1-ml. portions to AO solutions (0.01 *M*, initial volume 75 ml.) in the calorimeter. The measurement of the heat of decomposition of the complexes in acid (ΔH_T) was accomplished by the addition of small (1–2 ml.) portions of the complex solution of known concentration (0.02–0.04 *M*) to 75 ml. of 0.06 *M* HClO_4 in the calorimeter. Heats of dilution in all measurements were found to be small and were neglected. The heats of complex formation, represented by the equation $\text{Ni}_{\text{aq}}^{2+} + 2\text{AO}_{\text{aq}} \xrightarrow{\Delta H_f} [\text{Ni}(\text{AO})_2\text{-H}]_{\text{aq}}^+ + \text{H}_{\text{aq}}^+$ were calculated from the equation $\Delta H_f = 2\Delta H_p - \Delta H_T$.

The rates of all of the reactions studied were fast enough to be complete in 4 min. and under the conditions studied were better than 99% complete at equilibrium. The ionic strength was less than 0.002 for the protonation of the amines and 0.06 for the complex dissociation. In this region the ionic strength has

only a small effect on the reaction heats. Attempts were made to measure ΔH_f by direct formation of the complex. This gave variable results due to the slowness of the formation reaction.

Results

Table I contains the thermodynamic constants for the protonation of AO compounds.

Table I: Thermodynamic Data^a for $\text{AO}_{\text{aq}} + \text{H}_{\text{aq}}^+ \rightarrow \text{AOH}_{\text{aq}}^+$ at 25°, Molar Ionic Strength = 0.002

	$-\Delta G_p$, kcal./mole ^b	$-\Delta H_p$, kcal./mole	ΔS_p , cal./ deg.-mole
AO	12.4	12.7	-1
MeAO	12.6	10.3	+8
EtAO	12.6	10.6	+7
<i>n</i> -PrAO	12.4	10.8	+5
<i>n</i> -BuAO	12.4	11.0	+5
<i>i</i> -PrAO	12.5	10.6	+6
Allyl-AO	...	10.8	...

^a Errors in ΔG_p and ΔH_p estimated to be ± 0.1 kcal./mole, ΔS_p data were calculated from the corresponding ΔH_p and ΔG_p values. ^b ΔG_p was calculated from the equilibrium constants, ref. 8. The ionic strength used in these determinations was 0.02.

For comparison three simple amines were measured. In Table II results of this comparison are given at 25°.

Table II

	$-\Delta G_p$, kcal./mole	$-\Delta H_p$, kcal./mole	ΔS_p , cal./ deg.-mole
Methylamine	14.5 ^a	13.5	+3
Dimethylamine	14.7 ^a	12.2	+8
<i>n</i> -Butylmethylamine	14.5 ^b	13.1	+5

^a Values obtained from the work of Everett and Wynne-Jones, ref. 11. ΔH_p and ΔS_p were reported to be -13.09 and 4.7 for CH_3NH_2 and -11.88 and 9.5 for $(\text{CH}_3)_2\text{NH}$. ^b Determined by pH titration, $\mu = 0.02$.

Thermodynamic data for the formation of metal complexes of the formula $[\text{Ni}(\text{AO})_2\text{-H}]^+$ are tabulated in Table III.

(8) D. L. Lewis and R. K. Murmann, "Isotopic Exchange of Nickel(II) with α -Amineoximes," to be published.

(9) J. E. Bauman, Jr., and J. C. Wang, *Inorg. Chem.*, **3**, 368 (1964).

(10) H. M. Papee, W. J. Canady, and K. J. Laidler, *Can. J. Chem.*, **34**, 1677 (1956).

Table III: Thermodynamic Data^a for $M_{aq}^{2+} + 2AO \xrightarrow{\Delta H_f} [M(AO)_2-H]_{aq}^+ + H_{aq}^+$ and $[M(AO)_2-H]_{aq}^+ + 3H_{aq}^+ \xrightarrow{\Delta H_T} M_{aq}^{2+} + 2AOH_{aq}^+$

	$-\Delta H_T$, kcal./ mole	$-\Delta H_f$, kcal./ mole	$-\Delta G_f$, kcal./ mole	ΔS_f
$[Ni(AO)_2-H]^+$	16.9	8.5	8.3 ^b	-1
$[Ni(MeAO)_2-H]^+$	19.9	0.7	4.9 ^c	+14
$[Ni(EtAO)_2-H]^+$	23.8	-2.6		
$[Ni(n-PrAO)_2-H]^+$	23.6	-2.0	1.5 ^b	+12
$[Cu(AO)_2-H]^+$	14.1	11.3	10.7 ^b	-2
$[Cu(MeAO)_2-H]^+$	11.9	8.7	9.5 ^d	+3

^a Errors in ΔH_T , ΔH_f , and ΔG_f were estimated to be 0.1-0.2 kcal./mole. ΔS_f values were calculated from the corresponding ΔH_f and ΔG_f data; uncertainty in ΔS_f estimated to be ± 2 entropy units. ^b These values obtained from ref. 4. ^c Ref. 8. ^d Estimated from titration curves.

Discussion

$AO_{aq} + H_{aq}^+ \rightarrow AOH_{aq}^+$. From Table I it is apparent that the free energy changes remain nearly constant with increasing alkyl size. Thus changes in $-\Delta H_p$ are accompanied by appropriate ΔS_p changes resulting in relatively constant $-\Delta G_p$ values. In a comparison of the $-\Delta H_p$ values of the *n*-alkyl-substituted AO compounds, the secondary amines form a regular series MeAO = 10.3, EtAO = 10.6, PrAO = 10.8, BuAO = 11.0, while the primary amine has a considerably higher value, AO = 12.7. It is interesting that the three-carbon alkyl compounds have nearly the same heats of reaction, *n*-PrAO = 10.8, *i*-PrAO = 10.6, allyl-AO = 10.8.

Considering the straight-chain alkyl-substituted secondary amines, ΔS_p becomes less positive with increasing chain length. Although the individual points are within experimental error, the trend seems to be real.

The major modification in the thermodynamic quantities occurs in a comparison of AO with MeAO. Here $-\Delta H_p$ decreases by over 2 kcal./mole and ΔS_p increases by 9 e.u. with a methyl substitution. With H_{aq}^+ as the reference acid, steric hindrance due to compression of the alkyl groups by H_{aq}^+ is not likely to be of major importance. The decrease in $-\Delta H_p$ and increase in ΔS_p may be explained by considering changes in solvation of the protonated amine due to interaction between solvated water molecules and the alkyl groups.

Methylamine Series. The importance of solvation of amine ions on the basic strength of amines has been pointed out¹¹⁻¹⁵ and calculations have been made for some simple amines. In the treatment of Briegleb¹⁴ it was assumed that the change in hydration energy for

the protonated amine was nearly the same as that for the neutral amine when considering methyl substitution of a hydrogen. Using an analogous treatment but not the above approximation we consider the enthalpy terms of the association $N + H^+ \rightarrow NH^+$ (N = neutral amine, NH^+ = protonated amine) to be: $\Delta H_p - \Delta H_g = h_{NH^+} - h_{H^+} - h_N$ where ΔH_g = the over-all enthalpy change for the reaction in gaseous phase and h = heat of hydration (gas phase to aqueous phase).

Let us compare D, dimethylamine, with M, methylamine.

$$\Delta H_p^D - \Delta H_g^D = h_{NH^+}^D - h_{H^+} - h_N^D$$

$$\Delta H_p^M - \Delta H_g^M = h_{NH^+}^M - h_{H^+} - h_N^M$$

For D-M

$$\Delta(\Delta H_p) = \Delta(\Delta H_g) + \Delta(h_{NH^+}) - \Delta(h_N)$$

1 2 3 4

Term 1 is +1.3 kcal./mole from our data, term 3 is estimated from Pearson's data¹⁵ to be 8 kcal./mole, and term 4 is the difference in the heat of hydration of methyl *vs.* dimethylamine (-0.6 kcal./mole) from the data of Briegleb.¹⁴ This gives a value of -7.3 kcal./mole for term 2 which is the gas phase inductive effect due to the substitution of a methyl group for hydrogen. Thus, the rather small $\Delta(\Delta H_p)$ observed is due to a small difference in hydration energies of the neutral amines and to a small difference between two large terms: the inductive effect and the heat of hydration of the ammonium-type ions. The large difference in the heat of hydration of the NH^+ ions probably comes about because of a change in the number of hydrogens available for hydrogen bonding $CH_3NH_3^+$ compared to $(CH_3)_2NH_2^+$, the negative hydration enthalpy being greater with $CH_3NH_3^+$.

The heat of hydration of the neutral amines is more closely concerned with the inductive effect since water molecules would be bound primarily through the lone pair of electrons.

Comparing BuMeNH (Bu) with dimethylamine (D) in the order (Bu-D), $\Delta(\Delta H_p)$ is -0.9 kcal./mole experimentally. If the inductive effect of an *n*-butyl group is greater than that of a methyl substituent, the following changes are expected: (1) Δh_N : if the heats

(11) D. H. Everett and W. F. K. Wynne-Jones, *Trans. Faraday Soc.*, **35**, 1380 (1939).

(12) G. E. K. Branch and M. Calvin, "Theory of Organic Chemistry," Prentice-Hall, Inc., New York, N. Y., 1941, p. 229.

(13) A. F. Trotman-Dickenson, *J. Chem. Soc.*, 1293 (1949).

(14) G. Briegleb, *Z. Elektrochem.*, **53**, 350 (1949).

(15) R. G. Pearson and D. C. Vogelsong, *J. Am. Chem. Soc.*, **80**, 1038 (1958). Also see R. G. Pearson, *ibid.*, **70**, 204 (1948).

of hydration of the neutral amines are primarily determined by the polarizability of the lone pair of electrons, as suggested by the increase in $-h_N$ in the series NH_3 , CH_3NH_2 , $(\text{CH}_3)_2\text{NH}$, and $(\text{CH}_3)_3\text{N}$ ($-h_N = 8.0, 10.4, 11.0,$ and 11.3 kcal./mole, respectively),¹⁴ Δh_N (Bu-D) would be negative. This term would be expected to be small. (2) Δh_{NH^+} : the stronger inductive effect of the butyl group would decrease the effective charge of the protonated amine and thus decrease $-h_{\text{NH}^+}$. The decrease in $-h_{\text{NH}^+}$ for Bu compared with D also comes from its larger bulk. Therefore Δh_{NH^+} (Bu-D) would be positive. (3) $\Delta(\Delta H_g)$: this term is expected to be negative (Bu-D) because it is primarily determined by the inductive effect.

Since $\Delta(\Delta H_p)$ is found to be negative (-0.9 kcal./mole), the term $\Delta(\Delta H_g)$ is the predominating one in this case.

Amineoxime Series. A comparison of the enthalpies of reaction of the amineoximes shows the same general behavior and the same explanation is suitable. The slight increase in $-\Delta H_p$ in the series MeAO, EtAO, *n*-PrAO, and *n*-BuAO indicates a small increase in the inductive effect as the chain length of the alkyl group increases. The large decrease in $-\Delta H_p$ (approximately 2 kcal./mole) from the primary amine AO to the secondary amines RAO compounds is due to a large decrease in the negative heats of hydration of the protonated secondary amines compared with the heat of hydration of AOH^+ , as discussed previously in the cases of CH_3NH_2 and $(\text{CH}_3)_2\text{NH}$.

Nickel Complexes. The decrease in $-\Delta H_f$ upon the substitution of a methyl group for a hydrogen is considerably greater than those found by a further lengthening of the chain. Likewise, ΔS_f increases by 15 e.u. from the AO to MeAO complexes but a change of only 2 e.u. is found between MeAO and PrAO. The increase in ΔS_f is primarily due to the decreased hydration of the alkyl-substituted complexes and is of the same order of magnitude as that observed in the protonation of the amines.

The $-\Delta H_f$ changes are much larger than that found in the protonation reaction, probably indicating a large steric interaction between the N-alkyl groups. This ligand-ligand repulsion becomes important because of the *cis* configuration of the ligands imposed by the hydrogen bond.

These steric factors may be numerically evaluated if we consider that alkyl substitution makes three major changes in the complex: (a) decreases the hydrophilic character of the complex, (b) increases the polarizability of the nitrogen atoms coordinated with the metal ion (inductive effect), and (c) introduces ligand-ligand repulsion (steric effect). The first two of these quanti-

ties may be evaluated by assuming $\Delta(\Delta G)$ due to these two factors for the AO series to be the same as that observed with the bis-N-alkylethylenediaminenickel(II) complexes.¹⁶ (In the latter type complex the alkyl groups are expected to predominately occupy *trans* positions.) Thus, the values are estimated to be $\text{AO} \rightarrow \text{MeAO} = 1.3$ kcal./mole and $\text{AO} \rightarrow n\text{-PrAO} = 3.2$ kcal./mole. Subtracting these values from the respective $\Delta(\Delta G_f)$ values for the AO series, the changes in ΔG_f due to the steric effect (c) are found to be $\text{AO} \rightarrow \text{MeAO} = 2.1$ kcal./mole and $\text{AO} \rightarrow n\text{-PrAO} = 3.6$ kcal./mole.

Although $\Delta(\Delta H_f)$ and $\Delta(\Delta S_f)$ due to (a) and (b) can be evaluated in a similar way, the values for the bis-N-alkylethylenediamine complexes are not accurately known. However, if it is assumed that the $\Delta(\Delta S_f)$ values found in the AO system are not affected by term (c), then $\Delta(\Delta H_f)$ due to (a) and (b) can be estimated to be $\text{AO} \rightarrow \text{MeAO} = 7.8 - 2.1 = 5.7$ kcal./mole and $\text{AO} \rightarrow n\text{-PrAO} = 10.5 - 3.6 = 6.9$ kcal./mole.

It is interesting to note that the free energy or the enthalpy change due to ligand-ligand repulsion is less for a methyl than for a *n*-propyl substitution. Models suggest that if the two alkyl groups in the complex assume a *syn* position, the steric interaction changes with, lengthening of the chain. In the case of *i*-PrAO, however the complex, $[\text{Ni}(i\text{-PrAO})_2\text{-H}]^+$, does not form, presumably because of the large increase in interligand repulsion.

Copper Complexes. The general trends found with nickel are observed with copper. A major difference is the small magnitude of the change in ΔH_f . This is interpreted as evidence that in solution the *cis* configuration and the hydrogen bond are not present, and thus

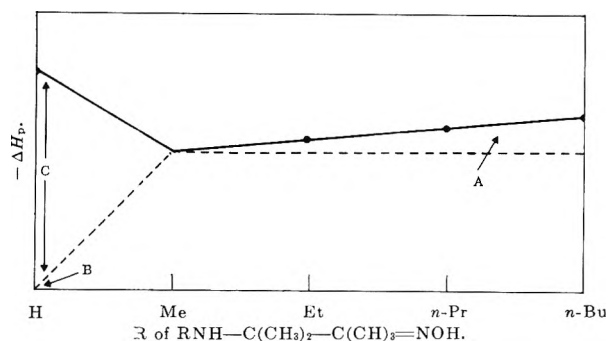


Figure 1. A, primarily due to the inductive effect; B, expected on basis of inductive effect only; C, due to hydration energy of RNH_3^+ ion.

(16) F. Basolo and R. K. Murmann, *J. Am. Chem. Soc.*, **74**, 5243 (1952).

the steric factor becomes unimportant. The change in ΔG_t of complex formation from AO to MeAO is found to be 1.2 kcal./mole, the same value is obtained for the change in ΔG of complex formation from en to N-Meen.¹⁷ Thus, $\Delta(\Delta G)$ steric is essentially zero and since $\Delta(\Delta S)$ steric is assumed to be zero, $\Delta(\Delta H)$ steric is zero.

Summary. The thermodynamic quantities involved in the reaction $R-AO + H_{aq}^+ \rightarrow RAOH_{aq}^+$ have been determined. An explanation of the changes in $-\Delta H$ and ΔS with changes in R has been given which involves hydrational and inductive effects. Changes in ΔH are described qualitatively in Fig. 1. The change in $-\Delta H_p$ with alkyl size, A, is primarily due to an alkyl inductive effect. Point B corresponds approximately to the expected $-\Delta H_p$ for the primary amine on the inductive effect of hydrogen as compared with an alkyl group. We suggest that the observed increase, C, is due to an increased hydrational energy of the RNH_3^+

ion due to the larger number of hydrogens available for hydrogen bonding.

The large differences in $-\Delta G_t$ for the formation of $[Ni(RAO)_2-H]^+$ complexes observed with alkyl group introduction are caused by (1) hydrophobic and inductive effects and (2) steric factors. The former increases by 6-7 and the latter by 2-4 kcal./mole with straight-chain alkyl groups. The hydrogen bond forces a *cis* configuration in the nickel(II) complexes causing a large steric effect. In contrast the copper(II) complexes show little or no steric effect suggesting a *trans* configuration in solution. With this metal ion the changes in $-\Delta G$ upon alkyl substitution of amineoximes are the same as found in the N-alkylethylenediamine series. The hydrogen bond and *cis* configuration of copper(II) amineoximes may, however, be present in the solid state.

(17) Calculated from data reported in Table III, ref. 16.

Energies of Disorientation in Solid Carbon Monoxide and Nitrous Oxide¹

by Marian Whitney Melhuish and Robert L. Scott

Contribution No. 1660 from the Department of Chemistry, University of California, Los Angeles 24, California
(Received April 3, 1964)

The f.c.c. structure of α -N₂, α -CO, CO₂, and N₂O is a consequence of the quadrupole-quadrupole interactions between the molecules. The classical electrostatic energies resulting from fixed dipoles and quadrupoles in these crystals have been calculated by summation over the first 449 shells on an electronic computer. Depending upon the somewhat uncertain values of the quadrupole moments, the quadrupole-quadrupole contribution ranges from 10 to 40% of the total lattice energy. The additional energy arising from the dipole-dipole interactions is very small, -4.5 and -10.7 cal. mole⁻¹ for α -CO and N₂O, respectively. The Curie temperatures for dipole orientation in these substances are thus around 5 and 11°K., at which temperatures the rate of the ordering process will be almost infinitesimally slow. Consequently, the disorientation entropy of $R \ln 2$ for these substances is always present above these temperatures and will in practice persist to the lowest temperatures.

Introduction

It is well known that the low temperature crystalline phases of carbon monoxide and nitrous oxide retain a residual entropy of approximately $R \ln 2$ per mole to the lowest temperatures at which heat capacities have been measured.^{2,3} The universally accepted explanation of these residual entropies is that the linear heteronuclear molecules CO and NNO (which are isoelectronic with NN and OCO, respectively) are distributed on their crystal lattices with no discrimination between their actually different opposite ends.

However, carbon monoxide and nitrous oxide do have small dipole moments; and it is obvious that at sufficiently low temperatures (*e.g.*, below 1°K.) the equilibrium state will be one in which the dipoles are oriented. While it is obvious that at these temperatures this equilibrium state would be approached at an almost infinitesimally rate, it is nonetheless of interest to attempt the calculation of the oriented and disoriented lattice energies and to estimate the Curie temperatures for the order-disorder transitions.

Crystal Structures and Parameters

CO₂, N₂O, and the low temperature phases α -N₂ and α -CO all have essentially the same crystal structure, an f.c.c. lattice in which the linear molecules are located at lattice sites and oriented along the body diagonals

(space group T_h⁶ or Pa³). This relatively complex structure arises from minimizing the electrostatic energy of the strong quadrupole-quadrupole interaction, which has the result of making the net contribution of the interaction between the weak dipoles even smaller.

The opposing influences of the quadrupolar and dipolar interactions are clearly illustrated in Table I, which shows the relative magnitudes of the electrostatic interactions between two isolated molecules in different orientations.

Table I: Electrostatic Energies for Different Pair Orientations

		Parallel 	Skew ·	Perpendicular —	Linear --
Dipoles	$u_{12}/\mu^2\tau^{-3}$	± 1	0	0	± 2
Quadrupoles	$u_{12}/\Theta^2\tau^{-6}$	$+9/4$	$+3/4$	-3	+6

The state of minimum energy (greatest attraction) for an isolated pair of point quadrupoles is the perpen-

(1) Paper presented before the Division of Physical Chemistry at the 146th National Meeting of the American Chemical Society, Denver, Colo. January, 1964.

(2) W. F. Giauque and J. O. Clayton, *J. Am. Chem. Soc.*, **54**, 2610 (1932); **55**, 5071 (1933).

(3) R. W. Blue and W. F. Giauque, *ibid.*, **57**, 991 (1935).

dicular orientation; but if the molecules have dipoles oriented along the principal axes of the quadrupoles, the dipolar energy is exactly zero since the vectors are orthogonal. Conversely, if the molecules assume the linear orientation most favorable for two dipoles ($\rightarrow \rightarrow$), the quadrupolar energy is repulsive. For a molecule like CO, with the parameters given in Table II, the dipolar energy in the most favorable (linear)

Table II: Lattice Parameters and Molecular Constants^a

	$a_0/10^{-8}$ cm.	x	y	$\mu/10^{-18}$ e.s.u.	$\Theta/10^{-28}$ e.s.u.
α -N ₂	(5.67) ^b 5.644 ^d	(0.070) ^b 0.0530 ^e	(0.039) ^b 0.0530 ^e	0	(+1.1) ^c
α -CO	5.63 ^f	(0.067) ^f	(0.042) ^f	0.112 ^g	(± 1) ^h
CO ₂	5.540 ⁱ	0.117 ⁱ	0.117 ⁱ	0	-4.1 ^j (± 4.8) ^c
N ₂ O	5.65 ^k	0.117 ^k	0.117 ^k	0.166 ^l	(-2.5) ^o

^a Where possible extrapolated to 0°K. ^b L. Vegard, *Z. Physik.*, **58**, 497 (1929). ^c A. D. Buckingham, *Quart. Rev.*, **13**, 183 (1959). ^d L. H. Bolz, M. E. Boyd, F. A. Mauer, and H. S. Peiser, *Acta Cryst.*, **12**, 247 (1959). ^e J. Donohue, *ibid.*, **14**, 1000 (1961). ^f L. Vegard, *Z. Physik.*, **61**, 185 (1930). ^g C. A. Burrus, *J. Chem. Phys.*, **28**, 427 (1958); **31**, 1270 (1959). ^h A. D. Buckingham, *Ann. Rept. Chem. Soc.*, **57**, 53 (1961). ⁱ W. H. Keesom and J. W. L. Kohler, *Physica*, **1**, 167 (1935); J. de S nedt and W. H. Keesom, *Proc. Roy. Acad. Sci. Amsterdam*, **27**, 839 (1924). ^j Ref. 7. ^k L. Vegard, *Z. Physik*, **71**, 465 (1931). ^l R. G. Shulman, B. P. Dailey, and C. H. Townes, *Phys. Rev.*, **78**, 145 (1950).

orientation is only 10% of the quadrupolar energy in its most favorable (perpendicular) orientation (both at the same distance of separation). Thus, it is not surprising that the quadrupolar interaction dominates and determines the structure. In the crystal, with its three-dimensional large lattice, the exact cancellation of the dipolar energy no longer obtains, but the qualitative feature remains: if the orientation is determined by minimizing the quadrupole-quadrupole energy, the dipole-dipole energy becomes very unimportant.

Table II summarizes the lattice parameters for the four crystals as determined from X-ray diffraction; a_0 is the length of the cubic unit cell, while the terminal nuclei of the molecule are at positions x, x, x and $-y, -y, -y$ (in units of a_0) from the lattice point. It is interesting to note that the space group T_h^6 requires that the molecules N₂ and CO₂ be centered on the lattice sites. Vegard reported that N₂ and CO were not so centered (space group T^4 in which $x \neq y$) but more recent work has largely disproved this for N₂ and we suspect that the similar data for CO were probably also in error. Nonetheless in our calculations we have ex-

amined the effect of displacing the dipoles and quadrupoles from the lattice sites.

Electrostatic Energy of the Lattices

Instead of calculating the electrostatic interaction energies of point dipoles and point quadrupoles in appropriate positions and orientations (as was done in an earlier paper by Jansen, Michels, and Lupton⁴), we instead assumed discrete dipolar and quadrupolar charge distributions for each molecule and summed over all the electrostatic interactions. These were ultimately expanded into inverse powers of the lattice parameter a_0 , so the final results are equivalent to one which starts with a multipole expansion.

The central dipole is assumed to consist of a charge δ^+ at position x, x, x corresponding to one end nucleus and a charge δ^- at position $-y, -y, -y$ corresponding to the other end nucleus; other dipoles are equivalently located at the other lattice sites.

Similarly the central quadrupole is assumed to arise from two charges q^- at x, x, x and $-y, -y, -y$, and a charge $2q^+$ at $(x-y)/2, (x-y)/2, (x-y)/2$, with other quadrupoles equivalently oriented.

Because of the symmetry of the lattice there is no net interaction between the dipoles and the quadrupoles. The energy of interaction between the central dipole and the rest of the (ordered) lattice is

$$u_{\text{dipole}} = \frac{\delta^2}{a_0} [A(x+y)^2 + B(x+y)^2(x-y)^2 + C(x+y)^4 + \dots] \quad (1)$$

while the corresponding energy of interaction between the central quadrupole and the rest of the lattice is

$$u_{\text{quadrupole}} = \frac{q^2}{a_0} [P(x+y)^4 + Q(x+y)^4(x-y)^2 + R(x+y)^6 + \dots] \quad (2)$$

The terms A, B, C, P, Q, R of the expansion of the energies (see Appendix) were evaluated for each of the first 449 shells⁵ with the aid of high speed electronic computers (a CDC 1640 at the University of California, San Diego, and an IBM 7090 at the University of California, Los Angeles); the coefficients for the first few shells (and the number n_s in each shell) and the sums are shown in Table III.

(4) L. Jansen, A. Michels, and J. M. Lupton, *Physica*, **20**, 1235 (1954). (We were unaware of this paper until this research was nearly complete.)

(5) By shell number, we mean $2r_0^2/a_0^2$ where r_0 is the distance between a member of the shell and the central molecule. The 450th shell is at distance $r_0 = 15a_0$ (indices 15, 0, 0). Some shells are empty (14, 30, 46, etc.), while others contain two or more subshells which are nonequivalent (9, 13, 17, etc.).

Table III: Energy Coefficients of Various Shells

Shell	n_s	A	B	C	P	Q	R
1	12	-33.94	-1272.8	-101.82	-241.83	14,223	827.3
2	6	0	0	42.00	-31.50	0	67.5
3	24	13.06	10.9	6.29	-2.00	-325	-11.2
4	12	0	0	-3.71	2.78	0	-19.4
5	24	-6.07	-4.7	-3.64	1.55	-18	-0.2
6	8	0	0	-2.40	1.80	0	3.4
7	48	-1.50	14.6	2.84	1.52	13	0.2
8	6	0	0	1.31	-0.98	0	0.5
9	12 + 24	2.93	-9.5	-1.53	-1.23	5	0.3
10	24	0	0	0.60	-0.45	0	-0.7
Sum 1-449		26.046	1260.43	60.214	-269.245	13,894.20	867.841
"Best value"		26.01	1260.43	60.214	-269.246	13,894.2	867.84
Estimated un- certainty		±0.04	±0.01	±0.001	±0.002	±0.1	±0.01

In Table III, the "best value" of each coefficient was selected after studying the variation of the sum over several hundred shells. There are fluctuations in the sums with long periods; thus, the sum over the 449 shells is not necessarily the best value. In particular the dipolar coefficient A converges slowly; the first shell contributes 130% of the total, and the sum over 10 shells is 96% of the total.

If we convert to the point multipoles, we may write for the dipole moment $\mu = \sqrt{3}\delta a_0(x + y)$, for the quadrupole moment $\Theta = 3qa_0^2(x + y)^2/2$, for the octopole moment $\Omega = 3\sqrt{3}\delta a_0^3(x + y)^3/4 = 3\mu a_0^2(x + y)^2/4$, and for the hexadecapole moment $\Xi = 9qa_0^4(x + y)^4 = 3\Theta a_0^2(x + y)^2/4$. If we substitute these and the numerical values of the coefficients into eq. 1 and 2, we obtain for the energy of a lattice of N molecules

$$E_{\text{dipoles}} = N \left[-4.34 \frac{\mu^2}{a_0^3} \{1 + 48.5(x - y)^2\} - 13.3 \frac{\mu\Omega}{a_0^5} + \dots \right] \quad (3)$$

$$E_{\text{quadrupoles}} = N \left[\frac{-59.99\Theta^2}{a_0^5} \{1 - 51.4(x - y)^2\} + 257.1 \frac{\Theta\Xi}{a_0^7} + \dots \right] \quad (4)$$

With the lattice parameters and moments of Table II we calculate the energies shown in Table IV. The lattice energy (E_{lattice}) is essentially the negative of the energy of sublimation at 0°K.⁶

If Vegard's unequal values of x and y were correct for CO, the factor $\{1 + 48.5(x - y)^2\} = 1.03$ and E_{dipoles} would be -4.64 cal. mole⁻¹. Similarly for the quad-

Table IV: Lattice Energies and Electrostatic Contributions, Cal. Mole⁻¹, Assuming $x = y$

	$\alpha\text{-N}_2$	$\alpha\text{-CO}$	CO ₂	N ₂ O
E_{lattice}	-1650	-1900	-6450	-5800
$E_{\text{dipole-dipole}}$	0	-4.39	0	-9.54
$E_{\text{dipole-octopole}}$	0	-0.12	0	-1.20
Total E_{dipoles}	0	-4.51	0	-10.72
$E_{\text{quadrupole-quadrupole}}$	(-160)	(-180)	-2800	(-940)
$E_{\text{quadrupole-hexadecapole}}$	(+6)	+7	+500	(+170)
Total $E_{\text{quadrupoles}}$	(-150)	(-170)	-2300	(-770)

rupolar energy $\{1 - 51.4(x - y)^2\}$ would be 0.97 for CO.

Jansen, Michels, and Lupton⁴ reported the dipolar energy for $\alpha\text{-CO}$ as -3.4 cal. mole⁻¹. Our value of -4.51 cal. mole⁻¹ differs from theirs (a) because they summed over the first four shells only and the coefficients (especially that for μ^2) converge slowly as the number of shells increases and (b) because they neglected the dipole-octopole term which contributes 3% of the total (11% in N₂O).

With the exception of CO₂, whose quadrupole moment has recently been determined by a direct measurement,⁷ all quadrupole moments are indirectly deduced and are consequently not very accurate. Nonetheless, it is apparent that the classical electrostatic interaction between point quadrupoles accounts for only a small part of the lattice energies of these crystals. The principal contribution to the energy must be the Lon-

(6) K. K. Kelley, U. S. Department of the Interior Bureau, of Mines Bulletin No. 383, 1935.

(7) A. D. Buckingham and R. L. Disch, *Proc. Roy. Soc., (London)*, **A273**, 275 (1963).

don dispersion effect ("van der Waals attraction") although there must be a quadrupole-induced quadrupole effect as well.

Order-Disorder Effects

When the orientations of the dipoles are distributed randomly between positive and negative directions, $E_{\text{dipoles}} = 0$, but $E_{\text{quadrupoles}}$ is unchanged. In other words the energy of disorientation is simply

$$\Delta E = E_{\text{disoriented}} - E_{\text{oriented}} = 0 - E_{\text{dipoles}} = -E_{\text{dipoles}} \quad (5)$$

In the zeroth approximation to the order-disorder problem (e.g., the Bragg-Williams theory⁸), the Curie temperature is related to the disorientation energy by the equation

$$NkT_c = 2\Delta E \quad (6)$$

which gives T_c for CO and N₂O as approximately 5 and 11°K., respectively. Since the energy of activation for rotating a dipole in the crystal lattice must be large (e.g., several kcal.), the rate at which the crystals might orient at temperatures below T_c must be utterly negligible.

One concludes therefore that a residual entropy of $R \ln 2 = 1.38 \text{ cal. deg.}^{-1} \text{ mole}^{-1}$ is to be expected in crystalline CO and N₂O at low temperatures.

The residual entropies determined by calorimetric studies^{2,3} (1.10 cal. deg.⁻¹ mole⁻¹ for CO and 1.14 cal. deg.⁻¹ mole⁻¹ for N₂O) are close to $R \ln 2$ but somewhat lower. Only a careful examination of the data (and probably additional experimental studies) can determine whether these discrepancies of about 0.1R are due to experimental error or to a slight amount of ordering in the crystals at low temperatures.

If additional examples of residual entropy of dipolar substances like CO and N₂O are to be found, they will be found only in crystals where a structure is essentially fixed by factors other than the dipole-dipole interactions and where, because of this, the dipole-dipole energy is very nearly negligible.

Acknowledgments. This research was supported in the greater part by the Petroleum Research Fund of the American Chemical Society and in a lesser part by the National Science Foundation. We thank Miss Judith Edwards for assistance with the computer work at the University of California, Los Angeles. We also thank the University of California, San Diego (where one of us (M.W.M.) was temporarily resident) for the use of the CDC 1640 computer.

Appendix

Equations for the Shell Coefficients. In the unit cell of the f.c.c. lattice there are four equivalent lattice points: (H, K, L) , $(H + 1/2, K + 1/2, L)$, $(H + 1/2, K, L + 1/2)$, and $(H, K + 1/2, L + 1/2)$ where H, K , and L are integers (not to be confused with the indices h, k, l of the reciprocal lattice). The even-numbered shells around a central molecule at $(0, 0, 0)$ arise from the first of these while odd-numbered shells arise from the permutations of the other three. In developing the power series which lead to the coefficients A, B, C, P, Q, R , one must distinguish between these two sets.

The following equations do *not* yield the energy of interaction between a central molecule and a molecule at lattice point (H, K, L) , etc., because the expressions have already been summed by permuting the indices through all the n_s members (6, 8, 12, 24, 48) of a particular subshell; a single representative set of indices suffices.

Even-Numbered Shells.

$$A = B = 0$$

$$C = -7n_s \{ 5(H^2K^2 + H^2L^2 + K^2L^2) - \rho^4 \} / \rho^9$$

$$P = 21n_s \{ 5(H^2K^2 + H^2L^2 + K^2L^2) - \rho^4 \} / 4\rho^9$$

$$Q = 0$$

$$R = 45n_s \{ 231H^2K^2L^2 - 21(H^2K^2 + H^2L^2 + K^2L^2)\rho^2 + 2\rho^6 \} / 8\rho^{13}$$

where $\rho^2 = r_0^2/a_0^2 = H^2 + K^2 + L^2$.

Odd-Numbered Shells.

$$A = n_s(3H^2 - \rho^2) / \rho^5$$

$$B = -15n_s \{ 7(H^2 + 2\kappa^2\lambda^2) - 4\kappa^2H^2 - \rho^4 \} / 2\rho^9$$

$$C = -n_s(35H^4 - 30H^2\rho^2 + 3\rho^4) / 2\rho^9$$

$$P = -3n_s \{ 35\kappa^2\lambda^2 + 5H^2\rho^2 - 4\rho^4 \} / 4\rho^9$$

$$Q = 45n_s \{ 231H^6 - 3003H^2\kappa^2\lambda^2 - (588H^4 - 273\kappa^2\lambda^2)\rho^2 + 378H^2\rho^4 - 31\rho^6 \} / 16\rho^{13}$$

$$R = -15n_s \{ 231H^2\kappa^2\lambda^2 + 21(H^4 - \kappa^2\lambda^2)\rho^2 - 21H^2\rho^4 + 4\rho^6 \} / 8\rho^{13}$$

where $\kappa = K + 1/2$, $\lambda = L + 1/2$, $\rho^2 = r_0^2/a_0^2 = H^2 + \kappa^2 + \lambda^2$.

(8) W. L. Bragg and E. J. Williams, *Proc. Roy. Soc. (London)*, **A145**, 699 (1934); **A151**, 540 (1935).

Activity Coefficients of Electrolytes at Intermediate Concentrations and the "Cube-Root" Law¹

by J. E. Desnoyers

Department of Chemistry, University of Sherbrooke, Sherbrooke Quebec, Canada

and B. E. Conway

Department of Chemistry, University of Ottawa, Ottawa, Ontario, Canada (Received April 4, 1964)

The experimental mean molal activity coefficients of simple electrolytes at concentrations below 1 *m* are regarded as being separable into three main contributions arising from interionic coulombic forces, ion-solvent, and ion-cavity interactions. The ion-solvent contribution is calculated from the theory of Robinson and Stokes and previously deduced hydration parameters. The ion-cavity contribution is based on a mutual salting-out effect in which each ion is assumed to interact with the cavities in the solvent associated with the presence of all the other ions. The experimental molal activity coefficients are first corrected for hydration and the above mutual salting-out effects. The remaining coulombic contribution to the activity coefficients for most alkali halides can then be shown to follow the relation $\log f_c = a - bc^{1/3}$ for *c* between 0.1 and 1 *m*. It is suggested that these linear plots can be interpreted in terms of a disordered lattice model.

Introduction

The nature of deviations from ideal behavior in very dilute electrolyte solutions are now reasonably well understood. The limiting theory of Debye and Hückel^{2a} for activity coefficients has been shown to be exact on statistical mechanical grounds by Kirkwood and Poirier^{2b} and the limit of validity of the Debye-Hückel model (in distinction to that of their mathematical approximations) has been set by Frank and Thompson³ at about 0.001 *m*. The necessity of using an adjustable parameter, *a*, the "distance of closest approach" in the Debye-Hückel theory, has been eliminated by Fuoss and Onsager⁴ when they showed, by integration of the Poisson-Boltzmann equation at small and large distances from the ion using Bjerrum's⁵ parameter for the critical distance, that the activity coefficient γ_{\pm} of a 1:1 electrolyte in dilute solution is independent of ion size.

The prediction of activity coefficients at intermediate concentrations is a much more difficult problem. In addition to long-range coulombic forces, shorter range interactions associated with solvation and finite size

of the ions become increasingly important. Also, Frank and Thompson⁶ have suggested that the spatial distribution of ions varies with concentration; while a continuous ionic cloud model is correct for very dilute solutions, a disordered lattice model would be more satisfactory at intermediate and high concentrations and lead to a cube-root law in salt concentration for $\ln \gamma_{\pm}$ which was demonstrated from *ca.* 0.001 to 0.1 *M* by these workers.^{3,6} At present, the formulation of a theory capable of accounting quantitatively for the activity coefficients of electrolytes at intermediate concentrations is presumptuous, and the aims of the

(1) Presented at the Symposium on Solvation sponsored by the Chemical Institute of Canada, Calgary, Alberta, Canada, 1963.

(2) (a) P. Debye and E. Hückel, *Physik. Z.*, **24**, 185, 305 (1923); (b) J. G. Kirkwood and J. C. Poirier, *J. Phys. Chem.*, **58**, 591 (1954).

(3) H. S. Frank and P. T. Thompson, *J. Chem. Phys.*, **31**, 1086 (1959).

(4) R. M. Fuoss and L. Onsager, *Proc. Natl. Acad. Sci. U. S. A.*, **47**, 818 (1961).

(5) N. Bjerrum, *Danske Videnskab. Selskab*, **7**, No. 9 (1926).

(6) H. S. Frank and P. T. Thompson, "The Structure of Electrolyte Solutions," W. J. Hamer, Ed., John Wiley and Sons, Inc., New York, N. Y., 1959, Chapter 8.

present paper will be restricted to an attempt to evaluate the contributions to the experimental activity coefficients of simple electrolytes in the range 0.1–1 *m*, which arise from the effects of hydration and mutual salting-out of ions and become significant in this range of concentrations. The resulting corrected activity coefficients should then reflect the nature of the distribution of ions in this concentration range and the presence of any other interactions neglected in this treatment.

Theoretical

1. *Introduction.* If we restrict the present study to solutions below 1 *m* in concentration, it is reasonable to assume that the experimental molal activity coefficient γ is separable into three main component terms (expressed as rational activity coefficients⁷)

$$\log \gamma = \log f_c + \log f_h + \log f_{so} \quad (1)$$

associated with coulombic, hydration, and mutual salting-out interactions.

The coulombic contribution f_c to the rational activity coefficient is the most important term in dilute solutions since it depends on long-range electrostatic forces. The hydration contribution f_h effectively takes into account the number of water molecules which are removed from their solvent role due to hydration of the ions and this term is equivalent to Hückel's " $c\mu$ " correction⁸ arising from the mutual salting-out effect associated with hydration also discussed by Butler.⁹ The term f_{so} is an extra salting-out term which allows for the fact that other ions distributed about a given ion occupy volume in the polar solvent medium but have less polarization than an equal volume of solvent in the field of the reference ion and therefore tend to be excluded from regions near the reference ions. This last term is closely linked with f_c in that both these coefficients deal with the distribution of particles around a reference hydrated ion. The coulombic term gives the distribution of ions taken as point charges while $\log f_{so}$ gives the distribution of ions taken as uncharged spheres, *i.e.*, as cavities of a medium of different polarizability from that of the solvent. In reality, we have a distribution of charged spheres, and consequently the above two terms can be regarded as additive only if $\log f_{so}$ is corrected for the effects of coulombic forces and $\log f_c$ for mutual salting-out effects.

2. *Hydration Contribution.* The relation between hydration parameters and activity coefficients has been dealt with principally by Robinson and Stokes⁷ using mole fraction statistics and by Glueckauf¹⁰ using volume fraction statistics. It has been difficult up to now to

choose between these two treatments since in both cases the hydration numbers and radii were treated as adjustable parameters which effectively took account of all other interactions except the Debye–Hückel electrostatic contribution. The hydration numbers obtained for individual ions are not additive and do not agree well with other values¹¹ obtained from partial molal volumes. In addition, the above treatments are based on the assumption that the coulombic contribution to the activity coefficient is given correctly by Debye and Hückel's theory for concentrations up to 4 *m* which is questionable.³ Despite the fact that the equations of Glueckauf and Robinson and Stokes cannot be used reliably to obtain primary hydration parameters¹² from activity data, these equations may still give the correct relation between activity and hydration data provided that known values for hydration numbers and radii are used. Hildebrand¹³ has presented arguments that mole fraction statistics are preferable to volume fraction ones when the dissolved electrolyte ions are spherical. It will also be shown below that better results are obtained with the theory of Robinson and Stokes than with that of Glueckauf. The relation derived by Robinson and Stokes will therefore be used to correct for the hydration contribution to $\log \gamma$, *viz.*

$$\log f_h = \frac{0.018hm\phi}{2.303} - \log [1 - 0.018(h - \nu)m] \quad (2)$$

where m is the molality, h the hydration number, ϕ the osmotic coefficient, and ν the total number of gram-ions arising from dissociation of 1 g.-mole of the electrolyte. The osmotic coefficient can be obtained experimentally and is known for most simple electrolytes as a function of m .⁷

The exact value of the hydration number to be used in a theoretical expression such as that above is always difficult to choose since hydration numbers depend to some extent on the property investigated. However, we have shown elsewhere¹¹ that primary

(7) Cf. R. A. Robinson and R. H. Stokes, "Electrolyte Solutions," Butterworth and Co. Ltd., London, 1959, Chapter 9. For a summary of Stokes and Robinson's numerical data, see B. E. Conway, "Electrochemical Data," Elsevier Publishing Co., Amsterdam, 1952.

(8) W. Hückel, *Physik. Z.*, **26**, 93 (1925).

(9) J. A. V. Butler, *J. Phys. Chem.*, **33**, 1015 (1929).

(10) E. Glueckauf, *Trans. Faraday Soc.*, **51**, 1235 (1955).

(11) J. E. Desnoyers and B. E. Conway, *Can. J. Chem.*, in press.

(12) B. E. Conway and J. O'M. Bockris, "Modern Aspects of Electrochemistry," Vol. I, J. O'M. Bockris and B. E. Conway, Ed., Butterworth and Co. Ltd., London, 1954, Chapter 2; J. O'M. Bockris, *Quart. Rev. (London)*, **3**, 173 (1949).

(13) K. Shinoda and J. H. Hildebrand, *J. Phys. Chem.*, **61**, 789 (1957).

hydration data¹² obtained from partial molal volume measurements are probably minimum values relevant to many of the physico chemical properties of ions (e.g., salting-out of nonelectrolytes,¹⁴ compressibilities) in ionic solutions while values from mobility data are maximum values. These two limiting values for hydration parameters (primary hydration numbers or primary hydration shell volumes) agree very well with the hydration data necessary for the interpretation of measured salting-out constants for nonelectrolytes and theoretical dielectric saturation effects near ions^{9,14} and polyions.¹⁴ It is therefore reasonable to assume that the hydration numbers required in eq. 2 should not be smaller than those obtained from partial molal volumes. The values of h and r_b , the radii of hydrated ions, are reproduced in Table I for alkali and alkaline earth halides. Utilization of these data should give the minimum influence of hydration effects on activity coefficients.

Table I: Hydration Radii and Numbers Calculated from Partial Molal Volumes at 25°^a

Ion	r_b , Å.	h	Ion	r_b , Å.	h
Li ⁺	2.18	2.6	Ca ²⁺	2.90	6.1
Na ⁺	2.61	4.0	Sr ²⁺	3.20	7.9
K ⁺	2.36	2.6	Ba ²⁺	3.45	9.0
Rb ⁺	2.30	2.1	Cl ⁻	2.21	1.1
Cs ⁺	2.27	1.6	I ⁻	2.16	0
Mg ²⁺	2.95	6.6	Br ⁻	2.23	0.8

^a From ref. 11; cf. also ref. 12.

3. Mutual Salting-Out. Ions in solution will attract or repel each other on account of the coulombic forces acting between their charges. Superimposed on these electrostatic interactions will be a certain amount of electrochemical exclusion between all ions as a result of mutual salting-out between ions of finite sizes^{2b} discussed above. This mutual salting-out interaction occurs beyond the primary hydration shell and is to be distinguished from the hydration salting-out effect associated with diminished activity of free solvent water. This latter contribution to activity coefficients is already accounted for in eq. 2 and in the Hückel term in the extended Debye-Hückel equation in which the linear empirical term in concentration, introduced in the latter equation for high concentrations, implicitly includes both effects.

The mutual salting-out contribution associated with ion cavities may be calculated by assuming that the only role of a dissolved ion without its charge is to occupy space. There will then be a preferential

attraction of a charged ion for polar solvent molecules rather than for the less polarizable cavities associated with the presence of the other ions. In considering the number dn_i of ions in an element of volume of thickness dr at distance r from a reference hydrated ion j , the effects of long-range coulombic forces and mutual salting-out will be taken into account by the relation

$$dn_i = C_0 \exp \left[- \frac{z_i e \psi_j}{kT} - \frac{\Delta u}{kT} \right] 4\pi r^2 dr \quad (3)$$

where C_0 is the average number of ions per unit volume, ψ_j the potential of the reference hydrated ion, and Δu the "salting-out energy" associated with the interaction of the field of the reference ion j with the polarizable cavity of the ion i . "Salting-out energy" has been previously derived for the problem of salting-out of nonelectrolytes by ions.¹⁴ It can be extended to mutual salting-out between ions by replacing the partial molal volume of the nonelectrolyte by that of each ion \bar{V}_i , and neglecting the polarizability of the cavity occupied by ion i . The energy leading to the tendency for mutual salting-out is then

$$\Delta u = \frac{z_j^2 e^2 \bar{V}_i}{8\pi N \epsilon r^4} \quad (4)$$

where ϵ is the relevant dielectric constant of water,¹⁴ e the electronic charge, and N Avogadro's number.

The distribution of ions dn_i^0 , in the case for which only long-range interionic coulombic forces are considered ($\Delta u = 0$), is given by

$$dn_i^0 = C_0 \exp \left[- \frac{z_i e \psi_j}{kT} \right] 4\pi r^2 dr \quad (5)$$

We may now treat the problem of the mutual salting-out effect in an analogous way to that involved in the case of nonelectrolytes.⁹ A solution element of volume dv near the reference ion j can be regarded as containing a real concentration n_i/dv of cavities (as defined in the sense above) of the other ions i , when the mutual salting-out effect is operating (Δu finite). In the absence of such salting-out effect an "ideal" concentration n_i^0/dv of such cavities would have arisen. The ratio of these two quantities gives a measure of the activity coefficient (cf. nonelectrolyte case) contribution arising from the mutual salting-out between the central ion j and all the other distributed ions i .⁹ That is

(14) B. E. Conway, J. E. Desnoyers, and C. A. Smith, *Phil. Trans. Roy. Soc. (London)*, in press.

$$\frac{1}{f_{ji}} = \frac{n_i}{n_i^0} = \frac{\int_{r_h}^{\infty} \exp \left[-\frac{z_i e \psi_j}{kT} - \frac{\Delta u}{kT} \right] 4\pi r^2 dr}{\int_{r_h}^{\infty} \exp \left[-\frac{z_i e \psi_j}{kT} \right] 4\pi r^2 dr} \quad (6)$$

The solution of this equation for all the possible combinations of j and i will give the mutual salting-out contribution to the rational activity coefficient corrected for the influence of long-range coulombic forces in the ion distribution.

An exact solution of eq. 6 is impossible but an approximate solution can be obtained if the following assumptions are made. Both $\Delta u/kT$ and $z_i e \psi_j/kT$ can be considered small compared with unity, so that the exponentials may be expanded as in the Debye-Hückel theory in a power series retaining the first term only. Also, since ψ_j appears only as a *correction factor*, it may be replaced by the Debye-Hückel potential even though it is known that the validity of this potential is doubtful at such high concentrations. Equation 6 thus becomes

$$\frac{1}{f_{ji}} = \frac{\int_{r_h}^{\infty} 4\pi r^2 dr - \int_{r_h}^{\infty} \frac{\Delta u}{kT} 4\pi r^2 dr - \int_{r_h}^{\infty} \frac{z_i e \psi_j}{kT} 4\pi r^2 dr}{\int_{r_h}^{\infty} 4\pi r^2 dr - \int_{r_h}^{\infty} \frac{z_i e \psi_j}{kT} 4\pi r^2 dr} \quad (7)$$

where¹⁵

$$\psi_j = \frac{z_j e}{\epsilon} \frac{e^{-\kappa a}}{1 + \kappa a} \frac{e^{-\kappa r}}{r} \quad (8)$$

and κ is the familiar Debye-Hückel parameter defined by

$$\kappa = \left(\frac{8\pi e^2 N}{1000 \epsilon kT} \right)^{1/2} \sqrt{I} \quad (9)$$

for an ionic strength I .

The first integral of eq. 7 represents the volume available to the central ion j , and thus the reciprocal of this term gives the number of ions j per unit volume, or

$$\int_{r_h}^{\infty} 4\pi r^2 dr = \frac{1000}{Nc_j} \quad (10)$$

where c_j is the concentration in gram-ions per liter.

The energy Δu and the potential ψ_j in eq. 7 may be replaced by the right-hand side values of eq. 4 and 8, respectively; the remaining integrals in eq. 7 can then be evaluated to give

$$\frac{1}{f_{ji}} = \frac{\frac{1000}{Nc_j} - \frac{(z_j e)^2 \bar{V}_i}{2\epsilon kTN} \frac{\bar{V}_i}{r_{h(i)}} - \frac{1000z_j z_i}{2NI}}{\frac{1000}{Nc_j} - \frac{1000z_j z_i}{2NI}} = 1 - \frac{(z_j e)^2 c_j \bar{V}_i}{1000\epsilon kT} \frac{\bar{V}_i}{r_{h(i)}} \frac{I}{2I - z_j z_i c_j} \quad (11)$$

Taking logarithms and using the approximation $\ln(1+x) = x$ when $x \ll 1$ leads to

$$\log f_{ji} = \frac{(z_j e)^2 c_j \bar{V}_i}{2303\epsilon kT} \frac{\bar{V}_i}{r_{h(i)}} \frac{I}{2I - z_j z_i c_j} \quad (12)$$

For a simple salt "MA" four interactions are possible; a central cation M may interact with the cavities of the anions leading to $\log f_{MM}$ and of the anions leading to $\log f_{MA}$, and conversely for a central anion A $\log f_{AA}$ and $\log f_{AM}$ terms will arise. The mean contribution of the mutual salting-out to the activity coefficient may be defined as

$$f_{so} = (f_M^{\nu_M} f_A^{\nu_A})^{1/\nu} \quad (13)$$

where $\nu = \nu_M + \nu_A$, $f_M = f_{MA} f_{MM}$, and $f_A = f_{AM} f_{AA}$.

Two cases will now be considered. For a 1:1 salt, $I = c_A = c_M = c$, and the mean salting-out activity coefficient contribution is

$$\log f_{so} = \frac{e^2 c}{4605\epsilon kT} \left\{ \frac{1}{3} \frac{\bar{V}_A}{r_{h(M)}} + \frac{\bar{V}_M}{r_{h(M)}} + \frac{1}{3} \frac{\bar{V}_M}{r_{h(A)}} + \frac{\bar{V}_A}{r_{h(A)}} \right\} \quad (14)$$

where c is the molar concentration. For a 2:1 salt (e.g., CaCl_2), the mean salting-out activity coefficient contribution is

$$\log f_{so} = \frac{e^2 c}{4605\epsilon kT} \left\{ \frac{\bar{V}_A}{r_{h(M)}} + \frac{4\bar{V}_M}{r_{h(M)}} + \frac{4/5\bar{V}_M}{r_{h(A)}} + \frac{2\bar{V}_A}{r_{h(A)}} \right\} \quad (15)$$

Discussion

We now have expressions for the hydration and mutual cavity salting-out contributions to the activity coefficient in terms of experimentally determinable parameters. The hydration data are taken from Table I and the partial molal volumes of individual ions from the compilation of Mukerjee¹⁶ (cf. ref. 9).

(15) Here the solution for the Debye-Hückel potential ψ_j is taken for the finite ion size boundary condition. However, this does not imply that any volume exclusion on account of finite size of ions has been allowed for in the Boltzmann distribution. This is unnecessary except at very high concentration. Cf. E. Wicke and M. Eigen, *Z. Elektrochem.*, **56**, 551 (1952); **57**, 319 (1953).

(16) P. Mukerjee, *J. Phys. Chem.*, **65**, 740 (1961).

The experimental molal activity and osmotic coefficients required in eq. 2 have been tabulated by Robinson and Stokes⁷ and the molalities have been converted into molarities from known densities.¹⁷ Therefore, the only unknown parameter in eq. 1 is the coulombic contribution to the nonideal, partial molal free energy of the salt related to $\log f_c$. This contribution may now be obtained as a function of concentration and was calculated for the alkali and alkaline earth halides in the concentration range 0.1–1 *m* at 25°. The results are summarized in Fig. 1, 2, 3, and 4 where $-\log f_c$ is plotted as a function of the *cube-root* of molar concentration.

Before discussing these results, it should be noted first of all that $\log f_{so}$ is a quite significant term, and with large univalent ions is even larger than $\log f_b$. In their study of the influence of ion-solvent interactions on activity coefficients, Robinson and Stokes⁷

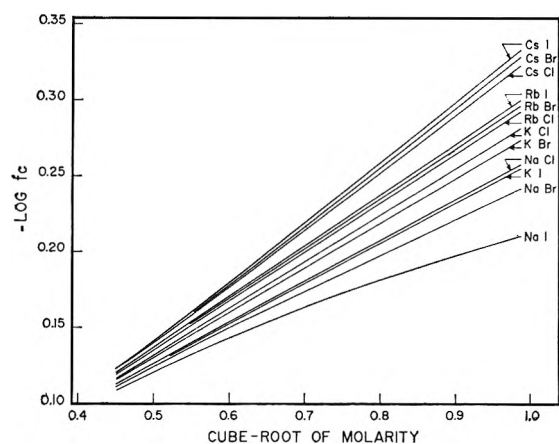


Figure 1. Plot of $-\log f_c$ as a function of cube root of molarity for certain alkali halides.

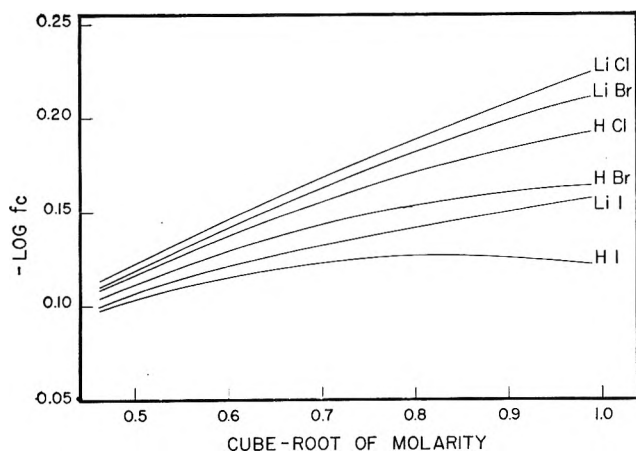


Figure 2. Plot of $-\log f_c$ as a function of cube root of molarity for hydrogen and lithium halides.

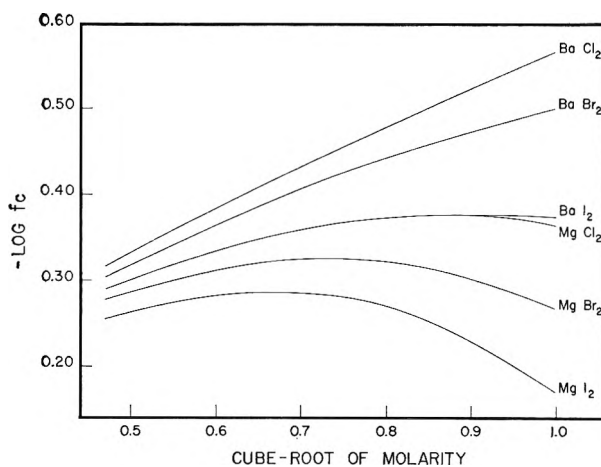


Figure 3. Plot of $-\log f_c$ as a function of cube root of molarity for Ba and Mg halides.

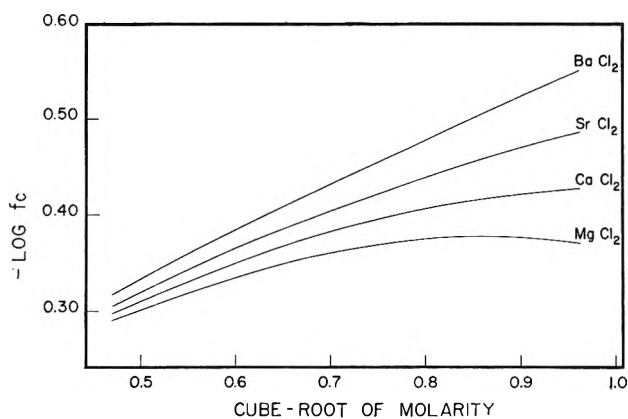


Figure 4. Plot of $-\log f_c$ as a function of cube root of molarity for alkaline earth chlorides.

have not considered this cavity mutual salting-out term. Consequently, they had to accept the deduction that hydration numbers of halide ions increased with increasing size of anions, a situation which is contrary to other experimental evidence.^{11,12} The introduction of a mutual salting-out term removes this anomaly.

The coulombic contributions to activity coefficients in Fig. 1 appear to be linear functions of the *cube root* of concentration for most of the alkali halides, NaI being an exception. At the lower concentrations, the data for some of the cesium and sodium salts also begin to deviate slightly from linearity in $c^{1/3}$, but this is not unexpected since all these $\log f_c$ plots must eventually follow a square-root relation in c at sufficiently low concentrations.¹⁸ The $\log f_c - c^{1/3}$ slopes obtained

(17) International Critical Tables, Vol. III, McGraw-Hill Book Co., New York, N. Y., 1928.

are only slightly dependent on the hydration parameter used; an increase or decrease in the value of hydration numbers by more than 0.2 molecule causes a positive or negative deviation from linearity of the $\log f_c$ functions at high concentration, but the slopes at lower concentrations are only slightly changed. These activity coefficients therefore follow a relation of the type $\log f_c = a - bc^{1/3}$, and the constants a and b are given in Table II.

Table II: Constants of the Equation $\log f_c = a - bc^{1/3}$ for Alkali Halides at 25°

Salt	a	b	Salt	a	b
CsI	0.061	0.400	KI	0.006	0.265
CsBr	0.057	0.391	KBr	0.019	0.297
CsCl	0.051	0.379	KCl	0.023	0.310
RbI	0.031	0.336	NaI
RbBr	0.029	0.330	NaBr	-0.010	0.235
RbCl	0.027	0.324	NaCl	0.018	0.270

This linear dependence of $\log f_c$ on $c^{1/3}$ lends support to the suggestion of Frank and Thompson⁶ that a disordered lattice model is preferable to an ionic cloud model at intermediate and high salt concentrations. It is interesting to note that the simple lattice theory suggested by Robinson and Stokes⁷ predicts a slope 0.29 for electrolytes with the "sodium chloride lattice." The satisfactory agreement between this rather simplified theory and the slopes deduced here again supports a disordered lattice model. At present no theory is available to explain why the slopes in Table II depend on the salts, but intuitively they must depend on the relative sizes of the ions constituting the salt.

The use of hydration data (radius and hydration number) other than those obtained from partial molal volumes removes the linearity between $\log f_c$ and $c^{1/3}$. It is therefore reasonable to assume that hydration effects associated with these two properties are closely related, since it has already been shown¹¹ that the hydration numbers obtained from the partial molal volume data are the minimum values characteristic of primary¹² hydration.

We have also attempted to calculate $\log f_h$ from Glueckauf's theory¹⁰ [volume fraction statistics] rather than from that of Robinson and Stokes,⁷ but linear plots of $\log f_c$ are not obtained if we use values of the hydration parameters equal to or larger than those given in Table I. It appears therefore that mole fraction statistics are preferable to those in terms of volume fractions in accounting for solvent effects.

While the plots shown in Fig. 1 satisfactorily demonstrate a linear relation between $-\log f_c$ and $c^{1/3}$ for the salts indicated, it was considered desirable to extend the calculation to data for other salts including 2:1 electrolytes in order to examine the generality of the behavior indicated in Fig. 1.

In Fig. 2, $-\log f_c$ is plotted against $c^{1/3}$ for lithium and hydrogen halides. The choice of hydration data for these small cations is more difficult. In a review of the literature, Conway^{19b} has shown that the most probable primary hydration number of the proton is 5 (H_3O^+ + 4 nearest neighbors) while the minimum value is obviously 1. The configuration suggested by Ackermann¹⁹ is H_9O_4^+ , *i.e.*, $h = 4$. Near the lithium ion probably two water molecules are adjacent to the ion and four more are attached through hydrogen bonds to these two inner water molecules. Also Bernal and Fowler estimate $h = 4-6$ for Li_{aq}^+ .²⁰ The hydration numbers were taken, respectively, as 5 and 6 for H^+ and Li^+ for the data in Fig. 2, and linear plots were not obtained for any of the pairs of ions. Moreover, no constant values of the hydration numbers of H^+ and Li^+ could be chosen to make all the relations linear. The same conclusion can be drawn with respect to the data for the alkaline earth halides; the values shown in Fig. 3 and 4 are those obtained from the hydration data recorded in Table I.

Two explanations may be put forward to explain the curvature in these relations. It may be possible that linear plots are to be expected only at higher concentrations, say from 0.5 *m* upward. The approximations made in deriving $\log f_c$ prevent us from investigating its dependence on $c^{1/3}$ beyond a concentration of 1 *m*. A more plausible explanation could be that the "distance of closest approach" is not important with most 1:1 electrolytes as suggested by Fuoss and Onsager⁴ but becomes more important with highly hydrated ions like Li^+ , H^+ , and all multivalent ions. Support for this tentative explanation is given by the fact that the largest deviation from linearity in the $-\log f_c - c^{1/3}$ relations occurs with salts of highly hydrated cations with large anions.

At the present time it would be premature to press the theory further to attempt to account semiquantitatively for the nonlinearity of the $-\log f_c$ vs. $c^{1/3}$ plots for the 2:1 electrolytes and the dependence of

(18) The transition conditions for a $c^{1/3}$ to a $c^{1/2}$ limiting law in ion concentration have been considered by Frank and Thompson.³

(19) (a) M. Ackermann, *Discussions Faraday Soc.*, 27, 180 (1957); (b) B. E. Conway, "Modern Aspects of Electrochemistry," Vol. III, J. O'M. Bockris and B. E. Conway, Ed., Butterworth and Co. Ltd., in press.

(20) J. D. Bernal and R. H. Fowler, *J. Chem. Phys.*, 1, 515 (1933).

the slopes of the relations for 1:1 electrolytes on the types of ions involved as also found for the lower range of concentrations by Frank and Thompson.^{3,6} It is clear that, at a given concentration, effects rather specific to the particular pairs of ions concerned are involved and are also observed with regard to other properties previously studied.²¹ This calls for further and better evaluation of individual ionic properties which can only be achieved by nonthermodynamic means such as have been discussed previously.^{11,14,16}

Conclusion

An expression has been derived to evaluate the mutual salting-out contribution, which arises from ion-cavity interaction effects, to activity coefficients. By correcting the experimental molal activity coefficients for hydration and the cavity mutual salting-out effects, the coulombic contribution to the rational activity

coefficient is obtained for different salts at 25° over the concentration range 0.1–1 *m*. This logarithmic activity coefficient, $\log f_c$, is a linear function of $c^{1/3}$ for most alkali halides in the concentration range investigated. Cube-root relations thus hold from 0.001 *m*^{3,6} to 1 *m* after appropriate corrections for hydration and related effects are made.

A theory capable of explaining the resulting dependence of $\log f_c$ on *c* would have to be based on a disordered lattice model and should take into account the relative size of each ion.

Acknowledgment. Grateful acknowledgment is made to the National Research Council for financial assistance. Thanks are also due Mr. M. Auray for his assistance with the calculations.

(21) E. A. Guggenheim and J. C. Turgeon, *Trans. Faraday Soc.*, 51, 747 (1955).

A Study of Irradiation-Induced Active Sites on Magnesium Oxide

Using Electron Paramagnetic Resonance

by Jack H. Lunsford

Lewis Research Center, National Aeronautics and Space Administration,
Cleveland, Ohio (Received April 6, 1964)

This investigation is a study of the ultraviolet irradiation-induced catalytic activity of MgO and the electron paramagnetic resonance spectra on the same sample. The data show that a correlation exists between the V_1 center concentration and the enhanced catalytic activity for the hydrogen-deuterium exchange reaction, $H_2 + D_2 \rightleftharpoons 2HD$. Samples were subjected to (a) degassing at 290 and 500°, (b) thermal decay at -79, 0, and 30°, (c) 2537-Å. ultraviolet as a function of time, and (d) several wave lengths of ultraviolet light. It is concluded that either a V_1 -type center existing on the surface is an active site for the exchange reaction, or the V_1 center formation is an integral step in the formation of the active site; that is, it is a hole trap that prevents recombination.

Introduction

Previous work¹ showed that the catalytic activity of MgO powders for the hydrogen-deuterium reaction $H_2 + D_2 \rightleftharpoons 2HD$ can be enhanced by ultraviolet irradiation provided that the catalyst is not completely degassed. The present investigation is a study of the induced catalytic activity and electron paramagnetic resonance (e.p.r.) spectra on the same sample. Magnesium oxide catalysts are particularly suitable for such studies since the e.p.r. spectra of MgO single crystals have been extensively explored by Wertz and co-workers.²⁻⁴

The role of unpaired electrons in adsorption on metals has been elucidated by the work of Selwood⁵ and others, who used magnetization techniques. Kohn⁶ observed the interaction between paramagnetic centers in silica gel and adsorbed gases, while Kokes⁷ made a similar study on zinc oxide. It follows that some such centers may act as catalytic sites. From a comparison of e.p.r. data on irradiated single crystals it was suggested in an earlier paper¹ that the active site following irradiation was Fe^{+3} . The present investigation has shown that the Fe^{+3} concentration actually decreases upon irradiation for the powders of catalytic interest. Subsequent data in this paper show, however, that a correlation does exist between the V_1 center concentration and the irradiation-induced catalytic activity.

The V_1 center is defined in Fig. 1 as a hole trapped at an anion adjacent to a positive ion vacancy. Several conditions must be satisfied for the V_1 center to be formed: (a) charge compensation for the positive ion vacancy, (b) quanta of light with sufficient energy to free an electron, and (c) an electron trap. Irradiation removes electrons from the valence band, and the resulting electron hole (called simply a hole) is then free to move through the lattice until it is trapped at the positive ion vacancy. This center now has an unpaired electron that may be detected by e.p.r. techniques.

Experimental

The catalysts used in this investigation were prepared from reagent grade MgO. Most of the experiments were carried out on pellets that were made from a paste of the powder and distilled water. The pellets,

- (1) J. H. Lunsford and T. W. Leland, *J. Phys. Chem.*, **66**, 2591 (1962).
- (2) J. W. Orton, P. Auzins, J. H. E. Griffiths, and J. E. Wertz, *Proc. Phys. Soc. (London)*, **78**, 554 (1961).
- (3) J. E. Wertz, P. Auzins, J. H. E. Griffiths, and J. W. Orton, *Discussions Faraday Soc.*, **26**, 66 (1958).
- (4) J. E. Wertz, J. W. Orton, and P. Auzins, *J. Appl. Phys. Suppl.*, **33**, 322 (1962).
- (5) P. W. Selwood, "Adsorption and Collective Paramagnetism," Academic Press, New York, N. Y., 1962.
- (6) H. W. Kohn, *J. Chem. Phys.*, **33**, 1588 (1960).
- (7) R. J. Kokes, *J. Phys. Chem.*, **66**, 99 (1962).

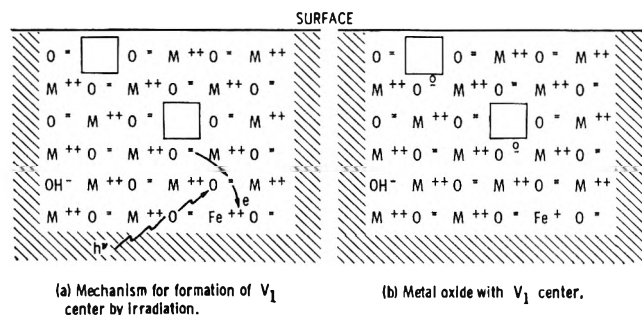


Figure 1. Metal oxide lattice showing V_1 center, electron trap, and charge compensating ion.

hereafter called P-1, were dried in air at 100° and evacuated at $290 \pm 5^\circ$ or $500 \pm 5^\circ$. Some data were obtained on the original powder, P-2, after evacuation at the elevated temperatures. A third sample, P-3, was doped by impregnation with 35 p.p.m. of Fe and fired at 800° *in vacuo*.

Batch reactions were carried out in quartz and Vycor reactors with a volume of about 10 cc. The pressure of the reacting mixture was 20 mm. All rate measurements reported here were carried out at -78° and are expressed by a first-order rate constant. The gas samples were analyzed for per cent HD with a mass spectrometer.

The ultraviolet lamps were of: (a) a hot-cathode-type, mercury-argon discharge tube with the inner wall coated with a conversion phosphor having its output in the range of 3100 to 4000 Å., and (b) a hot-cathode-type tube with peak output at 2537 Å. The longer wave length lamp was used in conjunction with a filter that removed the 3125-Å. lines from the spectrum. All irradiations were carried out at $23 \pm 3^\circ$.

The e.p.r. spectrometer used for this investigation was a Varian Model V-4500 equipped with a 100-kc. modulation unit. The cavity resonance frequency was about 9500 Mc./sec. Measurements were made near 77°K. by passing dry nitrogen gas through a liquid nitrogen heat exchanger and then past the sample.

Results

The E.p.r. Spectrum. If the trapped hole in Fig. 1 is localized upon one oxygen ion for a time that is long compared with 10^{-7} sec., then the defect shows axial electric field symmetry with the principal axis of the crystal as symmetry axis.⁴ Wertz⁴ has observed the spectrum of the V_1 center, which can be described by $g_{\parallel} = 2.0032$ (magnetic field along the symmetry axis) and $g_{\perp} = 2.0385$ (magnetic field perpendicular to the symmetry axis). The lines broaden at temperatures higher than 77°K. and cannot be observed after

the irradiated sample has been heated to 100° for a few minutes.

The shape of the paramagnetic resonance absorption curve for such a center in a polycrystalline sample is treated elsewhere.^{8,9} For $g_{\perp} > g_{\parallel}$ the derivative of the absorption curve will show a maximum at g_{\perp} and a minimum at g_{\parallel} .

The derivative spectrum of P-1 after ultraviolet irradiation at 2537 Å. is shown in Fig. 2. Arrows depict the g -components reported by Wertz. A symmetric line is slightly to the low-field side of the g_{\parallel} minimum. In addition to the similarity of g -values to those observed by Wertz, the relaxation times for the irradiation-induced center are so short that the spectrum can be observed only near 77°K. ; hence, one may conclude that the V_1 center is being observed in the catalyst sample. The line at the higher field is due to Cr^{+3} , which is saturated with microwave power.

At present, it is not clear whether there is any contribution to the spectrum from V_1 -type centers existing on the surface. By definition, the V_1 center cannot be a surface defect; however, a hole-trapping center at the surface, as shown in Fig. 1, may have an e.p.r. spectrum which is quite similar to the V_1 center in the bulk. Experimental evidence is not conclusive. At about 20 mm. pressure and -78° , H_2 , O_2 , or CO_2 have little or no effect on the spectrum shown in Fig. 2. On the iron-doped sample, P-3, H_2 and O_2 destroy the

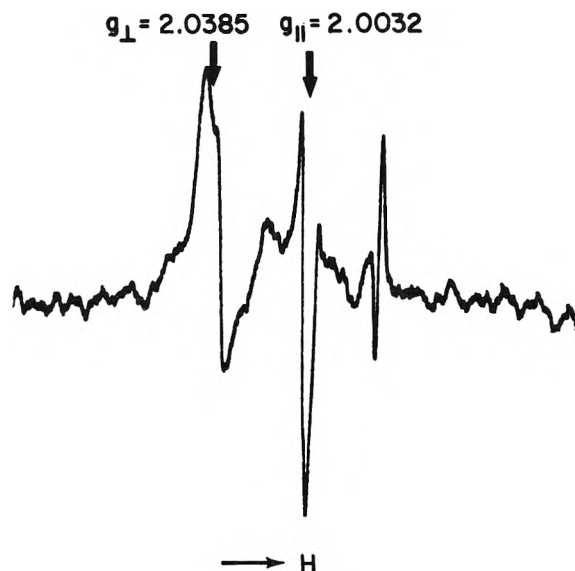


Figure 2. Spin resonance curve of MgO catalyst degassed at 290° *in vacuo* and irradiated with 2537-Å. ultraviolet light.

(8) R. H. Sands, *Phys. Rev.*, **99**, 1222 (1955).

(9) P. H. Kasai, *ibid.*, **130**, 989 (1963).

V_1 center spectrum in a few seconds. The V_1 centers are apparently formed in the iron-doped sample degassed at 800° because Fe^{+3} ions act as charge-compensating centers for the magnesium ion vacancy.

Response of V_1 Center Concentration and Catalytic Activity to Various Treatments. In an attempt to show that the enhanced catalytic activity is related to the V_1 center concentration, the samples were subjected to the following treatments: (a) degassing at 290 and 500° , (b) thermal decay at -79 , 0, and 30° , (c) 2537- \AA . ultraviolet light as a function of time, and (d) several wave lengths of ultraviolet light. Unless otherwise indicated, these treatments were carried out on P-1.

When the samples were degassed at 290° and then irradiated with 2537- \AA . ultraviolet light, the catalytic activity increased about tenfold over the unirradiated samples, and the V_1 center spectrum appeared. The catalytic activity of the samples degassed at 500° and irradiated showed no change in activity and no V_1 center spectrum. The effect of degassing at 290° is to remove partly surface and interlattice hydroxyl groups. The remaining hydroxyl ions probably act as charge-compensating centers for the positive ion vacancies. Their role as electron acceptors during irradiation is also possible. When these hydroxyl groups are removed by degassing at higher temperatures, the cation vacancies are no longer stable.

The decay in catalytic activity and V_1 center concentration was followed at three temperatures following 2537- \AA . ultraviolet irradiation. The sample had been degassed at 290° and in most cases the catalytic and e.p.r. measurements were made successively. To prevent bleaching with room lights, the samples were kept in partial darkness. Results of these thermal decay experiments are shown in Fig. 3, where Δk_0 and V_0 are the enhanced rate constant and V_1 center concentration immediately after irradiation respectively.

Response of the catalytic activity and V_1 center concentration to 2537- \AA . ultraviolet irradiation is shown in Fig. 4. In this case the sample was irradiated for 0.5, 4.5, and 45 min. with the e.p.r. spectrum recorded after each irradiation interval. The catalyst was then heated to 200° to remove any effects of the first ultraviolet treatment. Catalytic activity measurements were made after the same intervals of irradiation. While some scatter exists in the data, it is observed that more than half of the change takes place in the first 30 sec. of irradiation.

Various wave lengths of light were used for irradiation to determine qualitatively the threshold energy for the formation of the V_1 center and the enhanced activity. The intensity of the various portions of the

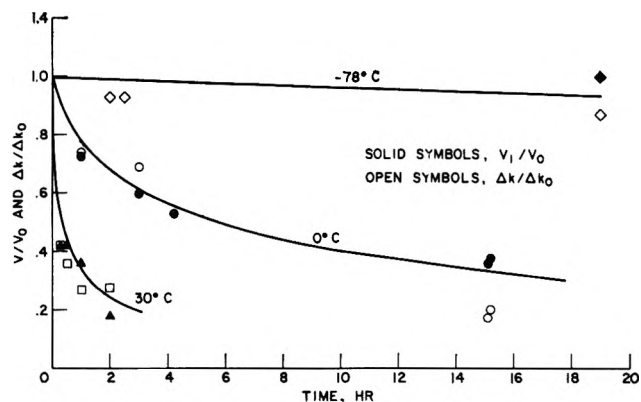


Figure 3. Thermal decay at three temperatures following 2537- \AA . ultraviolet irradiation. The curves at 0 and 30° represent eq. 3 with the constants C_1 and C_2 fitted to the experimental points.

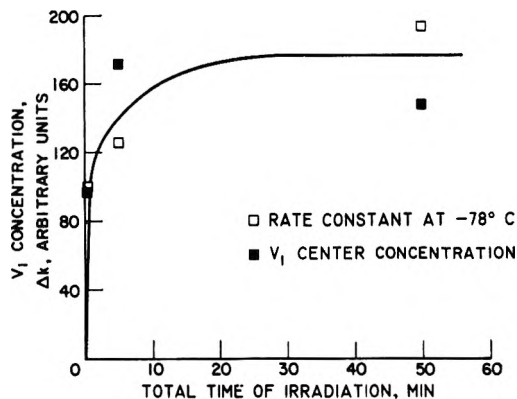


Figure 4. Response of catalytic activity and V_1 center concentration to 2537- \AA . irradiation at 23° .

spectra was not necessarily the same. The data show that a wave length of light less than 3200 \AA . is required to form the V_1 center and the active site. The cutoff wave length seems to be about 3100 \AA . or 4 e.v. This confirms earlier work¹⁰ which showed that a Pyrex reactor which acts as a filter of 50% efficiency for 3100- \AA . light reduces the enhanced catalytic activity considerably.

Catalyst P-2, which can be compared with that used in earlier work,¹ was subjected to similar tests, and qualitatively the agreement between catalytic activity and V_1 center concentration was substantiated. For this powder, however, a considerable error was introduced into the measurements since the V_1 center line was not more than five times the noise level. The preirradiation activation energy at -78° for the exchange reaction was 5 and 0.6 kcal./g.-mole for P-2 and P-1,

(10) J. H. Lunsford, Ph.D. Thesis, Rice University, 1961.

respectively. One would not necessarily expect the same response to irradiation for different catalysts.

Discussion of Results

Perhaps the strongest evidence that the active site for catalysis is closely related to the V_1 -type center comes from the thermal decay data. A decay scheme has been proposed for MgO single crystals by Soshea, Dekker, and Sturtz¹¹ that can be adapted to the present experiment. Irradiation with ultraviolet presumably produces a number of trapped electrons and holes resulting in a band scheme as shown in Fig. 5. At a given temperature the electrons trapped at E levels or holes at H levels (V_1 centers) will be released thermally.

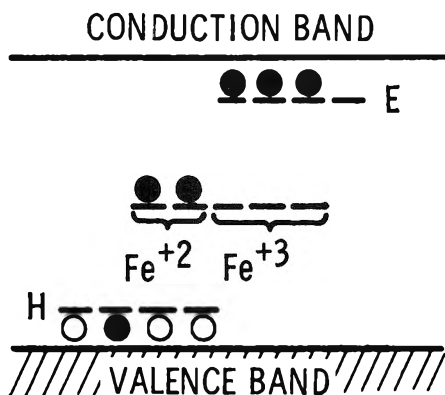


Figure 5. Schematic energy level diagrams for irradiated MgO. The levels E and H are, respectively, electron and hole traps. (After Soshea, Dekker, and Sturtz, ref. 11.)

Let N be the total number of E levels and let $n(t)$ of them be occupied by electrons. The probability for an electron thermally released from an E level to combine with a trapped hole is p ; the probability for this electron to return to an E level is then $1 - p$ where

$$p = \frac{\alpha n}{\alpha n + \beta(N - n)} \quad (1)$$

Here, α is the cross section for trapping of an electron by a V_1 center, and β is the same quantity for an E level. Equation 1 implies that the cross sections α and β are large compared with those of other electron sinks. Experiments on the catalysts indicate that this is the case for temperatures less than 100° . The rate of decay of electrons will therefore be equal to the rate of decay of V centers. This decay is determined by

$$dn/dt = -\gamma pn \quad (2)$$

where γ is a proportionality constant depending on temperature. The solution of the equation obtained by substituting (1) into (2) may be written as

$$t = C_1 \ln [n/n(0)] + (C_2/n)[1 - n/n(0)] \quad (3)$$

where $C_1 = (\beta - \alpha)/\gamma\alpha$ and $C_2 = \beta N/\gamma\alpha$. The curves for decay at 0° and 30° shown in Fig. 3 are eq. 3 fitted to the experimental data. It is important to note that while the loss of V_1 centers correlates quite well with the catalytic activity, there is a possibility that the E levels are the active sites. Wertz and co-workers¹² have shown that the formation and decay of Fe^+ ions in single crystals are similar to those of the V_1 center. They, along with others,^{11,13} have suggested that these ions might be the filled E levels. The author has also observed the Fe^+ ion spectrum in single crystals at $4^\circ K$. following ultraviolet irradiation, but the spectrum has not been found in powder samples that show the V_1 spectrum.

The problem is then to decide whether a V_1 -type center is the irradiation-induced active site for catalysis or whether it is related only in an indirect manner. The fact that the V_1 center interacts quite strongly with H_2 in the P-3 sample indicates an affinity of the center for H_2 . It is recognized, of course, that the formation of very strong bonds between the reaction products and adsorbent is not conducive to high catalytic activity. Perhaps, because of structural differences, the bonds between P-1 and H_2 are weaker than the bonds between P-3 and H_2 and the equilibrium reaction



is shifted to the left so that the change in the number of V_1 -type centers is not detected upon exposure of P-1 to the reactants. This is tantamount to saying that $H \cdot V$ is a reaction intermediate of low concentration.

In a more general sense, this work confirms that the enhanced catalytic activity is directly related to an electronic phenomenon. This proposition has been set forth by several investigators for insulator-type catalysts.¹⁴⁻¹⁶ Furthermore, in light of the results

(11) R. W. Soshea, A. J. Dekker, and J. P. Sturtz, *J. Phys. Chem. Solids*, **5**, 23 (1958).

(12) J. E. Wertz, P. Auzins, J. H. E. Griffiths, and J. W. Orton, *Discussions Faraday Soc.*, **28**, 136 (1959).

(13) W. T. Peria, *Phys. Rev.*, **112**, 423 (1958).

(14) H. W. Kohr and E. H. Taylor, *J. Phys. Chem.*, **63**, 500 (1959).

(15) H. W. Kohn and E. H. Taylor, *Proc. Intern. Congr. Catalysis, 2nd, Paris, 1960*, **2**, 1461 (1961).

(16) V. B. Kazanskii and Y. I. Pecherskaya, *Russ. J. Phys. Chem.*, **34**, 225 (1960).

reported here, it seems most difficult to support an alternative mechanism which supposes that irradiation simply moves OH groups from active sites to inactive sites, and that at some later time these poisons diffuse back. It is possible that hydroxyl groups at the surface act as the primary electron traps and that these are the active sites. Such centers would be expected to show an e.p.r. signal that could be correlated with the enhanced activity, but no such signal was observed in samples degassed at 290°.

Conclusions

1. The experimental data show that a correlation exists between the ultraviolet irradiation-enhanced catalytic activity and the V_1 center concentration.

2. This correlation strongly suggests that either a V_1 -type center existing on the surface is an active site for the hydrogen-deuterium exchange reaction, or the V_1 center formation is an integral step in the formation of the active site; that is, it is a hole trap which prevents recombination.

Electron Paramagnetic Resonance of Some Nitrogen-Bonded Copper Chelates¹

by A. K. Wiersema and J. J. Windle

Western Regional Research Laboratory,² Albany 10, California (Received April 6, 1964)

The electron paramagnetic resonance of copper chelates in which the central copper atom is bonded to two, three, or four atoms of nitrogen has been investigated. The spectra at room temperature and liquid nitrogen temperature show copper hyperfine structure and super-hyperfine structure of 5, 7, or 9 lines for coordination of copper to 2, 3, or 4 nitrogen atoms, respectively. The covalency of the bonding of copper to the ligand atoms was calculated from the copper and nitrogen hyperfine interactions independently. Both calculations indicate partial covalency of the copper-ligand bonds, but the degree of covalency calculated from the copper hyperfine structure is always found to be greater than that calculated from the nitrogen hyperfine structure. Deuteration of the amino groups of copper glycylglycylglycine and copper biuret did not produce a change in the spectra, indicating that amino protons do not contribute to the hyperfine spectra.

Introduction

Electron paramagnetic resonance (e.p.r.) has proved effective for investigating the bonding in cupric complexes and chelates. Information on the covalency of the bonding can be deduced from g values and the copper nuclear hyperfine interaction.³⁻⁵ In a few cases, the bonding parameters also have been determined from the ligand nuclear hyperfine interaction. Maki and McGarvey⁶ made the first such study on a copper complex of a dilute single crystal of copper salicylaldehydeimine in which the hyperfine interaction from two ligand nitrogen atoms was observed. They

applied molecular orbital theory in the interpretation of the spin Hamiltonian and found that the bonding information obtained from the nitrogen hyperfine

(1) Presented at the 144th National Meeting of the American Chemical Society, Los Angeles, Calif., April, 1963.

(2) A laboratory of the Western Utilization Research and Development Division, Agricultural Research Service, U. S. Department of Agriculture.

(3) A. H. Maki and B. R. McGarvey, *J. Chem. Phys.*, **29**, 31 (1958).

(4) H. S. Jarrett, *ibid.*, **28**, 1260 (1958).

(5) R. Rajan and T. R. Reddy, *ibid.*, **39**, 1140 (1963).

(6) A. H. Maki and B. R. McGarvey, *ibid.*, **29**, 35 (1958).

interaction agreed with that obtained from the copper interaction. Roberts and Koski^{7,8} observed nitrogen hyperfine interaction from four ligand nitrogen atoms in copper etioporphyrin(II) and in copper phthalocyanine, from which they drew some conclusions concerning the bonding properties of the odd electron. Kivelson and Neiman⁹ modified the theory of Maki and McGarvey and applied it to the interpretation of the e.p.r. spectra of a number of copper complexes. Gersmann and Swalen¹⁰ used a similar treatment in a recent study of several copper complexes in solution and as low temperature glasses.

E.p.r. has been applied with some success to the study of copper binding in proteins. Malmstrom and Vanngard¹¹ examined the e.p.r. spectra of several copper proteins and correlated the data qualitatively with the covalency of the copper bonding. Recent e.p.r. studies of copper conalbumins and transferrins showed nitrogen hyperfine structure in addition to the copper hyperfine structure, thereby establishing the bonding of copper to nitrogen in these proteins.^{12,13}

In the present study we obtained e.p.r. spectra from copper chelates in which copper is four-coordinated in a square planar arrangement to atoms of oxygen and nitrogen in various combinations. The spectra were obtained on aqueous or alcoholic solutions of these complexes at room temperature and on frozen solutions at liquid nitrogen temperature. At both temperatures the spectra show resolved hyperfine structure from both copper and nitrogen, making it possible to calculate independently the covalency of the bonding between the copper and the ligand atoms from the two different hyperfine interactions. These copper chelates were studied as model compounds for the e.p.r. investigation of more complicated molecules such as copper amino acid and copper-protein complexes.

Experimental¹⁴

The compounds employed in this study are listed in Table I. The samples were prepared by mixing stoichiometric amounts of $\text{Cu}(\text{NO}_3)_2$ and the chelating agents in water or ethanol to form 0.02 to 0.05 *M* solutions. Copper diphenylcarbazide was dissolved in chloroform. Two of the samples, copper biuret and copper glycyglycylglycine, were also deuterated by dissolving the solid chelates in 99.8% D_2O . N.m.r. measurements showed that the resulting chelates were 98% deuterated on nitrogen. The solutions were examined by e.p.r. at room temperature in capillary tubes, 1.2–1.5 mm. in diameter, and at liquid nitrogen temperature in quartz tubes, 3-mm. i.d.

The e.p.r. spectra were obtained with an X-band spectrometer of our own construction, which uses a

Varian 6-in. magnet and 100-kc. sec^{-1} multipurpose cavity. The first derivative of the absorption curve is plotted against the applied magnetic field utilizing an X-Y recorder. The *g* values were measured by comparison with the free radical standard diphenylpicrylhydrazyl. The magnetic field was calibrated with peroxyamine disulfonate and cycled to ensure reproducibility of sweep.

Results and Discussion

The results of the e.p.r. measurements at room temperature and liquid nitrogen temperature are summarized in Table I. The various chelating agents employed are listed along with the structures of the chelates formed, the number of nitrogen hyperfine lines observed, the *g* values, and the copper and nitrogen hyperfine coupling constants.

Figure 1 shows a typical e.p.r. spectrum obtained at room temperature for copper biuret. The spectrum consists of four lines due to the copper nuclear hyperfine interaction ($I = 3/2$) plus extra lines due to nitrogen (N^{14}) hyperfine interactions ($I = 1$). Each of the four copper hyperfine lines has a different width.

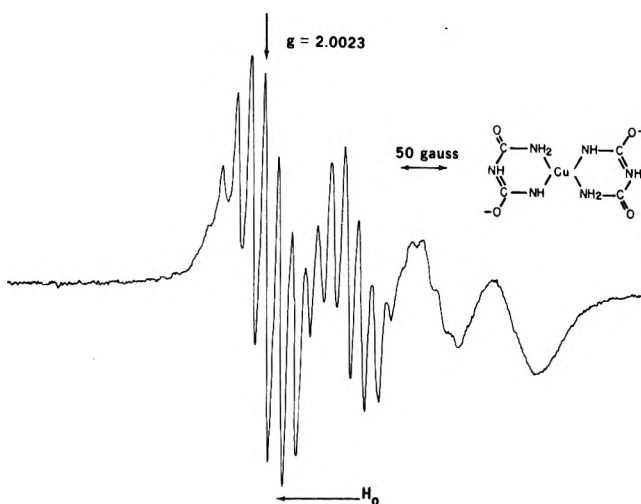


Figure 1. Room temperature spectrum of copper biuret.

(7) E. M. Roberts and W. S. Koski, *J. Am. Chem. Soc.*, **82**, 3006 (1960).

(8) E. M. Roberts and W. S. Koski, *ibid.*, **83**, 1865 (1961).

(9) D. Kivelson and R. Neiman, *J. Chem. Phys.*, **35**, 149 (1961).

(10) H. R. Gersmann and J. D. Swalen, *ibid.*, **36**, 3221 (1962).

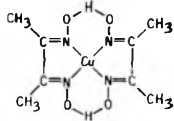
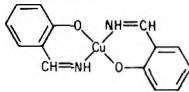
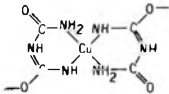
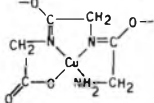
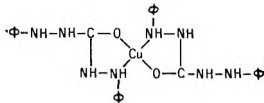
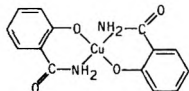
(11) B. G. Malmstrom and T. Vanngard, *J. Mol. Biol.*, **2**, 118 (1960).

(12) J. J. Windle, A. K. Wiersema, J. R. Clark, and R. E. Feeny, *Biochemistry*, **2**, 1341 (1963).

(13) R. Aasa, B. G. Malmstrom, P. Saltman, and T. Vanngard, *Biochim. Biophys. Acta*, **75**, 203 (1963).

(14) Reference to a company or product name does not imply approval or recommendation of the product by the U. S. Department of Agriculture to the exclusion of others that may be suitable.

Table I: Bonding, g Values, and Hyperfine Structure Constants for Copper Chelate Spectra

Chelating agent	Chelate structure	No. of nitrogen hyperfine lines	g values	$A_{\parallel} \times 10^4$ cm. ⁻¹	$A_{\perp} \times 10^4$ cm. ⁻¹
Dimethylglyoxime		9	$g_0 = 2.08$ $g_{\perp} = 2.05$ $g_{\parallel} = 2.15$	144 ± 10	14.6 ± 0.5
Salicylaldoxime		5	$g_0 = 2.11$ $g_{\perp} = 2.06$ $g_{\parallel} = 2.22$	163	14.0
Biuret		9	$g_0 = 2.09$ $g_{\perp} = 2.04$ $g_{\parallel} = 2.20$	158	13.5
Glycylglycylglycine		7	$g_0 = 2.10$ $g_{\perp} = 2.06$ $g_{\parallel} = 2.19$	168	12.4
Diphenylcarbazide		5	$g_0 = 2.12$ $g_{\perp} = 2.06$ $g_{\parallel} = 2.24$	140	11.0
Salicylamide		5	$g_0 = 2.12$ $g_{\perp} = 2.08$ $g_{\parallel} = 2.20$	156	10.8

Since the four lines have equal intensities, this increase in line width appears as a decrease in the amplitude with decreasing field. McConnell¹⁵ has explained the variation of line width for paramagnetic ions in solution on the basis of the tumbling of a microcrystalline unit. Because the copper hyperfine lines are narrower at high field, the nitrogen hyperfine lines are more clearly resolved on the high-field side of the spectrum.

The nitrogen hyperfine spectrum for copper biuret consists of nine lines with relative amplitudes of 1:2:8:14:19:14:8:2:1. This spectrum can be explained by assuming equal coupling of the unpaired electron with four nitrogen atoms, which would result in nine lines of relative intensities 1:4:10:16:19:16:10:4:1. The actual amplitude ratios are not the same as the theoretical ones because distortion of the nitrogen spectrum results from its superposition upon the copper spectrum, and because of line broadening due to noncoincidence of the underlying copper spectra from the isotopes, Cu⁶³ and Cu⁶⁵. The crystal structure of copper biuret has been determined by Freeman, Smith, and Taylor.¹⁶ They found that the copper atom is square-coordinated

by four amide nitrogen atoms belonging to two (biuret)²⁻ residues. Copper dimethylglyoxime has a similar nitrogen hyperfine spectrum of nine lines, showing that copper in this compound is also square-coordinated to four nitrogen atoms.

Copper glycylglycylglycine is a tetradentate chelate in which the copper is coordinated to three nitrogen atoms and one oxygen atom.¹⁷ Its spectrum is shown in Fig. 2. A seven-line nitrogen hyperfine spectrum is evident on the first two copper hyperfine lines, but the relative intensity ratios cannot be accurately determined because of poor resolution and distortion of the peaks. Equal coupling of the unpaired electron with three nitrogen atoms would produce a seven-line spectrum with intensity ratios of 1:3:6:7:6:3:1.

In the remaining three chelates, copper salicylaldoxime, copper diphenylcarbazide, and copper salicylamide, the copper is coordinated to two nitrogen atoms.

(15) H. M. McConnell, *J. Chem. Phys.*, **25**, 709 (1956).

(16) H. C. Freeman, J. E. W. L. Smith, and J. C. Taylor, *Acta Cryst.*, **14**, 407 (1961).

(17) T. Cooper, H. C. Freeman, G. Robinson, and J. C. Schoone, *Nature*, **194**, 1237 (1962).

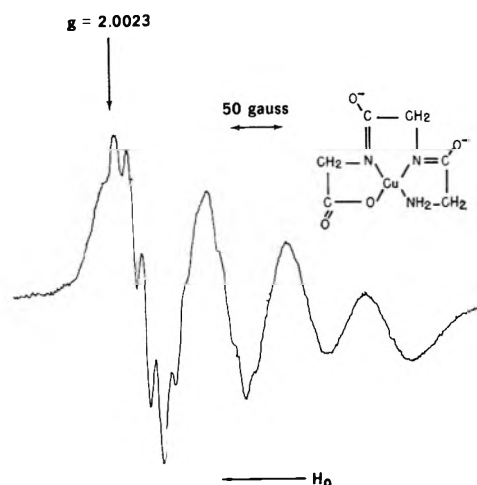


Figure 2. Room temperature spectrum of copper glycyglycylglycine.

Equal coupling with two nitrogen atoms will give a five-line hyperfine pattern with intensity ratios of 1:2:3:2:1. The spectra of these compounds exhibit a five-line nitrogen hyperfine pattern, but poor resolution of the components makes it difficult to determine the intensity ratios. An example of these spectra is shown in Fig. 3 for copper salicylaldoxime.

A typical spectrum at liquid nitrogen temperature is shown in Fig. 4 for copper salicylamide. The main features of the spectrum can be described in terms of an axially symmetric spin Hamiltonian

$$H = g_{\parallel}\beta H_z S_z + g_{\perp}\beta(H_x S_x + H_y S_y) + A_{\parallel}S_z I_z + A_{\perp}(S_x I_x + S_y I_y)$$

where the first two terms are the Zeeman interaction with an anisotropy in g , and the last two terms are the hyperfine interaction with their anisotropies. Two lines centered at g_{\parallel} and g_{\perp} , respectively, are expected. Each line will be split by the copper nuclear hyperfine interaction ($I = 3/2$) into four equally spaced components. This is clearly observed on the g_{\parallel} peak (Fig. 4) where three of the four components are visible; the fourth is hidden by the g_{\perp} peak which overlaps it. The splitting on the g_{\perp} peak is not resolved since A_{\perp} in copper complexes is usually found to be about one-tenth A_{\parallel} .¹⁰ In polycrystalline or glassy samples it has been found that an extra absorption peak will occur for certain values of g , A , and M_I .^{10,18} This peak does not add anything to our understanding of the spectra, but one should be aware of its presence in some spectra. An example of this extra absorption is shown in Fig. 4 on the high-field side of the spectrum.

In the low temperature spectra of all of the chelates, nitrogen hyperfine structure appears on the g_{\perp} com-

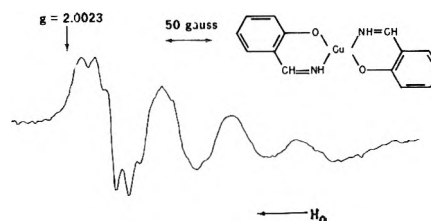


Figure 3. Room temperature spectrum of copper salicylaldoxime.

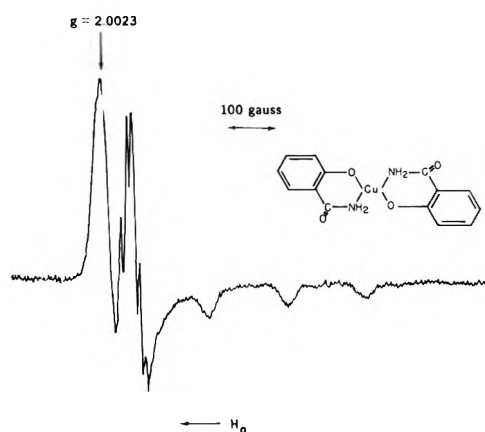


Figure 4. Low temperature spectrum of copper salicylamide.

ponent. The number and relative intensities of these lines are in each case the same as in the room temperature spectrum. The low temperature spectra were run to obtain values of g_{\parallel} and A_{\parallel} . The g_{\perp} values were then calculated from the equation $g_0 = 2/3g_{\perp} + 1/3g_{\parallel}$, the g_0 values having been obtained from the room temperature spectra.

We have analyzed these results according to the method developed by Kivelson and Neiman.⁹ This calculation assumes the copper to be coordinated to four ligand atoms in a square-planar arrangement. A linear combination of the 3d orbitals of copper and ligand sp hybrid orbitals of the same symmetry is employed. The ligand orbitals are of the form $\sigma = np + (1 - n^2)^{1/2}s$. For an sp^2 hybrid the value of n^2 is taken to be $2/3$. The odd electron is placed in the antibonding B_{1g} orbital in the ground state

$$B_{1g} = \alpha d_{x^2-y^2} - \alpha'/2(-\sigma_x^a + \sigma_y^b + \sigma_x^c - \sigma_y^d)$$

(The subscripts give the symmetry properties and the superscripts label the ligand atoms.)

The B_{1g} orbital is normalized by the equation of $\alpha^2 + \alpha'^2 - 2\alpha\alpha'S = 1$ in which S is the overlap between the copper $d_{x^2-y^2}$ orbital and the ligand orbitals. The value of S is 0.093. α^2 represents the degree of

(18) R. Neiman and D. Kivelson, *J. Chem. Phys.*, **35**, 156 (1961).

covalency of the bonding; $\alpha^2 = 1$ indicates a completely ionic bond and $\alpha^2 = 0.5$ indicates a completely covalent bond.

The values of α^2 based on the copper hyperfine spectra for our complexes were calculated using the approximate formula given by Kivelson and Neiman⁹

$$\alpha^2 = -(A_{\parallel}/P) + (g_{\parallel} - 2) + \frac{3}{7}(g_{\perp} - 2) + 0.04$$

where P , the coefficient of the hyperfine structure term, is given by the expression $P = 2\gamma\beta_0\beta_N\langle r^{-3} \rangle_0$, having the value of 0.035 cm.^{-1} .

Since nitrogen ligand atoms give rise to extra hyperfine structure, it is possible to calculate α^2 from the nitrogen interaction independently of the copper hyperfine parameters. The isotropic interaction energy between the unpaired electron and the nitrogen nuclei is given by the Fermi contact expression

$$W = (4\pi/9)\gamma\beta_0\beta_N\alpha'^2|\rho_N(0)|^2S_zI_z$$

γ is the magnetic moment of N^{14} , β_0 is the Bohr magneton, β_N is the nuclear magneton, α' is the ligand orbital coefficient for the ground state molecular orbital, and $|\rho_N(0)|^2$ is the value of the ligand $2s$ function at the ligand nucleus, having a value of $33.4 \times 10^{24} \text{ cm.}^{-3}$.⁶ The values of α^2 were obtained from the values of α'^2 calculated from the above equation using the normalization equation

$$\alpha^2 - 2\alpha\alpha'S + \alpha'^2 = 1$$

Table II shows the results of the calculations of covalency by the two different methods.

Table II: Values of Covalency of Copper Chelates Calculated from the Nitrogen and Copper Hyperfine Structure Parameters

Copper chelate	α^2 (N hfs)	α^2 (Cu hfs)
Dimethylglyoxime	0.76 ± 0.01	0.62 ± 0.04
Salicylaldoxime	.78	.75
Biuret	.79	.70
Glycylglycylglycine	.81	.73
Diphenylcarbazine	.84	.70
Salicylamide	.84	.72

The degree of covalency calculated from the copper hyperfine splitting is greater in every case than that calculated from the nitrogen hyperfine splitting, as has also been observed by others.⁹ This discrepancy falls outside the limits of uncertainty of our experiment and suggests that a modification of the theory is needed to bring the two sets of calculations into agreement.

The e.p.r. spectra of the copper glycylglycylglycine and copper biuret samples in which the NH_2 groups were deuterated were identical with the spectra of the undeuterated samples which indicates that any interaction of the unpaired electron with amino protons is too weak to contribute to the spectra. This conclusion is in accord with the observation of Maki and McGarvey⁶ on copper salicylaldehydeimine that an interaction occurred with protons on the carbon atoms adjacent to the bonding nitrogen but not with the imino protons.

Activity Coefficients in Aqueous Three-Component Electrolyte Solutions by Equilibrium Ultracentrifugation¹

by Richard M. Rush and James S. Johnson

Oak Ridge National Laboratory, Oak Ridge, Tennessee (Received April 6, 1964)

A procedure is outlined for determination of activity coefficients of solutes in three-component solutions. The procedure is limited to solutions of two electrolytes having a common monovalent ion. Free energy data for two-component solutions of the solutes in question are assumed to be available; the procedure for three components consists of finding, in the empirical equations for activity coefficients, thermodynamically consistent coefficients for terms involving the concentration of both solutes which will give the observed pattern. Experiments with interference optics can be carried out with concentrated two- and three-component solutions by using a background solution whose refractive index is brought close to that of the solution of interest with a solute of known activity coefficients; the background distribution can then be computed. Corrections for pressure on molal volumes and density may be made by a Tait-Gibson procedure, and on refractive indices by the Gladstone-Dale or Lorentz-Lorenz equations. The procedures are tested by determination of the activity coefficients of two-component $\text{BaCl}_2\text{-H}_2\text{O}$ solutions and of three-component $\text{HCl-BaCl}_2\text{-H}_2\text{O}$ solutions. Agreement with the literature is as good as can be expected.

It has been known for a long time that activity coefficients can be determined from the nonideality of equilibrium distribution of solutes in centrifugal fields.²⁻⁵ Application to systems of more than two components, however, apparently has not been attempted. The reason is hardly lack of interest in such systems; on the contrary, from a practical point of view, multicomponent systems are of considerably greater interest than those of two components. Most studies of complex equilibria, ion-exchange or solvent extraction phenomena, biochemical processes, not to mention attempts to estimate molecular weights of ionic systems by equilibrium ultracentrifugation or light scattering, involve at least two solute components. In spite of this, studies of free energies in systems of more than two components are relatively rare. The increasing difficulty of determinations as the number of components increases has discouraged research in this area, whatever the technique.

With respect to ultracentrifugation, the current methods of determining concentration distribution seem to offer further obstacles. The most precise

methods at present depend on the refractive index of the solutions, a property essentially nonspecific with respect to solute. In a three-component system, therefore, one is faced with the problem of resolving a pattern of refractive index as a function of radius into the contributions of the separate solute components, if the nonideality of their distributions, expressed as activity coefficients, is to be ascertained.

The problem is not as hopeless as it seems. The limiting situations are given by the activity coefficients of the two-component solutions of the separate solutes; a great many of these already are in the

(1) This document is based upon work performed for the United States Atomic Energy Commission at the Oak Ridge National Laboratory, operated by Union Carbide Corp. Presented in part at the 141st National Meeting of the American Chemical Society, Washington, D. C., March, 1962.

(2) K. O. Pedersen, *Z. physik. Chem.*, **A170**, 41 (1934).

(3) C. Drucker, *ibid.*, **A180**, 359, 378 (1937).

(4) T. F. Young, K. A. Kraus, and J. S. Johnson, *J. Chem. Phys.*, **22**, 878 (1954).

(5) J. S. Johnson, K. A. Kraus, and T. F. Young, *J. Am. Chem. Soc.*, **76**, 1436 (1954).

literature, and others of interest can be determined in a number of ways, including ultracentrifugation. Further, in a mixed system of components A and B, values are not independent; the Bjerrum restriction

$$\nu_A \left(\frac{\partial \log \gamma_{\pm A}}{\partial m_B} \right)_{m_A} = \nu_B \left(\frac{\partial \log \gamma_{\pm B}}{\partial m_A} \right)_{m_B} \quad (1)$$

where m is concentration in moles/kg. of solvent, γ_{\pm} the mean ionic activity coefficient, and ν the number of moles of ions/mole of solute, must be obeyed. With this limitation on the behavior of the separate solutes, interpretation of the pattern for the mixed system is possible.

We first obtain empirical equations for $\log \gamma_{\pm}$ of the two-component systems. In order to have a fit continuous into the low concentration range, these include a Debye-Hückel term and an integral power series in I (or m), with as many terms as necessary for an adequate fit to the data. Interpretation of the mixed system then involves determining the coefficients of as many cross terms, involving the concentrations of both solutes to various powers, as are necessary to reproduce satisfactorily the observed refractive index patterns. By eq. 1, these terms are not independent for the solutes. It seems to us more convenient to try to match the observed refractive index pattern in this fashion than to attempt to resolve directly the refractive index patterns into concentration distributions, as one normally does with two-component systems.^{3,5}

We have selected as a test HCl-BaCl₂-H₂O. The activity coefficients of HCl in this system have been carefully determined potentiometrically by Harned and Gary.⁶ Their results are given in terms of Harned's rule

$$\log \gamma_{\pm \text{HCl}} = \log \gamma_{\pm \text{HCl}(0)} - \alpha_{12} I_{\text{BaCl}_2} \quad (2)$$

where $\gamma_{\pm \text{HCl}(0)}$ is the activity coefficient of HCl in a two-component solution of the same total ionic strength

$$I = \frac{1}{2} \sum_i m_i z_i^2$$

and α_{12} is a constant for a given ionic strength. The relation is obeyed very closely by this system at $I = 1, 2,$ and 3 , the ionic strengths for which measurements are reported. The coefficient α_{12} is not constant with total ionic strength, though the variation is not great. If the activity coefficients of HCl in the two-component acid-water system and the value of α_{12} are known for a given ionic strength, the values of $\log \gamma_{\pm \text{HCl}}$ in the three-component system having the ionic strength in question may be immediately calculated from eq. 2;

conversely, to interpret the nonideality contribution to HCl distribution at centrifugation equilibrium, only this parameter would have to be considered.

The same is not true for the other solute, and the nonideality of BaCl₂ also affects the equilibrium refractive index pattern. A possible procedure is to assume that its activity coefficients vary linearly at constant total ionic strength with I_{HCl} , a rule analogous to that summarized by eq. 2; the activity coefficients of BaCl₂ would then be determined by the values for the two-component systems and of α_{12} .

Although there is evidence that this is at least approximately the case,⁶ we do not wish to make the assumption *a priori*. In an alternative procedure, by way of eq. 1, an expression for $\log \gamma_{\pm \text{BaCl}_2}$ can be obtained from the two-component activity coefficients for the salt, the values of α_{12} , and the partial derivative of α_{12} with respect to m_{BaCl_2} , which is given by the variation of α_{12} with I . It should be emphasized that the last must be considered. Two empirical equations for α_{12} as a function of I would imply the same values of $\log \gamma_{\pm \text{HCl}}$, at ionic strengths for which they happened to give the same values of α_{12} ; unless the slopes also happened to be the same, however, different values of $\log \gamma_{\pm \text{BaCl}_2}$ would be computed from the two equations.

In addition, because of sedimentation, ionic strength is not constant in a given ultracentrifugation experiment. It is therefore necessary in the interpretation of results to allow for a dependence of α_{12} on I . In the present study, we have done this in two ways. In one, experiments carried out at approximately the same ionic strength have been grouped in a least-squares computation, and a linear dependence of α_{12} on I , which should be valid over short ranges, has been assumed. In the other, computations for all experiments have been carried out at once, with a quadratic variation of α_{12} assumed. This quadratic variation appears consistent with the values reported by Harned and Gary,⁶ though since there are only three points available, other types of equations cannot be ruled out.⁷

Experimental

Details of centrifugation technique have been presented earlier.⁸ Centrifugations were carried out with a Spinco Model E ultracentrifuge at 25° using in most cases a six-hole rotor equipped with five 12-mm.

(6) H. S. Harned and R. Gary, *J. Am. Chem. Soc.*, **76**, 5924 (1954).

(7) W. J. Argersinger, Jr., and D. M. Mohilner, *J. Phys. Chem.*, **61**, 99 (1957).

(8) J. S. Johnson, G. Scatchard, and K. A. Kraus, *ibid.*, **63**, 787 (1959).

cells; for $I = 1$ a two-hole rotor equipped with one 30-mm. cell was used. The speeds used were 24,630, 20,410 and 16,200 r.p.m. Sedimentation was followed by the interference optical system standard with the machine. Light of 546 m μ , isolated with a Baird interference filter, was employed.

It is necessary that the effective light path through the solution and background compartments be approximately the same. Otherwise, the fringes will be washed out since the light is not completely monochromatic. The light paths are made approximately equal by putting HCl in the background compartment at such a concentration that the initial refractive index of the background solution is approximately the same as that of the HCl-BaCl₂-H₂O solution in the other compartment.

In reading the plates for analysis of the equilibrium interference patterns, it is necessary to correct for the effect of cell distortion on the fringes if the potential accuracy of the method is to be realized. The deviations of our results from those computed with the best values of the unknown parameters are only fractions of a fringe. Distortion of our cells, which have either quartz or sapphire windows and epoxy (not metal filled) centerpieces, varies from about a quarter fringe to well over a fringe in one case. These corrections are determined in a manner described before,⁸ by carrying out centrifugations with water in both compartments before and after the experiment in question.

The solutions were prepared by weighing solid BaCl₂·2H₂O or a stock solution of BaCl₂, a stock solution of HCl, and water into a volumetric flask. The stock BaCl₂ solutions were analyzed by evaporation to dryness and weighing as BaCl₂ and by precipitation of the chloride as AgCl. The stock HCl solutions were analyzed by precipitation of the chloride as AgCl and by measurement of the density. The solution concentrations and experimental conditions are summarized in Table I.

Computations

As we stated in the introduction, the procedure for interpretation is first to compute the distribution of the solutes for assumed values of activity coefficient parameters and then to compare the refractive index pattern predicted from the computed distribution with that observed. For convenience, we can divide the process into a number of steps; some steps must be carried out with initially assumed values of certain variables, the final solution being obtained by iteration.

1. *Concentration Distribution.* The equation describing the equilibrium distribution of a component,

AX_a (ionized as $A^{+a} + aX^-$ or $A^{-a} + aX^+$) in a centrifugal field is⁴

$$\ln \frac{(a_{AX_a})_j}{(a_{AX_a})_r} = \frac{M_{AX_a}\omega^2}{2RT} (x_j^2 - x_r^2) - \frac{1}{RT} \int_{P_r}^{P_j} (\bar{V}_{AX_a})_i dP \quad (3a)$$

or

$$\ln \frac{(m_A)_j}{(m_A)_r} = \frac{M_{AX_a}\omega^2}{2RT} (x_j^2 - x_r^2) - \frac{1}{RT} \int_{P_r}^{P_j} (\bar{V}_{AX_a})_i dP - a \ln \frac{(m_X)_j}{(m_X)_r} - \nu_A \ln \left[\frac{(\gamma_{\pm AX_a})_j}{(\gamma_{\pm AX_a})_r} \right]_{P_r} \quad (3b)$$

where a is activity; P , pressure; M , molecular weight; ω , angular velocity; R , gas constant; T absolute tem-

Table I: Experimental Conditions

Experiment	Solution		Background m_{HCl}	Speed of rotation, r.p.m.	α_{12}^0
	m_{HCl}	m_{BaCl_2}			
1a	0	0.6114	2.294	20,417	
1b	0	0.6114	2.294	16,204	
2a	0	0.9266	3.427	20,417	
2b	0	0.9266	3.427	16,204	
3a	0	1.2500	4.706	20,417	
3b	0	1.2500	4.706	16,204	
4a	0	1.2501	4.706	20,417	
4b	0	1.2501	4.706	16,204	
5a	0	1.5856	5.934	20,417	
5b	0	1.5856	5.934	16,204	
6	0.2496	0.2524	1.138	24,655	0.0689
7	0.5523	0.1530	1.138	24,656	0.0770
8	0.5191	0.5177	2.415	20,415	0.0538
9a	1.1732	0.3099	2.367	20,414	0.0650
9b	1.1732	0.3099	2.367	16,195	0.0631
10a	0.6434	0.8301	3.961	20,414	0.0662
10b	0.6434	0.8301	3.961	16,195	0.0648
11	1.5872	0.5273	3.539	20,415	0.0382
12 ^b	1.5872	0.5273	3.539	20,415	0.0681
13a	1.6230	0.5237	3.718	20,414	0.0671
13b	1.6230	0.5237	3.718	16,195	0.0664
14a ^c	1.6230	0.5237	3.718	20,414	0.0678
14b ^c	1.6230	0.5237	3.718	16,195	0.0678
15	0.4221	1.2614	4.961	20,415	0.0697
16a	1.0896	1.0580	5.442	20,414	0.0703
16b	1.0896	1.0580	5.442	16,195	0.0695

^a Estimated from deviations of slopes (Fig. 2) from zero.

^b Same solution as used in experiment 11 placed in a different cell. ^c Same solution as used in experiment 13 placed in a different cell.

perature; x , radius; m , concentration in moles/kg. of solvent; \bar{V} , partial molal volume; γ_{\pm} , mean ionic activity coefficient; and $\nu_A = (a + 1)$ is moles of ions/mole of AX_a . The subscripts j and r refer to two radial positions, r being a point taken as a reference. The volume required⁴ in eq. 3 is for the solution composition at position j and, for a complete solution, should be known as a function of pressure. The activity coefficient term, which will be discussed in more detail later, is primarily a function of the concentrations of the various solutes, but also depends on pressure; in eq. 3, it is evaluated for P_r . The meniscus would be a convenient reference point in some respects since then the activity coefficient ratio would be that for 1 atm. We have, however, located the reference near the center of the cell to make assignment of initial concentrations to the reference point a reasonable first approximation; we then make appropriate corrections of the activity coefficient ratios for pressure by standard thermodynamic equations.^{9a}

For a two component system, eq. 3b becomes

$$\ln \frac{(m_A)_j}{(m_A)_r} = \frac{M_{AX_a} \omega^2}{2\nu_A RT} (x_j^2 - x_r^2) - \frac{1}{\nu_A RT} \int_{P_r}^{P_j} (\bar{V}_{AX_a})_i dP - \ln \left[\frac{(\gamma_{\pm AX_a})_j}{(\gamma_{\pm AX_a})_r} \right]_{P_r} \quad (3c)$$

since electroneutrality must be maintained. If another solute, *e.g.*, BX_b , is present, however, equations for both electrolytes of the form (3a) or (3b) must be satisfied simultaneously with the electroneutrality condition

$$am_A + bm_B = m_X \quad (4)$$

Equations 3b for AX_a and BX_b are solved simultaneously by a Newton-Raphson method at the radii for which values are desired. The counterion concentration is given by eq. 4. The background distribution is computed by the same procedure with eq. 3c.

The present version of our computer program allows computations for electrolytic solutes with a common monovalent cation or anion (*e.g.*, $BaCl_2$ and $LaCl_3$). It does not permit analysis of data for systems having a common multivalent ion but different counterions (*e.g.*, $BaCl_2$ and $BaBr_2$), although there should be no great difficulty in writing a program for such a case. Solutions not having a common ion are not three-component systems. We do not consider cases for solutes in which multivalent ions of both charge signs are present.

In the following sections, the evaluation of other terms in eq. 3 is outlined.

a. Volumes. The empirical equations for partial molal volumes in terms of solute concentration are based on a mixture rule previously described.¹⁰ More density measurements on $BaCl_2$, HCl , and mixed solutions have accumulated since the earlier report and the parameters of the equations have been modified somewhat. The present equations for volumes (at 1 atm.) are as follows

$$\bar{V}_{HCl} = (18.052 + 1.5014\sqrt{I} - 0.13472I)y_{HCl} + (18.052 + 1.5948\sqrt{I} + 0.04301I)y_{BaCl_2} \quad (5a)$$

$$\bar{V}_{BaCl_2} = (24.023 + 5.0646\sqrt{I} + 0.1200I)y_{HCl} + (24.023 + 5.3448\sqrt{I} + 0.1342I)y_{BaCl_2} \quad (5b)$$

where $y_i = (I_i/I)$.

Corrections for the effect of pressure on partial molal volumes were made by a form of the Tait-Gibson equation.^{9b}

$$\bar{V}_{AX_a}^{(P_i)} = \bar{V}_{AX_a}^{(1)} - 434.3C \left(\frac{\partial P_e}{\partial m_{AX_a}} \right) \frac{1 - P_i}{(B + P_i + P_e)(B + 1 + P_e)} \quad (6)$$

where $C = 0.3071$, $B = 2923$ bars,¹¹ and P_e is the "effective" pressure exerted on the solution by the presence of solute. Values of P_e for HCl ¹² and $BaCl_2$ ¹³ were obtained from compressibility data. Since there are to our knowledge no data for compressibilities of three-component solutions, we have assumed that the total P_e for a solution is the sum of the values for the individual solutes. The contribution to the total P_e of the individual solutes is taken to be the value of P_e for a two-component solution of the solute in question at the same molality of that solute as in the three-component solution. Empirical expressions for P_e as a function of concentration were used. Over the small pressure ranges involved in these measurements, partial molal volumes vary little with pressure, and such variation as there is almost linear. We have therefore used for the

$$\int_{P_1}^{P_2} \bar{V} dP$$

in the centrifugation equations (and in correcting activity coefficients for pressure) the average of the

(9) H. S. Harned and B. B. Owen, "The Physical Chemistry of Electrolytic Solutions," 3rd Ed., Reinhold Publishing Corp., New York, N. Y., 1958: (a) p. 9; (b) Chapter VIII.

(10) R. M. Rush and G. Scatchard, *J. Phys. Chem.*, **65**, 2240 (1961).

(11) R. E. Gibson, *J. Am. Chem. Soc.*, **56**, 4 (1934).

(12) E. H. Lanman and B. J. Mair, *ibid.*, **56**, 390 (1934).

(13) R. E. Gibson, *ibid.*, **57**, 284 (1935).

volumes for the two pressures times the difference in pressure.

b. *Reference Concentrations. Molality-Molarity Conversion.* The average of the value of x^2 for the meniscus and the maximum radius is selected as the reference and, as a first approximation, the initial concentrations are assumed to occur at this point. These values are corrected iteratively by integration over the limits of the cell; for sector shaped cells, such as are used here

$$c_0(x_\omega^2 - x_\alpha^2) = \int_{x_\alpha^2}^{x_\omega^2} cd(x^2) \quad (7)$$

where c is concentration in moles/l.; the subscript α indicates meniscus; ω , maximum radius; and subscript 0, the initial concentration of the component in question. Concentrations are first computed at equal intervals of x^2 by eq. 3, the integral is evaluated by Simpson's rule, and adjustments are made in the reference concentrations until eq. 7 is satisfied to the desired convergence.

Solution density ρ is required for the conversion of molality to molarity and for other purposes. Values of density for 1 atm. are obtained with an equation derived by algebraic manipulation of the equations for partial molal volumes (see section a). A Tait-Gibson procedure,^{9b} analogous to that used to correct volumes for pressure, is used to correct densities for pressure. Molar concentrations in eq. 7 are corrected for pressure with the ratio of densities at the pressures in question. The initial concentration is likewise corrected by the ratio of its density at 1 atm. to its density at the pressure at the average value of x^2 .

c. *Pressure.* Pressure is evaluated by the equation

$$P_{II} - P_I = \int_{x_I}^{x_{II}} \rho \omega^2 x \, dx$$

It is customary in the interpretation of ultracentrifugation (except in density gradient work) to make the approximation that ρ is independent of radius. This procedure is satisfactory only for a first approximation. By iteration, a corrected table of P at the desired radii is obtained by summing elements of the integral for small increments of x^2 from the meniscus to the radius in question; in each element, the appropriate average value of ρ is used.

d. *Activity Coefficients.* Data for the limiting two-component solutions (HCl-H₂O and BaCl₂-H₂O) are already available, and the only problem they pose is to express them in a form suitable for machine computation. This is done by fitting literature activity coefficients by a least-squares procedure to an equation of the form

$$\nu_k \log \gamma_{\pm k} = (\text{DH})_k + b_{kk}m_k + d_{kkk}m_k^2 + f_{kkkk}m_k^3 + \dots \quad (8)$$

with as many terms in the power series as justified by the precision of the data. The symbol (DH)_k refers to a Debye-Hückel term

$$\frac{-\nu_k |z_{+k}z_{-k}| \mathcal{D}\sqrt{I}}{1 + a_k' \sqrt{I}}$$

where z is the charge of an ion; \mathcal{D} , the Debye-Hückel slope (0.50848 was used here); and a' , an empirical parameter sometimes associated with the distance of closest approach of the ions. In cases, such as the present, in which satisfactory representations of the two-component data can be obtained with a single value of a' (here 1.5), this form for (DH)_k is adequate. If a' for the two electrolytes is not the same, however, the Debye-Hückel term expressed in this fashion will not satisfy the cross differentiation restriction (eq. 1) and a more complicated form must be used.¹⁴

For HCl, in order to utilize the full precision of the available values for activity coefficients of HCl,¹⁵ terms linear, quadratic, and cubic in m were required. These are listed in Table II, and deviations between

Table II: Parameters in Activity Coefficient Eq. 8-10^a

	1 E.m.f. ^b	2 Isopiestic ^c	3 Ultra- centrifuge
a'	1.5 ^d	1.5 ^d	1.5 ^d
b_{AAA}	0.21080		
d_{AAA}	0.01320		
f_{AAAA}	-0.000836		
b_{BB}		0.2357	0.2522 ^e
d_{BBB}		0.0424	0.0338 ^e
f_{BBBB}		0 ^d	0 ^d
b_{AB}			0.2838
d_{AAB}			0.0280
d_{ALB}			0.0491
f_{AAAB}			-0.00198
f_{AABB}			-0.00437
f_{ABBB}			-0.00837

^a A is HCl, B is BaCl₂. ^b Ref. 15. ^c Ref. 16. ^d Set at indicated values. Agreement with experiment was not appreciably improved by varying these parameters. ^e From centrifugation of BaCl₂-H₂O solutions.

(14) G. Scatchard, *J. Am. Chem. Soc.*, **83**, 2636 (1961); see eq. 24.

(15) H. S. Harned and R. W. Ehlers, *ibid.*, **55**, 2179 (1933); G. Akerlöf and J. W. Teare, *ibid.*, **59**, 1855 (1937). The values used were taken from ref. 9, pp. 716 and 751. They did not agree at corresponding concentrations, but the ratios of γ_{\pm} for different concentrations did. We have therefore matched them in the region of concentration overlap.

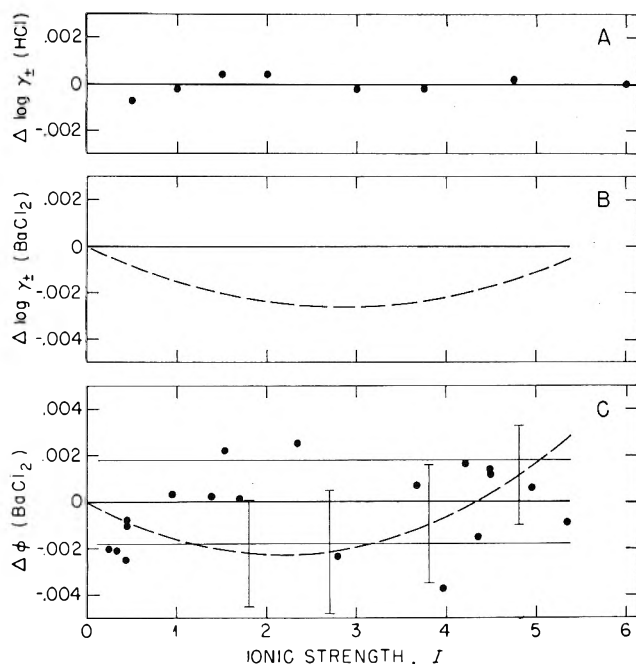


Figure 1. Precision of two-component data: (A) deviations of literature values (ref. 15) of $\log \gamma_{\pm \text{HCl}}$ (\bullet) from those computed by eq. 8 (—); (B) deviations of $\log \gamma_{\pm \text{BaCl}_2}$ computed with parameters obtained from ultracentrifuge data (---) (Table II, column 3) from those obtained from isopiestic data (—) (Table II, column 2); (C) deviations of ϕ_{BaCl_2} computed with parameters obtained from ultracentrifuge data (---) and experimental (\bullet) (ref. 16) from those computed with the parameters obtained from isopiestic data (—). Horizontal lines indicate one standard error on each side of the origin for isopiestic data, and vertical bars indicate one standard error on each side of the midpoint for ultracentrifuge data.

literature values and those computed from eq. 8 are given in Fig. 1A.

For BaCl_2 , an equation for activity coefficients was obtained from literature isopiestic data,¹⁶ measured against KCl solutions. (The values of ϕ for the KCl standard at molalities in isopiestic equilibrium with the BaCl_2 solutions were interpolated from the values listed by Robinson and Stokes¹⁷ at even molalities. This interpolation was accomplished by a least-squares fit of ϕ_{KCl} to an equation with a Debye-Hückel term¹⁸ and terms linear, quadratic, and cubic in molality.) Computed and experimental values of ϕ_{BaCl_2} are compared in Fig. 1C. The activity coefficient parameters¹⁹ corresponding to the fit of the ϕ -values are listed in Table II, column 2; terms linear and quadratic in molality were sufficient to represent the data within the precision of the measurements.

In expressions for the three-component solutions, the cross-differentiation requirement of eq. 1 can be met by equations in a Scatchard form²⁰

$$\begin{aligned} \nu_A \log \gamma_{\pm A} = & (\text{DH})_A + b_{AA}m_A + d_{AAA}m_A^2 + \\ & f_{AAAA}m_A^3 + b_{AB}m_B + 2d_{AAB}m_Am_B + \\ & d_{ABB}m_B^2 + 3f_{AAAB}m_A^2m_B + \\ & 3f_{AABB}m_Am_B^2 + f_{ABBB}m_B^3. \end{aligned} \quad (9)$$

and

$$\begin{aligned} \nu_B \log \gamma_{\pm B} = & (\text{DH})_B + b_{BB}m_B + d_{BBB}m_B^2 + \\ & f_{BBBB}m_B^3 + b_{AB}m_A + d_{AAB}m_A^2 + 2d_{ABB}m_Am_B + \\ & f_{AAAB}m_A^3 + 3f_{AABB}m_A^2m_B + 3f_{AABB}m_Am_B^2 \end{aligned} \quad (10)$$

In the particular application of interest, subscript A refers to HCl and B to BaCl_2 . Coefficients having in their subscripts only A's or B's are obtained from activity coefficient data of the two-component solutions of A and B.

Harned and Gary's⁶ values of α_{12} vary with ionic strength, and the variation is more than linear. If α_{12} is represented by a quadratic

$$\alpha_{12} = \alpha_{12}^\circ + \beta I + \delta I^2 \quad (11)$$

and eq. 2, representing Harned's rule, is rewritten in the form

$$\begin{aligned} \nu_A \log \gamma_{\pm A} = & (\text{DH})_A + \frac{b_{AA}}{S_A}I + \frac{d_{AAA}}{S_A^2}I^2 + \\ & \frac{f_{AAAA}}{S_A^3}I^3 - \nu_A \alpha_{12} I_B \end{aligned} \quad (2a)$$

where $S_A = I_A/m_A = (1/2)\mathbf{a}(\mathbf{a} + 1)$, it follows that the cross terms of eq. 9 and 10 are given by

$$\begin{aligned} b_{AB} &= S_B \left(\frac{b_{AA}}{S_A} - \nu_A \alpha_{12}^\circ \right) \\ d_{AAB} &= \frac{1}{2} S_B \left(\frac{2d_{AAA}}{S_A} - \nu_A S_A \beta \right) \\ d_{ABB} &= S_B^2 \left(\frac{d_{AAA}}{S_A^2} - \nu_A \beta \right) \\ f_{AAAB} &= \frac{S_B}{S_A} f_{AAAA} - \frac{\nu_A \delta S_A^2 S_B}{3} \end{aligned}$$

(16) R. A. Robinson, *Trans. Faraday Soc.*, **36**, 735 (1940).

(17) R. A. Robinson and R. H. Stokes, "Electrolyte Solutions," 2nd Ed., Butterworth and Co., Ltd., London, 1959, p. 476.

(18) G. Scatchard and L. F. Epstein, *Chem. Rev.*, **30**, 211 (1942).

(19) M. H. Lietzke and R. W. Stoughton, *J. Phys. Chem.*, **66**, 508 (1962).

(20) Equations of this form result from equations of ref. 14, followed by simplification of numerical coefficients; similar expressions were used in ref. 8.

$$f_{AABB} = \left(\frac{S_B}{S_A}\right)^2 f_{AAAA} - \frac{2}{3} \nu_A S_B^2 S_A \delta$$

$$f_{ABBB} = \left(\frac{S_B}{S_A}\right)^3 f_{AAAA} - \nu_A S_B^3 \delta$$

where $S_B = I_B/m_B = (1/2)\mathbf{b}(\mathbf{b} + 1)$.

It can be seen that in this case the parameters depend only on those of the limiting two-component solutions and those defining α_{12} .

e. Summary of Computation of Concentration Distribution. Equations 3 are first solved at equal intervals of x^2 for evaluation of the reference concentrations by integration. Iteration is continued until changes in the pressure table have no appreciable effect on concentration. With the converged values of reference concentration, eq. 3 is then solved for concentrations at the fringe radii in the solution compartment and concentrations of the radii in the background compartment from which light interferes with the solution compartment; on machines having unsymmetrical masks on the upper collimating lens, radii corresponding optically will be a little different in the two components.⁹ The pressure table is converged in the course of computations at the fringe positions also.

2. Computation of Refractive Index Pattern. Equations relating concentrations and refractive index of solutions of the two electrolytes in question (at 1 atm.) have been presented earlier.¹⁰ As with volumes, accumulation of data has led to slight modifications of the parameters; the equation used in analysis of results follows

$$\left(\frac{\Delta n}{c}\right)_{546} = (0.0085678 - 0.0001766c + 0.0000089c^2)x_{\text{HCl}} + (0.0309351 - 0.0018436c + 0.0002683c^2)x_{\text{BaCl}_2} + 0.000310x_{\text{HCl}}x_{\text{BaCl}_2}c \quad (12)$$

where $c = c_{\text{HCl}} + c_{\text{BaCl}_2}$ and $x_i = c_i/c$. For refractive index computations, molalities are converted to molarities by methods outlined in section 1b. The refractive indices of the solutions at 1 atm. are given by the equation

$$n^{(1)} = n_0^{(1)} + \left(\frac{\Delta n}{c}\right)c \quad (13)$$

where $n_0^{(1)}$ is the refractive index of water at atmospheric pressure.

Refractive indices of solutions are affected by pressure. With relatively dilute solutions, it has been sufficient to make a correction for the difference in

pressure between solution and background by assuming that the pressure effect on the refractive index of the solution in question was the same as for the solvent.⁵ This procedure turned out not to be adequate with the concentrated solutions used in this study, since the solutes affect the compressibility too greatly. To our knowledge there is no information in the literature concerning the effect of pressure on the refractive indices of solutions of even one solute. We have therefore estimated corrections from the Gladstone–Dale or the Lorentz–Lorenz equations.

If the Lorentz–Lorenz refractivity is assumed not to vary with pressure in the range of interest

$$\frac{[n^{(P)}]^2 - 1}{[n^{(P)}]^2 + 2} \frac{1}{\rho^{(P)}} = \frac{[n^{(1)}]^2 - 1}{[n^{(1)}]^2 + 2} \frac{1}{\rho^{(1)}} = \frac{L}{\rho^{(P)}} \quad (14)$$

and

$$n^{(P)} = \left[\frac{2L + 1}{1 - L}\right]^{1/2} \quad (15)$$

where the superscripts indicate the pressure.

A similar equation is readily obtained from the Gladstone–Dale equation, which holds well for the solvent.²¹ In the results reported here we have used eq. 15 to correct refractive indices for pressure, but use of the Gladstone–Dale approach instead did not affect the values of α_{12} significantly.

The refractive indices corrected for pressure were computed for solution and background at the radii corresponding to fringe positions. The computed difference between the two, corrected for the slight difference in cell thickness h of the two compartments in the direction of observation⁸

$$n^* = n_{\text{soln}} - \frac{h_{\text{bg}}}{h_{\text{soln}}} n_{\text{bg}}$$

was then obtained.

The fringe pattern gives the radial distances between points having differences in n^* of $\delta n^* = (\lambda/h_{\text{soln}})$, where λ is the wave length of the light. The experimental values of n^* to be compared with the computed values are obtained by assigning the computed value to a fringe near the center of the cell and adding or subtracting δn^* successively for the values at other fringe positions.

3. Evaluation of Parameters in the Activity Coefficient Equations. In an ideal case of no experimental error and a completely correct equation in form and values of parameters, there would be zero deviation of the values of $n^*_{\text{exp}} - n^*_{\text{comp}}$ with radius in all the ex-

(21) R. M. Waxler and C. E. Weir, *J. Res. Natl. Bur. Std.*, **67A**, 163 (1963).

periments. In practice, of course, one can only approach this situation. It is possible to proceed by adjusting the parameters for individual centrifugations, but we have found it profitable to devise a scheme for treating several runs at once. To do so, it is necessary to be able to summarize the results of a given centrifugation. Since it turns out that the deviations $n^*_{\text{exp}} - n^*_{\text{comp}}$ are usually approximately linear in x^2 , we have adopted the slope of this line, obtained by least-squares procedure, as the quantity to be minimized for all experiments.

The values of the slopes are used as the dependent variables for the Oak Ridge GLS nonlinear least-squares program.²² This program then adjusts those parameters being varied (here α_{12}° , β , and δ) to give the minimum least-squares deviations of the slopes of all runs from zero. Our programs will allow for equations for $\log \gamma_{\pm}$ up to cubic in concentration for the two-component systems and the cross terms (*i.e.*, up to $m_{\text{BaCl}_2} m_{\text{HCl}}^2$ or $m_{\text{BaCl}_2}^2 m_{\text{HCl}}$). In addition, the Debye-Hückel a' can be varied, if desired. The subroutine for calculating the activity coefficients will accept either the Harned's rule coefficients of eq. 11 or the coefficients of eq. 9 and 10.

The computations were carried out on an IBM 7090 computer.²³

Results and Discussion

1. *BaCl₂-H₂O*. To test some of the aspects of our computational procedure, particularly those involving compressibility, for which there are no data available for more than two components, we have carried out a series of centrifugations of BaCl₂-H₂O solutions. Previous measurements of two-component activity coefficients with interference optics in which the background compartment contained only the solvent were limited to dilute solutions since with concentrated solutions the refractive index difference between compartments becomes excessive (see Experimental section). In the method outlined above, this restriction is no longer necessary since any solute whose activity coefficients are known can be used in the background compartment.

We have centrifuged five BaCl₂-H₂O solutions at two speeds (Table I). In computation, to avoid division by zero or terms involving the logarithm of zero, the input values of HCl concentration in the solution compartment were set to a negligibly small value (m_{HCl} *ca.* 10^{-10}). The parameters obtained from the centrifugations at both speeds for the five solutions are listed in Table II and may be compared with the isopiestic values. Inclusion of a cubic term did not improve the fit appreciably. The deviation of ultra-

centrifuge values of $\log \gamma_{\pm \text{BaCl}_2}$ from those derived from the isopiestic data of Robinson¹⁶ are shown in Fig. 1B. For a comparison with isopiestic data, the deviation of values of ϕ_{BaCl_2} computed with coefficients corresponding to those summarizing the ultracentrifugation results (Table II, column 3) are plotted in Fig. 1C, along with the experimental osmotic coefficients. It is clear that the differences between the centrifuge and vapor pressure results are essentially within the scatter of the isopiestic results. An additional indication of the precision of the centrifuge method is given by the deviations between computed and experimental refractive index patterns (Fig. 2).

Since our objective is evaluation of the cross terms by ultracentrifugation we have used the BaCl₂-H₂O parameters obtained by ultracentrifugation in the analysis of three-component results; it is possible that small errors might drop out. However, use of the isopiastically obtained parameters for BaCl₂ (Table II, column 2) in the interpretation of ultracentrifugation does not affect activity coefficients obtained for three-component solutions greatly.

2. *HCl-BaCl₂-H₂O*. A total of nine solution compositions, some of which were centrifuged to equilibrium at two speeds, were examined (Table I). To check precision and reproducibility, two of the solutions of approximately the same composition (0.5 *M* BaCl₂-1.5 *M* HCl) were prepared from different stocks and centrifuged independently. Two samples of these solutions were placed in separate cells of the five-cell rotor. The other compositions were selected to provide two ratios of m_{HCl} to m_{BaCl_2} at each of the four ionic strengths (*ca.* 1, 2, 3, and 4). In total, with different speeds and identical solutions in more than one cell counted separately, there were two "observations" at $I = 1$, three at $I = 2$, eight at $I = 3$, and three at $I = 4$.

A least-squares analysis of all results, carried out in the manner described in the Computation section, gave an equation for the Harned coefficient

$$\alpha_{12} = 0.0581 + 0.00387I - 0.000263I^2 \quad (11a)$$

The cross terms of eq. 9 and 10 consistent with eq. 11a are listed in Table II, column 3.

An analysis of runs grouped according to the ionic strength was also carried out with the parameter δ of eq. 11 set at zero. Values of α_{12} obtained in this way are compared with those of Harned and Gary and those implied by eq. 11a in Fig. 3. It is seen that the

(22) W. R. Busing and H. A. Levy, Oak Ridge National Laboratory Report TM-271 (1962).

(23) Most of the program is written in the Fortran II language and symbolic card decks are available from the authors.

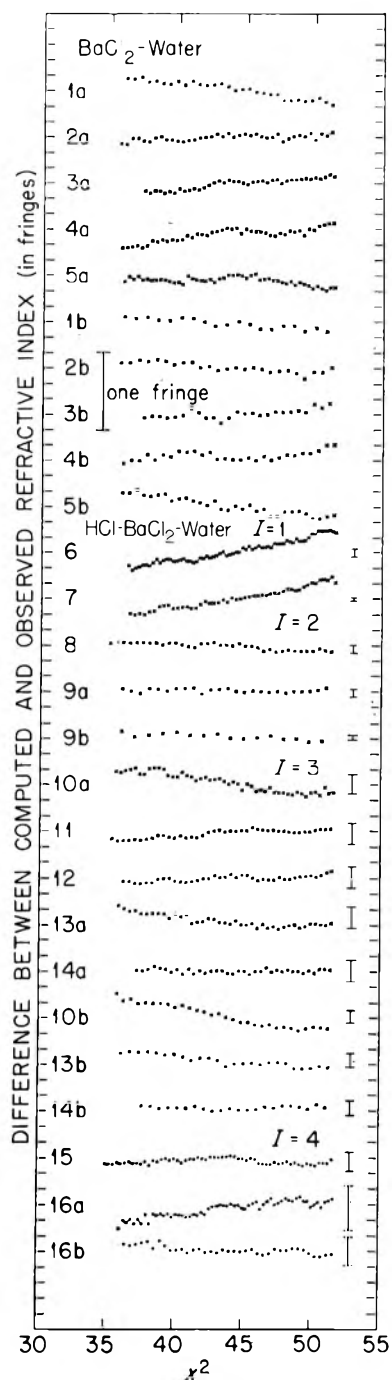


Figure 2. Deviations of observed from computed refractive indices for individual centrifugations. Numbers on the left refer to the experiment no. in Table I (a refers to 20,410 r.p.m. and b to 16,200 r.p.m.). Each vertical division represents 0.2 fringe. Bars on right represent fringe error across the cell equivalent to about 0.001 in α_{12} .

agreement between the two interpretations of the centrifuge results and the e.m.f. values is good at ionic strengths 2 and 3, but not so good at $I = 1$ and $I = 4$ (there are no e.m.f. values available at $I = 4$).

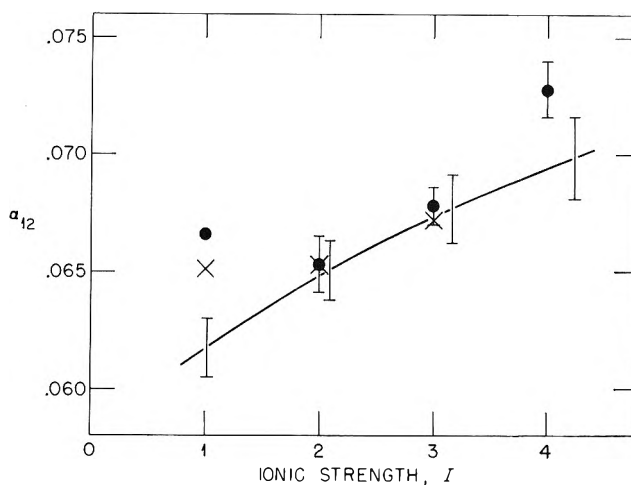


Figure 3. Comparison of values of α_{12} : X, e.m.f. (ref. 6); ●, ultracentrifugation, experiments grouped by ionic strength, linear variation of α_{12} with I ; (—) ultracentrifugation, all runs, quadratic variation of α_{12} with I (eq. 11a). Vertical bars indicate one standard error on each side of the midpoint and were obtained from the standard errors of the parameters and the correlation matrix.

The probable reason lies in the dependence, discussed in the introduction, of BaCl_2 activity coefficients on $d\alpha_{12}/dI$. The cross terms obtained from the ultracentrifugation experiment, in contrast to the values of α_{12} from e.m.f., are directly sensitive to the non-ideality of BaCl_2 , which in turn is sensitive to the variation of α_{12} with I . One and 4 m are at the extremes of the experimental ionic strength range and the derivatives are therefore probably not so well determined as in the middle of the range. In this respect, it is of interest that, if the 1 m experiments were omitted from the least-squares input, agreement was not nearly so good at $I = 2$ and 3 between the fit with α_{12} expressed as a quadratic in I and the other values. The derivatives $d\alpha_{12}/dI$, for the linear fit (runs grouped by ionic strength) compared with those given by the quadratic, eq. 11a, are as follows: $I = 1$, 0.00221, 0.00334; $I = 2$, 0.00299, 0.00272; $I = 3$, 0.00228, 0.00229; and $I = 4$, 0.00166, 0.00177. It is possible that the procedure of grouping runs of approximately the same ionic strength and fitting α_{12} to an equation linear in I gives better values of activity coefficients at the extremes of the concentration range. It seems so here at $I = 1$.

A perhaps more meaningful comparison of results from the two methods is given in Fig. 4, in which are plotted the deviations of $\log \gamma_{\pm \text{HCl}}$ computed from the ultracentrifugation parameters (Table II, column 3) from those given by the e.m.f. values of α_{12} (the HCl two-component parameters of Table II, column 1, were

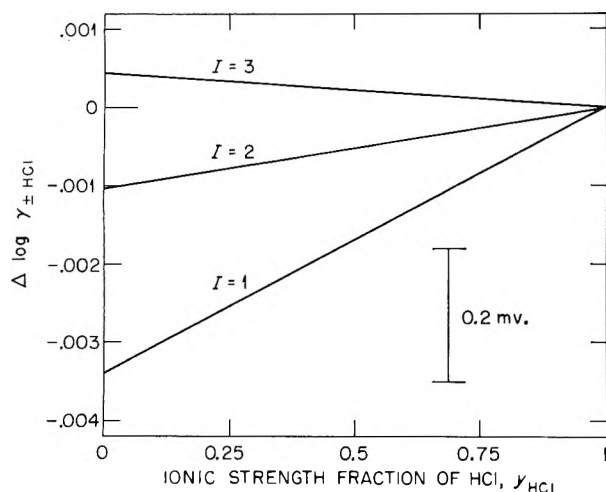


Figure 4. Deviations of $\log \gamma_{\pm \text{HCl}}$ given by ultracentrifuge results (Table II, column 3) from those given by e.m.f. (ref. 6).

used in both cases). The agreement is good, though not perfect; as expected it is seen to be better for ionic strengths in the middle of the concentration range.

Agreement of the experimental fringe patterns with those computed from the parameters of Table II, column 3, for individual centrifugations is shown in Fig. 2. The agreement is satisfactory in most cases, within ± 0.2 fringe; we believe our experimental uncertainty of locating fringe positions (based on reproducibility of water runs) to be about half of this range, and other uncertainties (see section 4) could account for the rest.

3. *Activity Coefficients of BaCl_2 .* On the assumption that Harned's rule was obeyed also by BaCl_2 , Harned and Gary⁶ derived values of the coefficient α_{21} for the salt from two-component osmotic coefficients and their measured values of α_{12} . Constancy of the sum ($\nu_1 S_1 \alpha_{12} + \nu_2 S_2 \alpha_{21}$) as a function of ionic strength was taken to indicate validity of the assumption.

Since the cross terms obtained by ultracentrifugation were obtained without such an assumption concerning the BaCl_2 behavior, it is of interest to see what they imply. Using the parameters of Table II, column 3, and eq. 10, values of α_{21} were obtained from $\log \gamma_{\pm \text{BaCl}_2}$ at $y_{\text{HCl}} = 0$ and 1 and are listed in Table III. The deviations of $\log \gamma_{\pm \text{BaCl}_2}$ at intermediate values of y_{HCl} from Harned's rule behavior (analogous to eq. 2) are also listed in Table III. It is seen that $\log \gamma_{\pm \text{BaCl}_2}$ at constant ionic strength is indeed to a good approximation linear with the fraction of ionic strength contributed by HCl. The slopes are similar to those reported by Harned and Gary⁶; they list $\alpha_{21} = -0.0716$, -0.0824 , and -0.0866 at $I = 1, 2$, and 3 , respectively.

Table III: Deviation of $\log \gamma_{\pm \text{BaCl}_2}$ from Linear Variation with I_{HCl}

I	α_{21}	I_{HCl}	Deviation
1	-0.0740	0.25	0.0000
		0.50	0.0000
		0.75	0.0000
2	-0.0801	0.50	0.0001
		1.00	0.0001
		1.50	0.0000
3	-0.0849	0.75	0.0006
		1.50	0.0006
		2.25	0.0003
4	-0.0883	1.00	0.0018
		2.00	0.0019
		3.00	0.0010

4. *Effect of Input Parameters.* It seemed of interest to see if the deviations between ultracentrifugation and e.m.f. results in Fig. 4 could be attributed to uncertainties in the two-component BaCl_2 parameters. Use of isopiestic values (Table II, column 2) gave average shifts in the deviations of *ca.* 0.001 in $\log \gamma_{\pm \text{HCl}}$, not enough to account for all the differences.

The analysis of results is so involved that it seemed worthwhile to test the influence of various experimental uncertainties on the results. The effect of variations of input parameters on α_{12} is indicated in Table IV for

Table IV: Effect of Various Input Parameters on α_{12} , Experiment 13a

	$\Delta \alpha_{12}$
Elimination of compressibility corrections	-0.0013
Equations from ref. 10 for refractive indices	0.0002
Equations from ref. 10 for partial molal volumes	0.0001
Isopiestic parameters for $\log \gamma_{\pm \text{BaCl}_2}$ (Table II, column 2)	-0.0010
Gladstone-Dale equation for $n^{(P)}$	-0.0002
Initial c_{BaCl_2} increased 1%	-0.0012
Optical magnification increased 0.3%	0.0004
R.p.m. increased 0.5%	-0.0014
Temperature increased 1°	0.0005
δ_s^* increased 0.5%	0.0007
Radius of center of cell increased 0.01 cm.	-0.0002

one of the observations (experiment 13a, Table I). These are evaluated from the shift of α_{12} necessary to give zero slope in a deviation plot similar to Fig. 2 and are somewhat approximate, though adequate for present purposes. (The individual values of α_{12} in Table I and the fringe error equivalents of α_{12} in Fig.

2 involve similar approximations.) It can be seen that the values of α_{12} obtained are affected trivially by use of the refractive index and volume parameters of eq. 12 and 5, rather than those of ref. 10. The same is true if correction for the effect of pressure on refractive index is made with the Gladstone–Dale equation instead of the Lorentz–Lorenz, or for likely errors in the concentrations of solutes (the error in concentrations should be much less than 1%). Neglect of pressure effects on volumes and refractive indices altogether, and use of the isopiestic parameters of $\log \gamma_{\pm \text{BaCl}_2}$, rather than those evaluated by ultracentrifugation, have a larger, but still small, effect; these effects were larger with a more concentrated solution (experiment 15, Table I).

The effect of uncertainties directly related to the ultracentrifugation experiment are in general small. The uncertainty in equilibrium temperature is only about 0.1°; in optical magnification, 0.1%; and the accuracy of location of the reference radius, 0.01 cm. The quantities whose errors have the largest effect on the results are probably the speed of rotation and the change in refractive index attributed to a fringe unit. The average r.p.m. is known to about 0.1%. Uncertainties in the measurement of the thickness of the column of solution in the direction of observation and in the isolation of the 546 m μ mercury line from the output of the pressure broadened source affect the relation of refractive index and fringes; the over-all uncertainty here is probably not more than 0.3%.

5. *Discussion.* The present results indicate that equilibrium ultracentrifugation can be a useful method for determination of activity coefficients of two electrolytic solutes in aqueous solution, at least in cases where one of the solutes is of fairly high molecular weight. It also appears that the assumptions made concerning compressibilities of three-component systems, and the techniques of correcting for pressure effects on refractive indices, are satisfactory. The deviations of the potentials from the linear relationship were within 0.05 mv.⁶ From the fact that ultracentrifugation parameters gave about as good agreement with fringe patterns as could be expected (Fig. 2), whereas the deviations of $\log \gamma_{\pm \text{HCl}}$ differ from the e.m.f. values by as much as 0.4 mv. (Fig. 4), it appears that ultracentrifugation is at present not so accurate as e.m.f. in those favorable cases for which reversible electrode systems are available.

There are, however, relatively few systems which can be studied by e.m.f. With respect to techniques of more general applicability, isopiestic errors in ϕ of 0.001 would correspond to ca. 0.05 mv.; such accuracy in ϕ should be attainable in the concentration range under discussion. Comparison of the ultracentrifugation and isopiestic results for two-component BaCl_2 (Fig. 1) is not so unfavorable for ultracentrifugation as this implies. It is difficult for us to estimate which technique involves greater effort, once one is set up. We come to different conclusions from the statements of different people experienced in isopiestic measurements, but suspect that ultracentrifugation probably requires somewhat greater exertion because of the auxiliary density and refractive index measurements required. These data have intrinsic interest, however. In cases where Harned's rule does not hold for either component, analysis of data for both methods may be more difficult since it likely will be necessary to determine more parameters. In the present case, we have experienced difficulty in obtaining convergent solutions by varying directly the cross terms of eq. 9 and 10.

Ultracentrifugation can be used in the relatively rare systems involving volatile solutes, as the isopiestic method of course cannot. Even in its present state of development, it should be useful as a confirmatory technique for particularly important cases (such as perchlorate solutes, in view of the wide use of such media in studies of complexing reactions). With consolidation of the many advances in ultracentrifugation technique now being made,²⁴ it seems possible that the method may become more attractive in the future.²⁵

Acknowledgment. We thank Kurt A. Kraus for suggesting this problem G. Scatchard for suggesting the method employed to correct refractive indices for pressure, and both for helpful discussion. We are indebted to Neva Harrison for technical assistance.

(24) See, for example, P. E. Hexner, R. D. Boyle, and J. W. Beams, *J. Phys. Chem.*, **66**, 1948 (1962); and H. K. Schachman, *Biochemistry*, **2**, 887 (1963).

(25) The most annoying experimental difficulty at present, and one much more serious if experiments are attempted at higher temperatures, is the tendency for drive oil to get on optical components. This difficulty seems to have been getting worse in recent years, presumably because of less rigorous reworking of drives by the manufacturer. There should be several remedies, though it may be necessary for individual users to work them out.

The Heat and Entropy of Formation of Boron(I) Fluoride(g)

by Jay Blauer, M. A. Greenbaum, and Milton Farber

*Research and Development Laboratories, Maremont Corporation,
Pasadena, California (Received April 6, 1964)*

The equilibrium $\frac{2}{3}\text{B}(c) + \frac{1}{3}\text{BF}_3(g) = \text{BF}(g)$ was studied in the temperature range 1307–1505°K. by means of transpiration at pressures below 300 μ . The enthalpy and entropy changes of the reaction in this temperature range were found to be 59.7 ± 2.6 kcal./mole and 25.1 ± 1.9 cal./deg./mole, respectively. The data have been interpreted and extrapolated to yield the second law heat of formation, $\Delta H_{f, 298^\circ\text{K.}} = -29.0 \pm 2.6$ kcal./mole, and entropy, $S_{298^\circ\text{K.}} = 47.6 \pm 1.9$ cal./deg./mole, of gaseous BF. Partial pressure studies indicate that the quantity of $\text{BF}_2(g)$ present under the experimental conditions is negligible.

Introduction

No experimental measurements of the heat of formation or entropy of gaseous BF have been reported to date. Estimated values of these functions have been reported.¹ These values are given as: $\Delta H_{f, 298} = -45.47$ kcal./mole and $S_{298} = 47.89$ cal./deg./mole. As a continuing part of our studies of the thermodynamic properties of the light metal compounds it was decided to undertake an experimental program to determine these thermodynamic values.

Experimental

Small pieces of crystalline boron (obtained from Kern Chemical Co.) of >99.5% purity were placed in a rhenium combustion boat. The boron and combustion boat had been weighed previously. The combustion boat was placed in a zirconia furnace tube with a 2.5-cm. i.d. The combustion tube was flushed continuously with a stream of argon gas during the loading operation. The furnace used in the present study was a Leco tube furnace with automatic temperature controls. The absolute temperature was established by means of a calibrated platinum-platinum-10% rhodium thermocouple. Once this was set the automatic controller maintained the temperature to $\pm 5^\circ$.

After the system had been evacuated, boron trifluoride (from Matheson Co.) having a purity in excess of 99.5% was admitted through a very fine metering valve. The gas was preheated by passage over a bed of alumina chips. No reaction was found to occur between the $\text{BF}_3(g)$ and Al_2O_3 chips over the tempera-

ture range specified. The total pressure of the system never exceeded 300 μ . Pressures were determined by means of a thermocouple gauge which was placed at the end of the furnace tube and which had been calibrated for the pressure at the center of the tube by means of a McLeod gauge. The transpired gases were collected in a cold trap cooled in liquid nitrogen.

At the end of each run the combustion boat was removed from the furnace and allowed to cool in an atmosphere of argon gas. The boron trifluoride in the cold trap was allowed to expand at room temperature and its pressure determined manometrically. The sample of boron chips was weighed separately due to the fact that the rhenium boat reacted to a slight extent with the boron trifluoride. However, the amount of this side reaction was quite small (less than 5%) and had no effect on the experimental results when the boron sample was weighed separately from the boat.

Treatment of Data

The theory for the molecular flow reaction method at very low pressures has been adequately described in a previous paper.²

If only BF(g) is formed under the experimental conditions considered, it is possible to show on the basis of the theory of molecular flow² that the following equation describes the conditions holding at equilibrium

(1) JANAF Thermochemical Tables, USAF Contract AF 33(616)-6149, Advanced Research Projects Agency, Washington 25, D. C.

(2) M. Farber and J. Blauer, *Trans. Faraday Soc.*, **58**, 2090 (1962).

$$K_p = \left(\frac{M_{BF}}{M_{BF_3}} \right)^{1/2} \left(\frac{\Gamma_{BF}}{\Gamma_{BF_3}} \right) P_{BF_3}^{2/3} \quad (1)$$

The symbols appearing in eq. 1 have the following definitions: K_p is the equilibrium constant, M_{BF} is the molecular weight of BF, M_{BF_3} is the molecular weight of BF₃, Γ_{BF} is the number of moles of BF escaping from the reaction zone per hour, Γ_{BF_3} is the number of moles of unreacted BF₃ escaping from the reaction zone per hour, and P_{BF_3} is the equilibrium pressure of BF₃. The calibration of the apparatus indicated that the following equation applies

$$P_{BF_3} = 0.00367 \Gamma_{BF_3} \quad (2)$$

where P_{BF_3} is expressed in units of atmospheres. A combination of eq. 1 and 2 yields eq. 3, namely

$$K_p = 0.02368 \frac{\Gamma_{BF}}{\Gamma_{BF_3}^{1/2}} \quad (3)$$

It was found that the reaction is markedly influenced by changing the surface area, or equivalently the weight, of the boron sample. It was found that the effect of surface area could best be described by means of the following equation

$$\log K_p = \log K_p^0 - \frac{J}{\omega} \quad (4)$$

where K_p^0 is the value of K_p at infinite surface area, J is a constant, and ω is the weight of the sample. It was further found that J is not temperature dependent. The over-all effect of both temperature and surface area upon the extent of the reaction was expressed by means of the following equation

$$\log K_p = \frac{\Delta S}{R} - \frac{\Delta H}{RT} - \frac{J}{\omega} \quad (5)$$

Results and Discussion

The experimental data are tabulated in Table I. The data taken at 1375°K. and at 1476°K. are shown plotted in Fig. 1 in the form described by eq. 4. The values of J and $\log K_p^0$ for these two temperatures were evaluated by the method of least squares and the results are tabulated in Table II. A variance ratio test³ indicates that the variances of J are statistically identical at the two temperatures; consequently, a Student's *t*-test can be applied to test the identity of the slopes themselves. The *t*-test indicates that within experimental error the slopes are identical and independent of temperature.

The values of the equilibrium constants for each run at 1375°K. have been corrected for surface effects by means of eq. 4 and tabulated in Table III as a function

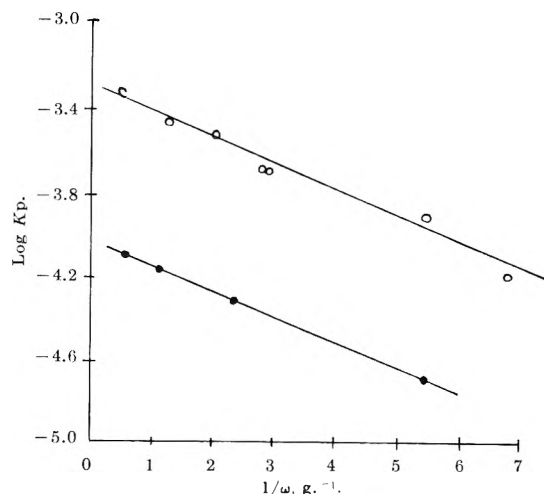


Figure 1. Effect of surface area upon the extent of reaction: O, data taken at 1476°K.; ●, data taken at 1375°K.

Table I: Experimental Data for the BF₃(g)-B(s) Reaction

Run no.	Γ_{BF} , moles/hr.	Γ_{BF_3} , moles/hr.	K_p , atm. ^{2/3}	$1/\omega$, g. ⁻¹	T , °K.
5	2.03×10^{-3}	3.97×10^{-2}	1.41×10^{-4}	2.19	1462
7	3.47×10^{-3}	8.58×10^{-2}	1.86×10^{-4}	2.09	1462
8	4.00×10^{-3}	8.48×10^{-2}	2.16×10^{-4}	1.16	1462
10	1.75×10^{-3}	5.99×10^{-3}	2.29×10^{-4}	1.52	1462
13	3.68×10^{-3}	5.99×10^{-2}	2.23×10^{-4}	1.35	1462
14	9.94×10^{-4}	8.36×10^{-2}	5.39×10^{-5}	1.07	1347
15	4.02×10^{-4}	7.00×10^{-3}	4.98×10^{-5}	1.24	1347
16	3.58×10^{-4}	2.29×10^{-2}	2.99×10^{-5}	1.20	1347
17	9.34×10^{-4}	6.55×10^{-3}	1.18×10^{-4}	1.17	1403
18	1.62×10^{-3}	7.94×10^{-2}	8.92×10^{-5}	1.56	1403
19	1.27×10^{-3}	6.77×10^{-3}	1.59×10^{-4}	1.65	1437
20	3.64×10^{-3}	7.49×10^{-2}	2.04×10^{-4}	0.89	1437
21	8.18×10^{-4}	2.11×10^{-2}	7.02×10^{-5}	1.09	1375
22	2.30×10^{-4}	2.24×10^{-2}	1.93×10^{-5}	5.38	1375
23	5.53×10^{-4}	2.12×10^{-2}	4.73×10^{-5}	2.34	1375
24	1.05×10^{-3}	2.00×10^{-2}	9.17×10^{-5}	0.52	1375
25	3.92×10^{-3}	1.79×10^{-2}	3.56×10^{-4}	1.26	1476
26	2.30×10^{-3}	1.90×10^{-2}	2.04×10^{-4}	2.77	1476
27	4.77×10^{-3}	1.85×10^{-2}	4.26×10^{-4}	0.52	1476
28	1.52×10^{-3}	1.95×10^{-2}	1.34×10^{-4}	5.39	1476
29	2.15×10^{-3}	1.83×10^{-2}	1.93×10^{-4}	2.77	1476
30	2.31×10^{-3}	4.99×10^{-3}	3.24×10^{-4}	2.04	1476
31	1.14×10^{-3}	7.48×10^{-2}	6.40×10^{-5}	6.70	1476
32	7.58×10^{-3}	6.77×10^{-2}	4.40×10^{-4}	0.99	1505
33	4.96×10^{-3}	3.41×10^{-3}	7.78×10^{-4}	0.51	1505
34	3.63×10^{-3}	1.58×10^{-2}	3.42×10^{-4}	2.46	1505
35	2.74×10^{-4}	6.06×10^{-3}	3.57×10^{-5}	0.99	1307

of the equilibrium pressure of BF₃. Since these equilibrium constants are not dependent upon the pressure it can be concluded that BF(g) was the only product

(3) A. Hald, "Statistical Theory with Engineering Applications," John Wiley and Sons, Inc., New York, N. Y., 1957, p. 574.

Table II: Effect of Sample Surface Area upon the Extent of Reaction

Temp., °K.	<i>J</i> , g.	log K_p^0	K_p^0 , atm. ^{2/3}
1375	0.136 ± 0.006	-3.99 ± 0.02	1.02 × 10 ⁻⁴ ± 0.02 × 10 ⁻⁴
1476	0.125 ± 0.013	-3.30 ± 0.05	5.02 × 10 ⁻⁴ ± 0.24 × 10 ⁻⁴

formed under the experimental conditions. In establishing the criteria for molecular flow,² when bimolecular collisions were involved lower pressures were necessary than for reactions with trimolecular collisions. Since the reaction under study here involves a trimolecular collision, the pressures involved are well within the molecular flow regime.

Table III: Data Corresponding to 1375°K. which Have Been Corrected for Surface Effects

Run no.	P_{BF_3} , μ	K_p^0 , atm. ^{2/3}
5	111	2.65 × 10 ⁻⁴
7	239	3.39 × 10 ⁻⁴
8	236	3.01 × 10 ⁻⁴
10	17	3.55 × 10 ⁻⁴
13	170	3.29 × 10 ⁻⁴

Equation 5 was fitted to the data by the method of least squares. The data yield a heat of reaction of 59.7 ± 2.6 kcal./mole, an entropy change of 25.1 ±

1.9 cal./deg./mole, and a surface parameter *J* of 0.125 ± 0.011 g. at an average temperature of 1433°K.

The entropies and heats of formation of crystalline boron and gaseous boron trifluoride are well known and have been compiled in the literature.¹ Accordingly, the heat of formation and entropy of gaseous BF can be evaluated from the results of the experimental data. The results indicate values for ΔH_f 1433°K. and S_{1433}^0 of -30.9 ± 2.6 kcal./mole and 60.0 ± 1.9 cal./deg./mole, respectively. The corresponding estimated values which have been reported¹ are -47.4 kcal./mole and 60.3 cal./deg./mole, respectively. As is to be expected for a diatomic molecule the agreement between estimated and experimental entropies is very good. The heat of formation obtained by means of an analysis of least squares compares favorably with the value of -30.5 ± 0.5 kcal./mole obtained by means of an average of the third law values.

Interpolations with estimated values of the heat capacities¹ of all species involved yields a second law heat of formation and entropy of BF(g) at 298°K. of -29.0 ± 3 kcal./mole and 47.6 ± 2 cal./deg./mole, respectively. An average of the third law values gives a heat of formation at 298°K. of -28.6 ± 1 kcal./mole.

The excellent agreement between second and third law heats of formation, coupled with near-perfect agreement between experimental and theoretical entropies and high precision of the data, lends considerable confidence to the assumption that the values reported here represent reliable values for these thermodynamic functions. As mentioned previously, these values represent the first experimental ones for the BF(g) molecule.

Sublimation and Thermodynamic Properties of Zinc Oxide

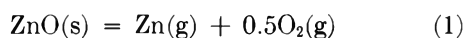
by Donald F. Anthrop and Alan W. Searcy

*Department of Mineral Technology and Lawrence Radiation Laboratory,
Inorganic Materials Research Division, University of California,
Berkeley, California (Received April 6, 1964)*

The sublimation of zinc oxide has been investigated by (a) Knudsen weight-loss measurements, (b) mass spectrometric measurements of the vapors effusing from Knudsen cells containing either zinc oxide or a mixture of a gold-zinc alloy with zinc oxide, and (c) transpiration measurements in streams of helium and zinc vapors. Zinc oxide was found to sublime congruently by dissociation to zinc atoms and oxygen molecules only. Limits for the dissociation energies of $\text{ZnO}(\text{g})$ and $\text{Zn}_2\text{O}(\text{g})$ are calculated to be $D_{298}^{\circ}(\text{ZnO}) \leq 66$ kcal. and $D_{298}^{\circ}(\text{Zn}_2\text{O}) \leq 127$ kcal. The probable source of the high transport rate reported in the literature for zinc oxide in zinc vapor is shown to be reaction of water vapor and/or carbon dioxide with the metal to yield hydrogen and/or carbon monoxide, which reduces the zinc oxide to zinc vapor with regeneration of water vapor and/or carbon dioxide.

Introduction

After examining the data available in 1951, Brewer and Mastick¹ concluded that under neutral conditions zinc oxide sublimes congruently by decomposition to the gaseous elements according to the reaction



Brewer calculated a limit for the heat of dissociation of $\text{ZnO}(\text{g})$ to the gaseous atoms of $\Delta H^{\circ}_0 < 92$ kcal./mole.²

Moore and Williams measured the rate of sublimation of zinc oxide in atmospheres of oxygen, nitrogen, and zinc gas by a transport method.³ The sublimation rates which they obtained in streams of oxygen and nitrogen are in general agreement with the rates calculated from the thermodynamic data for reaction 1. However, the sublimation rates which they measured in an atmosphere of zinc vapor were greater by a factor of 100 than rates obtained in atmospheres of oxygen and nitrogen, and greater by a factor of 10^9 than the rate calculated from the equilibrium constant for reaction 1. Moore and Williams hypothesized that the zinc vapor somehow catalyzed the decomposition of zinc oxide.

Using a static system, Secco studied the sublimation rate of zinc oxide under varied partial pressures and varied total pressures of gas.⁴ He reported an equilibrium constant for the dissociation of solid zinc oxide to the gaseous elements greater than the equi-

librium constant calculated from thermodynamic data by a factor of 10^8 .

Pillay reinvestigated the rate of sublimation of zinc oxide by the transport method in atmospheres of helium and zinc⁵ and obtained results in essential agreement with those of Moore and Williams.

Moore and Williams quote Inghram and Drowart as reporting that no gaseous zinc oxide molecules are present in zinc oxide vapor that could account for the reported rates of vaporization that far exceed the maximum rates calculated by application of the Langmuir equation to thermodynamic data for reaction 1. The tentative explanations of the high sublimation rates given by Moore and Williams and by Secco both amount to proposals that decomposition of unstable intermediate reaction products yields higher concentrations of zinc and oxygen vapors than calculated for reaction 1. Both proposals amount, therefore, to the assumption that the equilibrium for reaction 1 can be shifted by catalysis. Such proposals are at variance with accepted theory and with the preponderance

(1) L. Brewer and D. F. Mastick, *J. Chem. Phys.*, **19**, 834 (1951).

(2) L. Brewer, *Chem. Rev.*, **52**, 1 (1953).

(3) W. J. Moore and E. L. Williams, *J. Phys. Chem.*, **63**, 1516 (1959).

(4) E. A. Secco, *Can. J. Chem.*, **38**, 596 (1960).

(5) T. C. M. Pillay, *J. Electrochem. Soc.*, **109**, 76C, Abstract 134 (1962).

of experimental evidence. Further study that might yield a more acceptable explanation of the anomalous sublimation behavior appeared essential.

The present paper reports results of (a) Knudsen effusion measurements of the sublimation pressure of zinc oxide, (b) a mass spectrometric investigation of zinc oxide vapor under neutral and reducing conditions, and (c) new transport measurements.

Knudsen Effusion Studies

Method and Experimental Procedure. When an appreciable fraction (approximately 15%) of a zinc oxide sample was sublimed, no solid residue other than zinc oxide remained. This observation demonstrates that the vapor has the same over-all composition as the solid, *i.e.*, the solid sublimes congruently. At 1000° the composition of solid zinc oxide has been shown to differ from the stoichiometric composition by less than 10^{-2} atom % when the gas with which the solid is held in contact is varied in composition from pure oxygen at 1 atm. pressure to pure zinc vapor at 1 atm. pressure.⁶

Zinc oxide was shown in the mass spectrometric study to sublime to zinc atoms and oxygen molecules only. Since the ratio of zinc atoms to oxygen molecules in the vapor beam must therefore be 2:1, the partial pressures of oxygen and zinc in equilibrium with zinc oxide can be calculated from Knudsen weight-loss determinations, and these partial pressures can be compared with those calculated from the available thermodynamic data for reaction 1.

Zinc oxide from Johnson-Matthey Co. was used in all the experiments. Spectrographic examination showed 6 p.p.m. (by weight) of silicon, 1 p.p.m. of copper, 1 p.p.m. of iron, and less than 1 p.p.m. each of calcium, magnesium, and sodium.

One aluminum oxide and three silica effusion cells were used. Each cell was degassed until the weight loss of the empty cell became less than 0.02 mg. during a 10-hr. heating. The cells were weighed on an Ainsworth semimicrobalance with a reproducibility of 0.01–0.02 mg.

The alumina effusion cell was a crucible 1.3 cm. i.d. \times 1.8 cm. deep, which was fitted with an alumina lid which had a centered, cylindrical effusion orifice. This cell was contained in a tantalum cell 2.3 cm. i.d. \times 2.2 cm. deep, with a tantalum lid in which a centered 0.5-cm. diameter hole had been drilled. The tantalum cell was in turn contained in an open graphite crucible. The alumina cell was separated from the top and bottom of the tantalum crucible by rings made of 20-mil tungsten wire and from the side walls of the crucible by a 0.3-cm. gap.

In four experiments, an alumina plug was placed in the orifice of the effusion cell, and in one experiment a lid with no effusion orifice was used. The results are discussed in the next section.

Two silica cells had the same dimensions as the alumina cell. A third silica cell was 2.1 cm. i.d. \times 2.1 cm. deep. The lid of each cell was fused to its crucible to obtain a gas-tight seal. The silica cells were heated in an assembly similar to that used for the alumina cell.

The effusion cell assembly was heated in a glass vacuum system by a 500-kc. induction unit. During each experiment, the residual pressure inside the vacuum system was maintained below 1×10^{-5} torr by means of an oil diffusion pump and liquid nitrogen trap. Temperatures were measured with a calibrated optical pyrometer focused on the cell orifice through a window of known transmissivity.

No weight change was observed when an effusion cell that contained a sample of zinc oxide was exposed to air. However, to reduce to a minimum any possible pick-up of moisture by the finely divided sample, the cell was allowed to cool 10 hr. under high vacuum. Air, dried by passage over $\text{Mg}(\text{ClO}_4)_2$ and P_2O_5 and through a liquid nitrogen cold trap, was admitted to the vacuum system. The effusion cell assembly was removed from the system and stored over P_2O_5 for 8 hr. before the cell was weighed. Weight changes of samples stored for 2 days were within the reproducibility of the balance. Additional descriptions of equipment and procedure have been given by Searcy and McNees.⁷

Results. Data obtained with the alumina cell are summarized in Table I. The weight losses given in column 3 have been reduced by 23.2% to correct for the observed weight losses when zinc oxide was heated in a cell with no effusion orifice or with a plugged orifice.

Pressures inside a cell can be calculated from the weight loss through an orifice by means of the Knudsen equation⁸ when account is taken of the fact that the partial pressures of zinc and oxygen inside the cell are related by

$$P_{\text{Zn}} = 2P_{\text{O}_2}(M_{\text{Zn}}/M_{\text{O}_2})^{1/2} \quad (2)$$

where M_{Zn} and M_{O_2} are the molecular weights of zinc and oxygen. The calculated equilibrium constants are

(6) W. J. Moore and E. L. Williams, *Discussions Faraday Soc.*, **28**, 86 (1959).

(7) A. W. Searcy and R. A. McNees, Jr., *J. Am. Chem. Soc.*, **75**, 1578 (1953).

(8) Cf. J. L. Margrave, "Vapor Pressure," in "Physico-Chemical Measurements at High Temperatures," J. O'M. Bockris, J. L. White, and J. D. Mackenzie, Ed., Butterworth and Co. Ltd., London, 1959, p. 231.

Table I: ZnO Vapor Pressure Measurements in Al₂O₃ Cell

T, °K.	Time, min.	Weight loss, mg.	Area, ^a cm. ² × 10 ⁴	K × 10 ⁹
1341	266.6	5.45	8.517	27.3
1332	157.4	2.70	8.515	20.9
1374	163.6	7.26	8.521	89.0
1428	69.6	8.45	8.529	414.0
1404	120.9	9.42	8.525	210.0
1326	357.4	5.35	8.514	17.0
1282	704.8	3.90	8.509	3.73
1295	290.5	1.95	8.577	4.94
1368	142.7	4.26	8.587	48.2
1285	333.0	1.56	8.575	2.86
1324	225.5	2.43	8.580	10.2

^a Corrected for thermal expansion. The Clausius factor [D. A. Schulz and A. W. Searcy, *J. Chem. Phys.*, **36**, 3099 (1962)] was 0.2550 for the first seven experiments and 0.2557 for the remaining four.

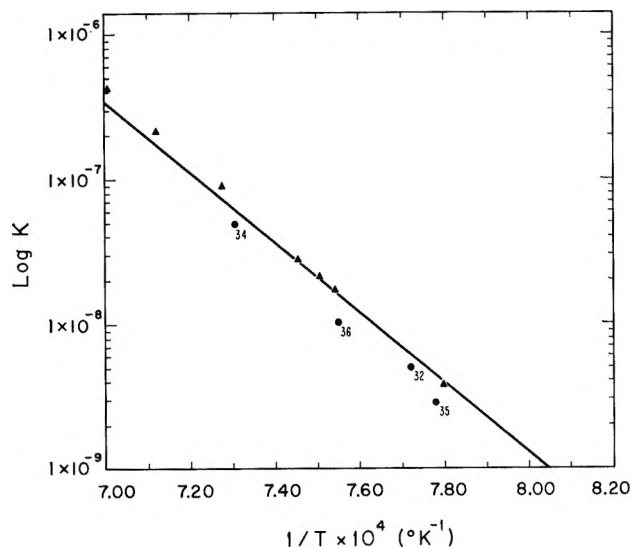


Figure 1. The equilibrium constant for the reaction $ZnO(s) = Zn(g) + 0.5 O_2(g)$ measured in alumina cells. The solid triangles are experimental determinations on zinc oxide alone. The line is plotted from the free energy of the reaction $ZnO(s) = Zn(g) + 0.5 O_2(g)$ that was calculated by Coughlin from the heats of formation of zinc oxide, the heat of vaporization of zinc, and from entropies and heat capacities. The numbered points were obtained when silica was added.

recorded in column 5 of Table I and plotted as functions of $1/T$ in Fig. 1. The last four measurements were made with particles of silica mixed with the zinc oxide sample. The reason for these four experiments, and the interpretation of the results, is presented in the Discussion section.

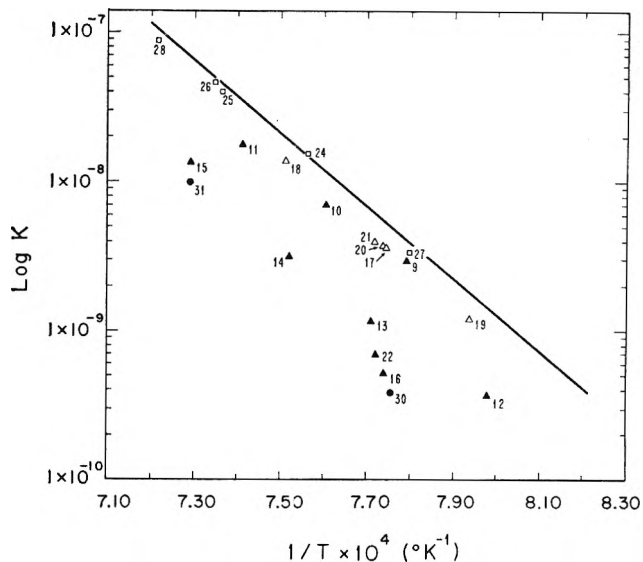


Figure 2. The apparent equilibrium constant for the reaction $ZnO(s) = Zn(g) + 0.5 O_2(g)$ measured in silica cells. The line is plotted from thermodynamic calculations of Coughlin. Points 24–28 were obtained with a cell that had a very small orifice. □ = quartz cell III; ▲ = quartz cell I; △ = quartz cell II; ● = quartz cell I with some Al₂O₃ added.

The apparent equilibrium constants obtained from the three silica effusion cells are plotted vs. $1/T$ in Fig. 2, together with an equilibrium line from thermochemical data.⁹ Nine measurements shown in Fig. 2 were made with the first silica cell. Five measurements were made with the second cell, and five measurements with the third. For the final two measurements, some crystals of alumina were mixed with the zinc oxide sample. The alumina crystals were very pure sapphire from the Aluminum Co. of America.

Mass Spectrometric Investigation

Equipment and Procedure. A Nuclide Analysis Associates high temperature mass spectrometer was used to determine the vapor species in equilibrium with solid zinc oxide. Cells from the weight-loss studies served as the beam sources. A cell was nested inside a tantalum crucible fitted with a tantalum lid having a centered hole of larger diameter than the Knudsen cell orifice. Radiation from two tungsten filaments was used to produce cell temperatures up to 1000°. Electron bombardment heating was necessary to obtain higher temperatures. Pressures between 1×10^{-7} and 7×10^{-7} torr were maintained in the

(9) J. P. Coughlin, "Heats and Free Energies of Formation of Inorganic Oxides," U. S. Department of the Interior, Bureau of Mines, Bulletin No. 342, U. S. Government Printing Office, Washington, D. C., 1954.

crucible region, and lower pressures were maintained in the analyzer region.

The temperature of the Knudsen cell was measured by a platinum-platinum-10% rhodium thermocouple which was inserted in a recess drilled in the bottom of the tantalum crucible.

Results of Zinc Oxide Experiments. The three most abundant isotopes of zinc have mass numbers 64, 66, and 68 and relative abundances 0.489, 0.278, and 0.186, respectively. When zinc atoms are subjected to 70-v. electron impact, some zinc atoms become doubly ionized. Since the mass-to-charge ratios of $^{64}\text{Zn}^{2+}$ and $^{16}\text{O}_2^+$ are the same, the presence of $^{64}\text{Zn}^{2+}$ in the ion beam interferes with measurements of the $I_{\text{O}_2^+}$. To overcome this difficulty, three ion currents, those for masses 66, 33, and 32, were measured at each temperature. From a measurement of the $^{66}\text{Zn}^+$ ion current, the total ion current of zinc can be calculated from the relation $I_{\text{Zn}^+} = I_{^{66}\text{Zn}^+}/0.278$. The $I_{^{66}\text{Zn}^{2+}}/I_{^{66}\text{Zn}^+}$ ratio was measured and assumed to be identical with the $I_{^{64}\text{Zn}^{2+}}/I_{^{64}\text{Zn}^+}$ ratio in correcting the measurements at mass 32 for doubly ionized zinc.

As discussed by Searcy, Williams, and Schissel, systems that sublime congruently can be used to calculate relative ionization cross sections.¹⁰ If, as in this research, an electron multiplier is used, the relative current-production efficiency of the apparatus for the vapor species can be calculated. The Knudsen weight-loss measurements demonstrated that the zinc and oxygen pressures are related by eq. 2. The ratio of the current-production efficiency measured in alumina cells was calculated to be 0.96 with an average deviation for two runs of about 0.04. The average of five runs in silica cells was 1.41 with an average deviation of 0.14. The relative ionization cross section calculated from the relationship given by Otvos and Stevenson is 0.411.¹¹ The difference in current-production efficiency for measurements made in the two cells probably reflects some reaction of the oxygen of the beam from the alumina cell, which leaked, with tantalum of the collimating system. From our data, it is not possible to conclude to what extent the difference between the ratio of current-production efficiency and the predicted ratio of ionization cross sections is due to imperfections in the Otvos and Stevenson theory, to what extent it is due to differences in dynode response, and to what extent to selective reactions of the beam components with the tantalum collimators. For calculation of pressures from current intensities, determination of the rate of effusion from the cells by means of the weight-loss experiments coupled with knowledge that the oxide sublimates congruently at a Zn/O₂ molecule ratio of 2:1 allows calibration of the

spectrometer intensities *vs.* pressures for zinc and oxygen with an uncertainty of less than 20%.

No gaseous zinc oxide molecules of any kind were detected. From the very low intensity of the background peak at mass 80, the ion current of $\text{ZnO}^+(\text{g})$ can be estimated to be less than 2.8×10^{-12} at 1249°K. At this temperature the measured ion currents of Zn^+ and O_2^+ were 3.2×10^{-8} and 1.8×10^{-8} , respectively. From known pressures for zinc and oxygen, measured ion currents, and ionization cross sections given by Otvos and Stevenson,¹¹ an upper limit of 1.2×10^{-10} atm. was calculated for the pressure of $\text{ZnO}(\text{g})$. From these partial pressures, from free energy functions for $\text{Zn}(\text{g})$ and $\text{O}_2(\text{g})$ given by Stull and Sinke,¹² and from estimated free energy functions for $\text{ZnO}(\text{g})$ given by Brewer and Chandrasekharaiah,¹³ a limiting dissociation energy of $\text{ZnO}(\text{g})$ was calculated to be $D_{298}^\circ < 66$ kcal.

The ion current of $\text{Zn}_2\text{O}^+(\text{g})$ was estimated to be less than 5.2×10^{-12} at 1258°K. from the very low intensity of the mass 148 peak. The zinc and oxygen ion currents were 3.60×10^{-8} and 1.65×10^{-8} . An upper limit of 1.3×10^{-10} atm. was calculated for the pressure of $\text{Zn}_2\text{O}(\text{g})$.

From these partial pressures, free energy functions for $\text{Zn}(\text{g})$ and $\text{O}_2(\text{g})$ given by Stull and Sinke,¹² and estimated free energy functions for $\text{Zn}_2\text{O}(\text{g})$, a limiting dissociation energy for $\text{Zn}_2\text{O}(\text{g})$ of $D_{298}^\circ < 127$ kcal. was calculated. Free energy functions for $\text{Zn}_2\text{O}(\text{g})$ were estimated to be identical with the functions by Cochran and Foster for Ga_2O .¹⁴

Gold-Zinc Alloy Plus Zinc Oxide Experiments. Since the very high sublimation rates of zinc oxide reported by other investigators³⁻⁵ were obtained when excess zinc vapor was present, and since two of these investigators hypothesized that the excess zinc vapor somehow catalyzed the evaporation of the zinc oxide, a mass spectrometric investigation of the zinc-zinc oxide system appeared desirable. The very high vapor pressure of zinc compared with that of zinc oxide precludes the use of a mixture of zinc oxide and zinc metal. However, a zinc-gold alloy that has a reduced zinc activity can be used successfully.

(10) A. W. Searcy, W. S. Williams, and P. O. Schissel, *J. Chem. Phys.*, **32**, 957 (1960).

(11) J. W. Otvos and D. P. Stevenson, *J. Am. Chem. Soc.*, **78**, 546 (1956).

(12) D. R. Stull and G. C. Sinke, "Thermodynamic Properties of the Elements," American Chemical Society, Washington, D. C., 1956.

(13) L. Brewer and M. S. Chandrasekharaiah, "Free Energy Functions for Gaseous Monoxides," Lawrence Radiation Laboratory Report UCRL-8713, April, 1959, unpublished.

(14) C. N. Cochran and L. M. Foster, *J. Electrochem. Soc.*, **109**, 144 (1962).

A 60% gold-40% zinc alloy was prepared as follows: a 1.0-cm. i.d. silica tube, containing 1.9522 g. of zinc and 8.8230 g. of gold, was evacuated and sealed. This sealed tube was heated in a furnace at 1123°K. for 4 hr., was removed, and was quenched.

For the mass spectrometer experiment, a silica effusion cell 1.7 cm. i.d. and 1.9 cm. deep, with two compartments, was used. One compartment was an open, cup-shaped crucible, 0.8 cm. i.d. and 0.6 cm. deep, which was centered on the bottom of the effusion cell. This compartment contained a zinc oxide sample. The region between the center crucible and the walls of the effusion cell formed the second compartment, which held 1.11 g. of the gold-zinc alloy. In the lid of the effusion cell was a centered, cylindrical effusion orifice. The silica cell was contained in a tantalum crucible which was heated by radiation from the filaments.

The pressure of zinc above the alloy at a given composition and temperature can be calculated from thermodynamic data for the alloy.¹⁵ From a measurement of the ion current of Zn^+ from the alloy at a known temperature, the sensitivity of the mass spectrometer for zinc can be calculated. At 703°K. the mass-66 peak became sufficiently intense for an accurate measurement of the ion current to be made. That the alloy did not change composition significantly during the measurements at 703°K. was indicated by the fact that the ion current of $^{66}Zn^+$ remained constant for more than 3 hr. When the temperature was raised to 806°K. the $^{66}Zn^+$ ion current decreased with time of the measurement, an indication that the composition of the alloy was changing.

The temperature was raised in steps to 1229°K. The alloy was by this time depleted in zinc, and the O_2^+ peak appeared. The subsequent variations of the ion current of O_2^+ with the ion current of Zn^+ were followed until the ion ratios reached the ratio characteristic of the congruently subliming oxide.

Results and Calculations. Thermodynamic data given by Hultgren, *et al.*,¹⁵ were used to calculate the partial pressure of zinc at 703°K. The current-production efficiency at mass 66 was then calculated from this pressure and from the measured current intensity. Activity coefficients and partial molal free energies are known for the alloy only at 1048°K. The regular solution approximation was used for both the solid and liquid alloy to calculate the activity of zinc at 703°K. The liquidus temperature for the 40% zinc alloy lies at 950°K. The entropy of fusion per g.-atom of alloy was estimated to be 3 e.u., and both ΔS_{fus} and ΔH_{fus} were assumed constant with temperature.

The calculation led to $P_{Zn} = 2.8 \times 10^{-7}$ for the 40% zinc alloy at 703°K.

The measured ion current is related to the pressure inside the Knudsen cell by

$$I^+ = SP = S^* \frac{P}{T} \quad (3)$$

where S is the sensitivity as usually defined and S^* is a constant independent of temperature. From I^+ and P at 703°K., S^* was calculated to be 3.50. As the temperature was subsequently raised and the composition of the alloy changed, the pressure of zinc was calculated from each measurement of I_{Zn^+} by means of eq. 3.

From the measurements of the ion current for the mass-33 peak made during the calibration with the alloy at 703°K., the ratios $I_{66Zn^2^+}/I_{66Zn^+}$ were evaluated as 7.42×10^{-2} . Ion currents for O_2^+ were calculated from the total intensity measured at mass 32 by the method previously described. Results of the

Table II: Summary of Pressure Calculations from Mass Spectrometer Data on the Zn-ZnO System

Time	T , °K.	Gaseous species	I^+ , ion current, $\times 10^6$	P , atm.
0:0	849	Zn	7.12	1.73×10^{-5}
4:48	991	Zn	19.0	5.40×10^{-5}
7:35	1088	Zn	13.8	4.31×10^{-5}
11:30	1185	Zn	0.809	2.74×10^{-6}
11:55	1185	O_2	0.0	
12:50	1194	O_2	0.0	
13:31	1207	O_2	0.0	
13:55	1225	Zn	12.0	4.22×10^{-5}
14:10	1229	O_2	0.0	
14:20	1229	O_2	0.022	5.8×10^{-8}
14:30	1229	Zn	0.576	2.02×10^{-6}
14:47	1229	O_2	0.043	1.1×10^{-7}
15:10	1229	O_2	0.046	1.2×10^{-7}
15:20	1230	Zn	0.396	1.39×10^{-6}
16:00	1255	Zn	10.4	3.74×10^{-5}
16:11	1257	O_2	0.0	
16:28	1257	O_2	0.189	5.04×10^{-7}
16:35	1257	Zn	0.529	1.90×10^{-6}
16:51	1258	O_2	0.281	7.48×10^{-7}
17:01	1258	O_2	0.386	1.03×10^{-6}
17:15	1258	Zn	0.518	1.86×10^{-6}
17:31	1258	O_2	0.342	9.12×10^{-7}
17:40	1258	O_2	0.357	9.51×10^{-7}
17:55	1258	Zn	0.468	1.68×10^{-6}
18:12	1259	Zn	0.400	1.44×10^{-6}
18:50	1259	O_2	0.360	9.61×10^{-7}

(15) R. R. Hultgren, "Selected Values for the Thermodynamic Properties of Metals and Alloys," Materials Research Laboratory, University of California.

pressure calculations are summarized in Table II. Equilibrium constants calculated from these pressure determinations are summarized in Table III.

Table III: Equilibrium Constants for the Vaporization Reaction $\text{ZnO(s)} + \text{Zn(g)} + 0.5\text{O}_2\text{(g)}$

T , °K.	P_{Zn} , atm.	P_{O_2} , atm.	K' from measured pressures	K eq. from thermo- dynamic data ^a
1229	1.39×10^{-6}	1.2×10^{-7}	4.8×10^{-10}	6.0×10^{-10}
1229	2.02×10^{-6}	1.1×10^{-7}	6.7×10^{-10}	6.0×10^{-10}
1259	1.44×10^{-6}	9.61×10^{-7}	1.4×10^{-9}	1.7×10^{-9}
1258	1.68×10^{-6}	9.51×10^{-7}	1.6×10^{-9}	1.7×10^{-9}
1258	1.86×10^{-6}	9.12×10^{-7}	1.8×10^{-9}	1.7×10^{-9}
1258	1.90×10^{-6}	7.48×10^{-7}	1.6×10^{-9}	1.7×10^{-9}
1257	1.90×10^{-6}	5.04×10^{-7}	1.5×10^{-9}	1.6×10^{-9}

^a See ref. 9.

No gaseous zinc oxide molecules of any kind were detected. From measurements of the background intensities at mass 80 and mass 148, upper limits for the pressure of ZnO(g) and $\text{Zn}_2\text{O(g)}$ were calculated. At 1151°K. the pressure of Zn(g) calculated from the measured ion current was 3.02×10^{-6} atm. The upper limits for the pressures of ZnO(g) and $\text{Zn}_2\text{O(g)}$ were 5.6×10^{-9} and 1.7×10^{-9} atm., respectively.

Transport Studies

Apparatus and Procedure. The Knudsen effusion experiments and the mass spectrometric investigation indicated that zinc oxide sublimates by dissociation to zinc atoms, and oxygen molecules at rates to be expected from the known thermodynamic data. Re-examination of the influence of zinc vapor on zinc oxide sublimation in a tube furnace seemed necessary to reveal the cause of the earlier, anomalous tube furnace results.

The experimental apparatus was deliberately designed to be similar to that used by Moore and Williams³ and by Pillay.⁵ Zinc oxide powder was pressed into disks 1.3 cm. in diameter and 0.3 cm. thick. Three of these disks were placed in a degassed alumina boat which, in turn, was placed in a horizontal mullite tube in a resistance furnace. The tube was 2.5-cm. i.d. with a 0.3-cm. wall thickness. The boat was 3.8 cm. long, 2.2 cm. wide, and 0.6 cm. deep. To one end of the tube a ground-glass joint was sealed. To this joint were sealed a gas inlet tube and a thermocouple protection tube. A rubber stopper, through which a gas outlet tube and a porcelain thermocouple protection tube were introduced, was placed in the other end.

Helium obtained from the U. S. Bureau of Mines was the carrier gas. The analysis furnished by the supplier showed no oxygen and a dew point of -60° . The helium passed in sequence through a $\text{Mg}(\text{ClO}_4)_2$ drying tube, a silica tube filled with copper turnings at 450° , a variable-area flow meter, and a liquid nitrogen cold trap before entering the furnace tube.

In an initial experiment, the boat containing the disks was placed in the gas inlet end of the tube. A helium flow was maintained while the furnace was heated to 1056° . The boat was then pushed with the thermocouple protection tube into the center of the hot zone.

For determination of the sublimation rate of zinc oxide in excess zinc vapor the procedure was the same as that just described, except that as soon as the boat had been pushed to the center of the heated tube, the ground-glass joint was unsealed and an aluminum oxide crucible containing some zinc metal was placed in the cool region of the tube near the joint. The joint was immediately resealed; and after the system had been flushed with helium for 1 hr., the crucible containing the zinc was slowly pushed into a hotter section of the tube by the thermocouple protection tube. The thermocouple inside this protection tube was used to monitor the temperature of the zinc. The approximate flow rate of zinc vapor was calculated from the weight loss of the alumina crucible containing zinc, in the known time of heating.

The zinc metal (purity at least 99.999%) used in this experiment was obtained from Johnson-Matthey Co. Upon heating, any hydrogen that might be dissolved in the zinc might be evolved and react with the zinc oxide to yield water vapor and zinc gas. Accordingly, the zinc metal was melted in an open alumina crucible at a pressure of less than 10^{-5} torr prior to use. This procedure should reduce the hydrogen content to a negligible level.

For two experiments the zinc was replaced in the tube furnace by iron wire (analytical grade). Iron has a negligible vapor pressure at the temperature to which it was heated (approximately 600°). A new furnace tube and a new thermocouple protection tube were used for these experiments to ensure that zinc from the previous experiments would not affect the results.

The iron wire (which was handled only with rubber gloves or forceps) was wound into a small wad, was inserted into the inlet end of the mullite tube, and was pushed into the hotter portion of the tube by the thermocouple protection tube.

The results of these experiments are given in Table IV. The rates of loss of the zinc oxide sample are

Table IV: Summary of Tube Furnace Experiments

System studied	Time, hr.	T , °C.	He flow rate, cm. ³ /min.	Wt. of Zn transported, g.	P_{Zn} , atm.	Wt. loss of ZnO, mg.	Rate of measured loss of ZnO, g./hr.	Rate of loss of ZnO expected for reaction 1, g./hr.
ZnO	44.4	1056	77.0	3.8	8.56×10^{-5}	1.31×10^{-4}
ZnO-Zn	19.97	1019	64.8	3.0046	1.45×10^{-2}	387.6	1.94×10^{-2}	3.7×10^{-12}
ZnO-Fe	22.8	1019	75.8	128.7	5.64×10^{-3}	5.79×10^{-5}
ZnO-Fe	26.3	1006	65.2	152.8	5.81×10^{-3}	3.72×10^{-5}

given in column 8. In column 9 are given the rates of loss of the zinc oxide calculated on the assumption that zinc oxide sublimes by dissociation to zinc atoms and oxygen molecules.

Discussion

Points in both Fig. 1 and 2 are labeled by run numbers to indicate the sequence of experiments in the Knudsen weight-loss studies. Equilibrium constants calculated from measurements made with silica cell I were lower than the constants calculated from Coughlin's data.⁹ Furthermore, the calculated constants decreased after each high temperature experiment, *i.e.*, after experiments 11 and 15. The sample was stirred before experiment 22 was made, but stirring had little effect on the apparent pressure. Since this behavior was not observed with the alumina effusion cell (Fig. 1), some kind of interaction between one kind of cell and zinc oxide appeared responsible. To determine whether the silica or the alumina caused the strange behavior, alumina powder was mixed with the zinc oxide in silica cell I, and experiments 30 and 31 were performed. The apparent equilibrium constants calculated from these two experiments continued to decrease. This fact implies that alumina has no effect on the zinc oxide evaporation.

Next, some particles of fused silica were mixed with the zinc oxide sample in the alumina cell. The apparent equilibrium constants measured after this addition (experiments 32, 34, 35, and 36) are lower than the constants measured in runs in which zinc oxide was exposed to alumina only (Fig. 1).

X-Ray diffraction showed no evidence of reaction products. Perhaps the surface of the zinc oxide acquired a coating of silica, which lowered the sublimation rate of the zinc oxide. Surface diffusion is the probable mechanism of such transport because surface diffusion is known to change catalytic activity at concentrations well below those at which bulk reactions occur,¹⁶ and the partial pressures of SiO₂(g) and SiO(g) were both less than 10⁻¹¹ atm., too low for significant vapor transport.

If the hypothesis that silica reduces the rate of sublimation of zinc oxide is correct, an increase in the ratio of sample surface area A to orifice area a might allow equilibrium to be attained in fused silica cells. Silica cell III was designed to have an A/a ratio 48 times as great as that in cell I. Small amounts of condensate of zinc oxide were deposited in the effusion channel of silica cell III during the experiments, and we estimate the total uncertainty in the equilibrium constant may be as high as 19%. However, the apparent equilibrium constants calculated from experiments made with cell III clearly agree well with constants calculated for the alumina cell, and with constants calculated for reaction 1, dissociation to Zn(g) plus 0.5O₂(g).

The mass spectrometer studies give further support to the conclusion that reaction 1 describes the sublimation of zinc under neutral conditions and furthermore give evidence that reaction 1 remains the equilibrium sublimation reaction in the presence of excess zinc vapor. No peaks that could be attributed to zinc oxide molecules were observed. Furthermore, in the experiments in which a gold-zinc alloy was heated with zinc oxide, the partial pressures calculated for zinc atoms and oxygen molecules yielded equilibrium constants for reaction 1 that were in excellent agreement with the constant calculated from thermochemical data for zinc oxide and sublimation data for zinc (Table III).

Zinc pressures as high as those used in the tube furnace experiments (10⁻³ atm. or more) could not be used in our mass spectrometer experiments; the highest zinc partial pressure used in the spectrometer for the zinc-zinc oxide systems was 5×10^{-5} atm. However, Pillay found no variation of the evaporation rate of zinc oxide with the partial pressure of zinc,⁵ and Secco found high rates of sublimation when the only source of zinc was the zinc oxide dissociation reaction itself. The zinc pressures in our mass spectrometer, therefore, should have been high enough to induce

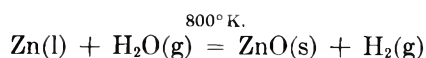
(16) A. J. E. Welch in "Chemistry of the Solid State," W. E. Garner, Ed., Butterworth and Co. Ltd., London, 1955, Chapter 12.

any effects that might have increased the rate of weight loss from zinc oxide.

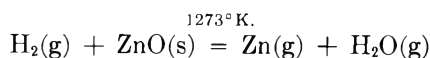
Our mass spectrometric study of zinc-zinc oxide did not reveal even low concentrations of gaseous molecules such as ZnO, ZnO₂, Zn₂O, or polymers thereof. Furthermore, the product $P_{\text{Zn}} \times P_{\text{O}_2}^{1/2}$ remained equal to the calculated equilibrium constant, while the zinc-to-oxygen pressure ratio varied from as high as about 15:1 to about 2.8:1, the ratio dictated for steady-state effusion by eq. 3. This fact appears to preclude the possibility that significant fractions of the zinc ion intensities measured in the spectrometer experiments were contributed by fragmentation of undetected zinc oxide molecules.

The explanation of the conflicting data reported by other investigators was revealed by our tube furnace experiments. The tube furnace design and procedure were deliberately similar to those used by Pillay⁵ and by Williams.³ The sublimation rate of zinc oxide in an atmosphere of flowing helium (Table IV) was, within the limits of uncertainty, that calculated for the dissociation reaction. In the presence of zinc vapor, the rate was increased, just as reported by Williams and by Pillay.

One possible explanation, first suggested by Cubicciotti,¹⁷ remained to be tested. This was that, despite the traps, water vapor was present in the tube furnaces in sufficient concentration to produce the observed zinc oxide volatilization. The reaction sequence could be



and



Our calculations showed that if water vapor were present this set of reactions could produce the observed behavior, and so could the corresponding equilibrium involving CO₂ and CO.

To test the possibility that water or CO₂ caused the observed behavior, iron wire was substituted for zinc. Iron has negligible volatility at the temperature of our experiments but can reduce water to hydrogen and carbon dioxide to carbon monoxide. The sublimation rates of zinc oxide measured when iron was heated in the gas stream were comparable to those obtained when zinc had been present. Furthermore, after each experiment the iron was severely oxidized.

The purification to which our carrier gas was subjected was as rigorous as the procedures followed in the earlier studies of Moore and Williams and of Pillay. We conclude that the increase in sublimation rate, attributed by Moore and Williams to a catalytic effect of zinc vapor on the sublimation of zinc oxide, in fact was caused by a reaction of hydrogen and/or carbon monoxide with the zinc oxide. In Secco's static experiments a trace of water and of a reducing agent coupled with a small temperature gradient may account for the high observed zinc oxide transport. On the other hand, in our mass spectrometer experiments the background pressures of water and CO₂ were too low to cause significant reactions.

Acknowledgments. We express sincere gratitude for the helpful suggestions offered by Dr. Daniel Cubicciotti, Dr. David J. Meschi, and Dr. Lies N. Finnie. This work was done under the auspices of the U. S. Atomic Energy Commission.

(17) D. D. Cubicciotti, Stanford Research Institute, private communication.

Kinetics of Reaction of Elemental Fluorine. II. The Fluorination of Hafnium Carbide and Hafnium Boride

by A. K. Kuriakose and J. L. Margrave

Department of Chemistry, Rice University, Houston, Texas 77001 (Received April 9, 1964)

The corrosion kinetics of high purity hafnium carbide and hafnium diboride in elemental fluorine under low fluorine partial pressures (2.8–52.5 torr) in helium have been investigated up to 890° for HfC and 1020° for HfB₂. Although HfC produces solid hafnium tetrafluoride from 300 to 500°, the tetrafluoride does not adhere to the HfC. HfB₂, on the other hand, breaks down in the same temperature range, apparently because of reaction at pre-existing cracks when the fluorine partial pressure is 13 torr. Due to the volatility of the fluorides around 600°, both HfC and HfB₂ begin to lose weight in fluorine with linear reaction rates and the samples stay unbroken even to the highest temperatures examined in this investigation. The reactions are highly exothermic and the surface temperatures of the samples increase rapidly, almost proportionally to the fluorine partial pressure in the system, as fluorine is admitted. For HfC the reaction rate varies directly as the fluorine partial pressure while for HfB₂ it varies directly as the square root of fluorine pressure. A comparison of the behavior of the carbides and diborides of zirconium and hafnium toward fluorine is given.

In the first paper of this series,¹ measurements of the fluorination rates of ZrC and ZrB₂ were reported. Because of the well-known close resemblances between zirconium and hafnium compounds, similar behaviors of HfC and HfB₂ with fluorine are to be expected. However, the slightly higher volatility of HfF₄ than ZrF₄ should make the Hf compounds slightly more reactive at lower temperatures.

Experimental

The apparatus and experimental procedure were essentially the same as for the fluorination of ZrC and ZrB₂. The HfC samples were prepared from an arc-melted piece of composition HfC_{0.962} with the following impurities (%): Zr, 0.035; N, 0.031; Fe, 0.005; O, 0.003; Ti and Si, 0.002 each; H, Cu, Mn, and Mg, 0.001 each. The HfB₂ specimens were cut from zone-refined cylindrical bars which had a composition HfB₂₋₀₃₅ with impurities: Zr, 0.01–0.1%; C, 0.16%; Cr, Cu, and Mg, 0.001% each; N, 42 p.p.m.; Ti and Fe, 30 p.p.m. each; O, 26 p.p.m.; and Si, 10 p.p.m. The surfaces were polished by mechanical means and their areas were calculated from geometrical dimensions.

Results

Both HfC and HfB₂ were found to withstand fluorine at room temperature to a pressure of 1 atm. The exposures at higher temperatures were done only at low fluorine partial pressures.

Fluorination of HfC. Experiments with HfC exposed to fluorine at 2.8 torr partial pressure indicated that a detectable reaction started at about 300°. There was formation of solid HfF₄, but the reaction rate could not be measured since the product was not adherent to the HfC surface up to 400°. The HfF₄ was collected at the bottom of the furnace and the HfC surfaces were practically clean. At 500°, however, the product was more adhesive; but still no reproducible rate data could be obtained because of the abrupt crumbling of the product layer. From a few initial readings at this temperature, the reaction rate appeared to be linear. At 565° the HfC began to lose weight, and the reaction became smoother. The rate data from 565 to 890° are given in Table I. The reaction rate was almost inde-

(1) A. K. Kuriakose and J. L. Margrave, *J. Phys. Chem.*, **68**, 290 (1964).

pendent of temperature above 650° and the calculated activation energy practically zero. At 565° the rate was considerably lower, probably due to the incomplete volatilization of the HfF_4 . The reaction rate was directly proportional to the fluorine partial pressure up to 52.5 torr above 600° (Fig. 1).

Table I: Rate Data for the HfC-F_2 Reaction

Temp., °C.	P_{F_2} , torr	k_1 , mg./cm. ² /min.	Temp., °C.	P_{F_2} , torr	k_1 , mg./cm. ² /min.
565 ^a	2.8	2.06	800	13.2	11.71
650 ^a	2.8	5.36	820	52.5	49.80
720	2.8	6.14	825	2.8	6.32
765	2.8	5.18	890	2.8	6.08
800	6.7	8.26			

^a Furnace temperature.

Fluorination of HfB_2 . Although no measurable reaction occurred between HfB_2 and fluorine at low fluorine pressures up to 500°, the samples broke down presumably at pre-existing cracks even at about 350° at 13.2 torr fluorine pressure. Small quantities of white HfF_4 were found within the cracks, but not on the outer surface. HfB_2 began to lose weight at about 550° but it stayed together even up to 1020°. The

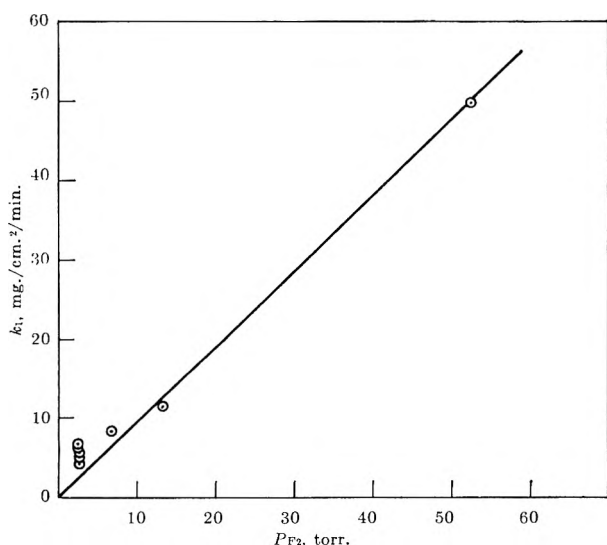


Figure 1. Effect of fluorine partial pressure on the HfC-F_2 reaction above 600°.

reaction was linear as expected and the rate constants under various conditions are recorded in Table II. Here again, temperature had practically no effect on

the reaction, but the fluorine partial pressure had a marked influence on the reaction.

Table II: Rate Data for the $\text{HfB}_2\text{-F}_2$ Reaction

Temp., °C.	P_{F_2} , torr	k_1 , mg./cm. ² /min.	Temp., °C.	P_{F_2} , torr	k_1 , mg./cm. ² /min.
765	2.8	5.31	610 ^a	13.2	9.82
830	2.8	5.24	835	13.2	7.94
900	2.8	4.86	880	13.2	9.62
975	2.8	5.16	985	13.2	11.87
810	6.7	6.92	610 ^a	30.6	13.56
840	6.7	6.15	890	30.6	12.95
940	6.7	9.37	950	30.6	15.77
1020	6.7	8.82	610 ^a	52.5	19.44

^a Furnace temperature.

As the fluorine pressure was increased, there was a proportional rise in the sample surface temperature and above 1000° sparks began to appear as the specimen was observed through the optical pyrometer. Shortly after the appearance of the sparks, the nickel wire burned up and the sample fell down. Although the sample surface temperatures rose above 1000°, the actual furnace temperature was never raised above about 900°. In Table III are shown the actual surface temperatures of a sample of weight about 0.7 g. and surface area about 1.3 cm.² under various fluorine partial pressures at a furnace temperature of 740°. Figure 2 is a plot of the rate constants against the square root

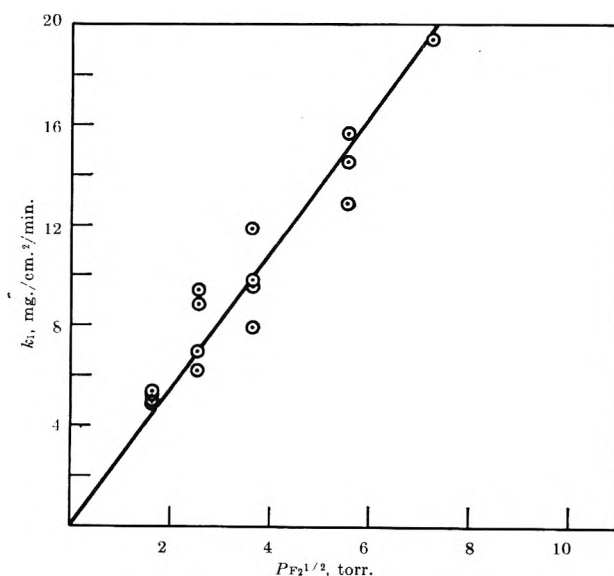


Figure 2. Effect of fluorine partial pressure on the $\text{HfB}_2\text{-F}_2$ reaction above 600°.

of fluorine partial pressure. The linearity of the plot indicates that the rate of fluorination of HfB_2 varies directly as the square root of the fluorine partial pressure.

Table III: Surface Temperatures of HfB_2 Samples with Various Fluorine Partial Pressures at a Furnace Temperature of 740°

P_{F_2} , torr	Surface temperature, $^\circ\text{C}$.
0	740
2.8	765
6.7	810
13.2	835
30.6	890

Discussion

As expected, the behaviors of both Zr and Hf carbides and borides toward fluorine are similar. The borides of both metals are more resistant to fluorine than the carbides. Whereas the carbides begin to react at around 300° under low fluorine partial pressure conditions forming solid products, the borides are attacked only above the volatilization points of the

metallic fluorides. Thus, a coating of the fluoride is never obtained on the ZrB_2 and HfB_2 . At temperatures above 600° all the reactions are gas diffusion controlled which is characterized by the insensitiveness of the rates to surface temperature changes.

ZrC differs from HfC in that while the former forms thick scales of ZrF_4 below 500° , the latter does not grow any scales on it. HfB_2 crumbles in fluorine even at low fluorine partial pressure at 350 – 550° , but the ZrB_2 stays undamaged up to 500° under the same conditions.

The fluorination of HfC and HfB_2 is much faster than that of ZrC and ZrB_2 . Even after converting the rate constants to moles, the HfC and HfB_2 are found to react with fluorine about four to five times faster than ZrC and ZrB_2 .

The dependence of the reaction rates on the fluorine partial pressure is also similar for both Zr and Hf carbides and borides, except that ZrC shows a 1.5 order with respect to fluorine while the HfC shows first order.

Acknowledgments. This research was supported, in part, by the United States Air Force under a subcontract with A. D. Little, Inc., and administered by Dr. Leslie A. McClaine. Samples of HfC and HfB_2 were furnished through the courtesy of Dr. George Feick.

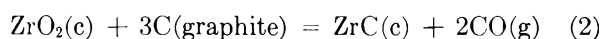
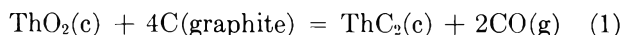
A Torsion Effusion Study of the Reaction of Graphite with Oxides of Thorium and Zirconium

by John R. Hollahan¹ and N. W. Gregory

Department of Chemistry, University of Washington, Seattle, Washington
(Received April 14, 1964)

The torsion effusion method is found to give useful results for the study of the solid-solid reaction between ThO₂ and graphite which produces ThC₂ and CO. Near equilibrium pressures do not appear to be established for the reaction of graphite with ZrO₂, however. Thermodynamic properties of ThC₂ are discussed.

A number of studies have been reported from this laboratory concerning the applicability of the effusion method for the study of vaporization processes in systems in which the condensed states are markedly different in molecular character from the equilibrium vapor.^{2,3} The present paper gives results of a torsion effusion study of the reaction between thorium oxide and graphite and a preliminary investigation of the similar reaction between zirconium oxide and graphite. There is much evidence to indicate that these reactions proceed according to the equations



For example Jackson, *et al.*,⁴ have observed, in mass spectrometric studies of the vaporization of ThC₂, that the dicarbide is the product of the direct reaction of thorium and carbon. Lonsdale and Graves⁵ prepared ThC₂ by reaction 1 and examined the product by X-ray diffraction as well as chemical analysis. Prescott and Hincke⁶ studied (1) using manometric methods and provide further evidence to support the formation of the products indicated. Nothing to suggest formation of solid solutions of oxide and carbide or of oxycarbide intermediates in either system at temperatures and pressures involved in our study has been reported.

The advantages of the torsion effusion method and its theory are well known.⁷ Its applicability to the study of solid-solid reactions has not been examined previously, to our knowledge. In general problems associated with diffusion of reactants to the reaction zone, nucleation and growth of product crystals, and

kinetics of the reaction itself suggest that rates of vaporization for such reactions may be insufficient to maintain steady-state pressures in the effusion cell which are near equilibrium values. However, our results for reaction 1, studied between 1560 and 1680°K., are encouraging and, we believe, lead to valid equilibrium results. Such does not appear to be the case for reaction 2, however.

Experimental

Materials used: spectroscopic grade graphite (90–95% through 200 mesh), National Carbon Co.; high purity (99.9%) thorium dioxide (4–10 μ particle size), American Potash and Chemical Corp.; 99.7% zirconium dioxide (40 μ), Zirconium Corp. of America.

Cylindrical effusion cells, *ca.* 19 mm. o.d. and 28 mm. long (internally 12.5 × 22), were fabricated from graphite rods (grade AUC, National Carbon Co.) or pyrolytic graphite blocks (Union Carbide Corp.). Table I

(1) Eastman Kodak Predoctoral Fellow, 1961–1962; du Pont Teaching Award Predoctoral Fellow, 1962–1963.

(2) E. Kay and N. W. Gregory, *J. Phys. Chem.*, **62**, 1079 (1958).

(3) (a) R. R. Hammer and N. W. Gregory *ibid.*, **66**, 1705 (1962); (b) *ibid.*, **68**, 314 (1964).

(4) D. D. Jackson, G. W. Barton, Jr., O. H. Krikorian, and R. S. Newbury, "Thermodynamics of Nuclear Materials," International Atomic Energy Agency, Vienna, 1962; and private communication.

(5) H. K. Lonsdale and J. N. Graves, "Thermodynamics of Nuclear Materials," International Atomic Energy Agency, Vienna, 1962.

(6) C. H. Prescott and W. B. Hincke, *J. Am. Chem. Soc.*, **49**, 2744 (1927).

(7) M. Volmer, *Z. physik. Chem., Bodenst. Festband*, 836 (1931); A. W. Searcy and R. D. Freeman, *J. Am. Chem. Soc.*, **76**, 5229 (1954).

Table I: Dimensions of Graphite Effusion Cells^a

Cell ^b	\bar{d} , cm.	$\bar{a}_0 \times 10^3$, cm. ²	k_{cell} $\times 10^2$, mm./radian	\bar{f} estd.
A-1	0.862	10.93	7.04	(0.898)
A-2	0.934	2.012	1.35	(0.850)
B-2	0.667	1.738	8.49	(0.97)
B-3	0.690	17.81	8.85	(0.97)
B-4	0.740	3.557	31.1	(0.97)

^a \bar{d} = average moment arm; \bar{a}_0 = average orifice area; \bar{f} = average nonideal effusion factor, estimated. ^b Cells A-1, B-3, and B-4 were suspended by a W wire 59.4 cm. long, 0.002-in. diameter, with a torsion constant of 1.750 dynes cm./radian; corresponding values for cell A-2: wire 53.7 cm., 0.001 in., 0.9914 dyne cm./radian; cell B-2: wire 19.4 cm., 0.001 in., 0.3877 dyne cm./radian.

lists cell geometrical and tungsten torsion wire characteristics. Zinc was used to calibrate the suspension system.⁸ The known vapor pressure and the observed angle of deflection, β_{Zn} , determine a cell-torsion wire constant, $k_c = P_{Zn}/\beta_{Zn}$ in mm./radian, from which subsequent measurements of β can be used to calculate the corresponding pressures. This method of calibration was considered more reliable than the absolute method because of the difficulty in the latter in determining the alignment of the suspension system.

The suspended cell was heated by a molybdenum resistance vacuum furnace, similar in design to that described by Austerman, Wolten, and Broman.⁹ The heating element, 8 in. long and 1.5 in. in diameter, was fabricated from 3-mil molybdenum sheet. A.c. power was supplied by a 25-kva. step-down transformer. The furnace assembly was covered by a steel "bell jar" with an O-ring seal at its base. Pressures as low as 2×10^{-6} mm. were obtained at room temperature and about 5×10^{-5} at 1650°K. The upper temperature limit of the furnace is ca. 2000°.

Temperatures ($\pm 5^\circ$) were measured by a microoptical pyrometer (Pyrometer Instrument Co., Bergenfield, N. J.) and were corrected¹⁰ for adsorption of radiation by the sight window. The pyrometer was sighted directly on the cell, assumed to be a black body. The validity of the temperature was checked by observing the melting points of nickel and gold, bracketed within a temperature range of 10°. The pyrometer was calibrated by the manufacturer; it was also compared with a Leeds and Northrup model and against an N.B.S. calibrated Pt-Pt-10% Rh thermocouple.

A small residual torque effect, similar to that reported by Schulz and Searcy,¹¹ was observed when the empty degassed cell was heated. The origin of this

effect has not been fully explained. It is reproducible and appears to be associated with an anisotropy of the torsion wire. The deflection is reversed in direction when the wire is reversed. With the 2-mil wire (torsion constant 1.75 dynes cm./radian, 59.4 cm. long) the correction is not very large (at 1600°, 0.010 radian); with the 1-mil wire (torsion constant 0.0992 dyne cm./radian), a correction at 1600°K. of 0.082 radian is necessary. At high effusion pressures the effect is not significant relative to the total deflection for the 2-mil wire; however, at the lowest pressures measured the correction approaches 30% for the 1-mil wire and 10% for the 2-mil wire.

The oxide and graphite powders were mechanically mixed in various mole ratios and, in some cases, pelletized in a press prior to addition to the cells. Above a certain minimum sample size (ca. 1.75 g. for the stoichiometric mixture of ThO₂ and graphite) the effusion steady-state pressures were independent of the amount of material in the cell. Samples were heated slowly (over a period of about 4 hr.) to the reaction temperature zone and then briefly to a temperature 40° above the highest experimental temperature of interest to ensure desorption of adsorbed gases. Cells were then cooled below the experimental range to check the null point before measurements were begun. An attractive feature of the furnace assembly is the very rapid adjustment after a change of voltage. Cell and furnace are in equilibrium again approximately 10 min. after a temperature change of 20°. Angular deflections were measured by means of the usual telescope and curved scale. Temperatures were selected randomly once a series of measurements was begun.¹² (For full details of the experimental set-up, see ref. 12.)

Results and Discussion

The ThO₂-C-ThC₂-CO System. Effusion pressures of CO from reaction 1, Fig. 1, are seen to depend on orifice area. Apparent equilibrium values were derived by extrapolation, using the expression

$$P_{ss}^{-1} = P_{eq}^{-1} + a_t C P_{eq}^{-1}$$

(8) R. F. Barrow, *et al.*, *Trans. Faraday Soc.*, **51**, 1354 (1955); K. K. Kelley, U. S. Department of the Interior, Bureau of Mines Bulletin, U. S. Government Printing Office, Washington, D. C., No. 383, 1935.

(9) J. B. Austerman, G. M. Wolten, and C. T. Broman, "A High Temperature Vacuum Furnace," *Atomics International Bulletin* NAA-SR-2312, June 15, 1958.

(10) H. J. Kostowski and R. D. Lee, "Theory and Methods of Optical Pyrometry," National Bureau of Standards Monograph, U. S. Government Printing Office, Washington, D. C., No. 41, March 1, 1962.

(11) D. A. Schulz and A. W. Searcy, *J. Phys. Chem.*, **67**, 103 (1963).

(12) J. R. Hollahan, Doctoral Dissertation, University of Washington, 1964.

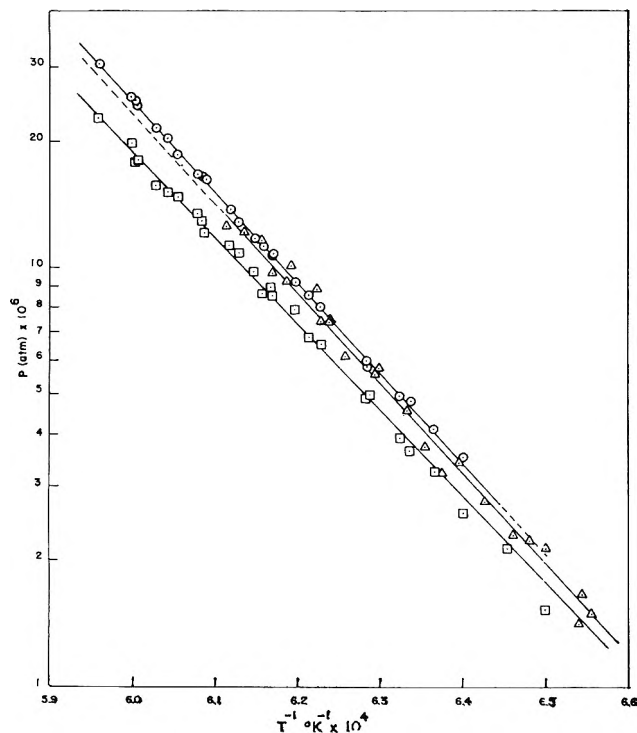


Figure 1. Carbon monoxide effusion pressures over $\text{ThO}_2 + \text{C} + \text{ThC}_2$: \square , cell A-1; Δ , cell A-2; \circ , apparent equilibrium.

where P_{ss} is the steady-state pressure, P_{eq} the apparent equilibrium pressure, a_t the total orifice area, and $C = f/\alpha a_s$ where f is an average nonideal effusion factor,¹³ α the condensation coefficient, and a_s the area of the sample. Values of the reciprocal pressure at zero orifice area were taken as P_{eq}^{-1} . The validity of such an extrapolation procedure is questionable. Only two cells were used; furthermore α and a_s must remain constant; other problems associated with such a treatment have been discussed elsewhere.¹⁴ A better model for extrapolation for a solid-solid reaction has not been found as yet. In this case the effective sample area must be determined by the area of interfacial contact and is probably a more critical function of the degree of reaction than in the case of simple vaporization. However, as seen in Fig. 1, the apparent equilibrium values obtained are virtually the same as those measured in cell A-2; the latter could be used directly as apparent equilibrium pressures without seriously changing the conclusions of our study.

Data in Fig. 1 may be correlated with equations of the form $\log P(\text{atm.}) = -AT^{-1} + B$. Values of the constants A and B and the corresponding mean enthalpies and entropies for the temperature interval 1560–1680°K. for reaction 1 are shown in Table II.

To calculate ΔH° at 298°K. for (1), heat capacity

Table II

	Apparent ΔH° , kcal.		Apparent ΔS° , cal. deg. ⁻¹	
	A	1620°K.	B	1620°K.
Cell A-1	20,651	189	7.67	70.2
Cell A-2	21,460	196	8.25	75.5
Apparent equil	21,830	200	8.44	77.2

data for graphite, $\text{CO}(\text{g})$, and $\text{Th}_2\text{O}_3(\text{c})$ as given by Kelley were used.¹⁵ The estimated heat capacity of ThC_2 , based on the method given by Krikorian,¹⁶ was taken from Jackson, *et al.*⁴ A plot of

$$\Sigma = -4.576 \log P_{\text{CO}^2}(\text{atm.}) - 0.2764 \log T - 1.19 \times 10^{-3}T + 2.75 \times 10^5 T^{-2}$$

vs. $1/T$ gave results leading to $\Delta H^\circ_{298} = 199$ kcal. and $\Delta S^\circ_{298} = 83.6$ cal. deg.⁻¹ for (1). The scatter of points suggests an uncertainty of 5% in slope which corresponds to ± 10 kcal. in the reaction heat.

These results may be compared with those predicted from free energy functions. Values for $\text{CO}(\text{g})$, $\text{ThO}_2(\text{c})$, and graphite were calculated from the data given by Kelley.^{15,17} Those for $\text{ThC}_2(\text{c})$ were taken from Jackson, *et al.*,⁴ based on Krikorian's estimated heat capacity (by comparison with UC_2) and standard entropy of 14 ± 3 at 298°K.¹⁶

$$\Delta H^\circ_{298} = -RT \ln P_{\text{CO}^2}(\text{atm.}) - \Delta(F^\circ_T - H^\circ_{298})$$

The resulting average value of $\Delta H^\circ_{298} = 217.5$ kcal. is significantly higher than the second law result. (The slight apparent trend of values with temperature, Table III, is very small relative to the experimental uncertainty in pressures.) Several reasons for the difference may be suggested: the accuracy of the estimated free energy functions for the carbide; the possibility of transitions in the solid phases in the intermediate tem-

(13) R. D. Freeman and A. W. Searcy, *J. Chem. Phys.*, **22**, 762 (1954).

(14) See, *e.g.*, M. Motzfeldt, *J. Phys. Chem.*, **59**, 139 (1955); L. Brewer and J. S. Kane, *ibid.*, **59**, 105 (1955); J. H. Stern and N. W. Gregory, *ibid.*, **61**, 1226 (1957); G. M. Rosenblatt, *J. Electrochem. Soc.*, **110**, 563 (1963).

(15) K. K. Kelley, "Contributions to the Data on Theoretical Metallurgy. XIII," U. S. Department of the Interior, U. S. Bureau of Mines Bulletin, U. S. Government Printing Office, Washington, D. C., No. 584, 1960.

(16) O. H. Krikorian, University of California Radiation Laboratory Report UCRL-6785, February 6, 1962.

(17) K. K. Kelley, "Contributions to the Data on Theoretical Metallurgy, XIV," U. S. Department of the Interior, U. S. Bureau of Mines Bulletin, U. S. Government Printing Office, Washington, D. C., No. 592, 1961.

Table III: Free Energy Function Treatment of Equilibrium Pressures

T, °K.	-log K. atm. ²	If S [°] ₂₉₈ (ThC ₂) = 14.0		If S [°] ₂₉₈ (ThC ₂) = 11.0	
		-Δ(F [°] T - H [°] ₂₉₈)/T	ΔH [°] ₂₉₈	-Δ(F [°] T - H [°] ₂₉₈)/T	ΔH [°] ₂₉₈
		1678	9.02680	88.58	217.9
1667	9.19754	88.59	217.8	81.18	205.5
1666	9.19620	88.59	217.6	81.18	205.4
1665	9.22772	88.59	217.8	81.18	205.5
1658	9.32908	88.60	217.7	81.19	205.4
1655	9.38372	88.60	217.7	81.19	205.4
1651	9.45818	88.60	217.7	81.19	205.5
1645	9.55926	88.61	217.7	81.20	205.5
1644	9.56766	88.61	217.6	81.20	205.5
1643	9.57084	88.61	217.6	81.20	205.4
1635	9.72088	88.62	217.6	81.23	205.5
1632	9.77278	88.62	217.6	81.23	205.6
1627	9.95184	88.63	217.6	81.25	205.5
1624	9.87936	88.63	217.4	81.25	205.4
1621	9.95020	88.64	217.5	81.25	205.5
1621	9.94124	88.64	217.4	81.25	205.4
1614	10.07166	88.65	217.5	81.27	205.6
1609	10.12888	88.66	217.2	81.29	205.4
1606	10.19110	88.66	217.3	81.29	205.4
1592	10.44806	88.67	217.3	81.30	205.4
1591	10.47254	88.67	217.3	81.30	205.6
1582	10.61412	88.68	217.1	81.36	205.5
1578	10.63788	88.68	216.8	81.36	205.2
		Average	217.5	Average	205.5

perature region; the assumed equilibrium pressures may be low by reason of an incorrect extrapolation procedure. It is interesting to note, however, that if the standard entropy of ThC₂ is taken as 11 at 298°K., that is at the lower limit of the uncertainty given by Krikorian, the free energy function calculation gives ΔH[°]₂₉₈ as 205 kcal., in good agreement with the second law treatment. The consistency of the data for this choice is shown in Table III. Hence, if we assume our pressures are equilibrium values, that no transitions occur in the intermediate temperature interval, and that the estimated heat capacity of the carbide is correct, an entropy of ThC₂ of ca. 11 is predicted.

The only other direct study of the equilibrium corresponding to (1) is that of Prescott and Hincke.⁶ Their experiment consisted of a manometric measurement of CO pressures at room temperature with the sample temperature in the range 2000–2500°K. Their pressures show a rather large scatter which makes a second law treatment subject to considerable uncertainty; using the same heat capacity data as in the preceding paragraphs, one obtains a value of ΔH[°]₂₉₈ of 181 kcal. This low value leads to an unreasonably large heat of

formation of the carbide. The free energy function treatment of Prescott and Hincke's data, comparable to that shown for our results in Table III, gives values of 208 and 191 kcal., respectively.

Considering all existing equilibrium data and their associated uncertainties, it appears reasonable to assign the values 201 ± 10 kcal. as ΔH[°]₂₉₈ and 85 ± 3 cal. deg.⁻¹ as ΔS[°]₂₉₈ as the best experimental values for reaction 1. This value for the enthalpy change, together with the well-established heats of formation of CO (-26.42 kcal. mole⁻¹) and ThO₂ (-293.2 kcal. mole⁻¹) leads to a value of -39.4 kcal. mole⁻¹ for the heat of formation of ThC₂ at 298°K. This may be compared with values deduced by independent methods: Jackson, *et al.*⁴ considering vaporization data relative to the carbide, give values ranging from -31.8 to -37 kcal. depending on the processes considered and whether the second law or free energy function method was used; Lonsdale and Graves,⁵ from carbide vaporization studies, give -46 kcal. mole⁻¹; from electrochemical measurements Egan and Bracker¹⁸ deduce a value of -37.3 kcal. mole⁻¹.

Effusion Pressure Characteristics of the Reacting Mixture. A number of special experiments were performed to test the dependence of the effusion pressures on certain factors. One sample was heated for a long period (42 hr.) to ascertain the effect of the degree of completion of the reaction on effusion pressures. After the pressure in the cell reached its initial steady-state value, it remained unchanged for about 10 hr. Then a gradual fall-off was observed. The sample was removed from the cell after 34 hr. of heating during which, according to the observed weight loss, about 70% of the oxide had been converted to the carbide, and after which the pressure had fallen to about 20% of its initial steady-state value. The sample was quickly broken up again into a fine powder and replaced in the cell. On reheating and after evolution of some products of hydrolysis, CO pressures at the original steady-state value were again observed for about 1 hr. after which a fall-off again occurred. The fall-off appears to be due largely to sample depletion with the available reacting interfaces becoming insufficient to saturate the cell with CO. The behavior observed, however, supports the assumption that no appreciable solid solution is formed between oxide and carbide. The heterogeneous nature of the samples was clearly visible. A Knudsen calculation of the average pressure of CO over the 34-hr. interval,

(18) J. J. Egan and J. Bracker. "The Standard Free Energy of Formation of ThC₂ from Electromotive Force Measurements," presented at the 2nd Conference on Nuclear Reactor Chemistry, Gatlinburg, Tenn., October 10–12, 1961; and private communication.

based on the weight loss (0.1266 g.), was in good agreement with that determined by the torsion effusion.

In a number of experiments the initial composition (moles of ThO_2 -moles of C) of the solid mixture was varied as 1:4, 1:3, and 1:2. The results showed no dependence on the initial composition.

It is difficult to estimate the magnitude of the condensation coefficient of CO on the carbide-oxide reaction interface because of the problem of assigning an effective area. If this area is taken to have a magnitude comparable to the cell cross section, the coefficient, as indicated by the variation of pressure with orifice area, appears to be of the order of 10^{-2} .

The ZrO_2 -C-ZrC-CO System. Here effusion pressures are significantly less than expected equilibrium values. Results of runs in three cells, for which the ratio of total orifice area was 1:2:10, are shown in Fig. 2. Results from the two cells with the smaller orifices, B-2 and B-4, are virtually indistinguishable. Pressures

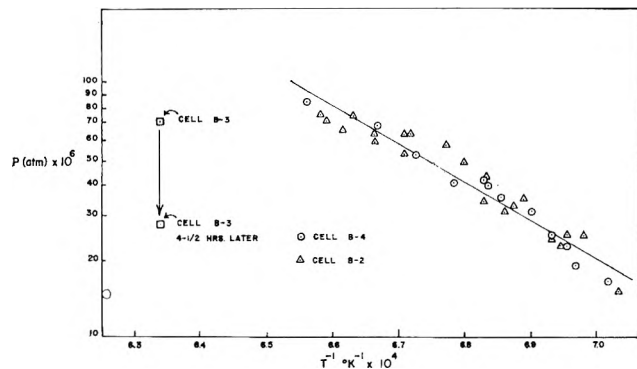


Figure 2. Carbon monoxide effusion pressures over $\text{ZrO}_2 + \text{C} + \text{ZrC}$.

in the cell with the largest orifice, B-3, fell off continuously from the first measured value; the change in 4.5 hr. is shown in Fig. 2. This behavior was observed for both a 1.05-g. powdered sample (reactants in the stoichiometric proportions) and a 2.64-g. pelletized sample; the latter was as large as could be physically accommodated in the cell. The pressures observed for the powdered sample, at corresponding time and temperature, were considerably below those of the pelletized sample.

A least-squares treatment of the combined data from cells B-2 and B-4, in the temperature range 1422–1520°K., gives the equation

$$\log P_{\text{CO}}(\text{atm.}) = -16,100T^{-1} + 6.55$$

which corresponds to an apparent reaction heat for (2) of 147 kcal. Prescott¹⁹ in a manometric study with

the sample at 1875–2225°K. obtained 152 kcal. His data may be represented by the equation

$$\log P_{\text{CO}}(\text{atm.}) = -16,580T^{-1} + 8.59$$

If the steady-state pressures from cells B-2 and B-4 are assumed to be equilibrium values, the entropy change for the reaction in the experimental temperature range is 60 cal. deg.⁻¹, or, using estimated heat capacity relationships,¹⁶ 64 cal. deg.⁻¹ at 298°K. This, together with well-known values for ZrO_2 (12.12), CO, and graphite, would require the entropy of ZrC to be -14.6, obviously impossible. One must conclude that the steady-state pressures in these cells are appreciably below the equilibrium values (by a factor of about 200) or that the equilibrium studied is not correctly represented by eq. 2. No other evidence to support the latter possibility has been found.

One would expect to have observed a significant difference in the steady-state pressures in cells B-2 and B-4, which differ in orifice area and hence rate of loss of CO by a factor of two, if the system is appreciably away from equilibrium. The temperature was varied randomly during each series of measurements and reproducible pressures were observed. It is also somewhat surprising that the apparent heat of reaction corresponds reasonably well with that observed by Prescott. This system seems to show a pseudo-equilibrium-like behavior in the effusion cell, somewhat similar to the situation observed earlier in the study of the decomposition of $\text{Mg}(\text{OH})_2$.¹

Conclusions

ZrC is classed as an interstitial carbide and is structurally quite different from the reactant ZrO_2 . On the other hand, ThO_2 and ThC_2 , while crystallographically different, appear more amenable to interconversion through reaction of graphite and carbon monoxide. One can visualize an interfacial region of these materials in contact with graphite at which the equilibrium interaction with the vapor phase is more easily facilitated in the thoria case than in the zirconia system for which the mono- rather than the dicarbide is formed. This appears to be the principal feature distinguishing the two systems.

Any more detailed consideration of the mechanism of the reaction in either system would be speculative. Diffusion paths, coefficients, and concentration gradients in the interaction region would be needed. Komarek, Coucoulas, and Klinger²⁰ indicate that the ThO_2 -

(19) C. H. Prescott, Jr., *J. Am. Chem. Soc.*, **48**, 2534 (1926).

(20) K. L. Komarek, A. Coucoulas, and N. Klinger, *J. Electrochem. Soc.*, **110**, 783 (1963).

graphite reaction follows a parabolic rate law, *i.e.*, plots of moles of CO produced *vs.* the square root of time are straight lines. They conclude that the process is diffusion controlled through a carbide layer. One might postulate that condensation of CO on the surface forms a chemisorbed oxycarbide intermediate from which, by diffusion, atoms migrate to the oxide and carbide crystalline phases, respectively.

It is apparent that one must be very cautious in the use of the effusion method to study vaporization processes in which gaseous species are produced through the interaction of nonvolatile solids. However, if the principal reactant and product solid phases are sufficiently similar, the method may be applicable. Such

seems to be the case for the $\text{ThO}_2\text{-C}$ reaction. In any case, careful study of the dependence of effusion pressures on orifice diameters, sample and particle size, solid-solid contact area, relative amounts of reactants, degree of conversion of the reactants, as well as verification of the nature of the equilibrium reaction involved, is necessary before results may be accepted with confidence.

Acknowledgment. This work was supported in part by grants from the Army Research Office, National Science Foundation, and the National Aeronautics and Space Administration (NSG 484), which are acknowledged with thanks.

The Near-Infrared Transitions of the Trivalent Lanthanides in Solution. III. Promethium(III)¹

by W. T. Carnall, P. R. Fields, and G. E. Toogood

Argonne National Laboratory, Argonne, Illinois (Received December 14, 1963)

The solution absorption spectrum of Pm^{+3} was measured both in molten $\text{LiNO}_3\text{-KNO}_3$ eutectic at 150° in the range $0.35\text{-}2.6\ \mu$ and in dilute DCl at 25° in the range $0.35\text{-}1.8\ \mu$. The results give the first experimental confirmation of calculations which place the two highest levels of the ground term multiplet, 5I_7 and 5I_8 , within the region of transparency of the nitrate melt in the near-infrared. A full intermediate coupling calculation for the f^4 configuration was also carried out, and all energy levels from 0 to $30,000\ \text{cm.}^{-1}$ are reported, based on the following values of the Slater integrals: $F_2 = 351\ \text{cm.}^{-1}$, $F_4 = 47.7\ \text{cm.}^{-1}$, $F_6 = 5.30\ \text{cm.}^{-1}$, and on a spin-orbit coupling constant, $\zeta = 1030\ \text{cm.}^{-1}$. Interpretation of the results in the visible region is offered based on these calculations and on recent theoretical treatments of the intensity of lanthanide spectra. A very intense transition of Pm^{+3} in the visible region in molten nitrate solvent was discovered, and this should aid in the analysis of the element in mixtures.

In the course of the present series of papers^{2,3} we have sought to interpret, when possible, the solution absorption spectra of the trivalent lanthanides in terms of the calculated field-free energy levels. We have been particularly interested in the near-infrared region

beyond $1.4\ \mu$ where water ceases to be transparent. Calculations show that the spectral range from 1.4 to $2.6\ \mu$ should contain one or more absorption bands for practically every lanthanide, and the $\text{LiNO}_3\text{-KNO}_3$ eutectic has proven to be a useful solvent in which to

observe these transitions. Most of them have not been observed previously in solution.

The last lanthanide to be considered, promethium, is also the only member of the series that does not possess a stable isotope. Chemical studies are normally conducted with Pm^{147} ($t_{1/2} = 2.6$ years).⁴ With this relatively short half-life, it is clear that any work with macro amounts of the element involves the handling of rather high levels of radioactivity. Thus, it is not surprising that few investigations of the absorption spectrum of Pm^{+3} have been reported, and practically all of these have been carried out in solution.⁵⁻⁹ Moreover, none has verified experimentally the calculations which show that transitions to the two highest levels of the ground-state multiplet should be observed in the 1.4–2.6 μ range.

This communication reports the results of experiments conducted with concentrations of promethium up to 60 mg./ml., which clearly demonstrate the existence of these levels. The characteristics of the absorption bands as observed in the visible range in the LiNO_3 – KNO_3 eutectic are discussed, and new data on the spectrum of Pm^{+3} in dilute DCl are included for comparison purposes. In addition, a full intermediate coupling calculation for the f^4 configuration was carried out using parameters which gave the best fit to the experimental results. This calculation, together with arguments based on intensity relationships, provided a basis for interpreting some of the observed absorption bands.

Experimental

The Pm^{147} sample used in this work was obtained from Oak Ridge National Laboratory as a chloride solution and contained 130 mg. of Pm^{147} , with 20 mg. of Nd, 4 mg. of Sm, and 4 mg. of Am^{241} as the principal contaminants.

Separation from americium was achieved at room temperature on a cation-exchange column (8% cross-linked zeolite resin with a settling rate of ~ 0.4 cm./min. in a 20 cm. long \times 1 cm. in diameter column), adsorbing the sample from 0.1 M HCl and eluting with 12 M HCl. The flow rate was ~ 0.5 ml./min.

Removal of samarium and neodymium was similarly carried out using a cation-exchange column run at 85°. The resin, 8% cross-linked zeolite with a settling rate of ~ 1.5 cm./min., was contained in a water-jacketed column 40 cm. long \times 1.7 cm. in diameter. The feed solution (< 0.1 M HCl) was preheated in a line that passed through the hot water jacket of the exchange column and was introduced after the resin had been ammoniated with hot 8 M NH_4OH and washed with several column volumes of hot water. The ad-

sorbed promethium was eluted with ammonium α -hydroxyisobutyrate (pH 6.4) using a flow rate of ~ 0.75 ml./min. The promethium butyrate fraction was made 1 M in HCl, adsorbed on a cation-exchange column similar to that used in the americium separation step, and then eluted with 6 M HCl. This separated practically all of the butyrate from the PmCl_3 . The latter was then refluxed with concentrated HNO_3 to destroy the last traces of butyrate plus any resin fines, reconverted to chloride, and then repeatedly evaporated to dryness in a micro still with 0.2 M DCl.

The final solution in 0.2 M DCl contained 119 mg. of promethium and 0.2 mg. of americium. Neither neodymium nor samarium was detected. Solutions were assayed for promethium by β^- -counting aliquots under standardized conditions in a 2π -proportional counter.

The americium gave a small shoulder near 0.5 μ on a much larger promethium absorption band that was centered near 0.493 μ . This shoulder was subtracted from the data shown in Fig. 1.

Absorption measurements were made using a Cary Model 14 recording spectrophotometer with 1-cm. path length borosilicate glass cells. After obtaining the absorption spectrum in DCl solution, the sample was transferred to a long-stemmed spectrophotometer cell and evaporated to dryness prior to dissolution in the molten nitrate salt. The details of the preparation of clear solutions of lanthanides in LiNO_3 – KNO_3 melts and the type of cells used have been described previously.¹⁰

The low energy (0.23 Mev.) $\text{Pm}^{147} \beta^-$ is not detected by many standard β - γ monitoring instruments, and this presents a hazard whenever one works with the pure isotope. In this connection, members of the instrument section of the Industrial Hygiene and Safety Division at Argonne National Laboratory have developed an extremely valuable modification of a gas-

(1) Based on work performed under the auspices of the U. S. Atomic Energy Commission.

(2) W. T. Carnall, D. M. Gruen, and R. L. McBeth, *J. Phys. Chem.*, **66**, 2159 (1962).

(3) W. T. Carnall, *ibid.*, **67**, 1206 (1963).

(4) F. P. Roberts, E. J. Wheelwright, and W. Y. Matsumoto, Hanford Laboratory Report HW-77296 (April, 1963).

(5) G. W. Parker and P. M. Lantz, *J. Am. Chem. Soc.*, **72**, 2834 (1950).

(6) W. F. Meggers, B. F. Schribner, and W. R. Bozman, *J. Res. Natl. Bur. Std.*, **46**, 85 (1951).

(7) D. C. Stewart, Argonne National Laboratory Report ANL-4812 (October, 1956).

(8) J. G. Conway and J. B. Gruber, *J. Chem. Phys.*, **32**, 1586 (1960).

(9) J. B. Gruber and J. G. Conway, *J. Inorg. Nucl. Chem.*, **14**, 303 (1960).

(10) W. T. Carnall, *Anal. Chem.*, **34**, 786 (1962).

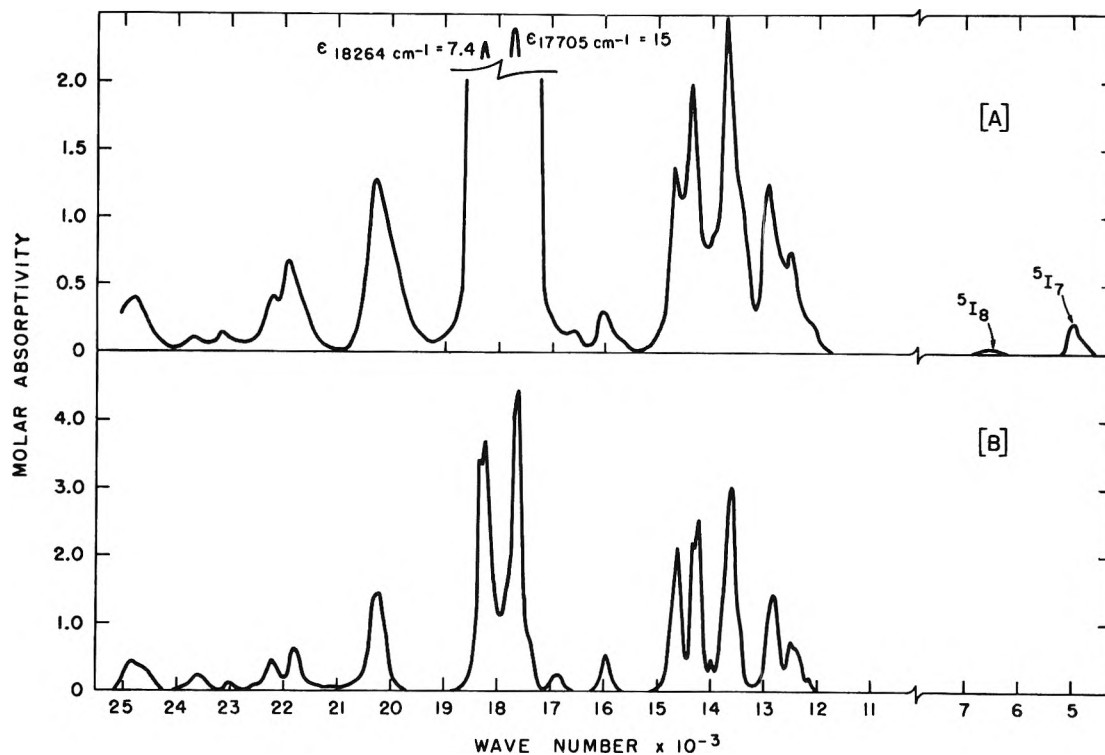


Figure 1. The absorption spectrum of Pm^{+3} in [A] $\text{LiNO}_3\text{-KNO}_3$ eutectic at 150° and [B] 0.2 M DCl at 25° .

flow portable α -monitor which provides a large area detector capable of detecting $\text{Pm}^{147}\beta^-$ with approximately 50% yield (the same yield as for α -particles).

Results and Discussion

The field-free ground term multiplet of Pm^{+3} can readily be calculated¹¹ to a fairly good approximation assuming pure Russell-Saunders coupling. Application of eq. 1 gives the results shown in Table I for the spin-orbit perturbation energy (E).

$$E = \frac{\lambda\zeta}{2} [J(J+1) - L(L+1) - S(S+1)] \quad (1)$$

where $\zeta = 1025\text{ cm.}^{-1}$ and $\lambda = 1/2S$. The rough value for the spin-orbit coupling constant (ζ) for Pm^{+3} was determined by linear extrapolation from known values of this constant for the other light lanthanides.

Assuming that the absorption bands occur with sufficient intensity, this calculation shows that transitions from the ground level 5I_4 to both 5I_7 and 5I_8 should be observed in the near-infrared transparency range of the molten $\text{LiNO}_3\text{-KNO}_3$ eutectic. One would also expect to observe 5I_8 in deuterated solvents. The absorption characteristics of H_2O , D_2O , molten $\text{LiNO}_3\text{-KNO}_3$, and borosilicate glass between 0.35 and $2.6\ \mu$ were given in ref. 2.

In their recent study of the absorption spectrum of

Table I: Calculated Field-Free Energy Levels of Pm^{+3}

Level	Energy, cm.^{-1}	Wave length, μ
5I_4	0	
5I_6	1280	(7.82)
5I_6	2820	(3.54)
5I_7	4610	(2.17)
5I_8	6660	(1.50)

Pm^{+3} in dilute DCl, Gruber and Conway did not observe a band near $1.5\ \mu$ while working in a concentration range of 30 mg. of $\text{Pm}^{+3}/5.23\ \text{ml.}^9$ We were also unable to obtain unequivocal evidence for the 5I_8 band in DCl even though we used considerably higher concentrations of promethium than Gruber and Conway; however, we clearly observed bands near the predicted energies for 5I_7 and 5I_8 in the $\text{LiNO}_3\text{-KNO}_3$ eutectic, as shown in Fig. 1. Both of these bands proved to be relatively weak compared to those observed in the visible range. They have not been observed previously, either in solution or in a crystal matrix. The fact that the 5I_8 band is very broad and

(11) J. P. Elliott, B. R. Judd, and W. A. Runciman, *Proc. Roy. Soc. (London)*, **A240**, 509 (1957).

Table II: Energy Levels of Pm^{+3}

Obsd. absorption peak, cm.^{-1}	Calcd. energy, cm.^{-1}	SLJ label	SL composition of states ^a	Obsd. absorption peak, cm.^{-1}	Calcd. energy, cm.^{-1}	SLJ label	SL composition of states
	0	$^5\text{I}_4$	97% ^5I	23,170	23,180	$^3\text{D}_1$	49% ^3D ; 47% ^3P
	1,515	$^5\text{I}_5$	98% ^5I	23,700	23,338	$^3\text{L}_5$	60% ^3L ; 20% ^3M ; 18% ^3K
	3,166	$^5\text{I}_6$	99% ^5I				
4,990	4,900	$^5\text{I}_7$	98% ^5I		24,173	$^3\text{G}_4$	60% ^3G ; 18% ^3H ; 12% ^5G
6,670	6,679	$^5\text{I}_8$	95% ^5I				
12,200	12,356	$^5\text{F}_1$	94% ^5F		24,261	$^3\text{H}_8$	64% ^3H ; 34% ^1I
12,570							
12,970	12,797	$^5\text{F}_2$	92% ^5F		24,266	$^3\text{L}_9$	75% ^3L ; 25% ^3M
13,720	13,674	$^5\text{F}_3$	95% ^5F		24,343	$^3\text{M}_8$	47% ^3M ; 34% ^1L ; 16% ^3L
14,380	14,366	$^5\text{S}_2$	93% ^5S				
14,700	14,611	$^5\text{F}_4$	89% ^5F		24,763	$^3\text{D}_3$	85% ^3D ; 10% ^3F
	15,938	$^3\text{K}_6$	98% ^3K	24,800	24,835	$^3\text{P}_0$	100% ^3P
16,070	15,958	$^5\text{F}_5$	91% ^5F	25,840 ^b	25,431	$^1\text{D}_2$	87% ^1D
	17,196	$^3\text{K}_7$	80% ^3K ; 17% ^3L		26,487	$^3\text{F}_4$	72% ^3F ; 12% ^3G ; 12% ^1G
	17,608	$^3\text{H}_4$	49% ^3H ; 21% ^3G ; 15% ^5G		26,615	$^3\text{G}_5$	69% ^3G ; 13% ^3H
17,705	17,903	$^5\text{G}_2$	92% ^5G		27,000	$^3\text{P}_1$	53% ^3P ; 45% ^3D
18,264	18,245	$^5\text{G}_3$	71% ^5G ; 25% ^3G		27,586	$^3\text{I}_5$	88% ^3I
	18,736	$^3\text{K}_8$	68% ^3K ; 16% ^3L		27,819	$^3\text{M}_9$	75% ^3M ; 25% ^3L
	19,919	$^3\text{H}_5$	46% ^3H ; 32% ^5G ; 15% ^3G		28,016	$^3\text{F}_2$	51% ^3F ; 35% ^3P
20,300	20,321	$^5\text{G}_4$	71% ^5G ; 25% ^3H		28,454	$^3\text{M}_{10}$	99% ^3M
	21,225	$^3\text{G}_3$	71% ^3G ; 25% ^5G		28,591	$^3\text{F}_3$	84% ^3F
21,950	22,116	$^3\text{D}_2$	59% ^3D ; 20% ^3P	29,070 ^b	28,752	$^3\text{I}_6$	92% ^3I
	22,172	$^3\text{G}_5$	61% ^5G ; 38% ^3H		29,193	$^1\text{L}_8$	56% ^1L ; 29% ^3M
22,250	22,198	$^3\text{L}_7$	82% ^3L ; 17% ^3K		29,252	$^3\text{I}_7$	74% ^3I ; 19% ^5I
	22,600	$^5\text{G}_6$	70% ^5G ; 29% ^3H	30,040 ^b	29,397	$^3\text{F}_2$	83% ^3F
					30,046	$^5\text{D}_0$	97% ^5D

^a Only components of 10% or greater are recorded. ^b Data from ref. 9.

weak in the nitrate melt helps to explain the difficulty in observing it in DCl, where this particular promethium absorption is somewhat obscured by the presence of a small D_2O band.

As an aid in interpreting the results, the matrix elements of the Coulomb and spin-orbit interactions in the f^4 configuration were calculated in terms of four parameters; the three Slater integrals F_2 , F_4 , and F_6 , and the constant ζ , using the Argonne CD-3600 computer. Similar calculations reported earlier^{12,13} were based entirely on observations of the solution absorption spectrum of Pm^{+3} in dilute DCl in the visible-ultraviolet region. The positions of the two highest levels of the ground term multiplet, which were observed in the near-infrared in the present investigation, are essentially determined by spin-orbit interaction, and their observation made possible the calculation of a much better value for ζ . The values for the three Slater integrals were then adjusted to give the best over-all fit to absorption bands observed in this work as well as that of Gruber and Conway.

The following set of parameters was used to generate the energy levels shown in Table II: $\zeta = 1030 \text{ cm.}^{-1}$, $F_2 = 351$, $F_4 = 47.7$, $F_6 = 5.30$.

The present experimental results, which indicate that there is no absorption due to promethium between approximately 1.4 and 0.82μ , are consistent with the calculation which places the first excited multiplet level ($^5\text{F}_1$) near 0.809μ . This is particularly useful confirmatory information in this case since the radioactive decay product of Pm^{147} is Sm^{147} , a very long-lived nuclide, which has a relatively intense absorption band near 1.25μ both in aqueous solution and in molten $\text{LiNO}_3\text{-KNO}_3$.² Thus, any absorption in a promethium sample at this wave length is definitely not due to promethium but may very likely be due to the samarium daughter.

A significant difference in the spectrum of Pm^{+3} in the nitrate melt as compared to that in DCl is found

(12) M. H. Crozier and W. A. Runciman, *J. Chem. Phys.*, **35**, 1392 (1961).

(13) S. Hüfner, *Z. Physik*, **165**, 397 (1961).

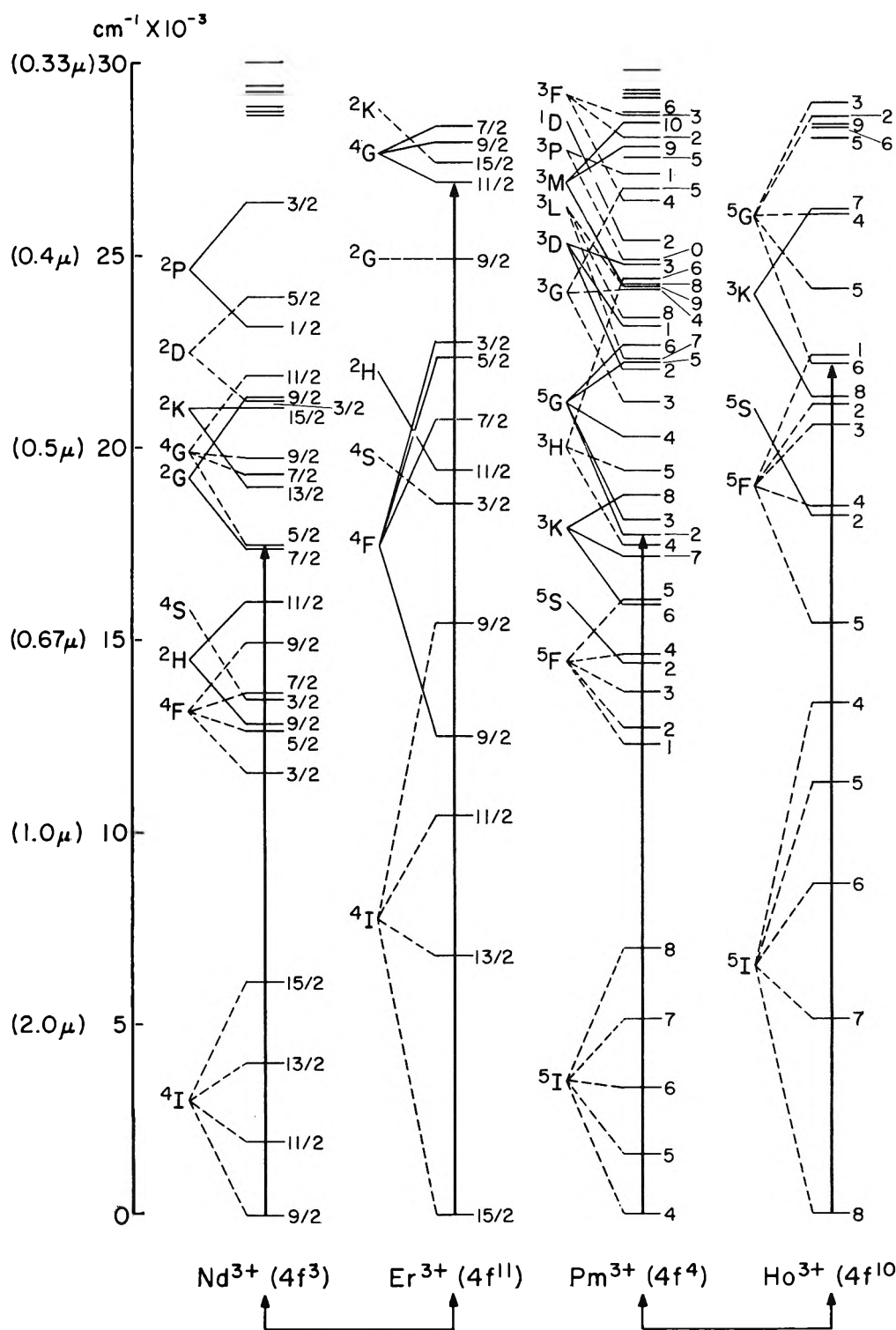


Figure 2. The field-free energy levels of Nd^{3+} , Er^{3+} , Pm^{3+} , and Ho^{3+} in the 0–30,000 cm^{-1} range as calculated in the present work and in ref. 12 and by B. G. Wybourne, *J. Chem. Phys.*, **32**, 639 (1960). The indicated transitions are those corresponding to the most intense bands observed in the visible region in the $\text{LiNO}_3\text{-KNO}_3$ melt.

in the visible range. Two bands, centered at 0.564 μ (17,705 cm^{-1}) and 0.548 μ (18,264 cm^{-1}), undergo a very large increase in intensity in the nitrate melt.

As can be seen from Fig. 1, these appear to be due to the same transitions that are responsible for the most intense bands of Pm^{3+} in the visible range in DCl

solution. The results of the intermediate coupling calculation indicate that the transitions involved in the 0.564- μ band are those from the ground state 5I_4 to a group of levels probably restricted to 3K_7 , 3H_4 , and 5G_2 , as shown in Fig. 2. It may be pointed out at this juncture that while the ground level is nominally designated as 5I , its composition is actually 97% 5I plus approximately 3% 3H . Thus, assuming that the selection rule $\Delta S = 0$ is rigidly adhered to, one cannot determine whether the intense absorption band at 0.564 μ is due primarily to a triplet to triplet or to a quintet to quintet transition without further information.

The discovery of these "super-allowed" bands in Pm^{+3} in the nitrate melt indicates that there is a pattern in this type of behavior in the lanthanides since earlier it was found that only Nd^{+3} , Ho^{+3} , and Er^{+3} exhibit the same type of phenomena.^{2,3} Each species, when dissolved in the nitrate melt, gave rise to one or two intense bands in the visible region. These bands do not always correspond to the most intense absorptions observed in aqueous solutions.^{2,3} However, it will be noted that the four elements form conjugate pairs; that is, $Nd^{+3}(f^3)$ and $Er^{+3}(f^{11})$, and $Pm^{+3}(f^4)$ and $Ho^{+3}(f^{10})$. Each pair has the same electrostatic energy level structure, but when the degeneracy of these levels is removed by spin-orbit coupling, the resulting levels are filled in reverse order. For example, Fig. 2 shows that both Pm^{+3} and Ho^{+3} have a 5I ground term, but in Pm^{+3} the order of the multiplet levels is from four to eight, while in Ho^{+3} the order is exactly the opposite. There appears to be no simple explanation as to why only these four elements develop the indicated intense absorption bands in the molten nitrate.

Recently Judd¹⁴ discussed the calculation of intensities of lanthanide absorption spectra and developed a theory which led to an expression for oscillator strength (P) as a function of the symmetry of the lanthanide ion (in terms of a complex function T_λ) and of the reduced matrix elements for the transition $\psi_J \rightarrow \psi'_{J'}$ of frequency ν

$$P = \sum_{\substack{\lambda \\ \text{even}}} T_{\lambda\nu}(\psi_J || U^{(\lambda)} || \psi'_{J'})^2$$

where $U^{(\lambda)}$ is a tensor operator of rank λ , and λ takes the values 2, 4, and 6. While no experimental results for Pm^{+3} were compared to the theory, Judd did compare the oscillator strengths determined from the solution absorption spectra of Nd^{+3} and Er^{+3} to those derived semiempirically, by calculating the reduced matrix elements and then treating the symmetry

functions (T_λ) simply as parameters to be adjusted to fit the experimental data.

These results indicated that T_2 was the part of the expression for the oscillator strength that was most sensitive to changes in environment. In the example cited, T_2 varied by a factor of two while T_4 and T_6 remained essentially invariant. A much better test of this generalization should result from calculating T_2 for Pm^{+3} in the molten nitrate system. In order to account for the obvious appreciable increase in oscillator strength of the band near 0.555 μ in the melt as compared to DCl solution, one might expect a very large value of T_2 for the transitions involved if T_4 and T_6 do not vary much from one medium to another.

The foregoing also suggests that one should in principle be able to use intensity arguments to determine which of several possible transitions is primarily responsible for a given intense absorption band. Thus, for Nd^{+3} the principal band in the nitrate melt has a maximum at 0.582 μ , which is consistent with a transition from $^4I_{5/2}$ to either $^4G_{5/2}$ or $^2G_{7/2}$; calculation places these two states at essentially the same energy (see Fig. 2). Now the value of the reduced matrix elements (RME), $(f^3[{}^4I_{5/2}] || U^{(\lambda)} || f^2[S'L'J'])$, will be the same for a given transition whatever the environment in which the Nd^{+3} is placed, and according to Judd's calculations for the specific case in point, the value of the RME for $\lambda = 2, 4$, and 6 is in every case larger for $^4G_{5/2}$ than for $^2G_{7/2}$. Thus, no matter what combination of values is taken for T_λ , the sum of the products of T_λ and (RME)² will always be larger for $^4G_{5/2}$. In $NdCl_3$ solution, for example, the oscillator strengths of $^4G_{5/2}$ and $^2G_{7/2}$ are 8.40×10^{-6} and 2.18×10^{-6} , respectively, and their sum is essentially equal to the experimental value for the band observed in $Nd(NO_3)_3$ solution between 0.575 and 0.578 μ .¹⁵ It seems reasonable to conclude that the transition $^4I_{5/2} \rightarrow ^4G_{5/2}$ is primarily responsible for the intense band of Nd^{+3} observed in a $NdCl_3$ solution and for the band seen in the nitrate melt at 0.582 μ . As mentioned earlier, a similar situation is observed with the most intense band of Pm^{+3} both in DCl solution and in the molten nitrate (0.564 μ). It appears reasonable to assume that the transitions involved are to 3H_4 , 5G_2 , and 3K_7 . A knowledge of the reduced matrix elements for these transitions, and a fitting of this data to the absorption spectrum of Pm^{+3} in DCl solution and in the nitrate melt, should make it possible to select which one of these transitions is primarily responsible

(14) B. R. Judd, *Phys. Rev.*, **127**, 750 (1962).

(15) J. Hoogschagen and C. J. Gorter, *Physica*, **14**, 197 (1948).

for the band. We plan to report the results of such calculations for Pm^{+3} and for the other lanthanides in future communications in this series.

It is clear that the intensification of the band structure that is observed in Pm^{+3} , Nd^{+3} , Ho^{+3} , and Er^{+3}

in fused nitrates should be of considerable help in detecting small amounts of these elements in mixtures.

Acknowledgment. We wish to thank Dr. B. G. Wybourne for numerous helpful discussions and aid in carrying out the calculations.

NOTES

Heat of Formation of $(\text{HOBO})_3$

by Jay A. Blauer and Milton Farber

Research and Development Laboratories, Maremont Corp., Pasadena, California (Received February 24, 1964)

In recent years there have been several attempts to give definitive values to the thermodynamic properties of $(\text{HOBO})_3(\text{g})$. Based upon data obtained by means of mass spectrometry, Chupka, *et al.*,¹ give a value of -540 ± 10 kcal./mole for its heat of formation at 298°K. This large uncertainty arises because about 99% of the volatile boron species in their apparatus was $\text{HOBO}(\text{g})$, leaving only about 1% as $(\text{HOBO})_3(\text{g})$. Randall, *et al.*,² give -537.5 ± 3 kcal./mole for the heat of formation of $(\text{HOBO})_3(\text{g})$ at 298°K. based upon transpiration experiments carried out at very high rates of flow (17 cm./min.). Whereas Randall, *et al.*,² were troubled with the need for making diffusion loss corrections, this was eliminated in the present study by employing a more suitable apparatus.

The apparatus consisted of a Vycor tube with an o.d. of 25 mm. equipped with a capillary inlet (i.d. 2 mm.) and constricted to an i.d. of 17 mm. at a distance of 12 mm. from the inlet. A hollow Vycor plug having a central orifice of 2-mm. diameter was fitted tightly against the constriction and held in place by means of a solid quartz weight (see Fig. 1). The capillary inlet was wrapped with heating tape and kept at a temperature in excess of 200°.

Nitrogen gas was passed through a heat exchanging coil immersed in a constant temperature bath and then through a fritted disk into distilled water, also heated by means of the bath. The gaseous mixture was then passed through the transpiration cell, over liquid B_2O_3

which was contained in a platinum combustion boat. The amount of transpired nitrogen, and consequently of water vapor, was determined by collecting the nitrogen over water at the end of the transpiration train. The rates of linear gaseous flow were in the neighborhood of 1 cm. per min. The combustion boat and its contents were weighed before and after each run.

The runs were made at varying gas flow rates. It was found that plots of $(\Gamma_{\text{B}_2\text{O}_3}/\Gamma_{\text{H}_2\text{O}})$ vs. $\Gamma_{\text{H}_2\text{O}}$, where Γ_x represents the number of moles of species x which passes out of the cell per hour, were linear and could be easily extrapolated to zero flow by means of the method of least squares (see Fig. 2 and 3).

The values of the ratios $(\Gamma_{\text{B}_2\text{O}_3}/\Gamma_{\text{H}_2\text{O}})$ were determined at zero flow for each of the values of the water vapor pressure considered. The values are tabulated in Table I, the degrees of statistical freedom being taken

Table I: Extrapolated Transpiration Data

T , °K.	$P_{\text{H}_2\text{O}}$, atm.	$\left(\frac{\Gamma_{\text{B}_2\text{O}_3}}{\Gamma_{\text{H}_2\text{O}}}\right)_{\omega=0}$ ^a	f^b
1147	0.704	0.0320 ± 0.0023^c	3
1147	0.308	0.0293 ± 0.0015	2
1147	0.488	0.0279 ± 0.0017	2
1147	0.132	0.0178 ± 0.0013	2

^a ω is the linear rate of gaseous flow. ^b Degrees of statistical freedom. ^c The uncertainties are the calculated standard deviations.

(1) W. A. Chupka, D. J. Meschi, and J. Berkowitz, *J. Chem. Phys.*, **33**, 530 (1960).

(2) S. P. Randall and J. L. Margrave, *J. Inorg. Nucl. Chem.*, **16**, 29 (1960).

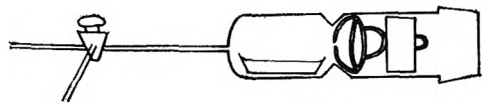
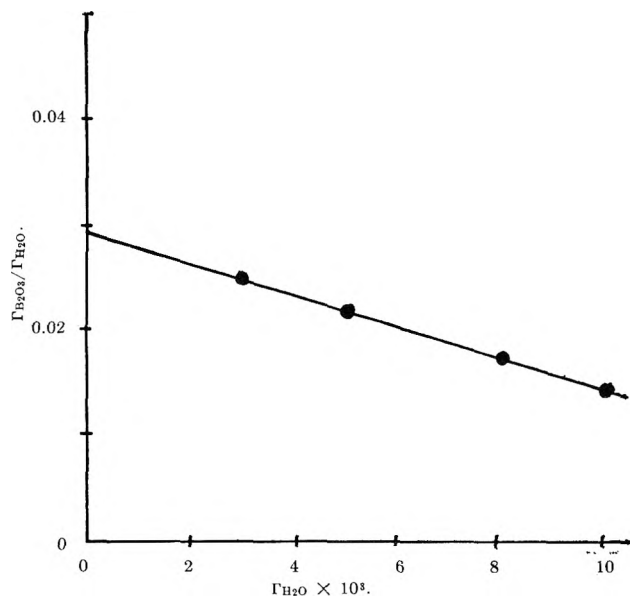
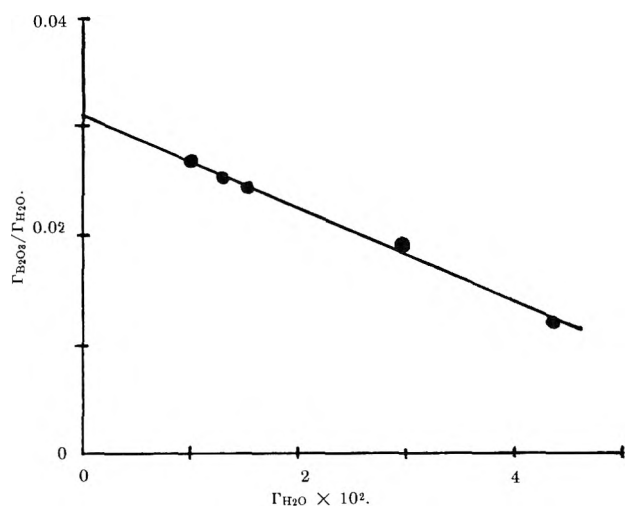
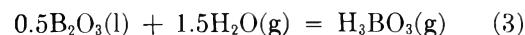
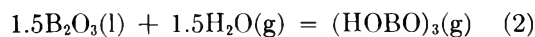
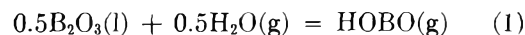


Figure 1. Schematic drawing of transpiration cell.

Figure 2. The effect of the rate of gaseous flow upon the extent of reaction; $P = 0.308$ atm.Figure 3. The effect of the rate of gaseous flow upon the extent of reaction; $P = 0.704$ atm.

as the quantity $(n - 2)$ where n is the number of datum points corresponding to a particular water vapor pressure.

In the analysis of our experimental data it was assumed that each of the following reactions occurs



On the basis of these three reactions it can be shown that the following equation describes the condition holding at equilibrium

$$\left(\frac{\Gamma_{B_2O_3}}{\Gamma_{H_2O}}\right)_{\omega=0} \sqrt{P_{H_2O}} = 0.5K_1 + (1.5K_2 + 0.5K_3)P_{H_2O} \quad (4)$$

where K_1 , K_2 , and K_3 are the equilibrium constants for reactions 1, 2, and 3, respectively. The data are shown plotted in the form prescribed by eq. 4 in Fig. 4.

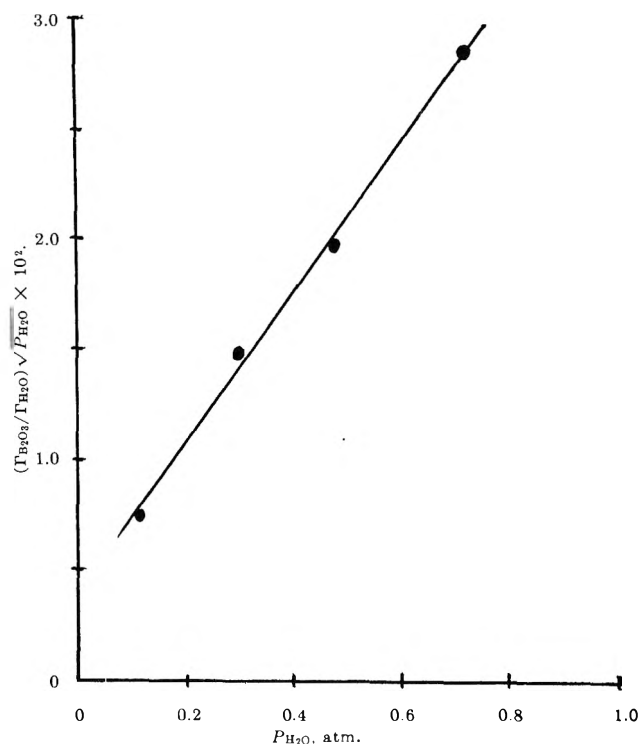


Figure 4. The data plotted in the manner prescribed by eq. 4.

The data were treated by the method of least squares and the resulting values of the slope and intercept are tabulated in Table II.

On the basis of a Students' t -test³ the value of the intercept does not differ significantly from zero; however, the value of the slope is highly significant and will allow further treatment. This indicates that within the pressure range considered in this study

(3) A. Hald, "Statistical Theory with Engineering Applications," John Wiley and Sons, Inc., New York, N. Y., 1957, p. 574.

Table II: Equilibrium Data

$0.5K_1$	t_1^a	$(1.5K_2 + 0.5K_3)$	t_2^b	f^c
0.0031 ± 0.0026	1.19(-)	0.0342 ± 0.0095	3.62(++)	7

^a Students' t-test for significance of intercept as compared to zero. ^b Students' t-test for significance of slope as compared to zero. ^c Degrees of statistical freedom $\left(\sum_{i=1}^4 f_i - 2\right)$.

the monomer, HOBO(g), is only a minor product in comparison to the trimer, (HOBO)₃(g).

Thermodynamic function is for H₃BO₃(g), H₂O(g), and B₂O₃(l) have been tabulated by the National Bureau of Standards.^{4,5} The entropy of (HOBO)₃(g) has been estimated by White, *et al.*⁶ On the basis of these tabulated functions the value of K_3 at 1147°K. is 0.0038 atm.^{-1/2}. On the basis of this value and the value of the slope of the line illustrated in Fig. 3, the value of K_2 is 0.0215 ± 0.0063 atm.^{-1/2}. Employing the entropy listed by White, *et al.*,⁶ the resulting heat of formation of (HOBO)₃(g) at 1147°K. is -544.8 ± 0.6 kcal./mole. Interpolations within the heat capacity data tabulated for (HOBO)₃(g) by White, *et al.*,⁶ leads to a value of -545.8 ± 2.0 kcal./mole for the heat of formation at 298°K. The uncertainty in this figure arises from the uncertainty in the heat capacity data.

(4) National Bureau of Standards (U. S.), Circular 500, U. S. Government Printing Office, Washington, D. C., 1952.

(5) National Bureau of Standards (U. S.), Report 7093, U. S. Government Printing Office, Washington, D. C., 1960.

(6) D. White, D. E. Mann, P. N. Walsh, and A. Sommer, *J. Chem. Phys.*, **32**, 488 (1960).

Appearance Potentials of the Difluoromethylene Positive Ion

by W. C. Steele

Department of Chemistry, Tufts University, Medford, Massachusetts
(Received February 24, 1964)

The continuing high level of interest in the chemistry of organic fluorine compounds has created a similar interest in the thermochemical properties of fluorocarbon radicals and ions. However, this area is characterized by a paucity of well established values. This is particularly true of the difluoromethylene posi-

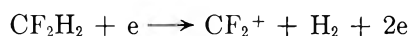
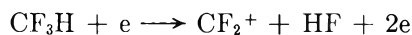
tive ion. Appearance potentials of CF₂⁺ from CF₃X, X = F, Cl, Br, and I, have been measured by Dibeler, Reese, and Mohler¹; and a separate set of these same measurements has been listed by Craggs and Massey,² who also included CF₂Cl₂. These two lists show considerable divergence and no consistent value for $\Delta H_f(\text{CF}_2^+)$ can be deduced from those few cases for which the necessary auxiliary data are available. A direct electron impact measurement of the ionization potential of the CF₂ radical has been reported by Reed and Snedden,³ who obtained a value of 13.3 e.v. We have now measured the appearance potential of CF₂⁺ from two new compounds, CF₃H and CF₂H₂. These measurements lead to a consistent value for $\Delta H_f(\text{CF}_2^+)$ and demonstrate that Reed and Snedden's value for $I(\text{CF}_2)$ is too high.

Appearance potentials were measured on a Consolidated Electrodynamics Corp. Model 21-103C mass spectrometer kindly made available by Harvard University. Ionization efficiency curves for the CF₂⁺ ions were not parallel to that of the calibration curve (argon) and the appearance potentials were obtained by conventional extrapolation of linear plots. Results are given in Table I.

Table I

Compound	$A_p(\text{CF}_2^+)$, e.v.	$\Delta H_f(\text{CF}_2^+)$, kcal. mole ⁻¹
CF ₃ H	14.7 ± 0.4	240 ± 10
CF ₂ H ₂	14.8 ± 0.4	234 ± 10

The heat of formation of the difluoromethylene positive ion has been calculated from the appearance potentials and known heats of formation of CF₃H,⁴ CF₂H₂,⁴ and HF,⁵ assuming the reactions



The resulting values (Table I) agree to well within experimental uncertainty. Added support may be found from the appearance potential data of Dibeler,

(1) V. H. Dibeler, R. M. Reese, and F. L. Mohler, *J. Res. Natl. Bur. Std.*, **57**, 113 (1956).

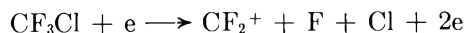
(2) J. D. Craggs and H. W. S. Massey in "Handbuch der Physik," S. Flügge, Ed., Vol. XXXVII/1, Springer-Verlag, Berlin, 1959, p. 314.

(3) R. I. Reed and W. Snedden, *Trans. Faraday Soc.*, **54**, 301 (1958).

(4) G. A. Neugebauer and J. L. Margrave, *J. Phys. Chem.*, **62**, 1043 (1958).

(5) H. M. Feder, W. N. Hubbard, S. S. Wise, and J. L. Margrave, *ibid.*, **67**, 1148 (1963).

Reese, and Mohler¹ for CF_2^+ from CF_4 and CF_3Cl , which, when combined with the required heats of formation⁶ and assuming the reactions



lead to values for $\Delta H_f(\text{CF}_2^+)$ of 249 and 245 kcal. mole⁻¹, respectively. In each of the four cases other reactions can be postulated, but these lead to widely divergent results. The above results show $\Delta H_f(\text{CF}_2^+) \leq 240 \pm 10$ kcal. mole⁻¹, which is an upper limit since excess energy may be present in all four dissociation processes.

Appearance potential studies of CF_2^+ from tetrafluoroethylene^{7,8} and the heat of formation of C_2F_4 ⁹ lead to the relation $\Delta H_f(\text{CF}_2^+) + \Delta H_f(\text{CF}_2) \leq 197$ kcal. mole⁻¹. Taken with the present result for $\Delta H_f(\text{CF}_2^+)$, this gives $\Delta H_f(\text{CF}_2) = -43$ kcal. mole⁻¹, which is within the established limits of -18 kcal. mole⁻¹^{10,11} and -45 kcal. mole⁻¹.¹² Furthermore, when taken with the lower limit for $\Delta H_f(\text{CF}_2)$, the present result allows calculation of an upper limit of 12.4 e.v. for $I(\text{CF}_2)$, which is well below the previous experimental value.³

(6) "Best values" from C. R. Patrick in "Advances in Fluorine Chemistry," Vol. II, M. Stacey, J. C. Tatlow, and A. G. Sharpe, Ed., Butterworth, Inc., Washington, D. C., 1961, p. 1.

(7) J. L. Margrave, *J. Chem. Phys.*, **31**, 1432 (1959).

(8) C. Lifshitz and F. A. Long, *J. Phys. Chem.*, **67**, 2463 (1963).

(9) G. A. Neugebauer and J. L. Margrave, *ibid.*, **60**, 1318 (1956).

(10) J. F. Reed and B. S. Rabinowitch, *ibid.*, **61**, 598 (1957).

(11) B. Atkinson, *J. Chem. Soc.*, 2684 (1952).

(12) B. A. Thrush and J. J. Zwolenik, *Trans. Faraday Soc.* **59**, 582 (1963).

Comparison of the Photo- and Radiation-Sensitized *cis-trans* Isomerizations of Polybutadiene

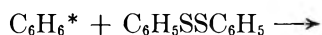
by Morton A. Golub

Stanford Research Institute, Menlo Park, California
(Received February 26, 1964)

Seely¹ has investigated the diphenyl disulfide sensitized *cis-trans* isomerization of polybutadiene in benzene and other solvents, using 3650-Å. light to photolyze the disulfide. He concluded that each thiyl radical thus formed isomerized about 370 polybutadiene double bonds. This number is very much lower

than that suggested for the isomerizing ability of the thiyl radical ($\sim 10^4$) produced in the analogous radiation chemical isomerization of polybutadiene.² Since the photo- and radiation-sensitized isomerizations are chain reactions with similar activation energies (3.67 and 2.3 kcal./mole, respectively) and with presumably the same type of free radical mechanism,^{1,2} there is no reason for the yields in these two cases to differ by so much. Actually, the number given in the radiation study² was only a rough estimate: it was based on assumptions made in the absence of definite information about energy transfer between benzene and diphenyl disulfide, or production of benzene triplet states. The purpose of this note is to re-examine the radiation yield with the aid of recent G values for excited benzene molecules,³⁻⁵ and to show that the thiyl radicals have, in fact, very similar isomerizing efficiencies whether produced by ultraviolet or by γ -rays. This finding is significant because it adds to the small but growing literature on detailed comparisons between photo- and radiation chemistry.⁶

From data on the radiation-induced *cis-trans* isomerization of 2-butene in benzene, Cundall and Griffiths^{3,4} concluded that $G(\text{C}_6\text{H}_6 \text{ triplet})$ was about 4.4. Moreover, 2-butene, at concentrations greater than 0.2 M , was considered to acquire virtually all of the excitation energy deposited in benzene. If our previous data on the diphenyl disulfide sensitized isomerization of polybutadiene² are replotted (see Fig. 1) in a form like that of Cundall and Griffiths (Fig. 1, ref. 4), we see an analogous approach to a limiting isomerization yield ($G_0 \sim 1400$ *cis* double bonds isomerized initially per 100 e.v. absorbed by the whole solution) at $[\text{C}_6\text{H}_5\text{SSC}_6\text{H}_5] > 0.14 M$. Consequently, the production of excited sensitizer molecules *via*



likewise can reach a saturation G value of about 4.4. Taking the energy deposited in the disulfide molecule to be 3.6 e.v. or 86 kcal./mole (corresponding to the lowest benzene triplet), which is somewhat greater than the energy imparted by 3650 Å. light (78 kcal./

(1) G. R. Seely, *J. Am. Chem. Soc.*, **84**, 4404 (1962).

(2) M. A. Golub, *ibid.*, **81**, 54 (1959).

(3) R. B. Cundall and P. A. Griffiths, *ibid.*, **85**, 1211 (1963).

(4) R. B. Cundall and P. A. Griffiths, *Discussions Faraday Soc.*, in press.

(5) W. Ando, K. Sugimoto, and S. Oae, *Bull. Chem. Soc. Japan*, **36**, 893 (1963).

(6) M. S. Matheson, *Proc. 2nd Intern. Conf. Peaceful Uses At. Energy, Geneva*, **29**, 385 (1958).

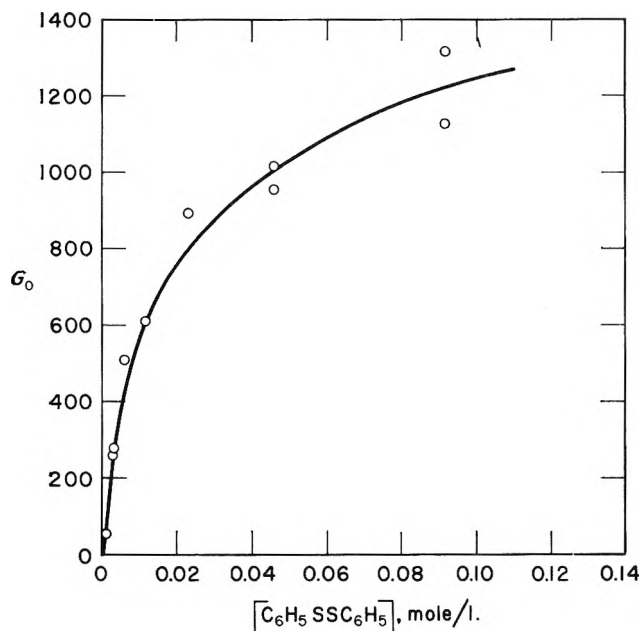


Figure 1. Dependence of the G value for isomerization of *cis*-polybutadiene (1% solution in benzene) on the sensitizer concentration.

mole), we may consider that $C_6H_5SSC_6H_5^*$ in (1) will dissociate with an efficiency which is at least as great as, and possibly even greater than, that obtained experimentally by Seely¹ for the diphenyl disulfide photolysis, *viz.*, 0.13. Accordingly, the limiting $G(C_6H_5S\cdot)$ is of the order of at least $4.4 \times 0.13 \times 2$ or 1.14, and may be closer to 1.40.⁷

An alternative route to this estimate stems from the work of Ando, Sugimoto, and Oae on the radiolysis of thiophenol in benzene in which they indicated a G value of 0.7 for the production of excited benzene molecules. Since this value was based on a kinetic approach where it was assumed that practically all of the benzene excitation energy is transferred to thiophenol, which then dissociates with an efficiency approaching unity, it would follow from their work that $G(-C_6H_5SH) = G(C_6H_5S\cdot) = 0.7$. Although these workers also studied the radiolysis of diphenyl disulfide in benzene, they did not provide sufficient data to permit a direct estimate of $G(C_6H_5S\cdot)$ for this reaction. However, by virtue of the close similarity of C_6H_5SH and $C_6H_5SSC_6H_5$, it is reasonable to consider that these compounds will radiolyze in benzene with comparable yields. Hence, $G(C_6H_5S\cdot)$ from $C_6H_5SSC_6H_5$ can be taken to be twice that from C_6H_5SH , or 1.4, which agrees very well with the value obtained from Cundall and Griffiths' work.

For a saturation $G(C_6H_5S\cdot)$ of ~ 1.1 – 1.4 , then, the limiting G_0 of around 1400 given above signifies that

~ 1000 – 1300 *cis* double bonds isomerize per thiyl radical (neglecting the minor contribution from direct radiolysis of the sensitizer). This chain length is of the same order of magnitude as that indicated by Seely, thus emphasizing the parallelism between the photo- and radiation-sensitized isomerization of polybutadiene in benzene; at the same time it represents a major revision of the previous crude estimate of 10^4 . If the chain length is largely independent of the sensitizer concentration at the dilutions considered, Fig. 1 provides a measure of the efficiency of energy transfer from $C_6H_6^*$ to $C_6H_5SSC_6H_5$, varying from about 5% at 0.001 *M* sensitizer to 90% at 0.1 *M*, and on up to 100% beyond 0.14 *M*.

Finally, it may be suggested that the number of double bonds isomerized per thiyl radical in Seely's work should be 750 instead of 370, which would bring the photo- and radiation-chemical values into even better agreement. The value of 750, corresponding to the ratio of rate constants for the isomerization and termination processes, and not one-half of it, should represent the chain length: although two $C_6H_5S\cdot$ radicals are formed in the initiation step, they both take part in isomerization and termination.

Acknowledgments. The author wishes to acknowledge helpful discussions with Drs. Theodore Mill and A. H. Samuel. This work was supported by Stanford Research Institute.

(7) It should be noted that Seely showed with the aid of a relation developed by R. M. Noyes, *Z. Elektrochem.*, **64**, 153 (1960), that the above dissociation efficiency of photoexcited diphenyl disulfide was quite reasonable obtaining a theoretical estimate of 0.10–0.15. An analogous calculation by the present author for the sensitized radiolysis of the disulfide yielded a value of 0.17.

The Effect of Pressure on the Benzylation of 1-Methyl-2-naphthoxide Ion

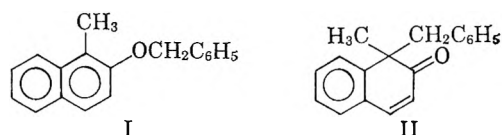
by W. J. le Noble

Department of Chemistry, State University of New York, Stony Brook, New York (Received February 26, 1964)

The effect of pressure on the product distribution in the reaction of phenoxide ion with allyl chloride was described in an earlier paper.¹ It was found that in protic solvents ring alkylation, particularly in the *para* position, was favored at high pressure. This

(1) W. J. le Noble, *J. Am. Chem. Soc.*, **85**, 1470 (1963).

fact was shown to be consistent with a suggestion made earlier² to the effect that the solvation sphere of an ambident anion might in certain cases have a decisive influence on its alkylation. In that system the hypothesis also suggests that the volumes of activation of these simultaneous reactions would not be so different in a solvent not particularly suited to solvate anions. On that score the evidence was inconclusive since allyl phenyl ether was the only detectable product in such solvents at any pressure. Clearly needed was information on the effect of pressure in an alkylation reaction in such a solvent in which both products are formed in easily measurable amounts. Kornblum and Derby³ had found that the reaction of benzyl bromide with lithium 1-methyl-2-naphthoxide in 1,2-dimethoxyethane gives substantial amounts of both benzyl-2-(1-methyl)naphthyl ether (I) and 1-benzyl-1-methyl-2-naphthalenone (II); this reaction is therefore well suited to illuminate that point.



Experimental

The preparation of 1-methyl-2-naphthol has been described.⁴ The 1,2-dimethoxyethane was dried by distillation from lithium aluminum hydride; a 0.1 *M* solution of the salt in this solvent was prepared from a solution of 2-methyl-1-naphthol and the equivalent amount of freshly pressed lithium ribbon. It was found that the salt was alkylated by benzyl bromide at 50.0° to the extent of 95% in 48 hr.; the benzylations of the salt in methanol (also 0.1 *M*) at 25.0° required about 24 hr. After neutralization of the residual base and removal of the solvent by flash evaporation, the residue could be chromatographed by elution of hexane-benzene and benzene-ether mixtures on alumina to give I, m.p. 65–70° (lit.³ m.p. 70–71°) and II, m.p. 57–61° (lit.³ m.p. 62–63). Infrared spectra were measured for the routine analysis of mixtures of these compounds; synthetic mixtures were prepared for comparison. In about half of the experiments the mixtures were also analyzed by the chromatographic technique described above. Both methods were found to be reliable to about 1%. The high pressure technique was described earlier.¹

Results

The difference in product distribution between the methanol and 1,2-dimethoxyethane reactions at 1 atm. is best explained as the result of more intense solvation in the former solvent and thus greater

shielding of the oxygen atom against the approach of the alkylating agent.² Since pressure facilitates the process of solvation, the carbon to oxygen (II/I) ratio in the alkylation reaction is expected to increase with pressure; this is indeed observed in methanol. On the other hand, 1,2-dimethoxyethane is not well suited for the solvation of anions, so that pressure should not affect the C/O ratio of the alkylation reaction very much in that solvent. The data in Table I bear out these expectations.

Table I: Product Distribution in the Reaction of Benzyl Bromide with Lithium 1-Methyl-2-naphthoxide

Solvent	Temp., °C.	<i>p</i> , kbar	% O, I	% C, II
1,2-Dimethoxyethane	50	0.00	79	21
1,2-Dimethoxyethane	50	1.24	80	20
1,2-Dimethoxyethane	50	2.47	80	20
1,2-Dimethoxyethane	50	3.79	78	22
1,2-Dimethoxyethane	50	4.84	78	22
1,2-Dimethoxyethane	50	6.72	78	22
1,2-Dimethoxyethane	50	8.41	80	20
Methanol	25	0.00	57	43
Methanol	25	1.41	52	48
Methanol	25	2.93	50	50
Methanol	25	4.17	49	51
Methanol	25	5.65	48	52

From the expression $(\partial \ln k/\partial p)_T = -\Delta V^*/RT$, one can readily show that at 1 atm. $V_{O^*} - V_{C^*} \approx 2-3$ ml./mole in methanol. In 1,2-dimethoxyethane, $V_{O^*} \approx V_{C^*}$; it had been anticipated, in fact, that the C/O ratio might show a small decrease in that solvent. Kornblum has shown that such ratios tend to decrease when various solvents of increasing dielectric constants are compared.⁵ Since the dielectric constants of liquids are pressure dependent, changes in the product distribution due to this effect are likely. However, the increase in *D* over the pressure range used in this work is so small (from 7 to 9, as estimated from the Owen-Brinkley equation⁶) that its effect is probably within the range of analytical uncertainty.

Acknowledgment. Support from the National Science Foundation for this work is gratefully acknowledged.

(2) N. Kornblum, P. J. Berrigan, and W. J. le Noble, *J. Am. Chem. Soc.*, **85**, 1141 (1963).

(3) N. Kornblum and R. Derby, unpublished results. The author is grateful to Professor Kornblum for making a number of experimental details available prior to publication.

(4) J. Cornforth, O. Kauder, J. E. Pike, and R. Robinson, *J. Chem. Soc.*, 3354 (1955).

(5) N. Kornblum, R. Seltzer, and P. Haberfield, *J. Am. Chem. Soc.*, **85**, 1148 (1963).

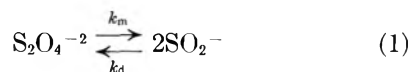
(6) B. B. Owen and S. R. Brinkley, Jr., *Phys. Rev.*, **64**, 32 (1943).

The Monomerization Rate of Dithionite Ion in Aqueous Solution

by S. Lynn, R. G. Rinker, and W. H. Corcoran

Chemical Engineering Laboratory, California Institute of Technology, Pasadena, California (Received February 26, 1964)

The presence of the SO_2^- radical ion in aqueous solutions of sodium dithionite has been previously reported.¹ Electron spin resonance (e.s.r.) measurements showed that the SO_2^- concentration varied as the square root of the dithionite concentration, suggesting a monomerization reaction of the form



This reaction has received significant polarographic study by Čermák² and chronopotentiometric studies by Fischer³ and co-workers. Based on experimental observation in a 0.1 *M* solution of sodium hydroxide, Čermák reported a value of 6×10^{-3} mole^{1/2} l.^{-1/2} sec.⁻¹ at 40° for the quantity k_m/\sqrt{K} where k_m is the rate constant for the monomerization as noted in eq. 1, and K is the equilibrium constant for the reverse of the reaction. The initial concentration of sodium dithionite in the studies by Čermák ranged from 3×10^{-4} to 3×10^{-3} *M*. Interpolation of Fischer's data for chronopotentiometric work in a buffered solution at a pH of 8.5 and for initial concentrations of dithionite of 0.92×10^{-3} and 4.94×10^{-3} *M* gives a value of 5×10^{-3} mole^{1/2} l.^{-1/2} sec.⁻¹ for k_m/\sqrt{K} at 40° which is in agreement with Čermák's data at the higher pH.

Only the ratio k_m/\sqrt{K} could be derived by Čermák and Fischer from their data. Evaluation of k_m then required determination of the value of K . That value was obtained at $25 \pm 2^\circ$ in e.s.r. studies in aqueous solution which was 0.1 *M* in sodium hydroxide and 5.0×10^{-3} *M* in the initial concentration of $\text{S}_2\text{O}_4^{-2}$ introduced as sodium dithionite. From the e.s.r. work in which a Cr^{+3} standard was used, a value of 1.8×10^{-6} *M* was established for the concentration of the radical ion SO_2^- to give a value of K of 1.6×10^9 mole⁻¹ l. Because Čermák's work was carried out under the same conditions of pH and concentration, his value for k_m/\sqrt{K} was used in the computation of k_m . Fischer's data were used as a guide in the extrapolation of Čermák's value to 25° by means of a plot of the logarithm of k_m/\sqrt{K} vs. $1/T$. The best estimate of k_m/\sqrt{K} at 25° using that procedure was 1×10^{-3}

mole^{1/2} l.^{-1/2} sec.⁻¹. A combination of that quantity with the measured value of K yields a value of 40 sec.⁻¹ for k_m at 25°, so that the monomerization reaction is moderately rapid.

Acknowledgment. Funds and facilities for the e.s.r. work were made available by the Dow Chemical Company while one of the authors, R. G. Rinker, was spending a year at their Western Division Laboratories. Their support is gratefully acknowledged.

(1) R. G. Rinker, T. P. Gordon, D. M. Mason, and W. H. Corcoran, *J. Phys. Chem.*, **63**, 302 (1959).

(2) V. Čermák, *Chem. Zvesti*, **8**, 714 (1954).

(3) O. Fischer, O. Dracka, and E. Fischerová, *Collection Czech. Chem. Commun.*, **25**, 323 (1960).

The Structure of Rhombohedral Sulfur

by J. Donohue and S. H. Goodman

Department of Chemistry, University of Southern California, Los Angeles, California (Received February 27, 1964)

In a paper recently received (in translation) in these laboratories, Soklakov¹ proposed, on the basis of X-ray powder patterns, that the rhombohedral polymorph of sulfur consists of spirally wound zigzag chains. This result is in sharp variance with previous work in which rhombohedral sulfur was shown to consist of discrete S_6 molecules.² We wish to point out that the structure proposed by Soklakov cannot be correct for the following reasons, any one of which, we feel, is sufficient to reject his proposed structure.

(1) Soklakov prepared his samples by annealing in the temperature range 80–100°. Rhombohedral sulfur, on the other hand, decomposes rapidly at these elevated temperatures; indeed, at room temperature, its conversion to a mixture of orthorhombic and plastic sulfur is virtually complete after 1.5 hr.^{3,4}

(2) Soklakov presents values for F_{meas} , as obtained from powder photographs, and for F_{calcd} , as obtained from the atomic coordinates of his proposed structure, and states that the average discrepancy, R , between the two is 19%. The value of R ,

(1) A. I. Soklakov, *Zh. Strukt. Khim.*, **3**, 559 (1962); *J. Struct. Chem.*, **3**, 538 (1963).

(2) J. Donohue, A. Caron, and E. Goldish, *J. Am. Chem. Soc.*, **83**, 3748 (1961); *Nature*, **182**, 518 (1958).

(3) C. Frondel and R. Whitfield, *Acta Cryst.*, **3**, 242 (1955).

(4) P. Bartlett, E. Cox, and R. Davis, *J. Am. Chem. Soc.*, **80**, 5064 (1958).

as calculated from his Table, is, in fact, 40%, a figure so high that it lends no confidence to the proposed structure.

(3) Soklakov states that rhombohedral sulfur is obtained by "crystallization from hot solutions of sulfur in benzene and toluene," perhaps in order to identify it with his own preparations which were made at 80–100°. Rhombohedral sulfur is in fact obtained from *ice-cold* solutions.^{5,6}

(4) Soklakov's preparations contain *ca.* 20 atomic % of arsenic. These can scarcely be termed "sulfur."

(5) It is not clear how Soklakov was able to arrive at values of F_{measd} for reflections with general values of (hkl) , since on powder photographs, as is well known, these are composed of two or more sets of nonequal F 's, and it is therefore impossible to calculate F 's from the observed composite intensities. It is equally unclear why Soklakov gave only one value for F_{calcd} for reflections of this type.

(6) Soklakov's observed powder pattern consists of 40 lines, 28 of which he attributed to rhombohedral sulfur on the basis of values of $\sin^2 \theta / \lambda^2$ calculated with the then available lattice constants³; his agreement between $(\sin^2 \theta / \lambda^2)_{\text{measd}}$ and $(\sin^2 \theta / \lambda^2)_{\text{calcd}}$ is not, however, outstanding, and, moreover, agreement just as good, if not better, is obtained when the observed values of Soklakov are compared with those observed for orthorhombic sulfur,⁷ and in view of the preparative methods mentioned by Soklakov it would not be surprising if his samples contained a large proportion of orthorhombic sulfur. (This seems as good a place as any to point out that while Soklakov attributed some of the lines in his pattern to monoclinic sulfur, the reference he gave to the powder pattern of that substance⁸ actually referred to orthorhombic sulfur, as will be seen from careful reading of the text of that reference, as opposed to merely reading its Table II.)

(7) Soklakov indexed his powder pattern by the use of the lattice constants obtained from single crystals,³ which are essentially the same as the lattice constants obtained in the later single crystal study.² The values of (hkl) assigned by Soklakov to his observed lines bear no resemblance to the indices of the reflections observed on the single crystal Weissenberg photographs (in particular, the space group extinction that $F = 0$ unless $h - k + l = 3n$, a condition suggested by the face development⁹ and observed in the single crystal study,² is consistently violated by the indices assigned by Soklakov). It must be concluded that the $\sin^2 \theta / \lambda^2$ agreement which Soklakov obtained is purely fortuitous.

(8) Soklakov's powder pattern bears no resemblance to one previously reported for rhombohedral sulfur.¹⁰

Soklakov dismisses that pattern and offers as an explanation for the difference between it and his own the possibility that the structure had broken down, and that the scattering of the breakdown products had been recorded by the authors of ref. 10. This "explanation" ignores the fact that the powder pattern of ref. 10 agrees in every respect with what is expected on the basis of other work on rhombohedral sulfur.²⁻⁶

We find it difficult to escape the conclusion that the evidence presented by Soklakov that rhombohedral sulfur consists of infinite chains should be disregarded.

Acknowledgment. This work was supported in part by a grant from the U. S. Army Research Office (Durham).

-
- (5) A. Aten, *Z. physik. Chem.*, **88**, 321 (1914).
 (6) E. Engel, *Compt. rend.*, **112**, 866 (1891).
 (7) H. E. Swanson, M. I. Cook, T. Isaacs, and E. H. Evans, National Bureau Standards (U. S.), Circular 539, Vol. 9, U. S. Government Printing Office, Washington, D. C., 1960, p. 54.
 (8) A. Pinkus, J. Kim, J. McAtee, and C. Concilio, *J. Am. Chem. Soc.*, **81**, 2652 (1959).
 (9) J. D. H. Donnay, *Acta Cryst.*, **8**, 245 (1955).
 (10) A. Caron and J. Donohue, *J. Phys. Chem.*, **64**, 1767 (1960).

The Photochemistry of α -Keto Acids and α -Keto Esters. III. Photolysis of Pyruvic Acid in the Vapor Phase

by George F. Vesley and Peter A. Leermakers

Hall Laboratory of Chemistry, Wesleyan University, Middletown, Connecticut (Received February 29, 1964)

Recent observations in these laboratories^{1,2} and an observation of an earlier worker³ concerning the photochemical behavior of pyruvic acid in solution have prompted us to investigate the vapor phase photochemistry of this simplest of the α -keto acids. In solution, the reaction path is highly dependent on the medium. In hydrogen-donating organic solvents photoreduction to dimethyltartaric acid predominates whereas in aqueous solution pyruvic acid is photodecarboxylated to yield acetoin (the head-to-head dimer of acetaldehyde) without any significant formation of acetaldehyde. Although being actively studied

-
- (1) P. A. Leermakers and G. F. Vesley, *J. Org. Chem.*, **28**, 1160 (1963).
 (2) P. A. Leermakers and G. F. Vesley, *J. Am. Chem. Soc.*, **85**, 3776 (1963).
 (3) W. Discherl, *Z. physiol. Chem.*, **219**, 177 (1933).

in these laboratories, the mechanism of the aqueous photodecarboxylation is not clear.

In the vapor phase, irradiation of pyruvic acid at 5 mm. pressure at a temperature of 80–85° with light of 3660 Å. leads to extremely efficient photodecomposition, quantum yield equal to 1.02 ± 0.06 and probably unity. Carbon dioxide is produced in quantitative yield, the other major product being acetaldehyde formed in 60–65% net yield. About 1–2% each of methane and carbon monoxide are also formed. Figure 1 shows the yields of carbon dioxide and acetaldehyde as a function of time from the photolysis of 0.723 mmole of pyruvic acid in the absence and presence of 50 mm. of nitrogen and oxygen. (Parallel experiments demonstrated that no dark reaction takes place after 2 hr. at the reaction temperature of 85°.)

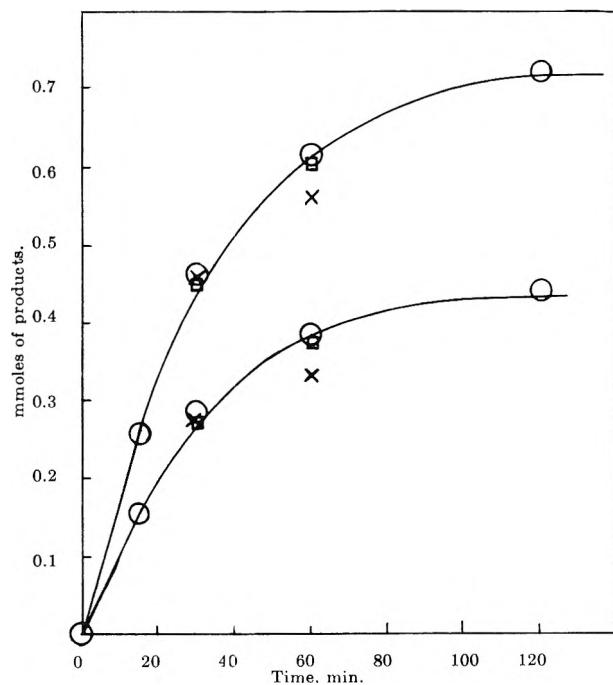
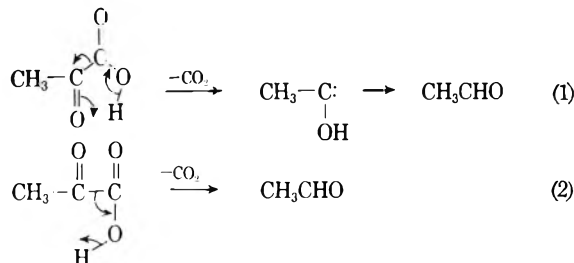


Figure 1. Variation of the yields of carbon dioxide and acetaldehyde from 0.723 mmole of pyruvic acid with time: O, no added gas; X, 50 mm. of N₂ added; □, 50 mm. of O₂ added.

From the data one sees that the ratio of acetaldehyde to carbon dioxide does not change with time, nor with the addition of added nitrogen and oxygen, and that the absolute yields (and hence quantum yields) are unaffected by the added gases. Fifty millimeters of ethylene is also ineffective at quenching the reaction. From the high yield of acetaldehyde and virtually insignificant yields of carbon monoxide and methane, and from the lack of an effect of 50 mm. of added oxygen,

we conclude that the primary photochemical process is a concerted decarboxylation from a cyclic transition state, and that acetaldehyde is *not* formed via a free radical path. We propose the following two possible mechanisms



Mechanism 1 is favored for the following reasons: (a) The configuration of the transition state is probably that of the ground state (for maximum hydrogen bonding), thus little rearrangement need take place in the excited state to get to the transition state. (b) The transition state is a five-membered rather than a four-membered ring. (c) Analogous to the Norrish type II process,⁴ hydrogen is initially becoming bonded to oxygen rather than to carbon. By analogy to photoreduction of $n-\pi^*$ states, initial bonding to oxygen is far more likely than to carbon. The initially formed divalent carbon intermediate would, of course, immediately rearrange to acetaldehyde at the pressure and temperature of the reaction.

As perhaps a side issue, the lack of an effect of oxygen also raises the question as to the nature of the excited state responsible for the photodecarboxylation. Calculations show that at 50 mm. pressure of oxygen the mean lifetime between collisions of pyruvic acid molecules with oxygen molecules is 2.5×10^{-9} sec. It has often been assumed that if pressures of oxygen as low as 10–15 mm. have no effect on a photochemical reaction (such as decomposition or isomerization of a ketone or conjugated olefin, etc.), then the triplet state is ruled out as the chemically active excited state. This may be quite valid in cases where chemical reaction is slow compared with collision lifetimes. However, the very high quantum efficiency of the pyruvic acid decomposition (unity) means that chemical reaction must be nearly two powers of ten faster than any de-excitation path. Thus, it is highly reasonable that the lifetime for chemical reaction could be in the order of 10^{-9} – 10^{-10} sec. after the chemically active excited state is reached. If this is the case, the lack of an effect of 15 or even 50 mm. of oxygen tells us nothing about the multiplicity of the reactive state.

(4) R. Norrish and M. Appleyard, *J. Chem. Soc.*, 874 (1934).

Porter claims evidence for the fact that intersystem crossing times for aromatic ketones such as benzophenone may be as short as 10^{-10} sec.⁵ This is substantially shorter than previous estimates in the order of 10^{-7} to 10^{-9} sec.⁶ Pyruvic acid undergoes exceedingly efficient intersystem crossing at 77°K. (the phosphorescence being even more intense than that of benzophenone²). Thus, if intersystem crossing time is comparable to benzophenone (and if the estimate cited by Porter is correct), intersystem crossing and subsequent decomposition of the triplet state of pyruvic acid could be occurring with combined lifetimes of less than 10^{-9} sec. Alternatively, decomposition could be taking place from an excited singlet faster than 10^{-10} sec.

Attempts were made to carry out runs at high oxygen pressures (500–700 mm.) where the presence or lack of an oxygen effect would be definitive (with respect to establishing the multiplicity), but the results were not conclusive due to the slow and incomplete vaporization of pyruvic acid.

Experimental

Materials. Pyruvic acid was Matheson Coleman and Bell, 99% reagent grade. It was distilled prior to use, b.p. 39–42° at 1 mm. Oxygen and nitrogen were Matheson high purity gases.

Determination of Products and the Effect of Added Gases. Irradiations were carried out in a 4-l. Pyrex vessel utilizing as a light source a Srinivasan–Griffin (Rayonet) type of reactor. The reactor is cylindrical in design with twelve 8-w. Westinghouse black lamps mounted around the interior surface. The radiation wave length was primarily 3660 Å. Photolyses were carried out on 50- μ l. samples of pyruvic acid at 80–85°, the elevated temperature being necessary to vaporize the keto acid. In the initial product runs pyruvic acid was placed in the reaction vessel and frozen out in a cold finger at the bottom of the vessel at Dry Ice temperatures. The vessel was then evacuated, sealed off, heated to volatilize the acid, and irradiated for 2 hr., and the products were subsequently frozen out at liquid nitrogen temperature. Infrared analysis of the condensed products (utilizing a 10-cm. path length gas infrared cell) indicated the presence of only carbon dioxide and acetaldehyde.

A similar sample of pyruvic acid was treated identically except that the irradiation was omitted. Analysis showed that no dark reaction ensued under the reaction conditions (85°, 2 hr.).

Quantitative analyses for the products were obtained by vapor chromatography. Pyruvic acid samples were frozen out, the vessel degassed, and the

system irradiated for varying periods of time (Fig. 1). Approximately 1 l. of helium was then injected into the system through a serum stopper, after which the gases were allowed to mix; 100-ml. samples were then withdrawn utilizing a Yale 100-ml. BD syringe with a blood stopcock between syringe and needle. The samples were injected into a dual column Aerograph gas chromatograph with Carbowax and silica gel columns in series. The latter column was placed between the two exit ports causing the gas stream to re-enter the instrument and pass through the reference part of the detector. In this way simultaneous analyses for both CO₂ and acetaldehyde were obtained. Runs in the presence of added gases were carried out identically except that after initial evacuation of the reaction vessel, the desired quantity of gas was bled in. In a separate experiment a 3.7-m. silica gel column was employed to obtain the yields of carbon monoxide and methane. In all cases authentic standards were injected to obtain absolute yields.

Quantum Yield Determination. The apparatus consisted of a standard optical bench, a PEK 500-w. high pressure mercury arc with appropriate power supply, columnating lens, and a Corning 7-39 filter to isolate primarily the 3660 Å. line. The amount of radiation absorbed by the pyruvic acid vapor was determined by an RCA 935 phototube in conjunction with a galvanometer. The reaction vessel was quartz, had a 30-cm. path length, and was wrapped with heating tape and asbestos to maintain elevated temperature (which was measured by a copper–constantan thermocouple). The light source was calibrated using uranyl oxalate actinometry.

Runs were carried out as follows: approximately 10 μ l. of pyruvic acid was vaporized in the reaction vessel, heated to 80°, and irradiated for 15 min. The vessel was attached to a vacuum system, and the gases were pumped off. Acetaldehyde was condensed out in a pentane–liquid nitrogen bath at –132°, and the other gases (mainly CO₂ with traces of CO and CH₄) were compressed in a sample cell by use of a mercury diffusion pump in series with a toepler pump.⁷ The gases were analyzed quantitatively by vapor chromatography with a 2-m. silica gel column.

Acknowledgment. This work has been supported by the Petroleum Research Fund of the American Chemical Society. Grateful acknowledgment is made to the donors of said fund.

(5) A. Beckett and G. Porter, *Trans. Faraday Soc.*, **59**, 2038 (1963).

(6) See, for instance, M. Kasha, *Radiation Res. Suppl.*, **2**, 253 (1960).

(7) The authors are indebted to Professor James N. Pitts for advice on the design of the gas analysis system.

The Rotatory Dispersion of Quartz¹

by Leonard I. Katzin

Chemistry Division, Argonne National Laboratory,
Argonne, Illinois (Received March 20, 1964)

Over a period of some years, Lowry and co-workers accumulated a body of data on the rotatory dispersion of quartz^{2,3} which, for precision and spectral span, is unmatched in the literature on this or any other substance. These data were fitted with an equation which described the degrees of rotation per mm. thickness of quartz, with wave length in microns

$$R_{\lambda} = 9.5639/(\lambda^2 - 0.0127493) - 2.3113/(\lambda^2 - 0.000974) - 0.1905 \quad (1)$$

The equation was first developed to fit the visible range but apparently agreed with observations over the whole wave length span to the order of thousandths of a degree. Actual rotation values varied from about 187° per mm. at 2327 Å. to 0.52° at above 3 μ.

Inasmuch as the full original data were available (thanks to the publishing policies of the day), it was considered useful to investigate whether with modern computer-based fitting methods^{4,5} it was really necessary to invoke a fifth parameter, and what the final parameters might show. A further goal of such an analysis would be to see how the parameters for optical activity dependent on crystal dissymmetry might relate to the parameters familiar from experience with asymmetric small molecules.

Procedure

At some point in the protracted course of Lowry and his co-workers' measurements on a 0.5-m. column of quartz, the sample was reground. On the basis of correspondence at selected points (the visible), the earlier data were corrected to match to the data obtained with the reground specimen. To avoid such questions as this procedure might raise, the analysis in this report is confined to the data obtained with the reground specimen directly. For the first paper,² this means some 250 points taken at from about 6707–2327 Å. All the infrared data of the Lowry and Snow report³ were obtained with the reground specimen.

Some errors in the computation of the original tabulation of results² were detected, generally because they gave bad errors in Lowry's results, and were corrected, thanks again to the data being available *in extenso*. No attempt was made, however, to correct or alter the wave length values given in Lowry's tables

to more modern values. The purpose of the investigation was to test the match to the data for which he had apparently already developed a good parametric fit, rather than to make the ultimate adjustment possible in the parameters. In the case of the rotations taken with the lines of the copper spectrum, Lowry preferred the wave length values of Huppers over those of Hasbach.² Our data fitting showed that the Huppers values actually gave poorer fits. We omitted the copper spectrum results completely in the final computations, to avoid this problem. The least-squares fitting program found to operate satisfactorily in earlier work^{4,5} was used, with the IBM 704 computer.

Results

With 250 points from 6707.846 to 2327.49 Å., and rotations from 16.535 to 187.247°, a two-term Drude equation can be fitted to the data with a root-mean-square deviation of ±0.017°, and no single deviation as high as 0.100°. However, there are unmistakable signs of systematic misfit to the data. Confining attention to the 150 points between 4820 and 3073 Å., these can be fitted by the equation

$$R_{\lambda} = 122.1035/(\lambda^2 - 0.00669422) - 114.9261/(\lambda^2 - 0.00599502) \quad (2)$$

to a root-mean-square deviation of ±0.0038°. Only one point deviates as much as 0.010°. A point-by-point comparison with the deviations from Lowry's equation indicates that, unrecognized by him, there existed a systematic preponderance of negative deviations (observed minus calculated) which our automated statistical fitting eliminates. This amounts to an approximately 0.004° shift, in the positive direction, of the individual deviations. The correspondence to these 150 points, by eq. 2, is as good as that using the five-parameter equation of Lowry and Coode-Adams.² Use of the eq. 2 parameters outside of the range of these points, however, predicts a rotation 0.065° too high at the 6707 Å. lithium line, and 0.925° too low at the 2327 Å. line. These are discrepancies of 0.39 and 0.5% respectively.

The 66 shortest wave length points, from 2327 to

(1) Based on work performed under the auspices of the U. S. Atomic Energy Commission.

(2) T. M. Lowry and W. R. C. Coode-Adams, *Phil. Trans., Roy. Soc. (London)*, **A226**, 391 (1927).

(3) T. M. Lowry and C. P. Snow, *Proc. Roy. Soc. (London)*, **A127**, 271 (1930).

(4) L. I. Katzin and E. Gulyas, *J. Phys. Chem.*, **66**, 494 (1962).

(5) L. I. Katzin and E. Gulyas, *J. Am. Chem. Soc.*, **86**, 1685 (1964).

2887 Å., with rotations 107–187°, are duplicated by the equation

$$R_\lambda = 134.4039/(\lambda^2 - 0.00931987) - 127.1814/(\lambda^2 - 0.00890141) \quad (3)$$

to a root-mean-square deviation of $\pm 0.006^\circ$. A group of 27 long wave length points from 6162 to 7741 Å. (data on the quartz *before* regrinding) fit the relation

$$R_\lambda = 374.7112/(\lambda^2 - 0.0022092) - 367.6544/(\lambda^2 - 0.00178683) \quad (4)$$

to $\pm 0.010^\circ$, which is about the experimental reliability claimed for these data.

It is easiest to compare and understand the implications of these relations if they are converted from the two-term Drude equation to the algebraically equivalent form^{4,5}

$$R_\lambda = [(A - B)\lambda^2 - (A\lambda_b^2 - B\lambda_a^2)]/(\lambda^4 - (\lambda_a^2 + \lambda_b^2)\lambda^2 + \lambda_a^2\lambda_b^2) \quad (5)$$

$$= [(A - B)(\lambda^2 - L) - C]/[(\lambda^2 - L)^2 - D]$$

where $L = (\lambda_a^2 + \lambda_b^2)/2$. The significant parameters,⁶ $(A - B)$ and L , for the several equations, are summarized in Table I, for easy comparison. The im-

Table I: Comparison of Principal Rotatory Dispersion Parameters

Spectral span	$(A - B)$	L
Full spectrum	7.1984	0.008351
6162-7741 Å.	7.0568	0.001998
3073-4820 Å.	7.1774	0.006345
2327-2887 Å.	7.2225	0.009111

portance of these parameters may be seen by considering that the dispersion curve for a two-term Drude relation is given approximately by the single Drude term, $(A - B)/(\lambda^2 - L)$, with the corrections to this representation given by the parameters C and D , as eq. 5 suggests. It is seen that there is a steady transition, with wave length, of the best parameters for a fit. Because of this, an attempt to match the full wave length span of the data with only four parameters results in the systematic mismatch already noted. The fact that the parameters of the shortest wave length section overestimate the rotation at the longer wave lengths, as do those of the central section also, necessitates consideration of an additional rotatory

contribution, with a negative sign, from a transition in the far-infrared. This is in fact the premise that Lowry had found necessary, though Drude had considered it negligible, and which was expressed as his fifth parameter. Our analysis has shown that it is not possible at all to represent the full quartz data accurately without such a term.

The infrared data of Lowry and Snow³ were combined with the Lowry and Coode-Adams² data to give 332 points ranging from 187.247° rotation at 2327.49 Å. to 0.520° at 32,100 Å. These were then analyzed according to the three-term Drude relation. A fit to a root-mean-square deviation of $\pm 0.00376^\circ$ is given by

$$R_\lambda = \frac{127.02476}{\lambda^2 - 0.009584310} - \frac{119.77145}{\lambda^2 - 0.009169645} + \frac{3.413 \times 10^4}{\lambda^2 - 1.8163 \times 10^6} \quad (6)$$

The actual significance of the last term is that, for data through 3–4 μ in wave length, it represents a constant, -0.1879 . This is because the critical wave length comes at some value sufficiently large that a λ^2 of 10 does not affect the value of the third term in (6) in the third decimal place (*i.e.*, to 0.001°). It can be seen that both parameters of this third term could be smaller by a factor of 10, or perhaps more, without altering the fit to 0.001° . Therefore, one may say that this term may represent an absorption somewhere in the region of 100 μ (100 cm.^{-1}), perhaps as low as 50 μ or as high as several hundred μ .

Discussion

The unique body of data on the optical rotatory dispersion of quartz, from 2327 Å. through 32,100 Å., left by Lowry and his co-workers, leaves no room for question that a Drude equation of three terms is required to describe the rotation. Because the data terminate at 3.2 μ , the parameters of the third (infrared) Drude term are known only as their ratio, leaving us an equation with five parameters. It may be pointed out that the two terms originating in the ultraviolet may, at 3 μ , be effectively represented, to 0.001° , by a single Drude term, $(A - B)/(\lambda^2 - L)$. Similarly, the term originating in the far-infrared may also be composed of two Drude terms. Data at much longer wave lengths would be required to make this resolution, and it would be highly desirable that such measurements be made.

The five parameters in Lowry's equation (eq. 1)

(6) Hereafter the parameters of eq. 5 will be called *polynomial* parameters, to distinguish them from the parameters of the Drude equation as normally written.

bear little direct resemblance to those in eq. 6, other than the values for the infrared term (-0.1905 and -0.1879 , respectively). Taking the ultraviolet terms in the polynomial form, however, (6) becomes

$$R_{\lambda} = \frac{7.2533\lambda^2 - 0.016845}{\lambda^4 - 0.018754\lambda^2 + 8.789 \times 10^{-5}} - 0.1879$$

and the Lowry equation (eq. 1) becomes

$$R_{\lambda} = \frac{7.2526\lambda^2 - 0.02015}{\lambda^4 - 0.013723\lambda^2 + 1.2418 \times 10^{-5}} - 0.1905$$

The resemblance is now more obvious. Allowing the computer to do a statistical refinement of the Lowry parameters, one obtains

$$\begin{aligned} R_{\lambda} &= \frac{9.70561}{\lambda^2 - 0.01265253} - \frac{2.45515}{\lambda^2 - 0.001178552} - 0.1871 \\ &= \frac{7.25046\lambda^2 + 0.0196254}{\lambda^4 - 0.0138311\lambda^2 + 1.4911 \times 10^{-5}} - 0.1871 \end{aligned} \quad (7)$$

The root-mean-square deviations between experimental values and this equation is $\pm 0.0036^{\circ}$ as against $\pm 0.00376^{\circ}$ for eq. 6. However, the latter showed 105 points fitting to better than $\pm 0.001^{\circ}$ and another 79 to better than $\pm 0.002^{\circ}$, whereas the refined Lowry parameters gave only 91 points better than $\pm 0.001^{\circ}$ and 83 more better than $\pm 0.002^{\circ}$. The improved root-mean-square deviation was obtained with poorer distribution of the errors because the worst accidental deviation in the former comparison, 0.016° , was thereby decreased somewhat, thus diminishing its large influence on the root-mean-square deviation.

We therefore believe that our eq. 6 gives a better match to the data than Lowry's equation, and that the wave lengths indicated give more realistic absorption wave length indication than that which would be deduced from Lowry's λ_2^2 value of 0.000974.

It is unmistakable that the optical rotatory dispersion of quartz is accurately described by a three-term Drude relation (with the possibility that the infrared term is composed of more than one component). The apparent origin of the infrared term, in the neighborhood of 50–200/ μ , is that of the quartz vibrational frequencies of 127, 207, 266, 357, and 370 cm^{-1} , which Kats⁷ has attributed to distortion vibrations. This is a reasonable relationship since the structural dissymmetry on which the optical rotation of quartz rests involves the fixed helical arrangement of oxygen atoms in the lattice, and it might be expected that distortion

of this arrangement should have repercussions in the optical rotation.

Gutowsky⁸ has published measurements purporting to show a rotational anomaly in the infrared, starting abruptly at wave lengths just longer than the longest of the Lowry and Snow data. In the region of overlap, there is concordance of results. It is very difficult to conceive of an anomaly that does not follow the usual dispersive relations and that thereby fails to register its presence in the data at 3.2 μ . The author is therefore very strongly inclined to West's interpretation⁹ of Gutowsky's results. This is another reason, however, for further investigation in the infrared region.

Data have been published on the far-ultraviolet rotatory dispersion of quartz, at wave lengths shorter than the Lowry and Coode-Adams results, by Duclaux and Jeantet¹⁰ and by Servant.¹¹ The precision of these data is considerably less than the former,² and comparison is thereby made uncertain. The parameters of eq. 6 predict rotations within 1° of those of Servant down to 1700 \AA . The deviations from about 1900 \AA . show a systematic bias, the computed values being greater than the reported. This may in part be remediable by tinkering with the parameters, and conceivably could also be in part in the measurements. The increasing deviations below 1700 \AA . could in largest part reflect entry into a region where deviation from the Drude relation, due to approach to the Cotton effect region, is dominant.

A summary of formulas which have been proposed by earlier workers to describe the rotatory dispersion of quartz has been given by Chandrasekhar¹² and need not be repeated here. They may be summarized as either having more parameters than the five that eq. 6 and the Lowry equation possess, or being obviously unable to fit the data satisfactorily through the whole range. One possible exception is an equation advocated strongly by Chandrasekhar himself and which is related to an earlier one by Lommel¹³

$$R = k\lambda^2/(\lambda^2 - \lambda_0^2)^2$$

Chandrasekhar gives the values $k = 7.19$ and $\lambda_0^2 = 0.00858$. The equation merits attention because it has only two parameters and because the author

(7) A. Kats, Thesis, University of Delft, Netherlands, 1961.

(8) H. S. Gutowsky, *J. Chem. Phys.*, **19**, 438 (1951).

(9) C. D. West, *ibid.*, **22**, 749 (1954).

(10) J. Duclaux and P. Jeantet, *J. phys.*, **7**, 200 (1926).

(11) R. Servant, *Ann. phys. (Paris)*, **12**, 397 (1939).

(12) S. Chandrasekhar, *Proc. Roy. Soc. (London)*, **A259**, 531 (1961).

(13) E. Lommel, *Ann. Phys. u. Chem.*, **20**, 578 (1883).

maintains that it shows "that terms of the Drude type do not contribute in any observable measures to the rotatory power in the visible and ultra-violet region of the spectrum."

It will be first noted that Chandrasekhar's parameters are very close to those in the first line of Table I, for $(A - B)$ and L , respectively. The reason for this correspondence is seen with the help of eq. 5. If one makes first the approximation $\lambda_a^2 = L = \lambda_b^2$, the denominator becomes $(\lambda^2 - L)^2$. If one then makes the further approximation that $(A\lambda_b^2 - B\lambda_a^2)$ in the numerator is zero, one is left with $(A - B)\lambda^2/(\lambda^2 - L)^2$, which is identically Chandrasekhar's expression. Therefore, contrary to his statement quoted above, he is in fact using the Drude relation, but in a doubly-approximate form.

The utility of the expression itself was tested by taking 96 of the shortest wave length points of the Lowry and Coode-Adams data, from 2327 to about 3570 Å., correcting for the infrared contribution, and doing a least-squares fitting to the Lommel-Chandrasekhar equation. The optimum parameters obtained were 7.2277 and 0.084597. There was an obvious systematic lack of fit to the data and the root-mean-square deviation approached 0.023° . Only 23 of the 96 points showed deviations as small as 0.010° , which is almost the worst deviation with the full Drude expression. The approximations are therefore not good enough to justify using the two-parameter form instead of the full expression.

Chandrasekhar¹² has placed considerable stress on Kuhn's summation rule¹⁴ as a criterion which equations have to meet to be considered valid. Kuhn himself has pointed out that one cannot place much emphasis on this because of the role of potential contributions outside the range of measurement. One can make this more explicit by pointing out that a Drude term at about 100μ with a numerator parameter equal and opposite in sign to that of the quartz ultraviolet $(A - B)$ would make a rotatory contribution of less than 0.001° in the region of measurement. One does not know what combination of terms goes into the infrared parameter, -0.1879° .

In summary, the rotatory dispersion of quartz is apparently exactly matched by a Drude equation. For the excellent data available from 0.23 to 3.2μ , a match to $\pm 0.0037^\circ$ per mm., root-mean-square deviation, is given by eq. 6 above. The infrared contribution summarized in the parameter -0.1879 is real.

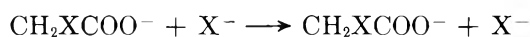
(14) W. Kuhn, *Z. physik. Chem.*, **B4**, 14 (1929).

The Kinetics of Bromine Exchange between Bromide and Bromoacetate Ions

by F. J. Johnston

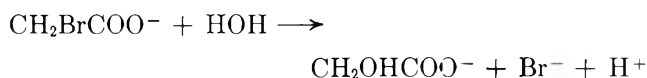
Department of Chemistry, University of Georgia, Athens, Georgia
(Received December 23, 1963)

Kinetics of the exchange reactions



for the chloroacetate-chloride¹ and iodoacetate-iodide^{2,3} systems have been previously described. The corresponding exchanges in the chloro-,⁴ bromo-,⁵ and iodoacetic^{2,5} acid systems have also been studied.

This report describes the kinetics of bromine exchange between bromide and bromoacetate ions at 0.100 ionic strength and compares the results for the different systems. Reaction rates for exchange in this system have been measured from 26.6 to 70.0° . The hydrolysis reaction



occurs simultaneously with the exchange reaction and for this reason experiments were carried out in the presence of sodium acetate to minimize the formation of molecular acid. The extent of the hydrolysis reaction during a given exchange series was small, corresponding always to less than 12% decomposition of the bromoacetate.

For a system in which exchange occurs and in which one of the exchanging species is being produced at the expense of the other, the fractional exchange as a function of time is given by^{1,4,6}

$$d[\ln(1 - F)]/dt = R(t)(a + b)/[a + p(t)] - [b - p(t)] \quad (1)$$

F is the fraction of equilibrium exchange at time t , a and b are initial concentrations of exchanging species, $p(t)$ is the extent of chemical change in the system, and $R(t)$ is the exchange rate at time t . For a process first order

(1) F. J. Johnston, *J. Phys. Chem.*, **66**, 1719 (1962).

(2) H. van der Stratten and A. H. Aten, *J. Am. Chem. Soc.*, **76**, 3798 (1954).

(3) R. C. Bond, M.S. Thesis, University of Georgia, 1963.

(4) R. A. Kenney and F. J. Johnston, *J. Phys. Chem.*, **63**, 1462 (1959).

(5) J. F. Hinton and F. J. Johnson, *ibid.*, **67**, 2557 (1963).

(6) C. P. Luehr, G. E. Challenger, and B. J. Masters, *J. Am. Chem. Soc.*, **78**, 1314 (1956).

Table I: Summary of Rate Constants for the Bromide-Bromoacetate Exchange Reaction at 0.10 Ionic Strength

Temp., °K.	(CH ₂ Br- COO ⁻) ₀ , M	(Br ⁻) ₀ , M	(CH ₂ - COO ⁻) ₀ , M	k _x , l. mole ⁻¹ sec. ⁻¹
343.1	0.0695	0.0205	0.0100	1.11 × 10 ⁻³
	0.0800	0.0103	0.0100	1.14
	Av. 1.12 × 10 ⁻³			
333.6	0.0101	0.0050	0.0850	0.483
	0.0400	0.0402	0.0200	0.475
	0.0501	0.0305	0.0200	0.475
	0.0500	0.0252	0.0250	0.491
	0.0700	0.0205	0.0100	0.489
	0.0800	0.0104	0.0100	0.483
Av. 0.483 × 10 ⁻³				
323.4	0.0350	0.0036	0.0600	0.179
	0.0500	0.0393	0.0100	0.177
	0.0650	0.0155	0.0200	0.178
	0.0750	0.0152	0.0100	0.189
Av. 0.180 × 10 ⁻³				
311.9	0.0445	0.0442	0.0100	0.594 × 10 ⁻⁴
	0.0497	0.0399	0.0100	0.572
	0.0700	0.0200	0.0100	0.572
	0.0750	0.0200	0.0062	0.602
	0.0800	0.0102	0.0100	0.602
Av. 0.589 × 10 ⁻⁴				
299.8	0.0552	0.0555	...	0.152
	0.0756	0.0256	...	0.148
Av. 0.150 × 10 ⁻⁴				

Experimental

Sodium bromoacetate was prepared by titration of Eastman White Label bromoacetic acid. Reagent sodium bromide solutions were labeled with potassium bromide-82 as obtained from Oak Ridge Isotope Sales Department. The sodium acetate added as buffer was reagent grade.

Reactions were carried out under conditions of temperature variations of less than ±0.05°. Titration with silver nitrate served to follow concentration changes in the system and to separate the reactants. Aliquots of the bromoacetate fractions were counted in a scintillation detector system and the fraction of equilibrium exchange evaluated from

$$F(t) = \frac{(\text{specific activity of CH}_2\text{BrCOO}^-)_t}{(\text{specific activity of total Br}^-)_{t=\infty}}$$

Counting rates were in every case high enough to allow a comparison of a reacted sample with a stock sample within a time sufficiently short that decay corrections for the 35-hr. bromine were unnecessary. Standard deviations of the net counting rates were less than 1%. Separation induced and background exchange were negligible.

Results and Discussion

Bromine Exchange. Rate constants for exchange, k_x , were calculated according to eq. 2. A summary of the results is given in Table I. The exchange reaction was satisfactorily described by a second-order rate law

Table II: Comparison of Exchange Parameters for the Haloacetate and Haloacetic Acid Systems

	System	ΔH^* , cal. mole ⁻¹ ^a	ΔS^* , cal. mole ⁻¹ deg. ⁻¹ ^a	k_x , l. mole ⁻¹ sec. ⁻¹ ^b
1	CH ₂ ClCOOH-Cl ^{-c}	23,700 ± 350	-10.9 ± 1.1	1.1 × 10 ⁻⁷
2	CH ₂ BrCOOH-Br ^{-d}	18,980 ± 100	-13.4 ± 0.2	0.92 × 10 ⁻⁴
3	CH ₂ ICOOH-I ^{-d,e}	15,980 ± 380 ^d 15,350 ^e	-14.6 ± 1.3 -17	0.78 × 10 ⁻²
4	CH ₂ ClCOO ⁻ -Cl ^{-f}	26,080 ± 300	-7.8 ± 0.9	0.96 × 10 ⁻⁸
5	CH ₂ BrCOO ⁻ -Br ⁻	19,700 ± 130	-16.6 ± 0.4	0.54 × 10 ⁻⁶
6	CH ₂ ICO ⁻ -I ^{-g,h}	15,940 ± 380 ^g 15,350 ^h	-19.3 ± 1.2 -20	0.79 × 10 ⁻³

^a Obtained by a least-squares computer programming of $k_x = kT/h \exp[\Delta S^*/R] \exp[-\Delta H^*/RT]$. The variations listed are standard deviations. The data for systems 1 and 4 were re-evaluated in this fashion. Where deviations are not given, sufficient data were not available to allow such a treatment. ^b Calculated for 298°K. ^c Ref. 4. ^d Ref. 5. ^e Ref. 2. ^f Ref. 1. ^g Ref. 3. The available data for this system are for 0.05 ionic strength.

with respect to each of the exchanging species, eq. 1 becomes

$$\ln(1 - F) = k_x(a + b)t \quad (2)$$

at all concentrations and temperatures studied. The parameters in the expression $k_x = kT/h \exp[\Delta S^*/R] \exp[-\Delta H^*/RT]$ were determined by a least-squares computer program for the data at an ionic strength of

0.100. It was found that $\Delta H^* = 19,700 \pm 130$ cal. mole⁻¹; the corresponding entropy of activation is $\Delta S^* = -16.6 \pm 0.4$ cal. mole⁻¹ deg.⁻¹. The variations listed are standard deviations obtained from the same program.

Comparison of the Different Systems. In Table II are summarized exchange constants for the haloacetic acid-halide and haloacetate-halide systems that have been studied. An essentially linear dependence of the exchange activation enthalpy upon bond strength in the haloacetic acid series has been previously noted.⁵ The difference in the exchange enthalpies for the chloroacetic acid and chloroacetate systems has been interpreted as due to electrostatic effects.¹ (The difference, approximately 2.4 kcal. mole⁻¹, is equivalent to the work done in bringing together two unit charges in water at 80° to a distance of 2 Å. apart.) For the bromide systems, however, the difference is 0.72 kcal. mole⁻¹ and for the iodide systems the enthalpies of activation are experimentally indistinguishable. These results suggest that electrostatic effects are less important in affecting the formation of the transition state than, for example, the relative degrees of hydration or polarizabilities of the haloacetic acid and haloacetate molecules.

Entropies of activation for exchange in the ionic series and in the acid series are in a direction consistent with steric hindrance of the replacement. The reason for the apparently significantly greater negative activation entropy for exchange of chloride with chloroacetic acid than with chloroacetate ion is not obvious.

Acknowledgments. Appreciation is expressed to Mr. James Fortson of the computer center for least-squares programming and analyses and to Michael Johnston for assistance with bromine-82 counting. This work was supported by A.E.C. Contract AT(40-1) 2826.

Association between Silver and Chloride Ions in Aqueous Solution

by M. J. Insley, G. D. Parfitt, and A. L. Smith

Chemistry Department, University of Nottingham, University Park, Nottingham, England (Received February 17, 1964)

In the course of a conductometric study of the precipitation of silver chloride from aqueous solution, which involved generating chloride ions homogeneously in the presence of silver nitrate, it was necessary to calcu-

late the concentrations of silver and chloride ions at any time and for this a knowledge of the formation constants of the various associated species present was required. Existing solubility data¹ seem to show that ion association is significant, with the formation constant for the uncharged species (AgCl) between 1000² and 2000³ and appreciable amounts of higher (mononuclear) complexes present in solutions containing a large excess of silver or chloride ions. In view of the doubt cast on the experimental procedure of some solubility determinations¹ and the rather surprising result that silver chloride cannot be considered as a strong electrolyte in aqueous solution, it was considered desirable to verify that the reported formation constants were consistent with conductance measurements.

The usual method by which conductance data over a range of concentration are analyzed by means, of *e.g.*, the Fuoss equation⁴ is not readily applicable to an electrolyte as sparingly soluble as silver chloride so that an alternative technique was used which, although not of great precision and unsuitable for detailed investigation of the higher complexes, is sufficiently sensitive to detect association of the order of that reported. This involves the homogeneous generation of chloride ions in an aqueous solution of silver nitrate by the hydrolysis of allyl chloride. The hydrolysis is sufficiently slow, at suitable concentrations, that an appreciable time elapses before precipitation of silver chloride occurs. During this time the rate of increase of conductance with time does not depart detectably from linearity if the carbonic acid dissociation is suppressed by keeping the pH to ~5. Association of Ag⁺ and Cl⁻ to form a nonconducting species will diminish the rate of increase of conductance relative to that in a control solution identical in every respect except that silver nitrate is replaced by potassium nitrate. Association in the latter, as measured conductometrically, is known to be small.

Experimental

Materials. The silver nitrate was Johnson, Matthey, and Co. Ltd. "Specpure" and the potassium nitrate was A.R. grade. The allyl chloride (British Drug Houses "Laboratory Reagent") was dried over calcium sulfate and then fractionated, with liberal rejection of the first and last portions, into brown stoppered bottles containing anhydrous calcium sulfate. Just prior to

(1) E. Berne and I. Leden, *Svensk Kem. Tidskr.*, **65**, 88 (1953).

(2) I. Leden, *ibid.*, **64**, 249 (1952).

(3) J. H. Jonte and D. S. Martin, *J. Am. Chem. Soc.*, **74**, 2052 (1952).

(4) R. M. Fuoss, *ibid.*, **81**, 2659 (1959).

use the allyl chloride was redistilled and the fraction boiling at 44° collected.

Ordinary distilled water was passed through a Biode-minrolite mixed bed ion-exchange column and then distilled twice from all-Pyrex stills. The final conductance, after equilibration with air, did not exceed 1.1×10^{-6} ohm⁻¹ cm.⁻¹.

Conductance Measurements. Conductance measurements were made at 25° using a thermostat filled with heavy liquid paraffin. The temperature was set by a resistance thermometer and the total variation was less than 0.005°.

Resistances were measured on a conventional shielded bridge operating at 1000 c.p.s. and equipped with a Wagner earth device. The detector was an oscilloscope preceded by a multistage amplifier and the balance point could be detected with a sensitivity of 0.001% at 10,000 ohms. The bridge was calibrated using Sullivan nonreactive resistances.

The cell, designed to conform with the requirements of Jones and Bollinger⁵ to avoid the Parker effect, was of Pyrex glass with bright platinum disk electrodes.

Procedure. Solutions of allyl chloride in water (approximately 10^{-4} mole l.⁻¹) were prepared by injecting an appropriate amount of the reagent from an Agla micrometer syringe into a large volume of conductance water with vigorous magnetic stirring. To equal volumes of such an allyl chloride solution equal volumes of equivalent solutions of silver and potassium nitrates were added to form a pair of solutions of as near as possible identical concentration, both in allyl chloride and salt. The volatility and sparing solubility of allyl chloride in water make this condition difficult to obtain by any other method. Resistance measurements were taken at 5-min. intervals, first on the solution containing silver nitrate so that at least 1 hr. elapsed after temperature equilibrium had been established before precipitation of silver chloride occurred, and then, after cleaning the cell, on the solution containing potassium nitrate.

Control experiments in which potassium nitrate was used in both solutions showed no detectable deviation from linearity of the increase of conductance with time over periods much longer than those used in the main part of the work, and no significant difference between the two solutions was observed.

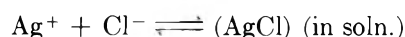
Analysis of Data

Because of the observed linearity of the conductance-time plots the concentration of hydrogen and chloride ions produced by the allyl chloride hydrolysis at time t may be written as $k't$ and their contributions (with no ion pairing) to the conductance κ as $kt\lambda_{H^+}$ and $kt\lambda_{Cl^-}$,

respectively ($k = k'/1000$). If ion-pair formation in solutions containing potassium nitrate is ignored and the ion conductances (λ) are taken as their values at infinite dilution (λ_0), then the slope S_1 of the conductance-time plot is given by

$$S_1 = d\kappa/dt = k\lambda_{\text{HCl}}^{\circ} \quad (1)$$

If ion pairing is assumed to occur between Ag⁺ and Cl⁻ in solutions containing silver nitrate then



and

$$K_A = [\text{AgCl}]/[\text{Ag}^+][\text{Cl}^-]f_{\pm}^2 = [\text{AgCl}]/c[\text{Cl}^-]f_{\pm}^2$$

where f_{\pm} is the mean ionic activity coefficient of Ag⁺ and Cl⁻, and c is the concentration of silver nitrate, being in great excess compared with that of the chloride ion and assumed constant over the course of an experiment. The activity coefficient of the uncharged species (AgCl) is taken as unity.

Thus, at time t

$$[\text{H}^+] = k't$$

$$[\text{AgCl}] - [\text{Cl}^-] = k't$$

$$[\text{AgCl}] = k'tK_Acf_{\pm}^2/(1 + K_Acf_{\pm}^2)$$

$$[\text{Cl}^-] = k't/(1 + K_Acf_{\pm}^2)$$

$$[\text{Ag}^+] = c - [\text{AgCl}]$$

giving the slope S_2 of the conductance-time plot as

$$S_2 = \frac{d\kappa}{dt} = k\lambda_{\text{H}^+} + \frac{k\lambda_{\text{Cl}^-}}{1 + K_Acf_{\pm}^2} - \frac{kK_Acf_{\pm}^2\lambda_{\text{Ag}^+}}{1 + K_Acf_{\pm}^2} \quad (2)$$

If $K_Acf_{\pm}^2 \ll 1$ this reduces to

$$S_2 = d\kappa/dt = k\lambda_{\text{HCl}} - kK_Acf_{\pm}^2\lambda_{\text{AgCl}} \quad (3)$$

A convenient parameter in terms of which the experimental results may be discussed is $(S_1 - S_2)/S_1c$ which the approximation (eq. 3) gives as $\lambda_{\text{AgCl}}K_Af_{\pm}^2/\lambda_{\text{HCl}}$. Assuming a value of $K_A = 1000$, $c = 1.4 \times 10^{-4} M$, $f_{\pm}^2 = 0.973$ (Debye-Hückel limiting law), and taking the equivalent conductances as at infinite dilution, $(S_1 - S_2)/S_1c$ becomes 278 mole⁻¹ l. from eq. 1 and 2 or 316 mole⁻¹ l. from the approximate expression. The precision of the method is such as to allow a difference between such values and zero, which corresponds to no association, to be readily detected.

Results and Discussion

The values of $(S_1 - S_2)/S_1c$ from Table I have a mean of -16 with a standard deviation of 88. It is evident

(5) G. Jones and G. M. Bollinger, *J. Am. Chem. Soc.*, **53**, 411 (1931).

Table I

[AgNO ₃] c, mole l. ⁻¹ × 10 ⁴	Slope S ₁ , ohm ⁻¹ cm. ⁻¹ min. ⁻¹ × 10 ⁸	Slope S ₂ , ohm ⁻¹ cm. ⁻¹ min. ⁻¹ × 10 ⁸	(S ₁ - S ₂)/ S _{1c}
1.40	1.160	1.188	-172
1.40	1.124	1.118	+38
1.40	1.078	1.080	-13
1.40	1.167	1.163	+26
1.40	1.120	1.127	-48
1.40	1.130	1.137	-47
1.40	1.144	1.145	-4
1.40	1.053	1.070	-119
1.40	1.095	1.093	+11
2.14	0.0574	0.0553	+171
2.14	0.0522	0.0524	-18

that the mean does not differ significantly from zero and the "t" test shows that the mean of $(S_1 - S_2)/S_{1c}$ at the 95% significance level lies in the range -16 ± 59 and at the 99% significance level, at -16 ± 84 . Since negative values of K_A are not possible this can be interpreted, using the approximate expression, as $K_A < 140$ at the 95% significance level and $K_A < 220$ at the 99% significance level.

These values of K_A may be compared with those found by the solubility method, $K_A = 2000$ by Jonte and Martin³ and $K_A = 1100$ as the "most probable value" quoted by Berne and Leden.¹

In the above analysis two factors have been ignored which could influence the apparent value of K_A . These are (a) higher association and (b) catalysis of the allyl chloride hydrolysis by silver nitrate. The justification for ignoring higher association (to, *e.g.*, $(Ag_2Cl)^+$) is twofold in that solubility data¹ suggest it to be negligible under the conditions obtaining in this work and, moreover, the formation of $(Ag_2Cl)^+$ from single ions would reduce the conductance to much the same extent as AgCl. It is possible that catalysis by silver nitrate has reduced the apparent value of K_A to around zero. Higher silver nitrate concentrations than those used in these experiments would then make the apparent value of K_A negative but this is difficult to test since precipitation of silver chloride would intervene unless the allyl chloride concentration were reduced and this in turn would considerably reduce the reproducibility of the method. Also higher association may cause complication. If such fortuitous cancellation is ignored, it remains to explain why the solubility method gives considerably higher values for K_A than the conductance method. It may be noted that the behavior of Ag^+ and Cl^- in aqueous solutions of more soluble salts, where conventional conductance measurements are possible, makes the low K_A values found in this work a

priori more likely than the higher figures found by the solubility method. The similar though rather more soluble salt, thallos chloride, has been found⁶ to have a $K_A \sim 3$.

It is possible that the solubility method involves some systematic error such as that colloidal silver chloride remains in suspension after filtration or centrifugation, and this possibility has been suggested by Berne and Leden¹ to explain the somewhat higher value of K_A found by Jonte and Martin.³ An alternative interpretation of the solubility data favoring the formation of $(Ag_2Cl)^+$ at the expense of AgCl would not reduce the discrepancy between the data from the two methods.

We conclude from our data that silver chloride in aqueous solution may not be so weak an electrolyte as has hitherto been supposed.

(6) R. A. Robinson and R. H. Stokes, "Electrolyte Solutions," 2nd Ed., Butterworth and Co. Ltd., London, 1959, p. 408.

Double Layer Capacity in the Presence of Leucoriboflavin

by T. Biegler and H. A. Laitinen

Noyes Chemical Laboratory, University of Illinois,
Urbana, Illinois (Received February 26, 1962)

Double layer capacity data have been used extensively for investigating adsorption of surface-active materials onto both mercury and solid electrodes.¹⁻⁶ Evaluation of surface coverages from capacity values extrapolated to zero frequency can be carried out with equations of purely thermodynamic origin⁷ but more commonly the nonthermodynamic assumption is made that either the capacity or the surface charge density is a linear function of coverage. Experimental verification of these assumptions has been obtained by comparing results with those derived from electrocapillary

(1) R. S. Hansen, R. E. Minturn, and D. A. Hickson, *J. Phys. Chem.*, **60**, 1185 (1956).

(2) R. S. Hansen, D. J. Kelsh, and D. H. Grantham, *ibid.*, **67**, 2316 (1963).

(3) H. A. Laitinen and B. Mosier, *J. Am. Chem. Soc.*, **80**, 2363 (1958).

(4) M. Breiter and P. Delahay, *ibid.*, **81**, 2938 (1959).

(5) W. Lorenz, F. Möckel, and W. Müller, *Z. physik. Chem.*, **25**, 10 (1960).

(6) M. W. Breiter, *Electrochim. Acta*, **7**, 533 (1962).

(7) F. W. Schapink, M. Oudeman, K. W. Leu, and J. N. Helle, *Trans. Faraday Soc.*, **56**, 415 (1960).

measurements.^{2,4} However, Parsons^{8,9} has concluded from theoretical considerations that unless adsorption obeys a simple Henry's law or Freundlich isotherm the capacity will not be a linear function of coverage by a neutral species except at high frequencies or potentials close to that of maximum adsorption.

Under conditions in which polarographic prewaves are observed it appears that the reduction products of compounds such as methylene blue and riboflavin form an insoluble film and accumulate at the mercury surface.¹⁰ Similar behavior occurs at a graphite electrode where anodic stripping was shown that a negligible amount of reduced methylene blue leaves the surface during pre-electrolysis times of up to 50 min.¹¹ These systems have, then, the useful property that an adsorbed film can be generated at an electrode surface and that the quantity of adsorbed product is easily calculated from the amount of current passed. Thus, for a diffusion controlled reduction at the dropping mercury electrode, the surface excess of reductant, Γ_t , at time t from the initiation of a drop is given by (cf. Koryta¹²)

$$\Gamma_t = 0.737 C_{OX} D_{OX}^{1/2} t^{1/2} \text{ moles cm.}^{-2} \quad (1)$$

where C_{OX} is the bulk concentration of oxidant in moles cm.^{-3} , D_{OX} is its diffusion coefficient, and the assumption is made that all of the reduction product remains adsorbed at the surface.

In this work the relationship between double layer capacity and coverage by leucoriboflavin, the reduced form of riboflavin, has been examined by measuring the capacity at various times during drop life with several concentrations of riboflavin and using eq. 1 to calculate the surface concentration of leucoriboflavin.

Experimental

Double layer capacities were measured with an a.c. bridge of conventional design (e.g., Grahame¹³). The bridge was fed by a General Radio Type 1301-A oscillator whose output was attenuated to give a bridge input signal of around 4 mv. The detector was a General Radio Type 1232-A tuned amplifier, and the amplified signal was displayed on a Tektronix 532 oscilloscope with a Type 53/54H plug-in amplifier. The time during growth of the mercury electrode at which the bridge reached balance was measured by a procedure somewhat different from those described in the literature. The presence of a logarithmic output feature on the tuned amplifier enabled convenient display of both the moment of drop detachment and a sharp balance point at a single oscilloscope sensitivity. An external time

base was provided by the triangular wave signal of a Hewlett Packard Type 202A low frequency function generator; the frequency was set at 0.25 c.p.s. and the amplitude adjusted so that the trace just filled the 10-cm. graticule. The required time between the two events could then be measured by noting the positions on the graticule at which they occurred and the intervening number of full sweeps. Accuracy of measurement was within ± 0.03 sec. This procedure gave somewhat more reliable results than use of the internal sweep of the oscilloscope which was neither as linear nor as reproducible as the signal from the function generator.

The dropping mercury electrode (d.m.e.) was drawn to a fine tip about 0.3 mm. o.d. Its characteristics were: $m = 1.67$ mg. sec.^{-1} and $t = 10.5$ sec. at -0.3 v. in the supporting electrolyte. The d.m.e. and a large cylindrical platinum counter electrode were connected to the bridge. The d.m.e. was polarized against a saturated NaCl calomel electrode with a Leeds and Northrup student potentiometer connected in series with a 200 Henry choke in order to block a.c. from the polarizing circuit. Frequency dispersion of the capacity for a pure electrolyte was typically less than 1% over the range 100–2000 c.p.s. D.c. polarograms were obtained with a Sargent Model XV polarograph.

Eastman riboflavin was used without further purification. The supporting electrolyte, 0.9 *N* NaClO_4 –0.1 *N* HClO_4 , was made up from appropriate quantities of reagent grade sodium hydroxide and perchloric acid. All experiments were carried out at $25 \pm 0.5^\circ$.

Results and Discussion

Measurement of polarographic diffusion currents led to a value of D_{OX} for riboflavin of 4.47×10^{-6} cm.^2 sec.^{-1} which was used in eq. 1 to calculate surface coverages. Plots of differential double layer capacity *vs.* surface coverage are shown in Fig. 1 for four potentials cathodic to the $E_{1/2}$ (-0.01 v.). Frequency dispersion was small and extrapolation to zero frequency of capacities at both partial and complete coverage gave values deviating less than 2% from those shown.

Except for Fig. 1D the plots consist of two straight lines intersecting at a common value of the surface excess. Some curvature near the points of intersection is noted in Fig. 1C. The implication of the constant

(8) R. Parsons, *Trans. Faraday Soc.*, **55**, 999 (1959).

(9) R. Parsons, *J. Electroanal. Chem.*, **5**, 397 (1963).

(10) W. Kemula, Z. Kublik, and A. Axt, *Roczniki Chem.*, **35**, 1009 (1961).

(11) S. P. Perone and T. J. Oyster, *Anal. Chem.*, **36**, 235 (1964).

(12) J. Koryta, *Collection Czech. Chem. Commun.*, **18**, 206 (1953).

(13) D. C. Grahame, *J. Am. Chem. Soc.*, **71**, 2975 (1949).

capacity branch is that full coverage has been reached. The two lines intersect at a value corresponding to the maximum surface excess which is estimated from these graphs to be $1.51 \pm 0.02 \times 10^{-10}$ mole cm^{-2} compared with 1.42×10^{-10} mole cm^{-2} calculated by Brdicka¹⁴ from the height of the polarographic prewave. Values in excess of this shown on the graphs have no physical significance since the assumption that all the product remains on the surface is obviously not correct here.

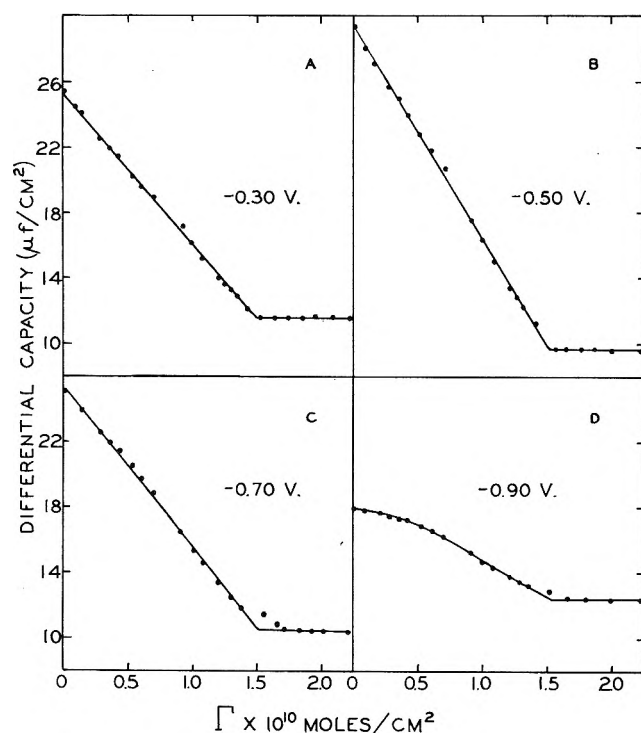


Figure 1. Dependence of double layer capacity, measured at 1000 c.p.s., on surface concentration of leucoriboflavin at potentials indicated.

The present results suggest an electrode reaction model in which reduction to an adsorbed product proceeds until surface coverage is reached. Until that time the rate of desorption is negligible and, except at the most cathodic potential examined, the lowering of capacity is proportional to the surface excess. After coverage either the desorption rate becomes rapid enough to allow the surface to accommodate all the product as it is formed or else reduction somehow occurs in the presence of a complete film. Assumption of fast desorption at or near maximum coverage would mean that reduction to the adsorbed species could continue unhindered as the surface approaches cover-

age, a conclusion contradicted by the appearance of a prewave. These considerations suggest that a necessary condition for a polarographic prewave controlled entirely by adsorption (*i.e.*, current is independent of concentration and proportional to mercury head) is that the desorption rate of product be negligible at all coverages; the commonly assumed requirement that the reduced species be much more strongly adsorbed than the oxidant is by itself inadequate.

The limiting surface concentration of leucoriboflavin does not appear to depend on potential even at -0.9 v. where it may be noted that intersection of the linear branches of Fig. 1D occurs at about 1.5×10^{-10} mole cm^{-2} . Despite this constancy the double layer capacity varies, reaching a minimum value somewhere in the vicinity of the point of zero charge where the lowering of capacity from the value for a clean surface is also greatest. Frumkin's suggestion¹⁵ that surface charge density at constant coverage depends linearly on potential and its corollary that the capacity of full coverage is independent of potential are therefore not substantiated with this system.

As mentioned above, the limiting capacity at -0.9 v. is reached at a surface excess comparable to that found at more positive polarizations. Curvature in the descending branch of Fig. 1D is therefore likely to reflect actual nonlinearity of the capacity-coverage relationship rather than a breakdown of the underlying assumption that the desorption rate is negligible. This result appears to support the recent work of Parsons.^{8,9}

Considering now the relationship between surface charge, q , and fractional coverage, θ , we note that

$$C = \frac{dq}{dE} = \left(\frac{\partial q}{\partial E} \right)_{\theta} + \left(\frac{\partial q}{\partial \theta} \right) \left(\frac{\partial \theta}{\partial E} \right) \quad (2)$$

where C is the differential double layer capacity. The contribution of the second term is probably small in the system being considered since coverage is found to be substantially independent of potential. It follows that at those potentials where linearity between C and θ was found, q was also a linear function of θ . On the other hand Fig. 1D indicates a nonlinear dependence of q on θ , a result similar to that found with the adsorption of phenol from perchloric acid solution.²

Acknowledgment. This work was supported by the National Science Foundation under Grant G-21049.

(14) R. Brdicka, *Z. Elektrochem.*, **48**, 686 (1942).

(15) A. Frumkin, *Z. Physik*, **35**, 792 (1926).

Limiting Isothermic Heats of Adsorption of *n*-Butane, *n*-Pentane, and *n*-Hexane on Graphitized Carbon Black

by G. C. Chirnside and C. G. Pope

Department of Chemistry, University of Otago, Dunedin, New Zealand (Received March 2, 1964)

Ross, Saelens, and Olivier¹ have recently applied a gas chromatographic technique to the determination of limiting isothermic heats of adsorption of a number of molecules on a graphitized carbon surface. The values reported for *n*-butane, *n*-pentane, and *n*-hexane did not agree well with results obtained from equilibrium experiments or from calculation.² The present work was undertaken to try to resolve these anomalies.

Experimental

A gas chromatograph of conventional design using nitrogen as carrier gas and incorporating a sample splitter and flame ionization detection was used. The amplified detector signal was recorded with a Honeywell Brown 1-mv. recorder (time for full scale deflection, 2 sec.). When measurements were intended for use in the calculation of isothermic heats of adsorption, the adsorbate was injected as part of a gas mixture which also contained methane.

The column was made from a 3-ft. length of copper tubing (i.d. 0.125 in.) and packed with 2.93 g. of Spheron 6 (2700°) graphitized carbon black (kindly donated by Dr. W. R. Smith of Godfrey L. Cabot, Inc.) which had been size graded to between 100 and 120 mesh. An air thermostat controlled the column temperature to within $\pm 0.2^\circ$.

The pressures at the ends of the column were measured with mercury manometers, and the carrier gas flow rate was obtained from separate experiments, using a soap bubble meter. Retention times were measured by stop watch and found to be reproducible to about ± 2 sec. Most measurements were in the range 250–600 sec.

Results and Discussion

The results were calculated using the method of Ross, Saelens, and Olivier.¹ In our work, the correction term arising from the compressibility of the gas stream proved to be significant. The most important experimental modifications were the substitution of 100–120 mesh Spheron 6 (2700°) (specific surface area 89.4 m.²/g.) for 60–100 mesh Sterling M.T. (3100°) (specific surface area 8.4 m.²/g.) as adsorbent, and

the replacement of the thermal conductivity detector by a flame ionization instrument.

With the new adsorbent the column H.E.T.P. was reduced to about 0.06 cm., while the retention volume has been greatly increased without an increase of dead volume. Both factors result in improved precision in retention time measurement.

Flame ionization detection allowed the use of much smaller adsorbate samples, so that the limiting condition of zero surface coverage was more closely approached. In addition to this, the gas phase within the column approximated very closely to pure carrier gas. This made the ideal gas equation a sufficiently accurate approximation to the gas phase behavior in the present work.

Methane was mixed with the adsorbate sample as an indicator of the behavior of a nonsorbed gas. At the lowest temperature used (45°) and a carrier gas flow rate of 15 cc./min., the methane peak emerged in 15–18 sec., whereas calculation based on the column geometry predicted that the retention time for a nonsorbed gas would be 10–12 sec. If a linear relationship exists between the logarithm of the corrected retention volume at constant temperature and the number of carbon atoms in the alkane molecule as is found in gas-liquid chromatography,³ and is consistent with our limited data on this system, methane would be held in the column for about 7 sec. due to adsorption. This is only about 0.5% of the retention time of *n*-butane under the same conditions so that this procedure should lead to small absolute error and an even smaller error in the comparison of retention volumes obtained at different temperatures.

The emergence of the very sharp peak maximum due to methane is easier to time than the moment of injection and allows one time interval to be used to determine the corrected retention time, instead of the two which are usually required.

It has been reported that Spheron 6 (2700°) shows some residual surface heterogeneity,⁴ and this could result in comparisons between our work and that of Ross and his co-workers,¹ or between our results and calculation for adsorption onto a graphite-like substrate, being of little significance. However, not all published isothermic heat curves show this initial heterogeneity with Spheron 6 (2700°)⁵ or differentiate be-

(1) S. Ross, J. K. Saelens, and J. P. Olivier, *J. Phys. Chem.*, **66**, 696 (1962).

(2) D. M. Young and A. D. Crowell, "Physical Adsorption of Gases," Butterworths and Co. Ltd., London, 1962, p. 31.

(3) J. F. Smith, *Nature*, **193**, 679 (1962).

(4) A. A. Isirikyan and A. V. Kiselev, *J. Phys. Chem.*, **66**, 205 (1962).

tween Sterling M.T. (3100°) and Spheron 6 (2700°).⁶ For this reason experiments were carried out to determine the effect of sample size on retention time, at constant temperature and flow rate (Fig. 1). The elution peaks obtained were symmetrical when less than about 0.07 cc. of *n*-butane was injected. With larger samples the peaks became progressively more skewed with steeper leading than trailing edges.

The maximum surface coverage caused by the adsorbate at the column exit can be calculated approximately from the shape of the elution peak, its retention time, and details of the column construction. A value of about 0.06 monolayer is obtained in this way as the result of injection of 0.1 cc. of *n*-butane under the operating conditions of Fig. 1. At the column inlet the situation is much less certain, but calculation based on the assumption that the sample is introduced at a constant rate during a period of 0.5 sec. leads to surface coverages at this position about ten times greater than those predicted above. The samples used during experiments to determine isosteric heats of adsorption always yielded maximum calculated coverages within the column of less than 0.05 monolayer.

If isotherm curvature on an ideal homotactic adsorbent at low surface coverage is attributed to the filling up of the available adsorption area, as it is, for instance, in the Langmuir model, the corrected retention volume should decrease almost linearly by about 10% when the surface concentration is increased from zero to 0.1 monolayer. Figure 1 shows, therefore, that the effects of residual surface heterogeneity have not become apparent over the range of low surface coverages used in this work, despite the fact that the results of Isirikyan and Kiselev⁴ for *n*-hexane adsorbed on Spheron 6 (2800°) at 20° indicate considerable heterogeneity at coverages less than about 0.15 monolayer. Our estimate of the limiting isosteric heat of adsorption for *n*-hexane at about 150° (11.2 kcal./mole) agrees reasonably well with the value (11.5 kcal./mole) obtained by linear extrapolation of Isirikyan and Kiselev's results from high to zero surface coverage, so as to eliminate the contribution to the heat of adsorption due to adsorbate-adsorbate interactions and surface heterogeneity, but is quite different from the value obtained by these workers at very low coverage (about 14.0 kcal./mole). This may indicate that the high energy sites are permanently filled with adsorbed material in our work, because the adsorbent cannot be outgassed under vacuum, prior to adsorption, as is usual in static experiments.¹

It is important to show that the effect described above does not arise from appreciable departures from equilibrium within the column. This was demon-

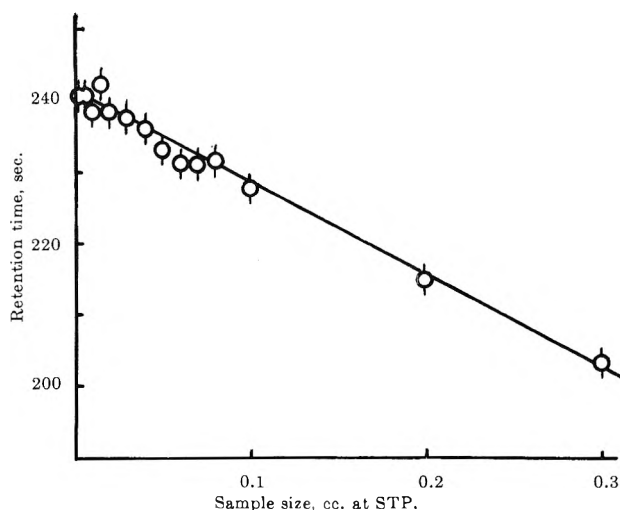


Figure 1. The effect of sample size on retention volume. Sample: *n*-butane at 96°; flow rate = 17 cc./mm.

strated in our work by the observation that no detectable change of retention volume was found over the range of flow rates used. The rather similar findings of Everett and Stoddart⁷ for a g.l.c. column, where equilibration would presumably be more sluggish due to the slow diffusion process occurring in the liquid phase during mass transfer,⁸ further confirmed this result.

Figure 2 shows a plot of log specific retention volume, corrected to zero flow rate, against reciprocal absolute temperature. Each point is the mean of three experiments, the average deviation between replicate determinations of retention time being 1.7 sec. The average slopes of the three straight lines and their probable errors were determined by least-squares analyses. The results are presented in Table I. Estimation of the precision of the individual measurements suggested that the isosteric heats should have a reproducibility of better than $\pm 1.5\%$. Also shown in Table I are the average energies of adsorption for the three adsorbates at 0°K. adsorbed on a graphite surface as calculated by Kiselev and his co-workers² using a Lennard-Jones 6-12 potential function, the results obtained by Ross with a chromatographic technique,³ and some results of equilibrium measurements.⁹ These latter figures refer to a surface coverage of 0.5 monolayer, and so

(5) R. A. Beeke and R. M. Dell, *J. Phys. Chem.*, **59**, 746 (1955).

(6) W. R. Spencer, C. H. Amberg, and R. A. Beeke, *ibid.*, **62**, 719 (1958).

(7) D. H. Everett and C. T. H. Stoddart, *Trans. Faraday Soc.*, **57**, 746 (1961).

(8) M. J. E. Golay, "Gas Chromatography," R. P. W. Scott, Ed., Butterworth and Co. Ltd., London, 1960, p. 139.

(9) A. V. Kiselev, *Quart. Rev. (London)*, **15**, 99 (1961).

Table I: Experimental and Calculated Limiting Isothermic Heats, Kcal./Mole, of Adsorption on Graphite

Adsorbate	This work	Temp. range, °C.	Ref. 1	Temp. range, °C.	Calculated	Equilibrium expt. at $\theta = 0.5$
<i>n</i> -Butane	7.88 ± 0.014	45-145	8.10	68-160	7.60	8.7, 8.3
<i>n</i> -Pentane	9.27 ± 0.07	118-160	8.61	99-190	9.30	10.2
<i>n</i> -Hexane	11.17 ± 0.014	130-200	9.83	99-190	11.00	12.1, 12.5

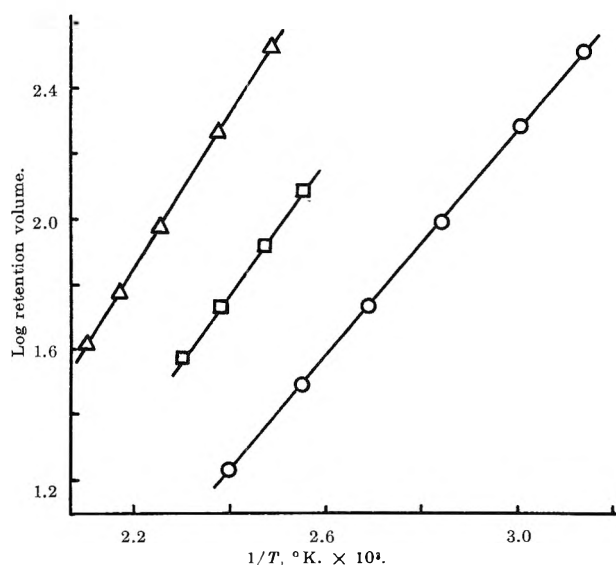


Figure 2. The variation of corrected retention volume with reciprocal absolute temperature: O, *n*-butane; □, *n*-pentane; Δ, *n*-hexane.

should exceed values at zero coverage by a lateral interaction energy which is probably about 1 kcal./mole, estimated on the basis of the data of Isirikyan and Kiselev.⁴

The uncertainties involved in the calculation, and the unknown effect of surface heterogeneity on the experimental results, make the close agreement in absolute magnitudes obtained of dubious significance. The differences in temperature between the experimental and calculated results should also, in principle, have been allowed for, although the correction term involved would probably be small.¹ The most promising feature of this work is that the differences between the three measured isothermic heats agree well both with calculation and with equilibrium experiments. Further work with more highly graphitized carbon black adsorbents will be necessary to examine the possible effects of surface heterogeneity more closely.

Acknowledgment. The authors wish to acknowledge the continued interest of Dr. A. G. Williamson in this work.

The Dipole Moments and Polarizabilities of Nitrogen Dioxide and Nitrogen Tetroxide¹

by James E. Boggs

Department of Chemistry, The University of Texas, Austin, Texas (Received March 4, 1964)

Interest in the polarity and polarizability of NO₂ and of N₂O₄ has been reawakened by the recent microwave Stark effect measurement of the dipole moment of NO₂ by Hodgeson, Sibert, and Curl.² Numerous discussions³⁻⁸ of the dielectric constant of NO₂-N₂O₄ mixtures have appeared in the literature, including three sets⁵⁻⁷ of accurate measurements. The independently determined experimental data are in fairly good agreement, but there is wide disagreement over the interpretation of the data. The problem is made difficult by the equilibrium existing between NO₂ and N₂O₄ and by the relatively narrow temperature range over which the system can be studied.

Zahn⁵ measured the dielectric constant of equilibrium mixtures of NO₂ and N₂O₄ between 297 and 397°K. and interpreted his results as indicating a dipole moment of 0.39 D. for NO₂ and of 0.55 D. for N₂O₄. There is now, however, overwhelming evidence^{9,10} that N₂O₄ is a planar molecule of D_{2h} symmetry so that it should have zero dipole moment. The observation¹¹ that isomeric forms of N₂O₄ can be formed

(1) This work was supported by a grant from the National Science Foundation.

(2) J. A. Hodgeson, E. E. Sibert, and R. F. Curl, Jr., *J. Phys. Chem.*, **67**, 2833 (1963).

(3) K. Bädcker, *Z. physik. Chem.*, **36**, 315 (1901).

(4) P. N. Ghosh and P. C. Mohanti, *Physik. Z.*, **30**, 531 (1929).

(5) C. T. Zahn, *ibid.*, **34**, 461 (1933).

(6) J. W. Williams, C. H. Schwingel, and C. H. Winning, *J. Am. Chem. Soc.*, **56**, 1427 (1934); **58**, 197 (1936).

(7) R. Schulz, *Z. Physik*, **109**, 517 (1938).

(8) C. C. Addison and J. Lewis, *J. Chem. Soc.*, 1869 (1953).

(9) G. M. Begun and W. H. Fletcher, *J. Mol. Spectry.*, **4**, 388 (1960).

(10) D. W. Smith and K. Hedberg, *J. Chem. Phys.*, **25**, 1282 (1956).

in various matrices at liquid helium temperatures would appear not to be relevant under the conditions of these experiments.

Williams, Schwingel, and Winning⁵ remeasured the dielectric constant of the system between 298 and 398°K. and, applying a different method of analysis to the data, concluded that N₂O₄ has a zero dipole moment, but that the dipole moment of NO₂ varies with temperature, ranging from 0.58 D. at 298°K. to 0.30 D. at 398°K. Various attempts to rationalize such a temperature variation have all failed.^{6,8}

Schulz⁷ made what is apparently the most accurate set of dielectric constant measurements and interpreted his data to show dipole moments of 0.32 D. for NO₂ and 0.42 D. for N₂O₄, both independent of temperature between 298 and 372°K. The interpretation of the dielectric constant measurements thus appears to be caught in a dilemma between the untenable calculation of a dipole moment for a symmetric molecule and the inexplicable postulation of a temperature-dependent dipole moment for NO₂.

The microwave Stark effect measurement by Hodgson, Sibert, and Curl² showed the dipole moment of NO₂ in the ground vibrational state to be 0.316 ± 0.01 D. This figure alone rules out the assumption of a temperature-dependent moment for NO₂, since all explanations of such behavior assumed a very large ground-state moment, with the moment of 0.3–0.6 D. at room temperature resulting from the presence of molecules in excited vibrational or electronic states. Moreover, the additional information provides the key to a re-evaluation of the older dielectric data.

The total polarization of a mixture of NO₂ and N₂O₄ can be written as the sum of the distortion and orientation polarizations of the two species

$$P = n_1 P_{d_1} + n_1 P_{o_1} + n_2 P_{d_2} + n_2 P_{o_2}$$

where n_1 and n_2 represent the mole fractions of the two species. In spite of the apparent high accuracy of Schulz's data,⁷ the range of temperature and concentration over which he was able to make measurements does not allow all four contributions to the total polarization to be evaluated independently. Attempts to do so lead to widely varying results depending on which combination of the data is used. Schulz chose to use the molar refractions measured by Cuthbertson and Cuthbertson¹² for the distortion polarizations of NO₂ and N₂O₄ and obtained the results $\mu_{\text{NO}_2} = 0.320$ D. and $\mu_{\text{N}_2\text{O}_4} = 0.415$ D. In an alternative calculation, they added 6% to the molar refraction to allow for the atomic polarization and obtained $\mu_{\text{NO}_2} = 0.286$ D. and $\mu_{\text{N}_2\text{O}_4} = 0.371$ D.

It is now known that the atomic polarization may

vary widely among different molecules and that the old practice of adding a fixed fraction of the electronic polarization has little justification. To understand the situation in the NO₂-N₂O₄ system, it would seem fruitful to reanalyze Schulz's data using $\mu_{\text{N}_2\text{O}_4} = 0$ and $\mu_{\text{NO}_2} = 0.316$ D. (the result obtained by Hodgson, Sibert, and Curl) and to calculate the distortion polarizations of the two species from the dielectric constant data. This can be done using the data from Table 8 of Schulz's paper in various combinations. The average values obtained using all combinations are $P_d = 7.61 \pm 0.09$ cc. for NO₂ and $P_d = 19.57 \pm 0.13$ cc. for N₂O₄, where the indicated uncertainties are the average deviations from the mean of the results using different combinations of data. The most accurate result should come from a combination of the measurements at the two temperature extremes, 298 and 372°K., where the variation in mole fraction of the two species is greatest. This result, $P_d = 7.64$ cc. for NO₂ and $P_d = 19.60$ cc. for N₂O₄, is not appreciably different from the mean of all the values.

The electronic polarization of NO₂, calculated from the refractive index measurements of Cuthbertson and Cuthbertson¹² at 6438 Å. and not extrapolated to infinite wave length, is 7.60 cc. If this value is accepted as correct, the distortion polarization of NO₂ of 7.61 cc. must be a little low, but the result indicates that the atomic polarization must certainly be small. The electronic polarization¹² of N₂O₄ is 16.77 cc. Comparison of this value with the total distortion polarization of 19.57 cc. indicates an atomic polarization of 2.82 cc., or nearly 17% of the electronic polarization. This factor, unaccounted for in earlier analyses, is presumably the cause of the confusion which has existed.

It is unfortunate that experimental measurements of the absolute infrared absorption intensities of NO₂ and N₂O₄ do not exist since these could be used to calculate the atomic polarizations directly.¹³ To an excellent approximation, the atomic polarization of a gas is given by

$$P_a = \frac{cV}{3\pi^2} \sum_n \frac{A_n}{\nu_n^2}$$

where V is the molar volume and A_n is the integrated intensity of the absorption band at frequency ν_n . Several of the vibration fundamentals of N₂O₄ occur

(11) W. G. Fately, H. A. Bent, and B. Crawford, Jr., *J. Chem. Phys.*, **31**, 204 (1959).

(12) C. Cuthbertson and M. Cuthbertson, *Proc. Roy. Soc. (London)*, **A89**, 361 (1913).

(13) A. B. Tipton, A. P. Deam, and J. E. Boggs, *J. Chem. Phys.*, **40**, 1144 (1964).

at very low frequency⁹ including the strong ν_7 vibration at 429 cm.^{-1} and the very strong ν_{12} vibration at 750 cm.^{-1} . Thus an atomic polarization of 2.82 cc. does not appear unreasonable for N_2O_4 .

From internal evidence, the work of Zahn⁵ appears to be less precise than that of Schulz.⁷ Under corresponding conditions of temperature and pressure, the results of Zahn are a little higher. On reanalysis of Zahn's data, it is found that dipole moments of 0.316 D. for NO_2 and 0 D. for N_2O_4 and distortion polarizations of 8.2 cc. for NO_2 and 22 cc. for N_2O_4 will reproduce the data with an average error of only about 1.5%. Again, a small atomic polarization for NO_2 and a large atomic polarization for N_2O_4 are indicated.

The data of Williams, Schwingel, and Winning⁶ also appear to have less precision than those of Schulz and, while they are roughly the same, they exhibit a pressure variation that is not compatible with the analysis suggested here nor with the data of Schulz or of Zahn.

It appears that the best dielectric constant data in the literature are compatible with the microwave dipole moment measurement for NO_2 and with a zero moment for N_2O_4 , and that previous difficulties in interpretation arose from ignoring the possibility that N_2O_4 might have a large atomic polarization. The atomic polarization of N_2O_4 is on the order of 3 cc., but a more precise determination must await measurements of infrared absorption intensities.

Generation of Acidity in Silica Gel by Ionizing Radiation

by C. Barter and C. D. Wagner

Shell Development Company, Emeryville, California
(Received March 20, 1964)

Irradiation of silica gel has been reported to cause the formation of hydrogen atoms^{1,2} and color centers.³ These entities, however, do not appear to be connected with the enhanced catalytic activity for hydrogen-deuterium exchange and ethylene hydrogenation shown by the irradiated gel⁴ since the hydrogen atoms are not stable above -120° ¹ and irradiated silica gel retains catalytic activity after color centers have been removed by chemisorption of hydrogen or bleaching by irradiation with ultraviolet. Recently, it has been reported that carbonium ions are formed when silica gel and certain adsorbed⁵ hydrocarbons are ir-

radiated simultaneously.⁵ On this basis it has been suggested that irradiation increases the acidity of silica gel and that this may account for its catalytic activity for hydrogen-deuterium exchange. However, the fact that carbonium ions were found when hydrocarbon and gel were irradiated together leaves open the question that acidity can be manifested in the gel in the absence of hydrocarbon.

The investigation reported here is a study of the effects of radiation on silica gel by chemical investigation after irradiation. Detection and measurement of acid sites is by indicators and by polymerization of isobutylene.

Experimental

Gel Preparation. Three grams of Davison 950 silica gel (surface area 625 $\text{m.}^2/\text{g.}$) was pretreated in air at 520° for several days and then was degassed at 520° under high vacuum for 20 hr. After the system was sealed off, the gel was irradiated at -196° with bremsstrahlung from the gold target of a 3-Mev. Van de Graaff to a total dose of 3×10^7 rads, in 1 hr. Irradiated samples were maintained at -196° until used.

Measurement of Acidity. One-tenth milliliter of a $5.4 \times 10^{-3} M$ solution of *p*-dimethylaminoazobenzene in carbon tetrachloride was degassed by successive freeze-thaw and pumping operations; it was added to the gel through a break-seal. Gel suspended in reagent was transferred by pipet to a spectrophotometer cell for recording of the absorption spectrum. Addition of pure *n*-butylamine, for titration purposes, was made by a micro hypodermic syringe directly to the optical cell.

In experiments with triphenylmethane and anthracene, the 50 mg. of hydrocarbon was distilled under vacuum onto the gel.

Measurement of Polymerization Activity. For this experiment, Phillips research grade isobutylene (8 ml.) was distilled *in vacuo* through a break-seal into the gel at -196° . The mixture was then warmed to -78° and stirred magnetically. After a specified time of polymerization, 10 ml. of *n*-hexane was added by distillation. The mixture was then brought to room temperature. The supernatant solution of

(1) V. B. Kazansky, G. B. Pariisky, and V. V. Voevodsky, *Discussions Faraday Soc.*, **31**, 203 (1961).

(2) P. H. Emmett, R. Livingston, H. Zeldes, and R. J. Kokes, *J. Phys. Chem.*, **66**, 921 (1962).

(3) H. W. Kohn, *Nature*, **184**, 630 (1959).

(4) H. W. Kohn and E. H. Taylor, *Proceedings of Second International Congress on Catalysis, Editions Technip, Paris, Vol. 2, 1962*, p. 1461.

(5) H. W. Kohn, *J. Phys. Chem.*, **66**, 1185 (1962).

polyisobutylene was decanted from the gel, and the solvent and unreacted isobutylene were removed by distillation. The weight of residue was taken after pumping on the residue until it reached constant weight.

Results and Discussion

Spectrophotometry of Acid Reactions. Absorption spectra of organic molecules adsorbed on silica gel are easily obtained with suspensions of the gel in a solvent of suitable refractive index. Spectra so obtained on gel with adsorbed *p*-dimethylaminoazobenzene in carbon tetrachloride are shown in Fig. 1. Spectra of the acid and base forms were obtained by adding small amounts of acetic acid or butylamine to the suspension of unirradiated gel in the indicator solution. Addition of the indicator alone to baked-out but unirradiated gel gives the spectrum shown with a small acid component (visually the color is yellow, however). Addition of the indicator to irradiated gel gives almost the typical acid spectrum. Addition of excess butylamine then gives a basic form. This basic form, though it is visually yellow, has a different absorption spectrum from the basic form on unirradiated gel, showing that the chemical properties of the surface are changed in ways other than just the production of strong acid. These changes are reversible, for heating irradiated gel at 500° for 10 hr. removed both effects of radiation.

The amount of strong acid generated in the gel was determined by titration with butylamine. Addition in small increments reduced the optical density at 5500 Å. approximately linearly until it reached the density characteristic of unirradiated gel. This amount was taken as the amount of acid generated by radiation. A dose of 3×10^7 rads produces about 3 μ moles of acid sites/g.

Distillation of triphenylmethane onto the colorless preirradiated silica gel resulted in an immediate yellow coloration. A similar effect was observed by Kohn,⁵ but as a result of the *simultaneous* irradiation of silica gel and triphenylmethane. In the present case an absorption spectrum of a slurry of the colored gel, in iso-octane solvent, showed that the yellow color was due to triphenylmethane cation,⁶ demonstrating that hydride abstraction from triphenylmethane had taken place.^{7,8}

Anthracene distilled onto preirradiated silica gel resulted in a green coloration, but in this case the absorption spectrum of the colored gel was not determined. Kohn⁵ observed a similar coloration following the simultaneous irradiation of silica gel and anthracene and concluded that the carbonium ion of anthracene had been formed since anthracene adsorbed on silica-

alumina results in a similar, visually green coloration. However, it has been pointed out⁹ that anthracene adsorbed on silica-alumina may be present as a positive molecule ion as well as in carbonium ion forms since the absorption spectrum of adsorbed anthracene shows a band at 7500 Å.¹⁰ which has been attributed to the positive molecule ion of anthracene.¹¹

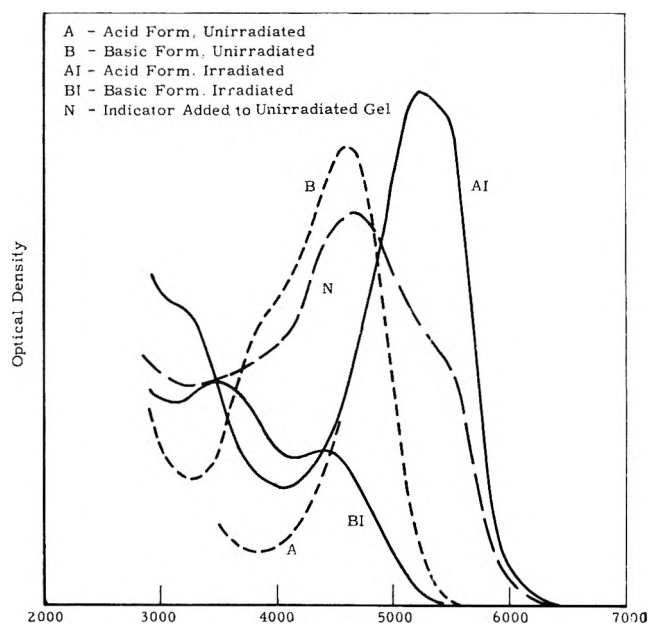


Figure 1. Absorption spectra of *p*-dimethylaminoazobenzene on irradiated and unirradiated silica gel.

Polymerization Studies. When polymerization was effected using 5 g. of isobutylene with 3 g. of irradiated gel, approximately 0.5 g. of polymer was obtained. Its molecular weight by ebullioscopic and osmometric methods was 2400. Correlation with the number of acid sites gives about 10–20 polymer molecules formed per acid site. Blank tests were made to determine whether polymerization could be effected by (1) unirradiated silica gel and (2) the irradiated flask with no silica gel. Less than 0.002 g. of polymer was formed in each blank experiment.

(6) L. C. Anderson, *J. Am. Chem. Soc.*, **57**, 1673 (1935).

(7) H. P. Leftin and W. K. Hall, ref. 4, Vol. 1, 1960, p. 1353.

(8) H. P. Leftin, *J. Phys. Chem.*, **64**, 1714 (1960).

(9) D. M. Brouwer, *Chem. Ind. (London)*, 177 (1960).

(10) R. M. Roberts, C. Barter, and H. Stone, *J. Phys. Chem.*, **63**, 2077 (1959).

(11) W. Y. Aalbersberg, G. J. Hoijtink, E. L. Mackor, and W. P. Weijland, *J. Chem. Soc.*, 3049 (1959).

A test of yield *vs.* time of polymerization with irradiated gel (3×10^7 -rad dose) showed the maximum yield to be approached asymptotically, with 90% of the maximum reached in 1 hr.

A study was made of the effect of dose; at a dose rate of 3×10^7 rads/hr., a maximum yield was again approached asymptotically, with 90% of the maximum value achieved at a dose of about 1.5×10^7 rads.

It was found that pretreatment of the gel is important in developing activity for polymerization by irradiation. Treatment of the gel *in vacuo* at 25° for 20 hr. prior to irradiation gave a gel completely inactive for polymerization. Baking out *in vacuo* at 520° for 20 hr. before irradiation gave only about half the polymerization activity attained by a bake-out time of 40 hr.

Decay of Acid Sites. Experiments were conducted in which irradiated gel was stored at 25 and 100° for specified periods before addition of *p*-dimethylaminobenzene or addition of isobutylene. The weight of polyisobutylene and the titration with butylamine to determine the amount of strong acid were used to determine relative activities. There was a parallelism between the two properties of the gel. Half-time for decay appeared to be about 2–3 hr. at 25° and 1–1.5 hr. at 100° . It is of interest to note that although the half-time for decay at -196° must be many hours, a saturation activity was reached upon irradiation for only 1 hr. This must mean that either there is a limited number of sites that can be made acidic, or there is a radiation-induced decay process which causes a steady-state activity to be reached in only short irradiation time.

The parallelism in decay rate of acid centers and those responsible for isobutylene polymerization probably means that the two types of centers are identical. Radiation-induced acidity in silica gel may well play an important role in its enhancement of *G*-value for certain radiation-induced polymerizations.¹²

The storage of chemically active centers generated by radiation in silica gel may be an effect similar to that noted by Hentz¹³ in silica-alumina; he found that irradiated silica-alumina could convert isopropylbenzene to benzene under conditions where it is normally inactive. Yamamoto¹⁴ observed evidence for acidity developed in Kaolinite by irradiation.

The Dipole Moment of Trifluoronitrosomethane¹

by James E. Boggs, DeWitt Coffey, Jr.,
and Jeff C. Davis, Jr.

*Department of Chemistry, the University of Texas,
Austin 12, Texas (Received April 9, 1964)*

From tabulated bond moment values² and any reasonable assumption about the C—N=O bond angle, the dipole moment of CF₃NO may be predicted to be in the range of 1.5–1.9 D., with the oxygen end of the molecule negative. An unsuccessful attempt to observe lines in the microwave spectrum of the compound in this laboratory suggested that the actual dipole moment is much less than this predicted value. We have, therefore, measured the molar polarization of CF₃NO and obtained an estimate of the dipole moment using the apparatus and methods described earlier.³ The sample used was prepared by the method of Mason and Dunderdale⁴ and purified by fractional distillation on a vacuum line. It was carefully shielded from light after purification to prevent dimerization.

The molar polarization of CF₃NO, extrapolated to high pressure,⁵ was found to be 14.0 ± 0.2 cc. at 296° , where the indicated uncertainty includes the effect of deviation from ideal gas behavior. The electronic polarization is estimated to be 10.9 ± 0.2 cc. This value is obtained using 1.83 cc. as the group refraction of C—F² and 5.4 ± 0.2 cc. as the group refraction of C—N=O, the latter based on the measured refractive indices of several halogenated aliphatic nitroso compounds.⁶ Using the standard assumption that the atomic polarization is approximately 10% of the electronic polarization, one may obtain a value of 0.31 ± 0.03 D. for the dipole moment of CF₃NO. The uncertainty does not include the uncertainty in estimating the atomic polarization, and, for reasons described below, 0.31 D. is probably an upper limit for the dipole moment.

(1) This work was supported in part by a grant from the National Science Foundation and in part by a grant from the Welch Foundation.

(2) C. P. Smyth "Dielectric Behavior and Structure," McGraw-Hill Book Co., New York, N. Y., 1955.

(3) A. B. Tipton, A. P. Deam, and J. E. Boggs, *J. Chem. Phys.*, **40**, 1144 (1964).

(4) J. Mason and J. Dunderdale, *J. Chem. Soc.*, 749 (1956).

(5) J. E. Boggs and A. P. Deam, *J. Chem. Phys.*, **32**, 315 (1960).

(6) J. D. Park, A. P. Stefani, G. H. Crawford, and J. R. Lacher, *J. Org. Chem.*, **26**, 3316 (1961); J. D. Park, A. P. Stefani, and J. R. Lacher, *ibid.*, **26**, 4017 (1961).

(12) R. Worrall and A. Charlesby, *Intern. J. Appl. Radiation Isotopes*, **4**, 84 (1958); R. Worrall and S. H. Pinner, *J. Polymer Sci.*, **34**, 229 (1959).

(13) R. R. Hentz, *J. Phys. Chem.*, **66**, 2714 (1962).

(14) D. Yamamoto, *Nippon Kagaku Zasshi*, **83**, 115 (1962).

In searching for an explanation for the low value of the dipole moment of CF_3NO , a comparison with the nitrosyl halides is fruitful. For NOF , NOCl , and NOBr , the nitrogen-halogen bond lengths are longer by 0.18, 0.29, and 0.30 Å., respectively, than would be expected for normal covalent single bonds.^{7,8} This observation has been explained by assuming appreciable contributions from an ionic structure, $(\text{N}\equiv\text{O})^+\text{X}^-$. Further evidence comes from an analysis⁸ of the vibrational force constant of nitrosyl chloride which yields an N-O bond order of 2.4. Furthermore, a microwave study⁸ of the Cl quadrupole coupling indicates 40% ionic character in the N-Cl bond.

Magnuson⁷ was able to measure the dipole moment components of NOF along the inertial axes and to resolve these into components in the bond directions. Using this procedure, he obtained a moment in the N-F direction of 1.75 D. and a moment in the N=O direction of -0.17 D. These measured values are strikingly different from the usual bond moments² of 0.17 D. for N-F and 2.0 D. for N=O, and are a clear indication of the shift of electron density in the direction of the halogen atom that is symbolized by the ionic structure.

We propose, on the basis of the unexpectedly low value for the dipole moment of CF_3NO , that this compound also has a structure which must be represented by an appreciable contribution from an ionic form, $(\text{N}\equiv\text{O})^+\text{CF}_3^-$, indicating a withdrawal of electron density by the "pseudo-halogen" CF_3 group.

In addition to the effect on the dipole moment, there should be two other observable effects of such a structure: an exceptionally long C-N bond length and a large positive chemical shift in the fluorine nuclear magnetic resonance. In view of the low dipole moment and the complications introduced by the expected very low barrier to internal rotation, the bond lengths will presumably have to await an investigation by electron diffraction techniques. If the C-N bond is very long, however, one would expect intense, low-frequency vibrations which would make unusually large contributions to the atomic polarization.³ For this reason, we suspect that the dipole moment of CF_3NO may be somewhat lower than the 0.31 D. calculated above.

We have measured the fluorine n.m.r. spectrum of CF_3NO at -100° and find a chemical shift of 89.83 ± 0.02 p.p.m. with respect to CFCl_3 , used as an internal reference. Table I compares this value with the chemi-

cal shift observed for other compounds containing the CF_3 group. The authors know of no compound containing the CF_3 group for which a more positive chemical shift has been reported.

Table I: Fluorine N.m.r. Chemical Shifts^a

Compound	Chemical shift, p.p.m.
CF_3NO	13.2
$(\text{CF}_3)_2\text{NCF}_2\text{CF}_3$	8.5
$\text{CF}_3(\text{CF}_2)_5\text{CF}_3$	7.5
CF_3H	6.3
CF_3COOH	0.00
$(\text{CF}_3-\text{BF}_3)^-$	-2.06
CF_3NONF	-7.0
$\text{CF}_3\text{N}(\text{CH}_3)_2$	-7.6
CF_4	-11.9
$\text{CF}_3\text{N}(\text{C}_2\text{H}_5)_2$	-17.3
$(\text{CF}_3)_2\text{NCF}_2\text{CF}_3$	-23.1
CFCl_3	-76.6

^a All values except that for CF_3NO taken from E. Fluck, "Die Kernmagnetische Resonanz und ihre Anwendung in der Anorganischen Chemie," Springer-Verlag, Berlin, Germany, 1963. Bold face type indicates the fluorine atom to which the listed chemical shift applies.

Further evidence for an abnormal structure for CF_3NO comes from the fact that CF_3NO dimerizes in an entirely different manner than does CH_3NO . We have prepared the dimer by allowing the monomer to stand exposed to light for a long period of time and have obtained its mass spectrum. The appearance of large peaks at $m/e = 168, 149, 133,$ and 114 corresponding to the fragments $(\text{CF}_3)_2\text{NO}$, $(\text{CF}_3)(\text{CF}_2)\text{NO}$, $(\text{CF}_3)(\text{CF}_2)\text{N}$, and $\text{C}_2\text{F}_4\text{N}$ shows that both CF_3 groups are attached to the same nitrogen atom. This provides additional confirmation of the structure $(\text{CF}_3)_2\text{N}-\text{O}-\text{N}=\text{O}$ which was suggested as a possibility by Jander and Haszeldine⁹ and later confirmed by the work of Mason¹⁰ and others.

(7) D. W. Magnuson, *J. Chem. Phys.*, **19**, 1071 (1951); D. F. Eagle, T. L. Weatherly, and Q. Williams, *ibid.*, **30**, 603 (1959); L. Pauling, "The Nature of the Chemical Bond," Cornell University Press, Ithaca, N. Y., 1960.

(8) D. J. Millen and J. Pannell, *J. Chem. Soc.*, 1322 (1961).

(9) J. Jander and R. N. Haszeldine, *ibid.*, 696 (1954).

(10) J. Mason, *ibid.*, 4531 (1963).

Can an inorganic chemist find success and happiness without INORGANIC CHEMISTRY?

Chances are he cannot. And most inorganic chemists apparently have discovered this fact already.

INORGANIC CHEMISTRY has received so many articles so fast that it is now a monthly publication with approximately 2,000 pages scheduled for 1964.

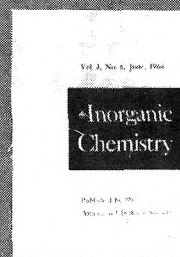
Total subscribers have risen to more than 4,000 in less than three years' time.

If you are that rare inorganic chemist who has not yet discovered these facts, make yourself happier by writing for and/or subscribing to INORGANIC CHEMISTRY.

1 year: ACS members \$11.00

All others 22.00

AMERICAN CHEMICAL SOCIETY 1155 Sixteenth Street, N.W., Washington, D.C. 20036



FERRO- AND ANTIFERROMAGNETISM STUDIES WITH EPR

(ELECTRON PARAMAGNETIC RESONANCE)

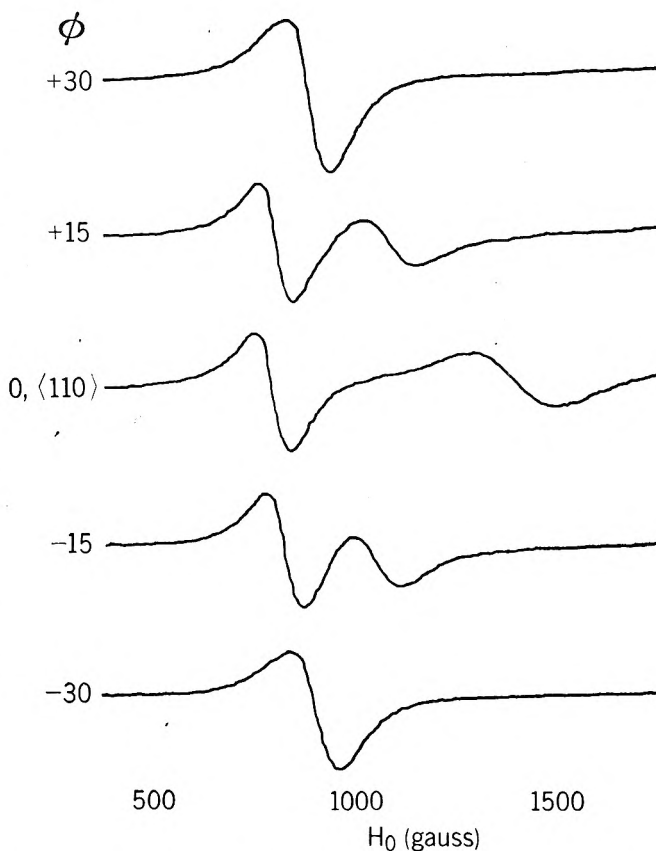
During the last few years many ferromagnetic and antiferromagnetic dielectrics have been discovered. The magnetic properties of these materials often permit observation of the electron spin resonance at microwave frequencies. The V-4502 EPR Spectrometer with the V-4545A Liquid Helium Accessory and rotating electromagnet proves to be quite useful in the understanding of magnetically ordered phenomena.

EXAMPLE

ELECTRON SPIN RESONANCE IN ANTIFERROMAGNETIC MATERIALS

The concept of antiferromagnetic ordering¹ was first proposed by Néel in 1932. Bitter presented a discussion in 1937; and Bizette, Squire, and Tsai in 1938 reported the first observation of this phenomenon in MnO. Van Vleck (1941), Anderson (1950) and Li (1950) subsequently presented extensive treatments on the magnetic ordering of the sublattice magnetizations. The theory of antiferromagnetic resonance (AFMR) was first discussed by Kittel² (1951) and by Nagamiya³ (1951). These two discussions treat the special case of uniaxial anisotropy and applied field H_0 less than the spin flop field H_c . This spin flop field, which is due to minimizing the free energy of the system, causes the sublattice magnetizations to reorient themselves perpendicular to the applied field. In 1952 Keffer and Kittel⁴, and Yosida⁵ treated the more general case of orthorhombic symmetry.

A particular example is the recent observation⁶ at liquid helium temperatures of AFMR in europium fluoride. The figure shows the AFMR at 4.2°K as a function of the orientation of H_0 . The data is taken at X-band in the (111) plane. With $H_0 < H_c$ the observed $(\cos \phi)^{-2}$ dependence is compatible with the existence of three equivalent easy or minimal energy directions in this plane. An independent measure of the static susceptibility permits determination of the anisotropy energy.



1. For a comprehensive review and an exhaustive reference list, refer to T. Nagamiya, K. Yosida and R. Kubo, *Advances in Physics* **4** (1955); B. Lax and K. J. Button, *Microwave Ferrites and Ferrimagnetics*, McGraw-Hill (1962); G. T. Rado and H. Suhl, editors, *Magnetism* Vol. 1-3, Academic Press (1963, 1964). 2. C. Kittel, *Phys. Rev.* **82**, 565 (1951). 3. T. Nagamiya, *Progr. Theoret. Phys. (Kyoto)* **6**, 342 (1951). 4. F. Keffer and C. Kittel, *Phys. Rev.* **85**, 329 (1952). 5. K. Yosida, *Progr. Theoret. Phys. (Kyoto)* **7**, 425 (1952). 6. Kenneth Lee (to be published).

For a collection of previous examples in this series and literature which fully explains the 100 kc EPR Spectrometer, write the Analytical Instrument Division. In Europe contact Varian A. G., Zug, Switzerland.



VARIAN associates
PALO ALTO 52, CALIFORNIA